

Photochromic Molecules for Biological Applications

Dissertation

Zur Erlangung des Doktorgrades der Naturwissenschaften

(Dr. rer. nat.)

an der Fakultät für Chemie und Pharmazie

der Universität Regensburg



vorgelegt von

Ulrike Wirth

aus Kastl

2023

The experimental work was carried out at the Institute of Organic Chemistry at the University of Regensburg under the supervision of Prof. Dr. Burkhard König between November 2018 and May 2022 and at the Institute of Biological Chemistry at the University of Vienna under the supervision of Prof. Dr. Markus Muttenthaler between June and August 2022.

Date of submission: 15.02.2023

Date of colloquium: 17.03.2023

Board of examiners:

Apl. Prof. Dr. Rainer Müller (chair)

Prof. Dr. Burkhard König (1st referee)

PD Dr. Max Keller (2nd referee)

Prof. Dr. Joachim Wegener (examiner)

INTRODUCTION

Design Strategies for Photoswitchable Small Molecules and Peptides

In the last few years, enormous progress has been made in the field of photopharmacology. This rather new approach uses light as the external trigger taking advantage of the properties it has to offer such as bioorthogonality, its non-invasive nature, and the high spatiotemporal precision that can be achieved.^[1] Therefore, a photochromic moiety which can be toggled between two (or more) isomers by light of different wavelengths is attached to or incorporated into a bioactive molecule. The switching results in a change in geometry, dipole moment, or electronic properties. The aim is to precisely control the activity of a bioactive molecule.^[1-3] One potential field of application are photoswitchable drugs. This would enable selective activation of a drug at the desired location in the body without flooding the whole body with the drug, therefore, limiting nonspecific side effects.^[2,4] Beyond that, these photoswitchable ligands can be utilized as ‘research tools’ to help investigate cellular processes and pathogenesis.^[5] Several biological processes have been made controllable by light, e.g. receptor function, enzyme activity, or ligand binding.^[1] To achieve the biggest possible on/off effect in activity the two isomers obtained upon switching have to show a certain difference in the overall structure and/or in its electronic properties (Figure 1A). The most important photochromic moiety for a geometric change is the class of azobenzenes (Figure 1C). They can be switched between their *trans* and their metastable *cis* isomer. Easy synthesis, high fatigue resistance, and relatively high photostationary states are just a few advantages that azobenzenes bring along.^[1,6,7]

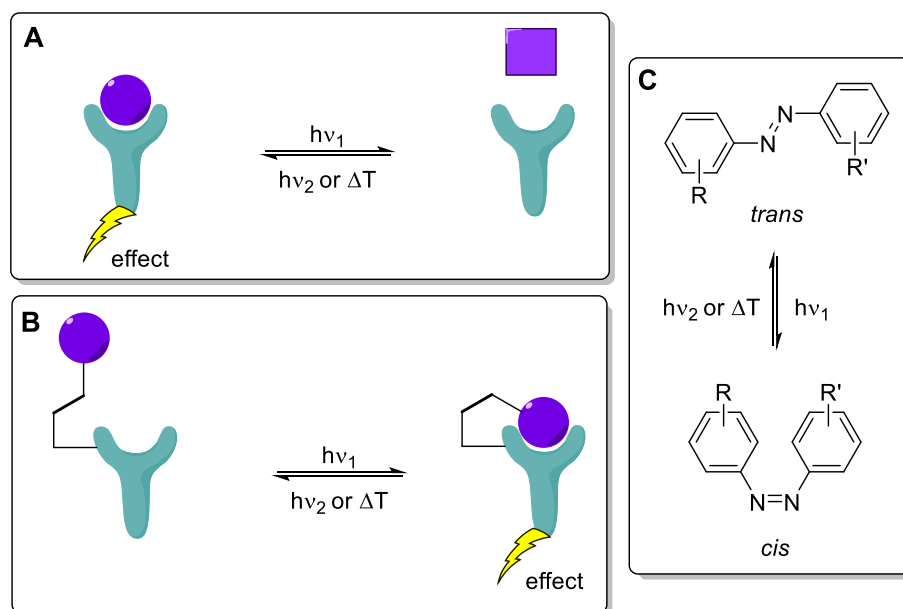


Figure 1. Principle of photoactive biological molecules (for both approaches also the other isomer can be the active isomer). **(A)** Photochromic ligands. **(B)** Photochromic tethered ligands. **(C)** Photoisomerization of azobenzenes.^[8-10]

All kinds of bioactive molecules can be and have been made photoswitchable, e.g. nucleic acids, lipids, small molecules, proteins, and peptides.^[1,11] In this thesis the focus lies on small molecules (chapters 1 & 2) and peptides (chapters 3 & 4). The design of photoswitchable probes should result in a molecule that is only active in one isoform and the pharmacological properties of this isomer should be as similar to the original compound as possible which is often challenging as already minor changes can lead to a loss of activity.^[5,12] When designing a photoswitchable small molecule based on a biologically active compound, there are two main ways how to incorporate an azobenzene moiety as the photoresponsive part. If a molecule has a certain motif, e.g., a stilbene, benzyl phenyl ethers, or diaryl esters, etc., the way to go is azologization.^[13] In this process, this motif is replaced by an azo group (Figure 2A). This results in a photoswitchable derivative that is similar in size and shape compared to the parent compound. As the isomerizable group is directly incorporated into the active molecule, ideally, switching results in a disruption of the structure that is responsible for binding or activation of the receptor, enzyme, ion channel, etc., which leads to a change in affinity or activity. If the molecule you want to modify does not have any of the above-mentioned motifs, the second approach can be applied in which an already existing phenyl ring is either extended to an azobenzene or the whole azobenzene moiety is attached to the bioactive molecule (Figure 2B).^[12] This way, the pharmacological core is not perturbed and the difference between the two isomers can be achieved by steric and electronic differences. An additional modification to these photoswitchable molecules is the extension by a covalent warhead (Figure 1B). This group can covalently bind to a protein via bioconjugation. One of the most used approaches are photochromic tethered ligands (PTLs) that bind to a cysteine or lysine residue close to the ligand binding site.^[8-10] These PTLs usually consist of the covalent warhead, a photochromic moiety, the pharmacophore, and linkers of varying lengths that connect these parts.^[10] This approach has been used, e.g., for ion channels^[14-16] or receptors^[10,17]. PTLs require the incorporation of an unnatural amino acid into the target protein that can act as an anchoring site but after this small alteration the protein is still very similar to its native state.^[10] This leads to a high selectivity for the receptor and furthermore, by covalently binding the ligand to the protein the concentration at the binding site is very high and the ligands are not diffusion limited.^[9,18,19]

A more modern approach to design photochromic ligands would be the use of computational methods. This way is less straightforward than azologization or azo extension, but it may result in structures that may have not been thought of just by the approaches mentioned above.^[12]

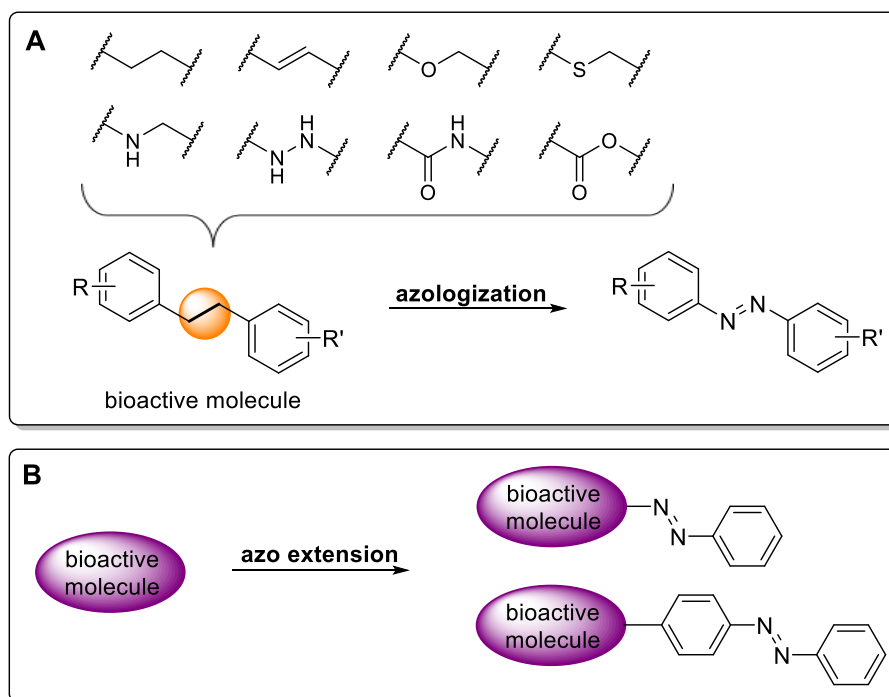


Figure 2. Approaches for the incorporation of azobenzenes into small molecules. **(A)** Azologization approach.^[1,3] **(B)** Azo extension approach.^[12]

Peptides represent another major class of bioactive molecules making them an interesting target for photopharmacology. Photoswitchable peptides can serve on the one hand as smaller motifs for bigger proteins and on the other hand, several bioactive peptides exist that play important roles in living systems, e.g. hormones such as insulin, neuropeptide Y, or oxytocin.^[20–22] Peptides often have a well-defined structure because of hydrogen bonds between the amide hydrogens and the carbonyl oxygens. These interactions result in two major secondary structures: α -helices and β -structures, including β -strands and β -turns that form β -sheets and β -hairpins.^[23] Still, peptides can also exist in an unordered way, the random coil.^[1] In which structure the peptides are present depends very much on the pH value, temperature and solvent.^[1,24] In the biological context these parameters are already fixed as cells or other living systems tolerate only very small changes in pH value and temperature, and water as the only solvent. One way to alter and interrupt these ordered structures of peptides is the incorporation of photoswitches. Different approaches exist on how to make peptides photoresponsive (Figure 3).^[1,11,20,21] In the first approach an unnatural amino acid with a photoswitchable side chain is incorporated into the peptide sequence (Figure 3A). To gain even more impact on the conformational control a photoswitch can also be inserted into the backbone of the peptide, either in a cyclic peptide or a linear peptide (Figure 3B). In the third approach, the side chains of two cysteines (more rarely used are lysine, glutamic or aspartic

acid) are connected via a photoswitch (Figure 3C).^[11] All three approaches have been successfully applied to photocontrol peptide structure and recognition.

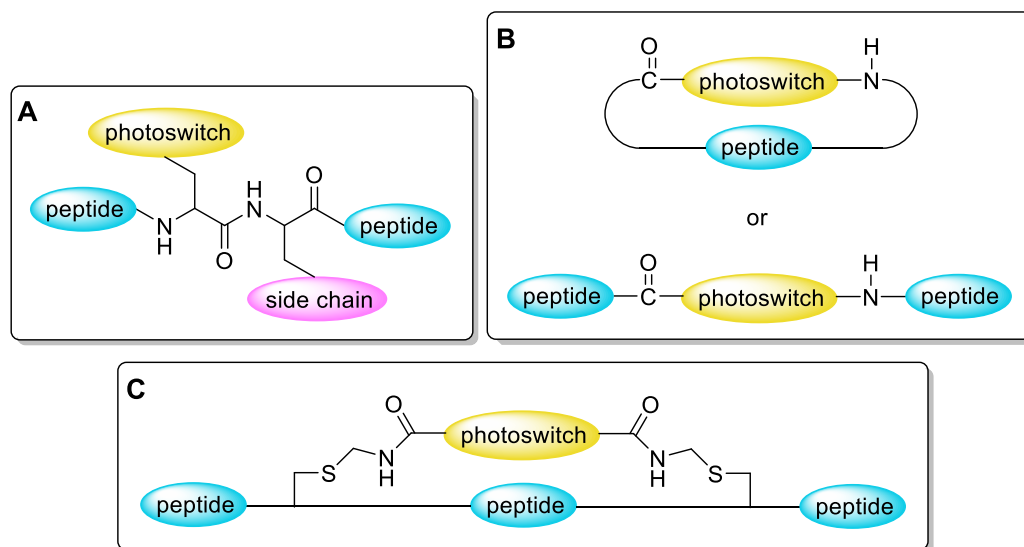


Figure 3. Approaches for the incorporation of photochromic moieties into peptides. **(A)** Photoswitch as an amino acid side chain. **(B)** Photoswitch incorporated into peptide backbone (cyclic or linear), **(C)** Cross-linking of two cysteines with a photoswitch.^[1,20,21]

Approach A has not been used as often as approaches B and C assuming that a photoswitchable amino acid residue does not have a large effect on the peptide backbone. Approaches B and C are more likely to induce a more dramatic conformational change in the overall peptidic structure than A. Yet, this approach can be useful when the photoswitchable peptide should be very similar to the parent peptide, e.g., because the peptide is prone to lose its activity upon changes. Even though the expected effect on the peptide backbone is rather small, in chapter 4 this approach led to the biggest differences in activity between *trans* and *cis* isomer.

In the second approach, the photoswitch is installed in the backbone of the peptide connecting the photochromic moiety at two opposite sides to the peptide. This can be done in linear, as well as in cyclic peptides.^[1,20,21] Compared to approach A, upon irradiation a more drastic change in the overall structure of the peptide is expected. This approach is preferably used to disrupt β -structures. A very common motif in proteins and peptides are β -turns. They cause a change in the direction of the peptide chain. A photochromic moiety can be incorporated and act as a β -turn element.^[25,26] In several examples it was shown that the *cis* isomer acts as a β -turn motif, while the *trans* isomer brings the peptide into a more extended form.^[27–29] A β -turn

can also induce the formation of a β -hairpin, two β -strands oriented in an antiparallel direction looking like a hairpin. By replacing the β -turn element with a photochromic moiety, upon irradiation this ordered structure can be disrupted.^[30–33]

α -Helices are the second important key structure in peptides. The predominant way to manipulate this structural element is approach C in which two cysteine residues are crosslinked by a photoswitchable moiety. In the best case, one isomer stabilizes the helical motif, whereas the other isomer leads to an unfolding of the peptide. Which isomer prevents the peptide from unfolding depends on the crosslinking sites and the length of the photoswitch backbone.^[1,20,22] In literature several different substituted azobenzenes are reported that crosslink two cysteines at various distances resulting in a change of α -helix content upon irradiation.^[34–39]

This introduction represents a brief overview over the design strategies that can be applied for small molecules and peptides to make them photoresponsive. Furthermore, the focus was only on azobenzenes, although of course other photochromic moieties can also be used for these purposes. A large part of the approaches was applied in this thesis. Chapter 1 covers the azologization approach and chapter 2 describes photoswitchable tethered ligands. In chapters 3 and 4 photoswitchable peptides were synthesized with photoswitchable amino acids and backbone incorporated photoswitches. All compounds were studied in a biological context, therefore, contributing to the ever-growing field of photopharmacology.

References

- [1] W. Szymański, J. M. Beierle, H. A. V. Kistemaker, W. A. Velema, B. L. Feringa, *Chem. Rev.* **2013**, *113*, 6114–6178.
- [2] W. A. Velema, W. Szymanski, B. L. Feringa, *J. Am. Chem. Soc.* **2014**, *136*, 2178–2191.
- [3] J. Broichhagen, J. A. Frank, D. Trauner, *Acc. Chem. Res.* **2015**, *48*, 1947–1960.
- [4] M. M. Lerch, M. J. Hansen, G. M. van Dam, W. Szymanski, B. L. Feringa, *Angew. Chemie Int. Ed.* **2016**, *55*, 10978–10999.
- [5] C. Brieke, F. Rohrbach, A. Gottschalk, G. Mayer, A. Heckel, *Angew. Chem. Int. Ed.* **2012**, *51*, 8446–8476.
- [6] F. A. Jerca, V. V. Jerca, R. Hoogenboom, *Nat. Rev. Chem.* **2021**, *6*, 51–69.
- [7] A. A. Beharry, G. A. Woolley, *Chem. Soc. Rev.* **2011**, *40*, 4422–4437.
- [8] M. Ricart-Ortega, J. Font, A. Llebaria, *Mol. Cell. Endocrinol.* **2019**, *488*, 36–51.
- [9] A. E. Berizzi, C. Goudet, *Adv. Pharmacol.* **2020**, *88*, 143–172.
- [10] J. Broichhagen, D. Trauner, *Curr. Opin. Chem. Biol.* **2014**, *21*, 121–127.
- [11] Z. L. Pianowski, *Molecular Photoswitches*, **2022**.
- [12] P. Kobauri, N. S. Galenkamp, A. M. Schulte, J. De Vries, N. A. Simeth, G. Maglia, S. Thallmair, D. Kolarski, W. Szymanski, B. L. Feringa, *J. Med. Chem.* **2022**, *65*, 4798–4817.
- [13] M. Schoenberger, A. Damijonaitis, Z. Zhang, D. Nagel, D. Trauner, *ACS Chem. Neurosci.* **2014**, *5*, 514–518.
- [14] M. Volgraf, P. Gorostiza, R. Numano, R. H. Kramer, E. Y. Isacoff, D. Trauner, *Nat. Chem. Biol.* **2005**, *2*, 47–52.
- [15] M. Banghart, K. Borges, E. Isacoff, D. Trauner, R. H. Kramer, *Nat. Neurosci.* **2004**, *7*, 1381–1386.
- [16] S. Berlin, S. Szobota, A. Reiner, E. C. Carroll, M. A. Kienzler, A. Guyon, T. Xiao, D. Trauner, E. Y. Isacoff, *Elife* **2016**, *5*.
- [17] P. C. Donthamsetti, N. Winter, M. Schönberger, J. Levitz, C. Stanley, J. A. Javitch, E. Y. Isacoff, D. Trauner, *J. Am. Chem. Soc.* **2017**, *139*, 18522–18535.
- [18] K. Hüll, J. Morstein, D. Trauner, *Chem. Rev.* **2018**, *118*, 10710–10747.
- [19] P. Leippe, J. Koehler Leman, D. Trauner, *Biochemistry* **2017**, *56*, 5214–5220.
- [20] L. Albert, O. Vázquez, *Chem. Commun.* **2019**, *55*, 10192–10213.
- [21] C. Renner, L. Moroder, *ChemBioChem* **2006**, *7*, 868–878.
- [22] R. J. Mart, R. K. Allemann, *Chem. Commun.* **2016**, *52*, 12262–12277.
- [23] M. M. Gromiha, *Protein Bioinforma.* **2010**, 1–27.
- [24] K. Pagel, S. C. Wagner, K. Samedov, H. Von Berlepsch, C. Böttcher, B. Kokschi, *J. Am. Chem. Soc.* **2006**, *128*, 2196–2197.
- [25] C. M. Wilmot, J. M. Thornton, *J. Mol. Biol.* **1988**, *203*, 221–232.
- [26] E. G. Hutchinson, J. M. Thornton, *Protein Sci.* **1994**, *3*, 2207–2216.
- [27] L. G. Ulysse, J. Chmielewski, *Chem. Biol. Drug Des.* **2006**, *67*, 127–136.
- [28] L. Ulysse, J. Cubillos, J. Chmielewski, *J. Am. Chem. Soc.* **1995**, *117*, 8466–8467.
- [29] M. Löweneck, A. G. Milbradt, C. Root, H. Satzger, W. Zinth, L. Moroder, C. Renner, *Biophys. J.* **2006**, *90*, 2099–2108.
- [30] S. L. Dong, M. Löweneck, T. E. Schrader, W. J. Schreier, W. Zinth, L. Moroder, C. Renner, *Chem. Eur. J.* **2006**, *12*, 1114–1120.
- [31] T. E. Schrader, T. Cordes, W. J. Schreier, F. O. Koller, S. L. Dong, L. Moroder, W.

-
- Zinth, J. *Phys. Chem. B* **2011**, *115*, 5219–5226.
- [32] A. A. Deeg, M. S. Rampp, A. Popp, B. M. Pilles, T. E. Schrader, L. Moroder, K. Hauser, W. Zinth, *Chem. Eur. J.* **2014**, *20*, 694–703.
- [33] C. Hoppmann, S. Seedorff, A. Richter, H. Fabian, P. Schmieder, K. Rück-Braun, M. Beyermann, J. C. Hoppmann, S. Seedorff, A. Richter, K. Rück-Braun, C. Hoppmann, P. Schmieder, M. Beyermann, H. Fabian, *Angew. Chemie Int. Ed.* **2009**, *48*, 6636–6639.
- [34] J. A. Ihalainen, B. Paoli, S. Muff, E. H. G. Backus, J. Bredenbeck, G. A. Woolley, A. Caflich, P. Hamm, *Proc. Natl. Acad. Sci. U. S. A.* **2008**, *105*, 9588–9593.
- [35] D. G. Flint, J. R. Kumita, O. S. Smart, G. A. Woolley, *Chem. Biol.* **2002**, *9*, 391–397.
- [36] A. A. Beharry, O. Sadovski, G. A. Woolley, *Org. Biomol. Chem.* **2008**, *6*, 4323–4332.
- [37] Z. Zhang, D. C. Burns, J. R. Kumita, O. S. Smart, G. A. Woolley, *Bioconj. Chem.* **2003**, *14*, 824–829.
- [38] A. M. Ali, G. A. Woolley, *Org. Biomol. Chem.* **2013**, *11*, 5325–5331.
- [39] F. Zhang, O. Sadovski, G. A. Woolley, *ChemBioChem* **2008**, *9*, 2147–2154.

TABLE OF CONTENTS

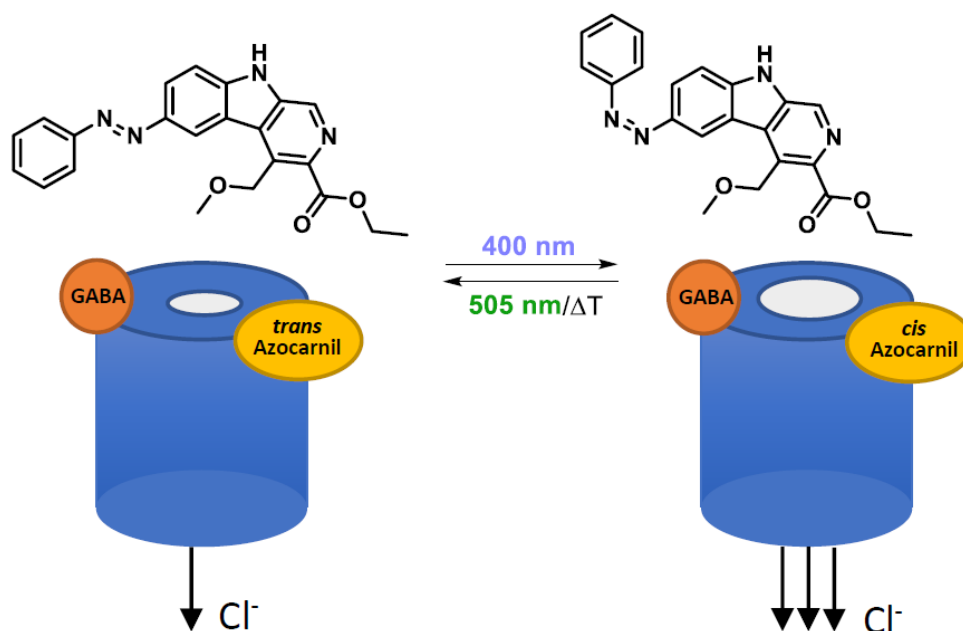
1	AZOCARNIL: A PHOTOSWITCHABLE POTENTIATOR OF THE GABA_A RECEPTOR	1
1.1	Introduction	3
1.2	Molecular Docking Studies.....	5
1.3	Synthesis	6
1.4	Photophysical Characterization.....	7
1.5	<i>In Vitro</i> Studies	9
1.6	Conclusion	11
1.7	Experimental Part.....	12
1.7.1	General Information.....	12
1.7.2	Synthetic Procedures	12
1.7.3	Molecular Docking	15
1.7.4	<i>In Vitro</i> Studies	16
1.8	Supporting Information	17
1.8.1	Purity.....	17
1.8.2	Photostationary States.....	18
1.8.3	Supplementary Figures to Molecular Docking Studies.....	19
1.8.4	Supplementary Figures to <i>In Vitro</i> Studies.....	21
1.8.5	NMR Spectra	22
1.9	References.....	28
2	SYNTHESIS AND CHARACTERIZATION OF NOVEL PHOTOSWITCHABLE COVALENT LIGANDS FOR THE β_2-ADRENERGIC RECEPTOR.....	31
2.1	Introduction	33
2.2	Design	33
2.3	Synthesis	35
2.4	Photophysical Characterization.....	37
2.5	Biological Characterization	39
2.6	Conclusion	41
2.7	Experimental Part.....	41
2.7.1	General Information.....	41
2.7.2	Synthetic Procedures	43

2.7.3	Biological Investigation	54
2.8	Supporting Information	56
2.8.1	Purity	56
2.8.2	Photophysical Characterization.....	58
2.8.2.1	UV/Vis Spectra and Cycle Performance.....	58
2.8.2.2	Photostationary States	61
2.8.2.3	Thermal Half-lives.....	66
2.8.3	Supplementary Information to Biological Investigation.....	68
2.8.4	NMR Spectra.....	73
2.9	References	105
3	MONITORING THE REVERSIBILITY OF GPCR SIGNALING BY COMBINING PHOTOCHROMIC LIGANDS WITH LABEL-FREE IMPEDANCE ANALYSIS	107
3.1	Introduction	109
3.2	Design	111
3.3	Synthesis.....	112
3.4	Photophysical Characterization	115
3.5	Ligand Binding and Functional Characterization.....	117
3.6	Impedance-Based Analysis of Y ₄ R Activation	121
3.7	Real-Time Monitoring of Light-Controlled Y ₄ R Agonism	124
3.8	Photoswitching Occurs inside Receptor Binding Pocket	128
3.9	Conclusion.....	129
3.10	Experimental Part	131
3.10.1	General Information	131
3.10.2	Synthetic Procedures.....	132
3.10.3	Biological Investigation	152
3.10.3.1	Ligand Binding and Functional Characterization	152
3.10.3.2	Impedance Studies	157
3.11	Supporting Information	161
3.11.1	Purity	161
3.11.2	Photophysical Characterization.....	166
3.11.2.1	UV/Vis Spectra and Cycle Performance.....	166
3.11.2.2	Photostationary States	170
3.11.2.3	Thermal Half-lives	181
3.11.3	Supplementary Information to Ligand Binding and Functional Characterization	183

3.11.4	Supplementary Information to Impedance Studies.....	187
3.11.5	NMR Spectra	190
3.12	References.....	213
4	PHOTOSWITCHABLE PROBES OF OXYTOCIN AND VASOPRESSIN.....	215
4.1	Introduction	217
4.2	Design	219
4.3	Synthesis	221
4.4	Photophysical Characterization	224
4.5	Biological Investigation	225
4.6	Conclusion	230
4.7	Experimental Part.....	231
4.7.1	General Information.....	231
4.7.2	Synthetic Procedures	232
4.7.3	Pharmacology	240
4.8	Supporting Information	242
4.8.1	Purity.....	242
4.8.2	Photophysical Characterization	254
4.8.2.1	UV/Vis Spectra and Cycle Performance	254
4.8.2.2	Photostationary States.....	258
4.8.2.3	Thermal Half-lives	264
4.8.3	Supplementary Figures.....	267
4.8.4	NMR Spectra	270
4.9	References.....	275
5	SUMMARY	281
6	ZUSAMMENFASSUNG	287
7	APPENDIX	293
7.1	Abbreviations	293
7.2	Curriculum Vitae.....	297
8	DANKSAGUNG	301
	EIDESSTATTLICHE ERKLÄRUNG.....	303

CHAPTER 1

1 Azocarnil: A Photoswitchable Potentiator of the GABA_A Receptor



This chapter is a manuscript in preparation for submission.

This chapter was in collaboration with the group of Prof. P. Gorostiza (Institute for Bioengineering of Catalonia, Barcelona Institute of Science and Technology, Barcelona, Spain), Prof. C. Rovira (University of Barcelona, Spain) and Prof. H. U. Zeilhofer (University of Zurich, Switzerland).

U. Wirth performed the synthesis and (photo-)chemical characterization of all compounds. A. Nin-Hill performed the docking studies. G. Malieieva performed the *in vitro* studies. M. Ranucci performs the *in vivo* studies.

U. Wirth, Dr. G. Malieieva, Dr. A. Nin-Hill and Prof. P. Bregestovski wrote the manuscript draft. Prof. König, Prof. Gorostiza, Prof. Bregestovski and Prof. Zeilhofer supervised the project.

1.1 Introduction

Utilizing chemical compounds that can change their conformation upon application of light of different wavelengths became a widely used approach for the optical control of behavior and function of different cells and tissues.^[1-3] This class of compounds is called photoswitches and contains a photochromic group that, upon illumination, undergoes a reversible change in its structure and properties. The most commonly used photoswitches are azobenzenes which isomerize between *trans* and *cis* conformation of the N=N double bond, resulting in changes in both length and dipole moment of the molecule.^[4-7] Incorporation of these molecular photoswitches into the structure of bioactive molecules paves the way for actively modulating the activity of specific biological molecules with very high spatiotemporal precision.^[8] Hence, these photoswitchable ligands represent promising research tools for investigating cellular processes and pathogenesis in life sciences.^[9-11] Two ionotropic receptors that are the object of current research are the GABA_A and glycine receptor, the major inhibitory neurotransmitter receptors in the mammalian brain and important targets in pharmaceutical research as they play a significant role in the treatment of e.g. epilepsy, anxiety, insomnia, hyperekplexia and autism.^[12-14]

During the last years, we developed several photochromic ligands capable of modulating the activity of GABA and glycine receptors. It has been shown that photoswitch Azo-NZ1, composed of a nitrazepam moiety merged to an azobenzene photoisomerizable group, is a soluble light-driven Cl-channel blocker, which allows photomodulation of the activity induced by anion-selective glycine and GABA receptors.^[15] Furthermore, we found Fulgazepam, a fulgimide that is also based on the benzodiazepine structure. But in contrast to Azo-NZ1, Fulgazepam in its closed form is able to act as a potentiator of the GABA_A receptor.^[16] Another compound, Glyght, is a negative allosteric modulator of glycine receptors. In its *cis*-configuration it stabilizes the closed state of the ion channel, while in the *trans*-configuration it can stabilize the open state.^[17,18] The effectiveness of Glyght as a light-controlled modulator of the activity of glycine receptors was proven at heterologous expression, in brain slices and *in vivo* observation on zebrafish.^[17,19] In the present study, we describe the synthesis, photophysical characterization and the *in vitro* biological investigation of azocarnil. This structure is based on abecarnil, a β -carboline, whereas all structures mentioned above were based on benzodiazepines. Abecarnil belongs to the class of nonbenzodiazepines and acts as a partial agonist with a high binding affinity.^[20,21] It shows anxiolytic and anticonvulsant effects,

but in contrast to benzodiazepines, it exerts weak or no sedative and ataxic actions.^[22–24] We demonstrate that the design that is based on an azologization approach and was confirmed by molecular docking studies resulted in a *cis*-active potentiator of the GABA_A receptor.

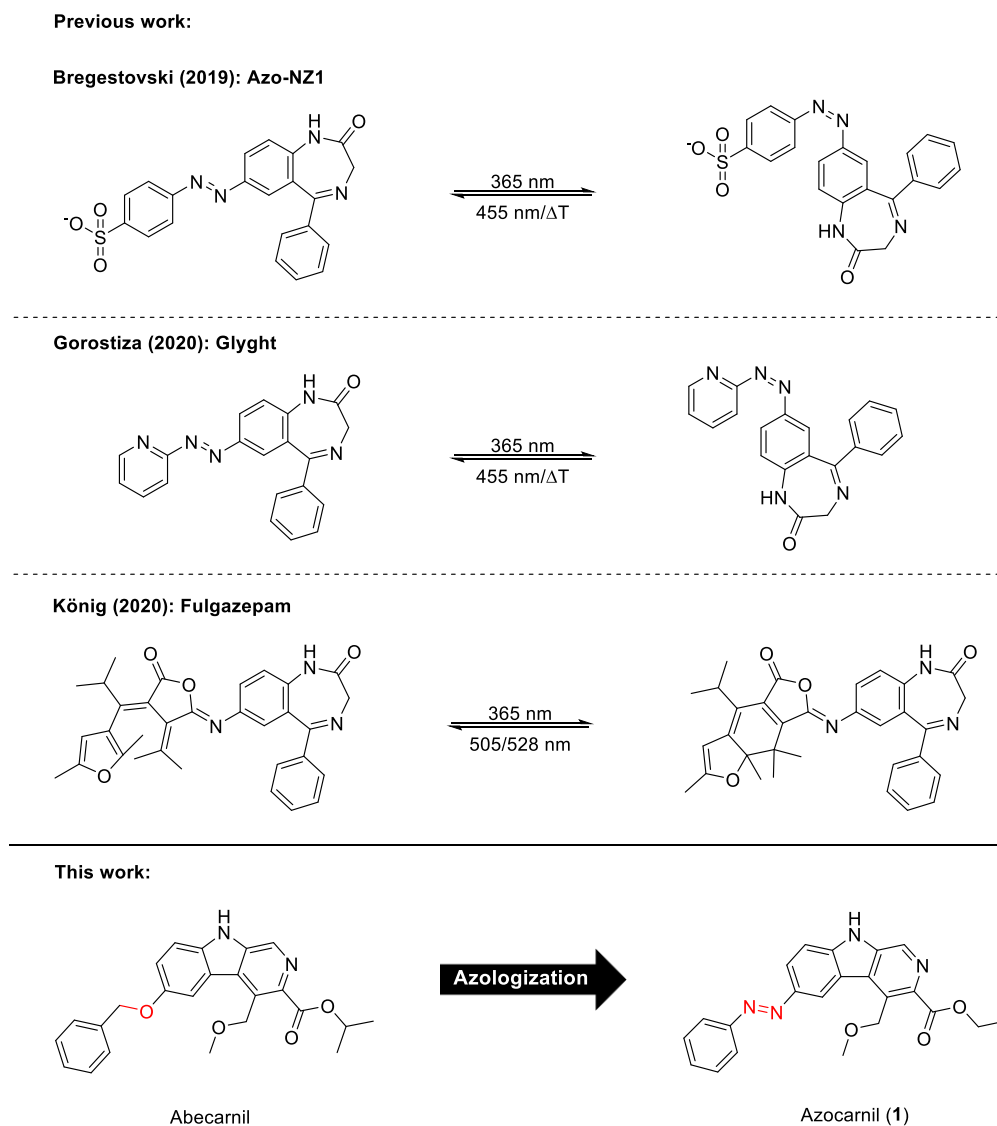


Figure 1. Previously reported photochromic ligands^[15–17] targeting GABA and glycine receptors and newly synthesized azocarnil (1).

1.2 Molecular Docking Studies

To get insight into the mechanism of action of azocarnil on the GABA_A receptor, molecular docking calculations were performed with both *cis* and *trans* conformations. We focused on the benzodiazepine binding site between the $\alpha 1(+)$ and $\gamma 2(-)$ subunits, as the parent compound, abecarnil, is a mixed full/partial agonist binding at this location.^[20,25] Docking of *cis*-azocarnil showed that the preferred binding pose resembles the diazepam binding found in the electron microscopy structure solved by Kim *et. al.*^[26] The azobenzene moiety of *cis*-azocarnil is oriented away from the membrane and towards the principal $\alpha 1(+)$ subunit, where the two benzene moieties are almost perfectly superimposed with the chlorophenyl and the pendant phenyl ring of the diazepam molecule. In this way, the interactions seen for the agonist diazepam molecule are conserved for *cis*-azocarnil, which also acts as a GABA_AR potentiator (Figure 1A). In contrast, the docking of *trans*-azocarnil shows a flipped orientation of the abecarnil moiety, placing the azobenzene group towards the membrane (Figure 1B). Such binding mode results in fewer interactions with the residues lining the benzodiazepine binding site compared to *cis*-azocarnil or diazepam, suggesting that binding of *trans*-azocarnil is less favourable. These results indicate that *cis*-azocarnil is more active, while *trans*-azocarnil is less active.

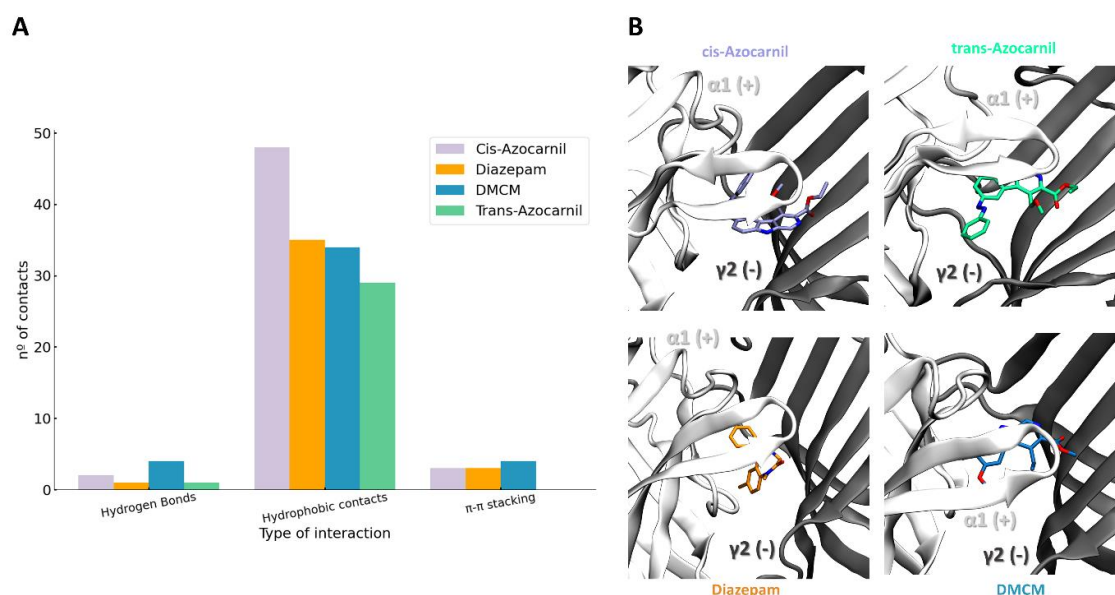
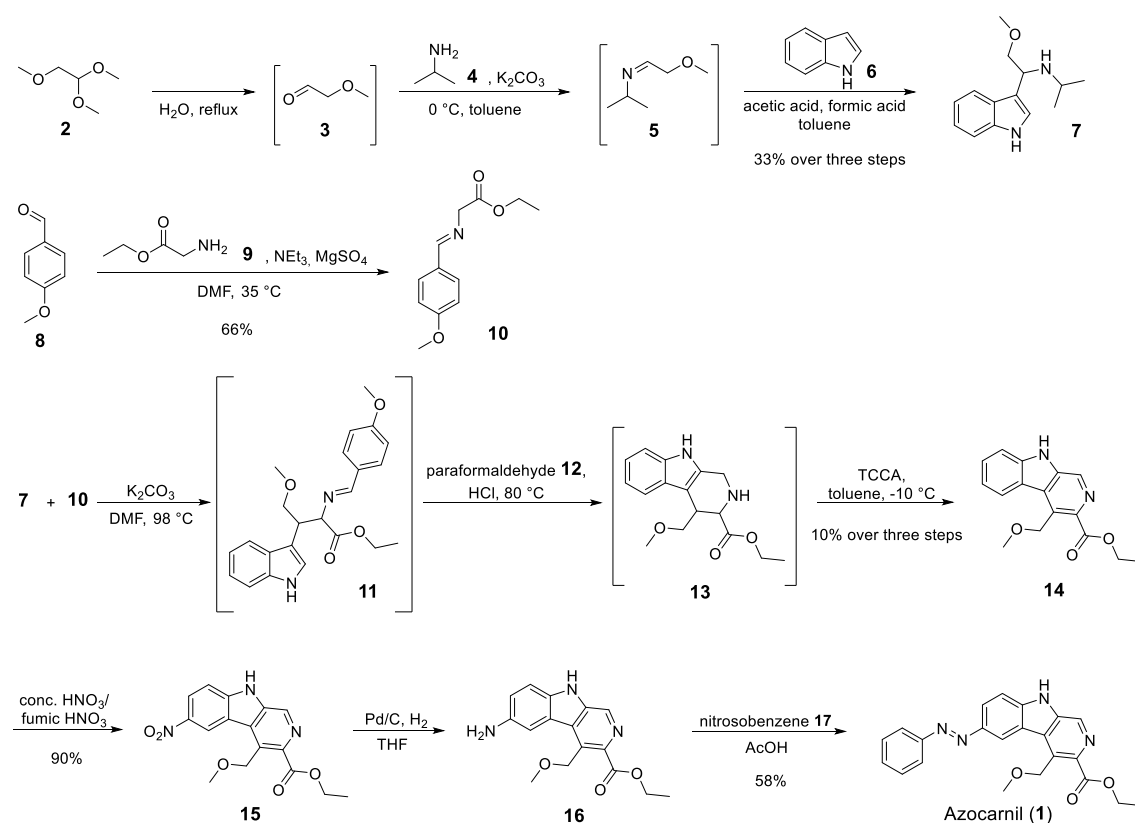


Figure 2. Molecular docking calculations of *cis*- and *trans*-azocarnil in the benzodiazepine binding site of the GABA_A receptor. **(A)** Number of interactions for *cis*-azocarnil (purple), *trans*-azocarnil (green), diazepam^[26] (orange, PDB: 6X3X) and DMCM^[27] (steel blue, PDB: 8DD3). **(B)** Preferred binding poses for the *cis*-azocarnil (purple) and *trans*-azocarnil (green) in the benzodiazepine binding site of GABA_AR (shown as new cartoon representation in white and gray). The diazepam (orange) and DMCM (steel blue) binding poses found in PDB 6X3X and 8DD3 are also shown.^[26,27] DMCM: methyl 6,7-dimethoxy-4-ethyl- β -carboline-3-carboxylate, PDB: protein data bank.

1.3 Synthesis

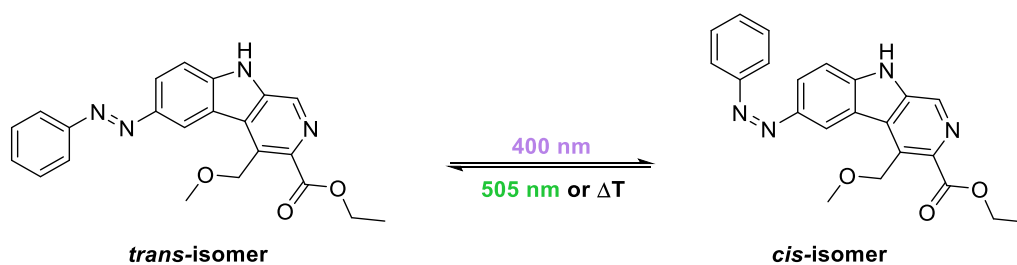
The two aromatic moieties in abecarnil are connected by an ether bond which was “replaced” by an azo group in order to make its photoswitchable analog (“azologization”). The second alteration was the replacement of the isopropyl group for an ethyl group because of synthetic reasons. The synthetic approach started from 1,1,2-trimethoxyethane (**2**) which was hydrolyzed to afford methoxyacetaldehyde (**3**) which was, due to its thermal instability and volatility, directly used in the reaction with isopropylamine (**4**) to form **5**.^[28,29] Intermediate **5** was, without further purification, reacted with indole (**6**) to give **7**.^[29] In a reaction executed in parallel, the reaction of 4-methoxybenzaldehyde (**8**) and glycine ethyl ester (**9**) gave imine **10**.^[30] The three-step synthesis towards β-carboline **14** starting from **7** and **10**, including the cyclization with paraformaldehyde (**12**) in a Pictet-Spengler reaction and oxidation with trichloroisocyanuric acid to obtain the fully aromatic scaffold, was done in one pot without isolation of the intermediates **11** and **13**.^[31] The next step involved the nitration of **14** with a mixture of concentrated and fuming nitric acid to get nitro compound **15**. Subsequent reduction of the nitro group led to the amine **16**. The photochromic moiety of **1** was installed in the last step performing a Mills reaction using nitrosobenzene (**17**) and amine **16** in acetic acid.



Scheme 1. Synthetic route towards azocarnil (**1**). TCCA: trichloroisocyanuric acid.

1.4 Photophysical Characterization

Azocarnil was investigated regarding its photophysical properties. It could be reversibly toggled between its *cis*- and *trans*-isomer in DMSO and aqueous buffer using wavelengths of 400 nm and 505 nm, respectively (Scheme 2).



Scheme 2. Photoisomerization of azocarnil (1).

The *trans*-isomer is indicated in green and showed the typical absorption maximum at around 360 nm, upon switching this maximum decreased and a new maximum in the visible range at around 450 nm appeared representing the *cis*-isomer (purple curve, Figure 3A). Azocarnil showed high fatigue resistance in both solvents, over ten cycles no decrease in absorbance was observed (Figure 3B). The thermal half-life in DMSO was 4.9 h which allowed the investigation of the photostationary states (PSS) by HPLC (Figure S2-S3). It exhibited a PSS of 87% for the *trans*- to *cis*-isomerization and 75% for the *cis*- to *trans*-isomerization. The thermal half-life of azocarnil in aqueous buffer was only 1.5 min (Figure 3C). Hence, the PSS could not be determined by HPLC or NMR.

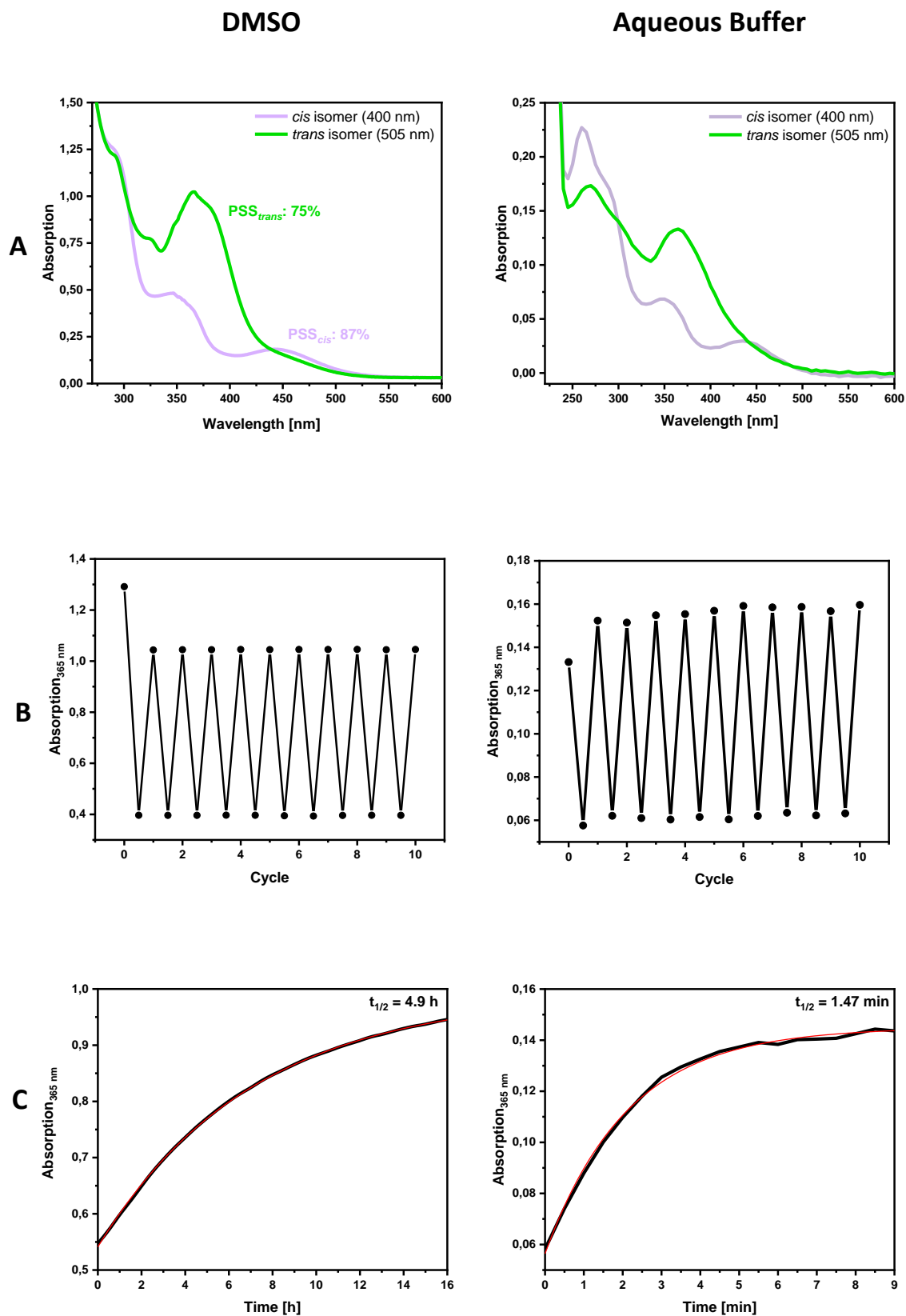


Figure 3. Photophysical characterization of **1** in DMSO (50 μ M, left) and aqueous buffer (25 μ M + 0.5% DMSO, right). **(A)** UV/Vis spectra of both isomers, **(B)** cycle performance, **(C)** thermal half-life.

1.5 *In Vitro* Studies

The effect of azocarnil (**1**) in *trans*- and *cis*-conformation was tested at the gabaergic currents in primary hippocampal cultured neurons. We noticed, that when light of 400 nm was applied in control conditions it was producing a deflection of the base line (Figure 4A, upper panel). Thus, in every experiment, before application of azocarnil, light of 400 nm and 505 nm, respectively, were applied to establish the amplitude of light-induced current for every cell. To calculate the increase of the amplitude of the current that was induced by co-application of azocarnil and light of 400 nm, experimentally recorder value was normalized to the amplitude of the current induced by the illumination with 400 nm alone.

Azocarnil in low concentrations of 500 nM and 1 μ M, upon illumination with 400 nm, produced small increase of the amplitude of the gabaergic currents to 1.17 ± 0.54 ($n = 4$ cells) and 1.79 ± 0.68 from control ($n = 3$ cells), respectively. When the concentration of azocarnil was increased to 10 μ M and 25 μ M its effect on the macroscopic gabaergic currents was found to be statistically significant: currents increased by 3.5 ± 1.4 times from control ($n = 5$ cells, $P < 0.05$) and 3.1 ± 0.49 ($n = 4$ cells, $P < 0.01$), respectively (Figure 4A, middle panel, Figure 4B). Addition of 0.5% DMSO combined with illumination with 400 nm was not producing an increase of the macroscopic gabaergic current (Figure S4C). To confirm that recorded currents were of gabaergic origin, after every experiment GABA_AR inhibitor bicuculine was applied (Figure 4A, lowest panel). Application of bicuculine was completely inhibiting gabaergic miniature inhibitory postsynaptic currents (mIPSCs) and significantly decreasing the amplitude of the macroscopic currents – the amplitude of the base line deflection induced by illumination with light of 400 nm was close to the control level – it comprised 1.3 ± 0.4 from control ($n = 4$; Figure 4C). When picrotoxin (PTX, 100 μ M) was used to block gabaergic receptors at the end of the experiment a complete inhibition of mIPSCs and macroscopic gabaergic currents that were induced by azocarnil and light of 400 nm was observed (Figure S4A, B).

We have as well studied the decay time of the mIPSCs at illumination with 400 nm before and after the application of azocarnil. Among all concentrations tested only the highest – 25 μ M induced a statistically significant increase in the decay time of the mIPSCs from 32 ± 11 ms to 43 ± 19 ms (Figure 4C, D; $P < 0.01$, total number of events that were analyzed – 78, from 4 independent experiments).

To investigate the selectivity of azocarnil its effect at the glutamatergic miniature excitatory postsynaptic currents (mEPSCs) was studied. Application of azocarnil in combination with light of 400 nm or 505 nm, respectively, have not induced or increased the amplitude of the macroscopic current (Figure 5A), nor increased the decay time of the mEPSCs (Figure 5B, C).

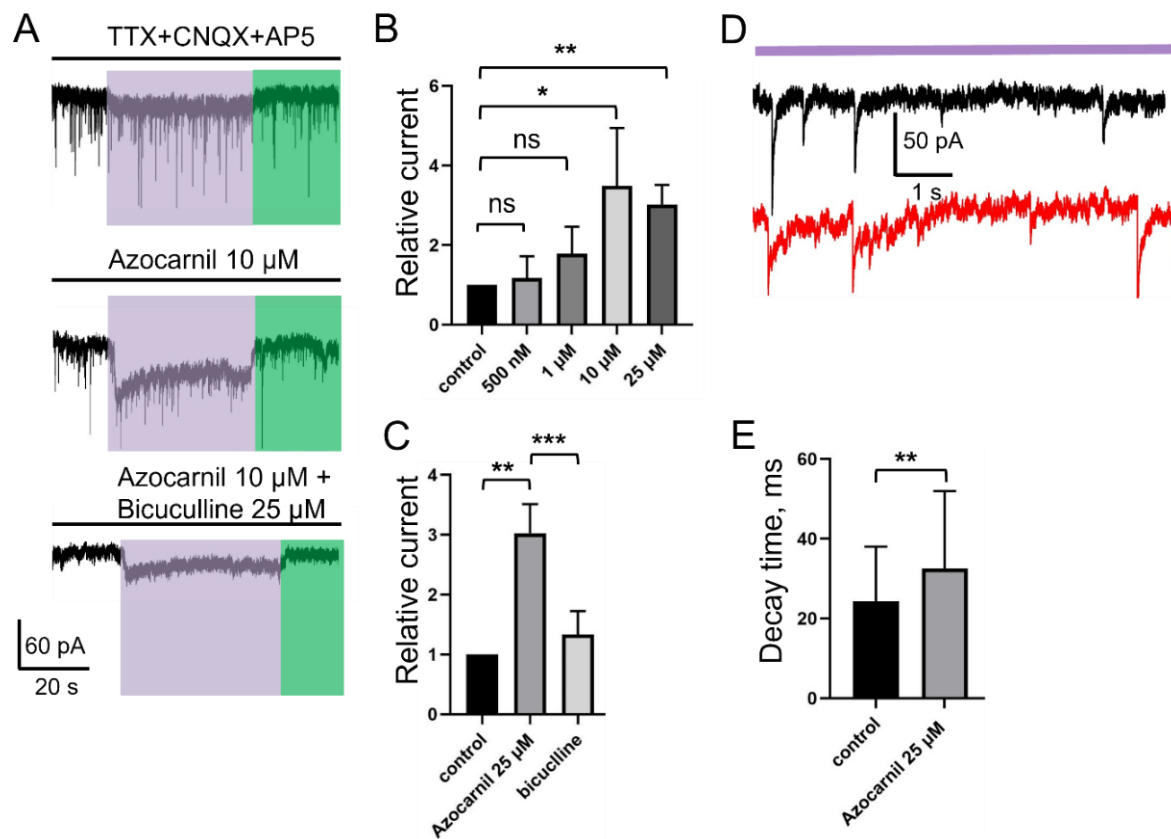


Figure 4. Effect of azocarnil on the gabaergic currents in cultured primary hippocampal neurons. **(A)** Voltage-clamp recordings of gabaergic currents in control (upper panel), during the application of azocarnil (10 μ M, middle panel) and during the application of the mixture of azocarnil (10 μ M) and bicuculline (25 μ M). Illumination with light of 400 nm is depicted by violet rectangle, illumination with light of 505 nm is depicted by green rectangle, $V_{\text{hold}} = -70\text{mV}$. **(B)** Cumulative graph demonstrating the relative amplitude of macroscopic gabaergic currents that were recorded during simultaneous application of different concentrations of azocarnil and illumination with 400 nm. Comparison was done using paired t-test, $n = 3-5$ cells for each concentration; ns – no significant, * - $P < 0.05$; ** - $P < 0.01$. **(C)** Cumulative graph demonstrating mean amplitude of macroscopic gabaergic currents in control, during application of azocarnil (25 μ M) and during application of azocarnil (25 μ M) and bicuculline (25 μ M) at illumination with 400 nm. **(D)** Azocarnil (25 μ M) in *trans*-conformation increased decay time of the mIPSCs. In black – recording of mIPSCs at illumination with 400 nm in control conditions, in red – recording of mIPSCs at illumination with 400 nm combined with application of azocarnil (25 μ M). **(E)** Cumulative graph demonstrating the effect of azocarnil (25 μ M) combined with light of 400 nm on decay time of mIPSCs in cultured hippocampal neurons. Comparison was done using unpaired t-test, ** - $P < 0.001$. TTX: tetrodotoxin, CNQX: 6-cyano-7-nitroquinoxaline-2,3-dione, AP5: (2R)-amino-5-phosphonovaleric acid.

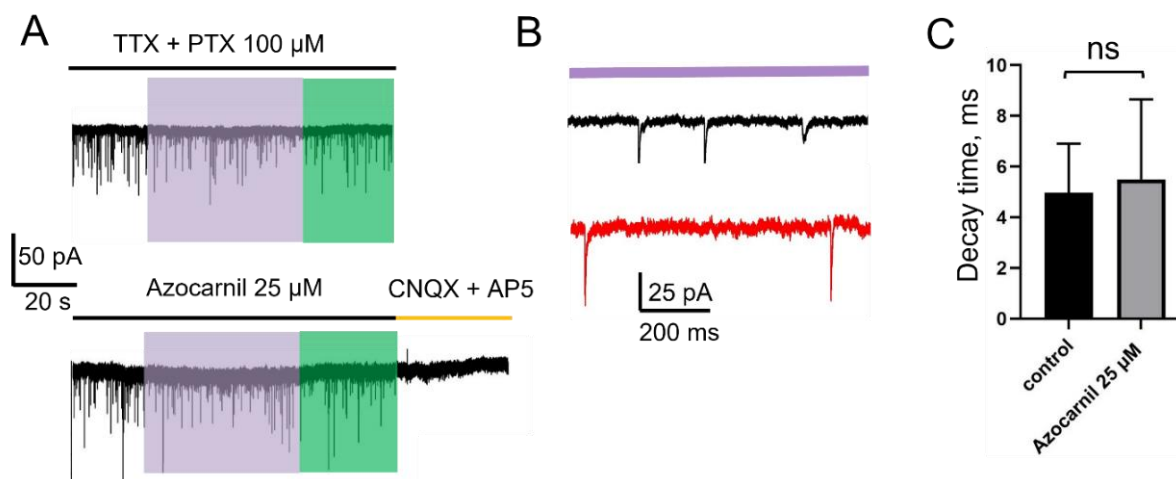


Figure 5. The effect of azocarnil on the glutamatergic currents in cultured hippocampal primary neurons. **(A)** Voltage-clamp recordings of glutamatergic currents in control (during the application of PTX (100 μ M)) and after addition of azocarnil (25 μ M). Duration of illumination (400 nm or 505 nm, respectively) are represented by colored rectangles. Application of the mixture of CNQX and AP5 is indicated by orange bar. **(B)** Magnified traces demonstrating single mEPSCs in control (black trace) and during application of azocarnil (25 μ M, red trace) at illumination with 400 nm indicated by violet bar. **(C)** Cumulative graph demonstrating the effect of azocarnil (25 μ M) during illumination with 400 nm on the decay time of mEPSCs. Comparison was done using unpaired t-test, ns – not significant. PTX: picrotoxin, TTX: tetrodotoxin, CNQX: 6-cyano-7-nitroquinoxaline-2,3-dione, AP5: (2R)-amino-5-phosphonovaleric acid.

1.6 Conclusion

We herein describe the synthesis of a photochromic GABA_A receptor potentiator on the basis of the known nonbenzodiazepine abecarnil called azocarnil. The design strategy was based on an azologization approach and was further supported by molecular docking studies predicting the *cis* isomer to be the more active isomer. The photophysical properties revealed reversible switching, and high fatigue resistance but a thermal half-life of only 1.5 min in aqueous buffer. By patch-clamp measurements we showed that the *cis* isomer indeed increased the amplitude of the gabaergic currents in cultured hippocampal neurons, whereas the *trans* isomer did not influence these currents. Blocking the ion channel after the experiments with the inhibitor bicuculline led to a decrease in the amplitude which proved that the currents are of gabaergic origin. Furthermore, azocarnil is selective towards the GABA_A receptor as it did not change glutamatergic currents. In conclusion, we showed that *in vitro*, azocarnil represents a promising photoswitchable tool to investigate the GABA_A receptor with high spatiotemporal control because the potentiating effect is only observed when azocarnil is in its *cis* configuration which can only be maintained under constant irradiation. To test the compound also in living animals *in vivo* studies are currently being conducted on mice.

1.7 Experimental Part

1.7.1 General Information

Starting materials and commercial reagents were purchased from Acros, Alfa Aesar, Fisher, Fluka, Fluorochem, Merck, Sigma-Aldrich, TCI and VWR and were used without further purification. Solvents were used in p.a. quality or dried according to common procedures if necessary. All reactions with oxygen- or moisture-sensitive reagents were carried out in glassware which was dried before use by heating under vacuum. Dry nitrogen or argon were used as inert gas atmosphere. NMR spectra were measured at room temperature using a Bruker Avance 400 (400 MHz for ¹H and 101 MHz for ¹³C) or a Bruker Avance 600 (600 MHz for ¹H and 151 MHz for ¹³C) NMR spectrometer. All chemical shifts are reported in δ-scale as parts per million [ppm] (multiplicity, coupling constant J, number of protons) relative to the solvent residual peaks. Coupling constants J are given in Hertz [Hz]. Abbreviations used for signal multiplicity: ¹H-NMR: s = singlet, d = doublet, dd = doublet of doublets, ddd = doublet of doublets of doublets, dt = doublet of triplets, t = triplet, td = triplet of doublets, q = quartet, and m = multiplet. Mass spectra were recorded on an Agilent Q-TOF 6540 UHD, Finnigan MAT SSQ 710 A, Jeol AccuTOF GCX or ThermoQuest Finnigan TSQ 7000 spectrometer. Absorption spectra were recorded on a UV/VIS Agilent Cary 50 spectrometer. Analytical thin layer chromatography (TLC) was performed on silica gel coated alumina plates (MN precoated TLC-sheets ALUGRAM® Xtra SIL G/UV254). Visualization was done by UV-light (254 nm or 366 nm) or staining with ninhydrin solution. Column chromatography was performed on a Biotage Isolera One automated flash purification system with UV/Vis detector. Analytical HPLC measurements were performed using an Agilent 1220 Infinity LC System (column: P/No 00F-4251-B0, Phenomenex Luna® 3 μm C18(2) 100 Å, LC column 150x2.0 mm). Purification by preparative HPLC was conducted on a preparative HPLC Agilent 1260 Infinity LC System (column: P/No 00G-4253-P0-AX, Phenomenex Luna® 10 μm C18(2) 100 Å, LC column 250x21.2 mm). The eluent systems were used as specified. After the purification process, solvents were removed by lyophilization.

1.7.2 Synthetic Procedures

2-Methoxyacetaldehyde (3). 1,1,2-Trimethoxyethane (**2**) (6.4 g, 7 mL, 54 mmol, 1.0 eq.) and water (15 mL) were refluxed overnight under nitrogen atmosphere. The mixture was cooled

to rt and was extracted with CH₂Cl₂. The combined organic layers were dried over MgSO₄ and the solvent was removed carefully. The product was used due to its volatility and instability without any further purification in the next step.

N-Isopropyl-2-methoxyethan-1-imine (5). Isopropylamine (6.7 g, 9.3 mL, 113 mmol, 2.1 eq.) was dissolved in toluene (20 mL) in a nitrogen atmosphere. The mixture was cooled to 0 °C and **3** was added. After 30 min K₂CO₃ (5 g) was added. Subsequently, the mixture was filtered. The solution containing the product was used as such in the next step without any further purification.

N-(1-(1H-Indol-3-yl)-2-methoxyethyl)propan-2-amine (7). Indole (**6**) (3.7 g, 31 mmol, 1.0 eq.) was suspended in toluene (20 mL), acetic acid (20 mL), formic acid (14 mL) and isopropyl amine (7.0 mL). The mixture was cooled to -10 °C and a solution of imine **5** (1.6 eq.) was added slowly. The mixture was stirred for 1 h at rt. Water (60 mL) was added and the pH was adjusted to 12. The aqueous phase was extracted with toluene. The combined organic phases were dried over MgSO₄ and the solvent was removed *in vacuo*. The crude product was purified by column chromatography (CH₂Cl₂/MeOH, 0-10%). **7** was obtained as an orange oil (4.2 g, 18 mmol, over three steps 33%). ¹H NMR (400 MHz, Chloroform-d) δ 10.16 (s, 1H), 9.62 (s, 1H), 7.86 (d, *J* = 2.7 Hz, 1H), 7.57 (d, *J* = 7.8 Hz, 1H), 7.47 – 7.43 (m, 1H), 7.25 – 7.16 (m, 2H), 4.79 (s, 1H), 4.00 (t, *J* = 9.8 Hz, 1H), 3.74 (dd, *J* = 10.2, 4.1 Hz, 1H), 3.42 (s, 3H), 3.25 (d, *J* = 9.2 Hz, 1H), 1.35 (dd, *J* = 8.2, 6.5 Hz, 6H). ¹³C NMR (101 MHz, CDCl₃) δ 135.9, 126.6, 125.8, 123.1, 120.9, 117.2, 112.3, 105.6, 72.7, 59.1, 52.8, 48.4, 20.5, 19.0. **ESI-MS:** *m/z* (%) = 233.17 (M+H)⁺.

Ethyl (E)-2-((4-methoxybenzylidene)amino)acetate (10). Glycine ethyl ester hydrochloride (**9**) (2.6 g, 25 mmol, 1.0 eq.) was dissolved in toluene (20 mL). 4-Methoxybenzaldehyde (**8**) (3.4 g, 3.0 mL, 25 mmol, 1.0 eq.) was added at rt. At 20 °C, triethylamine (2.8 g, 3.8 mL, 28 mmol, 1.1 eq.) was added dropwise and the resulting mixture was stirred at rt overnight. Then, water was added and the mixture was stirred for 15 min. The organic layer was separated, and the solvent was removed *in vacuo*. The crude product contained starting material and product but was used without further purification because the product decomposed during column chromatography. Yield: 66% (NMR analysis). ¹H NMR (400 MHz, Chloroform-d) δ 8.21 (d, *J* = 1.3 Hz, 1H), 7.75 – 7.68 (m, 2H), 6.95 – 6.89 (m, 2H), 4.35 (d, *J* = 1.2 Hz, 2H), 4.23 (q, *J* = 7.1 Hz, 2H), 3.83 (s, 3H), 1.29 (t, *J* = 7.1 Hz, 3H). ¹³C NMR (101 MHz, CDCl₃) δ 170.5, 164.8, 162.2, 130.3, 128.7, 114.1, 62.2, 61.1, 55.5, 14.3. **EI-MS:** *m/z* (%) = 221.10.

Ethyl 4-(methoxymethyl)-9H-pyrido[3,4-*b*]indole-3-carboxylate (14). Compound **10** (3.88 g, 17.5 mmol, 1.0 eq.) was dissolved in DMF (15 mL) and K₂CO₃ (6.0 g) was added. The mixture was stirred at 98 °C. A solution of **7** (4.1 g, 17.5 mmol, 1.0 eq.) in DMF (25 mL) was added dropwise over 1 h. The reaction mixture was stirred at 98 °C for further 1.5 h. After cooling to rt and standing overnight, the formed precipitated was filtered off and washed with DMF. To the filtrate water (15 mL) and conc. HCl (2.5 mL) were added and the mixture was stirred for 20 min. In a separate flask, paraformaldehyde (568 mg, 18.9 mmol, 1.1 eq.) was suspended in water (15 mL) and conc. HCl (0.3 mL) and heated to 80 °C for 30 min until the solution became clear. The formaldehyde solution was cooled to rt and was added to the reaction mixture over 30 min. Stirring was continued at rt overnight. Water (65 mL) and toluene (50 mL) were added and the solution was stirred for 10 min. The organic phase was separated and sodium bicarbonate was added to the aqueous phase until a pH of 8 was reached. The water layer was extracted with toluene and the organic phases were combined, washed with water and dried over MgSO₄. The volume was reduced to 45 mL. Then, the mixture was cooled to -15 °C and triethylamine (4.3 mL) was added in a nitrogen atmosphere. Under stirring, trichloroisocyanuric acid (2.44 g, 10.5 mmol) dissolved in ethyl acetate (60 mL) was added over 25 min, keeping the temperate below -8 °C. The mixture was stirred another 10 min at -10 °C and more triethylamine (5.1 mL) was added. The solution was stirred at rt overnight. Water was added (40 mL) and stirring was continued for 30 min. The organic phase was separated and the water phase was extracted with toluene. The organic phases were combined, washed with water and dried over MgSO₄. The solvent was removed *in vacuo* and the crude product was purified by column chromatography (PE/EtOAc, 50-100% and CH₂Cl₂/MeOH, 0-2%). Compound **14** was obtained as an off-white solid (516 mg, 1.8 mmol, 10% over three steps). ¹H NMR (400 MHz, Chloroform-*d*) δ 13.69 (s, 1H), 9.59 (s, 1H), 8.37 (dd, *J* = 8.3, 1.1 Hz, 1H), 7.82 (dt, *J* = 8.5, 1.0 Hz, 1H), 7.76 (ddd, *J* = 8.4, 6.9, 1.1 Hz, 1H), 7.47 (ddd, *J* = 8.2, 6.9, 1.1 Hz, 1H), 5.51 (s, 2H), 4.59 (q, *J* = 7.2 Hz, 2H), 3.52 (s, 3H), 1.54 (t, *J* = 7.1 Hz, 3H). ¹³C NMR (101 MHz, CDCl₃) δ 160.9, 144.7, 136.3, 133.2, 132.5, 132.1, 128.1, 127.1, 125.8, 122.8, 120.5, 114.0, 66.2, 63.9, 58.7, 14.0. **ESI-MS:** *m/z* (%) = 285.13 (M+H)⁺.

Ethyl 4-(methoxymethyl)-6-nitro-9H-pyrido[3,4-*b*]indole-3-carboxylate (15). At 0 °C, conc. nitric acid (14 mL) and fuming nitric acid (7 mL) were mixed carefully. Compound **14** (450 mg, 1.6 mmol, 1.0 eq.) was added portionwise. The reaction mixture was stirred for further 3 h at 5 °C. The solution was poured into ice water and neutralized with conc. ammonia solution. The precipitate was filtered, washed with water and dried to afford **15** as an off-white

solid (473 mg, 1.4 mmol, 90%). **¹H NMR** (400 MHz, DMSO-*d*₆) δ 12.75 (s, 1H), 9.12 (d, *J* = 2.3 Hz, 1H), 9.02 (s, 1H), 8.46 (dd, *J* = 9.1, 2.3 Hz, 1H), 7.83 (d, *J* = 9.1 Hz, 1H), 5.20 (s, 2H), 4.40 (q, *J* = 7.1 Hz, 2H), 3.39 (s, 3H), 1.37 (t, *J* = 7.1 Hz, 3H). **¹³C NMR** (101 MHz, DMSO) δ 166.7, 144.3, 140.9, 139.7, 138.0, 134.4, 127.5, 127.2, 123.5, 121.8, 120.0, 112.8, 67.4, 61.2, 57.6, 14.2. **ESI-MS**: *m/z* (%) = 330.11 (M+H)⁺.

Ethyl 6-amino-4-(methoxymethyl)-9*H*-pyrido[3,4-*b*]indole-3-carboxylate (16).

Compound **15** (433 mg, 1.3 mmol, 1.0 eq.) was dissolved in methanol (50 mL). Pd/C (10%, 130 mg) was added and the reaction mixture was stirred under hydrogen (1 bar) for 3 h at rt (TLC monitoring and staining with ninhydrin). The mixture was filtered over celite and the solvent was removed *in vacuo*. Amine **16** was used without further purification in the next step. **¹H NMR** (400 MHz, DMSO-*d*₆) δ 12.28 (s, 1H), 8.96 (s, 1H), 8.18 (d, *J* = 2.1 Hz, 1H), 7.78 (d, *J* = 8.7 Hz, 1H), 7.54 (dd, *J* = 8.7, 2.1 Hz, 1H), 5.16 (s, 2H), 4.39 (q, *J* = 7.1 Hz, 2H), 3.38 (s, 3H), 1.36 (t, *J* = 7.1 Hz, 3H). **ESI-MS**: *m/z* (%) = 300.13 (M+H)⁺.

Ethyl (*E*)-4-(methoxymethyl)-6-(phenyldiazenyl)-9*H*-pyrido[3,4-*b*]indole-3-

carboxylate (1). Compound **16** (363 mg, 1.21 mmol, 1.0 eq.) and nitrosobenzene (**17**) (130 mg, 1.21 mmol, 1.0 eq.) were stirred in AcOH (70 mL) and CH₂Cl₂ (10 mL) overnight at 40 °C. The solvent was removed *in vacuo*. Purification by preparative HPLC (column: Phenomenex Luna 10 μm C18(2) 100 Å, gradient 0-20 min: MeCN/0.05% aqueous TFA 10:90 – 98:2), evaporation, and lyophilization of the solvent yielded **1** (351 mg, 0.70 mmol, 58%) as a yellow solid. **¹H NMR** (400 MHz, DMSO-*d*₆) δ 12.47 (s, 1H), 8.97 (s, 1H), 8.83 (d, *J* = 1.9 Hz, 1H), 8.21 (dd, *J* = 8.9, 1.9 Hz, 1H), 7.98 – 7.90 (m, 2H), 7.82 (d, *J* = 8.9 Hz, 1H), 7.66 – 7.58 (m, 2H), 7.57 – 7.50 (m, 1H), 5.25 (s, 2H), 4.40 (q, *J* = 7.1 Hz, 2H), 3.42 (s, 3H), 1.37 (t, *J* = 7.1 Hz, 3H). **¹³C NMR** (101 MHz, DMSO) δ 166.9, 152.0, 146.1, 143.0, 139.3, 137.5, 133.9, 130.8, 129.4, 127.8, 127.1, 123.1, 122.3, 121.1, 120.8, 113.1, 67.5, 61.0, 57.6, 14.2. **HR-MS** (ESI): calc. for C₂₂H₂₀N₄O₃ (M+H)⁺, *m/z* 389.1608, found: 389.1613.

1.7.3 Molecular Docking

We used the homology model of the GABA_AR heteropentameric α1/β2/γ2 receptor from reference.^[32] The initial structures of the azocarnil compound (*cis*- and *trans*-isomers) were created employing Avogadro (version 1.1.1^[33]) and were optimized using quantum mechanical calculations. Such calculations were performed with the Gaussian09 (G09) programme package^[34] using density functional theory^[35,36], with the B3LYP functional^[34] and the 6–

31++G(d,p) basis set. The docking program used was Autodock Vina (version 1.1.2^[37]). We centered our search space in the benzodiazepine binding site, i.e. the binding site for the parent compound abecarnil.^[27] The ligand was allowed to change its geometry (by exploring all the possible ligand torsions) to optimize its fitting to the benzodiazepine site. The maximum energy difference between the best and worst binding modes and the exhaustiveness of the search algorithm were set to default values (3 and 8 kcal·mol⁻¹, respectively). Instead, the maximum number of modes was increase to 20 to increase the docking sampling. This protocol was repeated 10 times, starting with different random seeds, so that a total number of 200 binding modes were obtained. The ligand binding poses were clustered using the quality threshold algorithm implemented in VMD (<https://github.com/luisico/clustering>), and then the representative structure of the most populated cluster(s) was analysed using the Binana2.1 algorithm.^[38,39] The images of the modelling section were generated with VMD.^[40]

1.7.4 *In Vitro* Studies

Primary Hippocampal Cultures. Procedures were performed in accordance with the European guidelines for animal care and use in research and were approved by the Animal Experimentation Ethics Committee at the University of Barcelona.

Sprague-Dawley rats (P 1-3) were sacrificed by decapitation, hippocampal neurons were isolated and cultured as previously described.^[41] Neurons were plated on Poly-D-Lysine (PDL)-coated 16 mm coverslips ($0.5-1 \times 10^4$ cells) and incubated at 37 °C, 5% CO₂. On DIV 3 cultured cells were treated with 1 μM of Ara-C to prevent proliferation of non-neuronal cells. Electrophysiology experiments were performed at neurons older than 12 DIV which demonstrated intrinsic firing activity.

Electrophysiological Recordings and Data Analysis. Whole-cell recordings were performed at room temperature using an EPC-10 amplifier (HEKA Elektronik, Germany) and Patch Master software (HEKA). Cells were bathed with external solution containing (mM): 150 NaCl, 3 KCl, 2 MgCl₂, 10 HEPES, 10 D-glucose and 2 CaCl₂; pH was adjusted to 7.4 with NaOH. Recording pipettes were pulled from borosilicate glass capillaries (Harvard Apparatus Ltd, USA) and had resistance 5-10 MOhms. Solution used for filling patch contained (mM): 130 KCl, 10 HEPES, 1 MgCl₂, 3 Mg-ATP, 1 Na-GTP, 0.5 EGTA.

Miniature GABAergic inhibitory postsynaptic currents (mIPSCs) were recorded in voltage clamp configuration in the presence of tetrodotoxin (TTX, 1 μ M) and CNQX (10 μ M) and AP5 (40 μ M) to block AMPA and NMDA receptors-mediated currents. To block mIPSCs bicuculline 25 μ M was used, or picrotoxin (PTX). Recordings were made at holding potential of -70 mV.

Azocarnil and PTX were first dissolved in DMSO and then in the bath solution till the final concentration. TTX, CNQX, AP5 and bicuculline were first dissolved in MilliQ water and then in the bath solution till the final concentration.

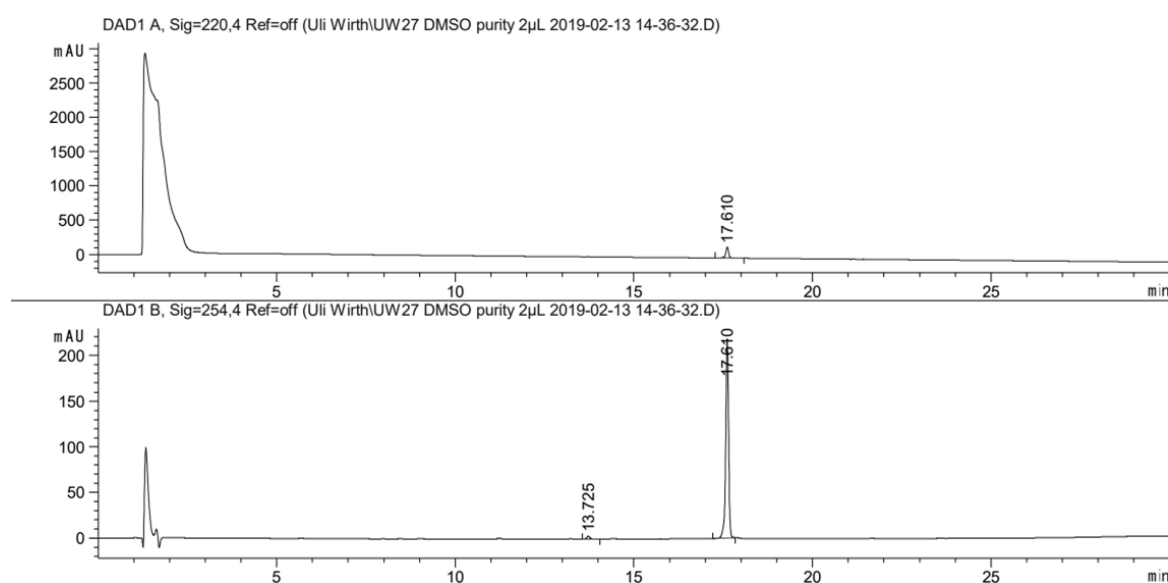
Data was analyzed using Igor Pro 6.05 (WaveMetrics, USA) and Prism 9 (GraphPad, USA) software. Results are represented as mean \pm SD. Statistical difference between groups was evaluated with paired and unpaired t-test and was considered significant at the value of P below 0.05.

1.8 Supporting Information

1.8.1 Purity

Purity was measured in DMSO at the detection wavelengths 220 nm and 254 nm.

Purity (220 nm): 100%, Purity (254 nm): 99%.



Signal 1: DAD1 A, Sig=220,4 Ref=off						Signal 2: DAD1 B, Sig=254,4 Ref=off							
Peak #	RetTime [min]	Type	Width [min]	Area [mAU*s]	Height [mAU]	Area %	Peak #	RetTime [min]	Type	Width [min]	Area [mAU*s]	Height [mAU]	Area %
1	17.610	BB	0.0841	912.38580	161.07248	100.0000	1	13.725	BB	0.0774	16.79308	3.29575	1.3674
Totals :				912.38580	161.07248		Totals :				1228.12132	221.57335	

Figure S1. Purity of **1** at 220 nm and 254 nm determined by analytical RP-HPLC.

1.8.2 Photostationary States

Photostationary states (PSS) were measured on analytical HPLC (flow: 0.3 mL/min, solvent A: H₂O (0.05% TFA), solvent B: MeCN). To determine the photostationary state of the photoswitch the samples (0.1 mM in DMSO) were irradiated first with 400 nm to get the *cis*-isomer. Afterwards, the sample was irradiated with 505 nm, to get back to the *trans*-isomer. The samples were measured at the isosbestic point (439 nm).

cis-Isomer: 87%

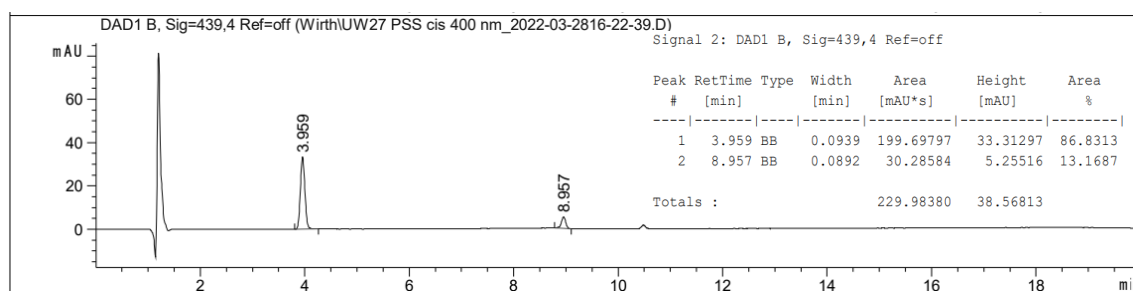


Figure S2. Photostationary state of **1** after irradiation with 400 nm.

trans-Isomer: 75%

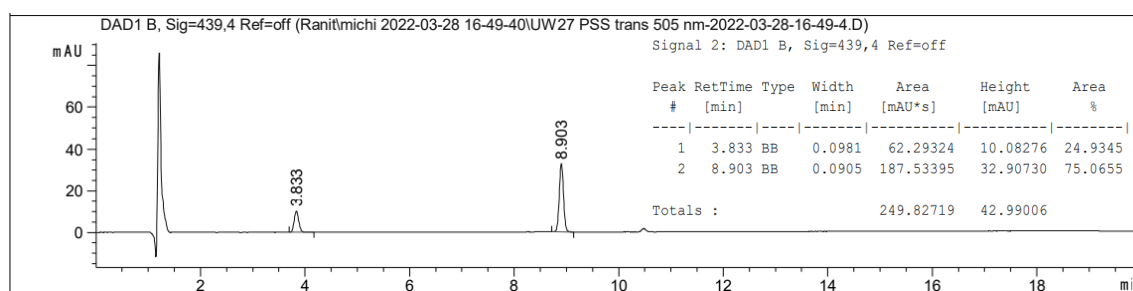


Figure S3. Photostationary state of **1** after irradiation with 505 nm.

1.8.3 Supplementary Figures to Molecular Docking Studies

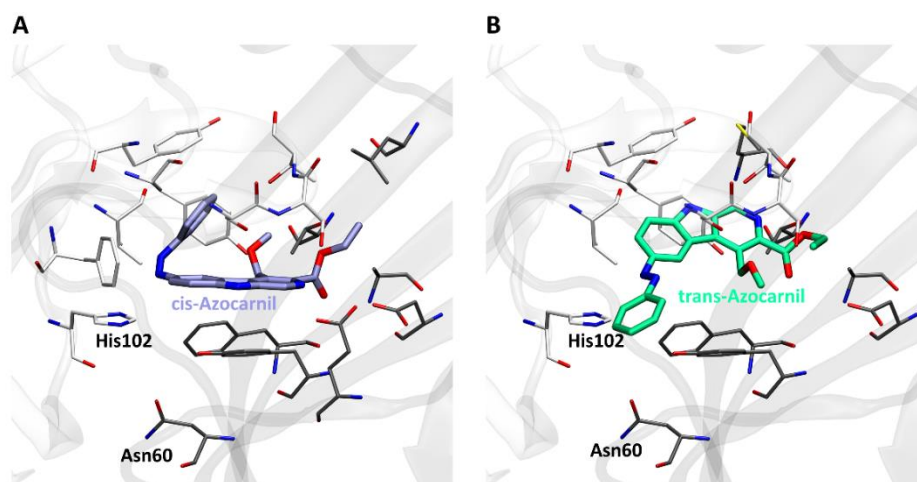


Figure S4. Preferred binding poses of the molecular docking calculations for *cis* and *trans* azocarnil in the benzodiazepine binding site of GABA_AR. **(A)** *Cis*-azocarnil (purple and thicker lines) and the interacting residues (white, for α 1 subunit, and gray, for γ 2 subunit) of GABA_AR are shown. The important residues His102 and Asn60 are labeled.^[26] **(B)** *Trans*-azocarnil (green and thicker lines) and the benzodiazepine binding site residues (white, for α 1 subunit, and gray, for γ 2 subunit) of GABA_AR are shown. The important residues His102 and Asn60 are labeled.^[26]

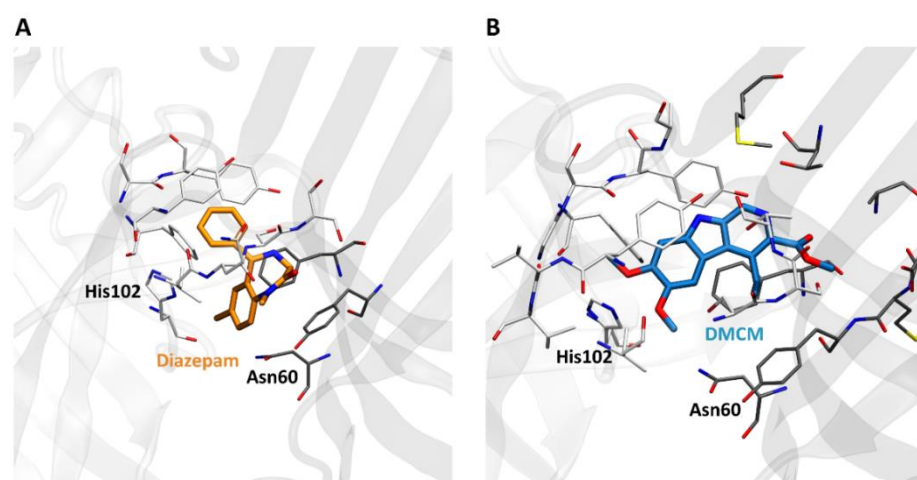


Figure S5. Binding poses of diazepam and DMCM in the benzodiazepine binding site of GABA_AR. **(A)** Diazepam (orange and thicker lines) and the interacting residues (white, for α 1 subunit, and gray, for γ 2 subunit) of GABA_AR are shown. Protein structure from PDB 6X3X.^[26] The important residues His102 and Asn60 are labeled.^[26] **(B)** DMCM (steel blue and thicker lines) and the benzodiazepine binding site residues (white, for α 1 subunit, and gray, for γ 2 subunit) of GABA_AR are shown. Protein structure from PDB 8DD3.^[27] The important residues His102 and Asn60 are labeled.^[26]

Table S1. Residues involved in each type of ligand-protein interaction found using Binana2.1^[39] for each system.

	<i>Cis</i> -Azocarnil	<i>Trans</i> -Azocarnil	Diazepam	DMCM
Hydrogen Bonds	α1 Ser206 α1 Ser205	α1 Thr207	α1 Ser205	γ2 Thr179 α1 His102 α1 Ser206
Hydrophobic	α1 Ser205 γ2 Tyr58 γ2 Phe77 α1 His102 α1 Val203 α1 Thr207 γ2 Ala79 γ2 Leu140 α1 Tyr160 α1 Tyr210 γ2 Thr142	α1 Ser205 α1 Tyr160 α1 Thr207 γ2 Met130 γ2 Thr142 α1 Tyr210 γ2 Ala79 α1 Ser206 α1 Val203 α1 His102 γ2 Tyr58	α1 Phe100 α1 His102 α1 Tyr210 α1 Tyr160 α1 Val203 γ2 Tyr58 γ2 Phe77 α1 Ser205	α1 Tyr210 α1 Tyr160 γ2 Met167 γ2 Phe114 α1 Phe100 α1 His102 α1 Gly158 α1 Ser159 α1 Ser205 γ2 Tyr95* α1 Val203
π-π stacking	γ2 Tyr58		α1 Tyr160 α1 Tyr210 γ2 Phe77	α1 Tyr160 α1 Tyr210 γ2 Phe114

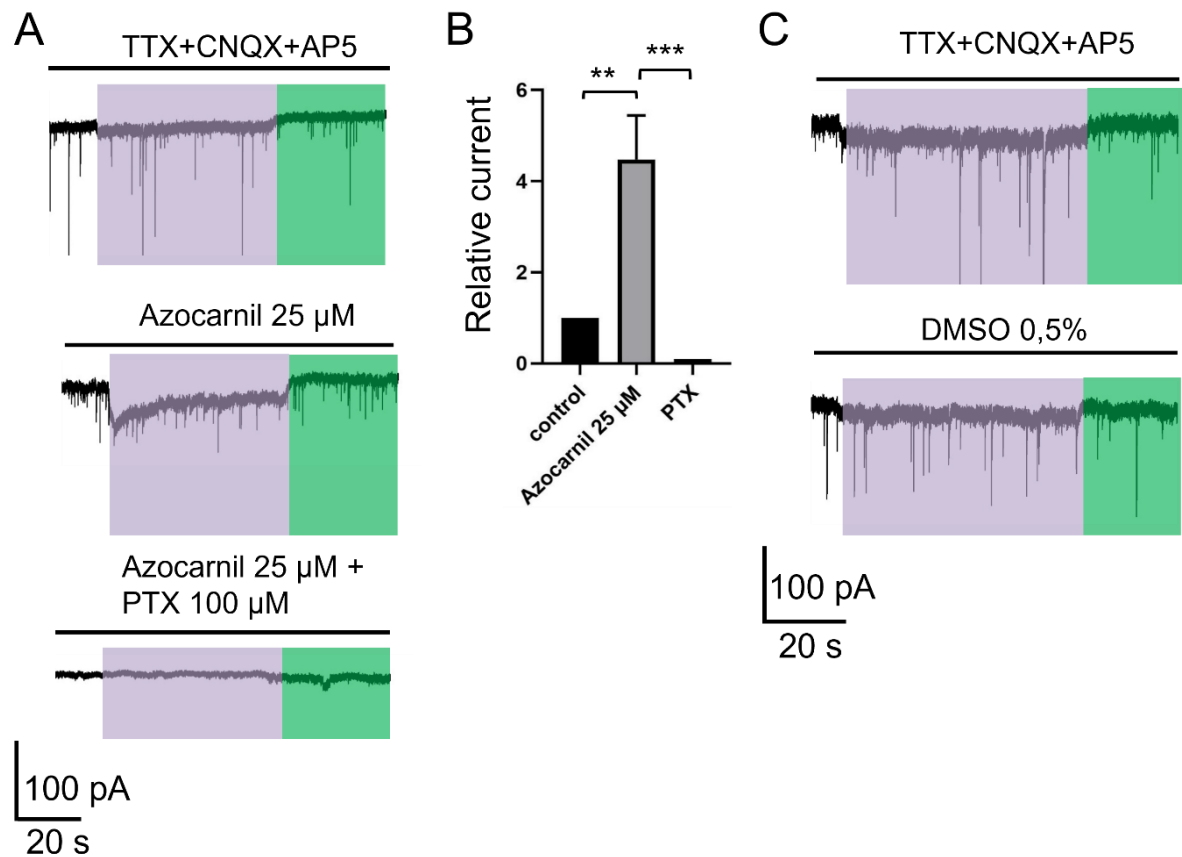
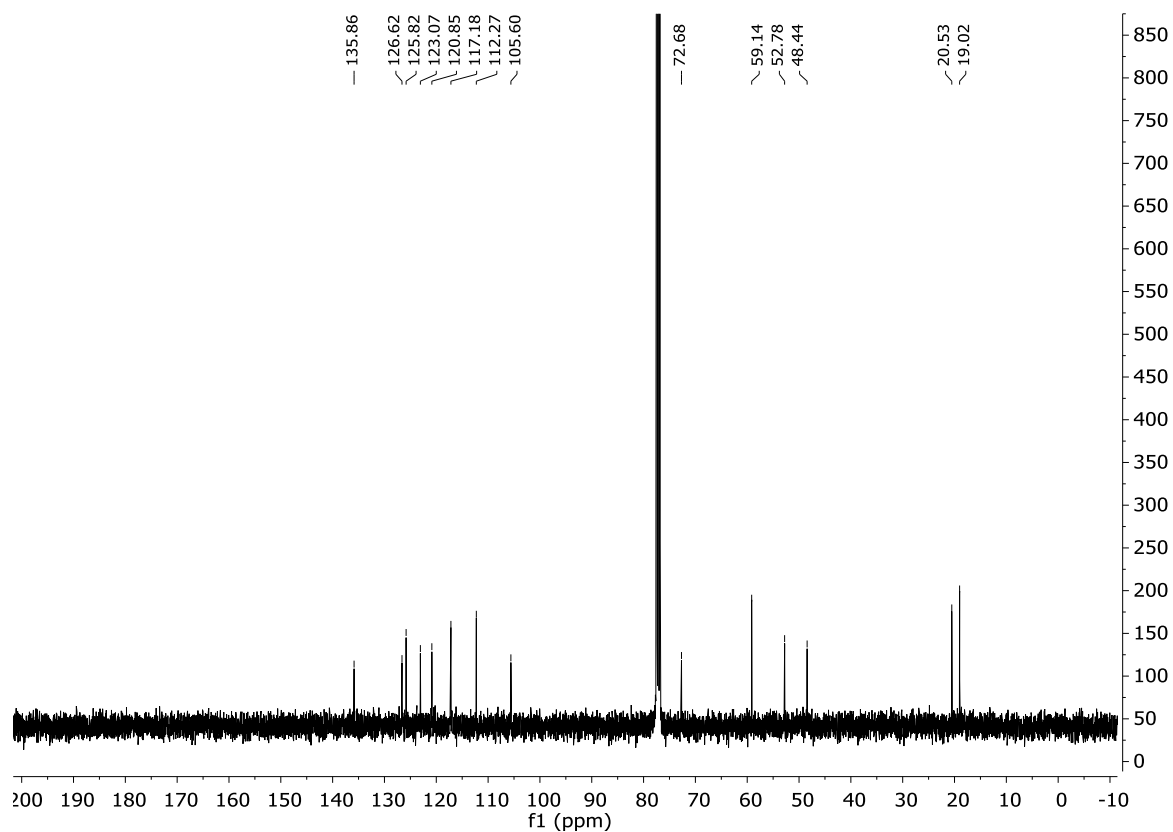
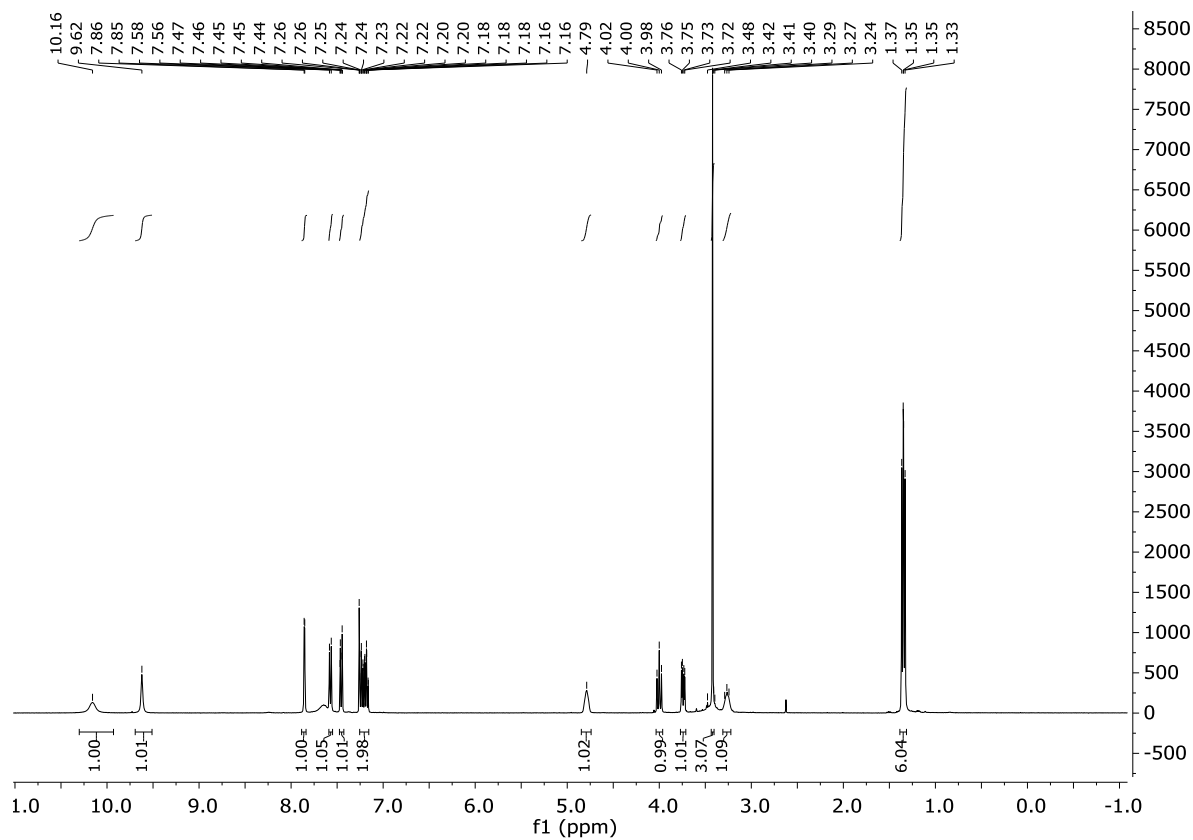
1.8.4 Supplementary Figures to *In Vitro* Studies

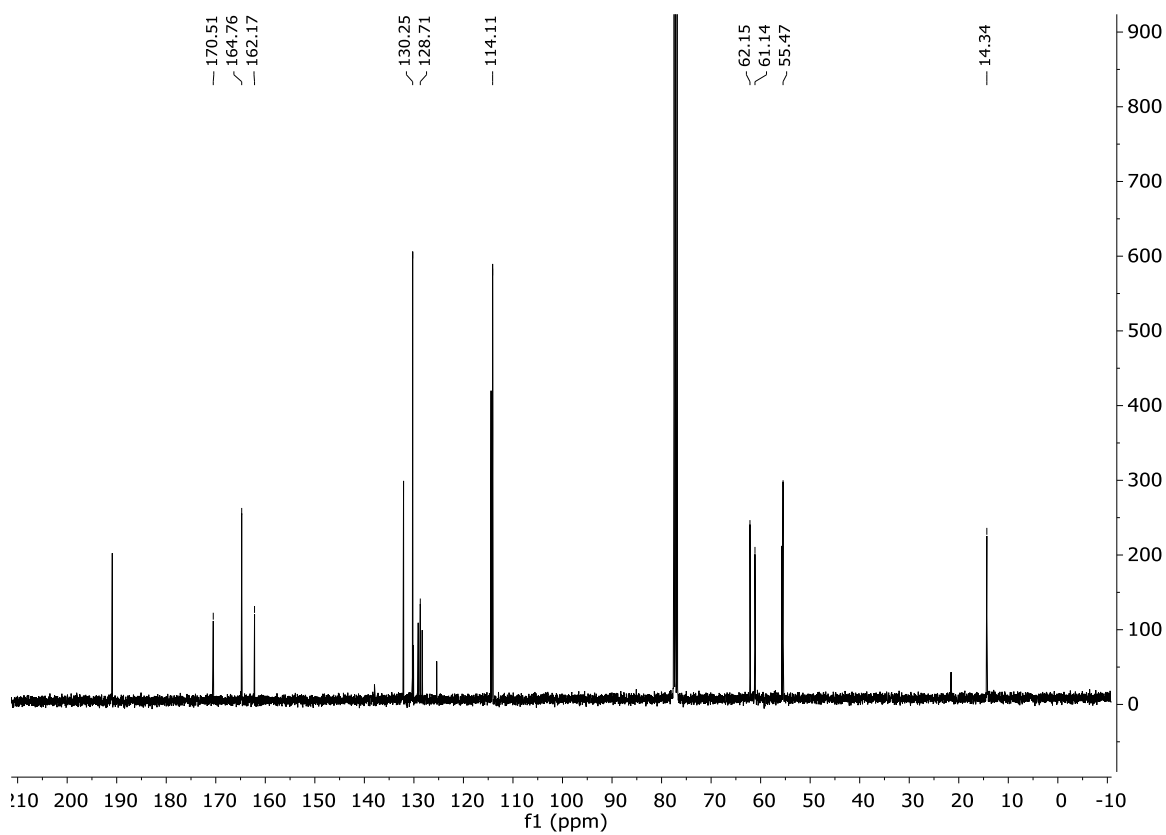
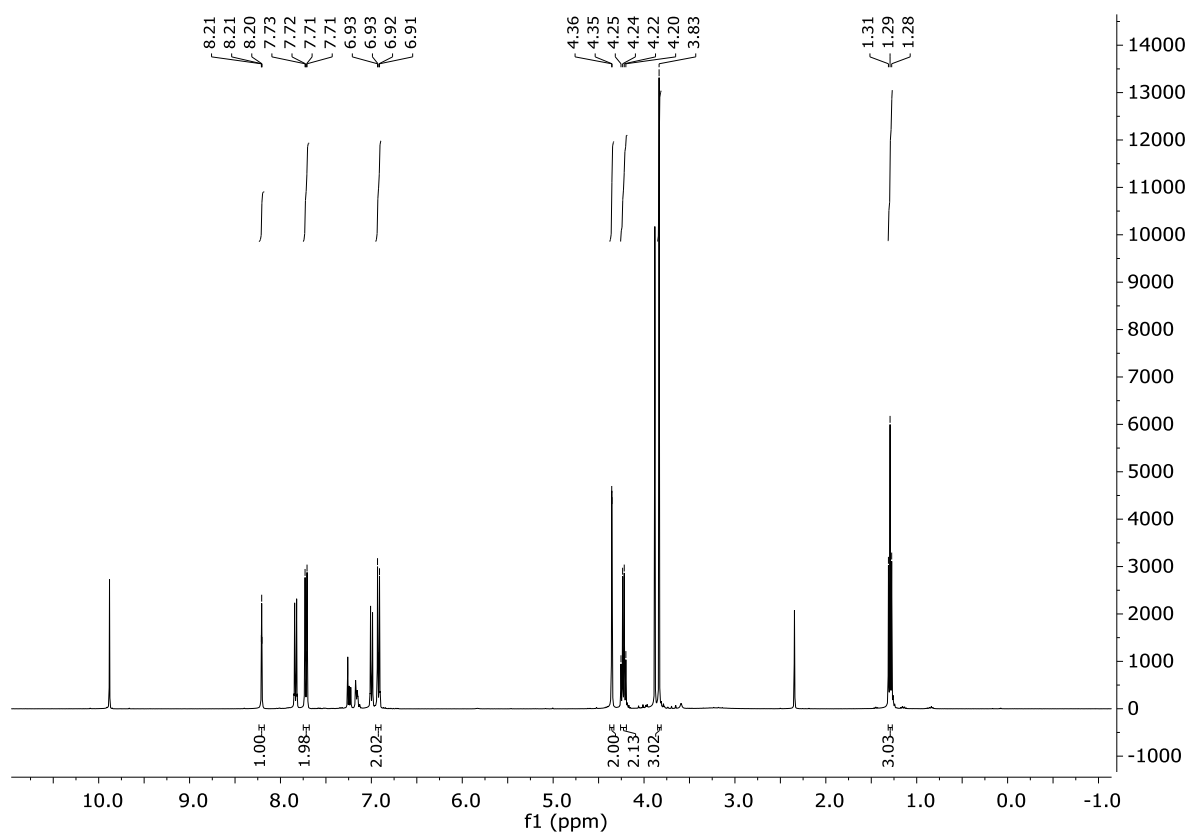
Figure S6. (A) Gabaergic currents in control (upper trace), after addition of azocarnil (25 μ M, middle trace) and after addition of PTX (100 μ M). Violet and green rectangles indicate illumination with 400 nm and 505 nm, respectively. (B) Cumulative graph demonstrating the differences in the amplitude of macroscopic currents in control, after addition of azocarnil (25 μ M) and PTX (100 μ M) at illumination with light of 400 nm. (C) Voltage-clamp recordings of gabaergic currents in control and after the addition of 0.5% of DMSO. Violet and green rectangles indicate illumination with 400 nm and 505 nm light, respectively.

1.8.5 NMR Spectra

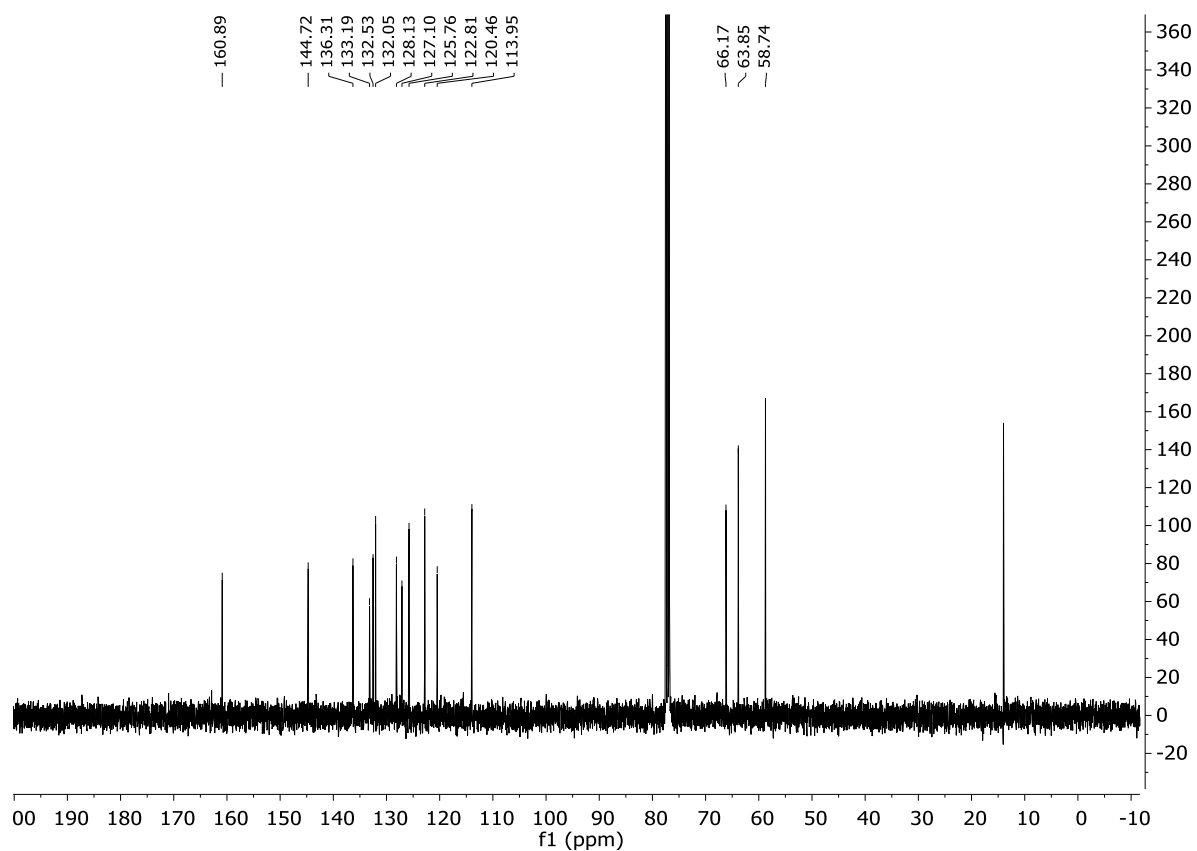
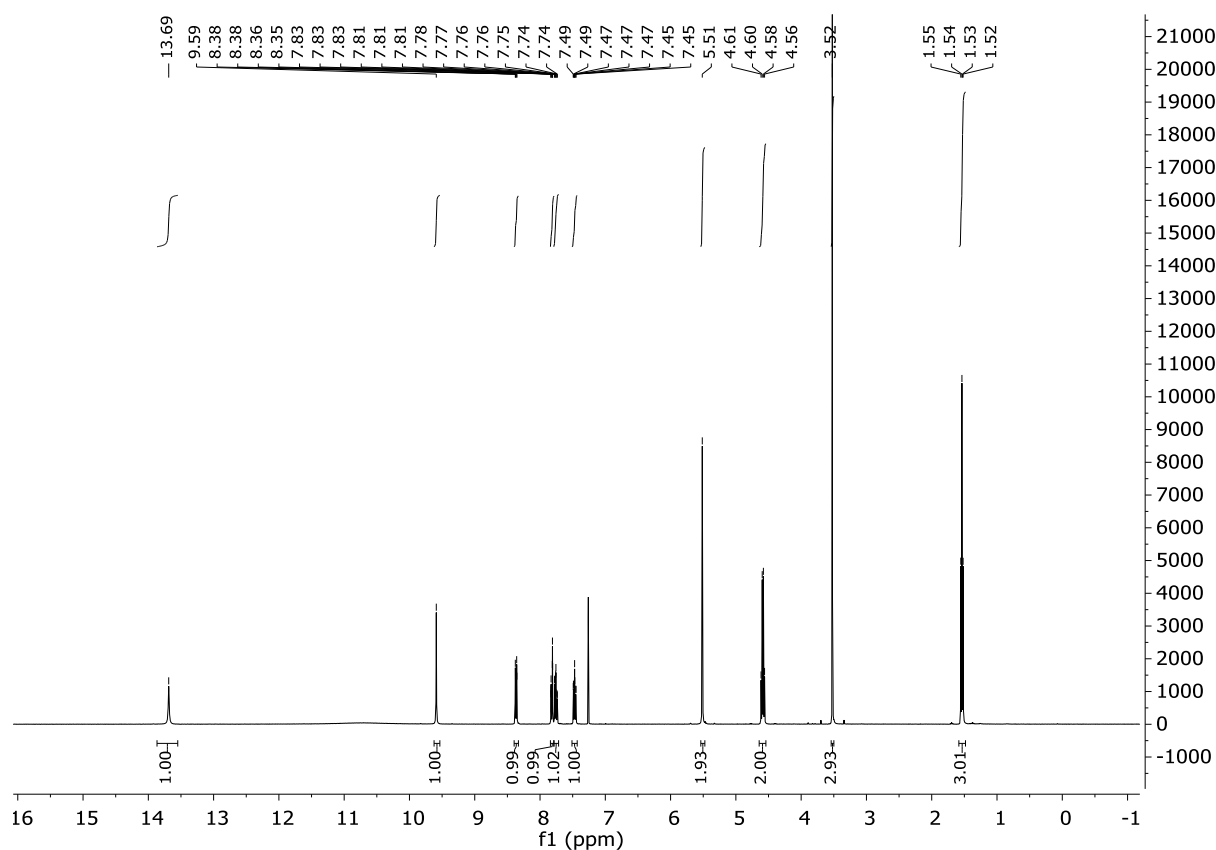
Compound 7



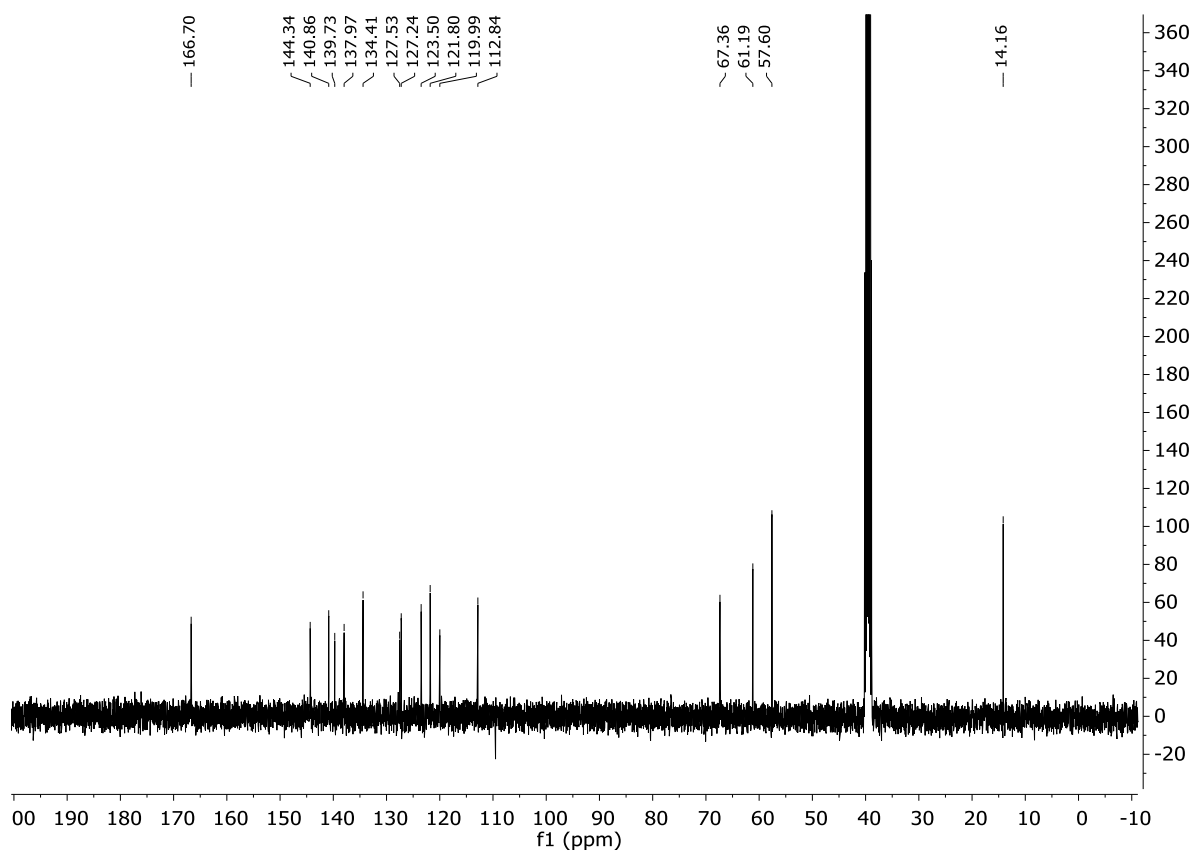
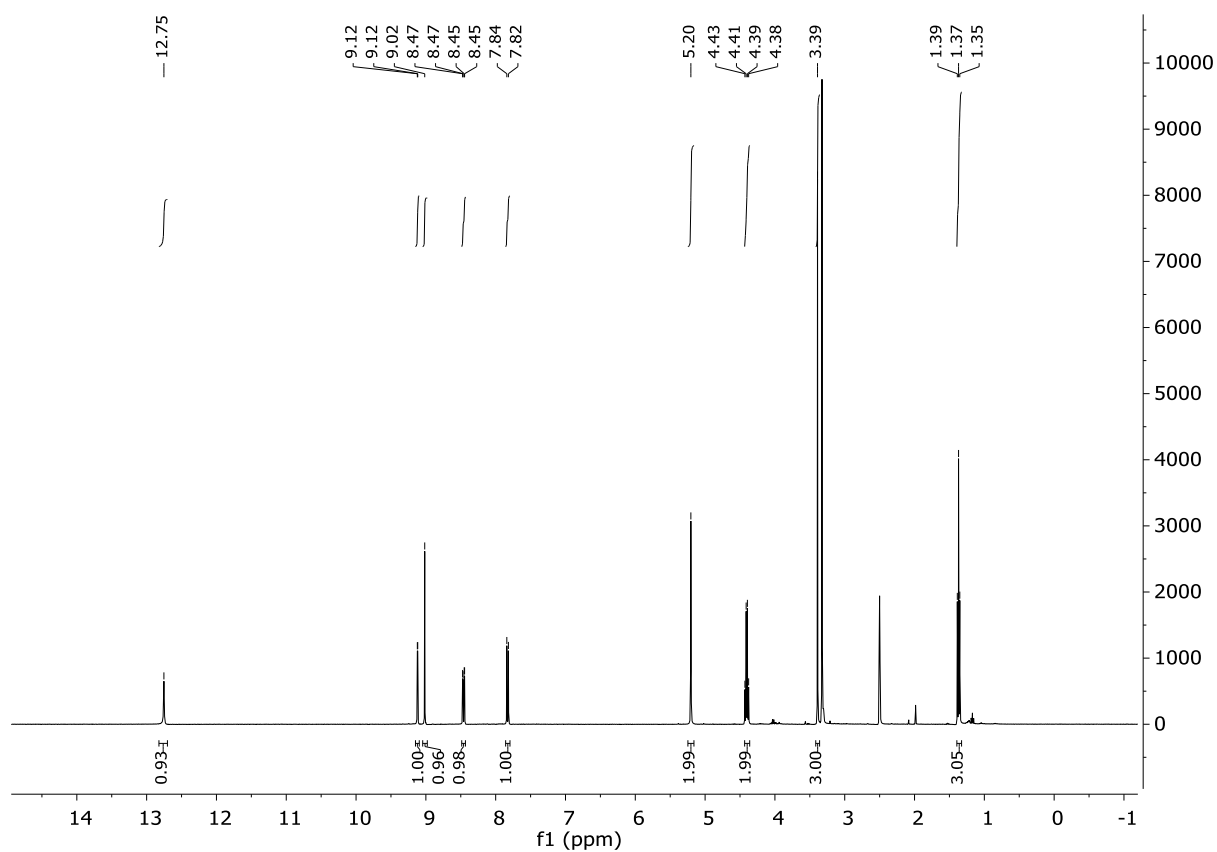
Compound 10



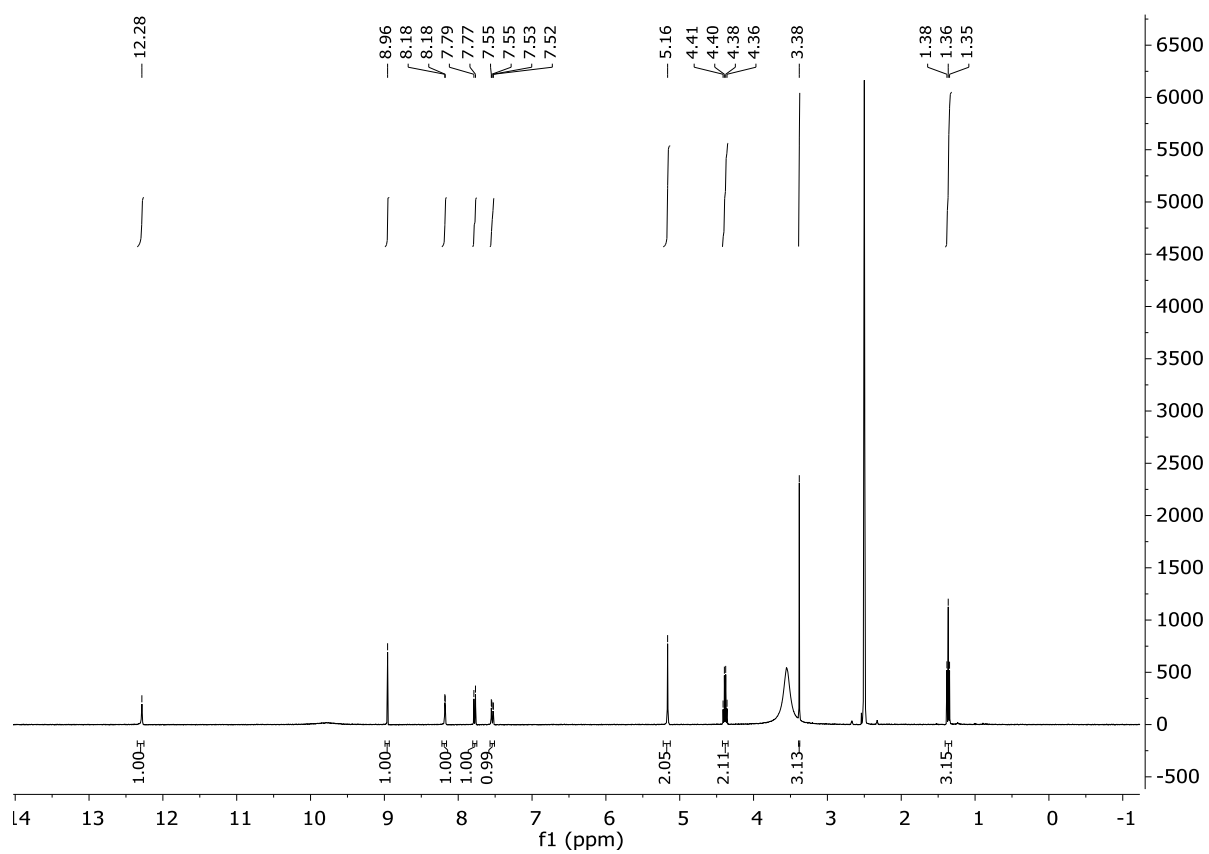
Compound 14



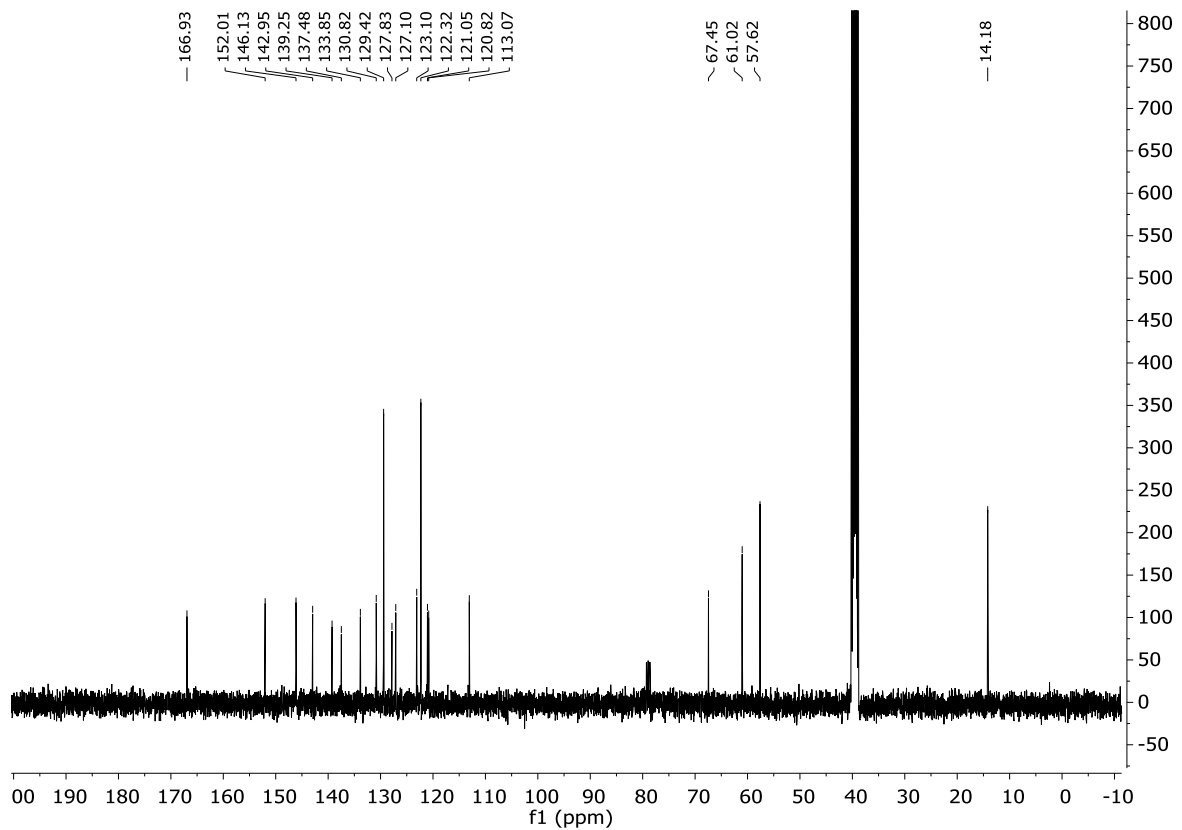
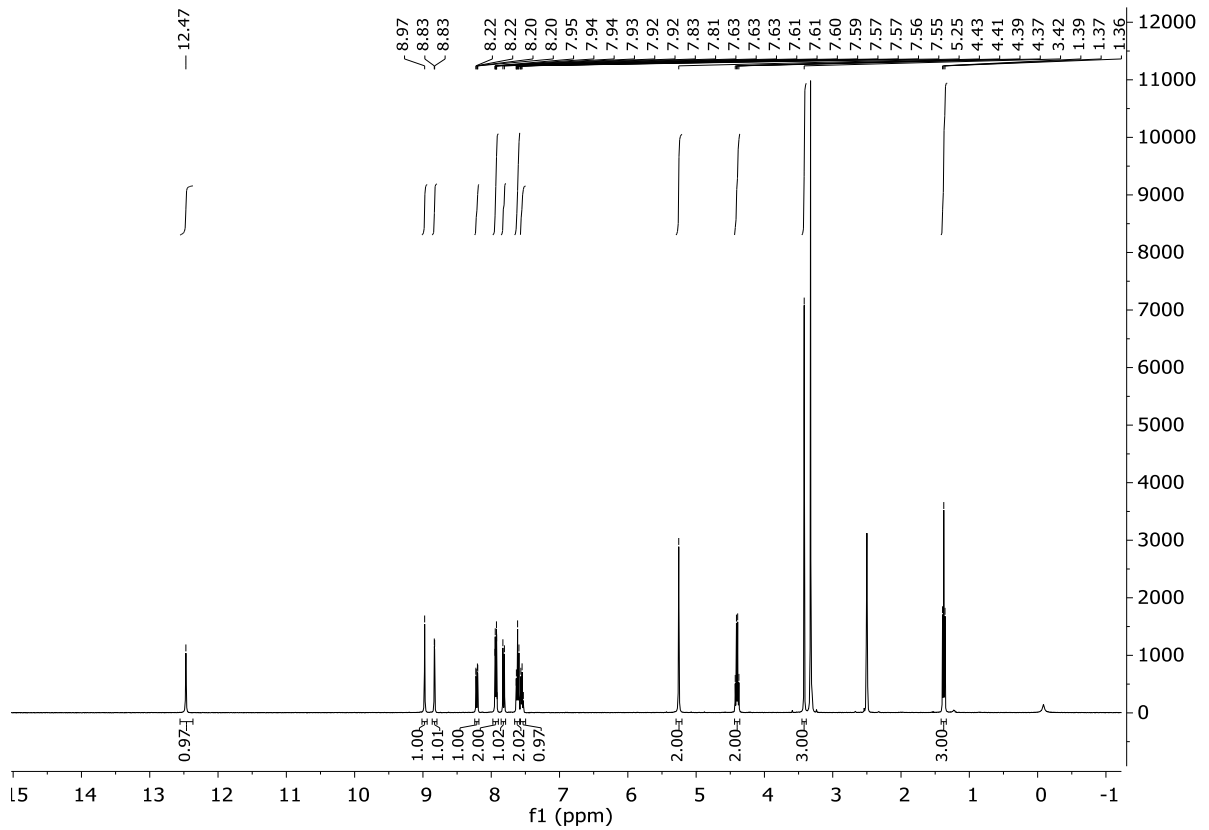
Compound 15



Compound 16



Azocarnil (1)



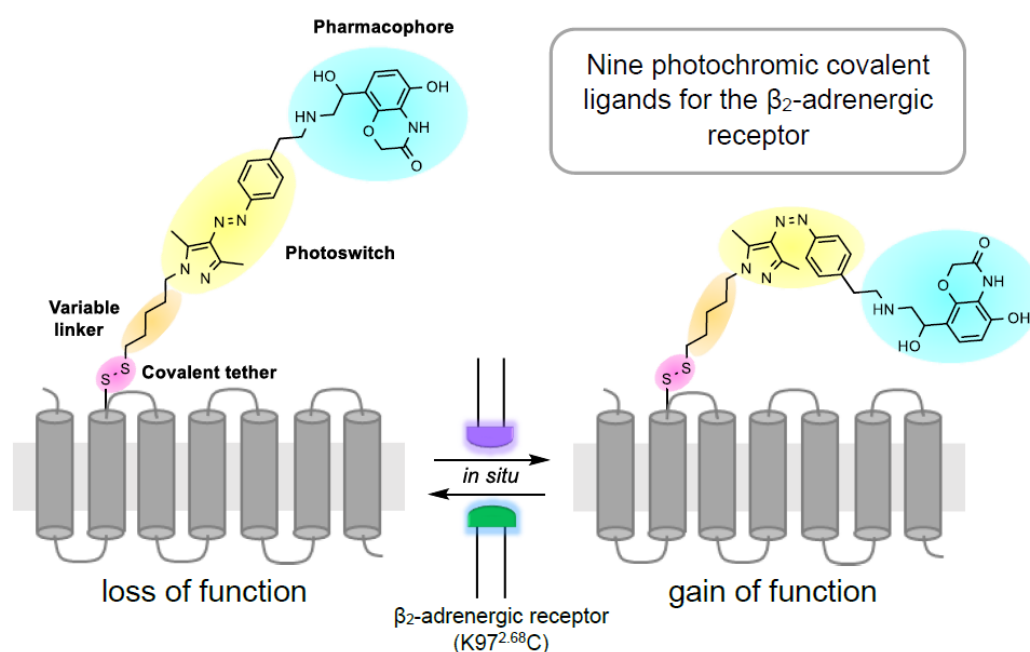
1.9 References

- [1] A. S. Lubbe, W. Szymanski, B. L. Feringa, *Chem. Soc. Rev.* **2017**, *46*, 1052–1079.
- [2] P. Paoletti, G. C. R. Ellis-Davies, A. Mourot, *Nat. Rev. Neurosci.* **2019**, *20*, 514–532.
- [3] M. H. Berry, A. Holt, J. Broichhagen, P. Donthamsetti, J. G. Flannery, E. Y. Isacoff, *Curr. Opin. Pharmacol.* **2022**, *65*, 102259.
- [4] P. Gorostiza, E. Isacoff, *Mol. Biosyst.* **2007**, *3*, 686–704.
- [5] C. K. McKenzie, I. Sanchez-Romero, H. Janovjak, *Adv. Exp. Med. Biol.* **2015**, *869*, 101–117.
- [6] P. Bregestovski, G. Maleeva, P. Gorostiza, *Br. J. Pharmacol.* **2018**, *175*, 1892–1902.
- [7] A. A. Beharry, G. A. Woolley, *Chem. Soc. Rev.* **2011**, *40*, 4422–4437.
- [8] I. M. Welleman, M. W. H. Hoorens, B. L. Feringa, H. H. Boersma, W. Szymański, *Chem. Sci.* **2020**, *11*, 11672–11691.
- [9] W. A. Velema, W. Szymanski, B. L. Feringa, *J. Am. Chem. Soc.* **2014**, *136*, 2178–2191.
- [10] C. Brieke, F. Rohrbach, A. Gottschalk, G. Mayer, A. Heckel, *Angew. Chem. Int. Ed.* **2012**, *51*, 8446–8476.
- [11] W. Szymański, J. M. Beierle, H. A. V. Kistemaker, W. A. Velema, B. L. Feringa, *Chem. Rev.* **2013**, *113*, 6114–6178.
- [12] C. D’Hulst, R. F. Kooy, *Trends Neurosci.* **2007**, *30*, 425–431.
- [13] E. R. Korpi, S. T. Sinkkonen, *Pharmacol. Ther.* **2006**, *109*, 12–32.
- [14] G. Maleeva, A. Nin-Hill, K. Rustler, E. Petukhova, D. Ponomareva, E. Mukhametova, A. M. Gomila, D. Wutz, M. Alfonso-Prieto, B. König, P. Gorostiza, P. Bregestovski, *eNeuro* **2021**, *8*, 1–17.
- [15] G. Maleeva, D. Wutz, K. Rustler, A. Nin-Hill, C. Rovira, E. Petukhova, A. Bautista-Barrufet, A. Gomila-Juaneda, P. Scholze, F. Peiretti, M. Alfonso-Prieto, B. König, P. Gorostiza, P. Bregestovski, *Br. J. Pharmacol.* **2019**, *176*, 2661–2677.
- [16] K. Rustler, G. Maleeva, A. M. J. Gomila, P. Gorostiza, P. Bregestovski, B. König, *Chem. Eur. J.* **2020**, *26*, 12722–12727.
- [17] A. M. J. Gomila, K. Rustler, G. Maleeva, A. Nin-Hill, D. Wutz, A. Bautista-Barrufet, X. Rovira, M. Bosch, E. Mukhametova, E. Petukhova, D. Ponomareva, M. Mukhamedyarov, F. Peiretti, M. Alfonso-Prieto, C. Rovira, B. König, P. Bregestovski, P. Gorostiza, *Cell Chem. Biol.* **2020**, *27*, 1425–1433.
- [18] A. Nin-Hill, N. P. F. Mueller, C. Molteni, C. Rovira, M. Alfonso-Prieto, *Int. J. Mol. Sci.* **2021**, *22*, 12072.
- [19] D. Petukhova, E.; Ponomareva, K. Rustler, B. Koenig, P. Bregestovski, *Int. J. Mol. Sci.* **2022**, *23*, 10553.
- [20] I. Pribilla, R. Neuhaus, R. Huba, M. Hillmann, J. D. Turner, D. N. Stephens, H. H. Schneider, *Psychopharmacol. Ser.* **1993**, *11*, 50–61.
- [21] V. S. Vorobjev, I. N. Sharonova, V. G. Skrebitsky, H. H. Schneider, D. N. Stephens, *Neuropharmacology* **1995**, *34*, 157–163.
- [22] M. Ozawa, Y. Nakada, K. Sugimachi, F. Yabuuchi, T. Akai, E. Mizuta, S. Kuno, M. Yamaguchi, *Jpn. J. Pharmacol.* **1994**, *64*, 179–188.
- [23] M. L. Barbaccia, G. Roscetti, F. Bolacchi, A. Concas, M. C. Mostallino, R. H. Purdy, G. Biggio, *Pharmacol. Biochem. Behav.* **1996**, *54*, 205–210.

-
- [24] B. Aufdembrinke, *Br. J. Psychiatry* **1998**, *173*, 55–63.
- [25] D. N. Stephens, L. Turski, G. H. Jones, K. G. Steppuhn, H. H. Schneider, *Psychopharmacol. Ser.* **1993**, *11*, 79–95.
- [26] J. J. Kim, A. Gharpure, J. Teng, Y. Zhuang, R. J. Howard, S. Zhu, C. M. Novello, R. M. Walsh, E. Lindahl, R. E. Hibbs, *Nature* **2020**, *585*, 303–308.
- [27] S. Zhu, A. Sridhar, J. Teng, R. J. Howard, E. Lindahl, R. E. Hibbs, *Nat. Commun.* **2022**, *13*, 1–13.
- [28] H. Wehlan, J. Oehme, A. Schäfer, K. Rossen, *Org. Process Res. Dev.* **2015**, *19*, 1980–1986.
- [29] K. Kuebler, Wolfgang; Haffer, Gregor; Wierzchowski, Reiner; Nickisch, *Preparation of 3-Alkylamino Methyl-Indole Derivatives from Indole Derivatives*, **1990**, DE4013907A1.
- [30] *Process for Producing 1-Arylimino-2-Vinylcyclopropanecarboxylic Acid Derivative*, **2015**, WO2015146881A1.
- [31] G. Rohlf, B. Vollert, *Isotopes Environ. Health Stud.* **1995**, *31*, 295–299.
- [32] R. Bergmann, K. Kongsbak, P. L. Sørensen, T. Sander, T. Balle, *PLoS One* **2013**, *8*, e52323.
- [33] M. D. Hanwell, D. E. Curtis, D. C. Lonie, T. Vandermeersch, E. Zurek, G. R. Hutchison, *J. Cheminform.* **2012**, *4*, 1–17.
- [34] P. J. Stephens, F. J. Devlin, C. F. Chabalowski, M. J. Frisch, *J. Phys. Chem.* **1994**, *98*, 11623–11627.
- [35] W. Kohn, L. J. Sham, *Phys. Rev.* **1965**, *137*, A1697.
- [36] P. Hohenberg, W. Kohn, *Phys. Rev.* **1964**, *136*, B864.
- [37] O. Trott, A. J. Olson, *J. Comput. Chem.* **2010**, *31*, 455.
- [38] J. Young, N. Garikipati, J. D. Durrant, *J. Chem. Inf. Model.* **2022**, *62*, 753–760.
- [39] J. D. Durrant, J. A. McCammon, *J. Mol. Graph. Model.* **2011**, *29*, 888–893.
- [40] W. Humphrey, A. Dalke, K. Schulten, *J. Mol. Graph.* **1996**, *14*, 33–38.
- [41] J. V. Halliwell, E. A. Grove, *Eur. J. Pharmacol.* **1989**, *163*, 369–372.

CHAPTER 2

2 Synthesis and Characterization of Novel Photoswitchable Covalent Ligands for the β_2 -Adrenergic Receptor



This chapter is a manuscript in preparation for submission.

This chapter was in collaboration with the group of Prof. P. Gmeiner (Institute for Chemistry and Pharmacy, Friedrich-Alexander-University Erlangen-Nürnberg).

U. Wirth performed the synthesis and (photo-)chemical characterization of 3-6, 8, 9, 11-18, 20-45, 47 and 48 . S. Feustel performed the synthesis and (photo-)chemical characterization of 1, 2, 7, 20-23, 26-33, 42, 44 and 46 and the biological studies of all final compounds. M. Schmidt performed the docking studies. D. Lachmann initiated this project.

U. Wirth, S. Feustel, Dr. H. Hübner and Prof. P. Gmeiner wrote the manuscript draft.

Prof. König, Prof. Gmeiner and Dr. Hübner supervised the project.

2.1 Introduction

The structural elucidation of GPCRs has made huge progress over the last years with techniques such as X-ray crystallography^[1,2] and cryo-electron microscopy^[3-5]. Nevertheless, these result in static pictures of the different states a receptor can adapt depending on the functional properties of the bound ligand. The elucidation of the dynamics and kinetics of a change in conformation is harder. A recent approach to unravel the mechanisms behind GPCR activation was the total internal reflection fluorescence (TIRF) based single-molecule analysis. This imaging technology gave insights into the conformational ensemble of the β_2 -adrenergic receptor (β_2 AR) induced by several different antagonists, agonists and partial agonists.^[6,7] The respective ligand affinity and binding kinetics have a major impact on the generation of a signal produced by the receptor.^[8] To study the dynamics of GPCR activation and signal transduction independent from ligand association and dissociation, a ligand with very slow off-kinetics is needed that can change its intrinsic activity by external control.^[9] These requirements are met by a photoswitchable ligand that is covalently bound to the target receptor. Photoswitch subunits are molecular structures controlled by an external light stimulus that vary the geometry or electronic properties of a molecule and, thus, the functional properties. These building blocks enable rapid and bistable ligand photoswitching between different intrinsic activities.^[10,11] Following this principle, reversibly binding photochromic ligands were developed for different GPCRs including CXCR3^[12], μ OR^[13], mGlu5^[14], CB1^[15], H3R^[16] and α_2 AR^[17]. For the β_2 AR, a photoswitchable antagonist was reported.^[18] In this project, the development of nine covalently binding photoswitchable ligands for the β_2 AR, a well-characterized and prototypical class A GPCR, was pursued. Interestingly, covalently binding agonists were already reported along with a β_2 AR co-crystal structure enabling us to design our ligand guided by those structures.^[9,19]

2.2 Design

The design of the covalent photoswitchable ligands was inspired by the previously reported compounds FAUC50 and FAUC37.^[9,19,20] These structures are composed of three main functional units, a pharmacophore, a phenyl linker and the covalent tether. The phenyl linker was replaced by a photoswitchable moiety (Figure 1). A wide variety of photoswitchable units has been used in photopharmacology. In this study, we used arylazopyrazoles as they exhibit

certain advantages compared to azobenzenes, like higher thermal half-lives and higher photostationary states (PSS).^[21] The three moieties were connected by short carbon spacers and the linker between photoswitch and covalent tether allowed us to fine-tune the molecules size according to the distance between the covalent anchoring site and the orthosteric binding site. The selected pharmacophores were on the one hand, norepinephrine (NE) as the endogenous ligand to ensure insights closer to the natural functions in the human body and on the other hand, BI-167107, a high-affinity synthetic agonist that was already used to support the crystallization of the active state of β_2 AR.^[22] We chose maleimides^[23,24] and disulfides^[9,19,20,25] as the covalently-binding units. Whereas disulfides selectively target cysteines, maleimides can interact with cysteines and lysines. Nine photoswitchable ligands were developed containing different linker lengths, pharmacophores, and warheads. As cysteines are not always present in the orthosteric binding sites, they had to be engineered to the receptor by point mutation. The positions His^{2.64}, Lys^{2.68} and Lys^{7.32} were considered suitable anchoring sites of the β_2 AR. The positions differ in the distance and in their relative spatial orientation to the basic nitrogen of the epinephrine head group or the BI-167107 group. Thus, depending on the anchoring site, the available space limits the size of the ligand and determines how much isomerization affects favorable ligand-receptor interactions. To probe different anchoring sites, a molecular docking study was pursued. The docking results proposed a cysteine to be introduced between the transmembrane loop 2 (TM2) to extracellular loop 1 (ECL1) (K97^{2.68}C). Alternatively, mutants including K305^{7.32}C or H93^{2.64}C were explored computationally. However, the docking poses of disulfide- and maleimide-based ligands did not align with the bioactive conformation of adrenaline, and no difference between *E* and *Z* isomers was observed.^[26]

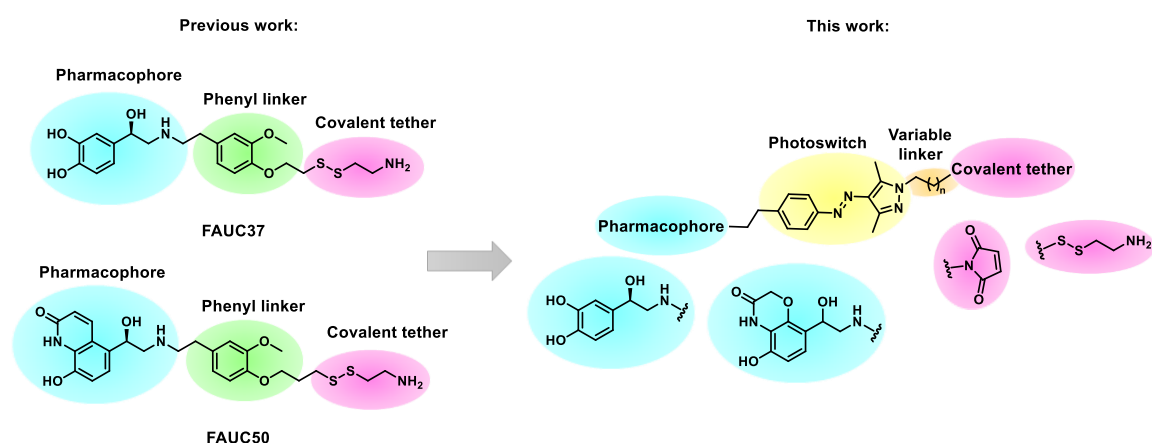
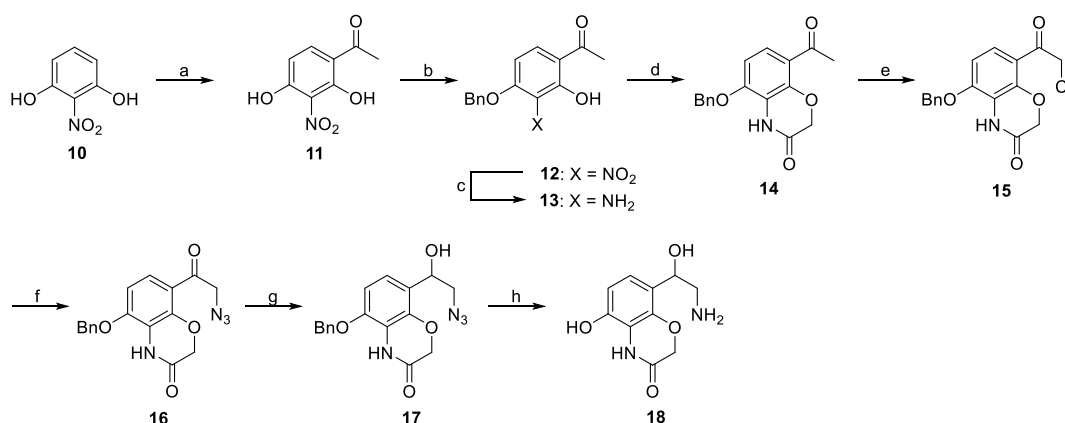


Figure 1. Design approach derived from FAUC37^[19] and FAUC50^[9].

2.3 Synthesis

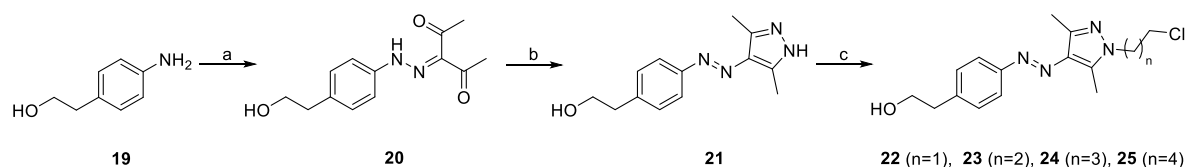
The photoswitchable ligands **1-9** were synthesized according to schemes 1-4.

The synthesis of the BI-167107 based pharmacophore was conducted according to Pappano *et al.*^[27] giving access to **16**. Ketone **16** was reduced to the corresponding alcohol using sodium borohydride. The azide **17** was simultaneously deprotected and reduced to obtain **18** in excellent yield (Scheme 1).



Scheme 1. Reagents and conditions: a) Ac_2O , AlCl_3 , nitrobenzene, $100\text{ }^\circ\text{C}$, 5 h, 97%; b) BnBr , NaHCO_3 , MeCN , reflux, 7 h, 90%; c) Zn dust, AcOH , rt, 2 h, 89%; d) 2-chloroacetyl chloride, NaHCO_3 , Cs_2CO_3 , DMF , $100\text{ }^\circ\text{C}$, 20 h, 79%; e) BTMA-ICl_2 , CH_2Cl_2 , AcOH , water, $65\text{ }^\circ\text{C}$, 20 h, 90%; f) NaN_3 , DMF , rt, 2 h, 78%; g) NaBH_4 , MeOH , $0\text{ }^\circ\text{C}$, 2 h, 73%; h) Pd/C , H_2 , AcOH , rt, 5 h, 94%.

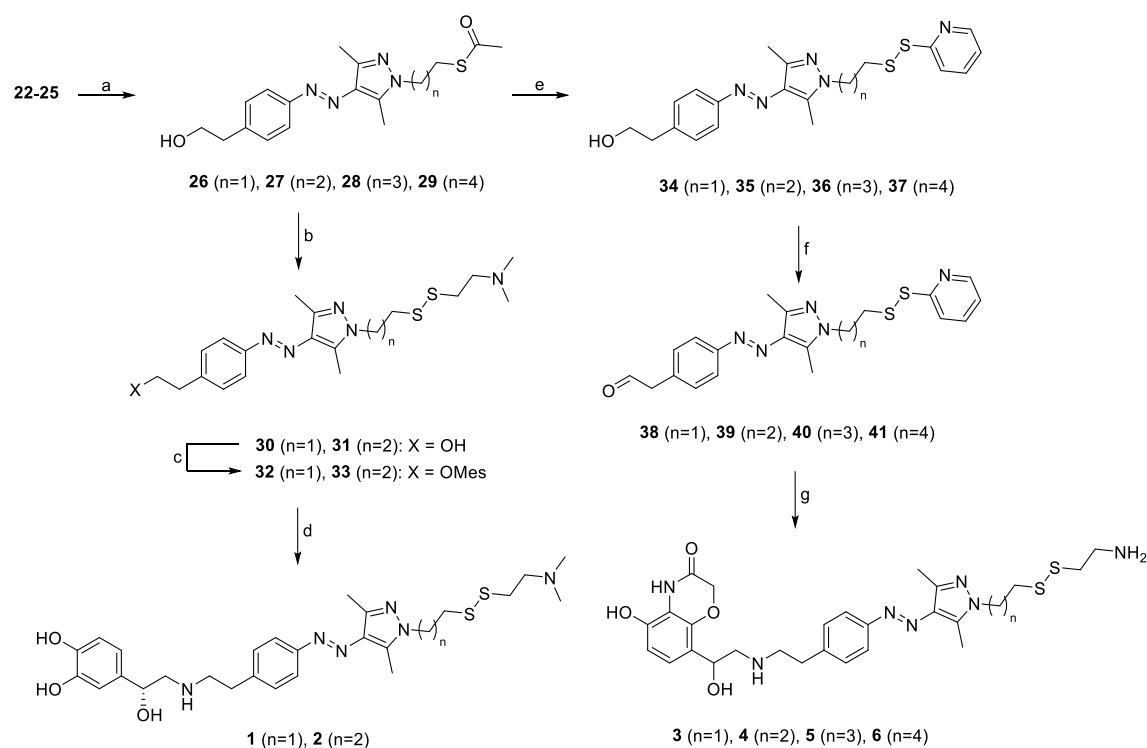
The synthesis of the photoswitchable part for the covalent ligands started from **19**. After diazotation and azo coupling **20** was obtained followed by condensation with hydrazine monohydrate to afford **21**. In the next step, the linkers were introduced. Due to elimination as the major side reaction, bromochloro-substituted compounds were favored over dibromo analogs. This way, linkers ranging from two to five carbon atoms were introduced yielding **22-25** (Scheme 2).



Scheme 2. Reagents and conditions: a) NaNO_2 , HCl , AcOH , $0\text{ }^\circ\text{C}$, 45 min, then pentane-2,4-dione, NaOAc , EtOH , rt, 30 min, 87%; b) hydrazine monohydrate, EtOH , reflux, 3 h, 93%; c) NaH , anhydrous DMF , rt, 30 min, then 1-bromo-2-chloroethane/1-bromo-3-chloropropane/1-bromo-4-chlorobutane/1-bromo-5-chloropentane, rt, 2 h, 60-83%.

Based on these compounds, the syntheses towards the disulfides and maleimides were done. Nucleophilic replacement gave the thioesters **26-29**. For the norepinephrine-based ligands, thioesters **26** and **27** were transferred to the thiopyridyl disulfides *in situ* and were directly converted to the disulfides **30** and **31**. Subsequent mesitylation and nucleophilic substitution with norepinephrine yielded the covalent ligands **1** and **2**.

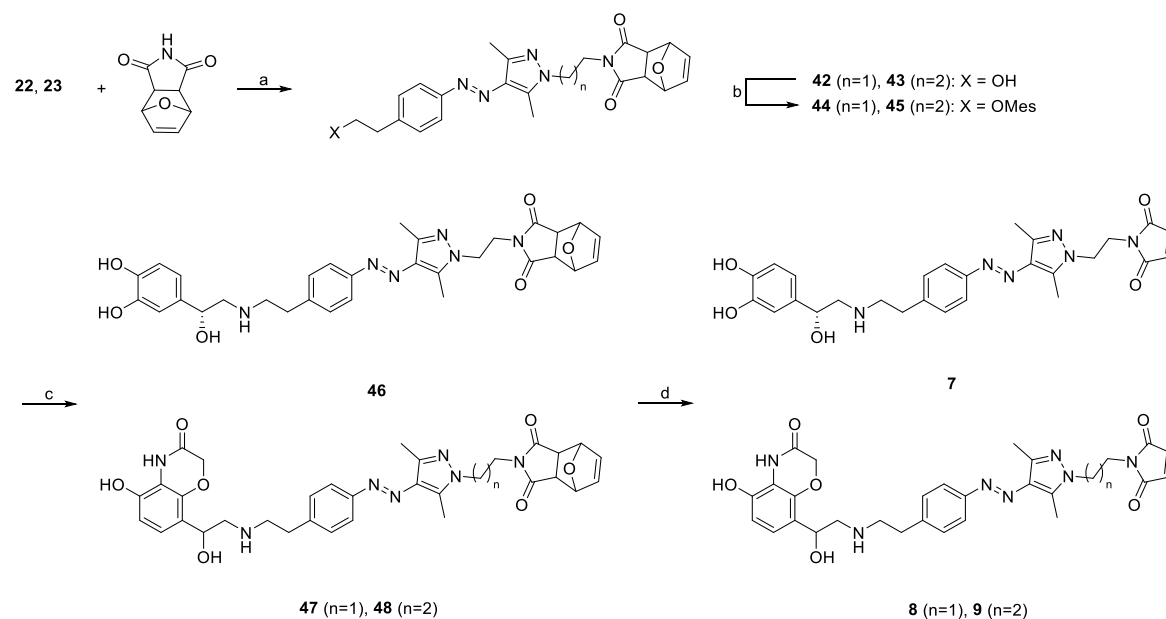
For the synthesis of the BI-167107 based ligands, the thioesters **26-29** were subjected to methanolysis and the thiopyridyl disulfides **34-37** were isolated. Oxidation with Dess-Martin Periodane yielded the aldehydes **38-41** which were subjected to a reductive amination reaction with **18**. After replacing the thiopyridyl group by cysteamine, the covalent ligands **3-6** were obtained (Scheme 3).



Scheme 3. Reagents and conditions: a) potassium thioacetate, THF, reflux, 16 h, 80-91%; b) 1: 2,2'-dithiodipyridine, MeOH, NaOCH₃, rt, 2 h, argon, 2: 2-(dimethylamino)ethanethiol hydrochloride, rt, 30 min, argon, 59-60% over two steps; c) MesCl, K₂CO₃, CH₂Cl₂, 0 °C to rt, 2 h, not isolated; d) norepinephrine, DMSO, argon, 70 °C, 19 h, 8-19%; e) 2,2'-dithiodipyridine, LiOH, MeOH, 40 °C, 4 h, 54-66%; f) DMP, CH₂Cl₂, 0 °C, 1.5 h, argon, not isolated; g) **18**, NaCNBH₃, MeOH, rt, 16 h, then cysteamine hydrochloride, rt, 1 h, 3-5%.

The ligands with a maleimide group as the covalent tether were synthesized starting from **22** and **23** which were brought to reaction with a protected maleimide to afford **42** and **43**. The hydroxy group was activated by mesitylation and replaced by norepinephrine or **18** and **46-48**

were obtained. In the last step, a Retro-Diels-Alder reaction was conducted to deprotect the maleimide to yield the ligands **7-9** (Scheme 4).



Scheme 4. Reagents and conditions: a) K_2CO_3 , DMF, 50 °C, 16 h, 45-50%; b) MeCl, NEt_3 , CH_2Cl_2 , 0 °C to rt, 4 h, not isolated; c) norepinephrine/**18**, DMSO, argon, 70 °C, 16 h, 10-18%; d) DMSO, argon, 110 °C, 3 h, 85-98%.

2.4 Photophysical Characterization

The photophysical properties of all photoswitches were investigated in aqueous buffer to mimic the conditions during the biological assays. All arylazopyrazoles could be reversibly toggled between *E* and *Z* isomer by irradiation with 365 nm and 528 nm, respectively (Figure 2). Switching over several cycles showed that the compounds exhibit high fatigue resistance. The UV/Vis spectra showed the typical absorptions of the *E* isomer (black curve) and *Z* isomer (purple curve). All compounds displayed high photostationary states (PSS) in both directions and long thermal half-lives that are typically for arylazopyrazoles.^[21] Table 1 summarizes the photophysical properties of all photoswitches.

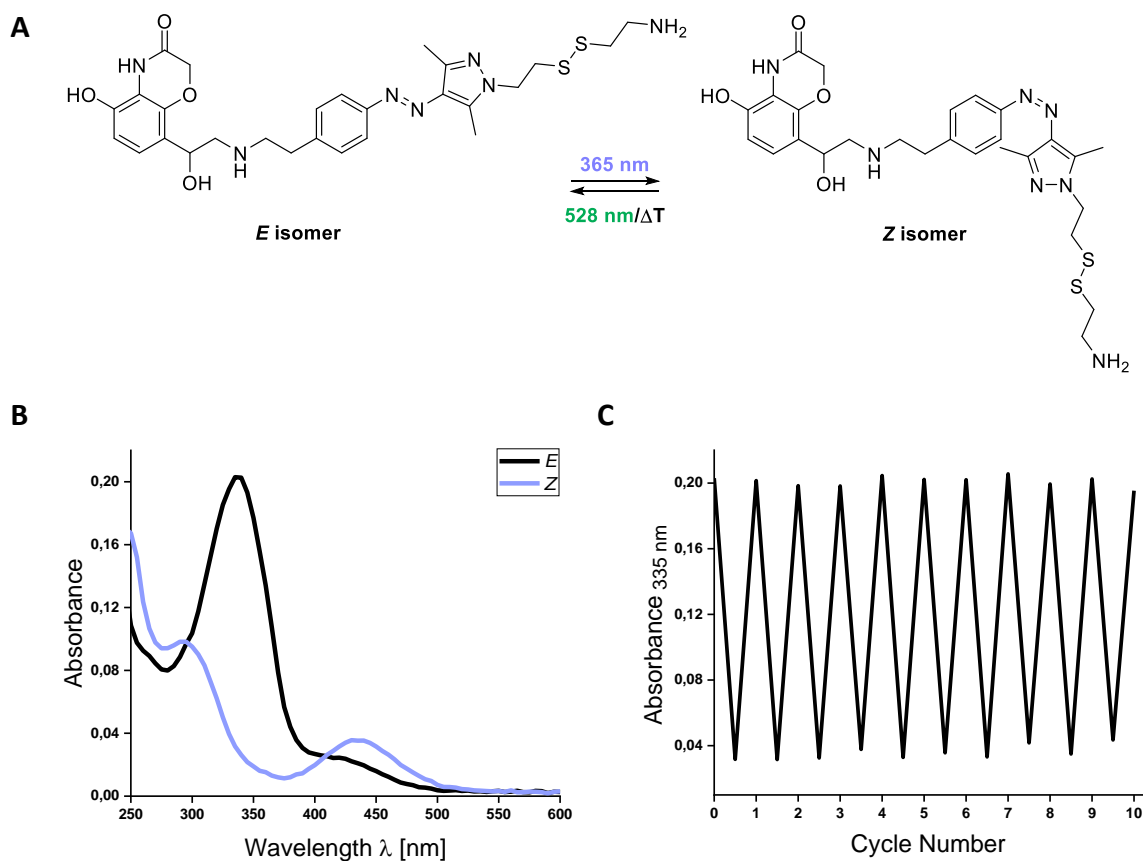


Figure 2. Photophysical characterization of **3** (10 μM + 0.5% DMSO in Tris buffer ((50 mM Tris, 1 mM EDTA, 1 mM MgCl_2 , pH 7.4))). **(A)** Light-induced *E/Z*-photoisomerization. **(B)** UV/Vis spectra of both isomers. **(C)** Cycle performance. Ligands **1**, **2**, **4-9** displayed similar photophysical properties (SI Figures S10-S18).

Table 1. Summarized photochemical properties of **1-9** in buffer^[a].

Compound	λ_{max} (<i>E</i>) [nm]	λ_{max} (<i>Z</i>) [nm]	λ_{iso} [nm]	$t_{1/2}$ [d]	PSS (<i>E</i> \rightarrow <i>Z</i>) ^[b]	PSS (<i>Z</i> \rightarrow <i>E</i>) ^[c]
1 (-S-S-/n=2)	335	435	295, 409	3.9	89%	90%
2 (-S-S-/n=3)	335	433	295, 409	4.9	89%	87%
3 (-S-S-/n=2)	337	434	295, 409	15.2	95%	89%
4 (-S-S-/n=3)	339	436	295, 411	15.7	96%	92%
5 (-S-S-/n=4)	338	436	298, 409	16.7	94%	92%
6 (-S-S-/n=5)	340	435	295, 411	13.3	95%	93%
7 (-mal-/n=2)	335	433	295, 409	4.5	92%	85%
8 (-mal-/n=2)	337	435	300, 400	18.6	95%	94%
9 (-mal-/n=3)	339	435	298, 405	20.4	95%	93%

[a] Buffer: Tris buffer: 50 mM Tris, 1 mM EDTA, 1 mM MgCl_2 ; [b] PSS determination was done by HPLC at the appropriate isosbestic points, irradiation with 365 nm; [c] PSS determination was done by HPLC at the appropriate isosbestic points, irradiation with 528 nm. Abbreviations: mal = maleimide, n = linker length.

2.5 Biological Characterization

Initial biological investigations were directed to the functional characterization of the photoswitches **1-9** at the β_2 adrenergic receptor (β_2 AR). To evaluate the differential effects of the pharmacophores, the photoswitchable entities, and the linker units on receptor activation, we performed functional studies. Hence, we conducted an IP accumulation assay (IP-One) in HEK293T cells transiently expressing the human β_2 AR and the hybrid G-protein $G\alpha_{qs}$ ($G\alpha_q$ protein with the five C-terminal amino acids replaced by the corresponding sequence of $G\alpha_i$, gifted from The J. David Gladstone Institutes, San Francisco, CA).^[28] Dose-response curves of the *E* and *Z* isomers showed agonist activity for all compounds with E_{max} values between 78 and 108% (Figure S38, Table S1). While the ligands with the BI-167107 pharmacophore (**3-6, 8, 9**) showed potencies in the low nanomolar range with EC_{50} values from 5.2 nM (**Z-3**) to 79 nM (**E-5**), the catechol derivatives **1, 2, 7** activated the receptor at micromolar concentrations ($EC_{50} = 0.48 \mu\text{M}$ (**Z-1**) to $EC_{50} = 4.3 \mu\text{M}$ (**Z-7**)). This data qualified all compounds for further experiments testing covalent receptor binding and photo-induced switching of the bound ligand. To facilitate disulfide formation or Michael addition of suitable covalent ligands, a β_2 AR mutant was constructed incorporating a reactive cysteine in position 2.68 at transmembrane helix 2 (TM2) instead of lysine (K97^{2.68}C). Evaluation of the K97^{2.68}C mutant showed activation properties of reference compounds that were similar to those toward wild-type receptor (norepinephrine: $EC_{50} = 3.2 \mu\text{M}$ (mutant)/ $EC_{50} = 0.98 \mu\text{M}$ (wild-type), epinephrine: $EC_{50} = 0.22 \mu\text{M}$ (mutant)/ $EC_{50} = 0.16 \mu\text{M}$ (wild-type)) (Figure S39).

To assess covalent binding to the receptor and subsequent switching of the bound isomer within the orthosteric binding site, we established a bioluminescence resonance energy transfer (BRET) based biosensor system expressing an RLuc-tagged β -arrestin 2 and the GFP-tagged enhanced bystander protein CAAX in HEK293T cells. The assay allowed us to determine receptor stimulated recruitment of β -arrestin to the β_2 AR and the bystander protein CAAX both located in the cell membrane.^[29] To facilitate covalent binding, $1 \mu\text{M}$ of the *Z* isomers of **1-9** were preincubated with the cells for 90 min. After removing all reversibly bound ligand in a washing step and the addition of propranolol as a blocking agent, the activation properties were determined after incubation for 15 min. To identify specific agonist effects for the *Z* and *E* isomer, cells were treated in two different ways after the blocking step. Hence, half of the cells were kept in the dark to maintain the *Z* isoform, while the second half was irradiated with light of 528 nm to induce switching from the *Z* to the *E* form. Detailed analysis of the BRET data revealed activation profiles with E_{max} values from 2-52% relative to the effect of

norepinephrine indicating a partial irreversible occupation of the receptor (Figure S40). While the catechol derivatives **1**, **2**, **7** showed only moderate E_{\max} values (2-19%), the highest intrinsic effect was determined for the four-carbon linker-substituted disulfide **5** ($E_{\max} = 52\%$) and its five-carbon analog **6** ($E_{\max} = 50\%$). Comparing the data of all *Z* isomers with the intrinsic effects determined after irradiation, resulting in formation of the *E* isoforms, compound **6** showed intrinsic effects with the greatest difference in E_{\max} (50% for *Z*-**6** and 39% for *E*-**6**). To confirm this interesting observation, we preincubated compound *E*-**6** followed by a comparative measurement of E_{\max} values for *E*-**6** (kept in the dark) and *Z*-**6** (irradiated at 365 nm) (Figure 3). In contrast to *Z*-**6** ($E_{\max} = 51\%$), the *E* isomer seemed to bind covalently at a higher amount to the β_2 AR (*E*-**6**: $E_{\max} = 73\%$) and the agonist activity increased when switched to *Z*-**6** ($E_{\max} = 86\%$) after irradiation with 365 nm. This confirms that the *Z* isomer is considerably more active than the *E* isoform.

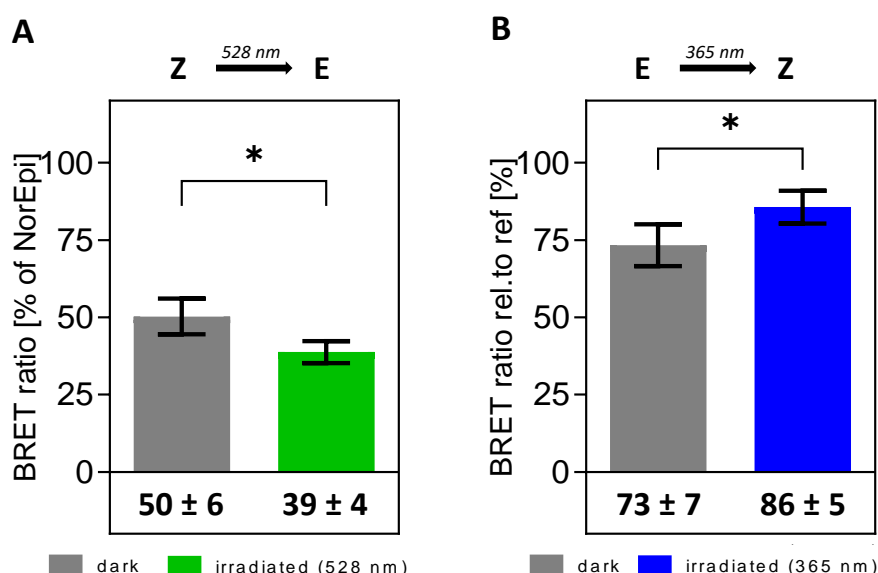


Figure 3. Intrinsic activity of compound **6** after photoswitching the covalently bound isoform at the β_2 adrenoceptor. **(A)** The efficacy of the covalently bound species of *Z* isomer of **6** (grey) is diminished after switching the ligand into the *E* isoform (green) by irradiation with 528 nm. **(B)** The E_{\max} for the covalent amount of the *E* isomer of compound **6** (grey) increases after switching the ligand to the *Z* form (blue) by light of 365 nm. Each bar represents mean E_{\max} values [in % \pm SEM] and is the result of 10 (A) or 12 (B) individual experiments, each done in quadruplicate, applying a biosensor-based β -arrestin recruitment assay and the β_2 AR mutant K972.68C. The significance of E_{\max} was analyzed by a paired t-test. The threshold for significance was set as a 99% confidence interval and displayed as p-value * ($p < 0.01$).

2.6 Conclusion

We describe the first β_2 adrenergic receptor (β_2 AR) ligand **6** that is photoswitchable in its receptor-bound state. The covalent ligand was synthesized by incorporating an arylazopyrazole moiety between its pharmacophore and a disulfide-functionalized tether. Hence, **6** complements retinal as a part of the rhodopsin system, which gets hydrolyzed and leaves the receptor after isomerization to the *trans*-isomer. For the next photoswitching cycle, opsin needs to bind another equivalent of *cis*-retinal.^[30,31] The system we herein describe is based on the β_2 AR incorporating a mutant with a cysteine anchor that is located adjacent to the orthosteric binding pocket (K97^{2.68}C). Hence, dissociation of the pharmacophore before or after photoswitching appears not possible for steric reasons. The photophysical characterization of our set of test compounds showed excellent properties like reversible switching and high fatigue resistance, high PSS and long thermal half-lives. As the wildtype receptor is lacking a free cysteine which is required for covalent binding, the ligands were tested on a point mutant (K97^{2.68}C). The percentage of receptor-bound ligand was determined by *in vitro* functional assays. The investigation of the ligands in a bystander BRET assay with irradiation after the incubation period revealed that **6** could still be switched while covalently bound to the receptor. Ligand **6** will serve as a lead compound for valuable research tools allowing us to study receptor kinetics and dynamics with high accuracy using single-molecule fluorescence microscopy techniques.

2.7 Experimental Part

2.7.1 General Information

Starting materials and commercial reagents were purchased from Acros, Alfa Aesar, Fisher, Fluka, Fluorochem, Merck, Sigma-Aldrich, TCI and VWR and were used without further purification. Solvents were used in p.a. quality or dried according to common procedures if necessary. All reactions with oxygen- or moisture-sensitive reagents were carried out in glassware which was dried before use by heating under vacuum. Dry nitrogen or argon were used as inert gas atmosphere. NMR spectra were measured at room temperature using a Bruker Avance 300 (300 MHz for ¹H and 75 MHz for ¹³C) or a Bruker Avance 400 (400 MHz for ¹H and 101 MHz for ¹³C) or a Bruker Avance 600 (600 MHz for ¹H and 151 MHz for ¹³C) NMR spectrometer. All chemical shifts are reported in δ -scale as parts per million [ppm] (multiplicity,

coupling constant J, number of protons) relative to the solvent residual peaks or relative to tetramethylsilane as the internal standard. Coupling constants J are given in Hertz [Hz]. Abbreviations used for signal multiplicity: $^1\text{H-NMR}$: s = singlet, d = doublet, dd = doublet of doublets, ddd = doublet of doublets of doublets, dt = doublet of triplets, t = triplet, td = triplet of doublets, q = quartet, and m = multiplet.

Mass spectra were recorded on an Bruker timsTOF, Agilent Q-TOF 6540 UHD, Finnigan MAT SSQ 710 A, Jeol AccuTOF GCX or ThermoQuest Finnigan TSQ 7000 spectrometer. HPLC-MS analyses were performed on a Thermo Scientific Dionex Ultimate 3000 HPLC system combined with a DAD detector (230 nm; 254 nm) and either using a Kinetex 2.6 μm mesh C8 100A (2.1 x 75 mm, 2.6 μm) or an Agilent ZORBAX Eclipse XDB-C8 (3.5 x 100 mm, 3.5 μm). For mass detection, a BRUKER amazon SL mass spectrometer using ESI ionization was incorporated. The solvent system was Methanol/H₂O + 0.1% formic acid (25% for 0.2 min, gradient 25 - 100% in 5.8 min, 100% for 2.5 min, gradient 100 - 25% in 0.5 min, 25% for 3 min) at a flow rate of 0.3 mL/min for Kinetex column and 0.4 mL/min for Agilent. Absorption spectra were recorded on a UV/VIS Agilent Cary 100 spectrometer or a Specord 200 Plus double-beam photometer. Thermal half-lives were measured on a 96-well plate in a Thermo Scientific Multiskan® Spectrum. Analytical thin layer chromatography (TLC) was performed on silica gel coated alumina plates (MN precoated TLC-sheets ALUGRAM® Xtra SIL G/UV254). Visualization was done by UV-light (254 nm or 366 nm) or staining with ninhydrin or KMnO₄ solution. Column chromatography was performed using normal-grade silica gel (SiO₂, 60 Å) under gravity flow conditions in a standard glass column setup with isocratic elution (composition of the mobile phase is given for each experiment) or on a Biotage Isolera One automated flash purification system with UV/Vis detector. Analytical RP-HPLC were measured on an Agilent 1200 Series HPLC system (column: Agilent ZORBAX Eclipse XCB-C8 (4.6 x 150 mm, 5 μm) and an Agilent 1220 Infinity LC System (column: P/No 00F-4251-B0, Phenomenex Luna® 3 μm C18(2) 100 Å, LC column 150x2.0 mm). Purification by preparative HPLC was conducted on a preparative HPLC Agilent Series 1100 system (column: Agilent ZORBAX XDB-C8 (21.2 x 150 mm, 5 μm)) and an Agilent 1260 Infinity LC System (column: P/No 00G-4253-P0-AX, Phenomenex Luna® 10 μm C18(2) 100 Å, LC column 250x21.2 mm). The eluent systems were used as specified. After the purification process, solvents were removed by lyophilization. Switching experiments were done with a 365 nm LED (SSC VIOSYS CUN66A1B, 700 mA, 1250 mW) and 528 nm LED (OSRAM Oslon SSL 80 green, 500 mA, 34 mW).

2.7.2 Synthetic Procedures

8-(2-Azido-1-hydroxyethyl)-5-(benzyloxy)-2*H*-benzo[*b*][1,4]oxazin-3(4*H*)-one (17). To a stirred solution of **16** (1.0 g, 2.9 mmol, 1.0 eq.) in anhydrous methanol at 0 °C, NaBH₄ (111 mg, 2.9 mmol, 1.0 eq.) was added. The mixture was stirred for 2 h at 0 °C and was then quenched with H₂O. After extraction with ethyl acetate the combined phases were dried over MgSO₄, filtered and the solvent was evaporated. The crude product was used for automated column chromatography (PE/EtOAc, 0-80%). The pure product was obtained as a beige solid (720 mg, 2.1 mmol, 73%). **¹H NMR** (400 MHz, DMSO-*d*₆) δ 10.12 (s, 1H), 7.56 – 7.51 (m, 2H), 7.36 (t, *J* = 7.3 Hz, 2H), 7.33 – 7.26 (m, 1H), 7.04 (d, *J* = 8.6 Hz, 1H), 6.77 (d, *J* = 8.7 Hz, 1H), 5.17 (s, 2H), 4.98 (dd, *J* = 6.6, 4.5 Hz, 1H), 4.53 (d, *J* = 3.7 Hz, 2H), 3.27 – 3.21 (m, 2H). **¹³C NMR** (101 MHz, DMSO) δ 164.4, 145.2, 140.8, 136.8, 128.2, 127.7, 127.6, 122.8, 120.1, 116.4, 106.6, 69.9, 67.0, 66.5, 56.1. **ESI-MS:** *m/z* (%) = 341.12 (M+H)⁺.

8-(2-Amino-1-hydroxyethyl)-5-hydroxy-2*H*-benzo[*b*][1,4]oxazin-3(4*H*)-one (18). Compound **17** (1.0 g, 2.9 mmol, 1.0 equiv.) was dissolved in acetic acid (40 mL). Pd/C (10 mol%, 309 mg) was added. The mixture was stirred for 5 h at rt in a hydrogen atmosphere (10 bar). The mixture was filtered over celite and the solvent was removed *in vacuo*. The residue was dissolved in MeOH and a spoon of Amerlite IRA-67 (ion-exchange resin) was added. The mixture was stirred for 2 h and afterwards filtered. The solvent was removed and **18** was afforded as an off-white solid (620 mg, 2.8 mmol, 94%). The product was used without further purification. **¹H NMR** (400 MHz, Methanol-*d*₄) δ 7.02 (d, *J* = 8.5 Hz, 1H), 6.57 (d, *J* = 8.5 Hz, 1H), 5.10 (dd, *J* = 9.1, 3.4 Hz, 1H), 4.58 (d, *J* = 3.5 Hz, 2H), 3.15 (dd, *J* = 12.6, 3.4 Hz, 1H), 2.98 (dd, *J* = 12.6, 9.1 Hz, 1H). **¹³C NMR** (101 MHz, MeOD) δ 166.7, 146.6, 142.7, 121.8, 120.8, 116.3, 110.1, 68.1, 65.5, 46.1. **ESI-MS:** *m/z* (%) = 225.09 (M+H)⁺.

3-(2-(4-(2-Hydroxyethyl)phenyl)hydrazineylidene)pentane-2,4-dione (20). 2-(4-Aminophenyl)ethanol (10.0 g, 73.0 mmol, 1.0 eq.) was dissolved in AcOH (109 mL) and conc. HCl (18 mL) and the mixture was cooled to 0 °C. NaNO₂ (6.0 g, 87.0 mmol, 1.2 eq.) was dissolved in a minimum amount of water and added to the cooled reaction mixture. The mixture was stirred for 45 min and subsequently transferred to a mixture of acetylacetone (9.7 mL, 95 mmol, 1.3 eq.) and NaOAc (17.9 g, 220 mmol, 3.0 eq.) in EtOH (73 mL). The mixture turned yellow and was stirred for further 30 min. Icewater was added and the obtained precipitate was filtered off, washed with EtOH/H₂O (1:1) and dried under vacuum to obtain a yellow solid (15.8 g, 63.7 mmol, 87%). **¹H NMR** (400 MHz, Chloroform-*d*) δ 14.67 (s, 1H),

7.30 – 7.24 (m, 2H), 7.20 – 7.17 (m, 2H), 3.78 (t, J = 6.5 Hz, 2H), 2.79 (t, J = 6.5 Hz, 2H), 2.50 (s, 3H), 2.39 (s, 3H). $^{13}\text{C NMR}$ (101 MHz, CDCl_3) δ 198.0, 197.3, 140.3, 136.7, 133.2, 130.4, 116.6, 63.7, 38.8, 31.8, 26.8. **ESI-MS:** m/z (%) = 249.12 (M+H) $^+$.

(E)-2-(4-((3,5-Dimethyl-1H-pyrazol-4-yl)diazenyl)phenyl)ethan-1-ol (21). Compound **20** (10.0 g, 40.3 mmol, 1.0 eq.) was dissolved in EtOH (200 mL). Then, hydrazine monohydrate solution (64% hydrazine monohydrate in water, 3.15 g, 3.05 mL, 40.3 mmol, 1.0 eq.) was added and the reaction mixture was refluxed for 3 h. The solvent was almost completely removed and the remaining volume was poured onto icewater and the formed precipitate was filtered off, washed with EtOH/ H_2O (1:1) and dried under vacuum to obtain a yellow solid (9.2 g, 37.7 mmol, 93%). $^1\text{H NMR}$ (400 MHz, DMSO-d_6) δ 7.65 – 7.60 (m, 2H), 7.37 – 7.30 (m, 2H), 3.64 (t, J = 7.0 Hz, 2H), 2.78 (t, J = 6.9 Hz, 2H), 2.44 (s, 6H). $^{13}\text{C NMR}$ (101 MHz, DMSO) δ 151.5, 141.4, 140.3, 134.1, 129.6, 121.2, 109.6, 62.0, 38.8, 11.9. **ESI-MS:** m/z (%) = 245.14 (M+H) $^+$.

General procedure for compounds 22-25. NaH (60% dispersion in mineral oil, 1.5 eq.) was added in portions at to a stirred solution of **21** (1.0 eq.) in anhydrous DMF under nitrogen. The solution was stirred for 30 min. Then the solution was added dropwise to a solution of 1-bromo-2-chloroethane/1-bromo-3-chloropropane/1-bromo-4-chlorobutane/1-bromo-5-chloropentane (3.0 eq.) in anhydrous DMF. The mixture was stirred for 2 h at rt. Then, water was added and the mixture was extracted with ethyl acetate. The organic phase was washed with water and brine. The organic phase was dried over MgSO_4 and the solvent was removed *in vacuo*. The crude product was purified by column chromatography (PE/EtOAc, 20-100%).

(E)-2-(4-((1-(2-Chloroethyl)-3,5-dimethyl-1H-pyrazol-4-yl)diazenyl)phenyl)ethan-1-ol (22). **Yield:** 60%. $^1\text{H NMR}$ (400 MHz, Methanol-d_4) δ 7.73 – 7.66 (m, 2H), 7.38 – 7.30 (m, 2H), 4.36 (t, J = 5.8 Hz, 2H), 3.94 (t, J = 5.8 Hz, 2H), 3.79 (t, J = 7.0 Hz, 2H), 2.87 (t, J = 7.0 Hz, 2H), 2.61 (s, 3H), 2.45 (s, 3H). $^{13}\text{C NMR}$ (101 MHz, MeOD) δ 153.4, 143.8, 142.5, 142.0, 135.7, 130.6, 122.8, 64.0, 50.9, 43.8, 40.0, 14.2, 9.9. **ESI-MS:** m/z (%) = 307.13 (M+H) $^+$.

(E)-2-(4-((1-(3-Chloropropyl)-3,5-dimethyl-1H-pyrazol-4-yl)diazenyl)phenyl)ethan-1-ol (23). **Yield:** 83%. $^1\text{H NMR}$ (400 MHz, Methanol-d_4) δ 7.72 – 7.67 (m, 2H), 7.36 – 7.31 (m, 2H), 4.23 (t, J = 6.8 Hz, 2H), 3.80 (t, J = 7.0 Hz, 2H), 3.58 (t, J = 6.2 Hz, 2H), 2.88 (t, J = 7.0 Hz, 2H), 2.62 (s, 3H), 2.45 (s, 3H), 2.34 – 2.25 (m, 2H). $^{13}\text{C NMR}$ (101 MHz, MeOD) δ 153.5, 143.5, 142.5, 141.0, 135.8, 130.7, 122.8, 64.0, 46.6, 42.4, 40.0, 33.6, 14.0, 9.7. **ESI-MS:** m/z (%) = 321.15 (M+H) $^+$.

(*E*)-2-(4-((1-(4-Chlorobutyl)-3,5-dimethyl-1*H*-pyrazol-4-yl)diazenyl)phenyl)ethan-1-ol (24). Yield: 80%. ¹H NMR (400 MHz, Methanol-*d*₄) δ 7.72 – 7.66 (m, 2H), 7.36 – 7.30 (m, 2H), 4.08 (t, *J* = 7.1 Hz, 2H), 3.79 (t, *J* = 7.0 Hz, 2H), 3.58 (t, *J* = 6.5 Hz, 2H), 2.87 (t, *J* = 7.0 Hz, 2H), 2.58 (s, 3H), 2.44 (s, 3H), 2.00 – 1.90 (m, 2H), 1.82 – 1.72 (m, 2H). ¹³C NMR (101 MHz, MeOD) δ 153.4, 143.2, 142.4, 140.4, 135.8, 130.6, 122.8, 64.0, 49.0, 45.1, 40.0, 30.7, 28.3, 14.0, 9.8. **ESI-MS:** *m/z* (%) = 335.16 (M+H)⁺.

(*E*)-2-(4-((1-(5-Chloropentyl)-3,5-dimethyl-1*H*-pyrazol-4-yl)diazenyl)phenyl)ethan-1-ol (25). Yield: 76%. ¹H NMR (400 MHz, Methanol-*d*₄) δ 7.71 – 7.66 (m, 2H), 7.35 – 7.30 (m, 2H), 4.05 (t, *J* = 7.2 Hz, 2H), 3.79 (t, *J* = 7.0 Hz, 2H), 3.55 (t, *J* = 6.6 Hz, 2H), 2.87 (t, *J* = 7.0 Hz, 2H), 2.57 (s, 3H), 2.44 (s, 3H), 1.89 – 1.73 (m, 4H), 1.51 – 1.42 (m, 2H). ¹³C NMR (101 MHz, MeOD) δ 153.4, 143.1, 142.4, 140.4, 135.8, 130.6, 122.8, 64.0, 49.6, 45.4, 40.0, 33.3, 30.2, 25.0, 14.0, 9.8. **ESI-MS:** *m/z* (%) = 349.18 (M+H)⁺.

General procedure for compounds 26-29. Compounds **22-25** (1.0 eq.) and potassium thioacetate (1.9 eq.) were refluxed in THF overnight. Solvent was removed under reduced pressure. The crude product was purified by column chromatography (PE/EtOAc, 30-100%).

(*E*)-S-(2-(4-((4-(2-Hydroxyethyl)phenyl)diazenyl)-3,5-dimethyl-1*H*-pyrazol-1-yl)ethyl)ethanethioate (26). Yield: 80%. ¹H NMR (400 MHz, Chloroform-*d*) δ 7.71 (d, *J* = 8.0 Hz, 2H), 7.30 (d, *J* = 8.3 Hz, 2H), 4.20 – 4.13 (m, 2H), 3.88 (d, *J* = 6.4 Hz, 2H), 3.30 – 3.24 (m, 2H), 2.90 (t, *J* = 6.6 Hz, 2H), 2.59 (s, 3H), 2.47 (s, 3H), 2.35 (s, 3H). ¹³C NMR (101 MHz, CDCl₃) δ 195.6, 152.4, 143.0, 140.3, 139.2, 135.0, 129.6, 122.0, 63.5, 47.8, 39.1, 30.7, 29.1, 14.1, 9.9. **ESI-MS:** *m/z* (%) = 347.15 (M+H)⁺.

(*E*)-S-(3-(4-((4-(2-Hydroxyethyl)phenyl)diazenyl)-3,5-dimethyl-1*H*-pyrazol-1-yl)propyl)ethanethioate (27). Yield: 91%. ¹H NMR (300 MHz, Methanol-*d*₄) δ 7.70 (d, *J* = 8.4 Hz, 2H), 7.34 (d, *J* = 8.4 Hz, 2H), 4.12 (t, *J* = 7.0 Hz, 2H), 3.79 (t, *J* = 7.0 Hz, 2H), 2.88 (td, *J* = 7.0, 1.5 Hz, 4H), 2.59 (s, 3H), 2.45 (s, 3H), 2.32 (s, 3H), 2.12 – 2.03 (m, 2H). ¹³C NMR (75 MHz, MeOD) δ 197.0, 153.4, 143.3, 142.4, 140.7, 135.9, 130.7, 122.8, 64.0, 40.0, 30.9, 30.7, 30.5, 26.8, 14.0, 9.8. **ESI-MS:** *m/z* (%) = 361.17 (M+H)⁺.

(*E*)-S-(4-(4-((4-(2-Hydroxyethyl)phenyl)diazenyl)-3,5-dimethyl-1*H*-pyrazol-1-yl)butyl)ethanethioate (28). Yield: 82%. ¹H NMR (400 MHz, Chloroform-*d*) δ 7.72 (d, *J* = 8.3 Hz, 2H), 7.31 (d, *J* = 8.1 Hz, 2H), 4.03 (t, *J* = 7.2 Hz, 2H), 3.89 (t, *J* = 6.6 Hz, 2H), 2.91 (dt, *J* = 10.6, 6.9 Hz, 4H), 2.57 (s, 3H), 2.48 (s, 3H), 2.32 (s, 3H), 1.91 (p, *J* = 7.4 Hz, 2H), 1.63 (p, *J* =

7.3 Hz, 3H). ^{13}C NMR (101 MHz, CDCl_3) δ 195.9, 152.6, 142.6, 140.1, 138.4, 135.2, 129.7, 122.1, 63.7, 48.5, 39.2, 30.8, 29.1, 28.6, 26.9, 14.1, 10.0. **ESI-MS:** m/z (%) = 375.19 ($\text{M}+\text{H}$) $^+$.

(E)-S-(5-(4-((4-(2-Hydroxyethyl)phenyl)diazenyl)-3,5-dimethyl-1H-pyrazol-1-yl)pentyl) ethanethioate (29). Yield: 87%. ^1H NMR (400 MHz, Chloroform-d) δ 7.69 (d, J = 8.3 Hz, 2H), 7.28 (d, J = 8.3 Hz, 2H), 3.97 (t, J = 7.2 Hz, 2H), 3.85 (t, J = 6.6 Hz, 2H), 2.89 (t, J = 6.6 Hz, 2H), 2.83 (t, J = 7.3 Hz, 2H), 2.54 (s, 3H), 2.47 (s, 3H), 2.29 (s, 3H), 1.82 (p, J = 7.4 Hz, 2H), 1.64 – 1.53 (m, 2H), 1.38 (tt, J = 10.2, 6.2 Hz, 2H). ^{13}C NMR (101 MHz, CDCl_3) δ 195.9, 152.4, 142.4, 140.2, 138.3, 135.0, 129.6, 121.9, 63.5, 48.7, 39.1, 30.7, 29.5, 29.2, 28.8, 25.8, 14.0, 9.9. **ESI-MS:** m/z (%) = 389.20 ($\text{M}+\text{H}$) $^+$.

General procedure for compounds 30 and 31. Compound **26** or **27** (1.0 eq.) and 2,2'-dithiodipyridine (1.2 eq.) were dissolved under argon in anhydrous methanol and solution of NaOCH_3 (0.5 M in methanol, 1.5 eq.) was added dropwise. The reaction mixture was stirred at rt for 2 h. 2-(Dimethylamino)ethanethiol hydrochloride (4.0 eq.) was added and stirring at room temperature was continued for another 30 min. The solvent was removed under vacuum and the residue was taken up in ethylene acetate. The organic phase was washed with 2 M NaOH and extracted with 2 M HCl solution. The acidic aqueous phase was brought to pH 10 and then extracted with ethylene acetate. The combined organic phases were dried over Na_2SO_4 and the solvent was evaporated. Purification was performed by flash column chromatography (dichloromethane/ethanol/ NH_3 conc., 85:14:1).

(E)-2-(4-((1-(2-((2-(Dimethylamino)ethyl)disulfaneyl)ethyl)-3,5-dimethyl-1H-pyrazol-4-yl)diazenyl)phenyl)ethan-1-ol (30). Yield: 60%. ^1H -NMR (400 MHz, Chloroform-d) δ 7.76 – 7.70 (m, 2H), 7.35 – 7.29 (m, 2H), 4.38 – 4.31 (m, 2H), 3.90 (t, J = 6.5 Hz, 2H), 3.15 – 3.09 (m, 2H), 2.93 (t, J = 6.5 Hz, 2H), 2.87 – 2.81 (m, 2H), 2.65 – 2.58 (m, 5H), 2.49 (s, 3H), 2.27 (s, 6H). ^{13}C -NMR (101 MHz, CDCl_3) δ 152.4, 142.9, 140.0, 139.3, 135.0, 129.6, 122.0, 63.6, 58.5, 47.5, 45.3, 39.0, 37.5, 36.7, 14.1, 10.0. **ESI-MS:** m/z (%) = 408.0 ($\text{M}+\text{H}$) $^+$.

(E)-2-(4-((1-(3-((2-(Dimethylamino)ethyl)disulfaneyl)propyl)-3,5-dimethyl-1H-pyrazol-4-yl)diazenyl)phenyl)ethan-1-ol (31). Yield: 59%. ^1H -NMR (400 MHz, Chloroform-d) δ 7.76 – 7.70 (m, 2H), 7.35 – 7.29 (m, 2H), 4.15 (t, J = 6.8 Hz, 2H), 3.90 (t, J = 6.6 Hz, 2H), 2.93 (t, J = 6.5 Hz, 2H), 2.83 – 2.78 (m, 2H), 2.69 (t, J = 6.9 Hz, 2H), 2.62 – 2.57 (m, 5H), 2.49 (s, 3H), 2.31 – 2.24 (m, 8H). ^{13}C -NMR (101 MHz, CDCl_3) δ 152.6, 142.8, 140.2, 138.8, 135.2, 129.7, 122.1, 63.7, 58.9, 47.0, 45.5, 39.2, 36.9, 35.3, 28.9, 14.1, 10.1. **ESI-MS:** m/z (%) = 422.1 ($\text{M}+\text{H}$) $^+$.

General procedure for compounds 32 and 33. Compound **30** or **31** (1.0 eq.) was dissolved under argon in anhydrous dichloromethane and cooled to 0 °C. Methanesulfonyl chloride (3.8 eq.) was added dropwise. The mixture was allowed to warm to rt and stirred for 2 h. If the reaction is not completed, K₂CO₃ was added (1.0 eq.). The reaction was quenched with a sat. NaHCO₃ solution, ethylene acetate was added and the organic phase was washed with sat. NaHCO₃ solution. The organic phase was dried over Na₂SO₄ and the solvent was removed under vacuum. The compounds were used without further purification.

General procedure for compounds 1 and 2. Compound **32** or **33** (1.0 eq.) was dissolved under argon and exclusion of light in anhydrous DMSO. The solution was added to norepinephrine (4.8 eq.) and the mixture was stirred under argon for 16 h at 70 °C. Water + 0.1% TFA was added and the solution was frozen and lyophilized. Purification was done with preparative HPLC (RP-C8, CH₃CN/water + 0.3% TFA 10-95% in 50 min).

(*R,E*)-4-(2-((4-((1-(2-((2-(Dimethylamino)ethyl)disulfaneyl)ethyl)-3,5-dimethyl-1*H*-pyrazol-4-yl)diazenyl)phenethyl)amino)-1-hydroxyethyl)benzene-1,2-diol (1). Yield: 19%. **¹H-NMR** (600 MHz, DMSO-*d*₆) δ 9.87 (s, 1H), 9.15 – 8.75 (m, 2H), 8.77 – 8.61 (m, 1H), 7.73 – 7.68 (m, 2H), 7.42 – 7.37 (m, 2H), 6.80 (d, *J* = 2.1 Hz, 1H), 6.73 (d, *J* = 8.1 Hz, 1H), 6.64 (dd, *J* = 8.1, 2.1 Hz, 1H), 4.75 (dd, *J* = 10.3, 3.0 Hz, 1H), 4.36 (t, *J* = 6.7 Hz, 2H), 3.38 (t, *J* = 7.8 Hz, 2H), 3.26 – 3.18 (m, 4H), 3.15 – 2.93 (m, 6H), 2.82 (s, 6H), 2.60 (s, 3H), 2.39 (s, 3H). **¹³C-NMR** (151 MHz, DMSO-*d*₆) δ 151.8, 145.2, 144.9, 140.9, 139.9, 138.8, 134.2, 132.4, 129.4, 121.6, 116.7, 115.3, 113.3, 68.0, 55.4, 53.4, 47.7, 47.0, 42.3, 36.6, 31.1, 30.8, 13.9, 9.3. **ESI-MS:** *m/z* (%) = 559.2 (M+H)⁺. **HR-MS** (ESI): calc. for C₂₇H₃₈N₆O₃S₂ (M+H)⁺, *m/z* 559.2520, found: 559.2525.

(*R,E*)-4-(2-((4-((1-(3-((2-(Dimethylamino)ethyl)disulfaneyl)propyl)-3,5-dimethyl-1*H*-pyrazol-4-yl)diazenyl)phenethyl)amino)-1-hydroxyethyl)benzene-1,2-diol (2). Yield: 8%. **¹H-NMR** (600 MHz, DMSO-*d*₆) δ 9.90 (s, 1H), 9.30 – 8.90 8.95 (m, 2H), 8.82 (s, 1H), 8.69 (s, 1H), 7.72 – 7.67 (m, 2H), 7.43 – 7.36 (m, 2H), 6.79 (d, *J* = 2.1 Hz, 1H), 6.73 (d, *J* = 8.0 Hz, 1H), 6.63 (dd, *J* = 8.1, 2.1 Hz, 1H), 6.00 (s, 1H), 4.77 – 4.70 (m, 1H), 4.15 (t, *J* = 6.9 Hz, 2H), 3.39 – 3.30 (m, 3H), 3.25 – 3.17 (m, 2H), 3.15 – 2.96 (m, 4H), 2.85 – 2.75 (m, 9H), 2.58 (s, 3H), 2.38 (s, 4H), 2.20 – 2.11 (m, 2H). **¹³C-NMR** (151 MHz, DMSO-*d*₆) δ 151.8, 145.1, 144.9, 140.6, 139.4, 138.7, 134.2, 132.4, 129.4, 121.5, 116.7, 115.3, 113.3, 68.0, 55.4, 53.4, 47.7, 46.6, 42.2, 34.2, 31.1, 30.7, 28.3, 13.9, 9.3. **ESI-MS:** *m/z* (%) = 573.3 (M+H)⁺. **HR-MS** (ESI): calc. for C₂₈H₄₀N₆O₃S₂ (M+H)⁺, *m/z* 573.2676, found: 573.2681.

General procedure for compounds 34-37. Compounds **26-29** (1.0 eq.) and 2,2'-dithiopyridine (1.2 eq.) were dissolved in methanol. Dropwise over 1 h aqueous LiOH solution (1 M, 1.2 eq.) was added. After 3 h at 40 °C, the reaction mixture was concentrated and purified by column chromatography (PE/EtOAc, 20-100%).

(E)-2-(4-((3,5-Dimethyl-1-(2-(pyridin-2-yl)disulfaneyl)ethyl)-1H-pyrazol-4-yl)diazenyl)phenyl)ethan-1-ol (34). Yield: 54%. ¹H NMR (400 MHz, Chloroform-d) δ 8.52 – 8.45 (m, 1H), 7.72 (d, J = 7.9 Hz, 2H), 7.64 (dq, J = 4.1, 1.3 Hz, 2H), 7.31 (d, J = 8.0 Hz, 2H), 7.15 – 7.07 (m, 1H), 4.37 (t, J = 6.8 Hz, 2H), 3.90 (t, J = 6.6 Hz, 2H), 3.26 (t, J = 6.8 Hz, 2H), 2.93 (t, J = 6.6 Hz, 2H), 2.58 (s, 3H), 2.48 (s, 3H). ¹³C NMR (101 MHz, CDCl₃) δ 159.3, 152.5, 150.0, 143.2, 140.2, 139.4, 137.3, 135.1, 129.7, 122.1, 121.2, 120.2, 63.7, 47.3, 39.2, 37.7, 14.2, 10.1. **ESI-MS:** m/z (%) = 414.14 (M+H)⁺.

(E)-2-(4-((3,5-Dimethyl-1-(3-(pyridin-2-yl)disulfaneyl)propyl)-1H-pyrazol-4-yl)diazenyl)phenyl)ethan-1-ol (35). Yield: 58%. ¹H NMR (400 MHz, Methanol-d₄) δ 8.37 (ddd, J = 4.9, 1.7, 1.0 Hz, 1H), 7.81 – 7.74 (m, 2H), 7.71 – 7.67 (m, 2H), 7.37 – 7.32 (m, 2H), 7.18 (ddd, J = 6.7, 4.9, 1.8 Hz, 1H), 4.18 (t, J = 6.8 Hz, 2H), 3.80 (t, J = 7.0 Hz, 2H), 2.88 (t, J = 7.0 Hz, 2H), 2.81 (t, J = 7.1 Hz, 2H), 2.58 (s, 3H), 2.42 (s, 3H), 2.24 (p, J = 6.9 Hz, 2H). ¹³C NMR (101 MHz, MeOD) δ 161.0, 153.4, 150.4, 143.3, 142.5, 140.6, 139.1, 135.9, 130.6, 122.8, 122.4, 121.3, 64.0, 48.0, 40.0, 36.1, 29.8, 14.0, 9.9. **ESI-MS:** m/z (%) = 428.16 (M+H)⁺.

(E)-2-(4-((3,5-Dimethyl-1-(4-(pyridin-2-yl)disulfaneyl)butyl)-1H-pyrazol-4-yl)diazenyl)phenyl)ethan-1-ol (36). Yield: 60%. ¹H NMR (400 MHz, Chloroform-d) δ 8.41 (ddd, J = 4.9, 1.9, 0.9 Hz, 1H), 7.72 – 7.67 (m, 2H), 7.65 (dt, J = 8.1, 1.1 Hz, 1H), 7.59 (td, J = 7.8, 1.8 Hz, 1H), 7.32 – 7.27 (m, 2H), 7.03 (ddd, J = 7.3, 4.8, 1.2 Hz, 1H), 3.98 (t, J = 7.0 Hz, 2H), 3.87 (t, J = 6.6 Hz, 2H), 2.90 (t, J = 6.6 Hz, 2H), 2.79 (t, J = 7.2 Hz, 2H), 2.50 (s, 3H), 2.46 (s, 3H), 1.97 – 1.88 (m, 2H), 1.72 (dq, J = 10.5, 7.4 Hz, 2H). ¹³C NMR (101 MHz, CDCl₃) δ 160.2, 152.4, 149.7, 142.5, 140.2, 138.3, 137.1, 135.0, 129.6, 122.0, 120.7, 119.8, 63.5, 48.4, 39.1, 38.3, 28.7, 26.1, 14.0, 9.9. **ESI-MS:** m/z (%) = 442.17 (M+H)⁺.

(E)-2-(4-((3,5-Dimethyl-1-(5-(pyridin-2-yl)disulfaneyl)pentyl)-1H-pyrazol-4-yl)diazenyl)phenyl)ethan-1-ol (37). Yield: 66%. ¹H NMR (400 MHz, Chloroform-d) δ 8.45 (dt, J = 5.0, 1.3 Hz, 1H), 7.74 – 7.70 (m, 2H), 7.70 – 7.67 (m, 1H), 7.62 (td, J = 7.7, 1.8 Hz, 1H), 7.31 (d, J = 8.2 Hz, 2H), 7.06 (ddd, J = 7.3, 4.8, 1.1 Hz, 1H), 3.99 (t, J = 7.2 Hz, 2H), 3.89 (t, J = 6.6 Hz, 2H), 2.92 (t, J = 6.6 Hz, 2H), 2.78 (t, J = 7.3 Hz, 2H), 2.54 (s, 3H), 2.48 (s, 3H), 1.83 (p, J = 7.4 Hz, 2H), 1.74 (t, J = 7.5 Hz, 2H), 1.49 – 1.40 (m, 2H). ¹³C NMR (101 MHz,

CDCl₃) δ 160.5, 152.6, 149.7, 142.5, 140.1, 138.3, 137.1, 135.1, 129.7, 122.0, 120.7, 119.8, 63.7, 48.8, 39.2, 38.7, 29.7, 28.6, 25.7, 14.1, 10.0. **ESI-MS**: m/z (%) = 456.19 (M+H)⁺.

General procedure for compounds 38-41. Compounds **34-37** (1.0 eq.) were dissolved in CH₂Cl₂ under an argon atmosphere and Dess Martin periodinane (1.5 eq.) was added. The mixture was stirred at 0 °C for 1.5 h. Then, EtOAc was added and the mixture was extracted with aqueous sat. Na₂S₂O₃, sat. NaHCO₃ and sat. NaCl. The combined organic layers were dried over MgSO₄ and after filtration the solvent was removed under reduced pressure to get the crude compound which was carried on to the reductive amination immediately without further purification.

General procedure for compounds 3-6. Compound **18** (1.0 eq.), **38-41** (1.5 eq.) and NaCNBH₃ (1.5 eq.) were dissolved in MeOH under an argon atmosphere. The mixture was stirred at rt for overnight. EtOAc was added and the solution was washed with sat. aqueous NaHCO₃ solution and H₂O. The organic layer was dried over MgSO₄, filtered and the solvent was removed *in vacuo*. The crude product was dissolved in MeOH and cysteamine hydrochloride (2.0 eq.) was added to stir the mixture for 1 h at rt. The solvent was removed *in vacuo* and the crude product was purified by preparative HPLC (column: Luna 10, 250 x 21 mm; flow: 22 mL/min, solvent A: H₂O (0.05% TFA), solvent B: MeCN; gradient A/B: 0-20 min: 90/10, 20-25 min: 2/98) to obtain a yellow solid.

(E)-8-(2-((4-((1-(2-((2-Aminoethyl)disulfaneyl)ethyl)-3,5-dimethyl-1H-pyrazol-4-yl)diazenyl)phenethyl)amino)-1-hydroxyethyl)-5-hydroxy-2H-benzo[*b*][1,4]oxazin-3(4H)-one (3). Yield: 5%. ¹H NMR (400 MHz, DMSO-d₆) δ 10.05 (s, 1H), 9.98 (s, 1H), 8.66 (s, 1H), 7.91 (s, 3H), 7.70 (d, J = 8.3 Hz, 2H), 7.39 (d, J = 8.4 Hz, 2H), 6.92 (d, J = 8.5 Hz, 1H), 6.56 (d, J = 8.5 Hz, 1H), 5.98 (s, 1H), 5.08 (d, J = 8.9 Hz, 1H), 4.53 (d, J = 2.2 Hz, 2H), 4.35 (t, J = 6.7 Hz, 2H), 3.18 (t, J = 6.6 Hz, 4H), 3.12 (d, J = 6.2 Hz, 4H), 2.97 (q, J = 8.7, 6.8 Hz, 4H), 2.59 (s, 3H), 2.38 (s, 3H). ¹³C NMR (151 MHz, DMSO) δ 164.2, 151.9, 144.9, 141.2, 140.9, 140.0, 138.9, 134.3, 129.5, 121.7, 120.0, 119.8, 115.3, 109.1, 67.0, 62.8, 52.2, 47.9, 47.1, 37.7, 36.5, 34.0, 31.1, 14.0, 9.4. **ESI-MS**: m/z (%) = 586.23 (M+H)⁺. **HR-MS** (ESI): calcd. for C₂₇H₃₅N₇O₄S₂ (M+H)⁺, m/z = 586.2265, found 586.2275.

(E)-8-(2-((4-((1-(3-((2-Aminoethyl)disulfaneyl)propyl)-3,5-dimethyl-1H-pyrazol-4-yl)diazenyl)phenethyl)amino)-1-hydroxyethyl)-5-hydroxy-2H-benzo[*b*][1,4]oxazin-3(4H)-one (4). Yield: 3%. ¹H NMR (400 MHz, DMSO-d₆) δ 10.15 (s, 1H), 9.96 (s, 1H), 8.99 (s, 1H), 8.76 (s, 1H), 8.08 (s, 3H), 7.69 (d, J = 8.0 Hz, 2H), 7.39 (d, J = 8.1 Hz, 2H), 6.92 (d, J

= 8.5 Hz, 1H), 6.58 (d, J = 8.5 Hz, 1H), 6.02 (s, 1H), 5.09 (dd, J = 10.1, 2.8 Hz, 1H), 4.53 (d, J = 2.2 Hz, 2H), 4.14 (t, J = 6.8 Hz, 2H), 3.22 (d, J = 8.3 Hz, 2H), 3.10 (q, J = 14.5, 10.8 Hz, 4H), 3.01 (dd, J = 15.3, 7.1 Hz, 2H), 2.93 (t, J = 7.1 Hz, 2H), 2.77 (t, J = 7.1 Hz, 2H), 2.57 (s, 3H), 2.38 (s, 3H), 2.15 (p, J = 7.0 Hz, 2H). **^{13}C NMR** (101 MHz, DMSO) δ 164.3, 151.9, 145.0, 141.2, 140.7, 139.5, 138.8, 134.3, 129.5, 121.7, 120.1, 119.8, 115.3, 109.2, 67.0, 62.9, 52.2, 47.9, 46.7, 37.9, 34.2, 33.9, 31.2, 28.6, 14.0, 9.4. **ESI-MS**: m/z (%) = 300.63 ($M+2H$)²⁺. **HR-MS** (ESI): calcd. for $\text{C}_{28}\text{H}_{37}\text{N}_7\text{O}_4\text{S}_2$ ($M+H$)⁺, m/z = 600.2421, found 600.2419.

(*E*)-8-(2-((4-((1-(4-((2-Aminoethyl)disulfaneyl)butyl)-3,5-dimethyl-1*H*-pyrazol-4-yl)diazanyl)phenethyl)amino)-1-hydroxyethyl)-5-hydroxy-2*H*-benzo[*b*][1,4]oxazin-3(4*H*)-one (5). Yield: 4%. **^1H NMR** (400 MHz, DMSO- d_6) δ 10.00 (d, J = 6.6 Hz, 1H), 9.98 (s, 1H), 8.84 (s, 1H), 8.68 (s, 1H), 7.93 (s, 3H), 7.72 – 7.67 (m, 2H), 7.43 – 7.37 (m, 2H), 6.93 (d, J = 8.5 Hz, 1H), 6.57 (d, J = 8.5 Hz, 1H), 5.98 (s, 1H), 5.08 (dd, J = 10.1, 2.8 Hz, 1H), 4.54 (d, J = 1.8 Hz, 2H), 4.08 (t, J = 7.0 Hz, 2H), 3.22 (s, 2H), 3.17 – 3.04 (m, 4H), 3.00 (dd, J = 14.7, 6.7 Hz, 2H), 2.89 (t, J = 7.0 Hz, 2H), 2.79 (t, J = 7.2 Hz, 2H), 2.57 (s, 3H), 2.37 (s, 3H), 1.86 (p, J = 7.1 Hz, 2H), 1.67 (p, J = 7.3 Hz, 2H). **^{13}C NMR** (101 MHz, DMSO) δ 164.2, 151.9, 144.9, 141.2, 140.5, 139.3, 138.7, 134.3, 129.5, 121.6, 120.0, 119.8, 115.3, 109.1, 67.0, 62.8, 52.2, 47.9, 47.8, 37.8, 36.8, 34.0, 31.1, 27.9, 25.5, 14.0, 9.4. **ESI-MS**: m/z (%) = 307.63 ($M+2H$)²⁺. **HR-MS** (ESI): calcd. for $\text{C}_{29}\text{H}_{39}\text{N}_7\text{O}_4\text{S}_2$ ($M+H$)⁺, m/z = 614.2578, found 614.2575.

(*E*)-8-(2-((4-((1-(5-((2-Aminoethyl)disulfaneyl)pentyl)-3,5-dimethyl-1*H*-pyrazol-4-yl)diazanyl)phenethyl)amino)-1-hydroxyethyl)-5-hydroxy-2*H*-benzo[*b*][1,4]oxazin-3(4*H*)-one (6). Yield: 5%. **^1H NMR** (400 MHz, DMSO- d_6) δ 10.03 (s, 1H), 9.97 (s, 1H), 8.86 (s, 1H), 8.69 (s, 1H), 7.94 (s, 3H), 7.73 – 7.66 (m, 2H), 7.42 – 7.36 (m, 2H), 6.93 (d, J = 8.5 Hz, 1H), 6.57 (d, J = 8.5 Hz, 1H), 5.98 (s, 1H), 5.09 (dd, J = 10.2, 2.8 Hz, 1H), 4.54 (d, J = 1.9 Hz, 2H), 4.04 (t, J = 7.1 Hz, 2H), 3.22 (s, 2H), 3.17 – 3.05 (m, 4H), 3.02 (d, J = 9.0 Hz, 2H), 2.89 (dd, J = 7.7, 6.4 Hz, 2H), 2.75 (t, J = 7.3 Hz, 2H), 2.56 (s, 3H), 2.37 (s, 3H), 1.78 (p, J = 7.3 Hz, 2H), 1.67 (p, J = 7.4 Hz, 2H), 1.42 – 1.33 (m, 2H). **^{13}C NMR** (101 MHz, DMSO) δ 164.2, 151.9, 144.9, 141.2, 140.4, 139.3, 138.7, 134.3, 129.5, 121.6, 120.0, 119.8, 115.3, 109.1, 67.0, 62.8, 52.2, 48.2, 47.9, 37.9, 37.3, 34.0, 31.1, 28.8, 28.1, 24.9, 14.0, 9.4. **ESI-MS**: m/z (%) = 314.64 ($M+2H$)²⁺. **HR-MS** (ESI): calcd. for $\text{C}_{30}\text{H}_{41}\text{N}_7\text{O}_4\text{S}_2$ ($M+H$)⁺, m/z = 628.2734, found 628.2734.

General procedure for compounds 42 and 43. Compound **22** or **23** (1.0 eq.) and 3a,4,7,7a-tetrahydro-1*H*-4,7-epoxyisoindole-1,3(2*H*)-dione (1.2 eq.) were dissolved in DMF. K_2CO_3

(3.0 eq.) was added and the mixture was stirred overnight at 50 °C. Water was added and the mixture was extracted with EtOAc. The organic phase was washed with water and brine. The combined organic phases were dried over MgSO₄ and the solvent was removed in vacuo. The crude product was purified by column chromatography (PE/EtOAc, 20-100%).

(*E*)-2-(2-(4-(((4-(2-Hydroxyethyl)phenyl)diazenyl)-3,5-dimethyl-1*H*-pyrazol-1-yl)ethyl)-3a,4,7,7a-tetrahydro-1*H*-4,7-epoxyisoindole-1,3(2*H*)-dione (42). Yield: 50%. ¹H NMR (400 MHz, Chloroform-*d*) δ 7.72 (d, *J* = 8.3 Hz, 2H), 7.31 (d, *J* = 8.3 Hz, 2H), 6.49 (s, 2H), 5.24 (s, 2H), 4.22 (t, *J* = 6.4 Hz, 2H), 3.93 – 3.85 (m, 4H), 2.92 (t, *J* = 6.6 Hz, 2H), 2.83 (s, 2H), 2.57 (s, 3H), 2.45 (s, 3H). ¹³C NMR (101 MHz, CDCl₃) δ 175.8, 152.5, 143.0, 140.2, 139.2, 136.7, 135.4, 129.7, 122.1, 81.0, 63.7, 47.6, 45.7, 39.2, 38.3, 14.1, 9.8. **ESI-MS:** *m/z* (%) = 436.20 (M+H)⁺.

(*E*)-2-(3-(4-(((4-(2-Hydroxyethyl)phenyl)diazenyl)-3,5-dimethyl-1*H*-pyrazol-1-yl)propyl)-3a,4,7,7a-tetrahydro-1*H*-4,7-epoxyisoindole-1,3(2*H*)-dione (43). Yield: 45%. ¹H NMR (400 MHz, Chloroform-*d*) δ 7.70 (d, *J* = 8.3 Hz, 2H), 7.30 (d, *J* = 8.3 Hz, 2H), 6.50 (s, 2H), 5.25 (s, 2H), 4.02 – 3.96 (m, 2H), 3.88 (q, *J* = 6.3 Hz, 2H), 3.59 (t, *J* = 6.7 Hz, 2H), 2.91 (t, *J* = 6.6 Hz, 2H), 2.81 (s, 2H), 2.52 (s, 3H), 2.46 (s, 3H), 2.21 – 2.11 (m, 2H). ¹³C NMR (101 MHz, CDCl₃) δ 176.2, 152.5, 142.5, 140.1, 138.7, 136.6, 135.2, 129.6, 122.1, 81.1, 63.7, 47.5, 46.5, 39.2, 36.6, 27.8, 14.1, 9.8. **ESI-MS:** *m/z* (%) = 450.21 (M+H)⁺.

General procedure for compounds 44 and 45. Compound **42** or **43** (1.0 eq.) was dissolved in CH₂Cl₂ and the mixture was cooled to 0 °C. Triethylamine (1.5 equiv.) and methanesulfonyl chloride (1.1 equiv.) were added and the mixture was warmed up to rt over 1 h. Water was added, and the aqueous phase was extracted with CH₂Cl₂. The solvent was removed *in vacuo*. The crude product was used in the next step without further purification.

General procedure for compounds 46-48. Compound **44** or **45** (1.0 eq.) and **18** or norepinephrine (3.0 equiv.) were dissolved in DMSO in an argon atmosphere. The solution was stirred overnight at 70 °C. The crude product was purified by preparative HPLC (column: Luna 10, 250 x 21 mm; flow: 22 mL/min, solvent A: H₂O (0.05% TFA), solvent B: MeCN; gradient A/B: 0-20 min: 90/10, 20-25 min: 2/98) to obtain a yellow solid.

2-(2-(4-((*E*)-4-(2-(((*R*)-2-(3,4-Dihydroxyphenyl)-2-hydroxyethyl)amino)ethyl)phenyl)diazenyl)-3,5-dimethyl-1*H*-pyrazol-1-yl)ethyl)-3a,4,7,7a-tetrahydro-1*H*-4,7-epoxyisoindole-1,3(2*H*)-dione (46). Yield: 10%. ¹H NMR

(400 MHz, DMSO- d_6) δ 8.95 (s, 2H), 8.67 (s, 2H), 7.70 (d, $J = 8.4$ Hz, 2H), 7.39 (d, $J = 8.4$ Hz, 2H), 6.79 (d, $J = 2.1$ Hz, 1H), 6.73 (d, $J = 8.1$ Hz, 1H), 6.63 (dd, $J = 8.1, 2.1$ Hz, 1H), 6.53 (s, 2H), 6.00 (s, 1H), 5.11 (s, 2H), 4.73 (dd, $J = 10.5, 2.9$ Hz, 1H), 4.17 (t, $J = 6.3$ Hz, 2H), 3.74 (t, $J = 6.3$ Hz, 2H), 3.21 (q, $J = 6.8$ Hz, 2H), 3.04 (ddt, $J = 22.1, 13.6, 6.4$ Hz, 4H), 2.53 (s, 3H), 2.34 (s, 3H). $^{13}\text{C NMR}$ (101 MHz, DMSO) δ 176.1, 151.9, 145.3, 145.0, 140.9, 140.0, 138.8, 136.5, 134.4, 132.5, 129.5, 121.7, 116.8, 115.4, 113.4, 109.5, 80.3, 68.2, 53.5, 47.8, 47.2, 45.4, 37.5, 31.2, 13.9, 9.1. **ESI-MS:** m/z (%) = 587.26 (M+H) $^+$.

(E)-2-(2-(4-((4-(2-((2-Hydroxy-2-(5-hydroxy-3-oxo-3,4-dihydro-2H-benzo[*b*][1,4]oxazin-8-yl)ethyl)amino)ethyl)phenyl)diazanyl)-3,5-dimethyl-1H-pyrazol-1-yl)ethyl)-3a,4,7,7a-tetrahydro-1H-4,7-epoxyisoindole-1,3(2H)-dione (47).

Yield: 17%. $^1\text{H NMR}$ (400 MHz, DMSO- d_6) δ 10.00 (s, 1H), 9.98 (s, 1H), 8.81 (s, 1H), 8.66 (s, 1H), 7.73 – 7.67 (m, 2H), 7.39 (d, $J = 8.4$ Hz, 2H), 6.93 (d, $J = 8.5$ Hz, 1H), 6.57 (d, $J = 8.5$ Hz, 1H), 6.53 (s, 2H), 5.97 (s, 1H), 5.10 (d, $J = 1.0$ Hz, 2H), 5.10 – 5.05 (m, 1H), 4.54 (d, $J = 2.2$ Hz, 2H), 4.18 (t, $J = 6.3$ Hz, 2H), 3.74 (t, $J = 6.3$ Hz, 2H), 3.22 (s, 2H), 3.18 – 3.06 (m, 2H), 3.04 – 2.98 (m, 2H), 2.93 (s, 2H), 2.53 (s, 3H), 2.34 (s, 3H). $^{13}\text{C NMR}$ (101 MHz, DMSO) δ 176.1, 164.2, 151.9, 144.9, 141.2, 140.9, 140.0, 138.8, 136.5, 134.4, 129.5, 121.7, 120.0, 119.8, 115.3, 109.1, 80.3, 67.0, 62.8, 52.2, 47.9, 47.2, 45.3, 37.5, 31.1, 13.9, 9.1. **ESI-MS:** m/z (%) = 642.27 (M+H) $^+$.

(E)-2-(3-(4-((4-(2-((2-Hydroxy-2-(5-hydroxy-3-oxo-3,4-dihydro-2H-benzo[*b*][1,4]oxazin-8-yl)ethyl)amino)ethyl)phenyl)diazanyl)-3,5-dimethyl-1H-pyrazol-1-yl)propyl)-3a,4,7,7a-tetrahydro-1H-4,7-epoxyisoindole-1,3(2H)-dione (48).

Yield: 18%. $^1\text{H NMR}$ (400 MHz, DMSO- d_6) δ 9.99 (d, $J = 10.4$ Hz, 2H), 8.80 (s, 1H), 8.66 (s, 1H), 7.69 (d, $J = 8.3$ Hz, 2H), 7.39 (d, $J = 8.2$ Hz, 2H), 6.92 (d, $J = 8.5$ Hz, 1H), 6.58 (s, 1H), 6.55 (d, $J = 1.3$ Hz, 2H), 5.97 (s, 1H), 5.14 (s, 2H), 5.08 (dd, $J = 10.0, 2.9$ Hz, 1H), 4.54 (d, $J = 2.3$ Hz, 2H), 3.99 (t, $J = 7.2$ Hz, 2H), 3.45 (d, $J = 7.5$ Hz, 2H), 3.21 (d, $J = 8.8$ Hz, 2H), 3.17 – 3.06 (m, 2H), 3.04 – 2.98 (m, 2H), 2.91 (s, 2H), 2.52 (s, 3H), 2.36 (s, 3H), 1.99 (p, $J = 7.2$ Hz, 2H). $^{13}\text{C NMR}$ (101 MHz, DMSO) δ 176.5, 164.2, 152.0, 144.9, 141.2, 140.6, 139.6, 138.7, 136.5, 134.3, 129.5, 121.7, 120.1, 119.8, 115.3, 109.2, 80.4, 67.0, 62.8, 52.2, 48.0, 47.2, 45.8, 35.6, 31.2, 27.0, 14.0, 9.2. **ESI-MS:** m/z (%) = 656.28 (M+H) $^+$.

General procedures for compounds 7-9. Compounds **46-48** were dissolved in DMSO under an argon atmosphere. The mixture was stirred at 110 °C for 3-4 h. The crude product was purified by preparative HPLC (column: Luna 10, 250 x 21 mm; flow: 22 mL/min, solvent A:

H₂O (0.05% TFA), solvent B: MeCN; gradient A/B: 0-20 min: 90/10, 20-25 min: 2/98) to obtain a yellow solid.

(*R,E*)-1-(2-(4-((4-(2-((2-(3,4-Dihydroxyphenyl)-2-hydroxyethyl)amino)ethyl)phenyl)diazenyl)-3,5-dimethyl-1*H*-pyrazol-1-yl)ethyl)-1*H*-pyrrole-2,5-dione (7). Yield: 85%. ¹H-NMR (600 MHz, DMSO-d₆) δ 8.94 (s, 2H), 8.63 (s, 2H), 7.73 – 7.67 (m, 2H), 7.41 – 7.37 (m, 2H), 7.03 (s, 2H), 6.79 (d, *J* = 2.1 Hz, 1H), 6.73 (d, *J* = 8.1 Hz, 1H), 6.63 (dd, *J* = 8.1, 2.1 Hz, 1H), 6.02-5.96 (m, 1H), 4.76-4.69 (m, 1H), 4.23 (t, *J* = 6.0 Hz, 2H), 3.78 (t, *J* = 5.9 Hz, 2H), 3.26 – 3.19 (m, 2H), 3.17 – 2.89 (m, 4H), 2.53 (s, 3H), 2.30 (s, 3H). ¹³C-NMR (151 MHz, DMSO-d₆) δ 171.1, 152.3, 145.7, 145.5, 141.3, 140.1, 139.3, 135.2, 133.0, 130.0, 122.2, 117.3, 115.8, 113.9, 68.6, 53.9, 48.2, 46.7, 37.2, 31.6, 14.2, 9.6. **ESI-MS:** *m/z* (%) = 519.2 (M+H)⁺. **HR-MS** (ESI): calc. for C₂₇H₃₀N₆O₅ (M+H)⁺, *m/z* = 519.2350, found: 519.2361.

(*E*)-1-(2-(4-((4-(2-((2-Hydroxy-2-(5-hydroxy-3-oxo-3,4-dihydro-2*H*-benzo[*b*][1,4]oxazin-8-yl)ethyl)amino)ethyl)phenyl)diazenyl)-3,5-dimethyl-1*H*-pyrazol-1-yl)ethyl)-1*H*-pyrrole-2,5-dione (8). Yield: 98%. ¹H NMR (400 MHz, DMSO-d₆) δ 10.00 (s, 1H), 9.98 (s, 1H), 8.81 (s, 1H), 8.66 (s, 1H), 7.70 (d, *J* = 8.2 Hz, 2H), 7.39 (d, *J* = 8.2 Hz, 2H), 7.03 (s, 2H), 6.92 (d, *J* = 8.5 Hz, 1H), 6.57 (d, *J* = 8.5 Hz, 1H), 5.97 (s, 1H), 5.12 – 5.02 (m, 1H), 4.54 (d, *J* = 2.2 Hz, 2H), 4.22 (t, *J* = 5.9 Hz, 2H), 3.78 (t, *J* = 5.9 Hz, 2H), 3.21 (d, *J* = 7.8 Hz, 2H), 3.12 (s, 2H), 3.04 – 2.97 (m, 2H), 2.52 (s, 3H), 2.30 (s, 3H). ¹³C NMR (101 MHz, DMSO) δ 170.6, 164.2, 151.9, 144.9, 141.2, 140.8, 139.7, 138.8, 134.7, 134.5, 129.5, 121.7, 120.0, 119.8, 115.3, 109.5, 67.0, 62.8, 47.9, 46.2, 46.2, 36.7, 31.1, 13.8, 9.2. **ESI-MS:** *m/z* (%) = 574.24 (M+H)⁺. **HR-MS** (ESI): calc. for C₂₉H₃₁N₇O₆ (M+H)⁺, *m/z* = 574.2409, found: 574.2419.

(*E*)-1-(3-(4-((4-(2-((2-Hydroxy-2-(5-hydroxy-3-oxo-3,4-dihydro-2*H*-benzo[*b*][1,4]oxazin-8-yl)ethyl)amino)ethyl)phenyl)diazenyl)-3,5-dimethyl-1*H*-pyrazol-1-yl)propyl)-1*H*-pyrrole-2,5-dione (9). Yield: 95%. ¹H NMR (400 MHz, DMSO-d₆) δ 9.99 (s, 1H), 9.98 (s, 1H), 8.79 (s, 1H), 8.65 (s, 1H), 7.70 (d, *J* = 8.4 Hz, 2H), 7.39 (d, *J* = 8.4 Hz, 2H), 6.99 (s, 2H), 6.92 (d, *J* = 8.5 Hz, 1H), 6.57 (d, *J* = 8.5 Hz, 1H), 5.97 (s, 1H), 5.08 (d, *J* = 9.8 Hz, 1H), 4.54 (d, *J* = 2.2 Hz, 2H), 4.05 (t, *J* = 6.9 Hz, 2H), 3.48 (t, *J* = 6.9 Hz, 2H), 3.22 (s, 2H), 3.18 – 3.04 (m, 2H), 3.00 (dd, *J* = 15.1, 7.1 Hz, 2H), 2.53 (s, 3H), 2.35 (s, 3H), 2.09 – 2.03 (m, 2H). ¹³C NMR (101 MHz, DMSO) δ 171.0, 164.2, 151.9, 144.9, 141.2, 140.5, 139.6, 138.7, 134.5, 134.3, 129.5, 121.7, 120.0, 119.8, 115.3, 109.1, 67.0, 62.8, 52.2, 47.9, 46.0,

35.0, 31.1, 27.6, 14.0, 9.3. **ESI-MS:** m/z (%) = 588.26 (M+H)⁺. **HR-MS** (ESI): calc. for C₃₀H₃₃N₇O₆ (M+H)⁺, m/z = 588.2565, found: 588.2573.

2.7.3 Biological Investigation

Mammalian cell culture.

Cell culture and transfection. HEK-293T cells (gift from the Chair of Physiology, FAU Erlangen-Nürnberg) were cultured in DMEM/F12 medium supplemented with 10% fetal bovine serum, 100 μ g/mL penicillin, 100 μ g/mL streptomycin, and 2 mM L-glutamine in culture dishes (10 cm). They were incubated at 37 °C and 5% CO₂ to a confluency of 70 – 100%. To prepare cells for the IP-One assay, HEK-293T cells were grown to a confluency of 70%. Transfection was done with the Mirus TransIT-293 reagent according to manufacturer's protocol when mixing the appropriate cDNA (β_2 AR wt or β_2 K97^{2.68}C and the hybrid G-protein G α_{qs} , a G α_q protein with the last five amino acids at the C terminus replaced by the corresponding amino acids of G α_s (gifted from The J. David Gladstone Institutes, San Francisco, CA) in a ratio of 1:3) with the Mirus TransIT-293 reagent in serum-free medium in a 1:3 ratio. After equal distribution of the mixture to the cells incubation was continued for 48 h before performing the assay. For BRET experiments, HEK cells were detached, diluted to a cell concentration of 250,000 cells/mL and transfected with 100 ng cDNA of the β_2 AR for β -arrestin recruitment (receptor: β -arrestin:GRK2:CAAX ratio 1:0.2:1:3) using linear polyethyleneimine (PEI, Polysciences, 3:1 PEI:DNA ratio). The DNA was complemented to a total amount of 1 μ g DNA per 3 · 10⁵ cells with ssDNA (Sigma Aldrich) and 20,000 cells per well were transferred into 96-well half-area plates (Greiner, Frickenhausen, Germany). Cells were incubated for 48 h before starting the assay.

Functional assays.

Irradiation of photoswitches. To adjust the photoswitchable compounds in the desired *E* or *Z* isoform a 100 μ M stock solution was irradiated with high-power LEDs emitting light with a wavelength of 365 nm (for 30 s to adjust the *Z* isomer) or 528 nm (for 120 s to switch to *E* isomer) directly before starting the assay.

IP-One accumulation assay. Evaluation of β_2 AR wild-type and mutant activation was performed applying the IP-One HTRF assay (PerkinElmer, Rodgau, Germany). The experiments were conducted according to the manufacturer's protocol. In brief, HEK-293T

cells were transiently co-transfected with appropriate cDNA and seeded into 384 well plates (Greiner Bio-One, Frickenhausen, Germany) and incubated for 24 h. For the assay test compounds in the range from 10 pM to 1 mM were added to the cells and incubated for 180 min followed by addition of IP1-d2 conjugate and 5 μ L anti-IP1-cryptate-TB conjugate to stop incubation and starting lysis. After further 60 min time resolved fluorescence resonance energy transfer (HTRF) was determined using the CLARIOstar[®] plate reader (BMG, Ortenberg, Germany) (Filter set: donor: 620-10 nm; acceptor: 665-10 nm). Data was analyzed by calculating the ratio of acceptor emission to donor emission. FRET ratio was normalized to the effect of buffer (0%) and the maximum effect of norepinephrine (100%) using GraphPad Prism 6.07 applying the equation for non-linear regression (dose-response curves (four parameters)). Mean values are the result of three to five independent experiments each done in duplicates.

Bioluminescence Resonance Energy Transfer (BRET) assay for recruitment of β -arrestin. For BRET assays microplates were coated with poly-*D*-Lysin (Sigma-Aldrich, Taufkirchen, Germany; MW: 70,000-150,000, 0.1 mg/mL aqueous solution) to improve cell adhesion. HEK-293T cells were transiently transfected with PEI as described above. Determination of receptor mediated β -arrestin recruitment was performed by addition of 1 μ M of test compound to the cells followed by incubation for 90 min. Preincubation was terminated by removing the incubation solution followed by a washing step with HBSS buffer. Buffer containing 10 μ M propranolol was added to block all free binding sites. One half of the wells were kept in the dark, the second half was irradiated at 528 nm for 120 s to enable the switching of the *Z* isomer to the *E* isomer. Incubation was continued for 10 min and 3 μ M of coelenterazine 400a was added for further 5 min. All incubation steps were performed at 37 °C. In parallel, control experiments were conducted with 1 mM of norepinephrine or buffer to derive reference values for normalization. BRET was monitored on a Clariostar plate reader (BMG, Ortenberg, Germany) with the appropriate filter sets (donor 410/80 nm, acceptor 515/30 nm) and was calculated as the ratio of acceptor emission to donor emission. Switching of compound **E-6** to **Z-6** after preincubation was done by irradiating the cells at 365 nm for 30 s. BRET ratio was normalized to the effect of buffer (0%) and the maximum effect of norepinephrine (100%). Mean E_{\max} values are the result of 3-12 independent experiments each done in quadruplicates. Significance of E_{\max} after switching compound **D** from *Z* to *E* and from *E* to *Z* was analyzed by paired t-test in Prism 6. The threshold for significance was set as 99% confidence interval and displayed as p-value ($p < 0.01$).

2.8 Supporting Information

2.8.1 Purity

The purity of all compounds was measured on analytical HPLC at a detection wavelength of 220 nm. Purity was measured either directly after purification or in DMSO.

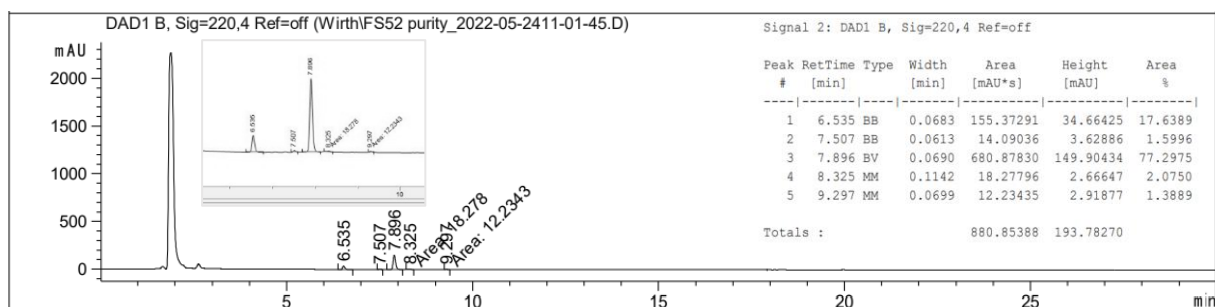


Figure S1. Purity of 1 (95%).

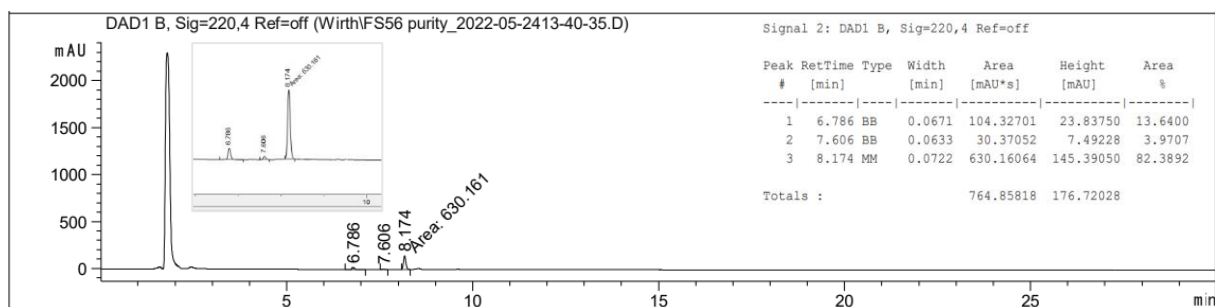


Figure S2. Purity of 2 (96%).

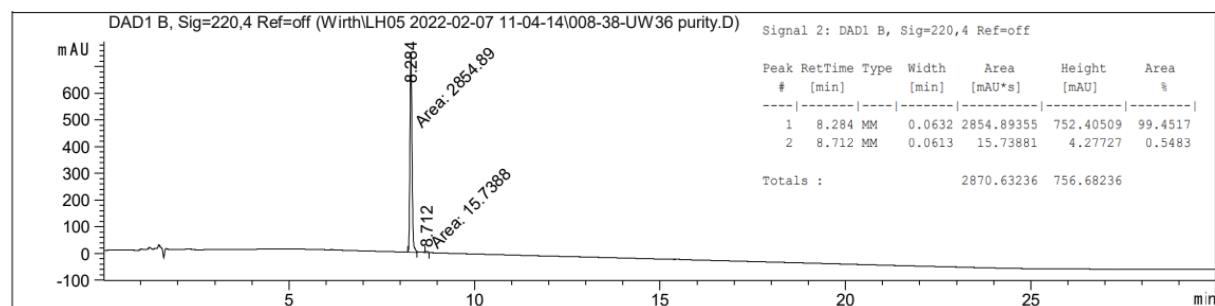


Figure S3. Purity of 3 (99%).

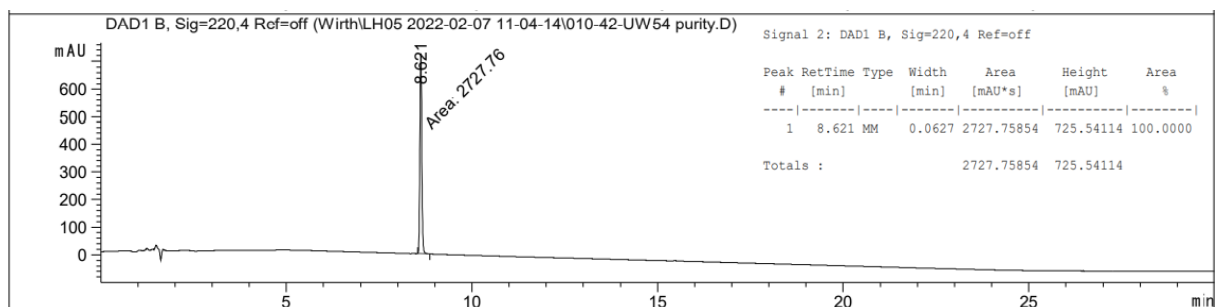


Figure S4. Purity of 4 (>99%).

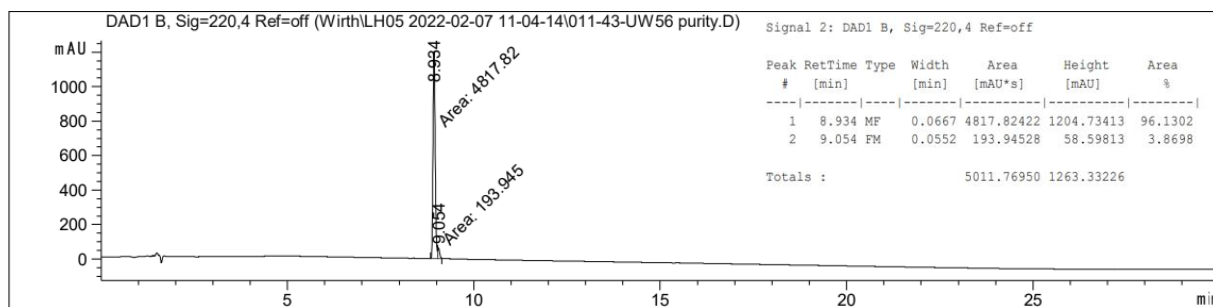


Figure S5. Purity of 5 (96%).

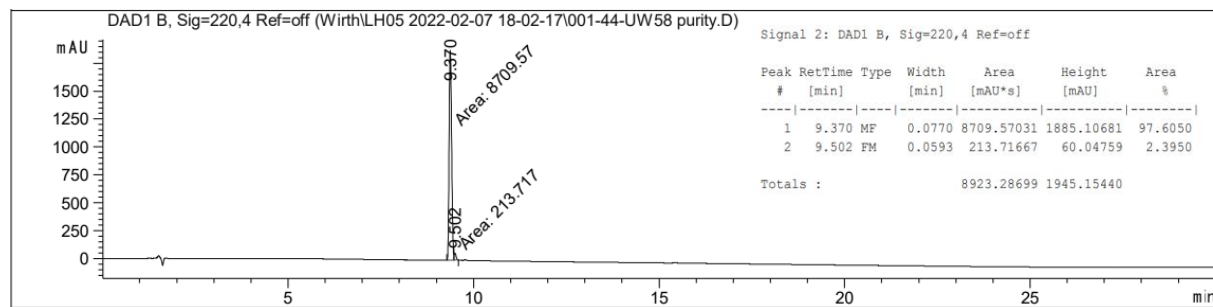


Figure S6. Purity of 6 (98%).

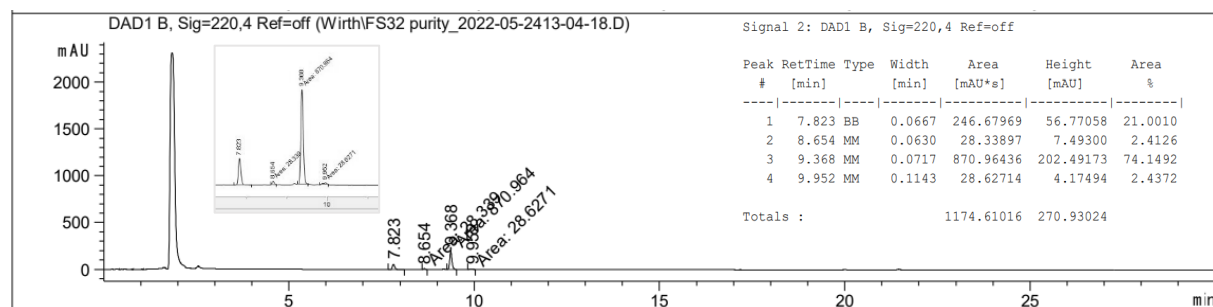


Figure S7. Purity of 7 (95%).

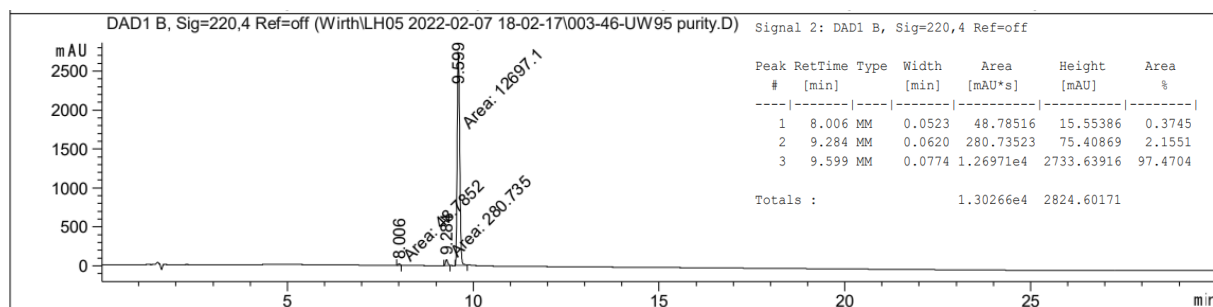


Figure S8. Purity of 8 (97%).

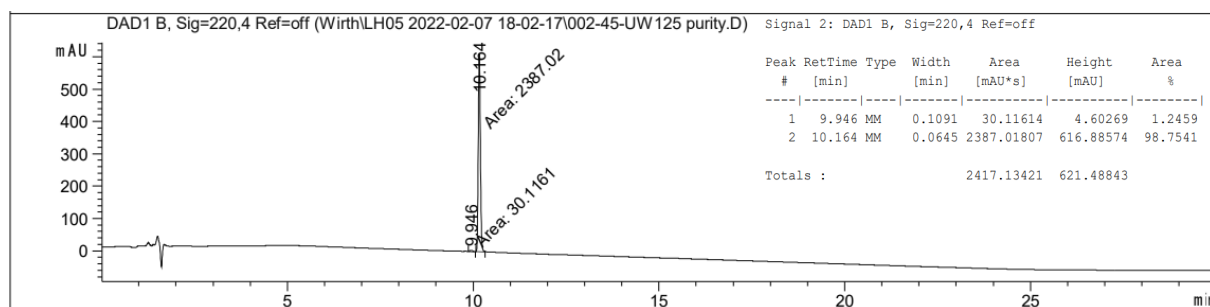


Figure S9. Purity of **9** (99%).

2.8.2 Photophysical Characterization

2.8.2.1 UV/Vis Spectra and Cycle Performance

UV/Vis absorption spectra were measured to characterize the photophysical properties of the synthesized photoswitches. The photoswitches were diluted with TRIS buffer (50 mM Tris, 1 mM EDTA, 1 mM MgCl₂, pH 7.4) to end up with a concentration of 10 μ M + 0.5% DMSO. The spectra were measured in a quartz glass cuvette after different illuminations with LED modules. First, the solution was illuminated with 365 nm light for 10 s to switch to the *Z*-isomer. After measuring the UV/Vis spectrum of the *Z*-isomer (purple curve), the solution was illuminated with 528 nm light for 120 s and the spectrum for the *E*-isomer (black curve) was measured. This cycle was repeated ten times to show the stability and repeatability of switching the compound. The isosbestic points could be determined from an overlay of the UV/Vis spectra of both isomers.

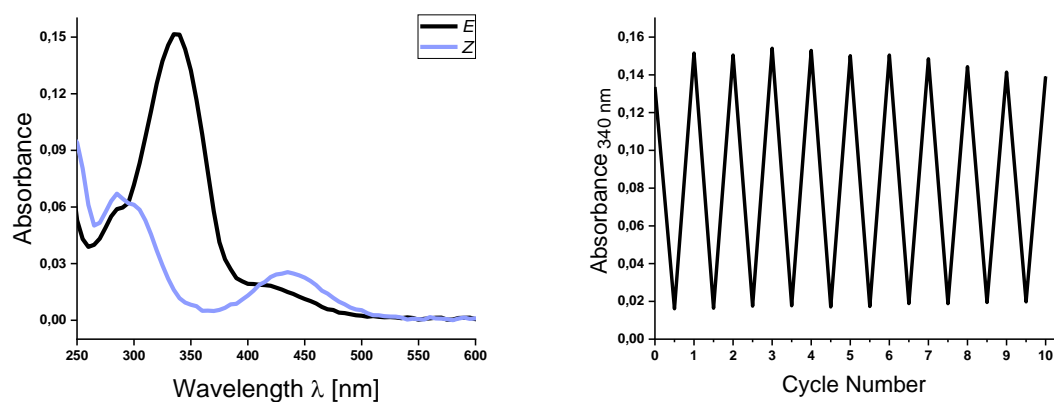


Figure S10. UV/Vis spectrum and cycle performance of **1**.

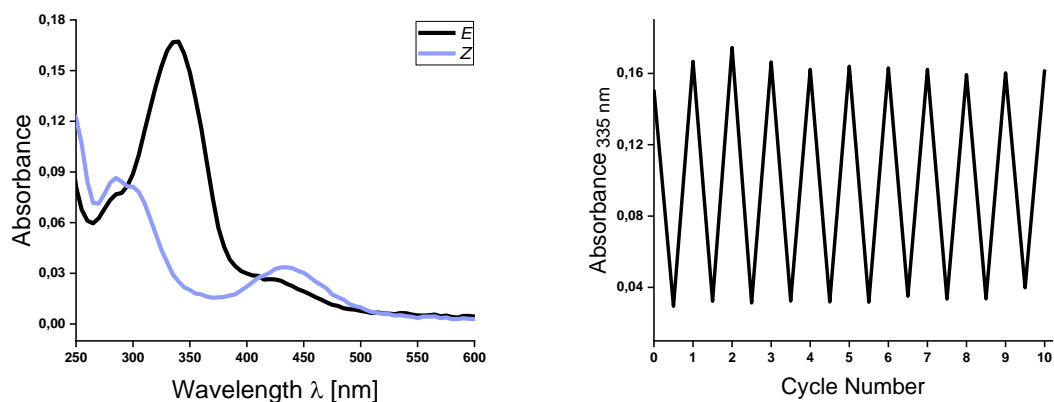


Figure S11. UV/Vis spectrum and cycle performance of 2.

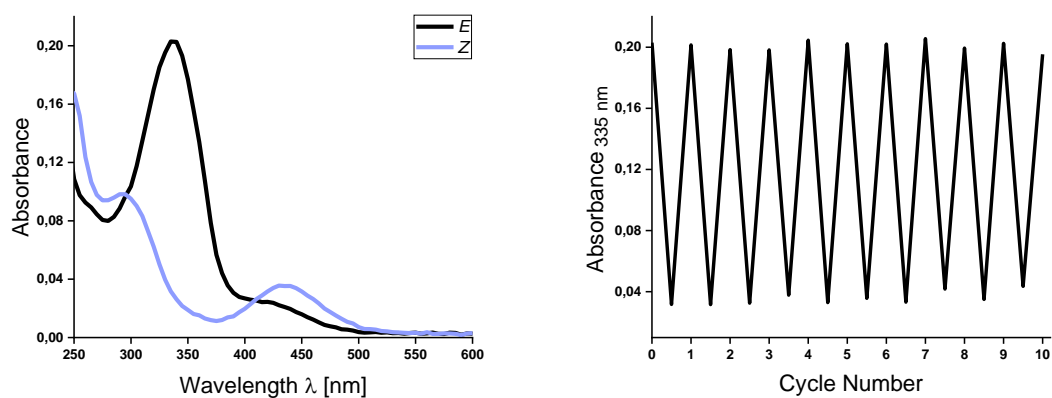


Figure S12. UV/Vis spectrum and cycle performance of 3.

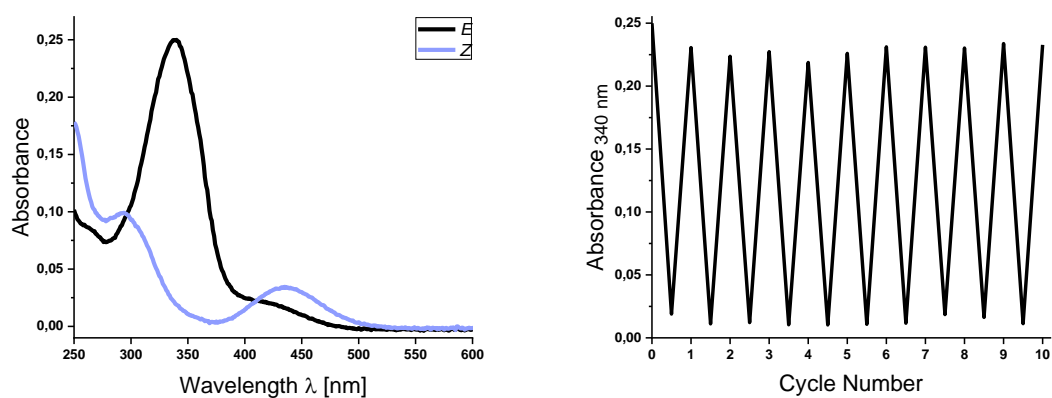


Figure S13. UV/Vis spectrum and cycle performance of 4.

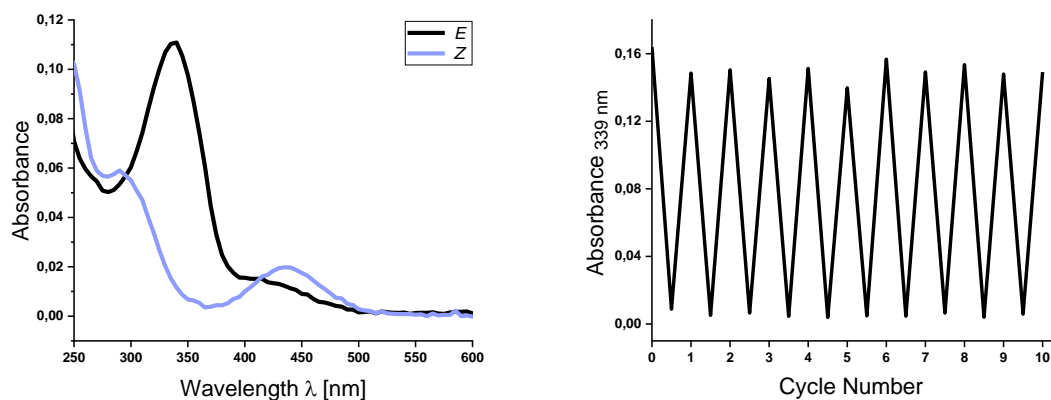


Figure S14. UV/Vis spectrum and cycle performance of 5.

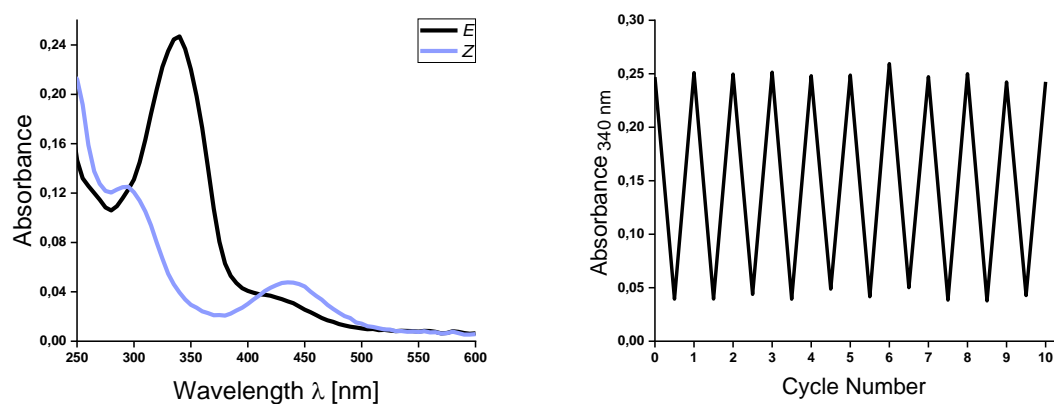


Figure S15. UV/Vis spectrum and cycle performance of 6.

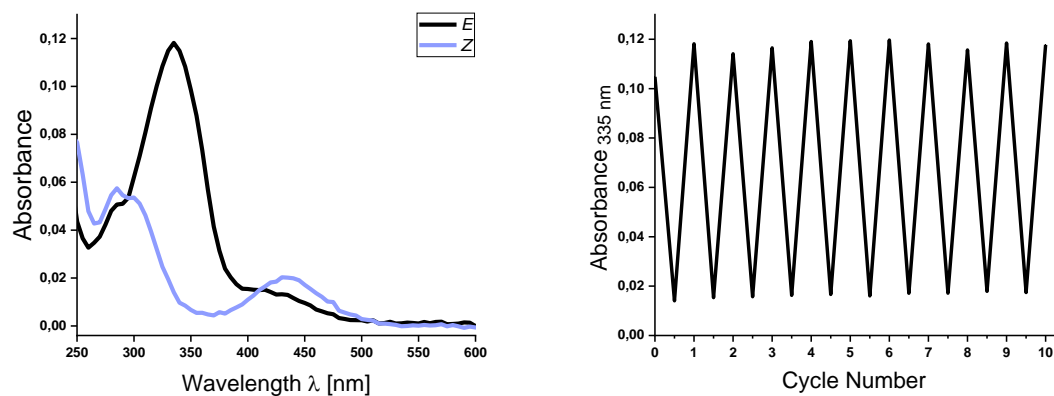


Figure S16. UV/Vis spectrum and cycle performance of 7.

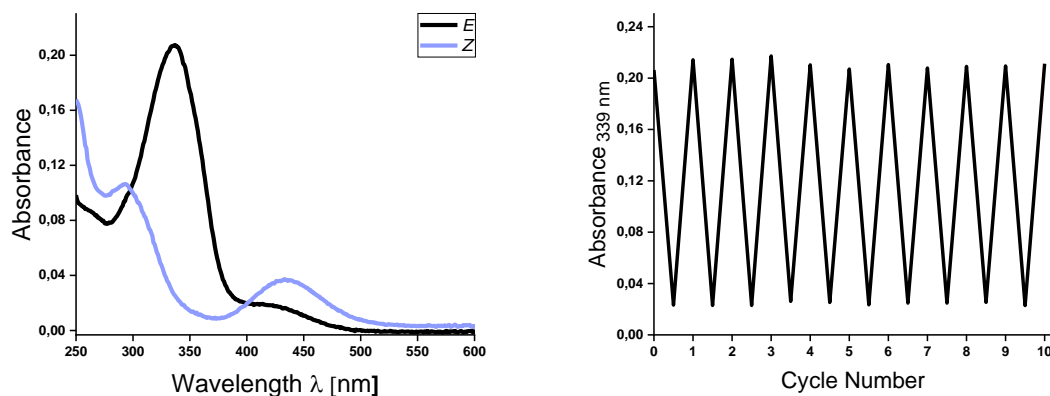


Figure S17. UV/Vis spectrum and cycle performance of **8**.

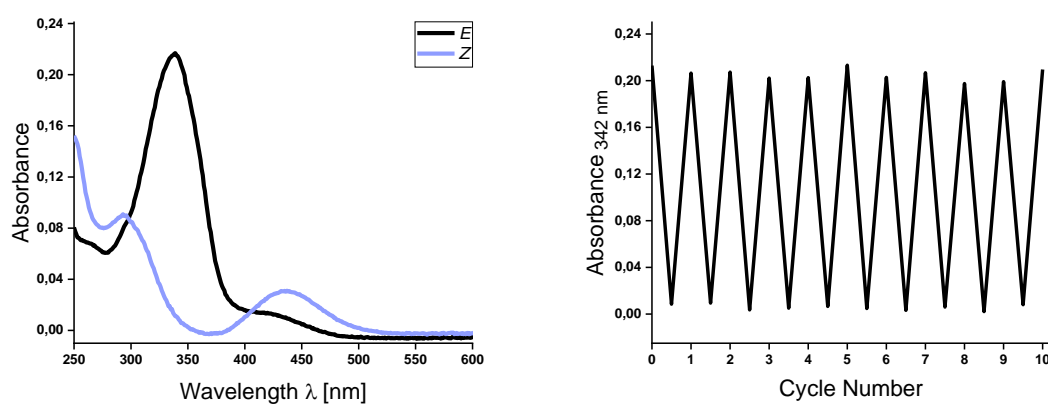


Figure S18. UV/Vis spectrum and cycle performance of **9**.

2.8.2.2 Photostationary States

Photostationary states (PSS) were measured on analytical HPLC. To determine the photostationary state of the photoswitches the samples (0.2 mM in Tris buffer + 2% DMSO) were irradiated first with 365 nm to get the *Z*-isomer (Peak 1). Afterwards, the sample was irradiated with 528 nm to get back to the *E*-isomer (Peak 2). The samples were measured at the isosbestic points.

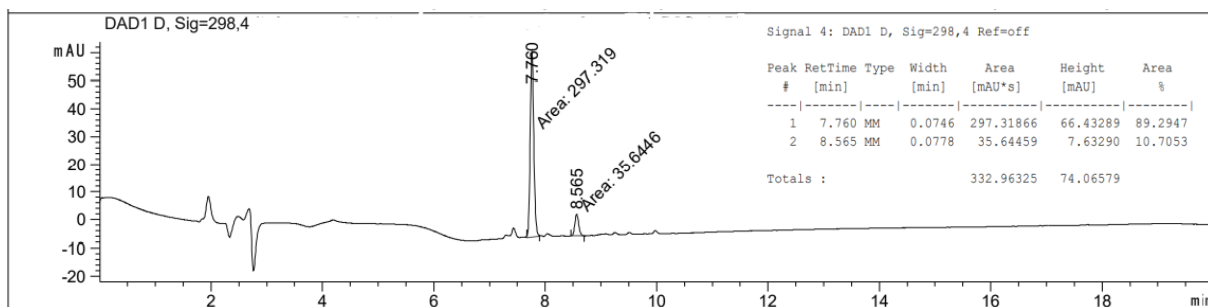


Figure S19. Photostationary state of **1** after irradiation with 365 nm (switching to the *Z*-isomer).

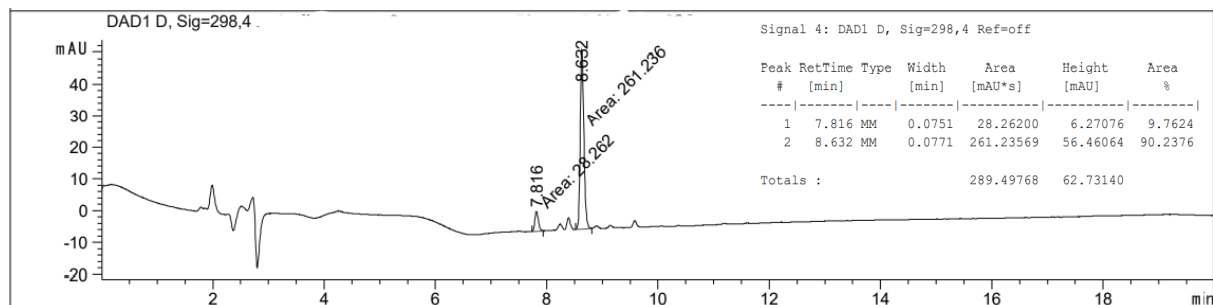


Figure S20. Photostationary state of **1** after irradiation with 528 nm (switching to the *E*-isomer).

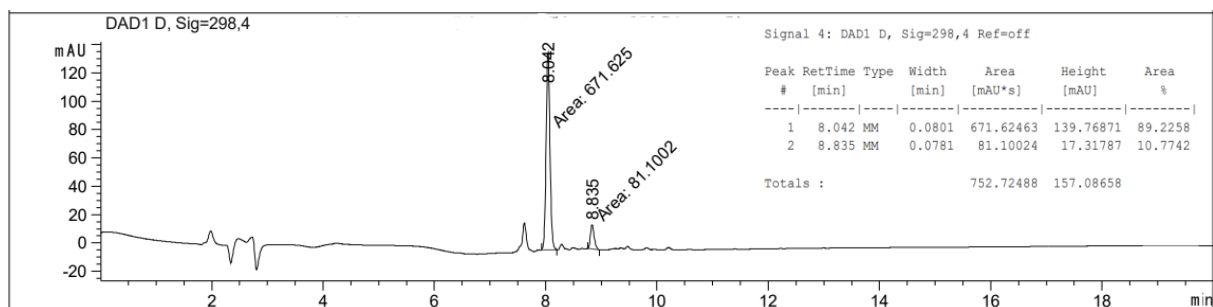


Figure S21. Photostationary state of **2** after irradiation with 365 nm (switching to the *Z*-isomer).

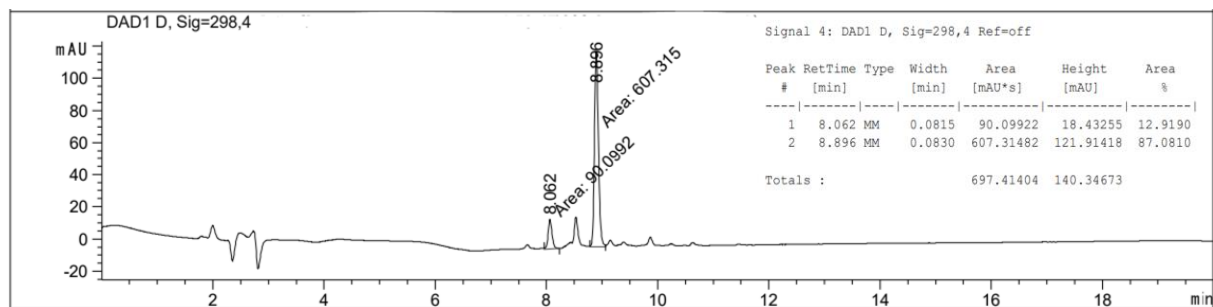


Figure S22. Photostationary state of **2** after irradiation with 528 nm (switching to the *E*-isomer).

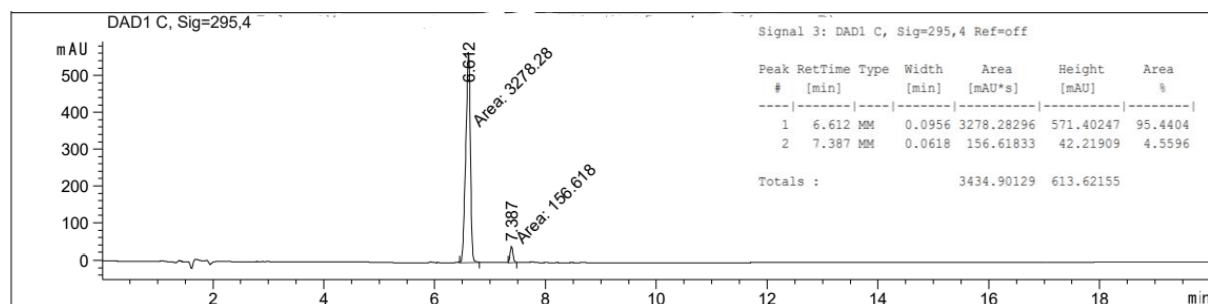


Figure S23. Photostationary state of **3** after irradiation with 365 nm (switching to the *Z*-isomer).

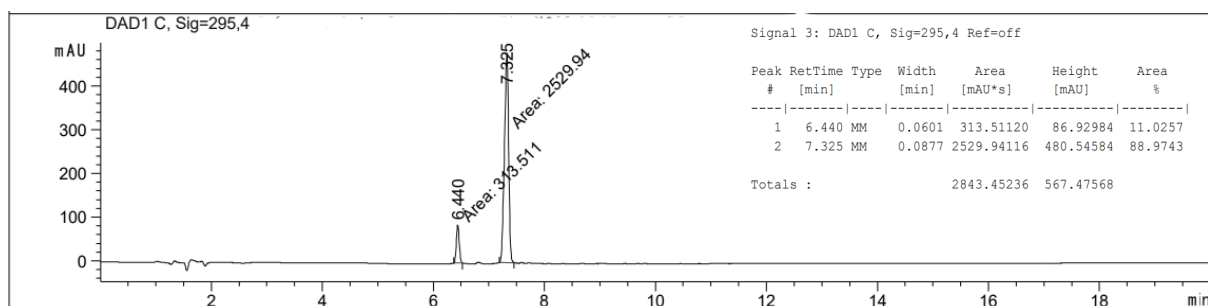


Figure S24. Photostationary state of **3** after irradiation with 528 nm (switching to the *E*-isomer).

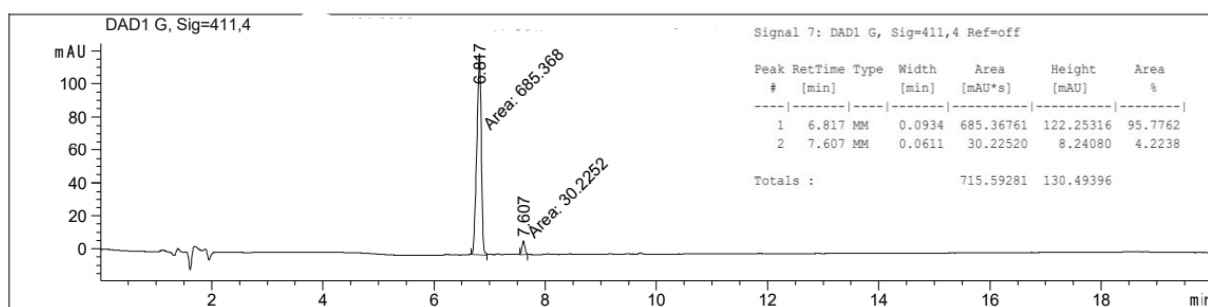


Figure S25. Photostationary state of **4** after irradiation with 365 nm (switching to the *Z*-isomer).

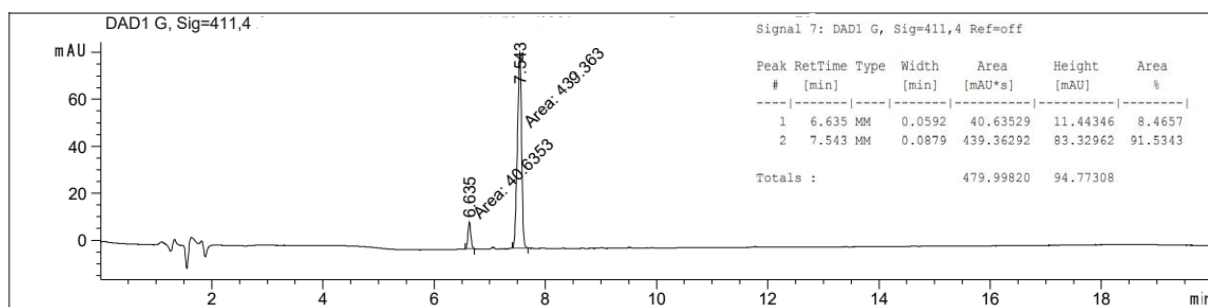


Figure S26. Photostationary state of **4** after irradiation with 528 nm (switching to the *E*-isomer).

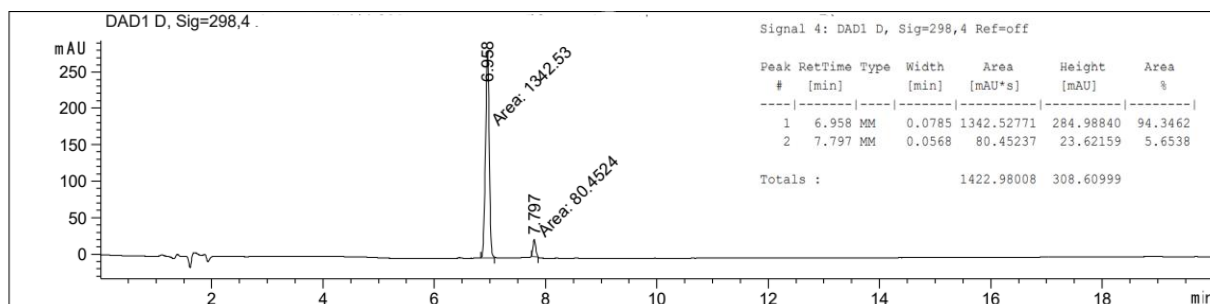


Figure S27. Photostationary state of **5** after irradiation with 365 nm (switching to the *Z*-isomer).

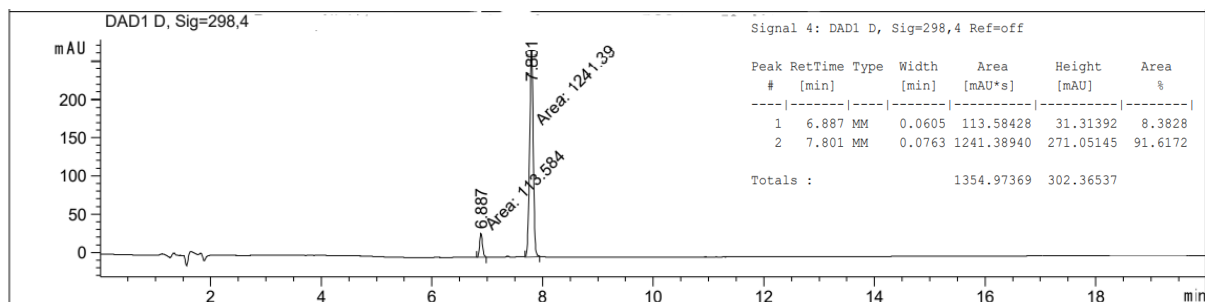


Figure S28. Photostationary state of **5** after irradiation with 528 nm (switching to the *E*-isomer).

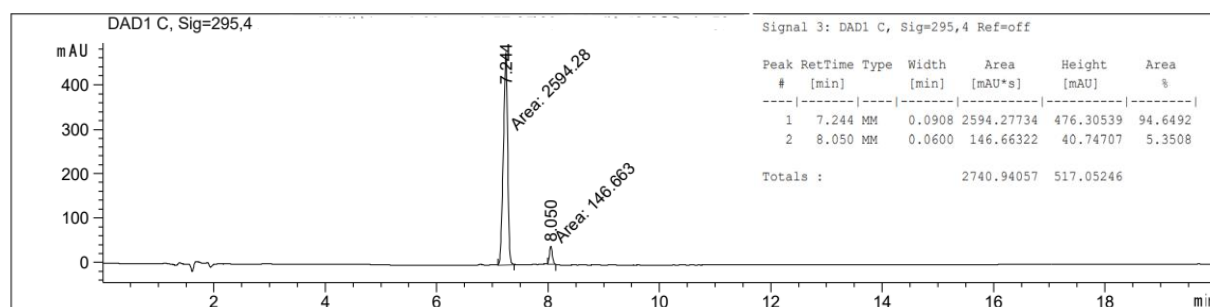


Figure S29. Photostationary state of **6** after irradiation with 365 nm (switching to the *Z*-isomer).

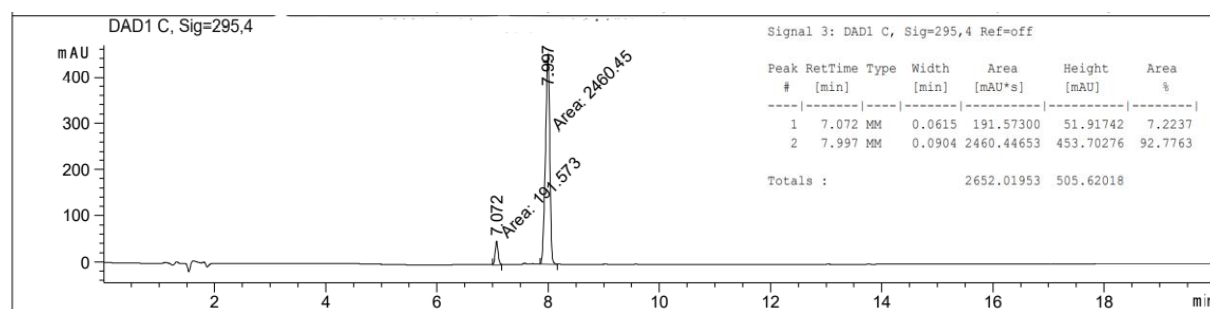


Figure S30. Photostationary state of **6** after irradiation with 528 nm (switching to the *E*-isomer).

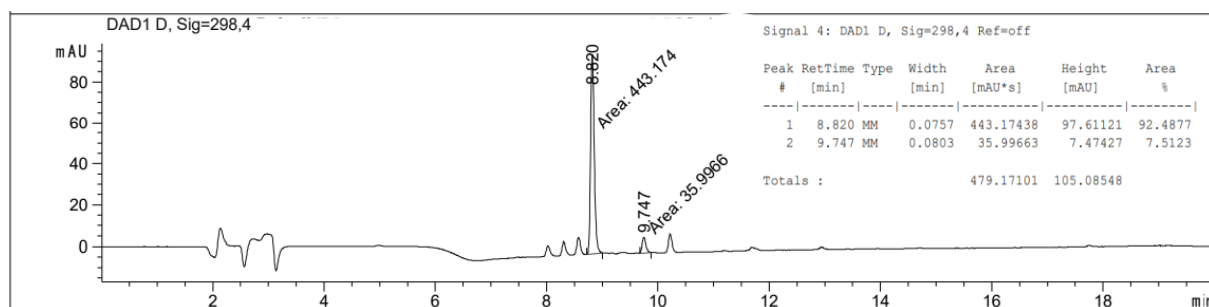


Figure S31. Photostationary state of **7** after irradiation with 365 nm (switching to the *Z*-isomer).

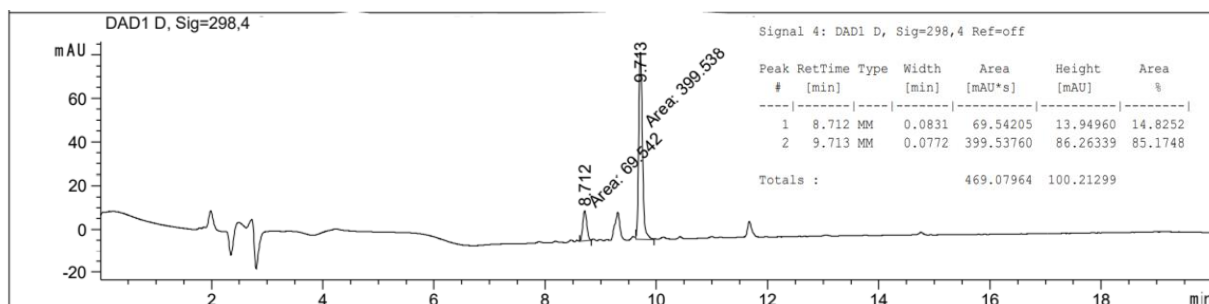


Figure S32. Photostationary state of **7** after irradiation with 528 nm (switching to the *E*-isomer).

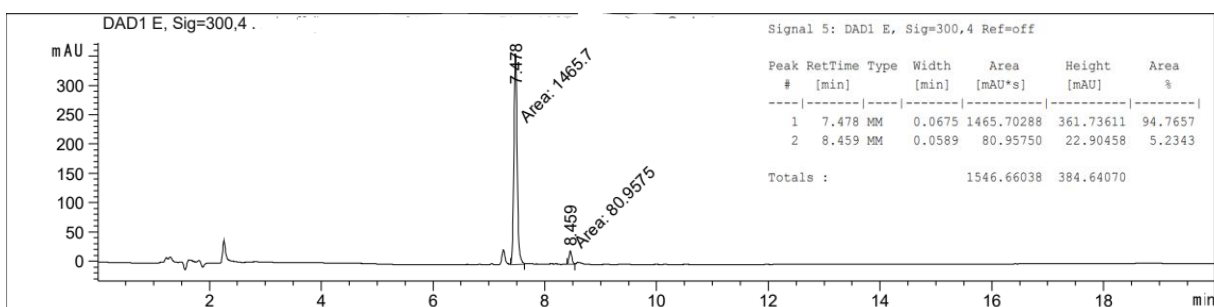


Figure S33. Photostationary state of **8** after irradiation with 365 nm (switching to the *Z*-isomer).

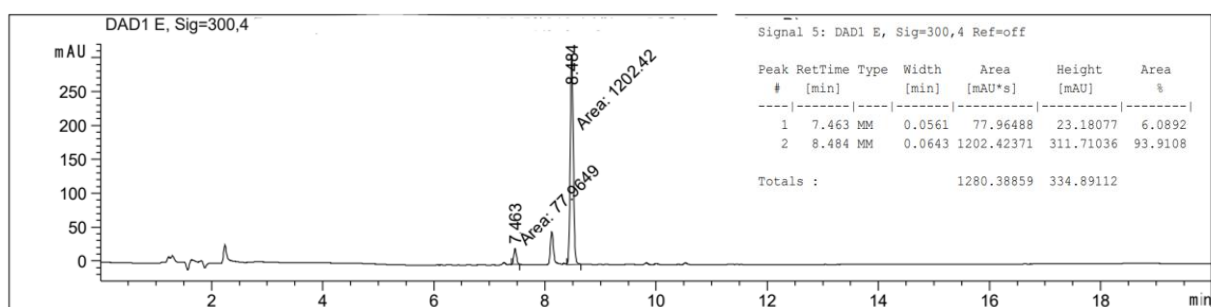


Figure S34. Photostationary state of **8** after irradiation with 528 nm (switching to the *E*-isomer).

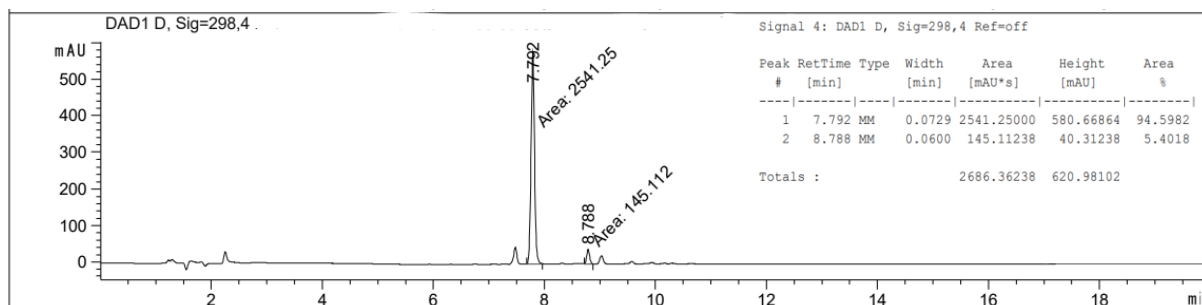


Figure S35. Photostationary state of **9** after irradiation with 365 nm (switching to the *Z*-isomer).

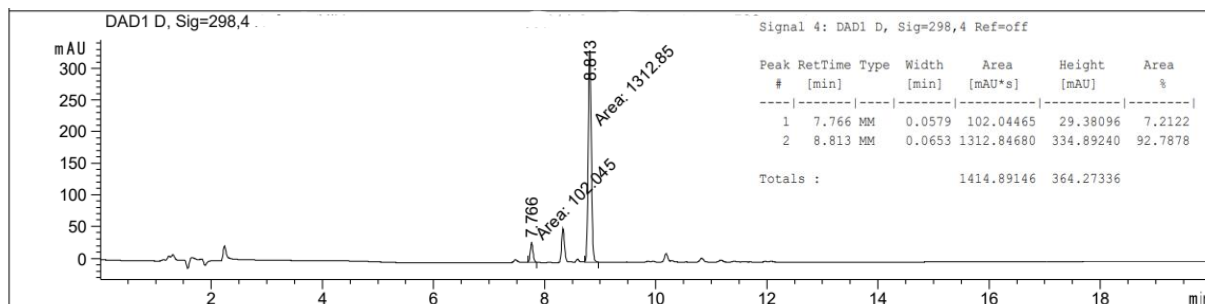
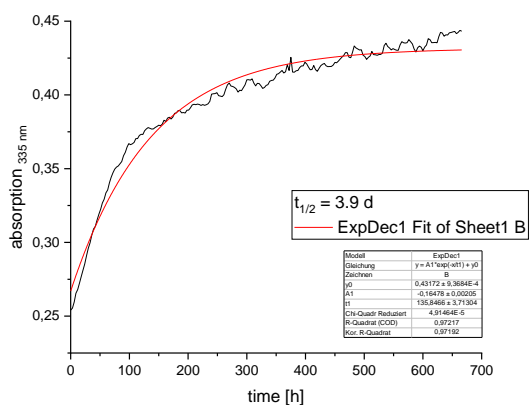


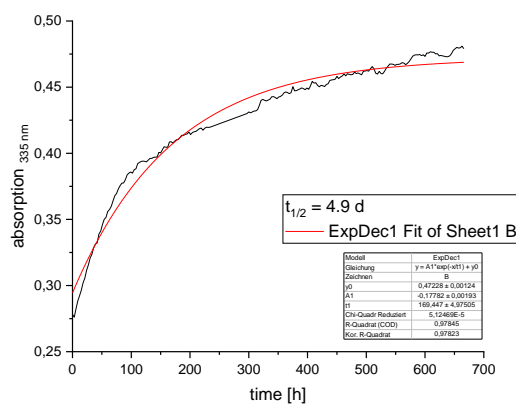
Figure S36. Photostationary state of **9** after irradiation with 528 nm (switching to the *E*-isomer).

2.8.2.3 Thermal Half-lives

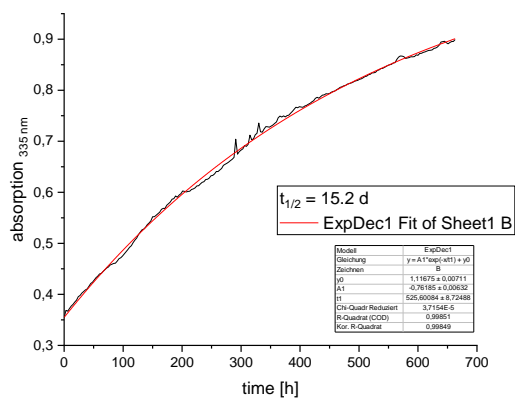
For the determination of the thermal stability of the metastable *Z* isomer a 50 μ M solution in Tris buffer + 0.5% DMSO was irradiated with 365 nm. For 4 weeks the absorption at 335 nm was measured every 3 h.



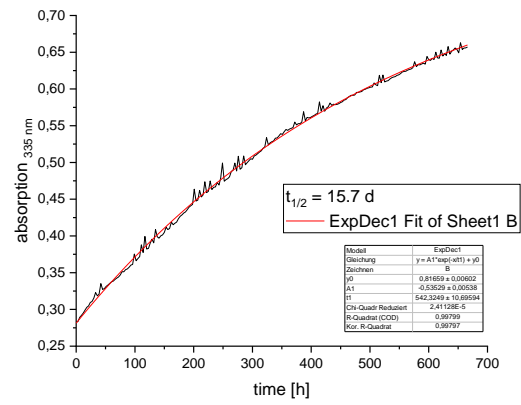
1



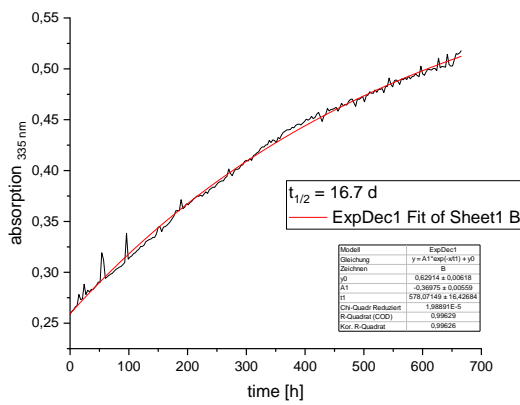
2



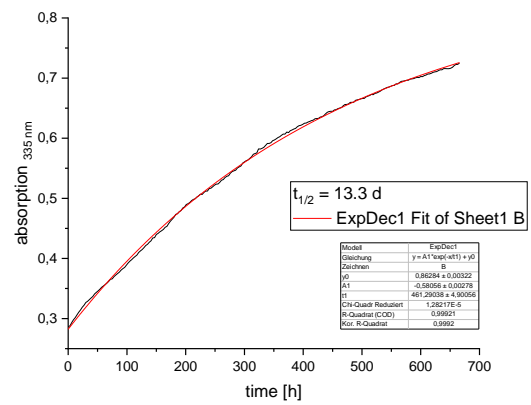
3



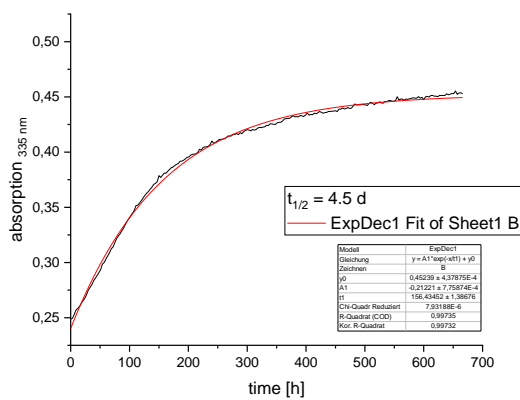
4



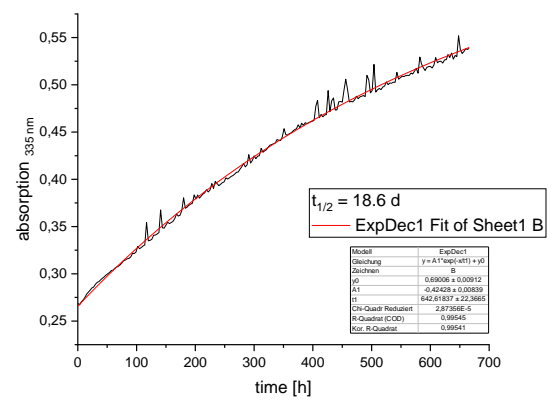
5



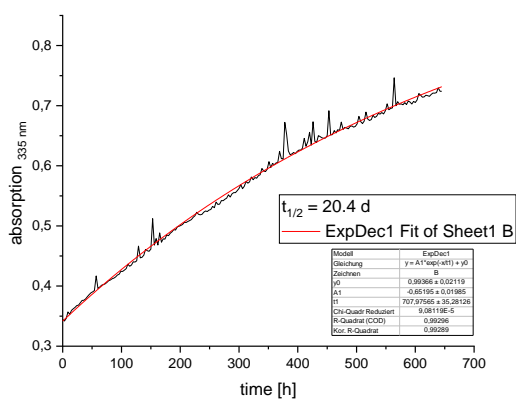
6



7



8



9

Figure S37. Thermal half-lives of compounds 1-9.

2.8.3 Supplementary Information to Biological Investigation

IP-One Assay on Functional Activity of the Photoswitches 1-9 at the β_2 adrenoceptor.

Functional activity of the photoswitches 1-9 were determined in the *E* and *Z* form applying an IP accumulation assay. HEK 293T cells were transiently co-transfected with the plasmids of the human β_2 adrenergic receptor and the hybrid G protein $G\alpha_{qs}$. Dose-response curves revealed intrinsic activity for all compounds in the range from 78-108% (Figure S38, Table S1). The BI-167107 derivatives 3-6, 8, 9 showed potencies in the range of $EC_{50} = 5.2$ nM (*Z*-3) to $EC_{50} = 79$ nM (*E*-5), while for the catechol derivatives 1, 2, 7 dose-response correlations resulted in potencies of $EC_{50} = 0.48$ μ M (*Z*-1) to $EC_{50} = 4.3$ μ M (*Z*-7).

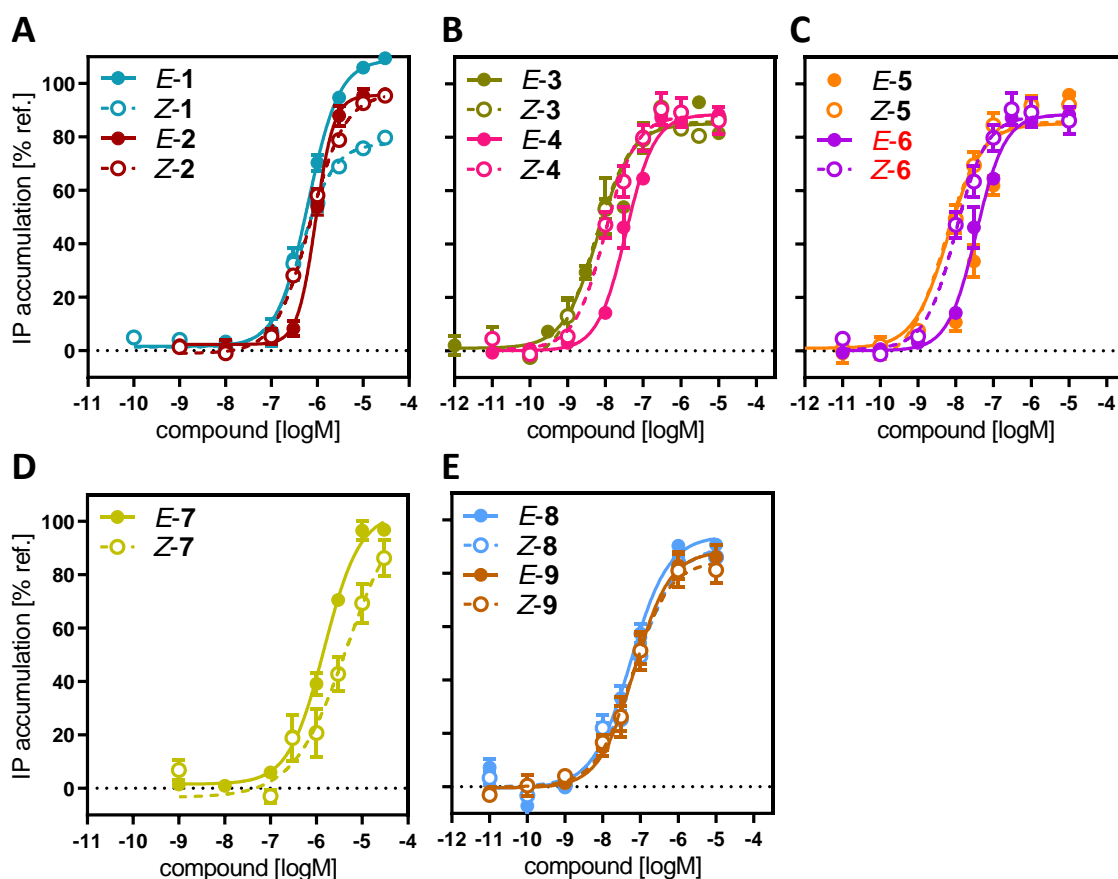


Figure S38. Functional activity of the photoswitches **1-9** at the β_2 receptor applying an IP-One assay. **(A)** Dose-response curves for the *E* and *Z* isomer of the catechol derivatives **1** and **2** revealed submicromolar potencies and intrinsic activities in the range from 78-108% relative to norepinephrine (NorEpi). Activation curves for the BI-167107 disulfide derivatives **(B)** **3** (with a two carbon linker), **4** (three carbon linker), **(C)** **5** (four carbon linker), and **6** (five carbon linker) show high potencies from 5.2 to 79 nM. Receptor activation curves for **(D)** the maleimide bearing catechol **7** and **(E)** the BI-167107 analogs **8**, **9**. Data represent mean \pm SEM from 3-5 independent experiments each conducted in duplicate.

Table S1. Functional properties of the photoswitches **1-9** at the wild type receptor β_2 AR.

compound	<i>E</i> isomer		<i>Z</i> isomer	
	EC ₅₀ [nM ± SEM] ^a	E _{max} [% ± SEM] ^b	EC ₅₀ [nM ± SEM] ^c	E _{max} [% ± SEM] ^b
1	630 ± 72	108 ± 3	480 ± 110	78 ± 0.5
2	940 ± 34	96 ± 2	700 ± 35	97 ± 1
3	7.2 ± 3.0	85 ± 2	5.2 ± 1.7	86 ± 0.2
4	39 ± 7.0	88 ± 3	9.8 ± 0.9	87 ± 5
5	79 ± 25	98 ± 1	9.9 ± 1.7	93 ± 4
7	1500 ± 78	103 ± 4	4300 ± 1300	101 ± 10
8	40 ± 16	97 ± 3	75 ± 2.3	90 ± 2
9	72 ± 12	88 ± 5	57 ± 8.5	85 ± 5

^a Potencies derived from 3 to 4 independent experiments each done in duplicates. ^b Maximum efficacy determined relative to the reference norepinephrine. ^c Potencies derived from 3 to 5 independent experiments each done in duplicates.

To evaluate the activation properties of the β_2 AR mutant β_2 K97^{2.68}C compared to the wild-type receptor an IP accumulation assay was performed applying the reference agonists norepinephrine and epinephrine. Norepinephrine showed an EC₅₀ of 3200 nM for the mutant. This was in the same range as an EC₅₀ of 1100 nM, which was determined for the wild-type receptor. Similar correlations could be observed for epinephrine revealing an EC₅₀ = 240 nM and an E_{max} = 109% for the mutant and an EC₅₀ = 190 nM and an E_{max} = 103% for the wild-type β_2 AR (Figure S39, Table S2).

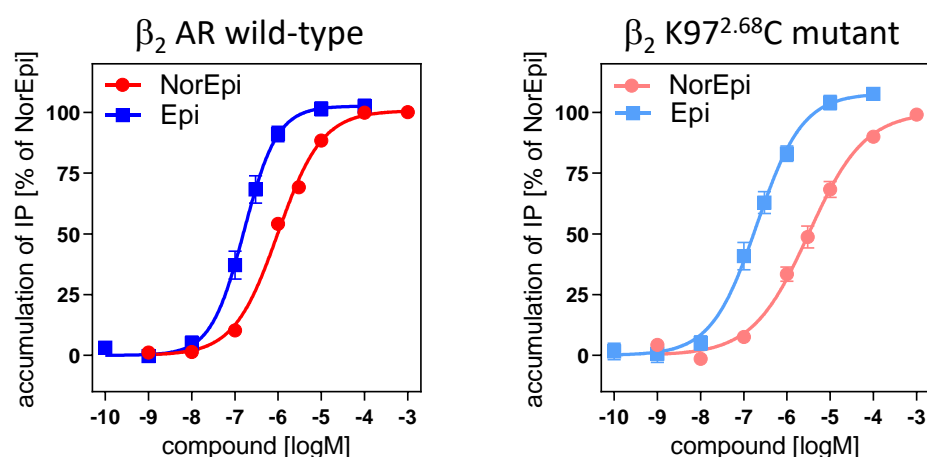


Figure S39. Evaluation of receptor activation for norepinephrine and epinephrine at the β_2 wt and the mutant β_2 K97^{2.68}C. An IP accumulation assay in HEK293T cells transiently transfected with β_2 wt or β_2 K97^{2.68}C and the hybrid G-protein $G\alpha_{qs}$ was conducted to get dose-response curves as mean from 10-14 individual experiments with β_2 wt and 5-6 single experiments with the mutant β_2 K97^{2.68}C.

Table S2. Functional properties of the reference compounds norepinephrine and epinephrine at the wild-type and the mutant β_2 AR.

compound	β_2 AR wild-type		β_2 AR K97 ^{2.68} C	
	EC ₅₀ [nM \pm SEM] ^a	E _{max} [%] ^b	EC ₅₀ [nM \pm SEM] ^c	E _{max} [%] ^b
norepinephrine	1100 \pm 109	100	3200 \pm 520	100
epinephrine	190 \pm 34	103 \pm 2	240 \pm 58	109 \pm 3

^a Potencies derived from 10 to 14 independent experiments each done in duplicates. ^b Maximum efficacy determined relative to the reference norepinephrine. ^c Potencies derived from 5 to 6 independent experiments each done in duplicates.

Determination of Receptor Activation after Covalent Binding and Photoswitching

Applying an Arrestin Recruitment Assay. Covalent binding to the receptor and subsequent switching of the bound isomer within the orthosteric binding site was determined with a bioluminescence resonance energy transfer (BRET) based biosensor system applying the enhanced bystander biosensor CAAX and the β_2 AR mutant K97^{2.68}C in HEK293T cells. To facilitate covalent binding, 1 μ M of the *Z* isomers of **1-9** was preincubated with the cells before washing and blocking any free receptor binding site. To measure the effect of the formed *E* isomer cells were irradiated with light of 528 nm. Determination of the resulting β -arrestin recruitment showed activation profiles with E_{max} values in the range of 2-52% relative to norepinephrine indicating a certain amount of irreversible occupation and subsequent activation of the receptor (Figure S40). The catechol derivatives **1**, **2**, **7** showed only moderate E_{max} values (2-19%). Greatest receptor activation was observed for the four-carbon linker-substituted disulfide **5** (E_{max} = 52%) and its five-carbon analog **6** (E_{max} = 51%). Comparison of the *Z* isomers and their corresponding *E* isomers, which have been formed after irradiation, yielded in compound **6** showing intrinsic effects with the greatest difference in E_{max} between *Z* and *E* (51% for **Z-6** and 38% for **E-6**).

β -arrestin recruitment after covalent binding and photoswitching at β_2 K97^{2.68}C

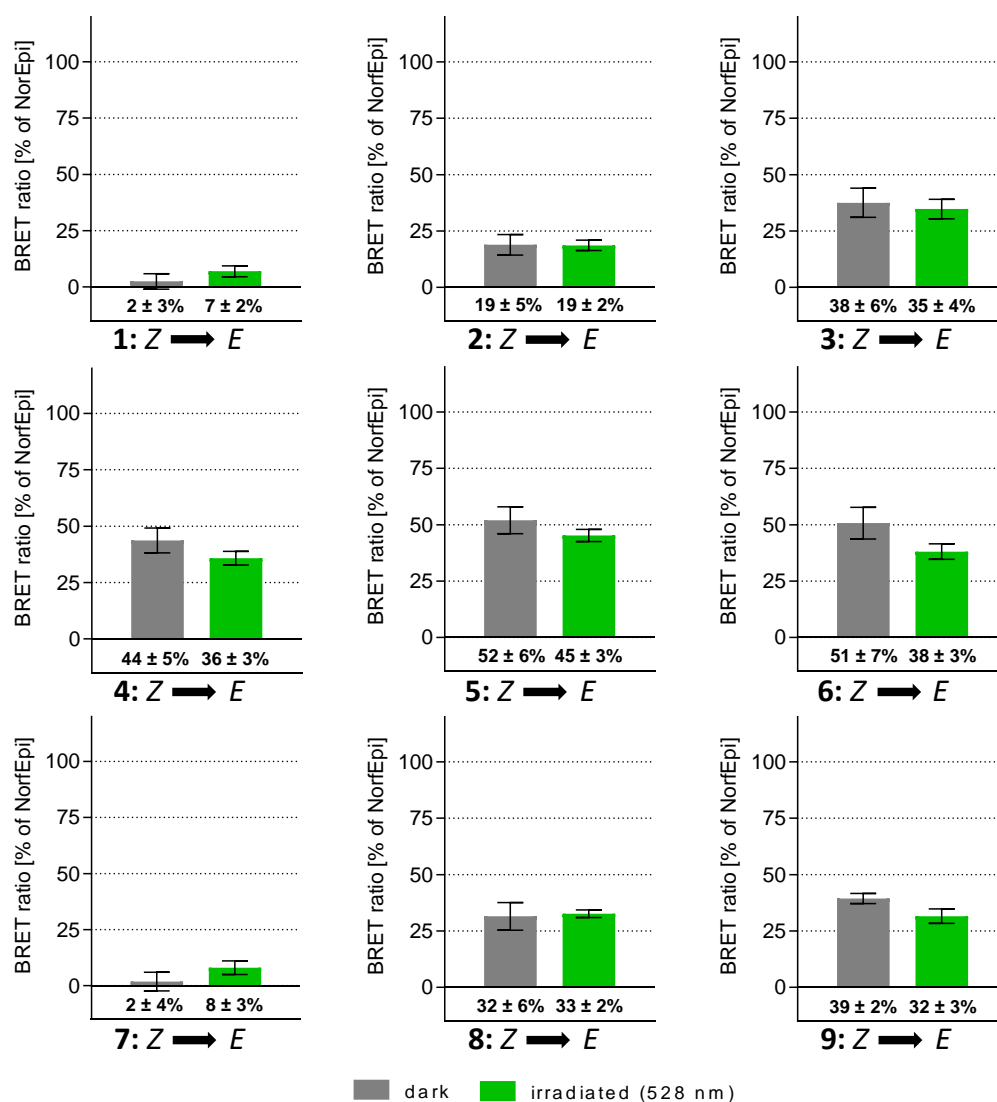
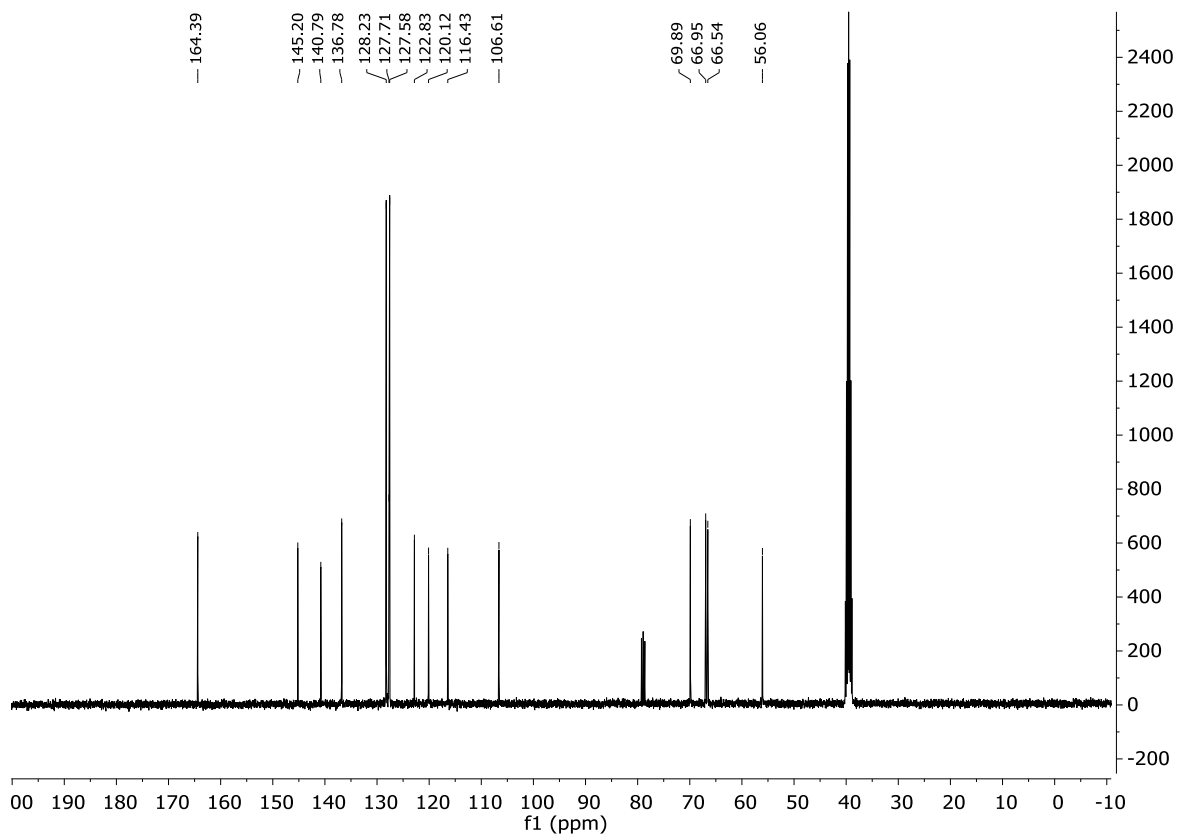
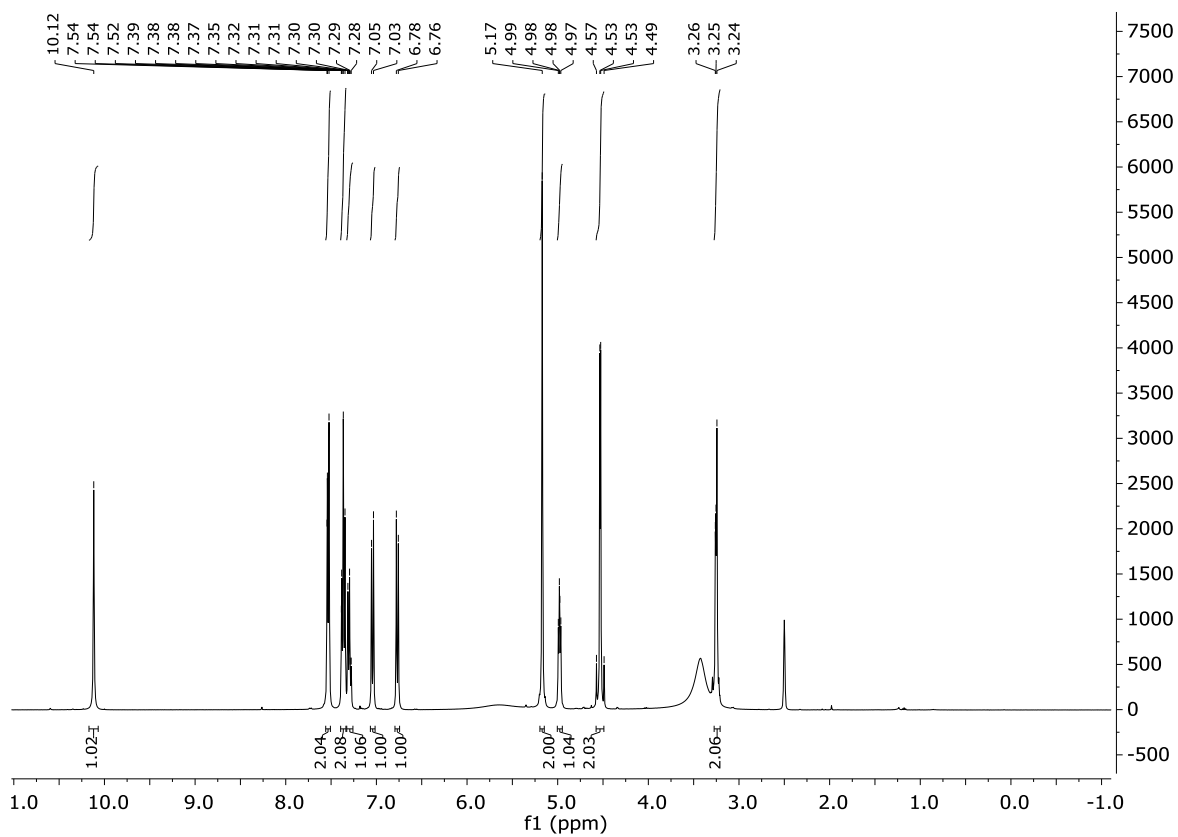


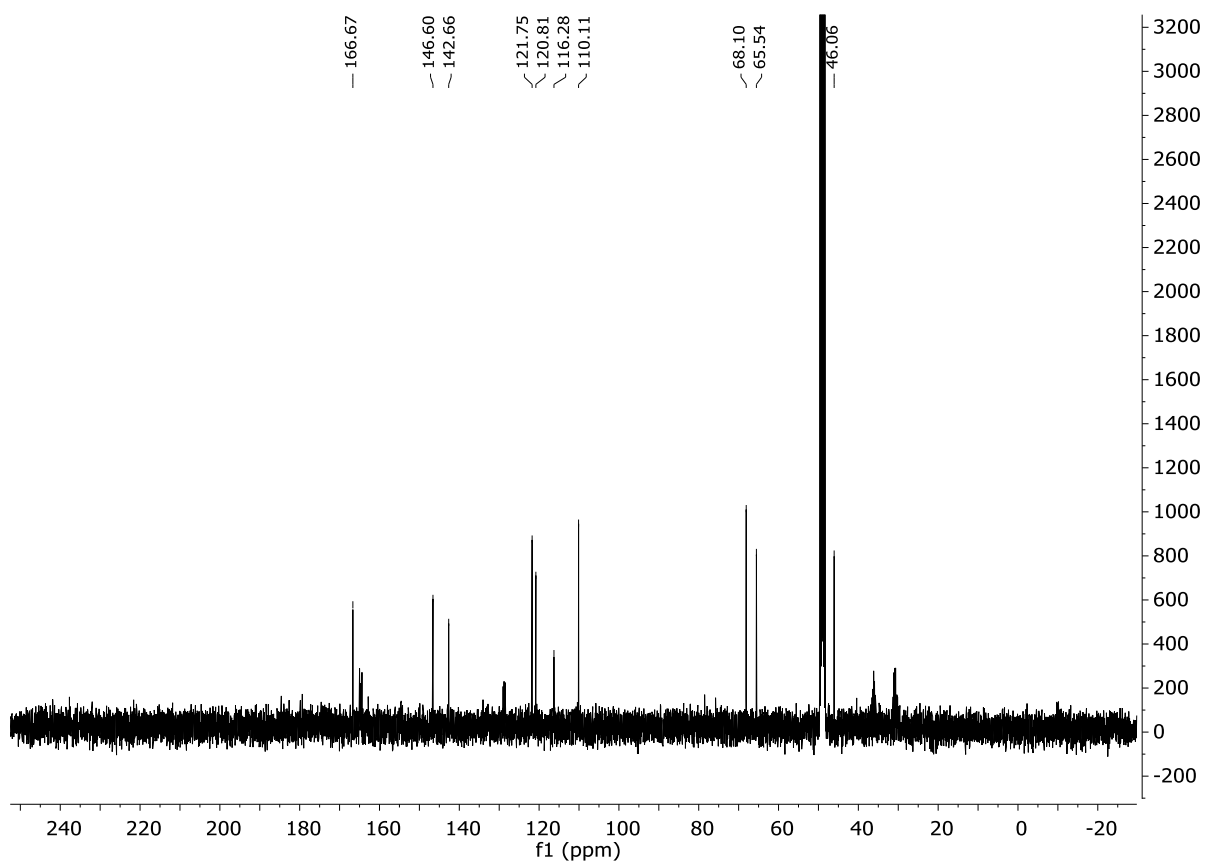
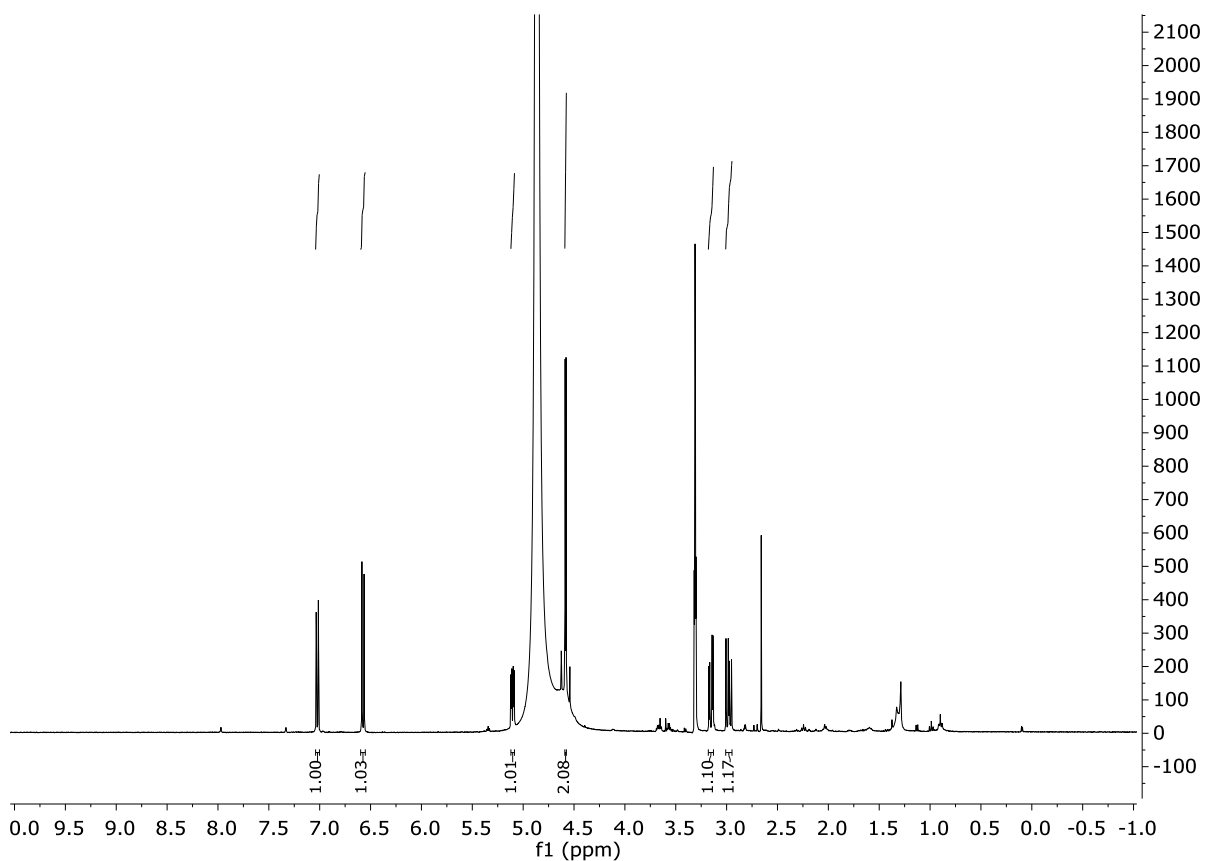
Figure S40. Intrinsic activity for the test compounds after covalent binding at the β_2 AR K97^{2.68}C mutant and irradiation with light of 528 nm. A β -arrestin recruitment assay based on the BRET enhanced bystander biosensor CAAX and the β_2 AR mutant K97^{2.68}C in HEK293T cells was performed for preincubation with 1 μ M of the Z isomers of 1-9. After washing and blocking of any free receptor binding site arrestin recruitment was measured after 15 min to get the maximum efficacy for each Z isomer (gray bars). Irradiation of cells after washing with light of 528 nm and subsequent incubation revealed maximum intrinsic activity for the corresponding E isomer (green bars). Data represent mean values \pm SEM and are derived from 3-8 independent experiments each conducted in quadruplicates.

2.8.4 NMR Spectra

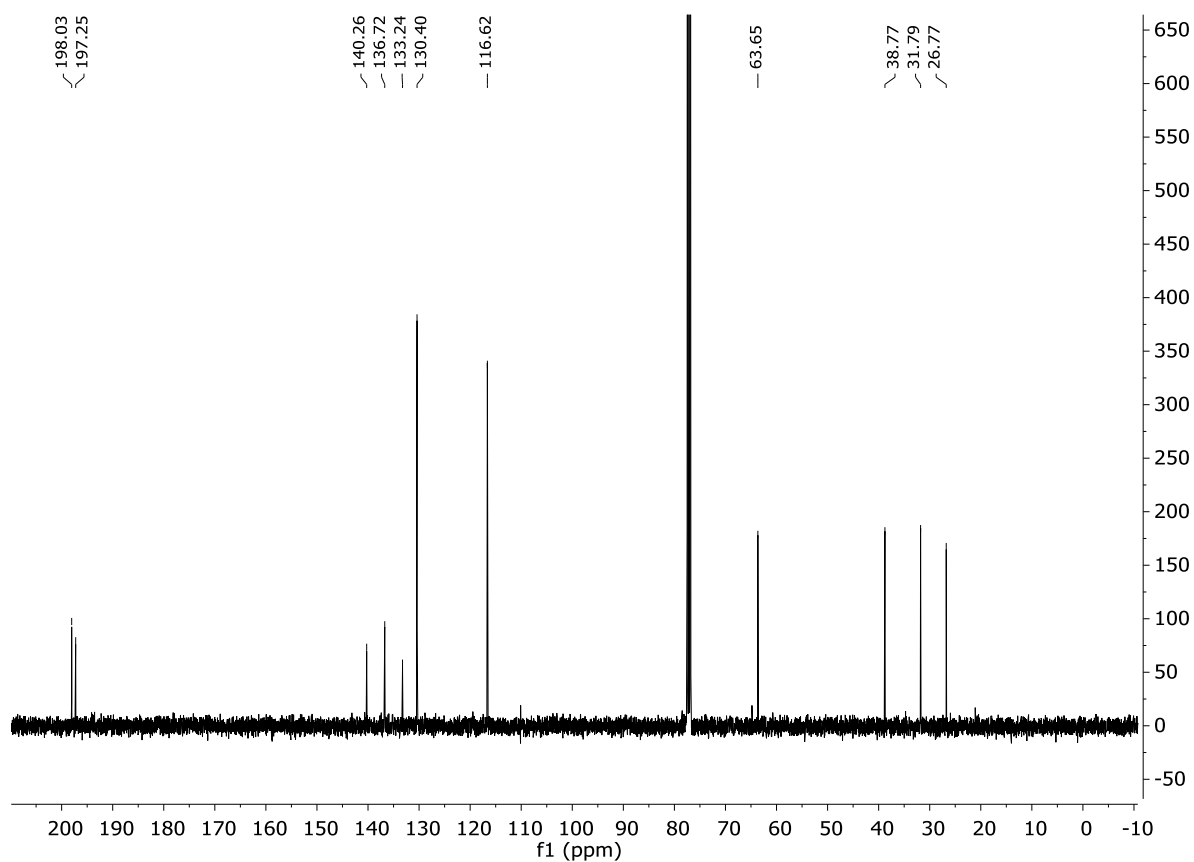
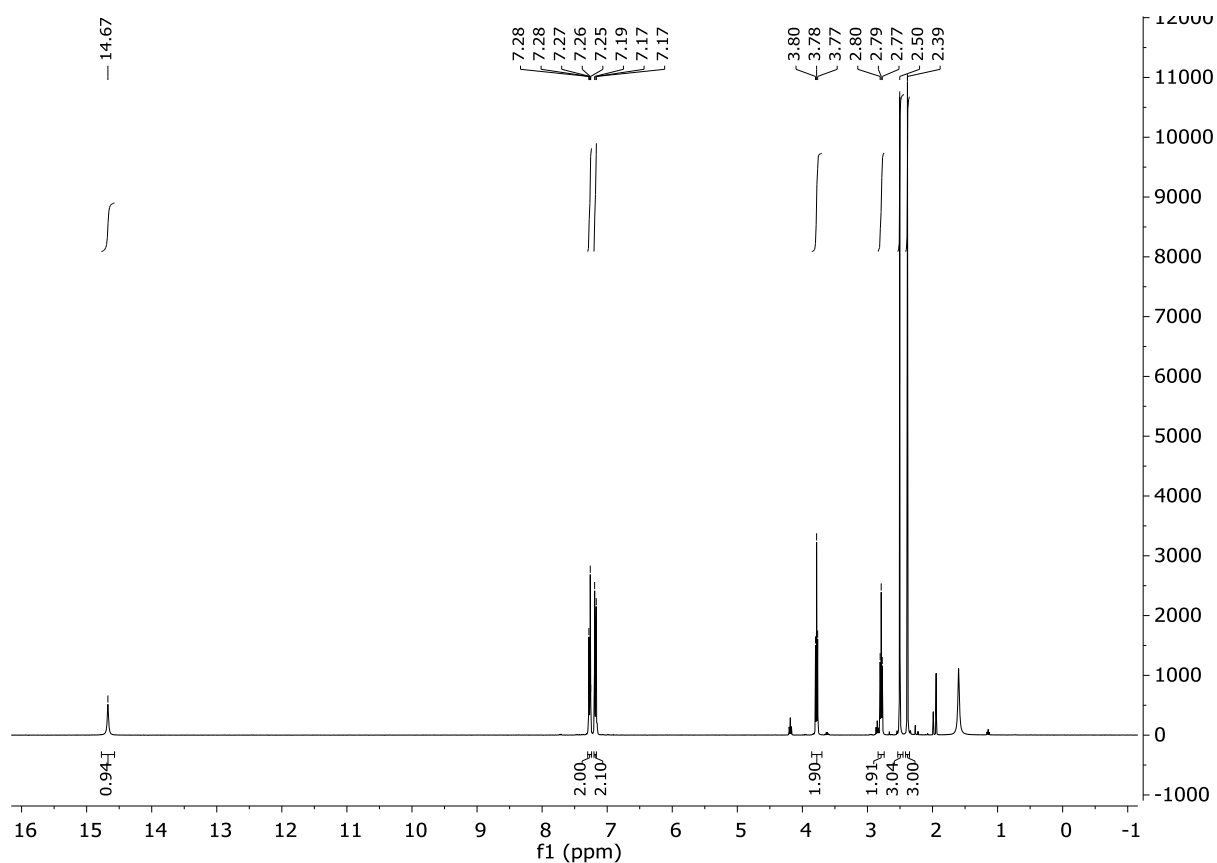
Compound 17



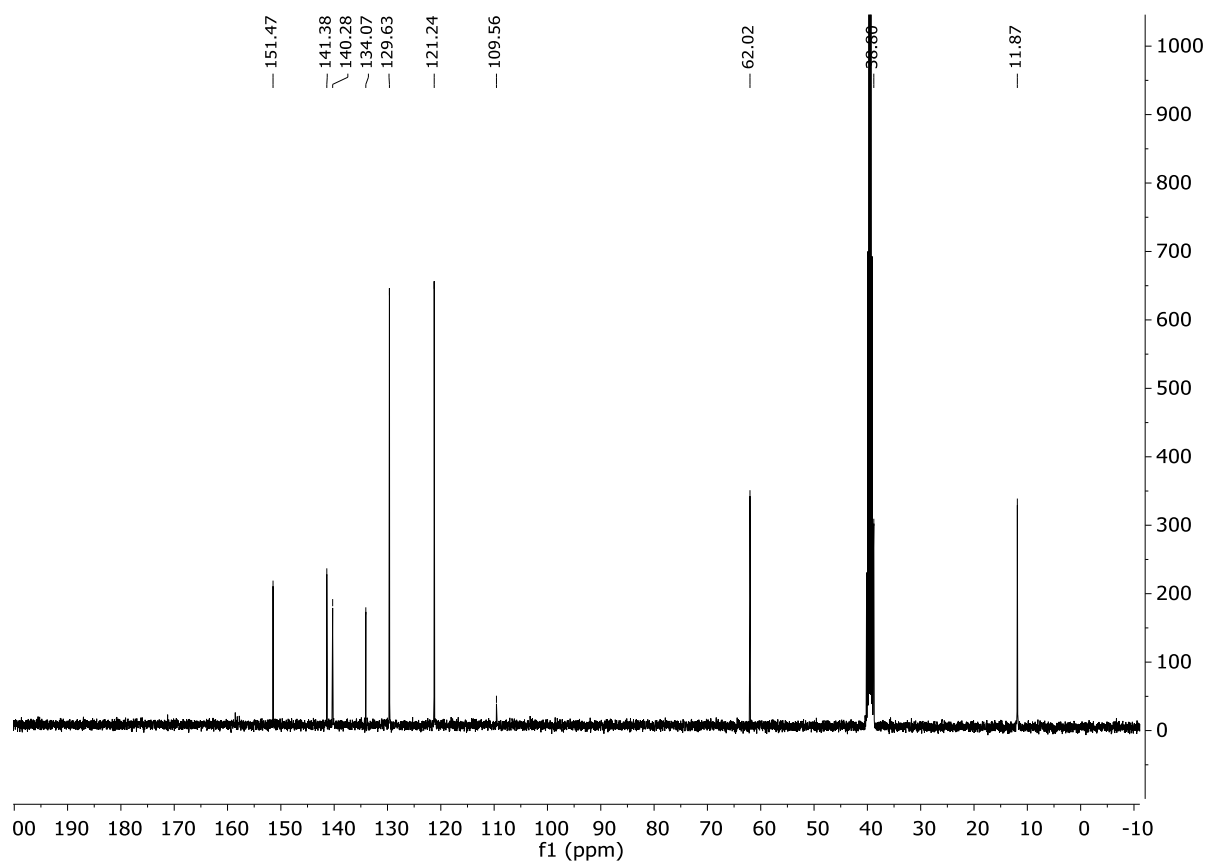
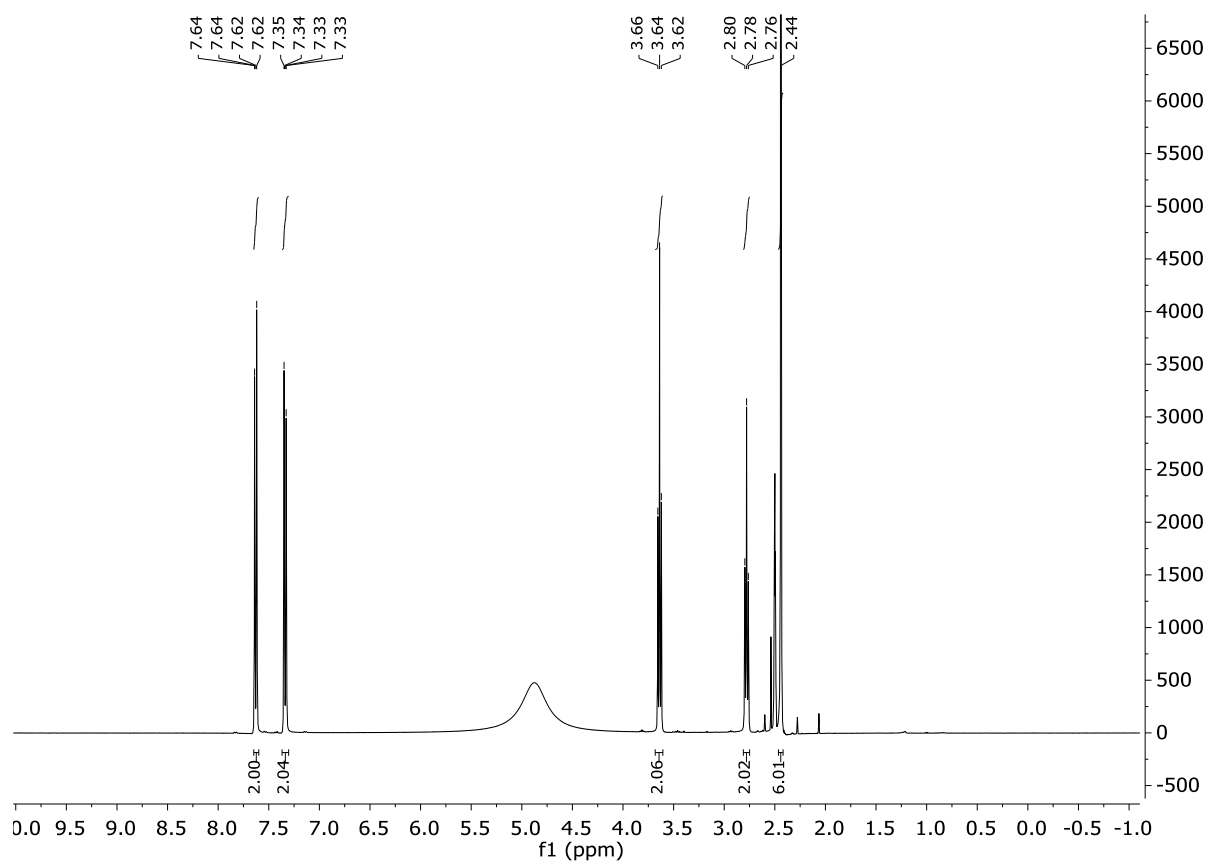
Compound 18



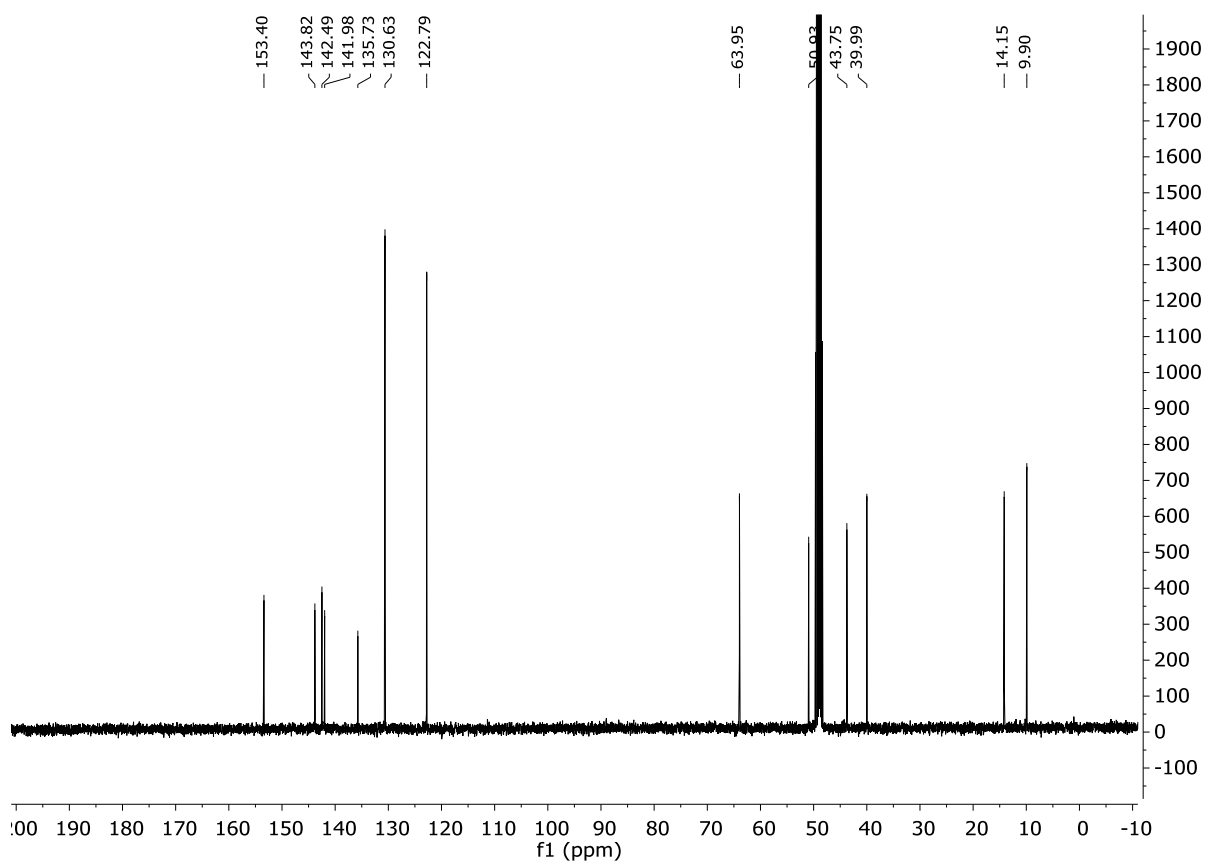
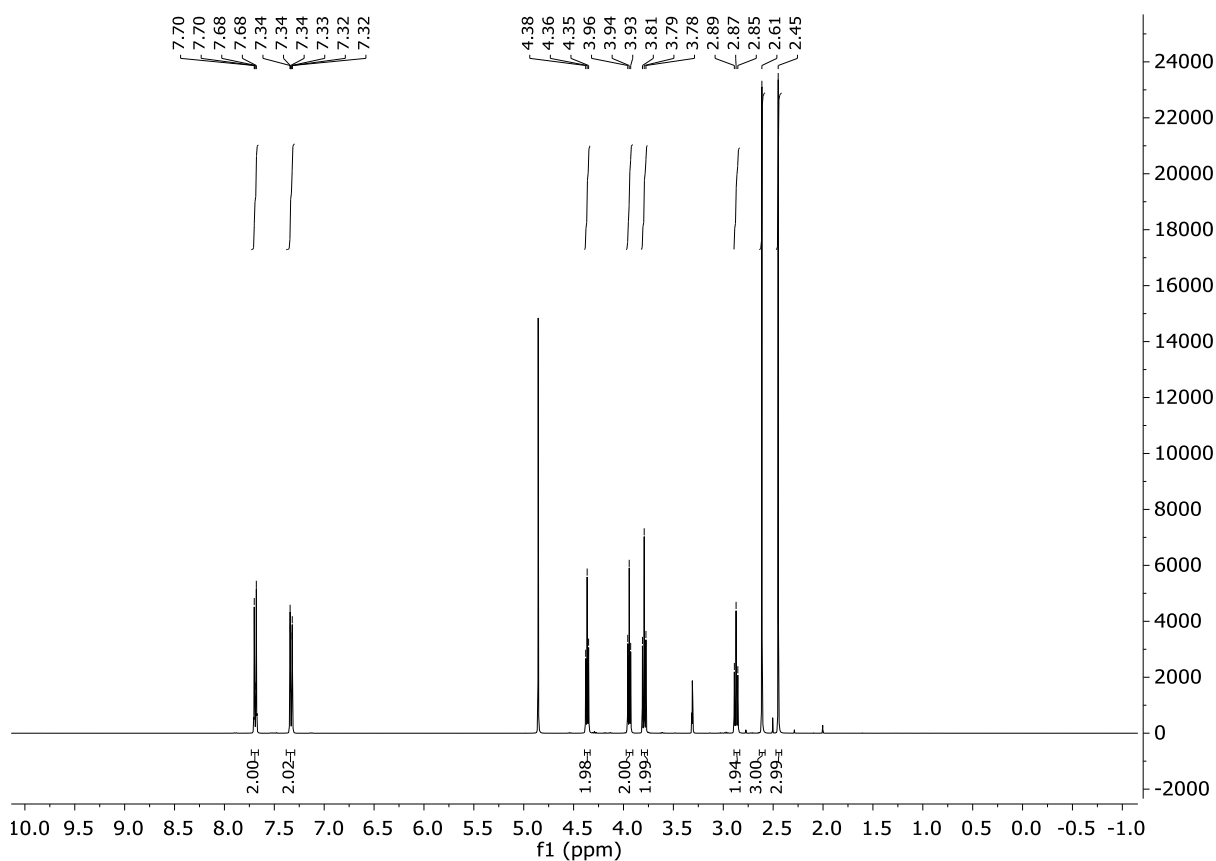
Compound 20



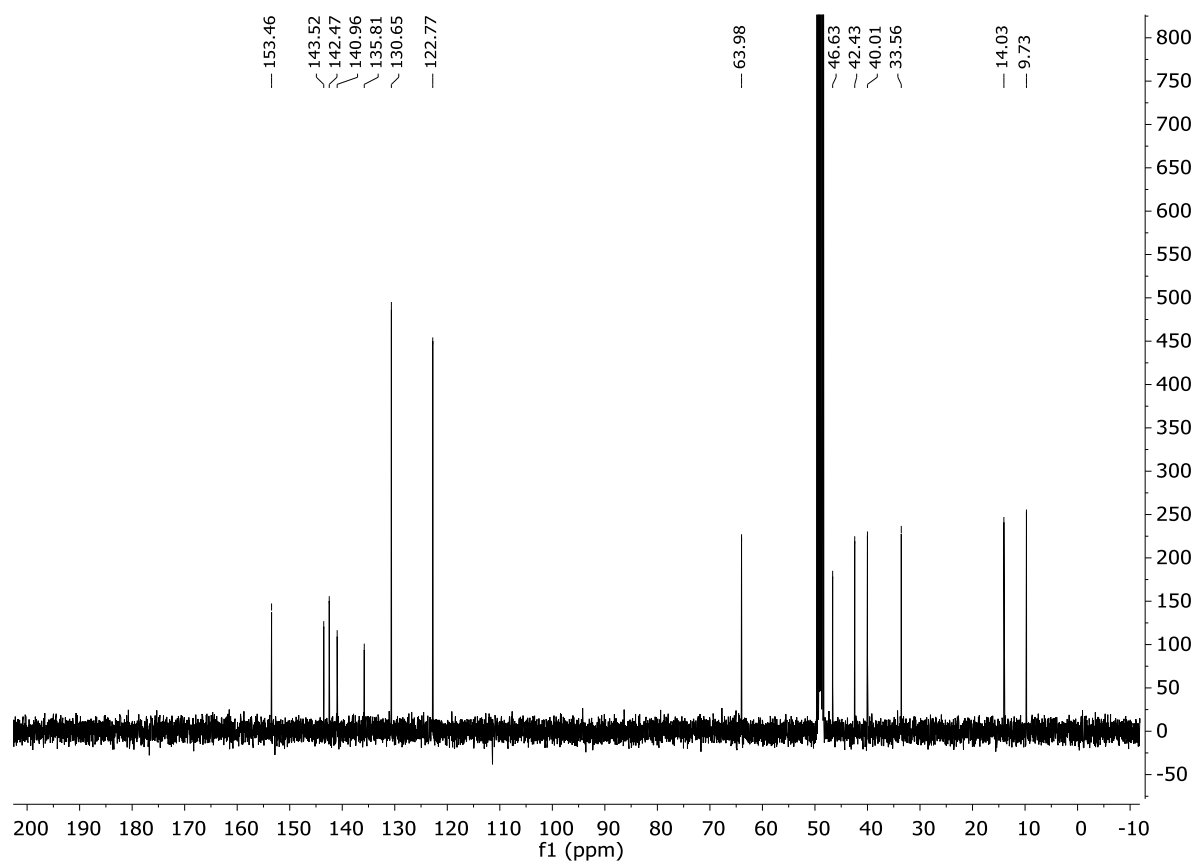
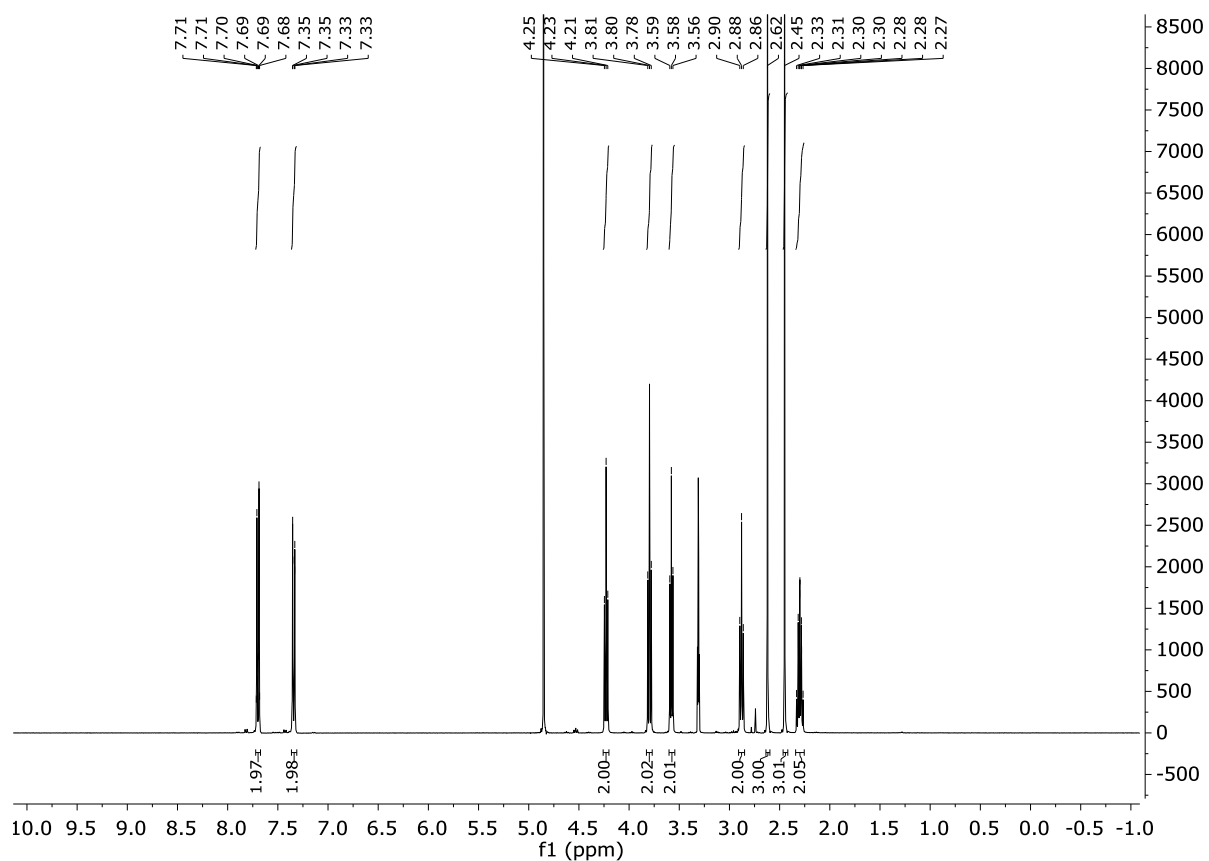
Compound 21



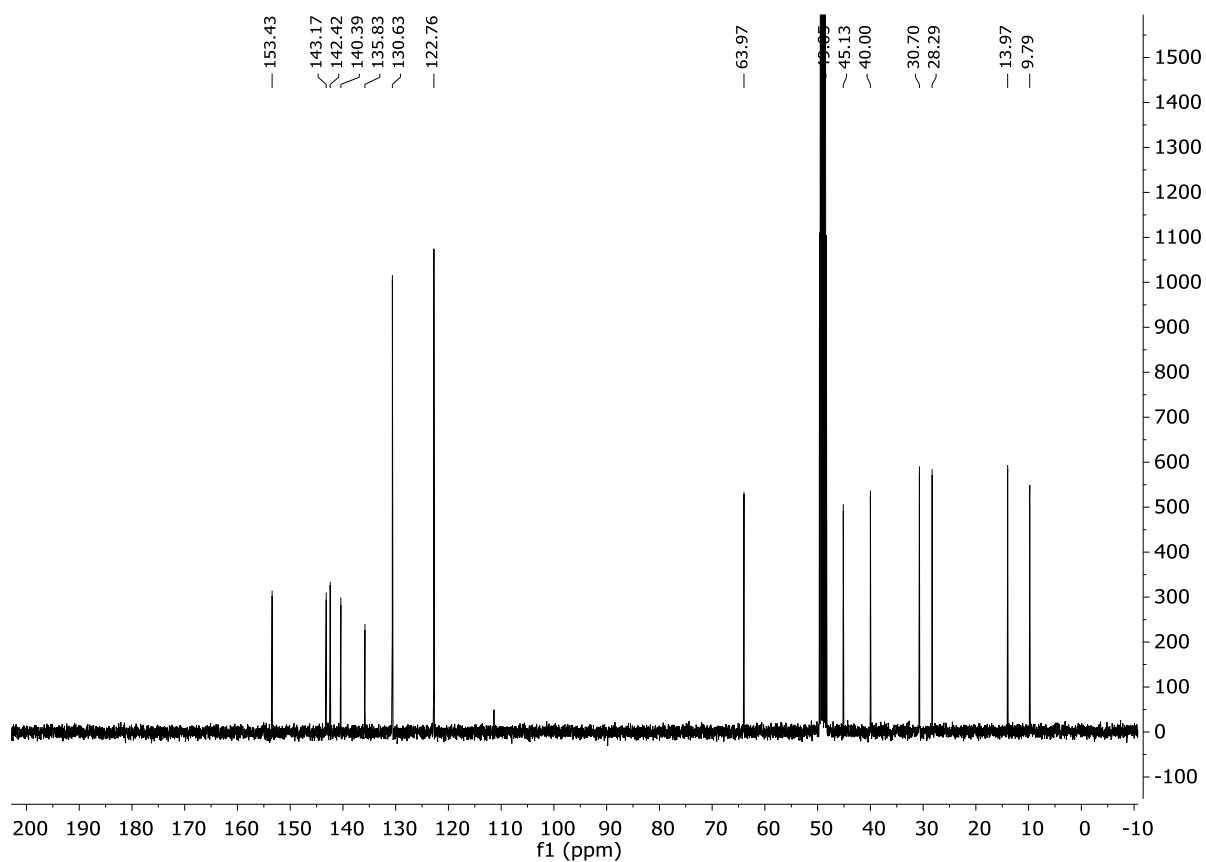
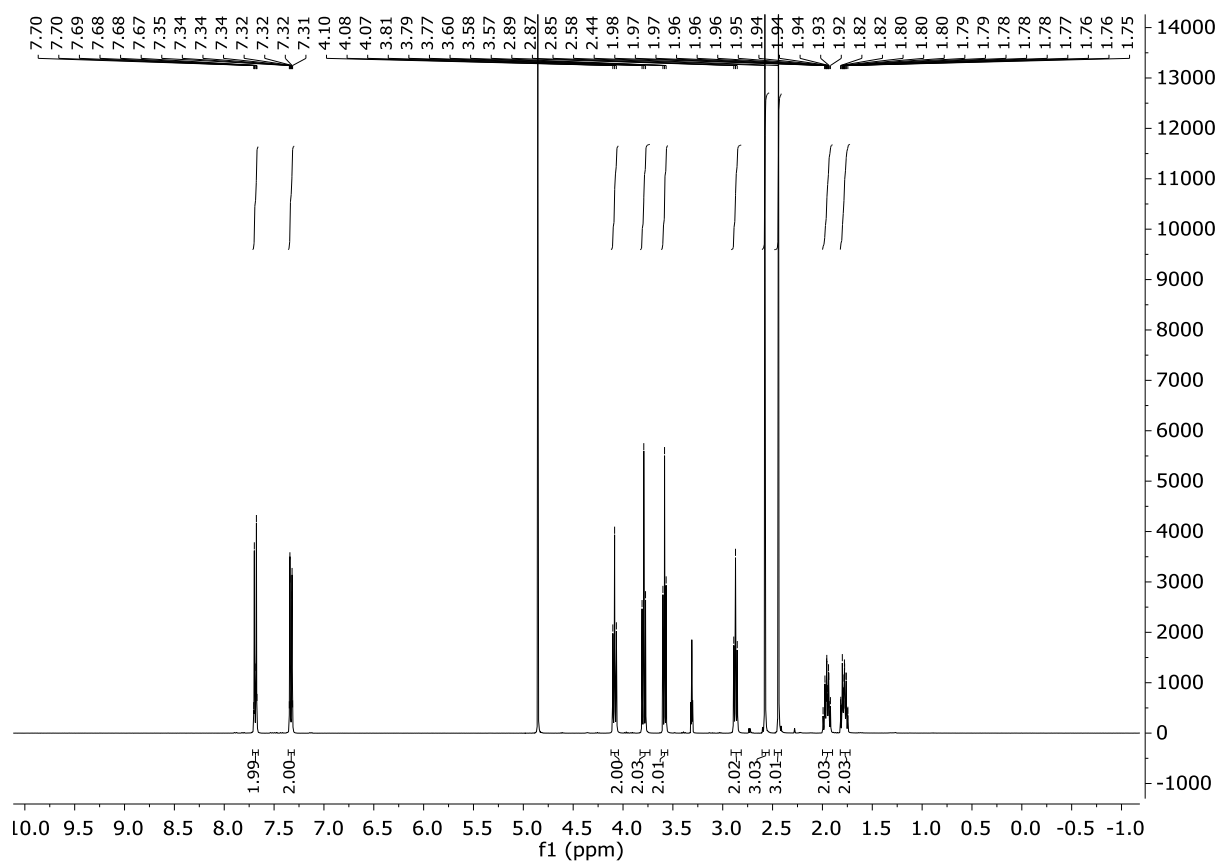
Compound 22



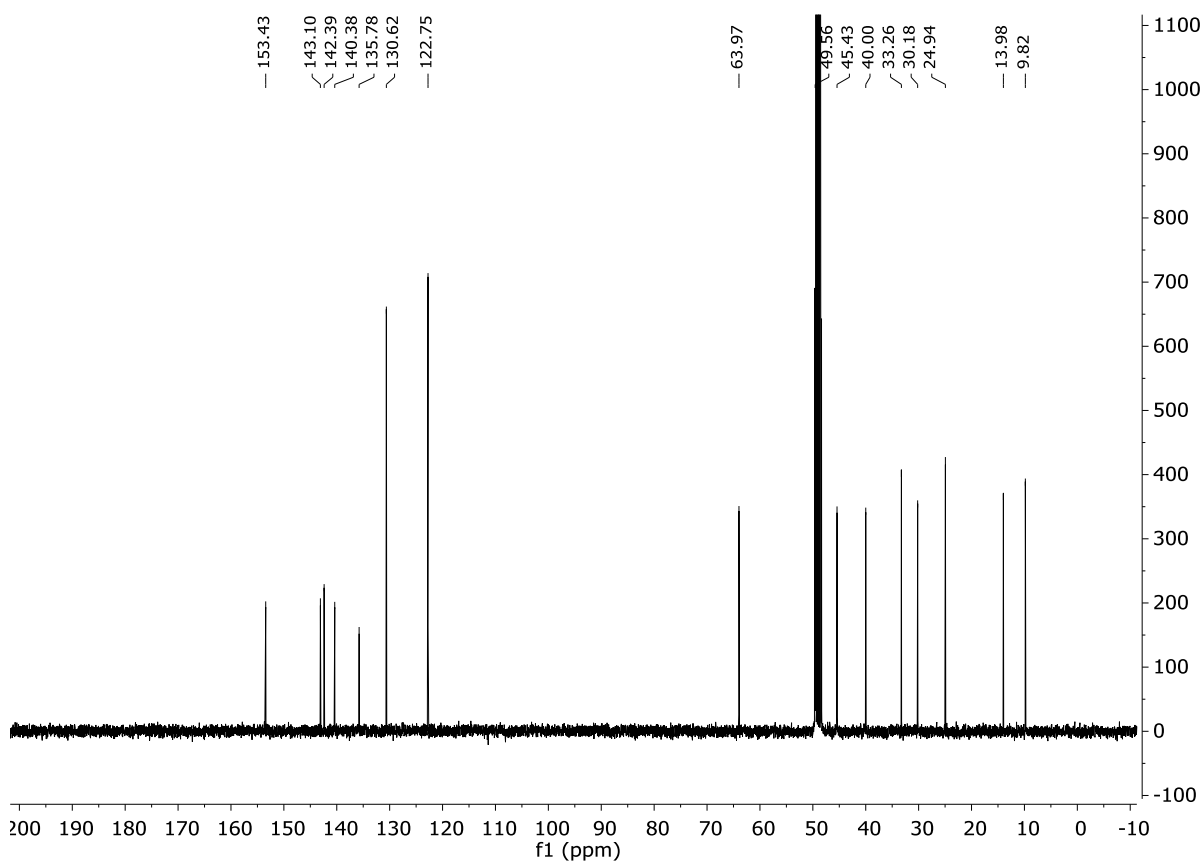
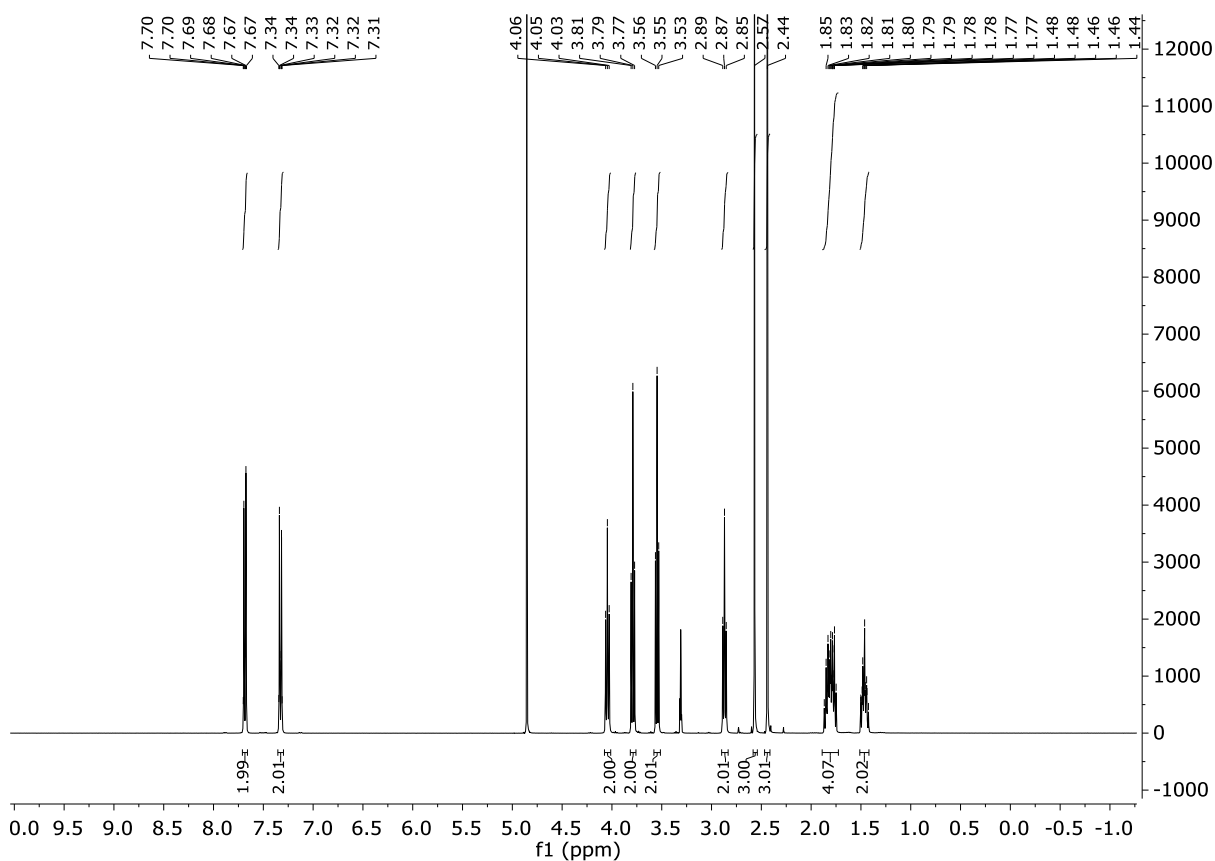
Compound 23



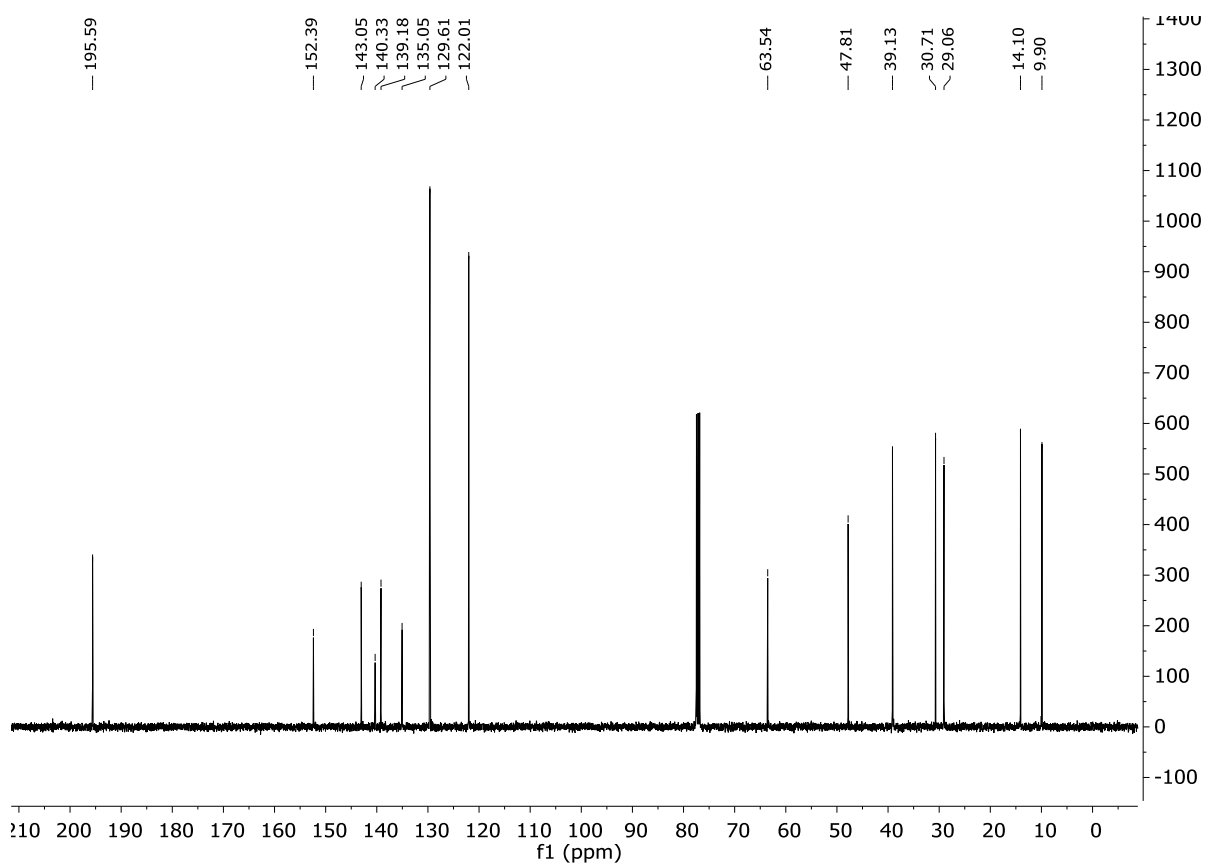
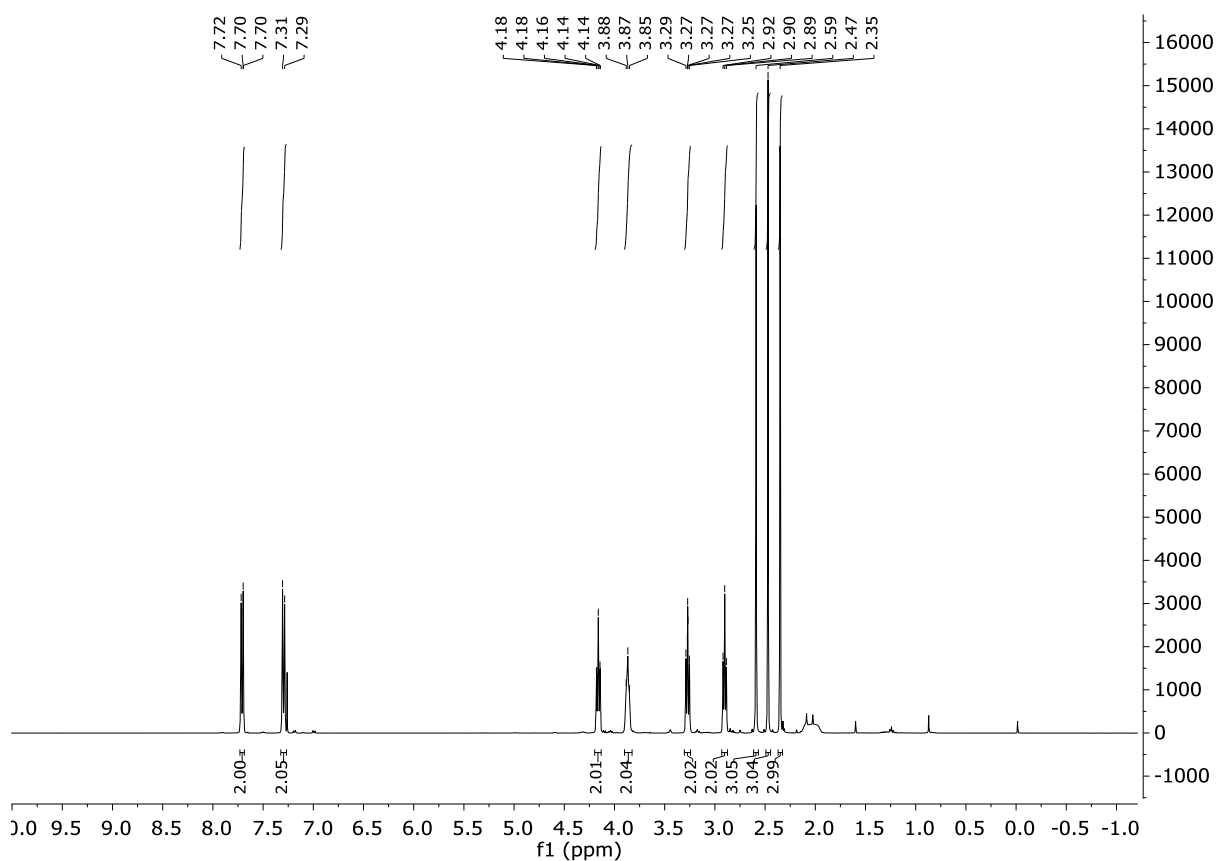
Compound 24



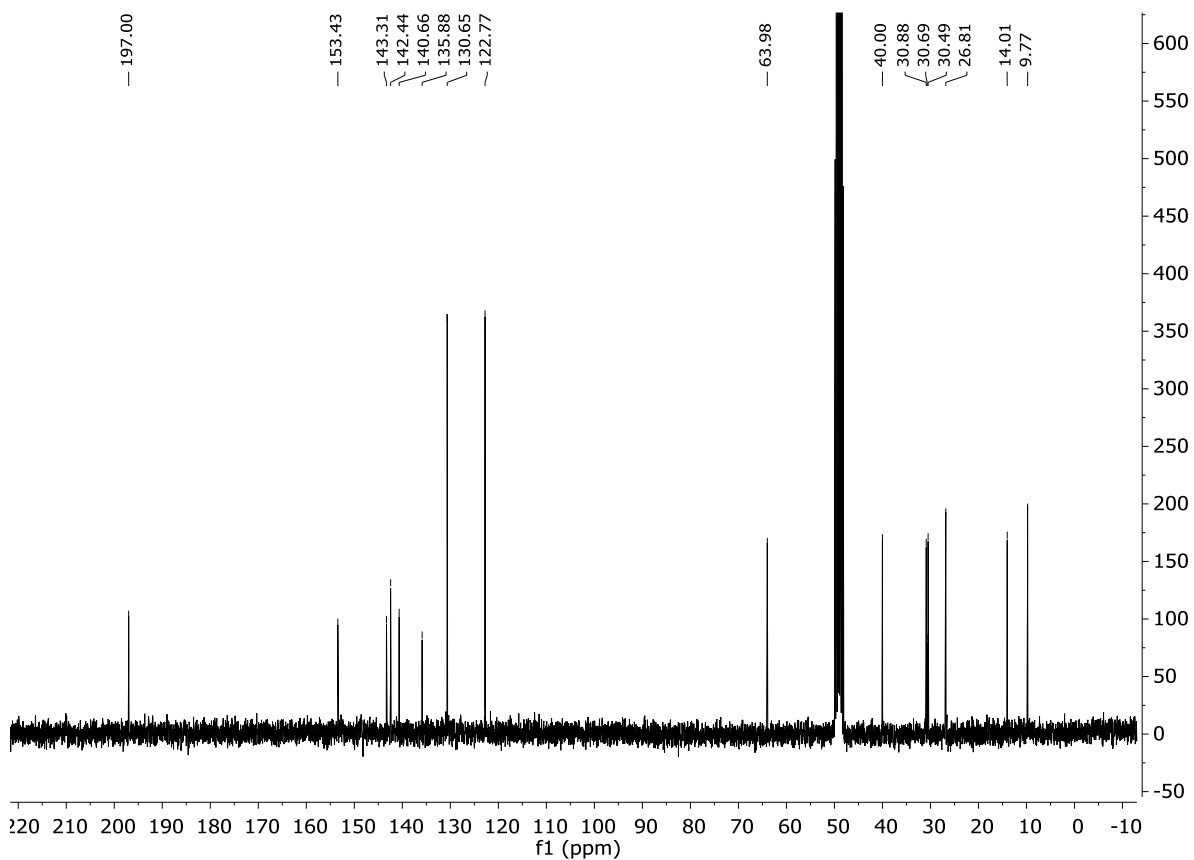
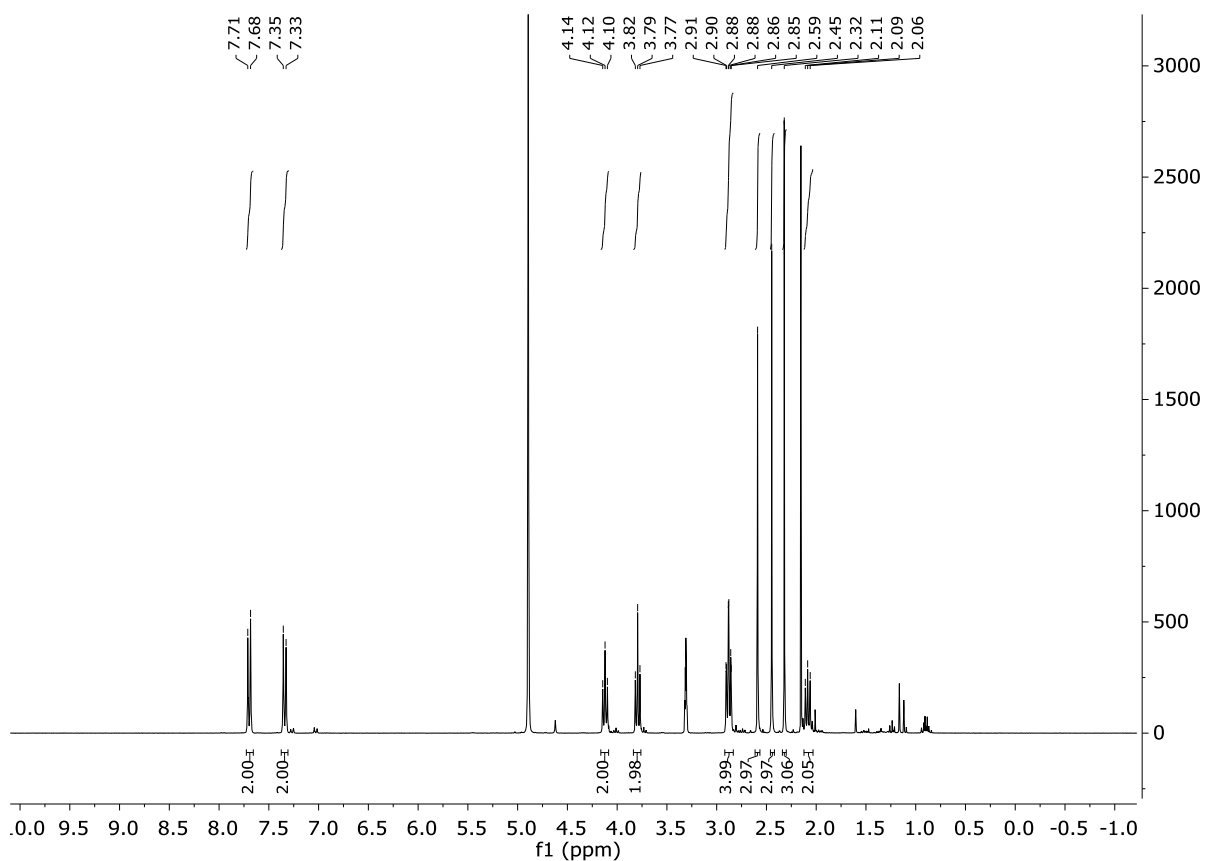
Compound 25



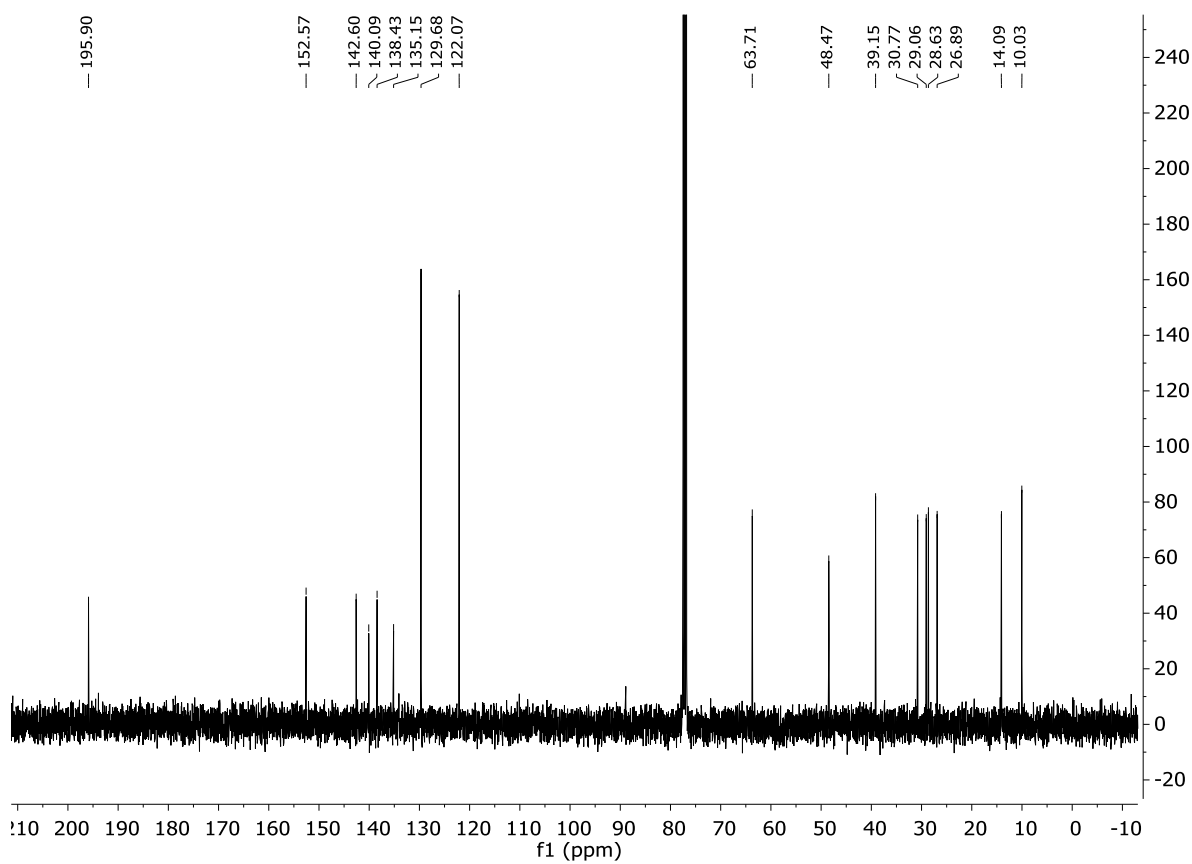
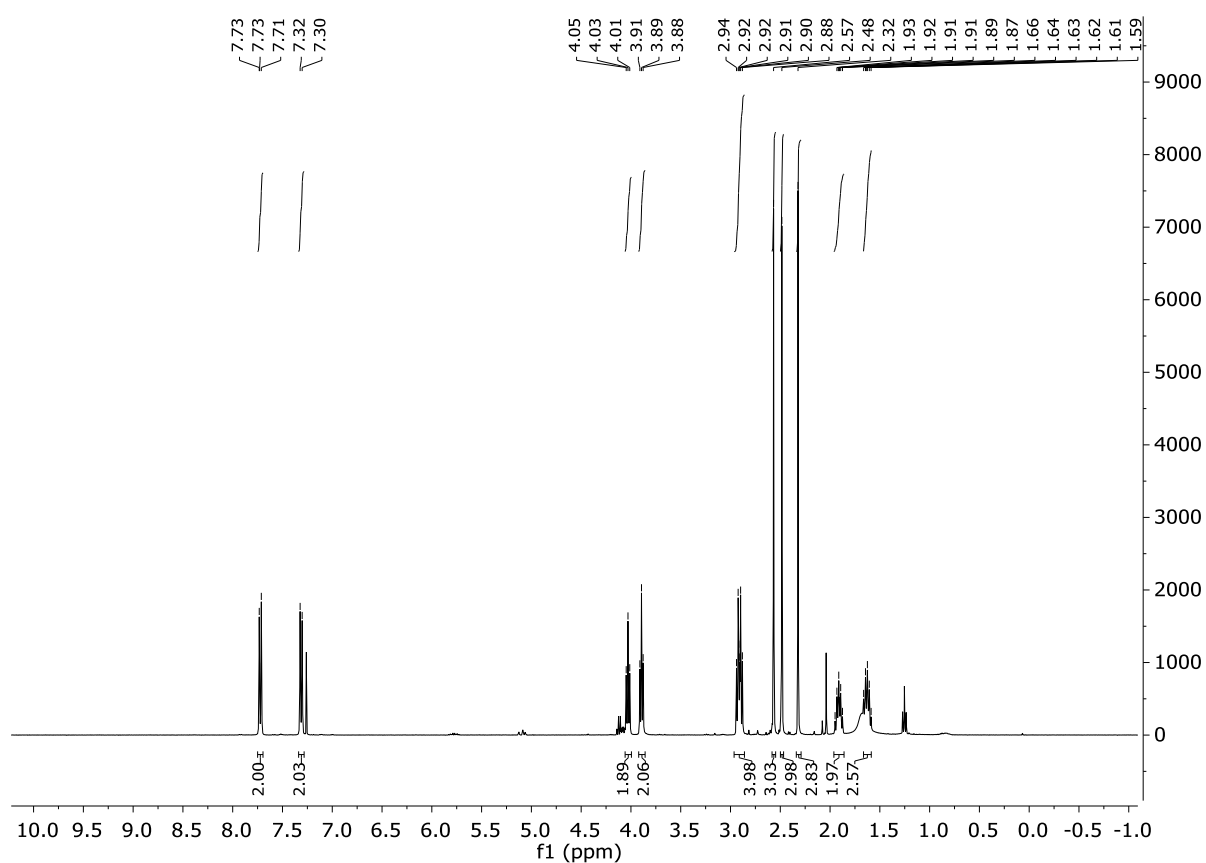
Compound 26



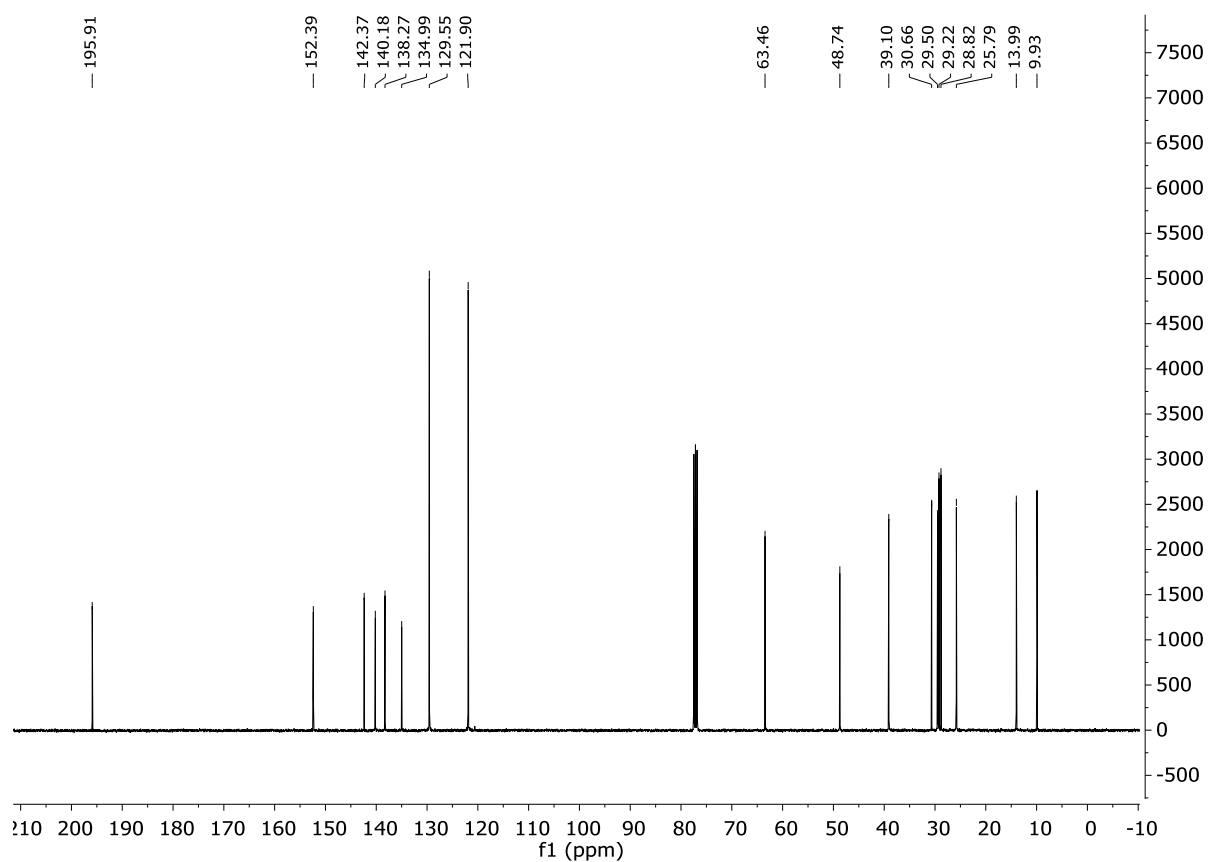
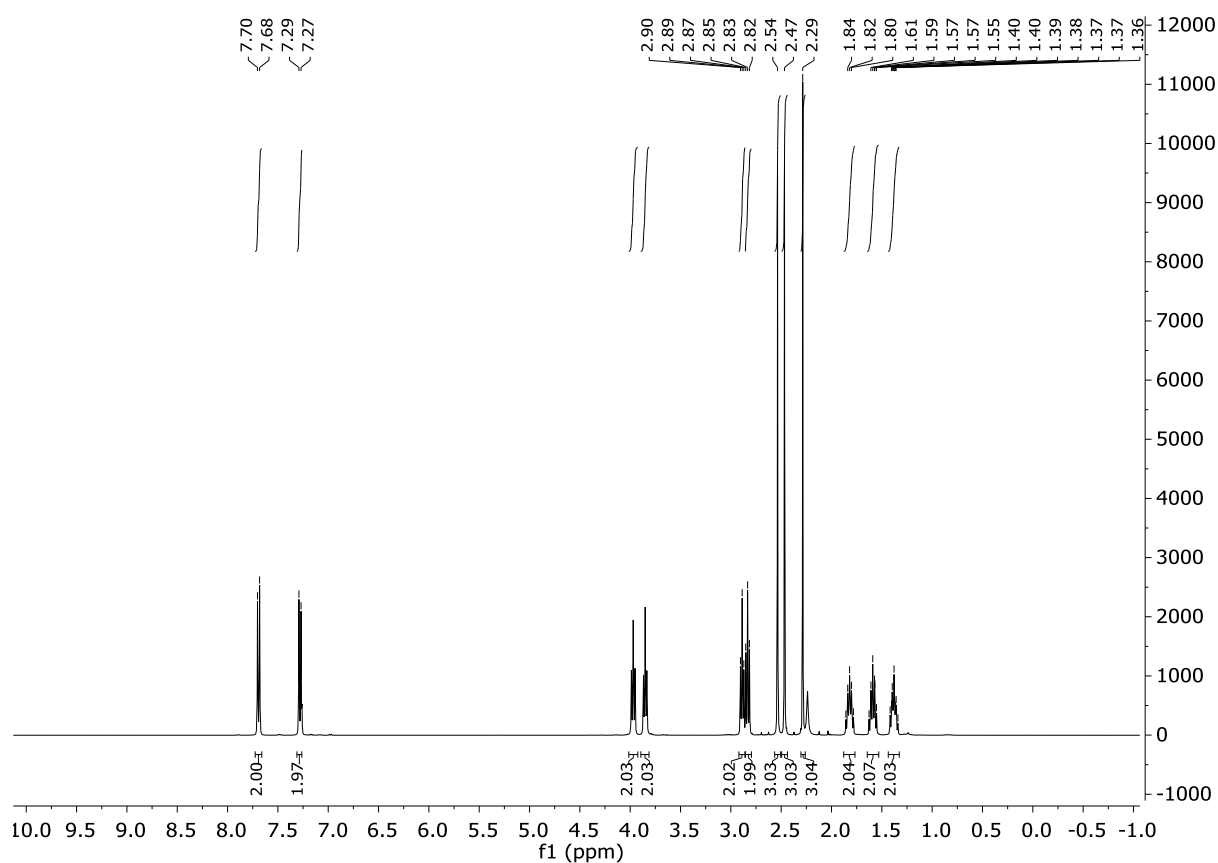
Compound 27



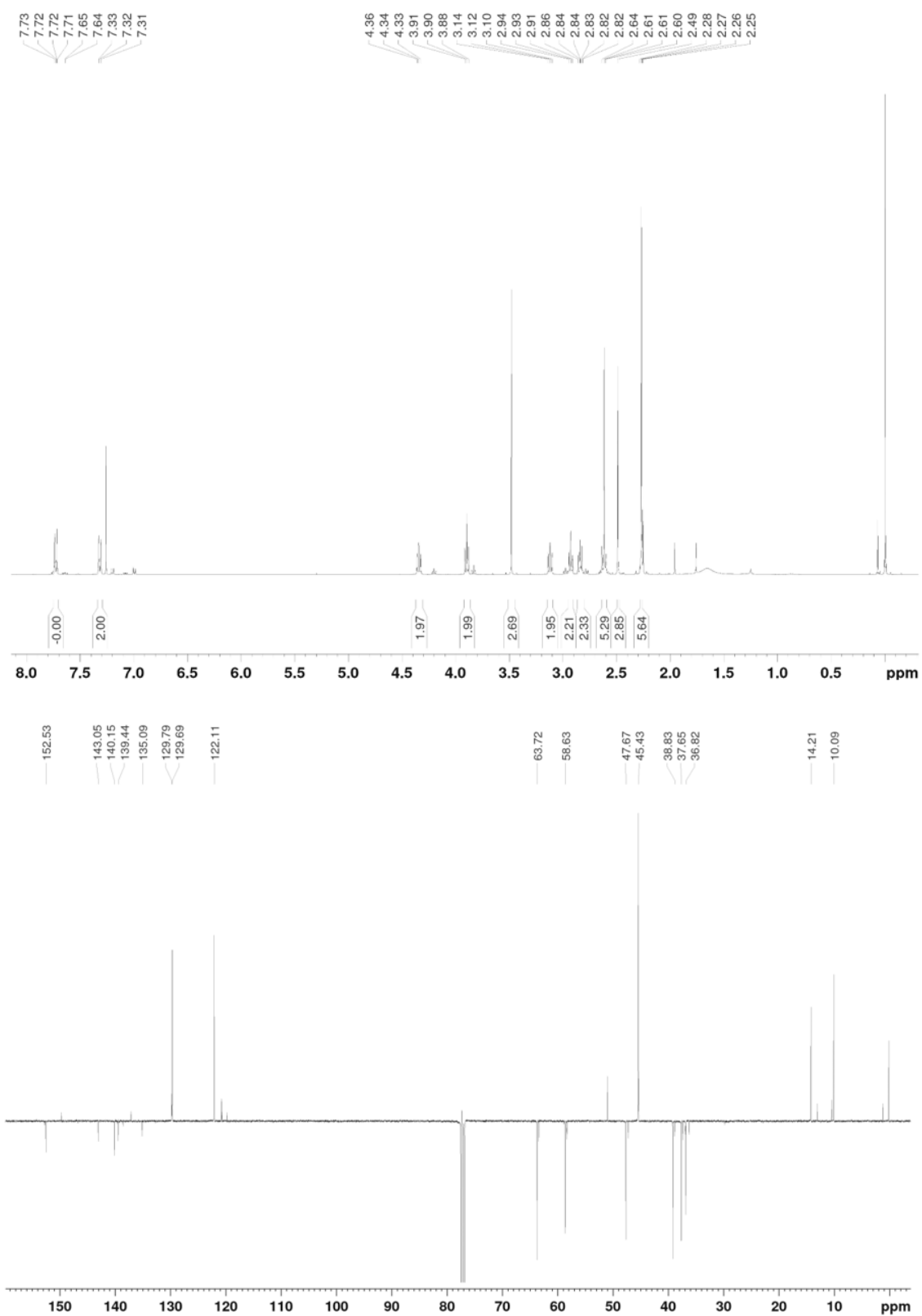
Compound 28



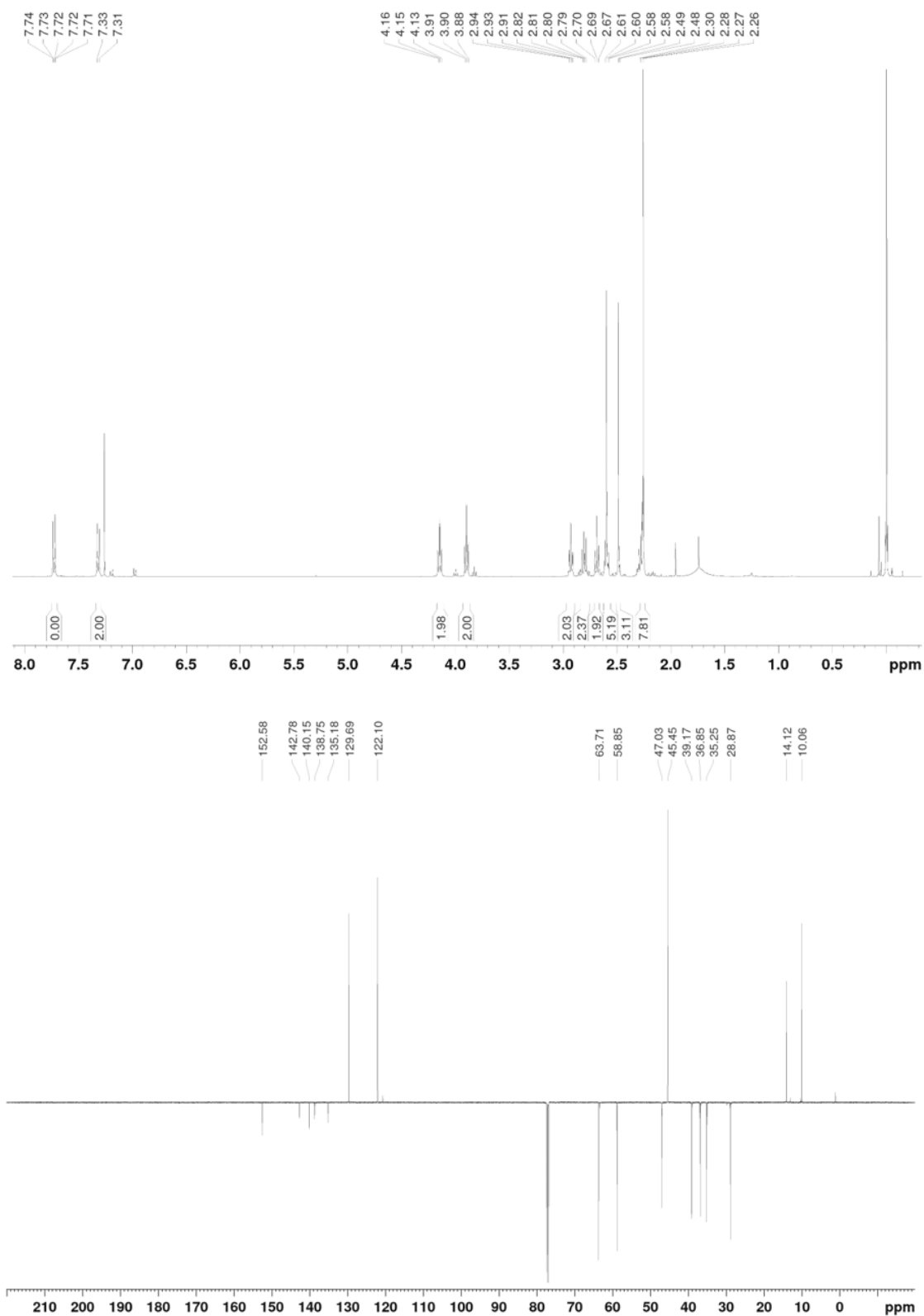
Compound 29



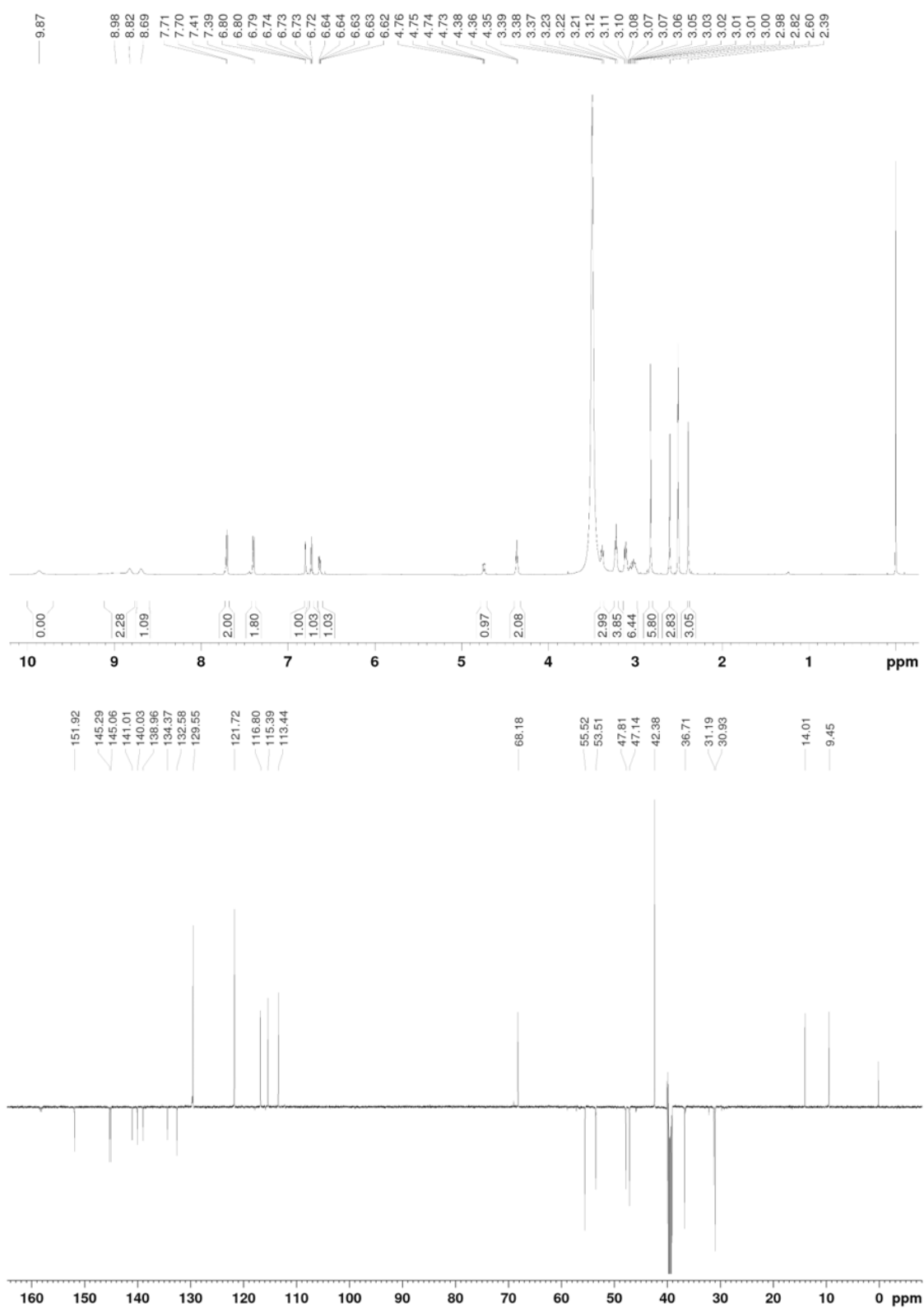
Compound 30



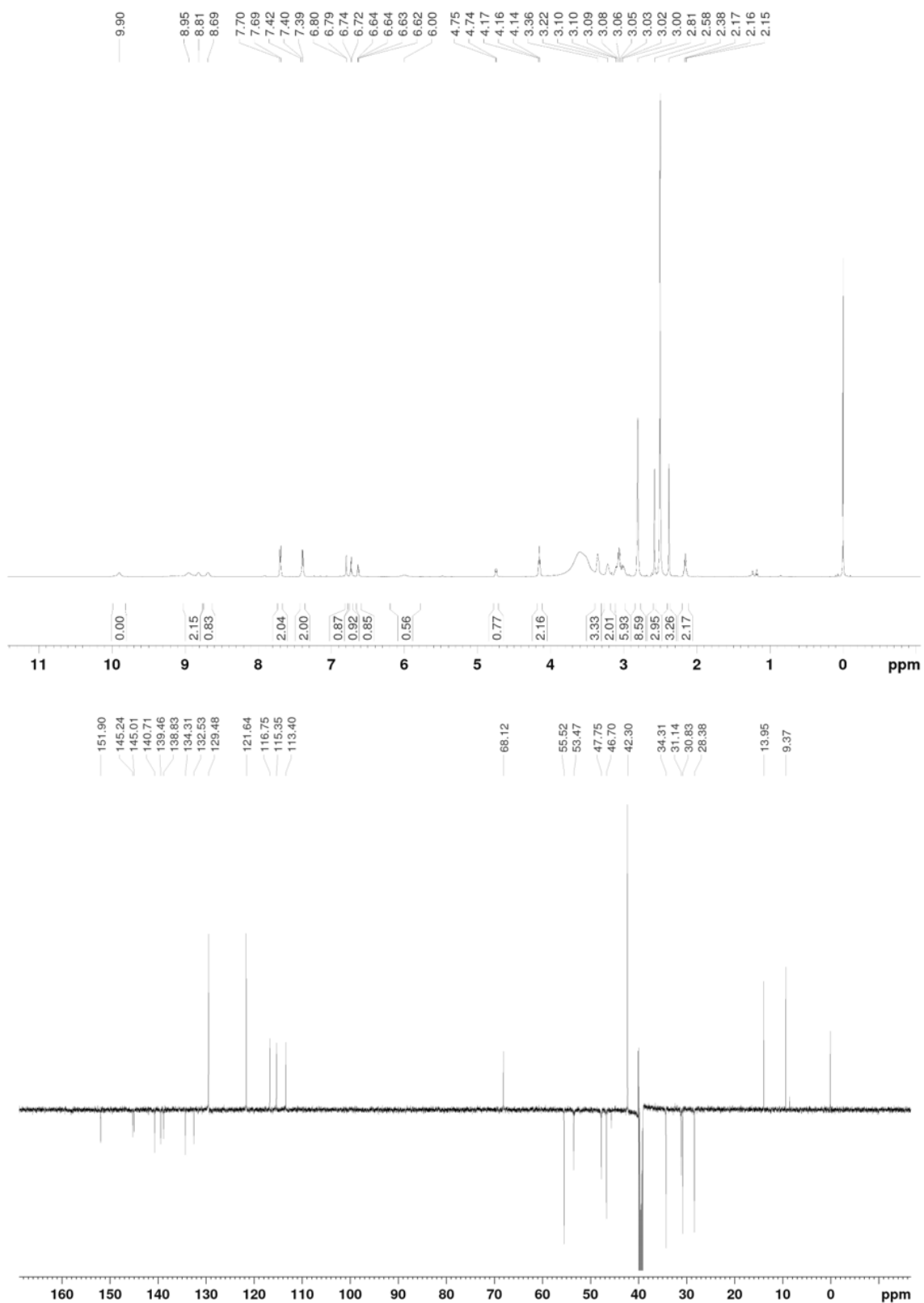
Compound 31



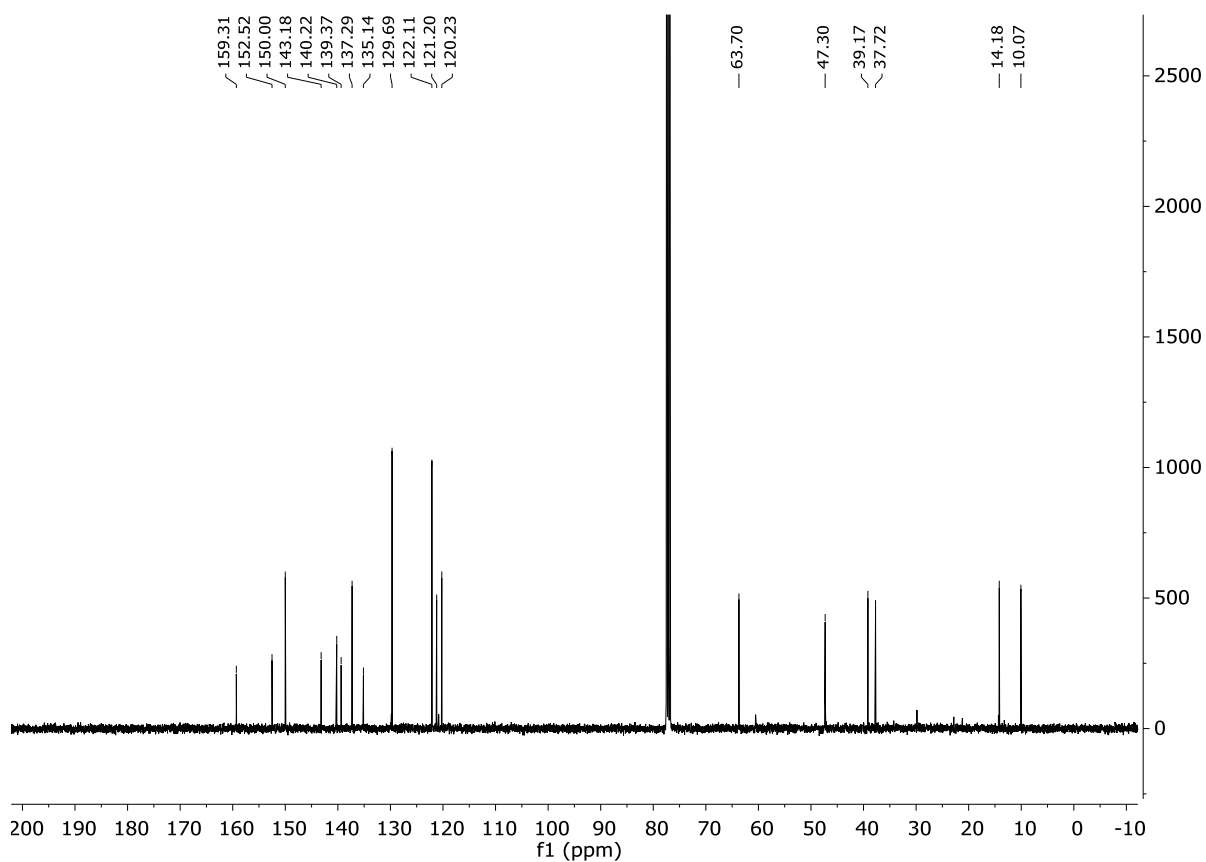
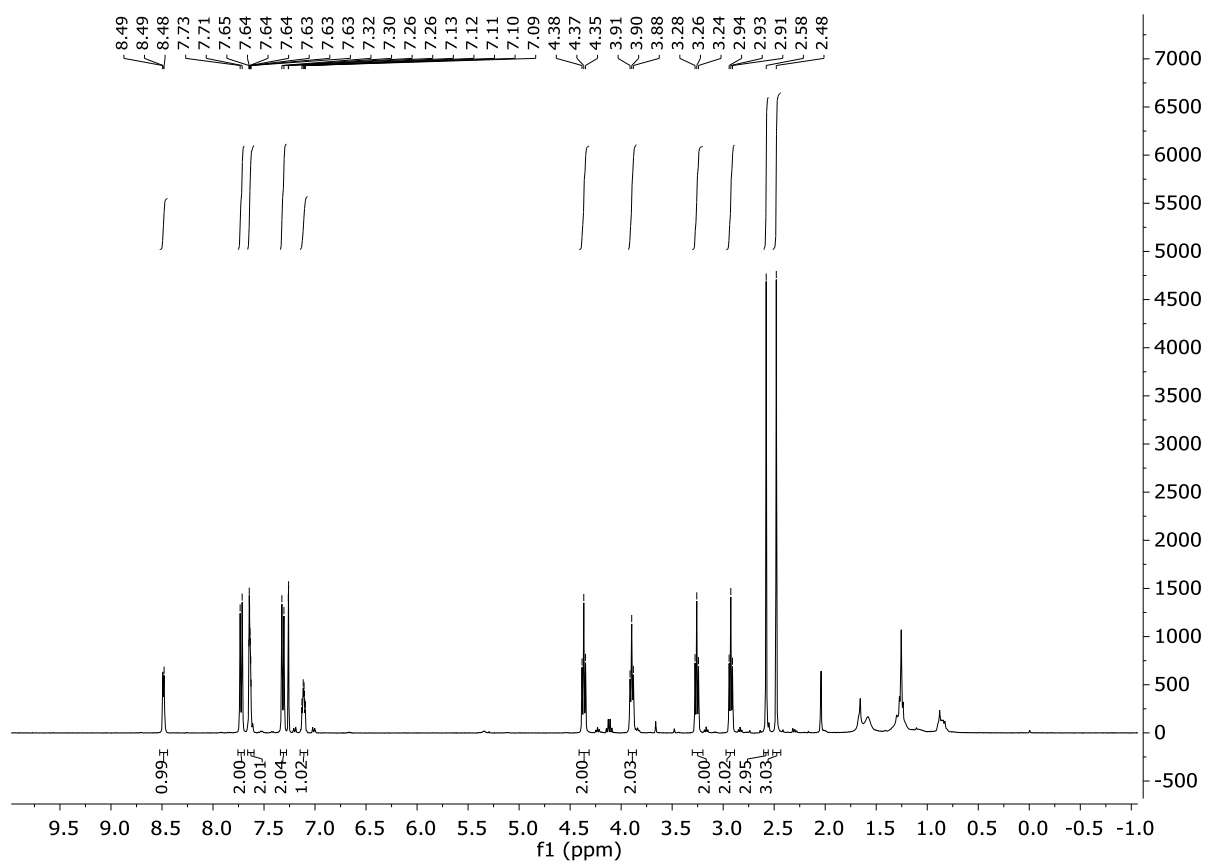
Compound 1



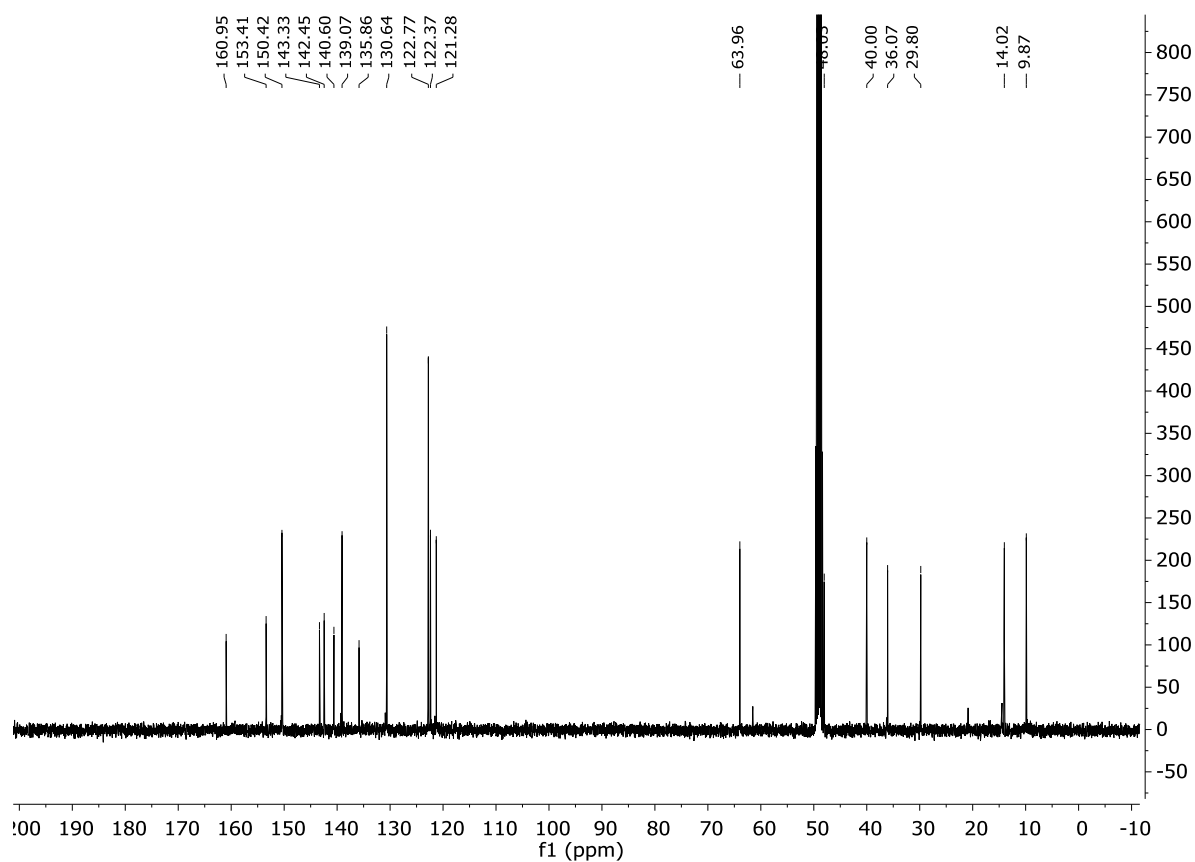
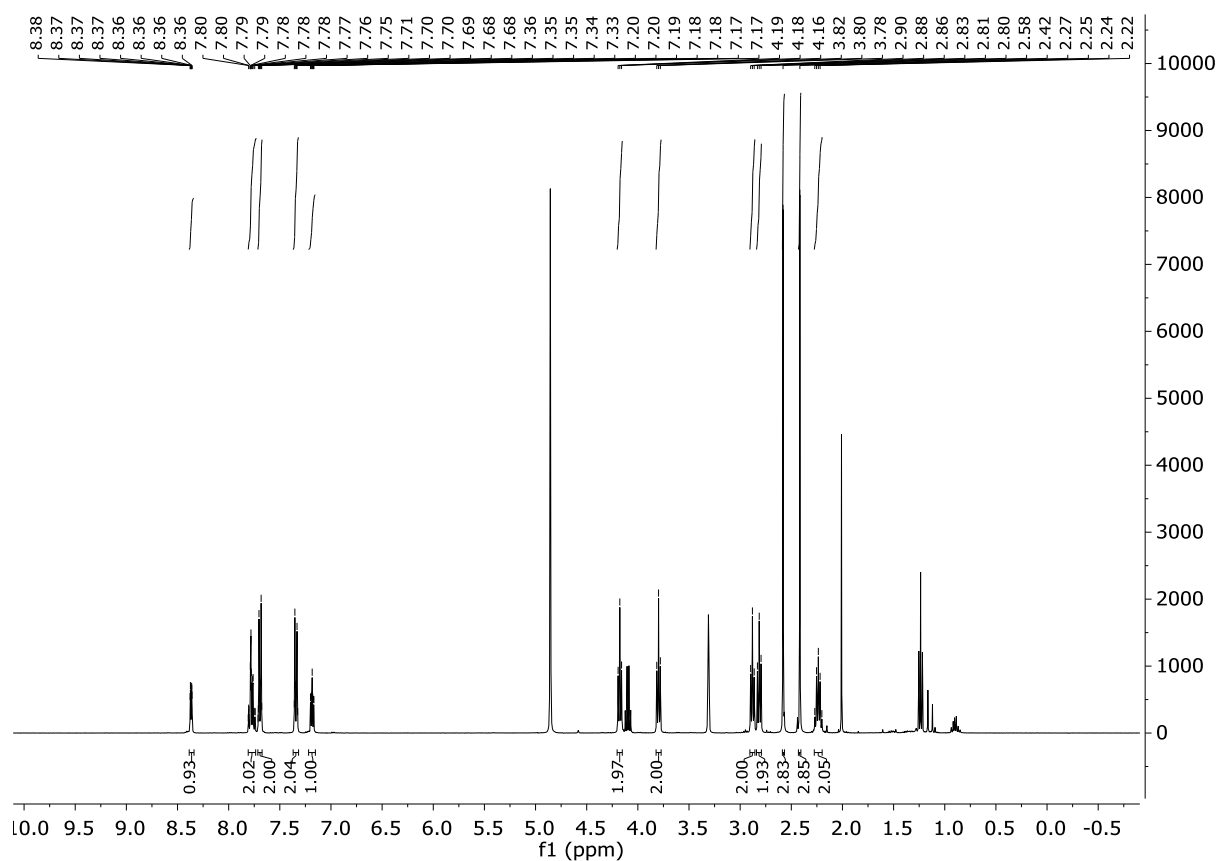
Compound 2



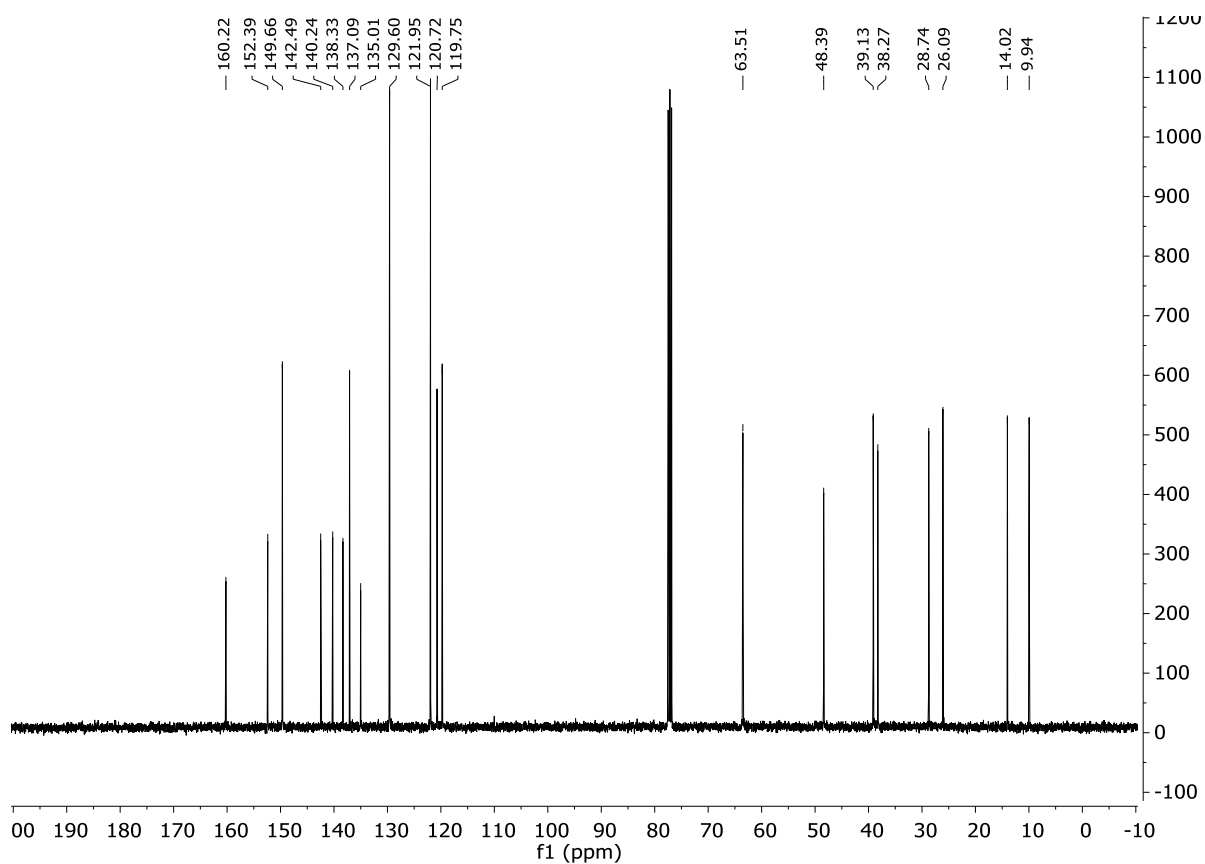
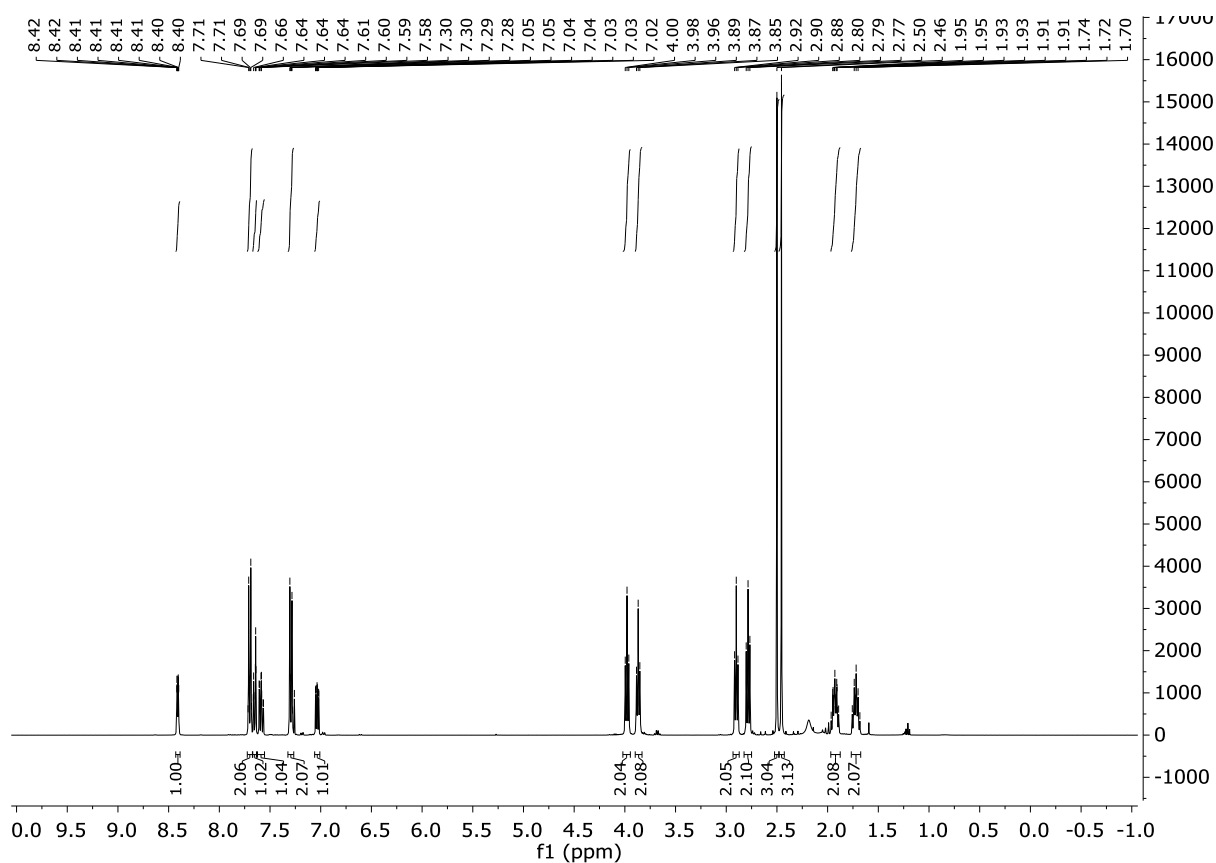
Compound 34



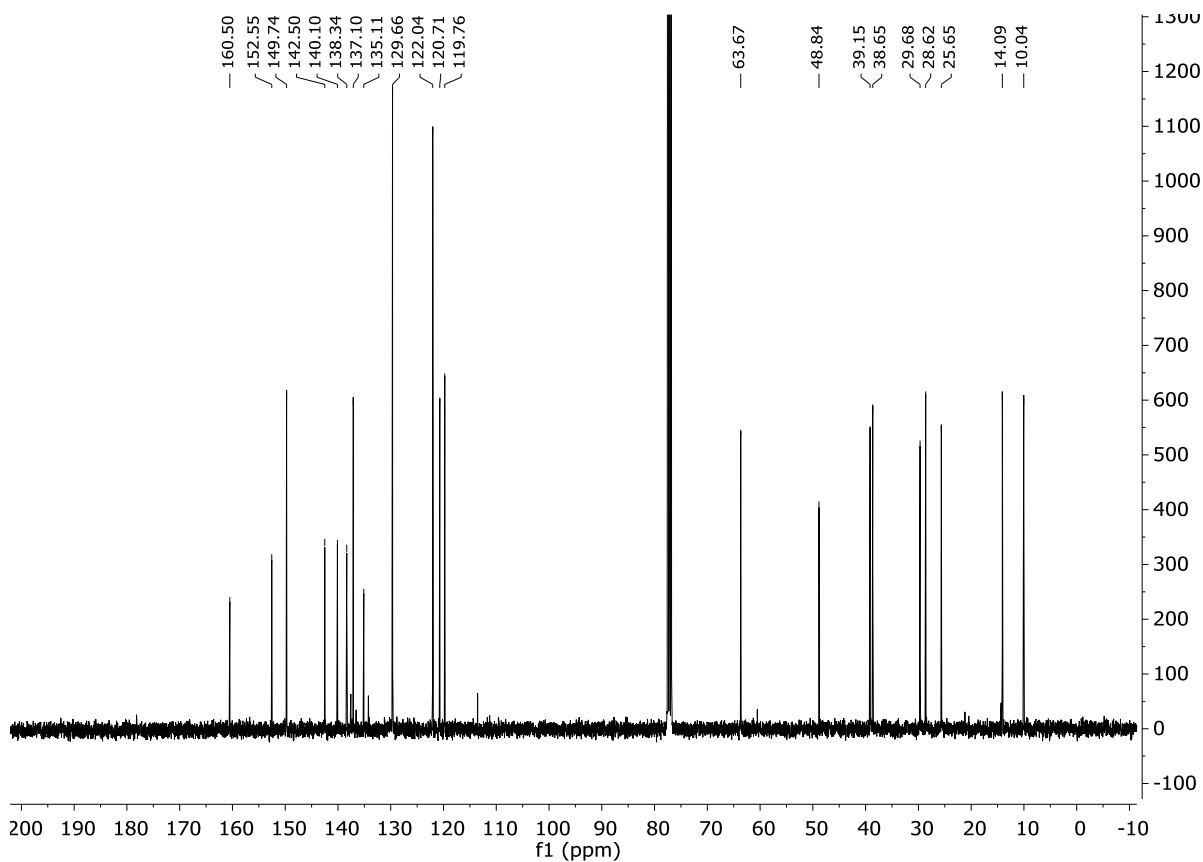
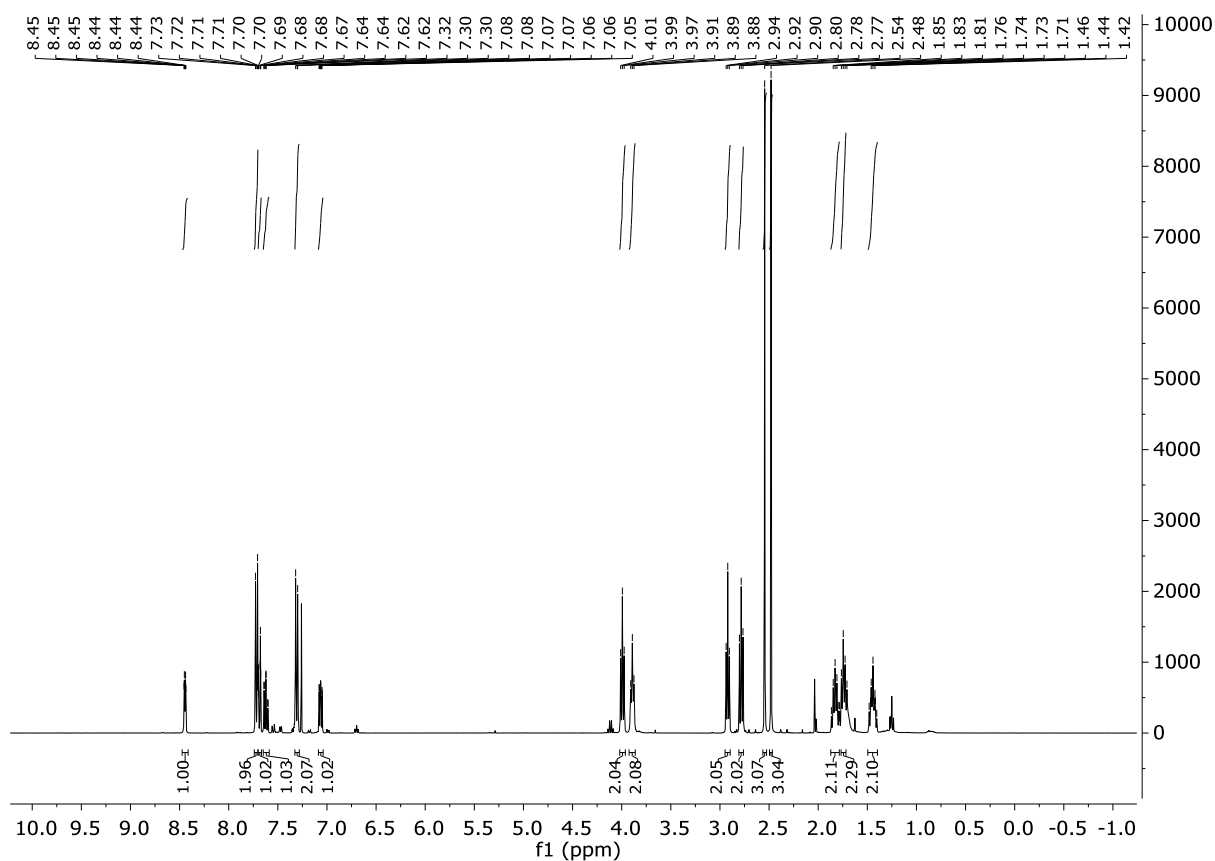
Compound 35



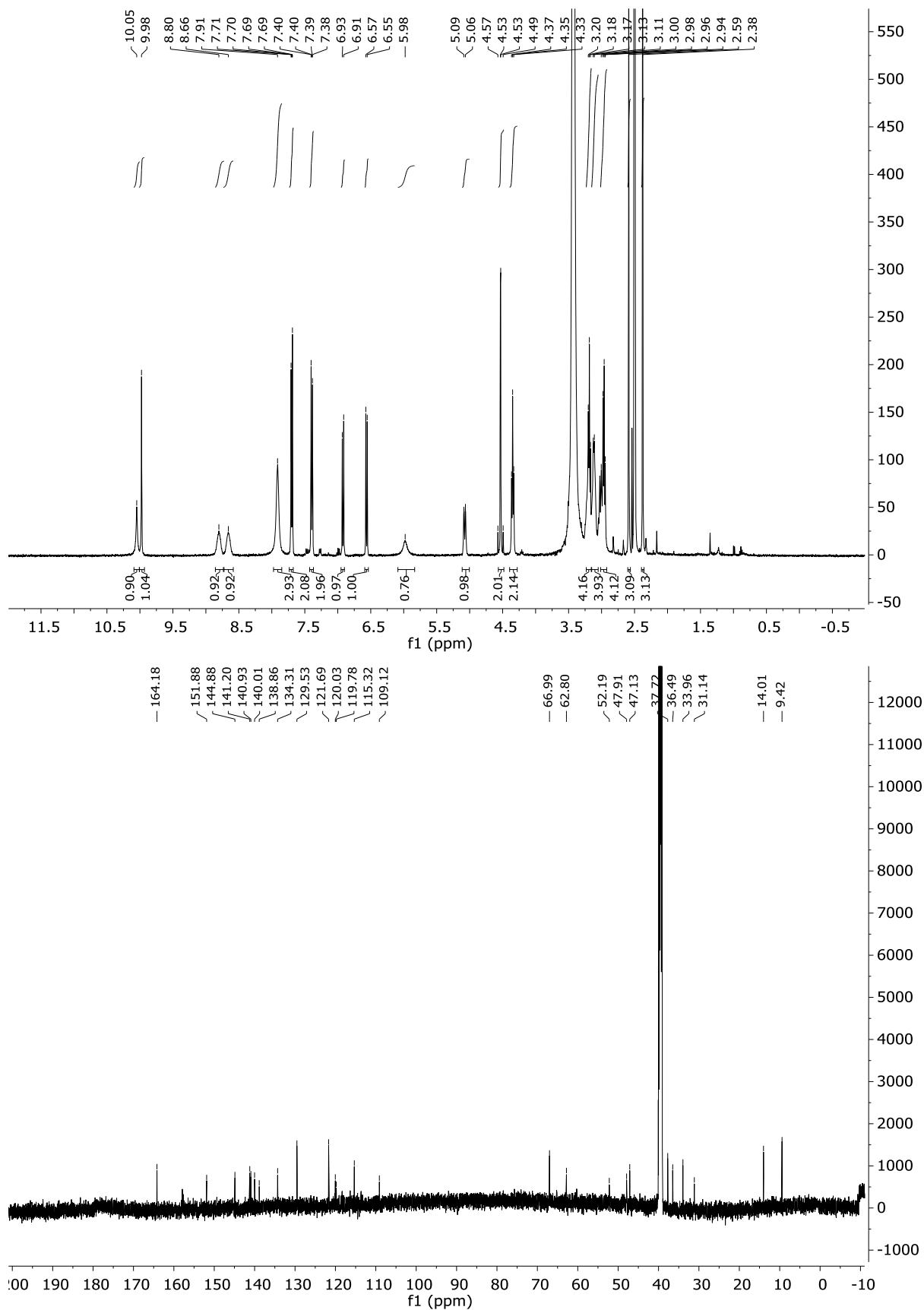
Compound 36



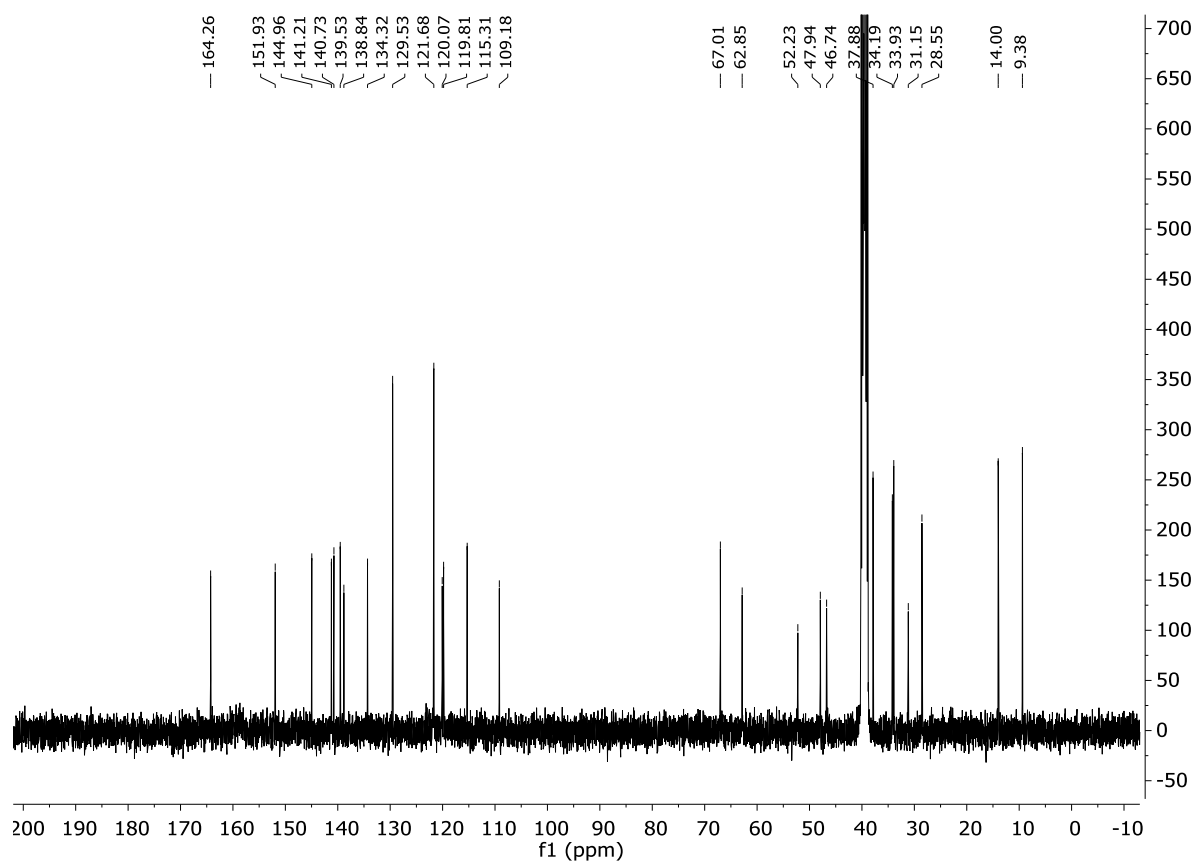
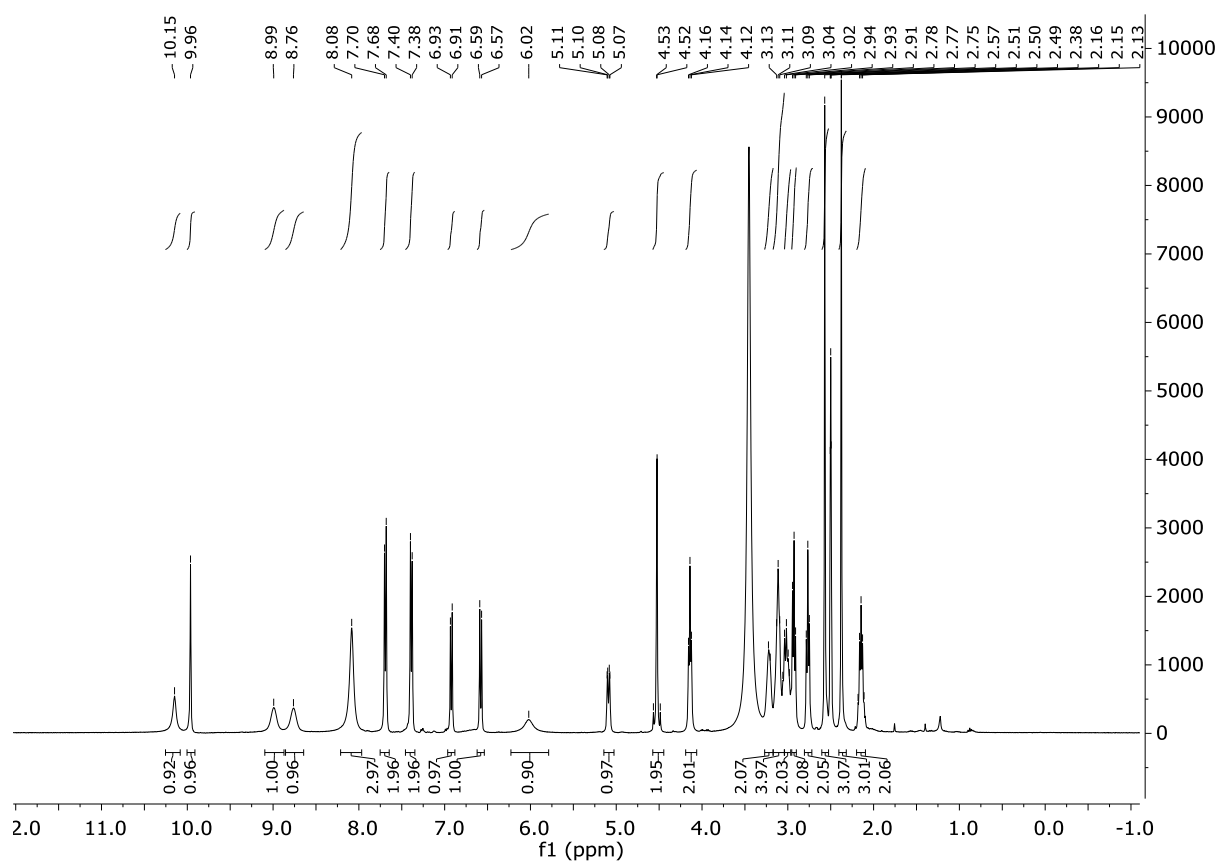
Compound 37



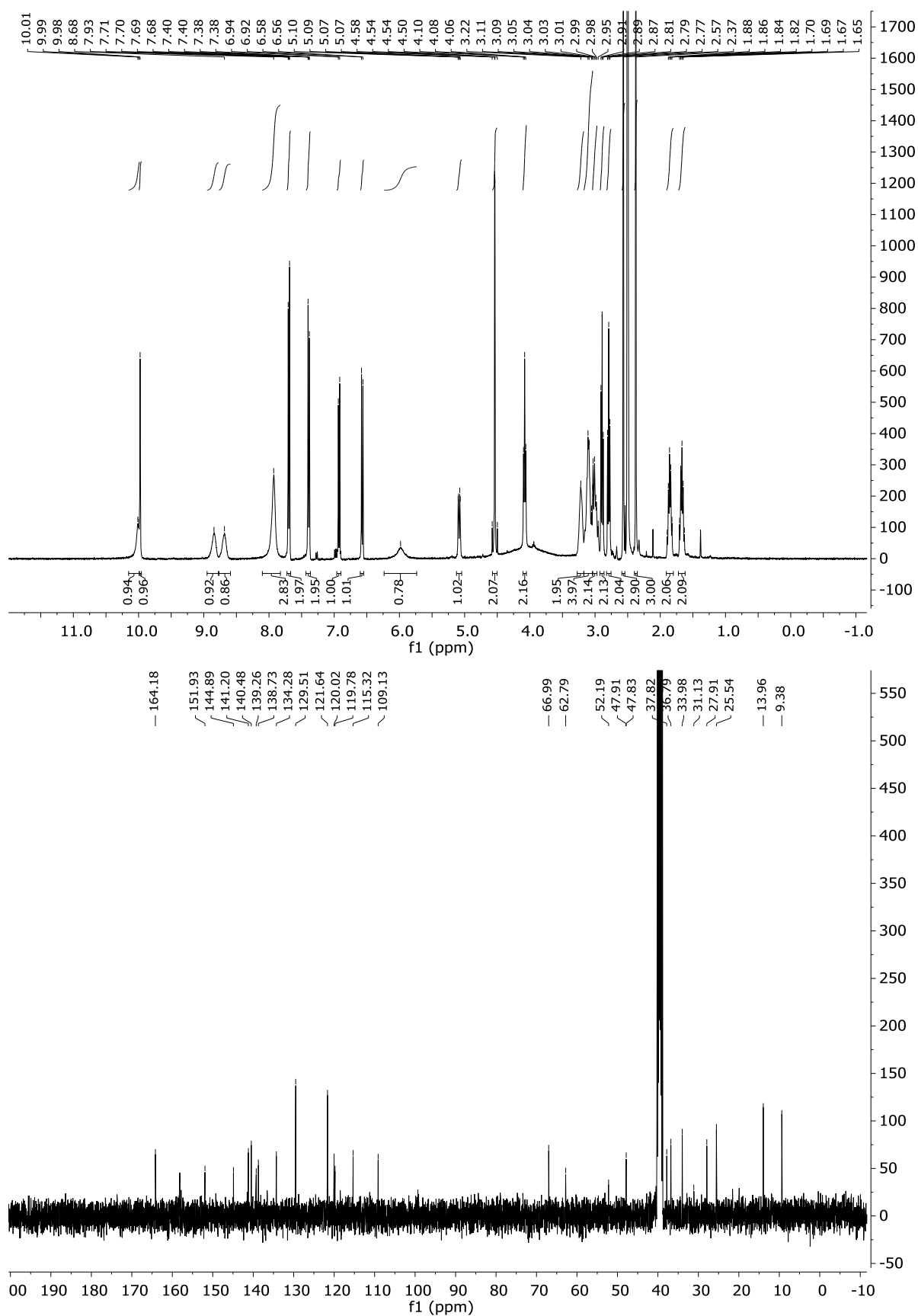
Compound 3



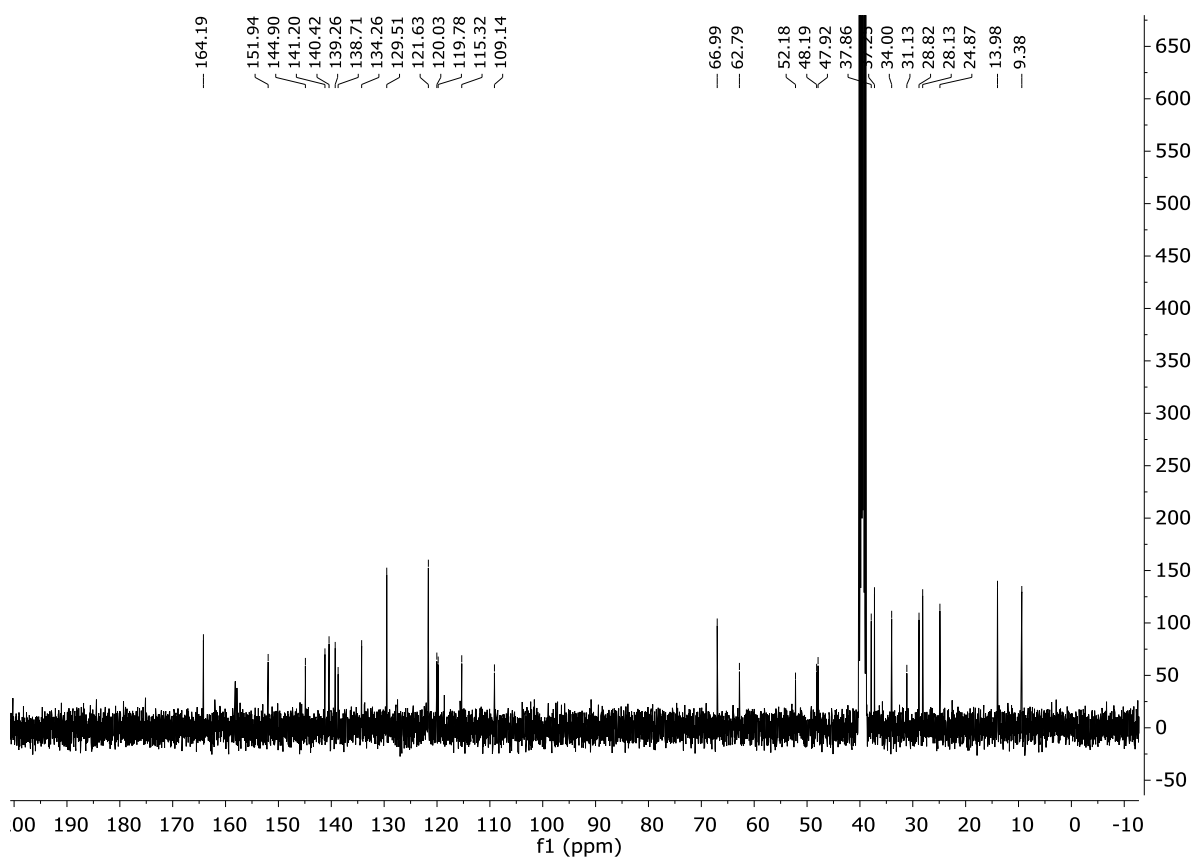
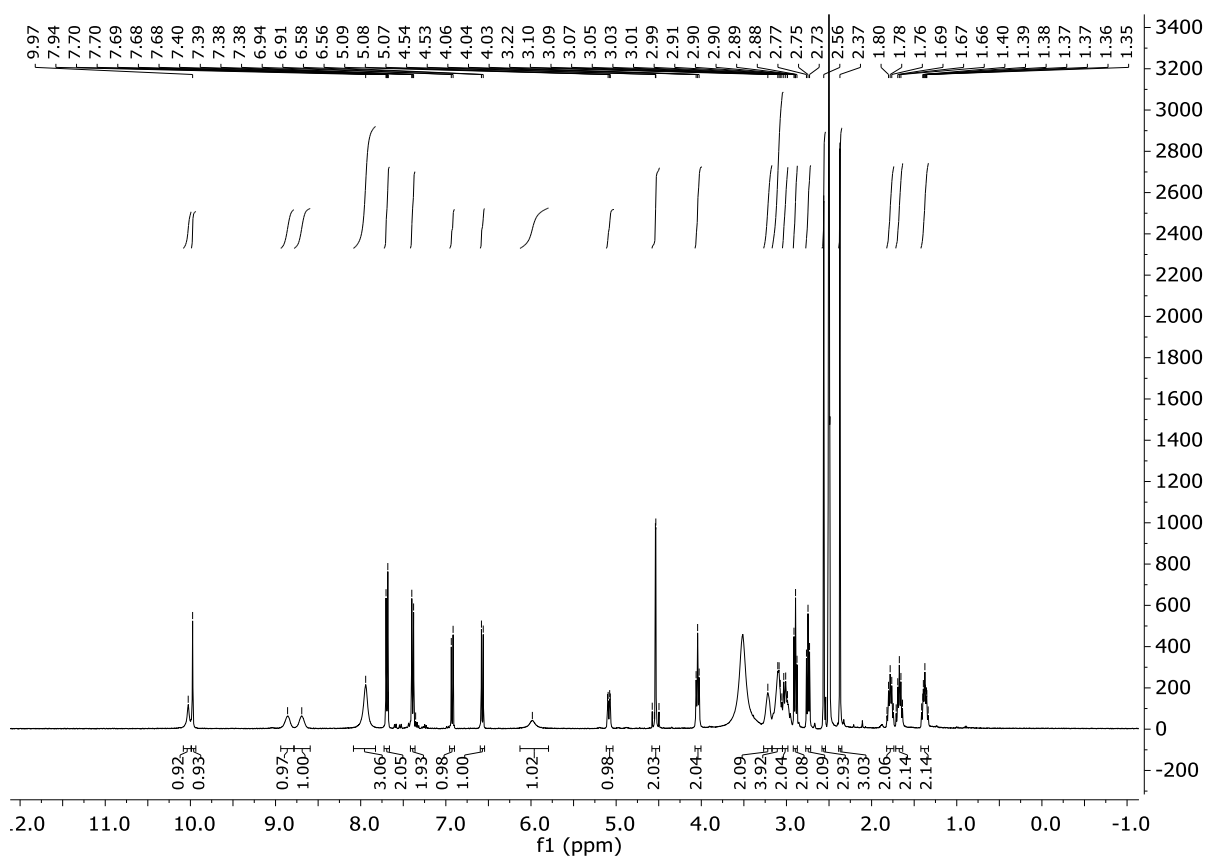
Compound 4



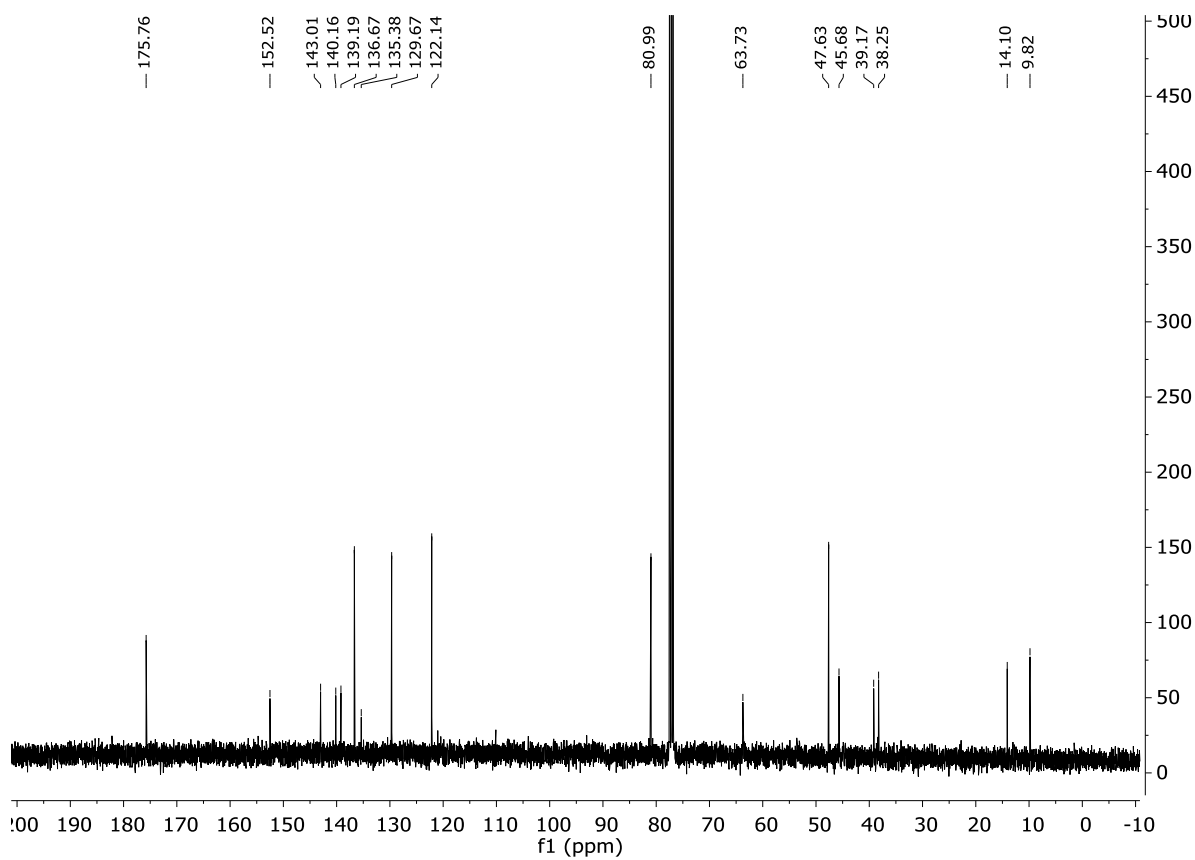
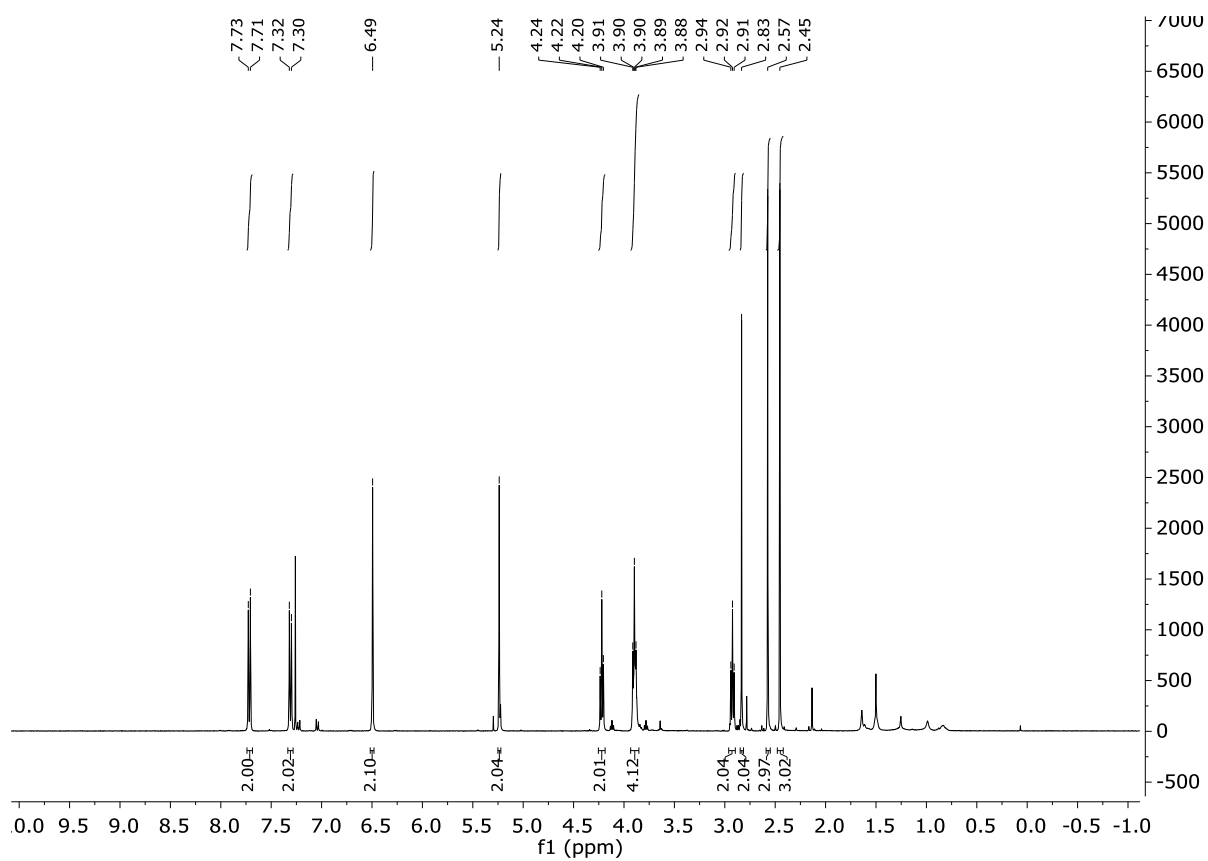
Compound 5



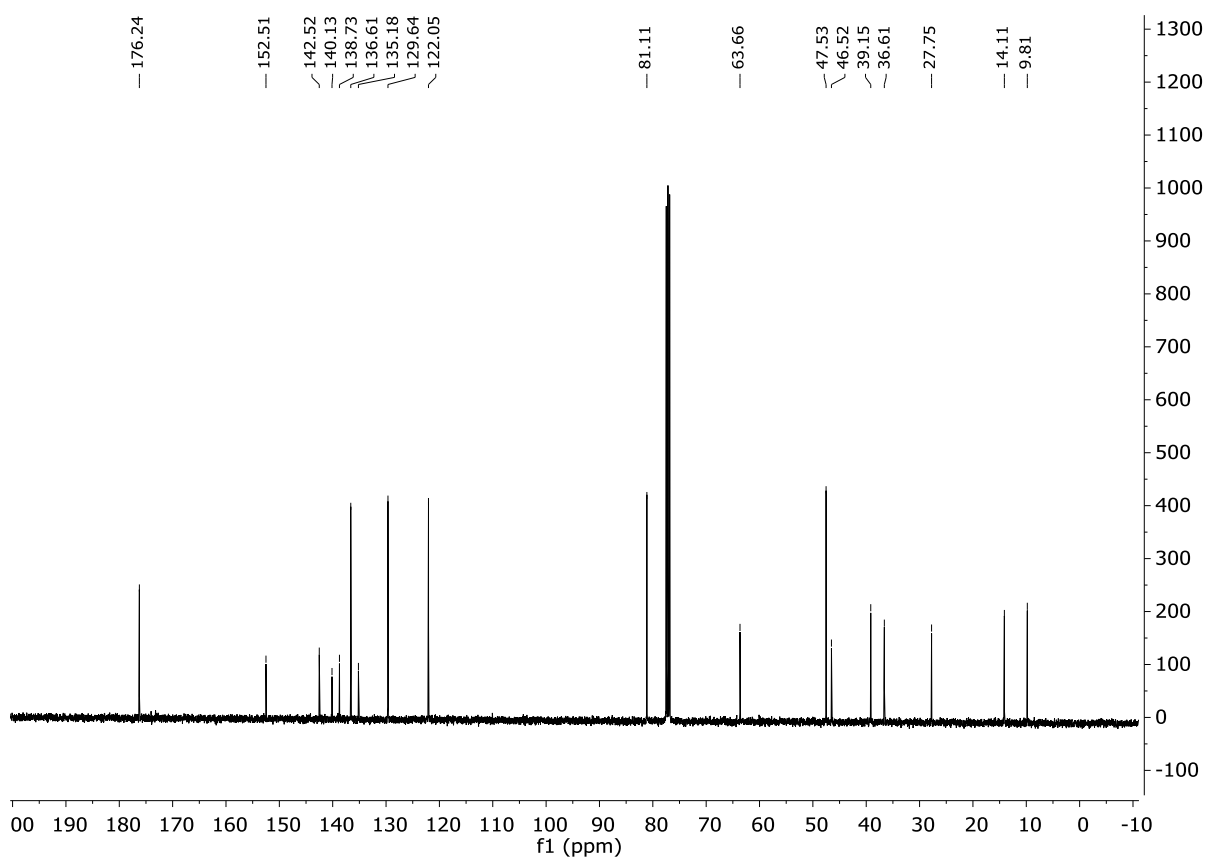
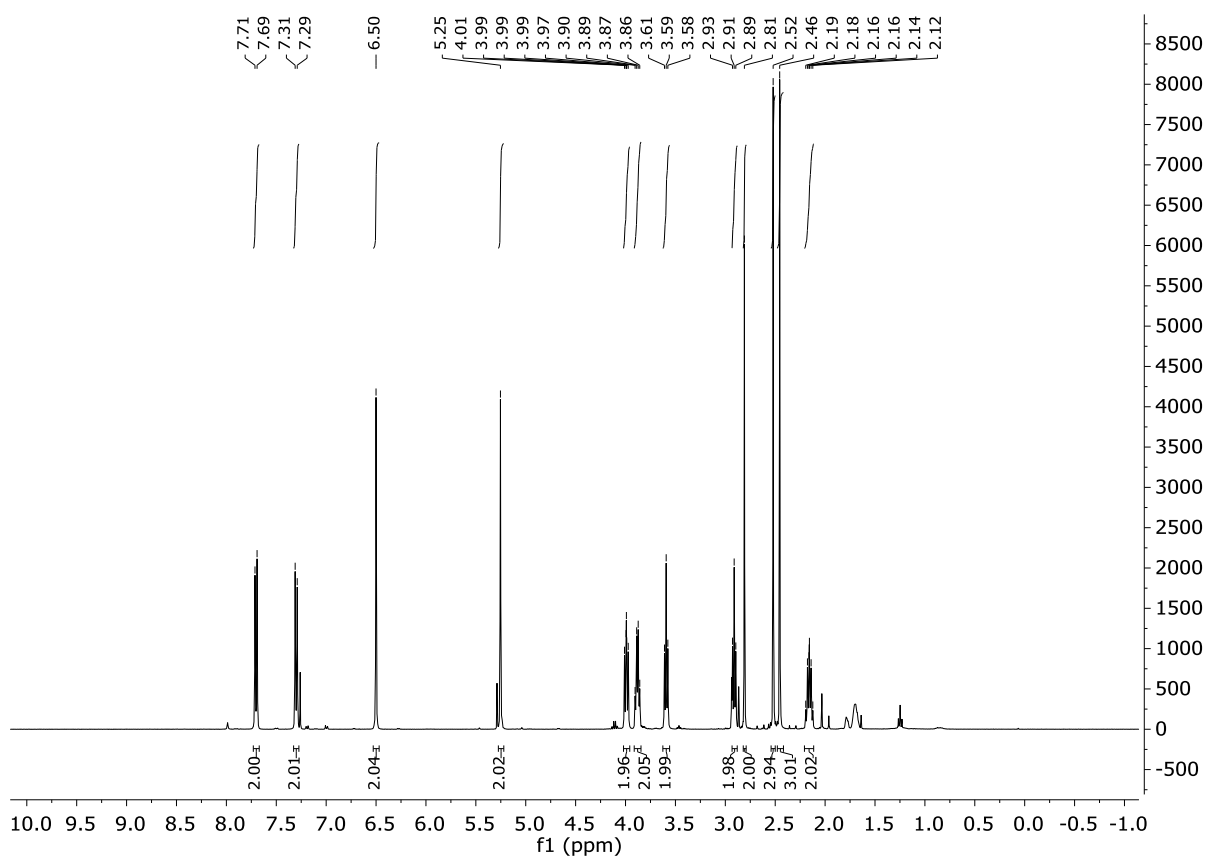
Compound 6



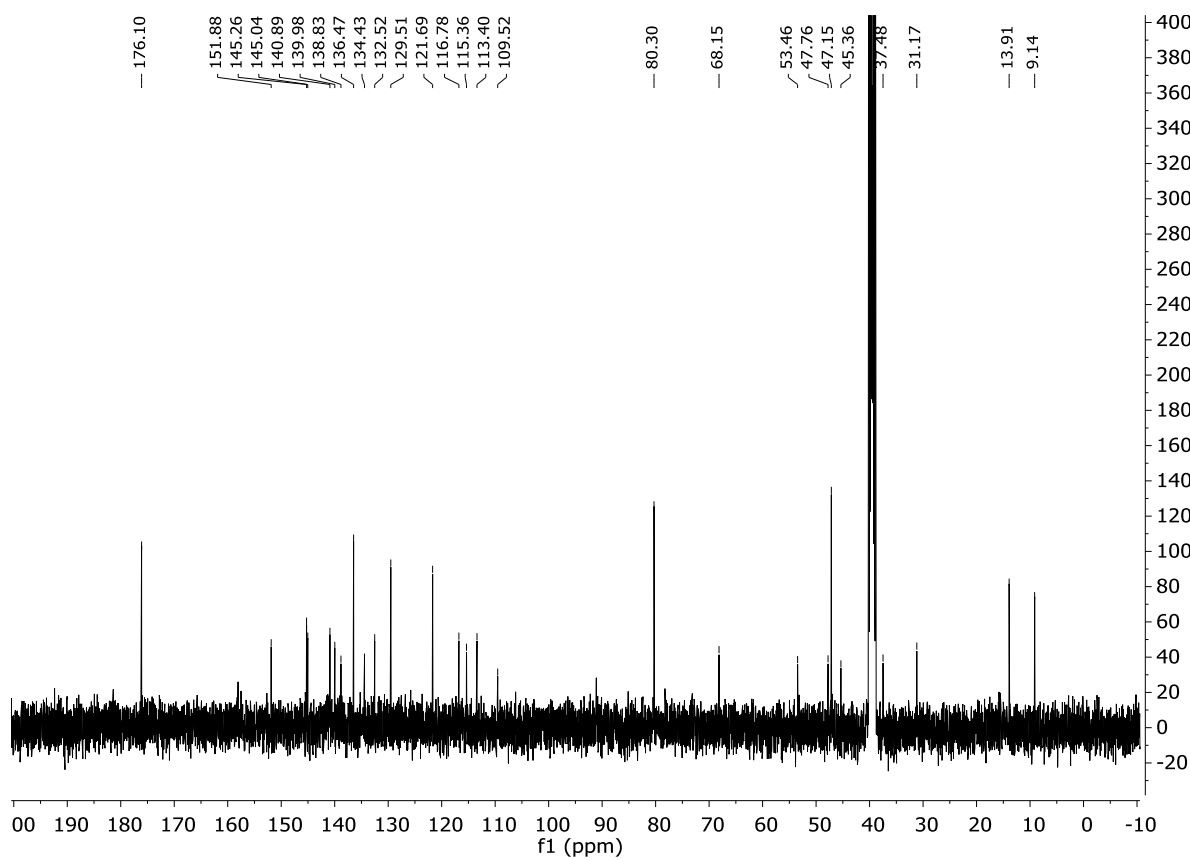
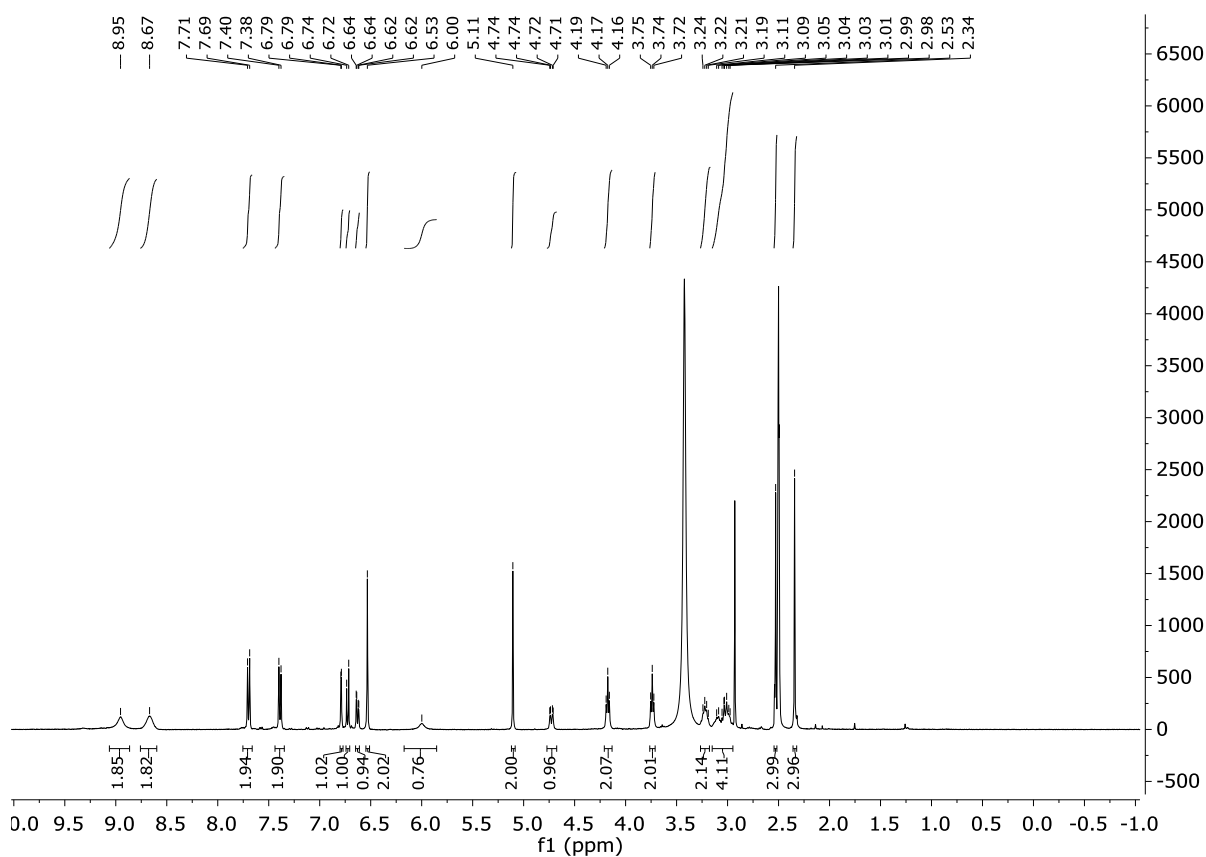
Compound 42



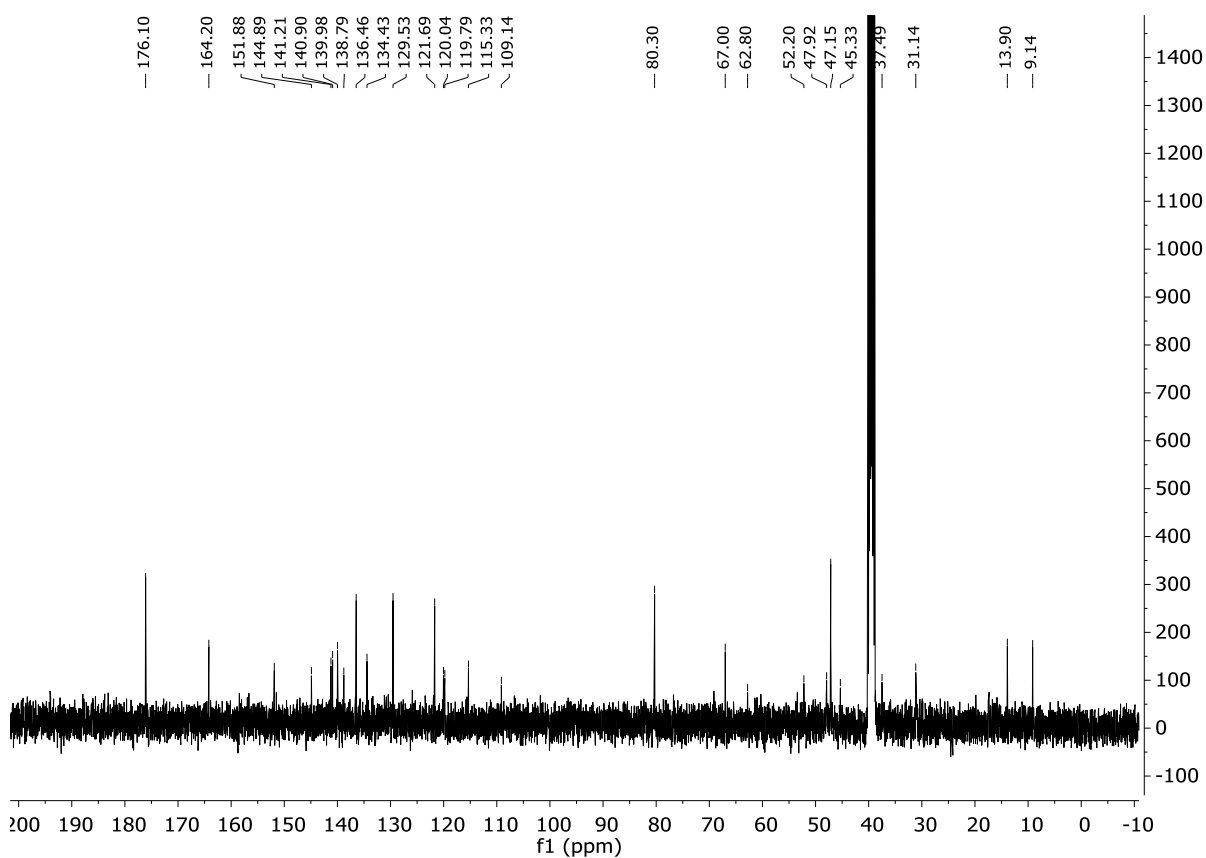
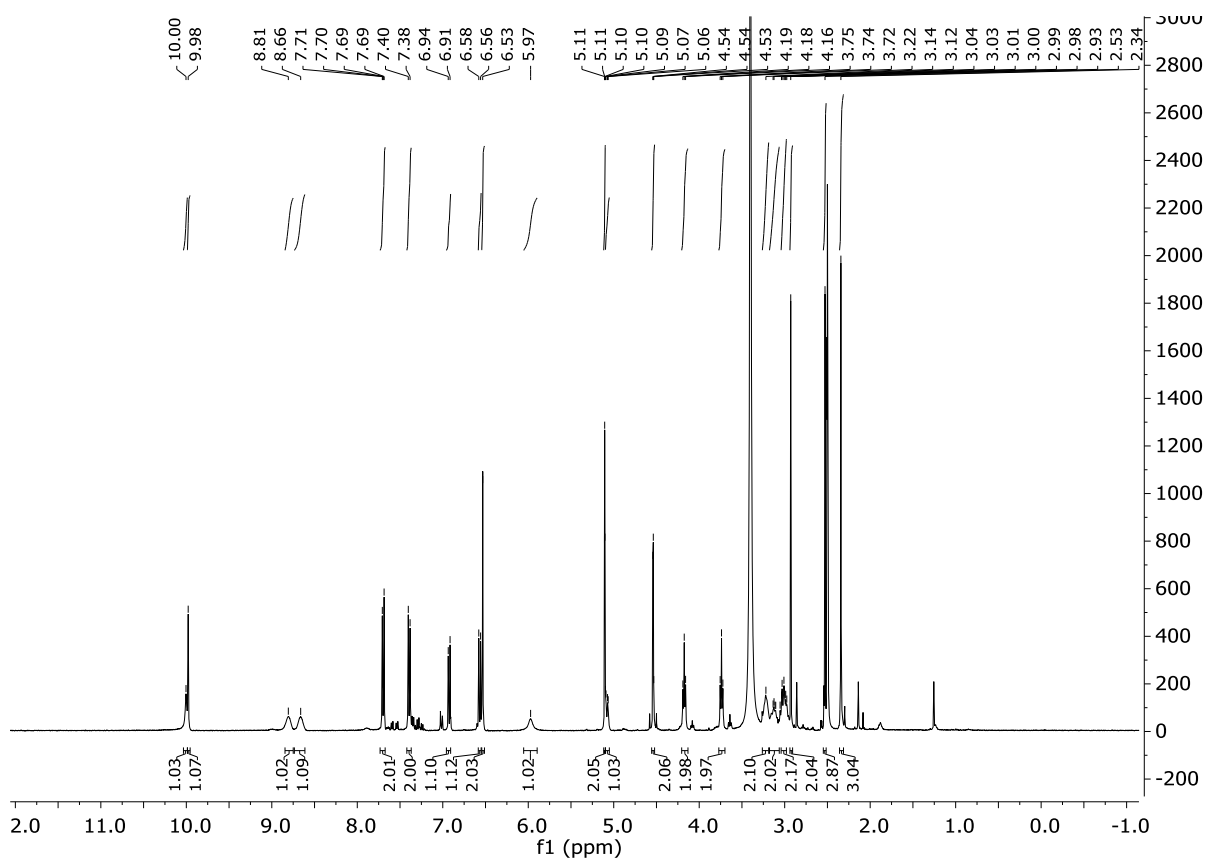
Compound 43



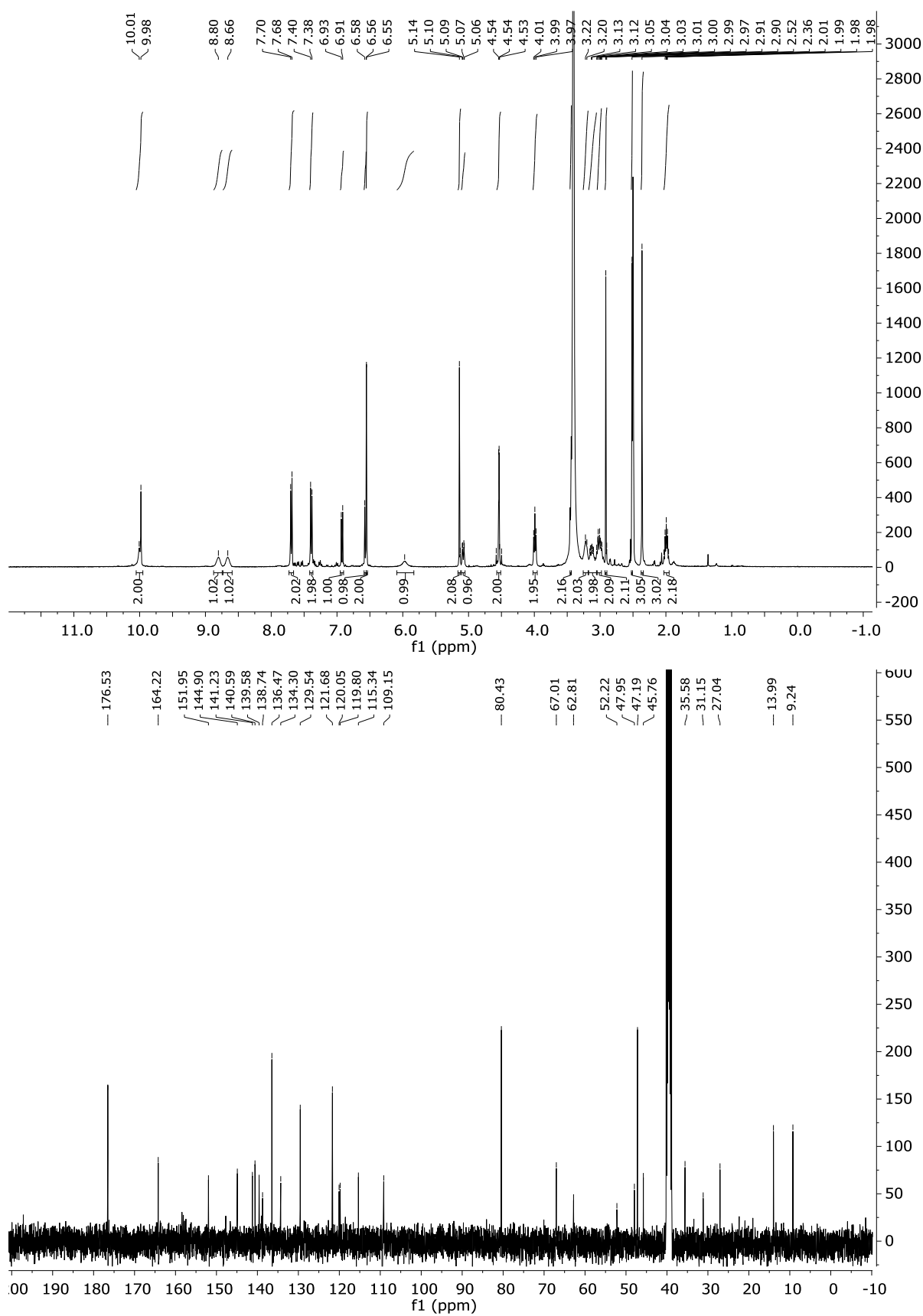
Compound 46



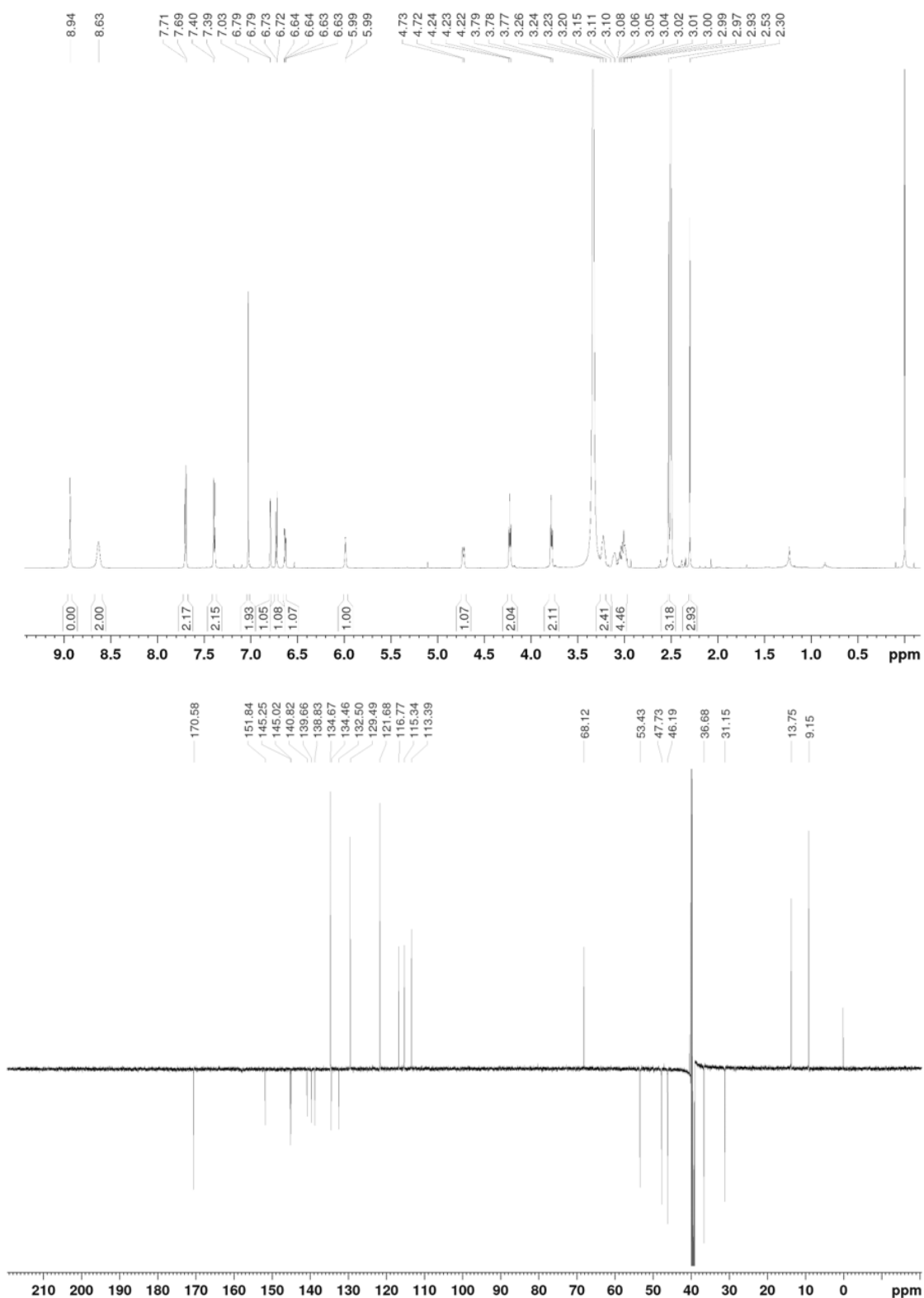
Compound 47



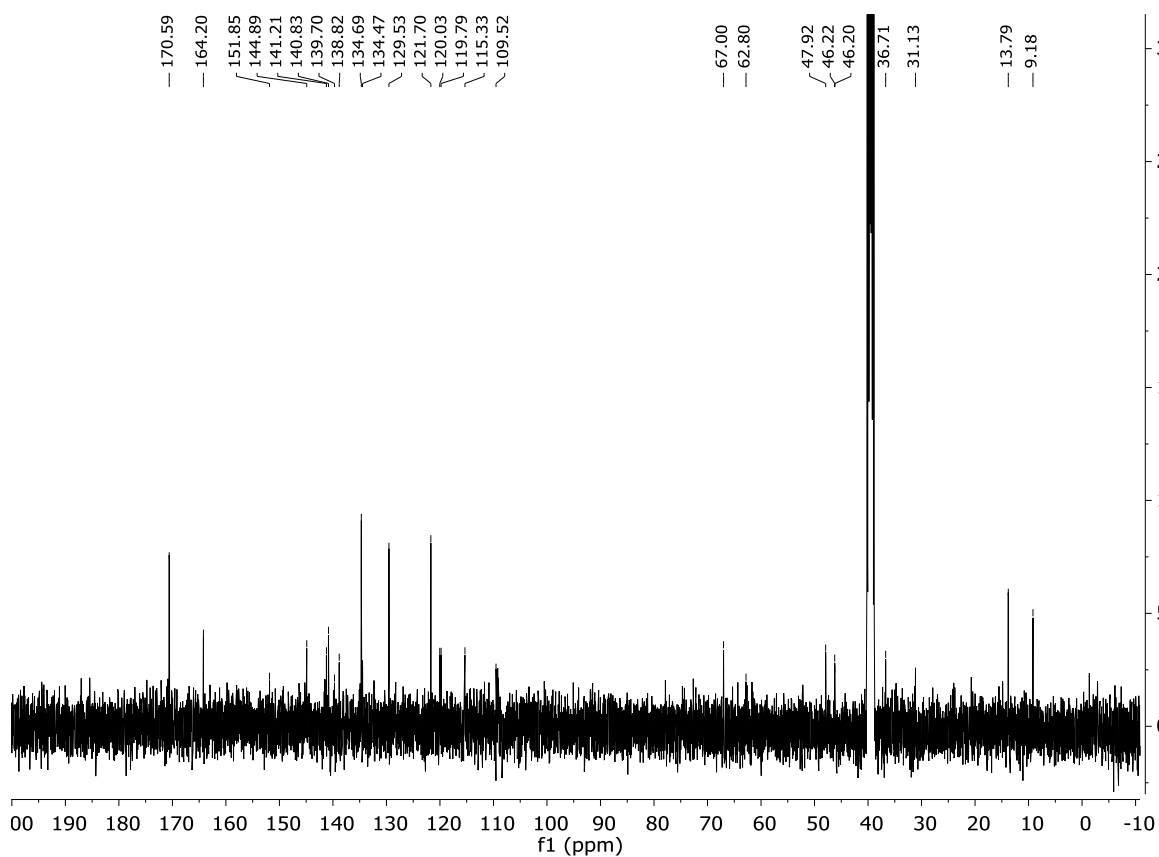
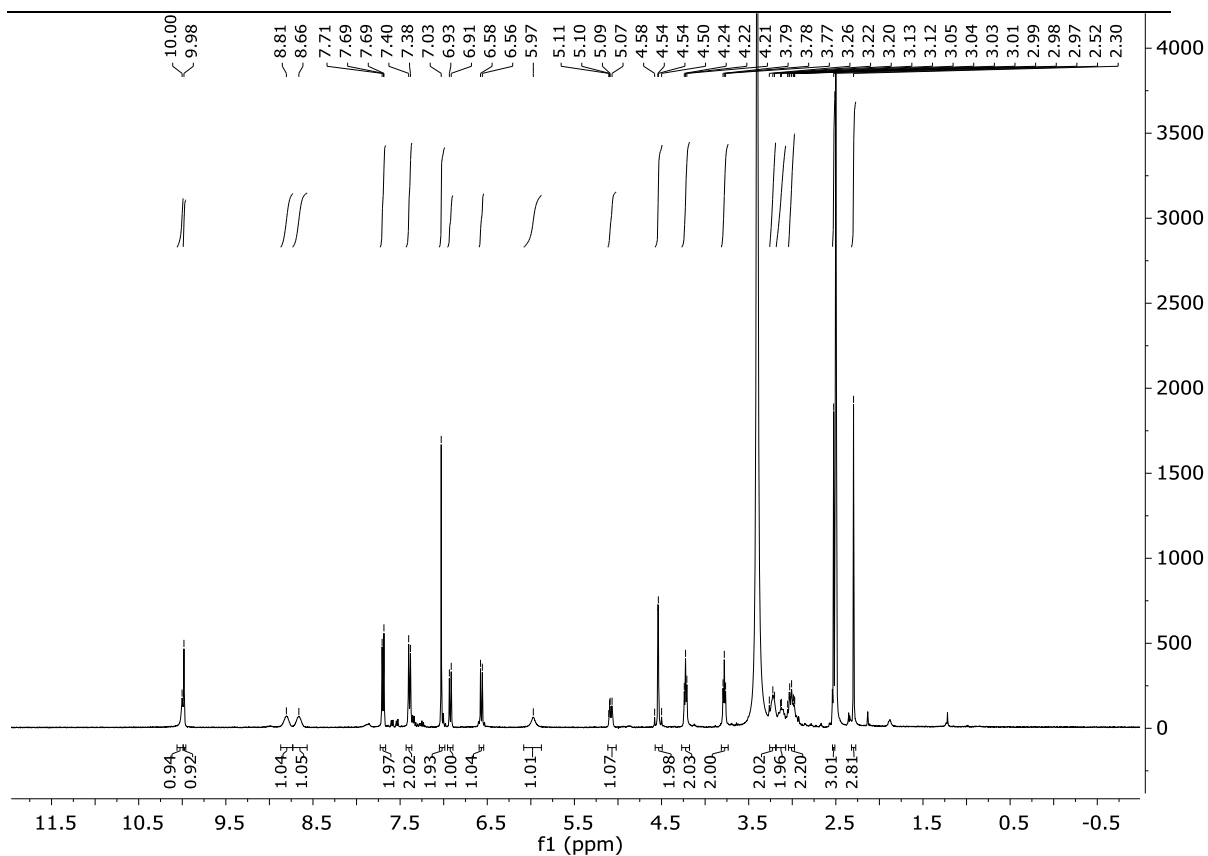
Compound 48



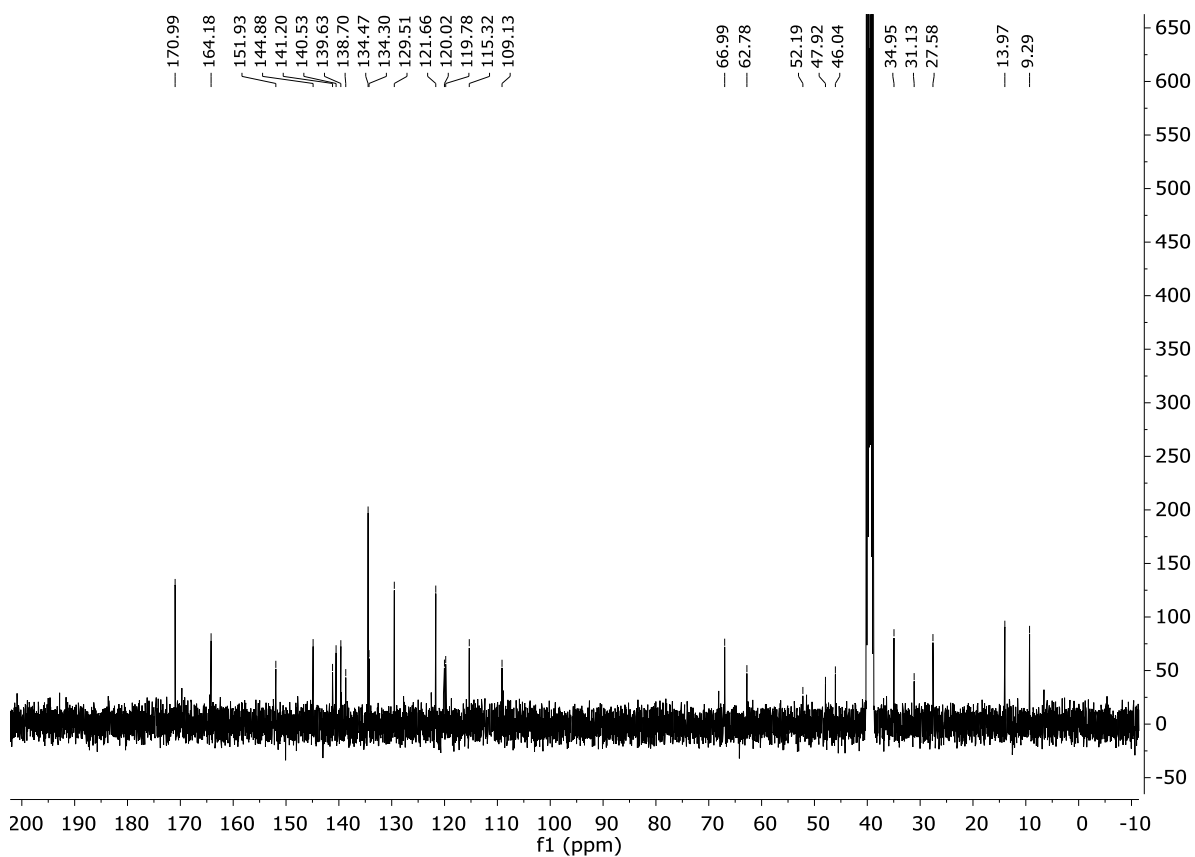
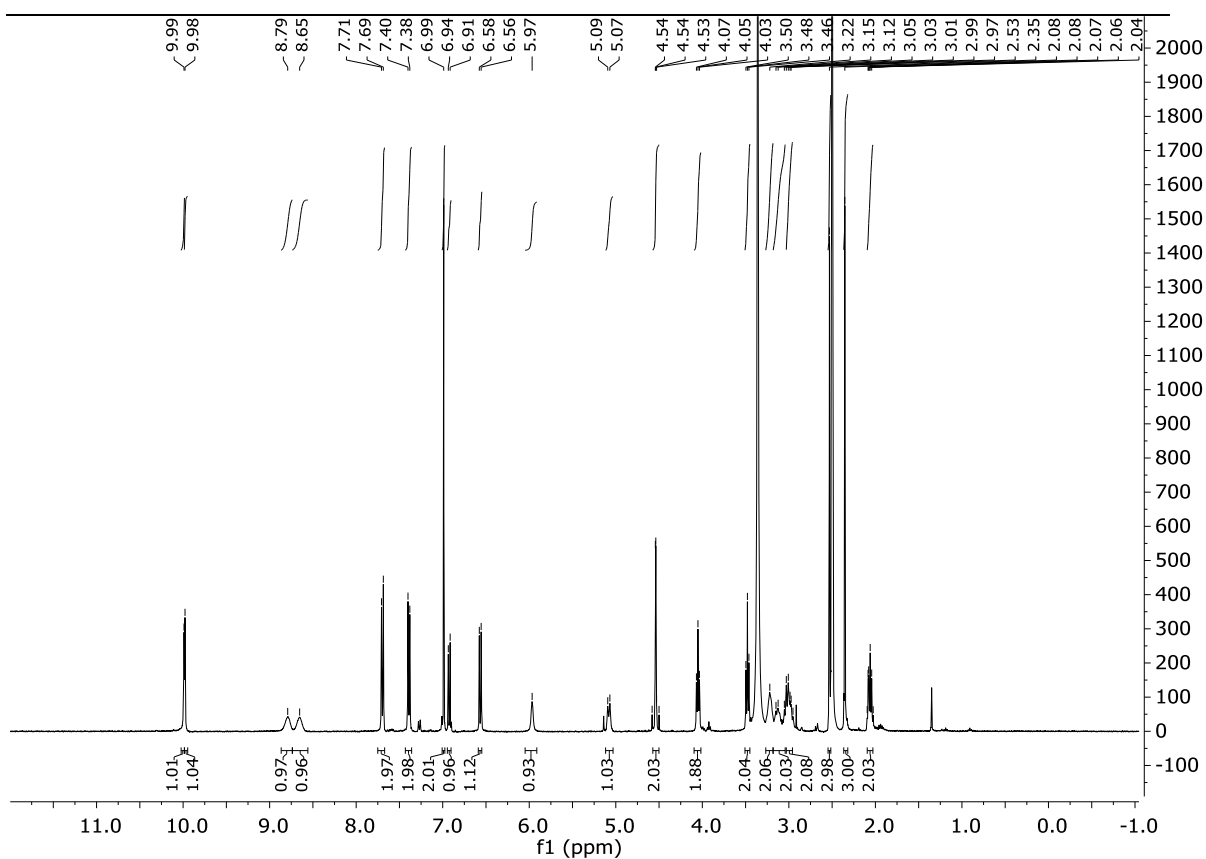
Compound 7



Compound 8



Compound 9



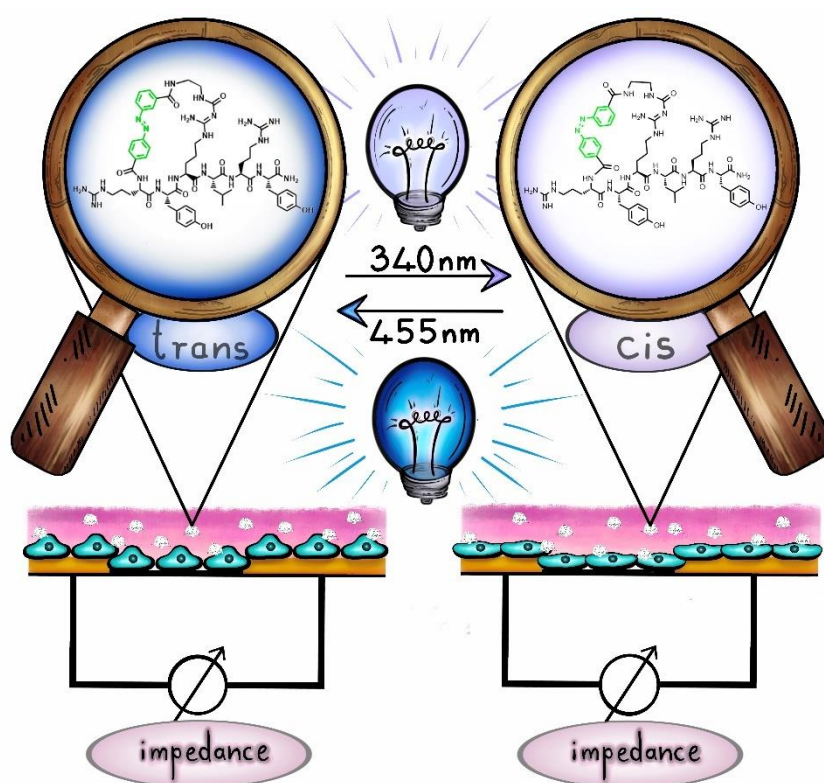
2.9 References

- [1] S. Topiol, M. Sabio, *Biochem. Pharmacol.* **2009**, *78*, 11–20.
- [2] K. A. Jacobson, S. Costanzi, *Mol. Pharmacol.* **2012**, *82*, 361–371.
- [3] J. García-Nafria, C. G. Tate, *Mol. Cell. Endocrinol.* **2019**, *488*, 1–13.
- [4] J. García-Nafria, C. G. Tate, *Biochem. Soc. Trans.* **2021**, *49*, 2345–2355.
- [5] X. Zhang, R. M. Johnson, I. Drulyte, L. Yu, A. Kotecha, R. Danev, D. Wootten, P. M. Sexton, M. J. Belousoff, *Structure* **2021**, *29*, 963–974.
- [6] M. Chen, N. V. Zaytseva, Q. Wu, M. Li, Y. Fang, *Appl. Phys. Lett.* **2013**, *102*.
- [7] Y. Fang, *Biosensors* **2015**, *5*, 223.
- [8] G. G. Gregorio, M. Masureel, D. Hilger, D. S. Terry, M. Juette, H. Zhao, Z. Zhou, J. M. Perez-Aguilar, M. Hauge, S. Mathiasen, J. A. Javitch, H. Weinstein, B. K. Kobilka, S. C. Blanchard, *Nature* **2017**, *547*, 68–73.
- [9] D. Weichert, A. C. Kruse, A. Manglik, C. Hiller, C. Zhang, H. Hubner, B. K. Kobilka, P. Gmeiner, *Proc. Natl. Acad. Sci. U. S. A.* **2014**, *111*, 10744–10748.
- [10] J. Broichhagen, J. A. Frank, D. Trauner, *Acc. Chem. Res.* **2015**, *48*, 1947–1960.
- [11] W. A. Velema, W. Szymanski, B. L. Feringa, *J. Am. Chem. Soc.* **2014**, *136*, 2178–2191.
- [12] X. Gómez-Santacana, S. M. de Munnik, P. Vijayachandran, D. Da Costa Pereira, J. P. M. Bebelman, I. J. P. de Esch, H. F. Vischer, M. Wijtmans, R. Leurs, *Angew. Chemie - Int. Ed.* **2018**, *57*, 11608–11612.
- [13] M. Schönberger, D. Trauner, *Angew. Chem. Int. Ed.* **2014**, *53*, 3264–3267.
- [14] S. Pittolo, X. Gómez-Santacana, K. Eckelt, X. Rovira, J. Dalton, C. Goudet, J. P. Pin, A. Llobet, J. Giraldo, A. Llebaria, P. Gorostiza, *Nat. Chem. Biol.* **2014**, *10*, 813–815.
- [15] M. V. Westphal, M. A. Schafroth, R. C. Sarott, M. A. Imhof, C. P. Bold, P. Leippe, A. Dhopeswarkar, J. M. Grandner, V. Katritch, K. Mackie, D. Trauner, E. M. Carreira, J. A. Frank, *J. Am. Chem. Soc.* **2017**, *139*, 18206–18212.
- [16] N. J. Hauwert, T. A. M. Mocking, D. Da Costa Pereira, A. J. Kooistra, L. M. Wijnen, G. C. M. Vreeker, E. W. E. Verweij, A. H. De Boer, M. J. Smit, C. De Graaf, H. F. Vischer, I. J. P. De Esch, M. Wijtmans, R. Leurs, *J. Am. Chem. Soc.* **2018**, *140*, 4232–4243.
- [17] D. Prischich, A. M. J. Gomila, S. Milla-Navarro, G. Sangüesa, R. Diez-Alarcia, B. Preda, C. Matera, M. Batlle, L. Ramírez, E. Giralt, J. Hernando, E. Guasch, J. J. Meana, P. Villa, P. Gorostiza, *Angew. Chem.* **2021**, *133*, 3669–3675.
- [18] A. Duran-Corbera, J. Catena, M. Otero-Viñas, A. Llebaria, X. Rovira, *J. Med. Chem.* **2020**, *63*, 8458–8470.
- [19] D. M. Rosenbaum, C. Zhang, J. A. Lyons, R. Holl, D. Aragao, D. H. Arlow, S. G. F. Rasmussen, H. J. Choi, B. T. Devree, R. K. Sunahara, P. S. Chae, S. H. Gellman, R. O. Dror, D. E. Shaw, W. I. Weis, M. Caffrey, P. Gmeiner, B. K. Kobilka, *Nature* **2011**, *469*, 236–242.
- [20] T. Schwalbe, H. Huebner, P. Gmeiner, *Bioorg. Med. Chem.* **2019**, *27*, 2959–2971.
- [21] C. E. Weston, R. D. Richardson, P. R. Haycock, A. J. P. White, M. J. Fuchter, *J. Am. Chem. Soc.* **2014**, *136*, 11878–11881.
- [22] S. G. F. Rasmussen, H. J. Choi, J. J. Fung, E. Pardon, P. Casarosa, P. S. Chae, B. T. Devree, D. M. Rosenbaum, F. S. Thian, T. S. Kobilka, A. Schnapp, I. Konetzki, R. K.

- Sunahara, S. H. Gellman, A. Pautsch, J. Steyaert, W. I. Weis, B. K. Kobilka, *Nature* **2011**, *469*, 175–181.
- [23] K. Renault, J. W. Freedy, P. Y. Renard, C. Sabot, *Bioconjug. Chem.* **2018**, *29*, 2497–2513.
- [24] J. M. J. M. Ravasco, H. Faustino, A. Trindade, P. M. P. Gois, *Chem. Eur. J.* **2019**, *25*, 43–59.
- [25] E. Buck, J. A. Wells, *Proc. Natl. Acad. Sci. U. S. A.* **2005**, *102*, 2719–2724.
- [26] M. Schmidt, Dissertation, **2022**.
- [27] R. F. Sweis, Z. Wang, M. Algire, C. H. Arrowsmith, P. J. Brown, G. G. Chiang, J. Guo, C. G. Jakob, S. Kennedy, F. Li, D. Maag, B. Shaw, N. B. Soni, M. Vedadi, W. N. Pappano, *ACS Med. Chem. Lett.* **2015**, *6*, 695–700.
- [28] J. R. Broach, J. Thorner, *Nature* **1996**, *384*, 14.
- [29] Y. Namkung, C. Le Gouill, V. Lukashova, H. Kobayashi, M. Hogue, E. Khoury, M. Song, M. Bouvier, S. A. Laporte, *Nat. Commun.* **2016**, *7*, 12178.
- [30] K. Palczewski, *Annu. Rev. Biochem.* **2006**, *75*, 743–767.
- [31] T. Okada, O. P. Ernst, K. Palczewski, K. P. Hofmann, *Trends Biochem. Sci.* **2001**, *26*, 318–324.

CHAPTER 3

3 Monitoring the Reversibility of GPCR Signaling by Combining Photochromic Ligands with Label-free Impedance Analysis



This chapter has been published as:

U. Wirth, J. Erl, S. Azzam, C. Höring, M. Skiba, R. Singh, K. Hochmuth, M. Keller, J. Wegener, B. König, *Angew. Chem.* **2023**, e202215547.

This chapter was in collaboration with the group of Dr. M. Keller (Institute of Pharmacy, University of Regensburg) and Prof. J. Wegener (Institute of Analytical Chemistry, University of Regensburg).

U. Wirth performed the synthesis and (photo-)chemical characterization of compounds **2**, **3**, **6-10**, **12**, **13**, **16-23**, **27-31**. R. Singh synthesized and characterized **24-26**, **32-34**. J. Erl performed the impedance studies, S. Azzam and M. Skiba did preliminary work on the impedance studies. C. Höring prepared the cells for the miniG_i recruitment assay and analysed the assay data. K. Hochmuth performed the ligand binding assays and the functional characterization.

U. Wirth, J. Erl, Dr. M. Keller, Prof. B. König and Prof. J. Wegener wrote the manuscript draft.

Dr. Keller, Prof. Wegener and Prof. König supervised the project.

3.1 Introduction

G protein-coupled receptors (GPCRs) form the largest family of cell surface receptors across the human body. Genes for about 800 GPCRs have been identified in the human genome.^[1] They all share the topology of seven transmembrane helices within one polypeptide chain, an extracellular ligand binding domain and an intracellular domain that transmits receptor activation by extracellular ligands into intracellular signaling cascades. Considering the number of genes encoding GPCRs, it is not surprising that they are involved in countless physiological processes and their dysfunction has been assigned to a myriad of severe diseases, such as diabetes, allergies, depression and certain forms of cancer.^[1-4] Accordingly, GPCRs are among the most highly addressed drug targets. Approximately 35% of all prescription pharmaceuticals on the market address GPCRs as agonists, antagonists or allosteric modulators.^[1]

Since the identification of new and selective ligands for specific GPCRs has gained an ever-growing interest in basic research and in drug discovery, a variety of different tools and assays has been developed that monitor or manipulate the complex interplay between ligand, receptor, and associated signal transduction either directly or indirectly. Most of them are used in combination with cultured cells (over)expressing the receptor of interest. A direct approach uses radio- or fluorescence-labeled ligands to determine the dissociation constants without disclosing whether the receptor is activated or blocked. Others probe the activation of the receptor at different stages along the intracellular signaling cascades by quantifying (second) messenger molecules, protein activation or protein-protein interactions. Genetically encoded sensors as used in protein fragment complementation or reporter gene assays have expanded the GPCR toolbox significantly in recent years. The entire pool of assays is reviewed comprehensively elsewhere.^[5-6] Most of them rely on optical readouts either via photo- or bioluminescence. A label-free alternative to monitor GPCR activation in cultured cells is based on non-invasive electrochemical impedance measurements. In these assays the cells expressing the receptor are grown on planar gold-film electrodes and the impedance is recorded at designated AC frequencies as a function of time. Due to the insulating nature of the plasma membrane, adherent cells force the current to flow around the cell bodies so that impedance readings become very sensitive to cell shape changes below the resolution of conventional light microscopy. It has been shown in the past that these kinds of impedance readings are well-suited to follow GPCR activation in real time^[7-11] even for cells with endogenous receptor

expression^[12]. Since the measurement integrates over the entire cell body, it benefits from intracellular amplification along the signaling cascades and it is often found to be more sensitive than assays reporting on molecular interactions confined to the receptor.^[13] On the downside, cell shape changes are a very generic indicator of receptor activation so that the missing molecular specificity needs to be compensated for by proper assay workflows and stringent controls.

Time-resolved impedance measurements become particularly valuable when light is used to control the activity of photochromic GPCR ligands as it avoids any interference with optical readouts. Photochromic GPCR ligands exist as two isomers that may get reversibly converted into each other upon irradiation with light of appropriate wavelengths. Ideally the two isomers provide significantly different pharmacological activities (photopharmacology) so that a precise spatio-temporal control of receptor activation becomes accessible and paves the way for external control of receptor function. Photochromic ligands have been described for a variety of GPCRs already.^[14-17] The analysis of their pharmacological activity is either conducted by endpoint assays, reporting only on receptor activation at a single time point, or by kinetic assays, continuously monitoring the status of receptor activation.^[18] Only the latter are capable of following any light-induced *in situ* switching between isomers to reveal a potential reversibility of receptor activation. Only two kinetic assays have proven their suitability for real time monitoring of photoswitching: (i) electrophysiology of G protein-coupled rectifying potassium channels (GIRK) and (ii) genetically encoded Ca²⁺ / cAMP sensors. The former are applicable to those GPCRs controlling GIRK ion channels, the latter inevitably require genetic engineering.^[18] Impedance analysis as performed in the current manuscript is not limited by these restrictions and may pave the way to real-time monitoring of photoswitchable GPCR ligands even for cells with endogenous expression of a wide variety of GPCRs.

This study presents a collection of cyclic peptide ligands targeting the Y₄ receptor, a member of the neuropeptide Y receptor family. Two different photochromic moieties based on azobenzene or arylazopyrazole have been introduced into the macrocycles providing *E/Z* isomers of each ligand. The ligands have been fully characterized with respect to their dissociation constants and agonistic activity by established assays. Impedance-based monitoring of the signaling cascade in Chinese Hamster Ovary (CHO) cells overexpressing the Y₄ receptor confirmed the individual agonistic activities of the isomers. Moreover, time-

resolved impedance profiles disclose the cellular response to receptor activation during single or repeated switching from one isomer to the other and vice versa. Our experiments suggest that isomerization of the ligands occurs in the binding pockets of the receptor rather than binding/dissociation of different isomers after photo-induced isomerization in the bulk phase. Combining photochromic GPCR ligands with real time and label-free impedance analysis significantly expands the available toolbox to directly monitor the dynamics and reversibility of GPCR signaling even in wild-type cells.

3.2 Design

The design of the photochromic ligands is based on the previously reported cyclic peptide UR-AK86c (**1**, Figure 1), showing picomolar affinity to the NPY Y₄R.^[19] In this work we synthesized photoswitchable derivatives based on this structure by incorporating the photochromic moiety either into the cyclic part or as an amino acid side chain. MD-simulations in the previous report showed that the cyclic part of UR-AK86c points towards the outside of the binding pocket giving this part of the molecule more space and freedom to alter its structure. Moreover, the cyclic part provides rigidity to the molecule so that by replacing the succinyl residue by a photoswitch that is integrated into the peptide on both sides, we hoped to see a big change in the overall structure of the molecule upon switching. Along this strategy we incorporated azobenzenes and arylazopyrazoles with different substitution patterns to create a small library of different ring sizes. As another modification strategy Tyr⁶ was replaced by the aromatic photoswitchable amino acid **16**. Since the linear C-terminus of the molecule reaches deep into the binding pocket, a change in structure could either lead to a complete loss of affinity or to a big difference between the two isomers. Furthermore, we have previously reported that a replacement of Leu⁴ by Trp led to antagonism of the linear precursor and partial agonism for the cyclic product. Therefore, **16** was incorporated in this position as well to see if switching could change the mode of action (agonism vs. antagonism). As a third modification we replaced Tyr² by **16**. When Tyr² was replaced by Trp in the original structure no affinity loss was observed, changes in that position seem to be well tolerated.^[19]

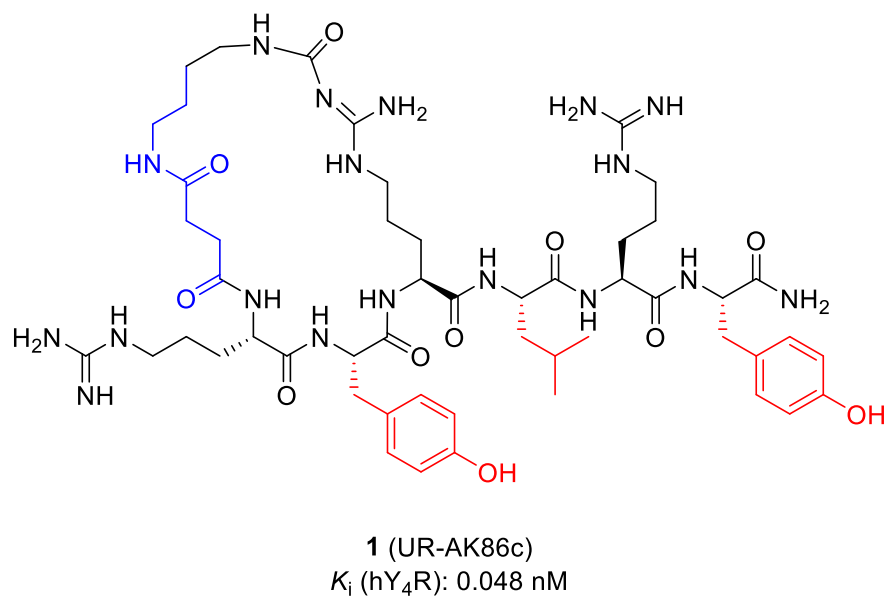
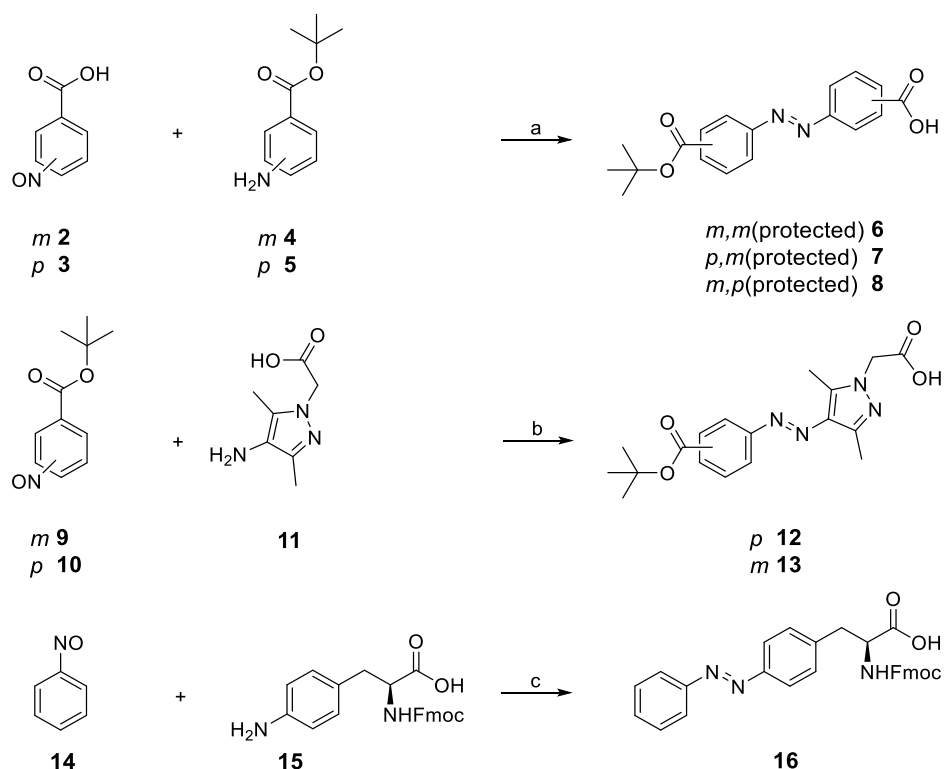


Figure 1. Structure of **1**^[19], incorporation sites for photochromic moieties **6-8**, **12** and **13** are shown in blue and for **16** in red.

3.3 Synthesis

To replace the succinyl moiety in the macrocycle, azobenzenes **6-8** and arylazopyrazoles **12** and **13** were prepared according to Scheme 1 providing a free and a protected carboxylic acid and an individual substitution pattern. Therefore, the nitroso compounds **2**, **3**, **9** and **10** were synthesized from the corresponding amines in an oxidation reaction with oxone by a literature known reaction.^[20] The Mills reaction that yielded the azobenzenes **6-8** was conducted in acetic acid over four days. For the preparation of the arylazopyrazoles **12** and **13**, the Mills reaction was performed under alkaline conditions in dichloromethane and triethylamine. The unnatural photoswitchable amino acid **16** was also synthesized in a Mills reaction. Starting from the amino-phenylalanine **15** and nitrosobenzene **14** the photoswitchable derivative of Fmoc-protected phenylalanine **16** was synthesized (Scheme 1).^[21]



Scheme 1. Synthesis of photoswitches **6-8**, **12**, **13** and **16**. Reagents and conditions: a) acetic acid, rt, 4 d, 22-25%, b) CH_2Cl_2 , NEt_3 , rt, 3 h, 10-57%, c) acetic acid, rt, 24 h, 59%.

The N^ω -carbamoylated arginine building blocks **17** and **18** (Figure 2), containing a dimethylene (**17**) or a tetramethylene (**18**) spacer, were used in solid phase peptide synthesis (SPPS) to incorporate the respective N^ω -carbamoylated arginine in position 3 in the hexapeptides. The original linker length of four carbons in **1** was shortened to two carbons for the incorporation of **6-8**, **12** and **13** to keep the ring size closer to the parental compound **1**. Compounds **17** and **18** were synthesized using previously reported procedures (Scheme S1).^[22]

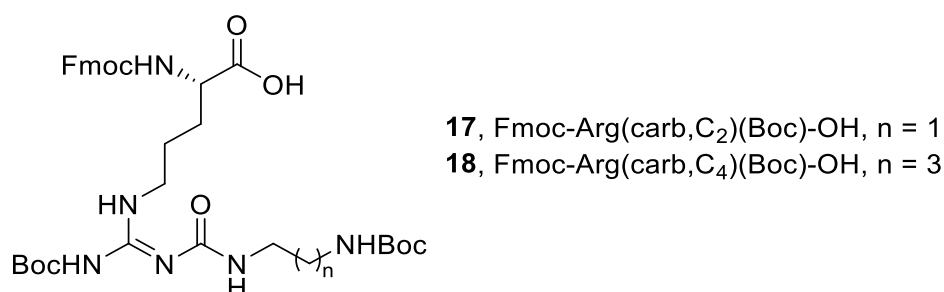
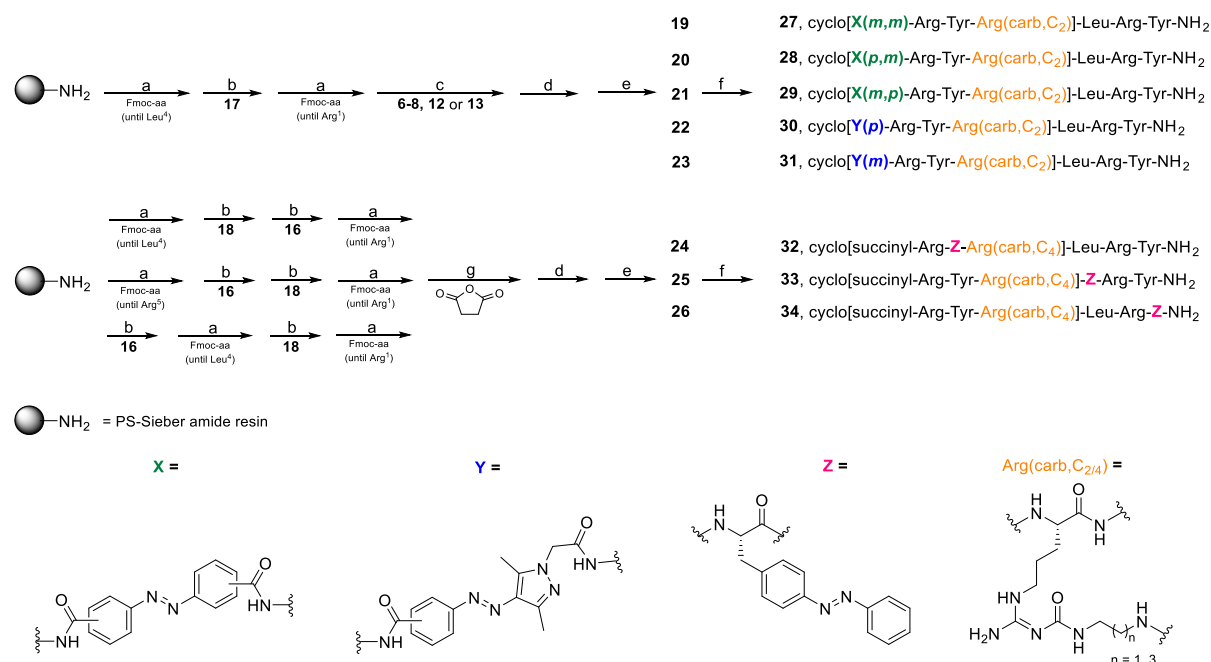


Figure 2. Structures of N^ω -carbamoylated arginine building blocks **17** and **18**.

The linear peptides **19-26**, precursors for the cyclic peptides **27-34**, were synthesized by Fmoc strategy SPPS using a Sieber amide resin (Scheme 2). 2-(1*H*-Benzotriazol-1-yl)-1,1,3,3-tetramethyluronium hexafluorophosphate (HBTU)/hydroxyl-benzotriazole (HOBt)/*N,N*-diisopropylethylamine (DIPEA) were used as coupling reagents for the natural amino acids as well as for the unnatural amino acids **16-18**. For the photoswitches **6-8**, **12** and **13**, benzotriazol-1-yloxytripyrrolidino-phosphonium hexafluorophosphate (PyBOP)/HOBt/DIPEA were used as coupling reagents. The natural amino acids were used in a “double coupling”, i.e. every coupling step was performed twice in 5-fold excess for 45 min at 35 °C. A “single coupling”, using 3-fold excess overnight at 35 °C, was applied for the unnatural amino acids **16-18** and photoswitches **6-8**, **12** and **13**. After the final Fmoc deprotection, either of the photoswitches **6-8**, **12** or **13** was coupled to the peptide. For peptides **24-26**, containing the photoswitch in the amino acid side chain, the resin was treated with succinic anhydride. Cleavage from the resin was achieved using a mixture of trifluoro acetic acid (TFA)/CH₂Cl₂ (1:3), followed by side chain deprotection using TFA/CH₂Cl₂ (1:1) and purification by preparative high performance liquid chromatography (HPLC) yielding the linear peptides **19-26**. The cyclization of the peptides was conducted in solution not exceeding a peptide concentration of 5 mM. The amide bond was formed between the primary amine of the N^ω-carbamoylated arginine residue and the carboxylic acid of the N-terminally attached photoswitchable moiety (**19-23**) or the N-terminal succinyl group (**24-26**). PyBOP/HOBt/DIPEA was used as coupling reagent and the reaction mixture was stirred at room temperature for 24 h. Purification of the final peptides was performed using preparative HPLC.



Scheme 2. Solid phase peptide synthesis. Reagents and conditions: a) peptide elongation, amino acid coupling: Fmoc-amino acid/HBTU/HOBt/DIPEA (5/5/4.9/10 eq.), DMF/NMP (8:2), 35 °C, 2 × 45 min (“double coupling”), Fmoc deprotection: 20% piperidine in DMF/NMP (8:2), rt, 2 × 10 min; b) **16-18**/HBTU/HOBt/DIPEA (3/3/2.95/6 eq.), DMF/NMP (8:2), 35 °C, 24 h (“single coupling”), Fmoc deprotection: 20% piperidine in DMF/NMP (8:2), rt, 2 × 10 min; c) photoswitches **6-8**, **12** or **13**/PyBOP/HOBt/DIPEA (3/3/3/6 eq.), DMF/NMP (8:2), 35 °C, 24 h (“single coupling”), Fmoc deprotection: 20% piperidine in DMF/NMP (8:2), rt, 2 × 10 min; d) cleavage from resin: TFA/CH₂Cl₂ (1:1), rt, 5 h, overall yields of linear peptides **19-26** after SPPS: 7-24%; f) PyBOP/HOBt/DIPEA (5/5/10 eq.), DMF/NMP (8:2), rt, 24 h, cyclization yields: 30-76%; g) succinic anhydride/DIPEA (10/10 eq.), DMF/NMP (8:2), 35 °C, 30 min.

3.4 Photophysical Characterization

The photophysical properties of all cyclic photoswitchable peptides and the linear peptides **20** and **25** were investigated in aqueous buffer to mimic physiological conditions. All compounds were switched to their *Z* isomers by irradiation at a wavelength of 340 nm. Whereas compounds **20**, **25**, **27-29** and **32-34**, containing an azobenzene, were switched back to the *E* isomer at a wavelength of 455 nm, arylazopyrazoles **30** and **31** were switched back to *E* by using light of a longer wavelength (528 nm) due to a slightly red-shifted absorption spectrum. Switching back and forth over several cycles showed that the compounds exhibit high fatigue resistance. No decomposition or side reactions seem to take place upon irradiation (Figure 3).

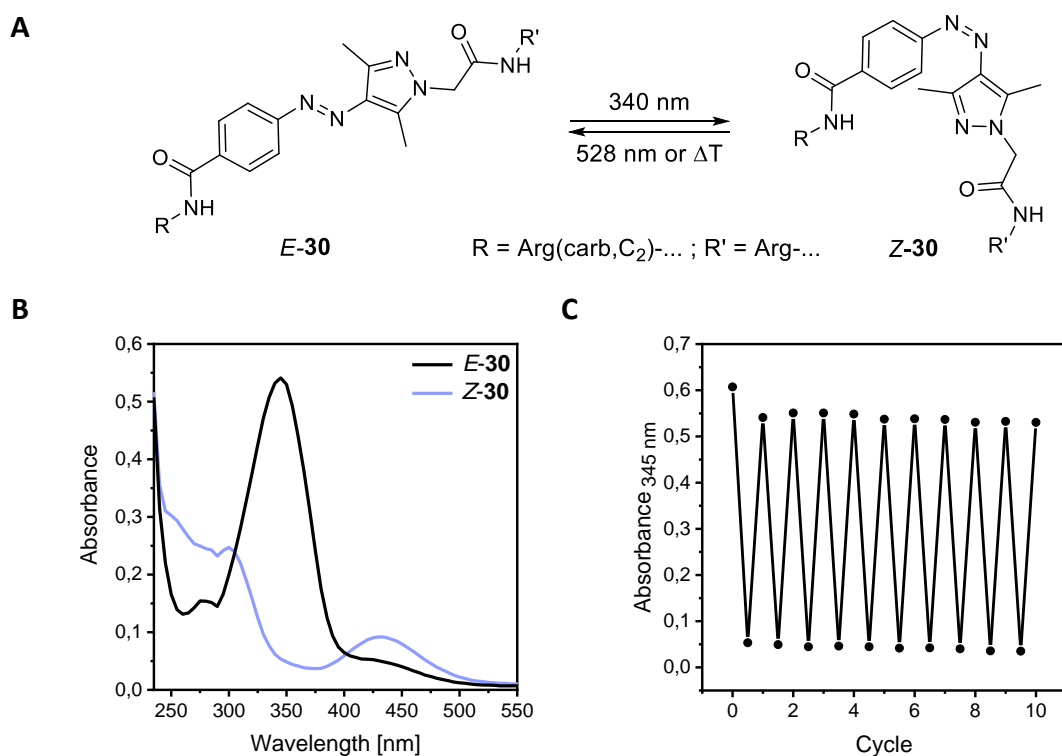


Figure 3. (A) Light-induced *E/Z* photoisomerization of **30**. (B) UV/Vis spectra of both isomers of compound **30**. (C) Cycle performance of compound **30** (20 μ M) in HEPES buffer (25 mM HEPES, 2.5 mM CaCl_2 , 1 mM MgCl_2 , pH = 7.4) + 0.1% DMSO. This compound is shown here as a representative. Compounds **20**, **25** and **27-34** showed similar photophysical properties (Figures S12-S21).

Furthermore, all photochromic peptides showed high photostationary states (PSS) when switched to the *Z* isomer ($\geq 90\%$). Switching back to the *E* isomer worked best for the arylazopyrazoles **30** and **31** with around 90%. Peptides **20**, **25**, **27-29** and **32-34** containing an azobenzene moiety could be switched back to the *E* isomer with 74-88%.

Thermal half-lives ($t_{1/2}$), describing how fast the thermal back-isomerization to the *E* isomer occurs, ranged between 7.5 and 52 days, which ensures that during the time required for the biological assays back-isomerization is not significant. Table 1 summarizes the photophysical properties of the photoswitchable peptides.

Table 1. Summary of experimental photophysical properties.^[a]

Compound	$t_{1/2}$ [d] ^[b]	PSS ($E \rightarrow Z$) ^[c]	PSS ($Z \rightarrow E$) ^[c]
20	13.3	90%	88%
27	31.5	95%	74%
28	23.7	92%	78%
29	22.6	91%	78%
30	7.5	94%	91%
31	52	97%	90%
32	9.3	92%	78%
25	9.4	94%	81%
33	12.6	94%	78%
34	9.8	94%	75%

[a] All Z isomers were obtained by irradiation with 340 nm. Irradiation using (i) 455 nm yielded the E isomers of **20**, **25**, **27-29**, **32-34** or (ii) 528 nm providing the E isomers of **30** and **31**. Concentration: 20 μ M in HEPES buffer (25 mM HEPES, 2.5 mM CaCl₂, 1 mM MgCl₂, pH = 7.4) + 0.1% DMSO. [b] Pre-irradiation to saturation with 340 nm. [c] PSS determination was done by analytical HPLC using UV/Vis detection at the individual isobestic points.

3.5 Ligand Binding and Functional Characterization

In the following paragraphs the term “E-isomer” refers to the ratio of isomers after irradiating the compound in thermal equilibrium with 455 nm and 528 nm, respectively. The term “Z-isomer” refers to the ratio of isomers after irradiating the compound in thermal equilibrium with 340 nm. To ensure the optimized ratio for each individual isomer in binding studies and functional assays, the compounds were always pre-illuminated with the corresponding wavelength. Assays were performed immediately afterwards in the dark.

The photochromic peptides **20**, **25** and **27-34** were investigated with respect to their Y₄R binding affinity by radioligand competition binding yielding pK_i values (Table 2). The incorporation of a photoswitchable moiety was well tolerated and binding affinities were still in the sub- to low-nanomolar range with **25** and **34** being the only exceptions. It was observed that for peptides **27-31**, with the photoswitch integrated in the cyclic part, the Z-isomers exhibited higher Y₄R affinities (lower K_i values) compared to their E-isomers. **Z-27** and **Z-30** showed the highest affinities, similar to the endogenous ligand human pancreatic polypeptide (hPP) and to **1**. Compound **28** displayed the biggest difference between the E and Z isomer

with an almost 10-fold difference in binding affinity (Figure 4A). In contrast, the *E*- and *Z*-isomer of its precursor **20** exhibited identical Y₄R affinities. The isomers of **27**, **30** and **31** exhibited seven- to eight-fold differences in Y₄R binding. Selected compounds were also subjected to radioligand competition binding studies for the NPY receptor subtypes Y₁, Y₂ and Y₅ (Table S1) revealing a clear selectivity for the Y₄R.

Moreover, the ligands were investigated in a miniG_i protein recruitment assay to study their capability of activating the Y₄R. A split-luciferase-based miniG_i protein sensor was recently reported as a tool to characterize ligands for histamine receptors.^[23] The Luciferase (NLuc) used for the histamine sensor shows a maximum emission around 470 nm. As the light emitted by NLuc may induce *cis*- to *trans*-isomerization under assay conditions for some of the ligands studied here, we developed a Y₄R split-luciferase miniG_i recruitment assay based on the click beetle red luciferase (CBR) with an emission maximum around 615 nm. Due to its broad emission spectrum, partial isomerization of the photochromic Y₄-peptides caused by CBR emission has to be considered. In order to keep the influence of CBR-induced photoisomerization as low as possible, dose-response curves were established based on the maximum of the signal time courses instead of using the area under the curve (AUC). The former were observed approximately 4 to 7 minutes after agonist addition, whereas the AUC integration is typically extended beyond the signal maximum and thereby increases the impact of CBR-induced back-isomerization (Figure S56). For comparison, compound **28** was studied in the NLuc-based and the CBR-based miniG_i recruitment assay. Whereas **E-28** exhibited a 5-fold lower potency than **Z-28** in the CBR-based miniG_i assay, the difference was less pronounced (2.5-fold) in the NLuc assay (Figure S54) indicating that NLuc-emitted light ($\lambda_{\max} \approx 470$ nm) may cause, to some extent, a back-isomerization from *Z* to *E*. All compounds were found to behave as partial agonists of the Y₄R in the CBR-based miniG_i recruitment assay, like the parental compound **1**.^[19] The arylazopyrazoles **30** ($\Delta E_{\max} = 38\%$) and **31** ($\Delta E_{\max} = 27\%$) and the peptide with the photoswitchable amino acid sidechain in position 4 (**33**, $\Delta E_{\max} = 39\%$) revealed the largest differences in efficacy (Table 2). Consistent with the results found in the binding studies, *Z*-isomers of **27-31** were more potent than their correspondent *E*-isomers. In contrast, peptide **33** displayed a higher potency in its *E*-configuration. Whereas peptides **27-31** exhibited slightly lower potencies than the endogenous ligand hPP, **33** and **34** showed a drastically reduced potency. The differences in EC₅₀ values between *E*- and *Z*-isomer were less pronounced than the differences in K_i values (Table 2). With a 5-fold difference in EC₅₀ values,

peptide **28** displayed the most pronounced change in potency for its two isomers, followed by **31** with an approximately 4-fold difference (**34** is not considered here because of the low potency and efficacy). The discrepancies between K_i values and EC_{50} values may be due to the absence or presence of sodium ions in the buffer composition used for binding and functional assays, respectively, as has been discussed previously.^[24,25] In addition to miniG_i recruitment assays, the *E*- and *Z*-isomer of **28** were also studied in a Ca²⁺ aequorin assay, measuring intracellular calcium mobilization upon Y₄R activation. In this functional assay **Z-28** also proved to be more potent than **E-28** by a factor of 3. However, compared to the data from the Y₄R CBR miniG_i recruitment assay, the efficacies were considerably lower (Figure S55). Likewise, the potencies were slightly lower, which is most likely due to the strong non-equilibrium character (rapid cellular response) of the Ca²⁺ assay.

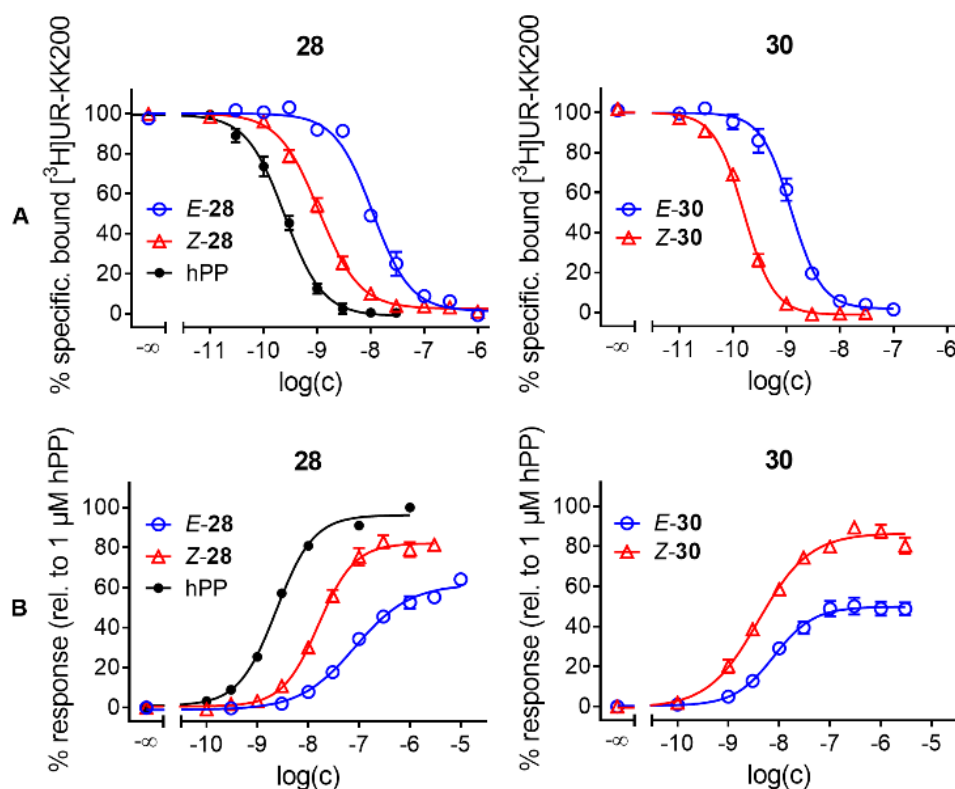


Figure 4. (A) Radioligand displacement curves and (B) Dose-response curves of both isomers of **28**, **30** and hPP (black) established from CBR miniG_i recruitment assays. For binding and dose-response curves of **20**, **25**, **27**, **29** and **31-34** see Figures S51 and S52. Data represent mean \pm SEM from at least three independent experiments performed in triplicate.

Table 2. Y₄R affinities (pK_i, K_i), Y₄R potencies (pEC₅₀) and efficacies (E) relative to hPP for *E/Z* isomers of compounds **20**, **25** and **27-34**. All *Z*-isomers were obtained by irradiation with 340 nm, whereas the *E*-isomers were obtained by irradiation using 455 nm or 528 nm, respectively.

	Y ₄ R binding ^[a]		Y ₄ R agonism ^[b]		
	pK _i ± SEM / K _i (nM)		pEC ₅₀ ± SEM / EC ₅₀ (nM)		
			efficacy E ± SEM (%)		
hPP	10.02 ± 0.06 / 0.10		8.59 / 2.6		100
<i>E</i>-20	9.76 ± 0.01 / 0.17		8.11 ± 0.06 / 7.8		77 ± 3
<i>Z</i>-20	9.74 ± 0.05 / 0.18		7.89 ± 0.06 / 13		81 ± 1
<i>E</i>-27	9.21 ± 0.02 / 0.62		7.95 ± 0.02 / 11		76 ± 5
<i>Z</i>-27	10.04 ± 0.05 / 0.09		8.47 ± 0.04 / 3.4		88 ± 3
<i>E</i>-28	8.37 ± 0.04 / 4.3		7.08 ± 0.02 / 84		62 ± 2
<i>Z</i>-28	9.35 ± 0.05 / 0.45		7.79 ± 0.04 / 16		83 ± 3
<i>E</i>-29	9.16 ± 0.09 / 0.73		7.88 ± 0.03 / 13		73 ± 3
<i>Z</i>-29	9.86 ± 0.02 / 0.14		8.29 ± 0.05 / 5.1		82 ± 1
<i>E</i>-30	9.31 ± 0.06 / 0.50		8.08 ± 0.06 / 8.3		50 ± 3
<i>Z</i>-30	10.19 ± 0.03 / 0.066		8.40 ± 0.06 / 4		88 ± 2
<i>E</i>-31	9.03 ± 0.04 / 0.94		7.65 ± 0.06 / 23		48 ± 3
<i>Z</i>-31	9.94 ± 0.03 / 0.11		8.21 ± 0.02 / 6.3		75 ± 2
<i>E</i>-32	9.58 ± 0.08 / 0.27		8.09 ± 0.06 / 8.2		82 ± 2
<i>Z</i>-32	9.81 ± 0.045 / 0.16		8.16 ± 0.04 / 7		81 ± 2
<i>E</i>-25	7.17 ± 0.07 / 69		n.d.		n.d.
<i>Z</i>-25	6.61 ± 0.09 / 260		n.d.		n.d.
<i>E</i>-33	8.76 ± 0.09 / 1.8		6.70 ± 0.13 / 201		78 ± 9
<i>Z</i>-33	8.07 ± 0.09 / 8.9		6.07 ± 0.04 / 849		39 ± 2
<i>E</i>-34	7.30 ± 0.05 / 51		5.72 ± 0.17 / 1914		32 ± 2
<i>Z</i>-34	7.98 ± 0.07 / 11		6.40 ± 0.04 / 397		12 ± 1

[a] Determined by competition binding with [³H]UR-KK200 (K_d = 0.67 nM, p⁴ c = 1 nM) at CHO-hY₄R-mtAEQ-Gq₅ cells. [b] Determined in a miniG_i protein recruitment assay performed with HEK293T-CBRN-mG_{si}/Y₄R-CBRC cells. Efficacies E were determined relative to the effect of 1 μM hPP. Data represent mean values from at least three independent experiments performed in triplicate (standard error of the mean (SEM) given for pK_i, pEC₅₀ and α values). n.d.: not determined.

3.6 Impedance-Based Analysis of Y₄R Activation

Both isomers of compounds **28** and **30** were analysed by time-resolved impedance measurements with respect to the response of adherent CHO cells overexpressing the Y₄ receptor. These two compounds belong either to the azobenzene (**28**) or arylazopyrazole (**30**) family of photoswitches used in this study. In these experiments the cells were grown to confluence in 96-well plates with integrated, planar gold-film electrodes in every well. The impedance magnitude $|Z|$ was recorded at an AC frequency of 12 kHz using non-invasive voltage amplitudes (40 mV) to induce a weak AC current in the μA range. As has been shown previously, activation of GPCR signalling cascades are readily monitored by the impedance time course that mirrors the associated changes in cell morphology.^[10-12] Figure 5 summarizes a typical experiment using **E-30**, **Z-30** (1 nM), the endogenous ligand hPP (100 nM) and a vehicle control (DMSO, 0.01% v/v). The impedance magnitudes of the individual electrodes have been zeroed to the impedance of the cell-covered electrodes immediately before adding the agonists.

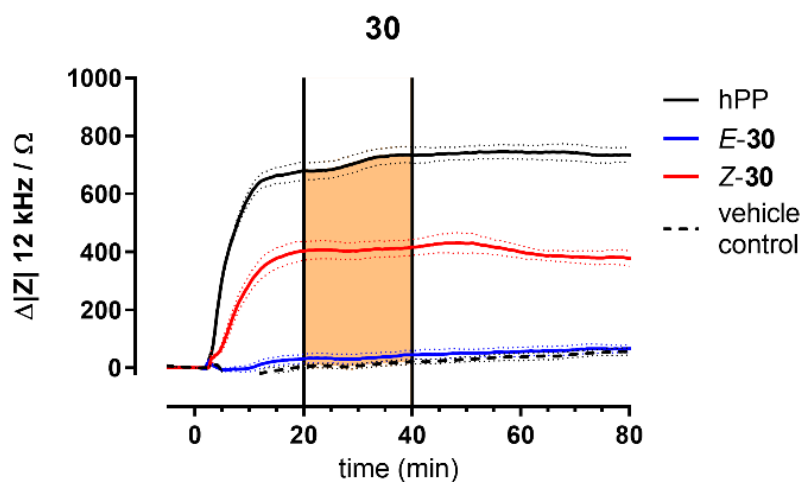


Figure 5. Typical impedance time courses at an AC frequency of 12 kHz along the stimulation of CHO-Y₄R cells with different agonists (blue: **E-30**, red: **Z-30**, $c = 1.0$ nM; solid black: hPP, $c = 100$ nM, dashed black: vehicle control DMSO, 0.01% v/v). Impedance magnitude $|Z|$ was zeroed immediately before agonist addition. Vertical lines at $t = 20$ min and $t = 40$ min indicate limits of integration used to determine the area under the curve (AUC, orange box). Cells were pre-stimulated with forskolin (0.4 μM) for 30 min (not shown). Mean \pm SEM ($n=3$).

In these experiments **30** was irradiated with light of 528 nm or 340 nm to yield **E-30** or **Z-30**, respectively, prior to cell exposure. Saturating the receptor with the endogenous ligand hPP (100 nM) induced an impedance change of approximately 650 Ω within 20 min and it remained

stable within the observation time of 80 min. The corresponding DMSO control (0.01% v/v) increased the impedance just by 20 Ω along the entire observation time. The two isomers **Z-30** and **E-30** showed distinctly different impedance responses when applied in 1 nM concentrations. Whereas **Z-30** induced an impedance increase of approximately 400 Ω with a similar time course as hPP, **E-30** was not significantly different from the DMSO control. For a more quantitative analysis we used the area under the curve (AUC) for each impedance time course in the time interval from 20 min to 40 min using the DMSO control as the lower border of integration (see orange area in Figure 5). AUC has proven to yield a more robust readout than the maximum impedance change in particular for non-monotonic time courses.^[13] Therefore, AUC analysis was applied to experiments conducted with increasing concentrations of both isomers of compounds **28** and **30** to reveal their individual dose-response relationships as summarized in Figure 6.

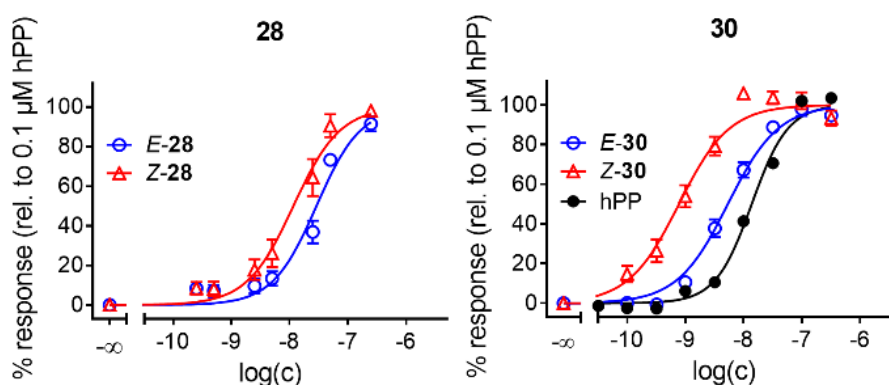


Figure 6. Dose-response curves of E/Z-isomers of **28** and **30** obtained by AUC calculation of impedance time courses at 12 kHz. hPP is included for comparison. Mean \pm SEM from at least three independent experiments performed in triplicate.

For both compounds **28** and **30**, we found the *Z*-isomer to be more potent than the *E*-isomer, which is in line with the radioligand competition binding and the miniG_i recruitment assay (Table 2). pEC₅₀ values as determined from impedance-based cell monitoring are summarized in Table 3. At saturating concentrations both compounds showed the same intrinsic activity as the endogenous ligand hPP. This phenomenon is often observed for integrative assays capturing the very end of the signalling cascade.^[26,27]

Table 3. Y₄R agonistic potencies (pEC₅₀) for *E/Z* isomers of compounds **28** and **30**. hPP is included for comparison.

	Y ₄ R ^[a]
	pEC ₅₀ ± SEM / EC ₅₀ (nM)
hPP	7.86 ± 0.04 / 13
<i>E</i>-28	7.54 ± 0.07 / 29
<i>Z</i>-28	7.94 ± 0.06 / 12
<i>E</i>-30	8.27 ± 0.03 / 5
<i>Z</i>-30	9.11 ± 0.05 / 0.8

[a] Determined from the time course of impedance by calculating the AUC between 20 and 40 min of exposure as illustrated in Figure 5 performed with CHO-Y₄R cells. pEC₅₀ values represent mean values from at least three independent experiments performed in triplicate.

K_i values of **28** and **30** determined from radioligand competition binding differed by a factor of approximately 10 between the isomers (*E/Z*). In miniG_i recruitment, this difference was less pronounced. The factor between EC₅₀ values of the isomers was just 5 for **28** and 2 for **30**. In impedance measurements **30** was found to show the bigger difference in potency between *E*- and *Z*-isomers with an approximately 6-fold difference, whereas the factor for **28** was only 2.5. It is important to recognize that miniG_i-recruitment assays report on signalling events that are localized directly at the receptor (proximal) while label-free wholistic measurements like impedance analysis integrate over the entire cell body and the entire signalling cascade (distal) similar to experiments performed with entire organs.^[28] This integrative character together with the inherent amplification along the signalling cascade is also responsible for the fact that impedance measurements do not reveal any significant difference in efficacy for the two isomers relative to hPP in contrast to miniG_i recruitment.^[27] In impedance-based assays, both isomers of **28** and **30** are considered full agonists. Another result is noteworthy: in impedance-based analysis both isomers of **30** are significantly more potent than hPP. The other two assays do not report a similar behaviour. A potential explanation is functional selectivity (biased agonism).^[29] The concept of functional selectivity proposes that different ligands are capable of triggering different signaling cascades to different degrees upon binding to the same receptor. Whereas competition binding and G-protein recruitment assays report on molecular changes close to the receptor, impedance measurements are very distal integrating over all signaling cascades that might be involved as discussed above. As such, impedance measurements might be affected by functional selectivity whereas the other two readouts are not.

The observed impedance increase may report on two potential changes in cell morphology that are indistinguishable from the current data: (i) strengthening of cell-cell interactions which leads to a reduced width of the intercellular cleft; (ii) enhancement of cell-matrix interactions which reduces the width of the narrow electrolyte-filled channel between lower cell membrane and electrode surface; or (iii) both. In either case, the pathways for ionic current flow are reduced which translates into an increase in impedance. Recording the impedance at a set of distinct frequencies instead of just one would allow for a clear assignment of the morphology changes^[30] but was not in the scope of this study.

3.7 Real-Time Monitoring of Light-Controlled Y₄R Agonism

From the dose-response studies (Figure 6) the optimum concentrations for **28** (50 nM) and **30** (1 nM) were selected to perform *in situ* switching from one isomer to the other while the impedance is continuously monitored. Figure 7 summarizes the outcome of these *in situ* switching experiments for all four compounds: (A) **Z-28**, (B) **E-28**, (C) **Z-30** and (D) **E-30**. For easy comparison, each graph contains the time courses of impedance for 100 nM hPP (solid black line) and the 0.01% (v/v) DMSO vehicle control (dashed black line), which define the upper and lower limit of impedance values in this assay. Time course data for the pure isomers are given in red (Z) or blue (E). The green curve represents the isomer that was switched *in situ* by irradiation with the proper wavelength at the time indicated by the vertical dotted lines. When **Z-28** (Figure 7A) was added to the CHO cells at time zero, impedance increased to about 80% of the values recorded for 100 nM hPP in line with the dose-response data. Irradiating the system with 455 nm after 20 min of agonist exposure induced a sharp decrease of impedance and stabilization at values recorded for **E-28** at this time point. Impedance did not change for almost 50 min indicating that the cells were equilibrated with these conditions. Subsequent irradiation with 340 nm almost 80 min after initial ligand exposure led to a pronounced increase again that does not quite reach the impedance levels of pure **Z-28** but stabilized again. Repeating this sequence of light-induced isomerization yielded similar cell responses with some signs of fatigue within the reversibility of the signalling cascades or cell physiology in general as the signal changes became smaller. We take the fact that the impedance of all cell populations slightly drifted to lower values along the experiment as an indicator, that the prolonged stimulation in a buffer with a minimum of nutrients tires

the cells out. In the same line, we have previously observed reduced cell responses to GPCR stimulation when we applied a cumulative dosing protocol during which the cells were sequentially exposed to increasing agonist concentrations.^[11] According to the *in vitro* characterization of the ligands, the observed phenomenon is not due to a limited reversibility of photo-induced isomerization but we cannot exclude changes in photostability in the binding pocket of the receptor. Figure 7B summarizes the opposite experiment. This time **E-28** (green curve) was applied to the CHO cells before the system was irradiated with 340 nm to induce isomerization. Under these conditions impedance did not increase to values recorded for the *Z*-isomer at the same time but showed a minor rise that stabilized close to the values of the pure *E*-isomer. After the opposite *in situ* switching using 455 nm, the impedance dropped significantly as expected when going from *Z* to *E* and stabilized at a new steady state. When the switching cycle is repeated, the impedance increased and decreased as expected from dose-response data even though the absolute values showed some offset relative to the isomers that were exposed to light prior to the experiment. Figures 7C and 7D summarize similar *in situ* irradiation experiments for compound **30** demonstrating the reversible switching between two distinct agonistic activities in this assay monitoring the integrated cell response.

In these experiments the recorded impedance showed some drifting to lower values along the observation time as well. Since (i) the experiments were performed in serum-free buffer with a minimum of nutrients and (ii) impedance measurements are rather sensitive to morphological changes coupled to energy metabolism, we assign the impedance drift to assay conditions and length of experiment. In control experiments we carefully ensured that there neither is an impact of the light itself (i) on resting cells (ii) nor on cells stimulated with a non-photochromic ligand (iii) nor on the electrodes that may lead to misinterpretations. We therefore performed *in situ* irradiation with the intensities and wavelengths as used for photoswitching with confluent CHO-Y₄R cells on the electrodes, but in absence of the photochromic ligands (Figure S59A) or in presence of the ligands but without cells on the electrodes (Figure S59B). In a third control experiment cells were stimulated with the non-photochromic endogenous ligand hPP and irradiated with light of the different wavelengths (Figure S59C). In either case, impedance recordings did not show any significant change upon irradiation with light of wavelength 340 nm, 455 nm or 528 nm. Neither the cells without photochromic ligands nor the ligands without cells induced any measurable impedance shift upon light irradiation

supporting our understanding that the individual interactions of the photochromic ligands with Y₄R are responsible for the distinct impedance profiles.

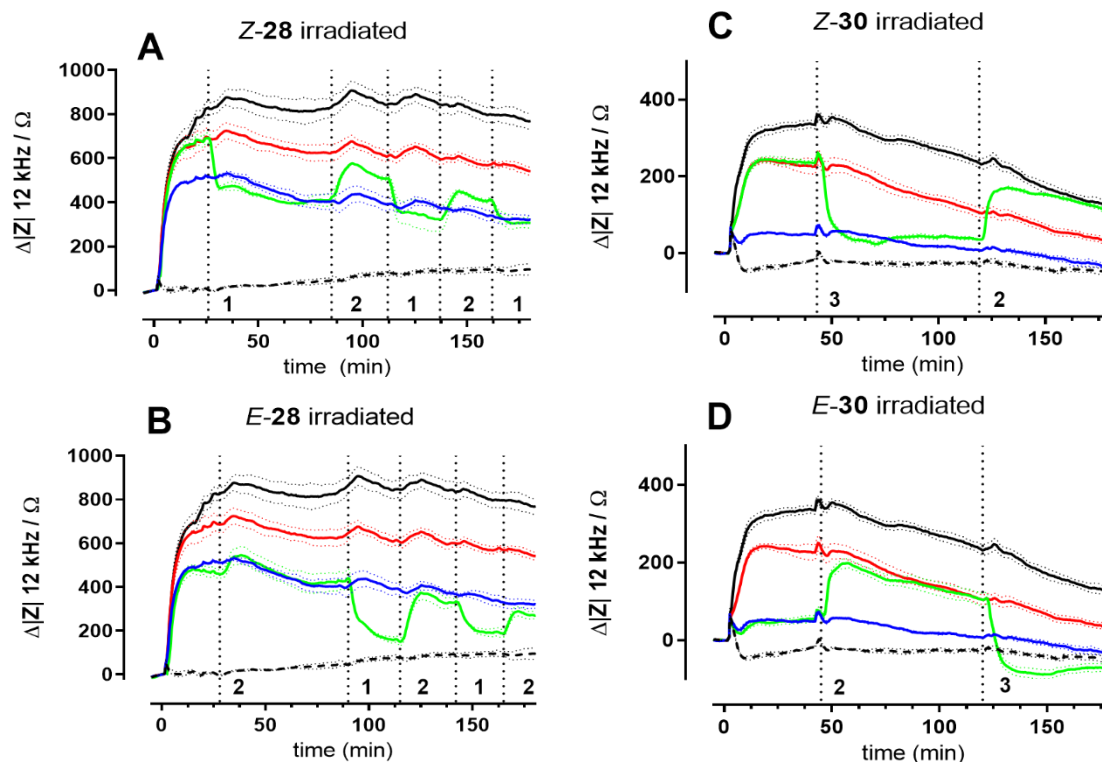


Figure 7. Impedance time courses at an AC frequency of 12 kHz when confluent CHO-Y₄R cells were stimulated with different agonists combined with repeated *in situ* irradiation at wavelengths specified below. Impedance was zeroed in for the last data point prior to agonist addition. Control cells were either incubated with hPP (solid black line; *c* = 100 nM) or DMSO (dashed black line; *c* = 0.01% (v/v)). The red curves represent the unperturbed Z-isomer of **28** (50 nM) and **30** (1 nM) whereas the blue curves stand for the corresponding unperturbed E-isomer. All green curves correspond to the isomer indicated in the header during light-induced *in situ* (re)isomerization. Times of irradiation are indicated by dashed vertical lines (1= 455 nm; 2 = 340 nm; 3 = 528 nm). Cells were pre-stimulated with forskolin (0.4 μM) for 30 min (not shown). Mean ± SEM (*n*=3).

A physiological interpretation of the impedance data during the switching cycles requires a closer look into the details of the Y₄R-dependent signal transduction. The canonical coupling of the Y₄R is reported to rely on G_{α_i} signalling and was verified by the miniG_{α_i} recruitment assay. Once G_{α_i} is released from the heterotrimeric G-protein, it binds to adenylate cyclase (AC) and inhibits cAMP formation. At the same time, cAMP is constantly degraded by cAMP-dependent phosphodiesterase (PDE). In resting cells constitutive activity of AC and PDE establish a dynamic equilibrium of cAMP production and degradation yielding a steady state concentration of cAMP. This energy consuming process is seemingly useless but allows very quick changes of cAMP concentrations in response to external triggers. Since cAMP levels are

low (< 50 nM)^[31] in resting cells and get even lower from G_{α_i} activity, it is generally difficult to monitor Y_4R activation by reading cAMP concentrations or downstream signalling events. Accordingly, it is common practice to pre-stimulate the cells by micromolar concentrations of forskolin, a receptor-independent, membrane permeable activator of AC isolated from plants. Forskolin increases intracellular cAMP concentrations to a level that facilitates experimental analysis of signalling mechanisms that lead to its reduction.^[32] Thus, a similar protocol was applied in impedance-based assays as performed in this study. Prior to adding the ligands, the cells were pre-stimulated by 0.4 μ M forskolin. The subsequent forskolin-induced cAMP net production led to a significant decrease of the cell impedance by 400 Ω from values recorded for the resting cells. After the cells had equilibrated to these conditions within 30 min, the different ligands were applied and monitored for their impact on cell impedance (Figure 6,7). Since forskolin concentrations were kept constant in all buffers and all phases of the experiment, release of G_{α_i} from the complete G-protein after receptor activation led to a competitive regulation of adenylate cyclase. Whereas forskolin – constantly present in all cell culture fluids – led to an activation of AC, G_{α_i} reduced its activity in a concentration-dependent manner. So, when the Y_4 receptor and the associated signalling cascade were fully activated by the endogenous ligand hPP or high concentrations of the synthetic ligands, cAMP is efficiently reduced by over-compensating the forskolin activity bringing impedance back up to values of the resting cells or higher. Any partial activation of the receptor led to a reduced release of G_{α_i} activity and thus, to a competitive regulation of AC between forskolin and G_{α_i} that may be simply controlled by their individual concentrations and activities. If this interpretation applies, the *in situ* switching between the isomers and the associated change in receptor activation led to a fine-tuning of AC activity and all processes dependent thereof explaining the reversibility of the cell response during switching. For the CHO cells studied here, it seems that impedance measurements mirror the time-dependent cAMP concentrations inside the cell most likely via a cAMP-regulated protein or protein network that is involved in cell shape control. The response time of impedance readings to forskolin or agonist addition is in the order of 10-20 minutes. Accordingly, the cell response as reported by impedance is not dependent on changes in gene expression as the latter would require more time. The cell response is more likely determined by changes in functional activity of existing proteins.

3.8 Photoswitching Occurs inside Receptor Binding Pocket

In the experiments described in preceding sections, the ligands were added to the cells at time zero and were continuously present throughout the experiment. The question arose whether isomerization of the ligands upon irradiation occurs (i) in the bulk phase with subsequent competition for the receptor binding site between the bound ligand and its free isomer in solution or (ii) whether isomerization occurs in the binding pocket of the receptor without any ligand exchange. The average residence time for similar, radiolabeled Y_4R ligands was found to be rather dependent on the experimental conditions and ranged between 5 and 30 min^[24] so that either mechanism is compatible with the impedance time courses. To gain more insight, we revisited the two isomers **Z-28** and **E-28** but adapted the experimental workflow by including a washing step after the ligands were incubated with the cells for 20 min (Figure 8).

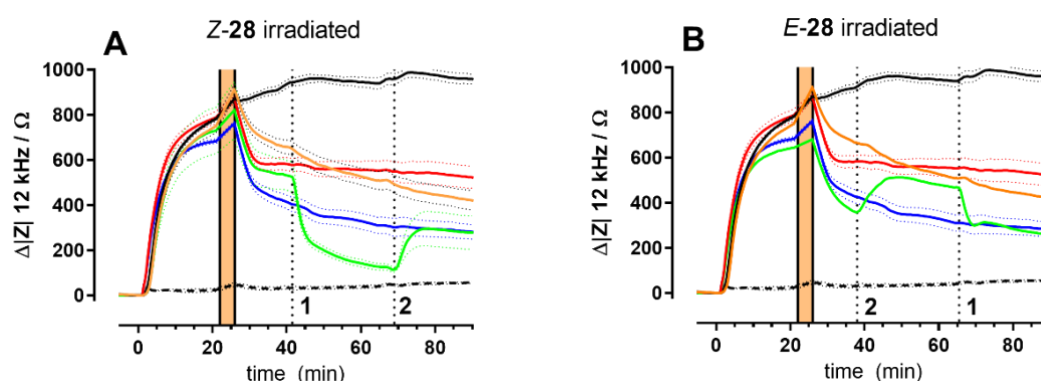


Figure 8. Time courses of impedance (12 kHz) during stimulation of CHO-Y₄R cells with different agonists combined with repeated *in situ* irradiation at wavelengths specified below. Impedance was zeroed in for the last data point prior to agonist addition. Control cells were either incubated with hPP (without washing solid black line; with washing solid orange line $c = 100$ nM) or a vehicle control (dashed black line; $c = 0.01\%$ (v/v) DMSO). The red curves represent the unperturbed **Z-28** (50 nM) whereas the blue curves stand for the corresponding unperturbed *E*-isomer. All green curves correspond to the isomer indicated in the header during light-induced *in situ* (re)isomerization. Times of irradiation are indicated by dashed vertical lines (1 = 455 nm; 2 = 340 nm). Time needed to wash out unbound ligands is indicated by the orange area. Cells were pre-stimulated with forskolin (0.4 μ M, $t = -30$ min, not shown). Mean \pm SEM ($n=3$).

The time interval needed for washing is indicated by the orange box. The colour code of the impedance time courses is as before. The endogenous ligand hPP (100 nM) is represented by (i) a black solid line when the liquid was not exchanged or (ii) an orange solid line, when the liquid with the free ligand was replaced by buffer. The vehicle control (DMSO, 0.01% v/v, no washing) is indicated by a black dashed line. The impedance response for **Z-28** is shown in

red, the one for **E-28** in blue. Both isomers were applied in 50 nM concentrations as before. The green curve corresponds to **Z-28** in Figure 8A and **E-28** in 8B. Only the cell population represented by the green curve was exposed to light (A: **Z-28**, 455 nm; B: **E-28**, 340 nm) at the time indicated by vertical dotted lines. As suggested by the red and blue curves in Figures 8A and B, washing led to a significant decrease of the impedance presumably due to a loss of a fraction of ligands from the receptor binding pockets when the bulk concentration was experimentally set to zero by washing. The mechanical load on the cells imposed by liquid handling may also contribute to the observed impedance decrease. *In situ* switching of the remaining **Z-28** to the less potent **E-28** after 40 min led to a significant and step-like reduction of impedance which is in line with the dose-response relationship of both ligands (Figure 8A). Re-isomerization to **Z-28** was induced by irradiation with 340 nm after 70 min of experimental time. It was associated with an increase in impedance. However, values did not recover to those of the *Z*-isomer that has not been switched at all. When the corresponding experiment was performed with **E-28** (Figure 8B), the outcome was similar. Initial isomerization of **E-28** to **Z-28** increased impedance almost to the values of the unperturbed *Z*-isomer. Re-isomerization by irradiation at 455 nm reduced impedance back to values of the unperturbed *E*-isomer. It is noteworthy that in these experiments no ligand was present in the bulk phase. Any dissociation from the binding pocket led to a practically infinite dilution so that any re-association of a formerly bound ligand back into the binding pocket was elusive. Conducting this washing/*in situ* photoswitching experiment with compounds **E-30** and **Z-30** returned very similar impedance time courses (data not shown). Taken together, these experiments demonstrate that *in situ* switching of the signalling cascade is possible even after unbound ligands have been washed out. Accordingly, the data provides evidence that isomerization is likely to occur with the ligand bound in the binding site of the receptor.

3.9 Conclusion

Photochromic ligands for cell surface receptors have significantly expanded the experimental toolbox for an in-depth analysis of ligand-receptor interactions. In combination with real time impedance measurements these molecules allow controlling GPCR signaling cascades starting from the conformational change of the receptor but entirely unaffected by the association or dissociation kinetics of the agonist. Ligand binding may get separated in time from a precisely

controllable change in agonistic activity. With systems as described here, it will become possible (i) to activate the receptor periodically with different frequencies, (ii) to study the minimum activation time needed to trigger signaling events downstream of the receptor or (iii) to test whether reducing agonistic activity after a certain amount of time will stop receptor internalization or desensitization. When switching of photochromic ligands is performed on a microscope stage with microscopic precision, they provide an unmet temporal and spatial control of receptor activation or modulation to study how activation of receptors in a fraction of cells affects the ensemble. Two general conditions need to be fulfilled to exploit the ligands' full analytical potential: (i) When optical readouts are being used to monitor the biological model system, the light that is used for photo-switching must not show spectral overlap with the light that is used for detection. (ii) The experimental setup must allow for *in situ* switching of the photochromic moieties. Label-free impedance measurements of adherent cells grown on planar gold-film electrodes are particularly well-suited to monitor the switching of bioactive photochromic probes as it provides an orthogonal readout with no interference by the light-induced switching. As the readout is sensitive to such a global indicator of cell state as morphology, it is applicable to a wide variety of receptors and signaling cascades. On the downside, impedance time courses do not contain any molecular information but only report on the integrated cell response. Molecular information requires the use of specific pharmacological modulators of the signaling cascades under test. The measurement itself is non-invasive and provides time resolutions that may be tailored to experimental needs from milliseconds to days or weeks. Since the gold electrodes are an integral part of the growth substrate, a typical setup provides a maximum of space to place light sources for switching. The data presented in this study illustrate how photochromic ligands in combination with tailored dosing/washing protocols may be used to unravel mechanistic details of receptor activation or signaling. The future combination of photochromic ligands with microfluidic chips to host the cells, specialized dosing protocols (e.g. stopped or pulsed flow), spatio-temporal control of bioactivity with the help of structured illumination and label-free detection will enable a new generation of assays to unravel dynamic properties of cellular signaling that are not available today.

3.10 Experimental Part

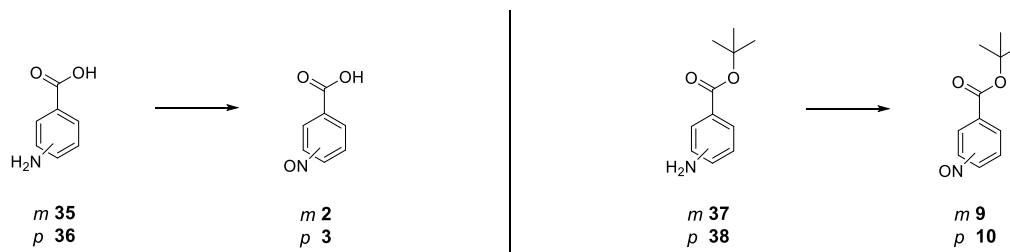
3.10.1 General Information

Starting materials and commercial reagents were purchased from Acros, Alfa Aesar, Fisher, Fluka, Fluorochem, Merck, Sigma-Aldrich, TCI and VWR and were used without further purification. Solvents were used in p.a. quality or dried according to common procedures if necessary. Reactions with oxygen- or moisture-sensitive reagents were carried out in glassware which was dried before use by heating under vacuum. Dry nitrogen or argon were used as inert gas atmosphere. NMR spectra were measured at room temperature using a Bruker Avance 400 (400 MHz for ^1H and 101 MHz for ^{13}C) or a Bruker Avance 600 (600 MHz for ^1H and 151 MHz for ^{13}C) NMR spectrometer. Chemical shifts are reported in δ -scale as parts per million [ppm] (multiplicity, coupling constant J, number of protons) relative to the solvent residual peaks. Coupling constants J are given in Hertz [Hz]. Abbreviations used for signal multiplicity: ^1H -NMR: s = singlet, d = doublet, dd = doublet of doublets, ddd = doublet of doublets of doublets, dt = doublet of triplets, t = triplet, td = triplet of doublets, q = quartet, and m = multiplet. Mass spectra were recorded on an Agilent Q-TOF 6540 UHD, Finnigan MAT SSQ 710 A, Jeol AccuTOF GCX or ThermoQuest Finnigan TSQ 7000 spectrometer. Absorption spectra were recorded on a UV/VIS Agilent Cary 50 spectrometer. Thermal half-lives were measured on a 96-well plate in a Thermo Scientific Multiskan[®] Spectrum. Analytical thin layer chromatography (TLC) was performed on silica gel coated alumina plates (MN precoated TLC-sheets ALUGRAM[®] Xtra SIL G/UV254). Visualization was done by UV-light (254 nm or 366 nm) or staining with ninhydrin solution. Column chromatography was performed on a Biotage Isolera One automated flash purification system with UV/Vis detector. Analytical RP-HPLC were measured on an Agilent 1220 Infinity LC System (column: P/No 00F-4251-B0, Phenomenex Luna[®] 3 μm C18(2) 100 Å, LC column 150x2.0 mm). Purification by preparative HPLC was conducted on a preparative HPLC Agilent 1260 Infinity LC System (column: P/No 00G-4253-P0-AX, Phenomenex Luna[®] 10 μm C18(2) 100 Å, LC column 250x21.2 mm). The eluent systems were used as specified. After the purification process, solvents were removed by lyophilization. Switching experiments were done with a 340 nm LED (SSC VIOSYS CUD4AF1B, 500 mA, 55 mW), 455 nm LED (Oslon SSL 80 LDCQ7P-2U3U, 700 mA, 1480 mW) and 528 nm LED (OSRAM Oslon SSL 80 green, 500 mA, 34 mW).

3.10.2 Synthetic Procedures

Compound **16** was synthesized according to literature.^[21]

General procedure for the synthesis of nitroso compounds **2, **3**, **9** and **10**.**^[20]



Amines **35-38** (1.0 eq.) were dissolved in CH_2Cl_2 . To this solution Oxone (2.0 eq.) dissolved in water was added. The solution was vigorously stirred under nitrogen at rt until TLC monitoring indicated complete consumption of the starting material. The carboxylic acids **2** and **3** formed a precipitate which was filtered off, washed with water and dried. For the esters **9** and **10** the organic phase was washed with 1 M HCl, sat. NaHCO_3 and brine. The solvent was removed *in vacuo*. The products were used without further purification directly in the next step.

General procedure for the synthesis of azobenzenes 6-8. Nitroso **2** or **3** (1.0 eq.) and amine **4** or **5** (1.0 eq.) were dissolved in AcOH and stirred at rt for 4 d. The solvent was removed *in vacuo* and the crude product was purified by column chromatography (MeCN/EtOH, 0-30%).

(E)-3-((3-(tert-Butoxycarbonyl)phenyl)diazenyl)benzoic acid (6). Yield: 24%. $^1\text{H NMR}$ (400 MHz, DMSO-d_6) δ 8.40 (d, $J = 1.9$ Hz, 1H), 8.36 (d, $J = 1.9$ Hz, 1H), 8.21 – 8.06 (m, 4H), 7.74 (td, $J = 7.8, 2.0$ Hz, 2H), 1.58 (s, 9H). $^{13}\text{C NMR}$ (101 MHz, DMSO) δ 166.7, 164.2, 151.7, 132.7, 132.5, 132.2, 131.9, 130.0, 130.0, 127.4, 126.9, 122.7, 122.5, 81.5, 27.8. **ESI-MS:** m/z (%) = 327.14 ($\text{M}+\text{H}$)⁺.

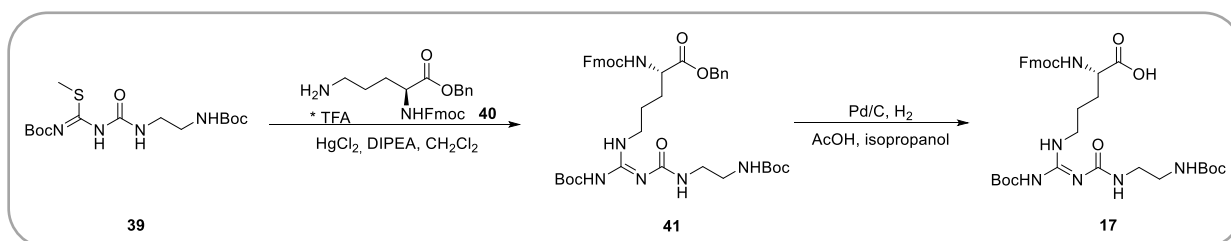
(E)-4-((3-(tert-Butoxycarbonyl)phenyl)diazenyl)benzoic acid (7). Yield: 22%. $^1\text{H NMR}$ (400 MHz, DMSO-d_6) δ 8.36 (t, $J = 1.8$ Hz, 1H), 8.21 – 8.14 (m, 3H), 8.11 (dt, $J = 7.7, 1.4$ Hz, 1H), 8.04 – 7.95 (m, 2H), 7.75 (t, $J = 7.8$ Hz, 1H), 1.59 (s, 9H). $^{13}\text{C NMR}$ (101 MHz, DMSO) δ 166.8, 164.2, 153.9, 151.8, 133.9, 132.7, 132.1, 130.6, 130.1, 126.9, 122.8, 122.7, 81.5, 27.7. **ESI-MS:** m/z () = 327.14 ($\text{M}+\text{H}$)⁺.

(*E*)-3-((4-(*tert*-Butoxycarbonyl)phenyl)diazenyl)benzoic acid (8). Yield: 25%. $^1\text{H NMR}$ (400 MHz, DMSO- d_6) δ 8.41 (d, $J = 1.8$ Hz, 1H), 8.21 – 8.09 (m, 4H), 8.02 (d, $J = 8.4$ Hz, 2H), 7.76 (t, $J = 7.8$ Hz, 1H), 1.58 (s, 9H). $^{13}\text{C NMR}$ (101 MHz, DMSO) δ 166.7, 164.3, 154.1, 151.8, 133.6, 132.5, 130.4, 130.1, 127.6, 122.8, 122.5, 81.4, 27.8. **ESI-MS:** m/z (%) = 327.13 (M+H) $^+$.

General procedure for the synthesis of arylazopyrazoles 12 and 13. Nitroso 9 or 10 (5.2 mmol, 1.0 eq.) in DCM was added to (4-amino-3,5-dimethyl-1*H*-pyrazol-1-yl)acetic acid dihydrochloride hydrate (11) (1.35 g, 5.2 mmol, 1.0 eq.) dissolved in DCM. Then NEt_3 was added dropwise until the solution turned yellow. The mixture was stirred for 3 h. The solvent was removed *in vacuo* and the crude product was purified by column chromatography (MeCN/EtOH, 0-30%).

(*E*)-2-(4-((4-(*tert*-Butoxycarbonyl)phenyl)diazenyl)-3,5-dimethyl-1*H*-pyrazol-1-yl)acetic acid (12). Yield: 10%. $^1\text{H NMR}$ (400 MHz, DMSO- d_6) δ 8.03 (d, $J = 8.4$ Hz, 2H), 7.81 (d, $J = 8.4$ Hz, 2H), 4.91 (s, 2H), 2.53 (s, 3H), 2.39 (s, 3H), 1.57 (s, 9H). $^{13}\text{C NMR}$ (101 MHz, DMSO) δ 169.0, 164.5, 155.6, 152.6, 141.8, 141.0, 135.0, 131.5, 81.0, 50.9, 27.8, 13.9, 9.5. **ESI-MS:** m/z (%) = 359.17 (M+H) $^+$.

(*E*)-2-(4-((3-(*tert*-Butoxycarbonyl)phenyl)diazenyl)-3,5-dimethyl-1*H*-pyrazol-1-yl)acetic acid (13). Yield: 57%. $^1\text{H NMR}$ (400 MHz, DMSO- d_6) δ 8.19 (t, $J = 1.8$ Hz, 1H), 7.95 (ddt, $J = 9.7, 7.8, 1.2$ Hz, 2H), 7.63 (t, $J = 7.8$ Hz, 1H), 4.87 (s, 2H), 2.52 (s, 3H), 2.39 (s, 3H), 1.57 (s, 9H). $^{13}\text{C NMR}$ (101 MHz, DMSO) δ 169.2, 164.5, 153.0, 141.2, 140.8, 134.6, 132.4, 129.6, 129.6, 125.4, 121.8, 81.1, 51.2, 27.8, 13.9, 9.5. **ESI-MS:** m/z (%) = 359.17 (M+H) $^+$.



Scheme S1. Synthesis route towards 17.

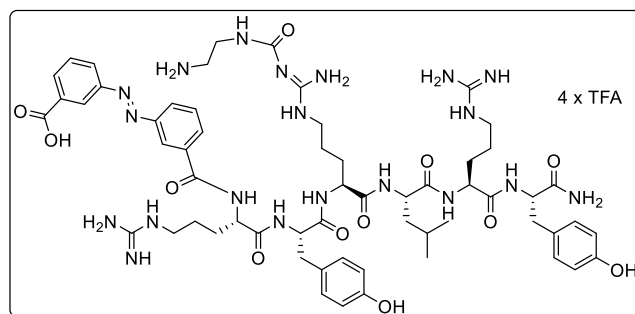
Benzyl (*S,E*)-16-((((9*H*-fluoren-9-yl)methoxy)carbonyl)amino)-11-((*tert*-butoxycarbonyl)amino)-2,2-dimethyl-4,9-dioxo-3-oxa-5,8,10,12-tetraazaheptadec-10-en-17-oate (41**).** HgCl₂ (2.93 g, 10.8 mmol, 1.5 eq.) and DIPEA (2.8 g, 3.74 mL, 21.5 mmol, 3.0 eq.) were added to a stirred solution of **40** (4.0 g, 7.2 mmol, 1.0 eq.) and **39** (2.7 g, 7.2 mmol, 1.0 eq.) in anhydrous CH₂Cl₂ (70 mL). The mixture was stirred for 1.5 h at rt. Afterwards, the solids were centrifuged off. The solvent was removed in vacuo and the crude product was purified by column chromatography (PE/EtOAc, 10-50%). Product **41** was obtained as a white solid (3.46 g, 4.48 mmol, 62%). ¹H NMR (400 MHz, DMSO-d₆) δ 12.43 (s, 0.5H), 11.13 (s, 0.5H), 9.13 (t, *J* = 4.8 Hz, 0.5H), 8.16 (s, 0.5H), 7.89 (d, *J* = 7.5 Hz, 3H), 7.71 (d, *J* = 7.4 Hz, 2H), 7.41 (d, *J* = 14.8 Hz, 2H), 7.32 (d, *J* = 7.5 Hz, 7.5H), 6.90 (s, 0.5H), 6.83 (s, 0.5H), 6.75 (s, 0.5H), 5.13 (s, 2H), 4.30 (dd, *J* = 6.2, 3.1 Hz, 2H), 4.22 (t, *J* = 6.9 Hz, 1H), 4.13 (dt, *J* = 8.7, 4.3 Hz, 1H), 3.26 (q, *J* = 6.6 Hz, 2H), 3.08 (d, *J* = 6.0 Hz, 1H), 2.99 (dt, *J* = 15.8, 5.9 Hz, 3H), 1.77 – 1.62 (m, 2H), 1.55 (dd, *J* = 13.1, 7.2 Hz, 2H), 1.44 (d, *J* = 11.4 Hz, 6H), 1.40 (s, 4H), 1.36 (d, *J* = 3.6 Hz, 9H). ¹³C NMR (101 MHz, DMSO) δ 172.1, 172.1, 164.4, 162.7, 156.5, 156.2, 156.1, 155.6, 154.7, 153.1, 152.3, 143.8, 143.7, 140.7, 135.9, 128.4, 128.0, 127.7, 127.6, 127.0, 125.2, 120.1, 82.0, 77.7, 77.6, 77.4, 65.9, 65.7, 53.8, 53.7, 46.6, 30.7, 28.2, 28.1, 27.7. **ESI-MS:** *m/z* (%) = 773.39 (M+H)⁺.

(*S,E*)-16-((((9*H*-Fluoren-9-yl)methoxy)carbonyl)amino)-11-((*tert*-butoxycarbonyl)amino)-2,2-dimethyl-4,9-dioxo-3-oxa-5,8,10,12-tetraazaheptadec-10-en-17-oic acid (17**).** Compound **41** (3.0 g, 3.88 mmol) was dissolved in acetic acid (12.5 μL) in 2-propanol (50 mL) and Pd/C (10%, 453 mg) was added. The solution was stirred in a hydrogen atmosphere (balloon, 1 bar) for 4.5 h (additional catalyst was added after 2.5 h (226 mg) and 3.5 h (149 mg)). The catalyst was removed by centrifugation. Water (150 mL) was added to the filtrate, and the mixture was lyophilized. The product was purified by column chromatography (MeCN/EtOH, 3-10%). After completion of elution, the eluate was immediately diluted with water (300 mL) and lyophilized. Compound **17** was obtained as a white solid (1.61 g, 2.36 mmol, 61%). ¹H NMR (400 MHz, DMSO-d₆) δ 12.52 (d, *J* = 64.1 Hz, 0.5H), 11.14 (s, 0.5H), 9.14 (t, *J* = 5.4 Hz, 0.5H), 8.16 (t, *J* = 5.4 Hz, 0.5H), 7.94 (d, *J* = 5.8 Hz, 0.5H), 7.88 (d, *J* = 7.5 Hz, 2H), 7.72 (d, *J* = 7.4 Hz, 2H), 7.62 (q, *J* = 6.6 Hz, 1H), 7.41 (t, *J* = 7.5 Hz, 2H), 7.32 (t, *J* = 7.4 Hz, 2H), 6.93 (t, *J* = 5.6 Hz, 0.5H), 6.83 (t, *J* = 5.7 Hz, 0.5H), 6.76 (d, *J* = 5.7 Hz, 0.5H), 4.30 – 4.20 (m, 3H), 3.97 (q, *J* = 4.0 Hz, 1H), 3.27 (q, *J* = 5.8 Hz, 2H), 3.08 (d, *J* = 7.3 Hz, 1H), 3.05 – 2.95 (m, 3H), 1.72 (dd, *J* = 9.2, 3.9 Hz, 1H), 1.65 – 1.52 (m,

3H), 1.45 (s, 5H), 1.40 (s, 4H), 1.37 (s, 9H). ^{13}C NMR (101 MHz, DMSO) δ 173.9, 173.9, 164.6, 164.5, 162.7, 156.5, 156.1, 155.6, 154.7, 153.9, 153.2, 152.4, 152.4, 143.9, 143.8, 140.7, 127.6, 127.1, 125.3, 120.1, 82.1, 82.0, 77.7, 77.6, 77.4, 65.6, 53.8, 46.7, 28.4, 28.2, 28.1, 27.7. **ESI-MS:** m/z (%) = 683.33 (M+H) $^+$.

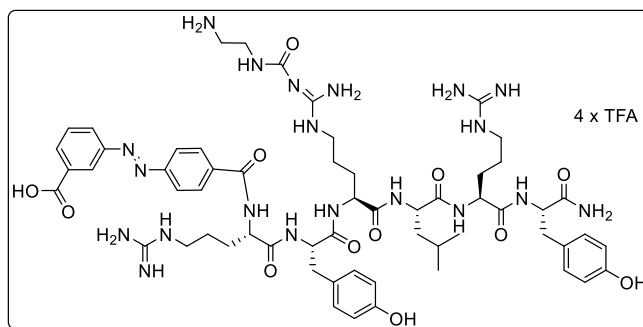
General procedure for the synthesis of peptides 19-26. Peptides were synthesized by manual SPPS according to the Fmoc strategy using Fmoc-PS-Sieber Resin. 2-mL Discardit II syringes equipped with polyethylene frits were used as reaction vessels. DMF/NMP (8:2 v/v) was used as solvent for the coupling reactions and the cleavage of Fmoc groups. For initial Fmoc deprotection of the resin and swelling, the resin was treated with 20% piperidine in solvent at rt for 2×20 min. Protected natural L-amino acids were used in 5-fold excess and preactivated with HBTU (4.9 eq.)/HOBt (5 eq.)/DIPEA (10 eq.) in polypropylene reaction vessels for 5-7 min prior to addition to the resin (volume of the solvent: ca. 2.2 mL/mmol Fmoc-amino acid). In the case of standard (natural) Fmoc-amino acids, “double” coupling (2×45 min) was performed at 35 °C. Amino acids **16-18** were used in 3-fold excess, preactivated with HBTU (2.95 eq.)/HOBt (3 eq.)/DIPEA (6 eq.) (volume of solvent: ca. 1.6 mL/mmol of **16-18**), and the reaction was performed at 35 °C for overnight (“single” coupling). During coupling reactions, syringes were shaken using a HLC BlockThermostate and ThermoMixer. After completed coupling of an Fmoc-aa, the resin was washed with solvent (4 \times) and treated with 20% piperidine in DMF/NMP (8:2 v/v) at rt for 2×10 min followed by washing the resin with solvent (6 \times). After coupling and Fmoc deprotection of the final amino acid either photoswitches **6-8**, **12**, **13** used in 3-fold excess, preactivated with PyBOP (3 eq.)/HOBt (3 eq.)/DIPEA (6 eq.) were added to the resin and the reaction proceeded at 35 °C for overnight. Or the resin was treated with succinic anhydride (10 eq.)/DIPEA (10 eq.) at 35 °C for 30 min. Afterwards, the resin was washed with solvent (6 \times) and CH_2Cl_2 (4 \times) followed by cleavage off the resin with CH_2Cl_2 /TFA (3:1 v/v) at rt (2×20 min, performed in the syringe). After completed cleavage, the resin was washed once with CH_2Cl_2 /TFA (3:1 v/v). The collected liquid phases were combined in a round-bottom flask and the volatiles were removed by rotary evaporation. The residue was dissolved in CH_2Cl_2 /TFA (1:1 v/v), the mixture was stirred at rt for 5 h (full side chain deprotection) and transferred to a 100-mL round-bottom flask containing water (40 mL) followed by lyophilization and subsequent purification by preparative HPLC (column: Luna 10, 250 x 21 mm; flow: 22 mL/min, solvent A: H_2O (0.05% TFA), solvent B: MeCN; gradient A/B: 0-20 min: 97/3, 20-25 min: 2/98).

3-((*E*)-(3-(((6*S*,9*S*,12*S*,15*S*,18*S*)-1,23-Diamino-6-(((*S*)-1-amino-3-(4-hydroxyphenyl)-1-oxopropan-2-yl)carbamoyl)-12-(3-((*E*)-2-((2-aminoethyl)carbamoyl)guanidino)propyl)-15-(4-hydroxybenzyl)-1,23-diimino-9-isobutyl-8,11,14,17-tetraoxo-2,7,10,13,16,22-hexaazatricosan-18-yl)carbamoyl)phenyl)diazenyl)benzoic acid (19).



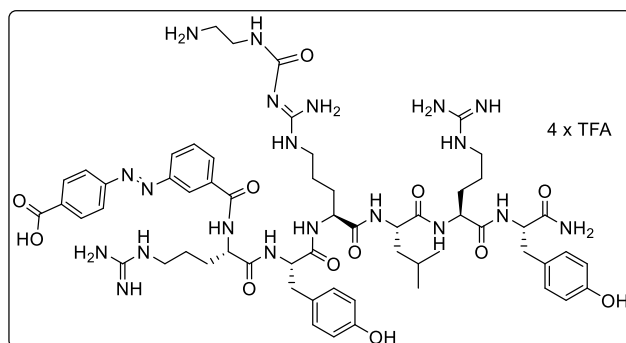
Overall yield: 14%. **¹H NMR** (400 MHz, DMSO-*d*₆) δ 13.35 (br, 1H), 10.60 (s, 1H), 9.15 (d, *J* = 14.7 Hz, 2H), 8.99 (s, 1H), 8.80 (d, *J* = 7.6 Hz, 1H), 8.75 – 8.30 (br, 2H), 8.44 (d, *J* = 14.2 Hz, 2H), 8.26 – 8.09 (m, 4H), 8.07 (d, *J* = 7.7 Hz, 2H), 8.02 – 7.68 (m, 8H), 7.57 (dd, *J* = 13.1, 6.6 Hz, 3H), 7.50 – 6.70 (br, 8H), 7.36 (s, 1H), 7.05 (s, 1H), 6.96 (dd, *J* = 8.3, 5.4 Hz, 4H), 6.58 (dd, *J* = 28.2, 8.4 Hz, 4H), 4.50 (q, *J* = 7.7 Hz, 1H), 4.41 (q, *J* = 7.7, 7.2 Hz, 1H), 4.30 (tt, *J* = 13.3, 6.2 Hz, 3H), 4.18 (q, *J* = 7.2 Hz, 1H), 3.22 (s, 2H), 3.05 (d, *J* = 8.3 Hz, 4H), 2.95 – 2.80 (m, 4H), 2.70 (dd, *J* = 14.4, 7.4 Hz, 2H), 1.56 (dd, *J* = 71.7, 34.7 Hz, 15H), 0.84 (dd, *J* = 9.8, 6.4 Hz, 6H). **¹³C NMR** (151 MHz, DMSO) δ 172.7, 172.1, 171.3, 171.1, 171.1, 170.9, 166.7, 166.0, 158.8, 158.6, 156.8, 155.8, 154.4, 153.8, 151.8, 151.7, 135.2, 134.8, 132.4, 132.2, 130.8, 130.2, 130.1, 129.7, 127.7, 127.5, 127.4, 125.0, 123.7, 122.3, 122.2, 120.1, 118.1, 116.1, 114.9, 114.9, 114.6, 114.1, 53.9, 53.9, 53.6, 52.4, 52.2, 51.0, 40.7, 40.6, 40.5, 40.1, 38.5, 37.2, 36.8, 36.6, 29.0, 28.3, 25.4, 25.0, 24.2, 23.1, 21.4. **ESI-MS:** *m/z* (%) = 421.89 (M+3H)³⁺. **HR-MS** (ESI): calcd. for C₅₉H₈₂N₂₀O₁₂ (M+3H)³⁺, *m/z* = 421.8880, found 421.8890.

3-((*E*)-4-(((6*S*,9*S*,12*S*,15*S*,18*S*)-1,23-Diamino-6-(((*S*)-1-amino-3-(4-hydroxyphenyl)-1-oxopropan-2-yl)carbamoyl)-12-(3-((*E*)-2-((2-aminoethyl)carbamoyl)guanidino)propyl)-15-(4-hydroxybenzyl)-1,23-diimino-9-isobutyl-8,11,14,17-tetraoxo-2,7,10,13,16,22-hexaazatricosan-18-yl)carbamoyl)phenyl)diazenyl)benzoic acid (**20**).



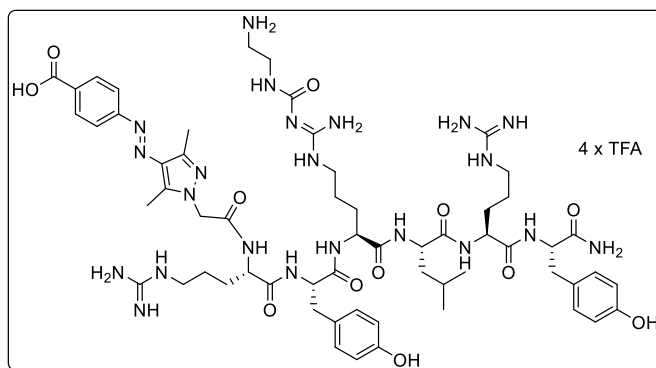
Overall yield: 24%. **¹H NMR** (600 MHz, DMSO-*d*₆) δ 13.35 (br, 1H), 10.72 (s, 1H), 9.19 (d, *J* = 6.5 Hz, 2H), 9.04 (s, 1H), 8.74 (d, *J* = 7.8 Hz, 1H), 8.69 – 8.30 (br, 2H), 8.43 (t, *J* = 1.9 Hz, 1H), 8.26 – 8.21 (m, 1H), 8.21 – 8.18 (m, 1H), 8.16 (dt, *J* = 7.7, 1.5 Hz, 1H), 8.10 – 8.02 (m, 4H), 7.91 (d, *J* = 7.9 Hz, 1H), 7.85 (t, *J* = 7.2 Hz, 4H), 7.80 – 7.76 (m, 1H), 7.72 (d, *J* = 7.9 Hz, 1H), 7.65 (t, *J* = 5.6 Hz, 1H), 7.59 (t, *J* = 6.0 Hz, 2H), 7.55 – 7.14 (br, 4H), 7.37 (s, 1H), 7.14 – 6.69 (br, 4H), 7.05 (s, 1H), 6.98 (t, *J* = 9.0 Hz, 4H), 6.65 – 6.61 (m, 2H), 6.59 – 6.53 (m, 2H), 4.54 – 4.39 (m, 2H), 4.36 – 4.25 (m, 3H), 4.20 (q, *J* = 7.3 Hz, 1H), 3.29 – 3.17 (m, 3H), 3.09 (dp, *J* = 19.4, 6.9 Hz, 4H), 2.91 (t, *J* = 6.8 Hz, 3H), 2.85 (dd, *J* = 13.9, 5.5 Hz, 1H), 2.72 (ddd, *J* = 13.7, 8.4, 4.0 Hz, 2H), 1.85 – 1.33 (m, 15H), 0.90 – 0.81 (m, 6H). **¹³C NMR** (151 MHz, DMSO) δ 172.7, 172.0, 171.2, 171.1, 171.1, 170.8, 166.6, 166.0, 159.0, 158.8, 158.6, 158.4, 156.8, 156.7, 155.8, 154.4, 153.7, 153.3, 151.9, 136.4, 132.4, 132.3, 130.2, 130.1, 130.1, 128.9, 127.7, 127.5, 127.4, 122.5, 122.3, 120.1, 118.1, 116.1, 114.9, 114.8, 114.1, 53.9, 53.8, 53.5, 52.4, 52.1, 51.0, 40.8, 40.5, 40.5, 40.1, 38.5, 37.2, 36.8, 36.6, 29.0, 28.3, 25.4, 24.9, 24.2, 23.1, 21.4. **ESI-MS:** *m/z* (%) = 421.89 (*M*+3*H*)³⁺. **HR-MS** (ESI): calcd. for C₅₉H₈₂N₂₀O₁₂ (*M*+3*H*)³⁺, *m/z* = 421.8880, found 421.8897.

4-((*E*)-(3-(((6*S*,9*S*,12*S*,15*S*,18*S*)-1,23-Diamino-6-(((*S*)-1-amino-3-(4-hydroxyphenyl)-1-oxopropan-2-yl)carbamoyl)-12-(3-((*E*)-2-((2-aminoethyl)carbamoyl)guanidino)propyl)-15-(4-hydroxybenzyl)-1,23-diimino-9-isobutyl-8,11,14,17-tetraoxo-2,7,10,13,16,22-hexaazatricosan-18-yl)carbamoyl)phenyl)diazenyl)benzoic acid (**21**).



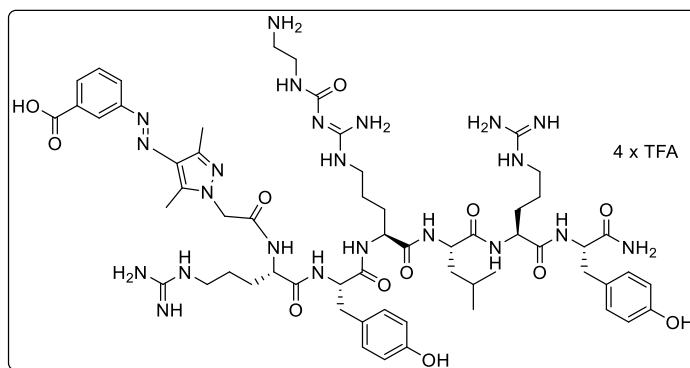
Overall yield: 14%. **¹H NMR** (600 MHz, DMSO-*d*₆) δ 13.39 (br, 1H), 10.78 (s, 1H), 9.20 (d, *J* = 20.5 Hz, 2H), 9.04 (s, 1H), 8.83 (d, *J* = 7.6 Hz, 1H), 8.76 – 8.24 (br, 2H), 8.45 (s, 1H), 8.21 (d, *J* = 7.9 Hz, 1H), 8.19 – 8.14 (m, 2H), 8.13 – 8.04 (m, 3H), 8.03 – 7.98 (m, 2H), 7.94 – 7.84 (m, 5H), 7.74 (q, *J* = 7.5 Hz, 2H), 7.69 (t, *J* = 5.6 Hz, 1H), 7.66 – 7.58 (m, 2H), 7.50 – 6.80 (br, 8H), 7.36 (s, 1H), 7.05 (s, 1H), 6.97 (t, *J* = 8.3 Hz, 4H), 6.63 (d, *J* = 8.5 Hz, 2H), 6.56 (d, *J* = 8.4 Hz, 2H), 4.50 (td, *J* = 8.2, 4.1 Hz, 1H), 4.43 (td, *J* = 8.4, 5.3 Hz, 1H), 4.31 (dtd, *J* = 22.2, 12.0, 10.0, 6.2 Hz, 3H), 4.19 (q, *J* = 7.5 Hz, 1H), 3.23 (p, *J* = 6.6 Hz, 3H), 3.08 (dq, *J* = 20.0, 6.7 Hz, 4H), 2.91 (q, *J* = 7.5, 5.4 Hz, 3H), 2.85 (dd, *J* = 13.9, 5.5 Hz, 1H), 2.72 (ddd, *J* = 13.9, 8.6, 5.4 Hz, 2H), 1.77 – 1.58 (m, 5H), 1.57 – 1.49 (m, 5H), 1.44 (dtd, *J* = 16.8, 8.9, 4.3 Hz, 5H), 0.85 (dd, *J* = 16.0, 6.5 Hz, 6H). **¹³C NMR** (151 MHz, DMSO) δ 172.7, 172.1, 171.3, 171.1, 171.1, 170.9, 166.7, 166.0, 159.3, 159.1, 158.8, 158.6, 156.8, 156.8, 155.9, 154.4, 154.2, 153.7, 151.8, 135.3, 133.2, 131.0, 130.7, 130.2, 130.1, 129.7, 127.5, 127.4, 125.2, 122.7, 122.3, 120.0, 119.7, 118.0, 116.1, 114.9, 114.9, 114.1, 53.9, 53.9, 53.6, 52.4, 52.2, 51.0, 40.7, 40.6, 40.5, 40.1, 38.5, 37.2, 36.8, 36.6, 29.0, 28.3, 25.4, 25.0, 24.2, 23.1, 21.4. **ESI-MS:** *m/z* (%) = 421.89 (*M*+3*H*)³⁺. **HR-MS** (ESI): calcd. for C₅₉H₈₂N₂₀O₁₂ (*M*+3*H*)³⁺, *m/z* = 421.8880, found 421.8899.

4-((*E*)-1-((6*S*,9*S*,12*S*,15*S*,18*S*)-1-Amino-6-(((*S*)-1-amino-3-(4-hydroxyphenyl)-1-oxopropan-2-yl)carbamoyl)-12-(3-((*E*)-2-(2-aminoethyl)carbamoyl)guanidino)propyl)-18-(3-guanidinopropyl)-15-(4-hydroxybenzyl)-1-imino-9-isobutyl-8,11,14,17,20-pentaoxo-2,7,10,13,16,19-hexaazahenicosan-21-yl)-3,5-dimethyl-1*H*-pyrazol-4-yl)diazenyl)benzoic acid (**22**).



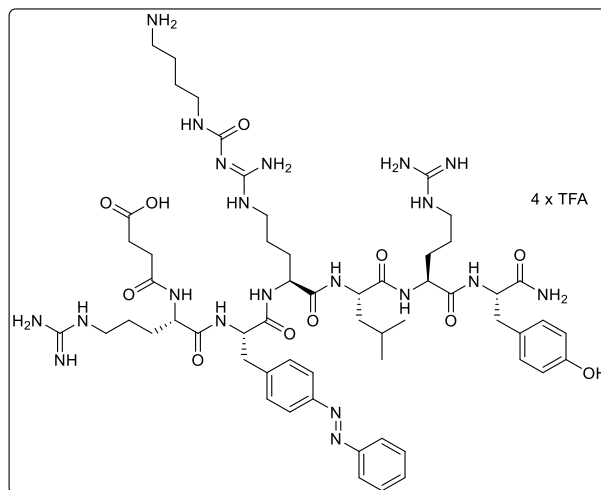
Overall yield: 7%. **¹H NMR** (600 MHz, DMSO-*d*₆) δ 13.10 (br, 1H), 10.70 (s, 1H), 9.19 (d, *J* = 8.9 Hz, 2H), 9.02 (s, 1H), 8.70 – 8.25 (br, 2H), 8.44 (d, *J* = 8.0 Hz, 1H), 8.22 (d, *J* = 7.8 Hz, 1H), 8.11 – 8.05 (m, 3H), 7.93 (dd, *J* = 32.1, 7.8 Hz, 2H), 7.84 (s, 2H), 7.81 – 7.79 (m, 2H), 7.72 (d, *J* = 7.8 Hz, 1H), 7.59 (dt, *J* = 21.5, 5.7 Hz, 3H), 7.51 – 6.71 (br, 7H), 7.37 (d, *J* = 2.2 Hz, 1H), 7.06 (d, *J* = 2.1 Hz, 1H), 7.01 – 6.95 (m, 5H), 6.63 (dd, *J* = 8.5, 3.1 Hz, 4H), 4.93 – 4.78 (m, 2H), 4.48 (td, *J* = 8.2, 4.0 Hz, 1H), 4.31 (dtd, *J* = 23.4, 7.5, 4.0 Hz, 4H), 4.20 (td, *J* = 7.7, 6.0 Hz, 1H), 3.24 (s, 2H), 3.06 (q, *J* = 7.0 Hz, 4H), 2.92 (d, *J* = 11.3 Hz, 3H), 2.85 (dd, *J* = 13.9, 5.5 Hz, 1H), 2.70 (ddd, *J* = 19.9, 14.0, 8.4 Hz, 2H), 2.51 (s, 3H), 2.38 (s, 3H), 1.71 – 1.40 (m, 15H), 0.86 (dd, *J* = 17.8, 6.5 Hz, 6H). **¹³C NMR** (151 MHz, DMSO) δ 172.7, 172.0, 171.1, 171.1, 171.1, 170.8, 166.9, 166.2, 158.9, 158.7, 158.5, 158.3, 156.7, 155.9, 155.8, 155.5, 142.1, 141.1, 135.0, 131.1, 130.5, 130.1, 130.0, 127.5, 127.4, 121.4, 118.1, 116.2, 114.9, 53.9, 52.4, 52.1, 51.5, 50.9, 40.8, 40.5, 40.4, 40.1, 38.5, 37.1, 36.8, 36.6, 29.3, 29.0, 25.0, 24.9, 24.2, 23.1, 21.4, 14.0, 9.6. **ESI-MS:** *m/z* (%) = 432.57 (*M*+3*H*)³⁺. **HR-MS** (ESI): calcd. for C₅₉H₈₆N₂₂O₁₂ (*M*+3*H*)³⁺, *m/z* = 432.5671, found 432.5685.

3-((*E*)-1-((6*S*,9*S*,12*S*,15*S*,18*S*)-1-Amino-6-(((*S*)-1-amino-3-(4-hydroxyphenyl)-1-oxopropan-2-yl)carbamoyl)-12-(3-((*E*)-2-((2-aminoethyl)carbamoyl)guanidino)propyl)-18-(3-guanidinopropyl)-15-(4-hydroxybenzyl)-1-imino-9-isobutyl-8,11,14,17,20-pentaoxo-2,7,10,13,16,19-hexaazahenicosan-21-yl)-3,5-dimethyl-1*H*-pyrazol-4-yl)diazenyl)benzoic acid (23).



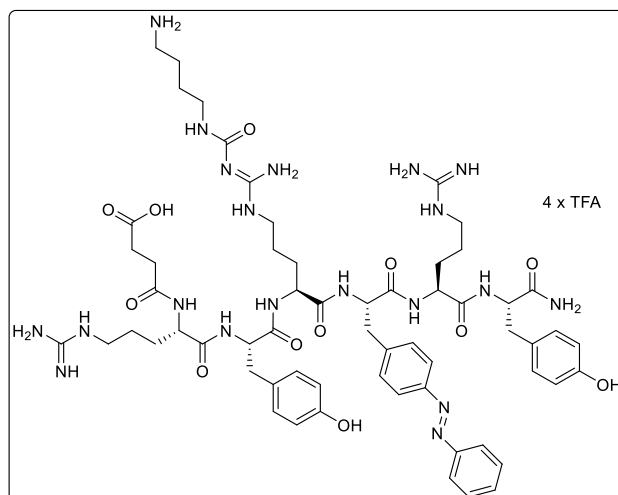
Overall yield: 7%. **¹H NMR** (600 MHz, DMSO-*d*₆) δ 13.23 (br, 1H), 10.75 (s, 1H), 9.20 (d, *J* = 6.8 Hz, 2H), 9.04 (s, 1H), 8.70 – 8.25 (br, 2H), 8.44 (d, *J* = 8.0 Hz, 1H), 8.28 – 8.20 (m, 2H), 8.09 (d, *J* = 7.7 Hz, 1H), 8.00 (dt, *J* = 7.7, 1.5 Hz, 1H), 7.97 – 7.89 (m, 3H), 7.82 (d, *J* = 35.2 Hz, 3H), 7.73 (d, *J* = 7.8 Hz, 1H), 7.67 – 7.56 (m, 4H), 7.54 – 6.71 (br, 7H), 7.38 – 7.36 (m, 1H), 7.07 – 7.04 (m, 1H), 7.01 – 6.95 (m, 5H), 6.63 (dd, *J* = 8.5, 3.5 Hz, 4H), 4.91 – 4.65 (m, 2H), 4.48 (dd, *J* = 8.5, 4.3 Hz, 1H), 4.36 – 4.23 (m, 4H), 4.20 (q, *J* = 7.5 Hz, 1H), 3.24 (s, 2H), 3.06 (q, *J* = 7.1 Hz, 4H), 2.92 (d, *J* = 9.9 Hz, 3H), 2.85 (dd, *J* = 13.9, 5.5 Hz, 1H), 2.70 (ddd, *J* = 19.8, 13.9, 8.4 Hz, 2H), 2.51 (s, 3H), 2.39 (s, 3H), 1.71 – 1.39 (m, 15H), 0.86 (dd, *J* = 17.6, 6.5 Hz, 6H). **ESI-MS:** *m/z* (%) = 324.68 (M+4H)⁴⁺. **HR-MS** (ESI): calcd. for C₅₉H₈₆N₂₂O₁₂ (M+4H)⁴⁺, *m/z* = 324.6772, found 324.6779.

(13*S*,16*S*,19*S*,*E*)-1,8-Diamino-13-(((*S*)-1-(((*S*)-1-(((*S*)-1-amino-3-(4-hydroxyphenyl)-1-oxopropan-2-yl)amino)-5-guanidino-1-oxopentan-2-yl)amino)-4-methyl-1-oxopentan-2-yl)carbamoyl)-19-(3-guanidinopropyl)-6,15,18,21-tetraoxo-16-(4-((*E*)-phenyldiazenyl)benzyl)-5,7,9,14,17,20-hexaazatetracos-7-en-24-oic acid (**24**).



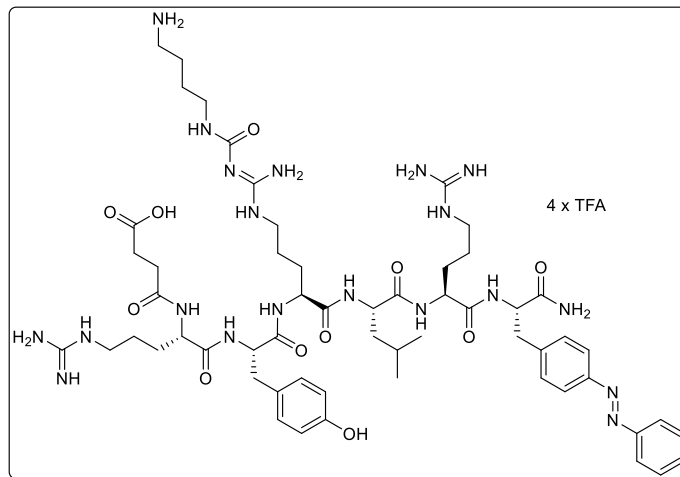
Overall yield: 36%. $^1\text{H NMR}$ (400 MHz, DMSO- d_6) δ 12.19 (br, 1H), 10.57 (s, 1H), 9.22 (d, $J = 14.9$ Hz, 1H), 9.04 (s, 1H), 8.47 (s, 2H), 8.29 – 8.02 (m, 3H), 7.93 (d, $J = 7.6$ Hz, 1H), 7.88 – 7.84 (m, 2H), 7.77 (dq, $J = 11.5, 7.9, 5.7$ Hz, 5H), 7.64 (s, 2H), 7.62 – 7.56 (m, 3H), 7.55 – 6.85 (br, 9H), 7.42 (d, $J = 8.2$ Hz, 2H), 7.36 (s, 1H), 6.97 (d, $J = 8.4$ Hz, 2H), 6.84 – 6.69 (m, 1H), 6.68 – 6.60 (m, 2H), 4.60 (dt, $J = 12.8, 5.8$ Hz, 1H), 4.40 – 4.26 (m, 3H), 4.19 (dq, $J = 12.5, 7.4$ Hz, 2H), 3.25 (s, 2H), 3.18 – 2.99 (m, 7H), 2.99 – 2.89 (m, 1H), 2.89 – 2.69 (m, 4H), 2.46 – 2.34 (m, 4H), 1.77 – 1.34 (m, 19H), 0.92 – 0.79 (m, 6H). **HR-MS** (ESI): calcd. for $\text{C}_{57}\text{H}_{86}\text{N}_{20}\text{O}_{11}$ ($\text{M}+\text{H}$) $^+$, $m/z = 1227.6858$, found 1227.6853.

(13*S*,16*S*,19*S*,*E*)-1,8-Diamino-13-(((*S*)-1-(((*S*)-1-(((*S*)-1-amino-3-(4-hydroxyphenyl)-1-oxopropan-2-yl)amino)-5-guanidino-1-oxopentan-2-yl)amino)-1-oxo-3-(4-((*E*)-phenyldiazenyl)phenyl)propan-2-yl)carbamoyl)-19-(3-guanidinopropyl)-16-(4-hydroxybenzyl)-6,15,18,21-tetraoxo-5,7,9,14,17,20-hexaazatetracos-7-en-24-oic acid (25).



Overall yield: 25%. **¹H NMR** (600 MHz, DMSO-*d*₆) δ 12.21 (br, 1H), 10.28 (s, 1H), 9.20 (d, *J* = 5.3 Hz, 2H), 8.95 (s, 1H), 8.41 (s, 2H), 8.32 (d, *J* = 7.8 Hz, 1H), 8.08 (d, *J* = 7.7 Hz, 1H), 7.89 (dd, *J* = 29.2, 7.9 Hz, 2H), 7.80 (dt, *J* = 5.7, 1.8 Hz, 2H), 7.76 (d, *J* = 8.2 Hz, 2H), 7.71 (d, *J* = 9.2 Hz, 4H), 7.56 (dq, *J* = 11.5, 5.8 Hz, 5H), 7.42 (d, *J* = 8.1 Hz, 3H), 7.37 – 6.72 (br, 6H), 7.27 (t, *J* = 7.8 Hz, 1H), 7.17 – 7.10 (m, 2H), 7.10 – 7.04 (m, 2H), 7.02 – 6.94 (m, 5H), 6.79 – 6.68 (m, 1H), 6.65 – 6.63 (m, 2H), 6.61 – 6.57 (m, 2H), 4.65 (td, *J* = 8.4, 4.2 Hz, 1H), 4.38 (dt, *J* = 10.1, 6.2 Hz, 2H), 4.26 (t, *J* = 7.8 Hz, 2H), 4.16 – 4.10 (m, 1H), 3.18 (s, 2H), 3.08 (qd, *J* = 12.5, 7.9, 6.7 Hz, 4H), 3.01 (t, *J* = 6.5 Hz, 2H), 2.87 (dt, *J* = 16.2, 8.1 Hz, 3H), 2.78 (q, *J* = 7.5, 6.9 Hz, 3H), 2.44 (q, *J* = 6.4, 5.7 Hz, 2H), 2.40 – 2.34 (m, 2H), 1.69 – 1.62 (m, 2H), 1.53 – 1.36 (m, 14H). **HR-MS** (ESI): calcd. for C₆₀H₈₄N₂₀O₁₂ (M+2H)²⁺, *m/z* = 639.3362, found 639.3368.

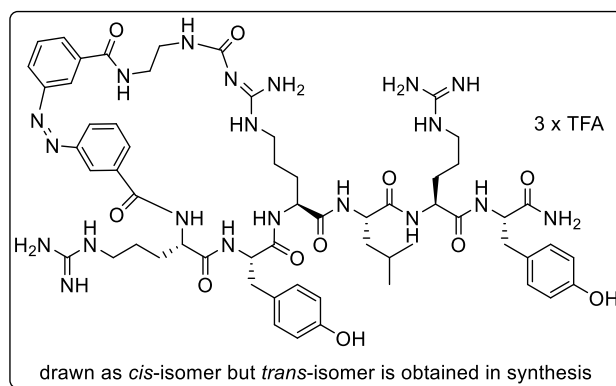
(13*S*,16*S*,19*S*,*E*)-1,8-Diamino-13-(((*S*)-1-(((*S*)-1-(((*S*)-1-amino-1-oxo-3-(4-((*E*)-phenyldiazenyl)phenyl)propan-2-yl)amino)-5-guanidino-1-oxopentan-2-yl)amino)-4-methyl-1-oxopentan-2-yl)carbamoyl)-19-(3-guanidinopropyl)-16-(4-hydroxybenzyl)-6,15,18,21-tetraoxo-5,7,9,14,17,20-hexaazatetracos-7-en-24-oic acid (**26**).



Overall yield: 33%. **¹H NMR** (400 MHz, DMSO-*d*₆) δ 12.18 (br, 1H), 10.54 (s, 1H), 9.21 (d, *J* = 15.0 Hz, 1H), 9.03 (s, 1H), 8.43 (d, *J* = 26.0 Hz, 2H), 8.27 – 7.97 (m, 3H), 7.94 – 7.84 (m, 3H), 7.76 (dd, *J* = 15.6, 7.8 Hz, 5H), 7.67 – 7.55 (m, 5H), 7.45 – 6.85 (m, 9H), 7.42 (d, *J* = 8.2 Hz, 2H), 7.35 (s, 1H), 6.99 – 6.95 (m, 2H), 6.76 (dd, *J* = 35.4, 7.8 Hz, 1H), 6.64 (dd, *J* = 8.0, 5.8 Hz, 2H), 4.60 (q, *J* = 7.5 Hz, 1H), 4.38 – 4.24 (m, 3H), 4.20 (dq, *J* = 13.5, 7.9, 7.4 Hz, 2H), 3.25 (s, 2H), 3.17 – 2.99 (m, 7H), 2.94 (dd, *J* = 13.8, 8.9 Hz, 1H), 2.88 – 2.69 (m, 4H), 2.40 (dq, *J* = 19.3, 7.2 Hz, 4H), 1.69 – 1.34 (m, 19H), 0.92 – 0.79 (m, 6H). **¹³C NMR** (101 MHz, DMSO) δ 174.1, 172.7, 172.0, 171.8, 171.5, 171.1, 170.8, 170.6, 158.9, 158.6, 158.3, 156.8, 155.8, 152.0, 150.6, 141.5, 131.4, 130.3, 130.0, 129.5, 128.9, 127.5, 122.4, 122.3, 119.9, 119.8, 118.6, 115.6, 114.9, 53.9, 53.5, 52.5, 52.3, 52.2, 51.1, 40.7, 40.5, 40.4, 40.4, 38.6, 38.5, 37.1, 36.8, 30.0, 29.2, 29.0, 28.7, 26.0, 25.0, 24.9, 24.6, 24.4, 24.2, 23.1, 21.5. **HR-MS** (ESI): calcd. for C₅₇H₈₆N₂₀O₁₁ (M+2H)²⁺, *m/z* = 614.3465, found 614.3464.

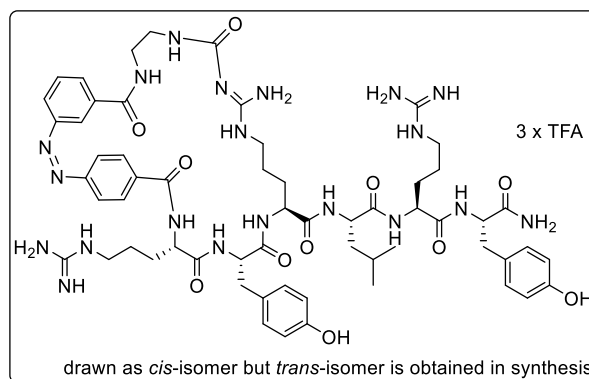
General procedure for the cyclization of peptides 27-34. Peptides **19-26** (1 eq.), HOBT (5 eq.) and DIPEA (10 eq.) were dissolved in DMF/NMP 8:2 v/v (100 μL/μmol of peptide) in an Eppendorf tube. Under stirring, a solution of PyBOP (5 eq.) in DMF/NMP 8:2 v/v (100 μL/μmol of peptide) was added and the mixture was stirred at rt overnight. The crude product was purified by preparative HPLC (column: Luna 10, 250 x 21 mm; flow: 22 mL/min, solvent A: H₂O (0.05% TFA), solvent B: MeCN; gradient A/B: 0-20 min: 97/3, 20-25 min: 2/98).

(2*E*,11*E*,17*S*,20*S*,23*S*)-12-Amino-*N*-(((*S*)-1-(((*S*)-1-(((*S*)-1-amino-3-(4-hydroxyphenyl)-1-oxopropan-2-yl)amino)-5-guanidino-1-oxopentan-2-yl)amino)-4-methyl-1-oxopentan-2-yl)-23-(3-guanidinopropyl)-20-(4-hydroxybenzyl)-5,10,19,22,25-pentaoxo-2,3,6,9,11,13,18,21,24-nonaaza-1,4(1,3)-dibenzenacyclopentacosaphane-2,11-diene-17-carboxamide (27).



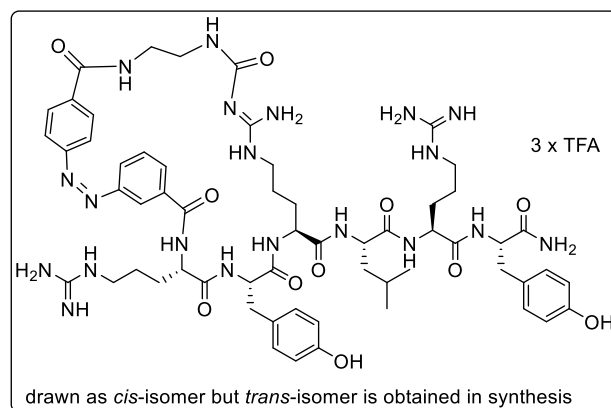
Yield: 47%. **¹H NMR** (600 MHz, DMSO-*d*₆) δ 10.19 (d, *J* = 73.6 Hz, 1H), 9.20 (d, *J* = 11.9 Hz, 2H), 9.06 (s, 1H), 8.87 (t, *J* = 5.6 Hz, 1H), 8.58 (s, 1H), 8.55 – 8.48 (br, 1H), 8.46 (d, *J* = 1.9 Hz, 1H), 8.36 (s, 1H), 8.26 (d, *J* = 7.9 Hz, 1H), 8.13 (d, *J* = 7.9 Hz, 1H), 8.06 (td, *J* = 6.8, 6.2, 3.0 Hz, 4H), 7.85 (d, *J* = 7.9 Hz, 1H), 7.73 (dt, *J* = 12.7, 7.8 Hz, 3H), 7.61 (t, *J* = 5.6 Hz, 2H), 7.55 (t, *J* = 5.7 Hz, 1H), 7.51 – 7.15 (br, 4), 7.39 – 7.35 (m, 1H), 7.15 – 6.7 (br, 4H), 7.06 (d, *J* = 8.2 Hz, 3H), 6.98 – 6.95 (m, 2H), 6.69 – 6.58 (m, 4H), 4.44 (s, 2H), 4.36 – 4.28 (m, 2H), 4.21 (dt, *J* = 14.2, 6.7 Hz, 2H), 3.48 (s, 1H), 3.44 – 3.40 (m, 1H), 3.32 – 3.21 (m, 3H), 3.16 (d, *J* = 4.5 Hz, 1H), 3.08 (dq, *J* = 19.9, 6.6 Hz, 4H), 2.96 – 2.81 (m, 2H), 2.76 – 2.63 (m, 2H), 1.86 – 1.36 (m, 15H), 0.86 (ddd, *J* = 17.5, 11.9, 6.8 Hz, 6H). **¹³C NMR** (151 MHz, DMSO) δ 172.7, 172.0, 171.2, 171.1, 171.1, 170.8, 166.6, 166.0, 159.0, 158.8, 158.6, 158.4, 156.8, 156.7, 155.8, 154.4, 153.7, 153.3, 151.9, 136.4, 132.4, 132.3, 130.2, 130.1, 130.1, 128.9, 127.7, 127.5, 127.4, 122.5, 122.3, 120.1, 118.1, 116.1, 114.9, 114.8, 114.1, 53.9, 53.8, 53.5, 52.4, 52.1, 51.0, 40.8, 40.6, 40.5, 40.1, 38.5, 37.2, 36.8, 36.6, 30.7, 29.0, 28.3, 25.4, 24.9, 24.6, 24.2, 23.1, 21.4. **ESI-MS:** *m/z* (%) = 415.89 (M+3H)³⁺. **HR-MS** (ESI): calcd. for C₅₉H₈₀N₂₀O₁₁ (M+3H)³⁺, *m/z* = 415.8845, found 415.8854.

(2*E*,11*E*,17*S*,20*S*,23*S*)-12-Amino-N-(((*S*)-1-(((*S*)-1-(((*S*)-1-amino-3-(4-hydroxyphenyl)-1-oxopropan-2-yl)amino)-5-guanidino-1-oxopentan-2-yl)amino)-4-methyl-1-oxopentan-2-yl)-23-(3-guanidinopropyl)-20-(4-hydroxybenzyl)-5,10,19,22,25-pentaoxo-2,3,6,9,11,13,18,21,24-nonaaza-1(1,4),4(1,3)-dibenzencyclopentacosaphane-2,11-diene-17-carboxamide (28).



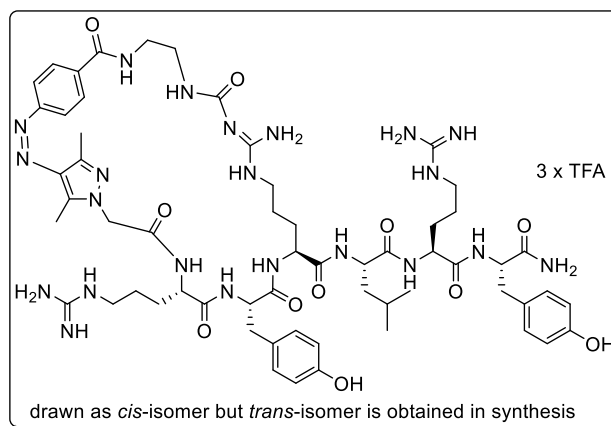
Yield: 43%. **¹H NMR** (600 MHz, DMSO-*d*₆) δ 10.35 (s, 1H), 9.24 – 9.15 (m, 2H), 9.00 (d, *J* = 6.3 Hz, 1H), 8.85 (s, 1H), 8.69 (s, 1H), 8.48 (s, 1H), 8.11 – 8.06 (m, 2H), 8.02 (dd, *J* = 13.8, 7.6 Hz, 2H), 7.96 – 7.82 (m, 4H), 7.78 – 7.69 (m, 2H), 7.69 – 7.57 (m, 2H), 7.54 (q, *J* = 6.8, 5.7 Hz, 1H), 7.47 (s, 1H), 7.44 – 7.11 (br, 4H), 7.36 (d, *J* = 3.9 Hz, 1H), 7.11 – 6.68 (br, 4H), 7.08 – 7.05 (m, 1H), 6.97 (dd, *J* = 8.7, 2.9 Hz, 2H), 6.89 (d, *J* = 8.0 Hz, 2H), 6.67 – 6.53 (m, 4H), 4.42 (q, *J* = 7.4 Hz, 1H), 4.32 (td, *J* = 7.8, 5.7 Hz, 1H), 4.27 (ddd, *J* = 10.3, 7.6, 4.8 Hz, 1H), 4.25 – 4.08 (m, 3H), 3.44 (s, 2H), 3.20 – 2.88 (m, 7H), 2.85 (dd, *J* = 13.9, 5.5 Hz, 1H), 2.72 (dt, *J* = 13.8, 8.2 Hz, 2H), 1.78 – 1.28 (m, 15H), 0.91 – 0.80 (m, 6H). **ESI-MS:** *m/z* (%) = 415.89 (*M*+3*H*)³⁺. **HR-MS** (ESI): calcd. for C₅₉H₈₀N₂₀O₁₁ (*M*+3*H*)³⁺, *m/z* = 415.8845, found 415.8850.

(2*E*,11*E*,17*S*,20*S*,23*S*)-12-Amino-N-(((*S*)-1-(((*S*)-1-(((*S*)-1-amino-3-(4-hydroxyphenyl)-1-oxopropan-2-yl)amino)-5-guanidino-1-oxopentan-2-yl)amino)-4-methyl-1-oxopentan-2-yl)-23-(3-guanidinopropyl)-20-(4-hydroxybenzyl)-5,10,19,22,25-pentaoxo-2,3,6,9,11,13,18,21,24-nonaaza-1(1,3),4(1,4)-dibenzenacyclopentacosaphane-2,11-diene-17-carboxamide (29).



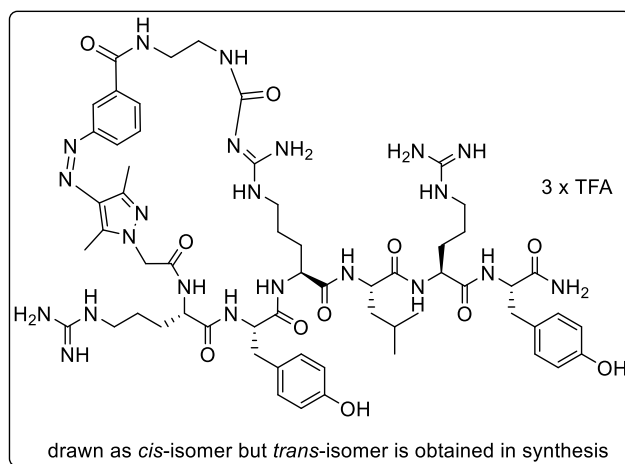
Yield: 76%. **¹H NMR** (600 MHz, DMSO-*d*₆) δ 10.20 (s, 1H), 9.29 – 9.11 (m, 2H), 9.10 – 8.90 (m, 2H), 8.48 (t, *J* = 5.8 Hz, 1H), 8.32 – 8.14 (br, 1H), 8.23 (d, *J* = 1.9 Hz, 1H), 8.12 – 8.08 (m, 1H), 8.05 (d, *J* = 7.7 Hz, 1H), 8.01 (d, *J* = 7.5 Hz, 1H), 7.99 – 7.87 (m, 5H), 7.80 – 7.71 (m, 2H), 7.68 – 7.58 (m, 2H), 7.51 (t, *J* = 5.7 Hz, 1H), 7.48 – 7.13 (br, 4H), 7.34 (s, 2H), 7.13– 6.67 (br, 4H), 7.07 – 7.05 (m, 1H), 6.97 – 6.94 (m, 2H), 6.90 (d, *J* = 8.1 Hz, 2H), 6.67 – 6.58 (m, 4H), 4.47 (td, *J* = 8.3, 4.4 Hz, 1H), 4.35 – 4.26 (m, 2H), 4.23 (q, *J* = 10.2, 8.6 Hz, 1H), 4.16 (q, *J* = 7.3 Hz, 1H), 4.10 (d, *J* = 7.5 Hz, 1H), 3.53 (dt, *J* = 14.5, 6.8 Hz, 1H), 3.30 – 3.14 (m, 2H), 3.05 (ddt, *J* = 37.4, 15.1, 8.3 Hz, 6H), 2.85 (dd, *J* = 13.9, 5.5 Hz, 1H), 2.71 (dt, *J* = 14.1, 7.7 Hz, 2H), 1.88 – 1.34 (m, 15H), 0.90 – 0.75 (m, 6H). **ESI-MS:** *m/z* (%) = 415.88 (M+3H)³⁺. **HR-MS** (ESI): calcd. for C₅₉H₈₀N₂₀O₁₁ (M+3H)³⁺, *m/z* = 415.8845, found 415.8855.

(1⁴*E*,2^Z,11*E*,17*S*,20*S*,23*S*)-12-Amino-*N*-(((*S*)-1-(((*S*)-1-(((*S*)-1-amino-3-(4-hydroxyphenyl)-1-oxopropan-2-yl)amino)-5-guanidino-1-oxopentan-2-yl)amino)-4-methyl-1-oxopentan-2-yl)-23-(3-guanidinopropyl)-20-(4-hydroxybenzyl)-1³,1⁵-dimethyl-5,10,19,22,25-pentaoxo-11*H*-2,3,6,9,11,13,18,21,24-nonaaza-1(4,1)-pyrazola-4(1,4)-benzenacyclohexacosaphane-2,11,4)-diene-17-carboxamide (30).



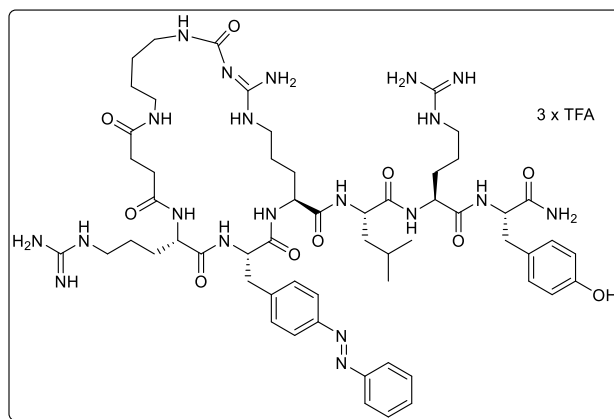
Yield: 30%. **¹H NMR** (600 MHz, DMSO-*d*₆) δ 10.07 (s, 1H), 9.23 – 9.16 (m, 2H), 8.93 (s, 1H), 8.35 (d, *J* = 23.2 Hz, 2H), 8.24 (s, 2H), 8.14 (d, *J* = 7.6 Hz, 1H), 7.96 (d, *J* = 7.6 Hz, 1H), 7.86 (d, *J* = 8.2 Hz, 2H), 7.72 (dd, *J* = 25.3, 8.2 Hz, 3H), 7.57 (s, 1H), 7.51 (s, 1H), 7.48 – 7.19 (br, 2H), 7.44 (s, 1H), 7.38 (s, 1H), 7.31 (s, 1H), 7.18 – 6.68 (br, 4H), 7.09 – 7.05 (m, 1H), 6.98 – 6.89 (m, 3H), 6.67 – 6.60 (m, 4H), 4.89 (s, 2H), 4.55 (q, *J* = 8.3, 7.8 Hz, 1H), 4.36 – 4.29 (m, 2H), 4.30 – 4.07 (m, 2H), 3.92 (q, *J* = 7.0 Hz, 1H), 3.51 (d, *J* = 0.9 Hz, 1H), 3.24 – 2.95 (m, 6H), 2.91 (dd, *J* = 14.2, 4.2 Hz, 1H), 2.85 (dd, *J* = 13.9, 5.6 Hz, 1H), 2.69 (ddd, *J* = 26.7, 13.9, 8.0 Hz, 2H), 2.49 – 2.34 (m, 6H), 1.68 – 1.35 (m, 15H), 0.86 (dt, *J* = 19.9, 7.3 Hz, 6H). **ESI-MS:** *m/z* (%) = 426.56 (M+3H)³⁺. **HR-MS** (ESI): calcd. for C₅₉H₈₄N₂₂O₁₁ (M+3H)³⁺, *m/z* = 426.5636, found 426.5646.

(1⁴*E*,2*E*,11*E*,17*S*,20*S*,23*S*)-12-Amino-*N*-(((*S*)-1-(((*S*)-1-(((*S*)-1-amino-3-(4-hydroxyphenyl)-1-oxopropan-2-yl)amino)-5-guanidino-1-oxopentan-2-yl)amino)-4-methyl-1-oxopentan-2-yl)-23-(3-guanidinopropyl)-20-(4-hydroxybenzyl)-1³,1⁵-dimethyl-5,10,19,22,25-pentaoxo-1¹*H*-2,3,6,9,11,13,18,21,24-nonaaza-1(4,1)-pyrazola-4(1,3)-benzenacyclohexacosaphane-2,11-diene-17-carboxamide (31).



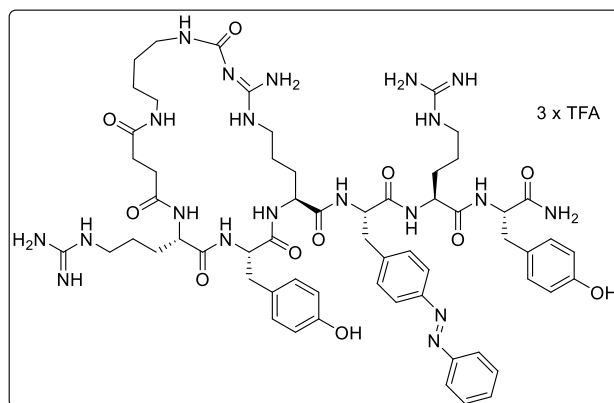
Yield: 39%. **¹H NMR** (600 MHz, DMSO-*d*₆) δ 10.10 (d, 1H), 9.26 – 9.14 (m, 2H), 8.95 (s, 1H), 8.67 (s, 1H), 8.41 (s, 2H), 8.24 (s, 1H), 8.07 (s, 1H), 8.01 (d, *J* = 8.7 Hz, 1H), 7.85 (dd, *J* = 14.6, 7.8 Hz, 4H), 7.72 (dd, *J* = 16.7, 7.9 Hz, 1H), 7.68 – 7.56 (m, 2H), 7.51 (t, *J* = 7.0 Hz, 2H), 7.45 (d, *J* = 7.2 Hz, 1H), 7.41 – 7.16 (br, 3H), 7.36 (d, *J* = 12.3 Hz, 1H), 7.16 – 6.69 (br, 4H), 7.06 – 7.04 (m, 1H), 6.98 – 6.94 (m, 4H), 6.66 – 6.60 (m, 4H), 4.88 (s, 2H), 4.45 – 4.07 (m, 5H), 3.98 (q, *J* = 6.2 Hz, 1H), 3.49 – 3.38 (m, 2H), 3.10 – 2.98 (m, 9H), 2.85 (dt, *J* = 13.8, 5.2 Hz, 1H), 2.72 (ddd, *J* = 21.7, 14.2, 8.8 Hz, 2H), 2.39 (s, 3H), 1.65 – 1.35 (m, 15H), 0.88 – 0.81 (m, 6H). **ESI-MS:** *m/z* (%) = 426.56 (M+3H)³⁺. **HR-MS** (ESI): calcd. for C₅₉H₈₄N₂₂O₁₁ (M+3H)³⁺, *m/z* = 426.5636, found 426.5642.

(9*S*,12*S*,15*S*,*E*)-4-Amino-*N*-((*S*)-1-(((*S*)-1-(((*S*)-1-amino-3-(4-hydroxyphenyl)-1-oxopropan-2-yl)amino)-5-guanidino-1-oxopentan-2-yl)amino)-4-methyl-1-oxopentan-2-yl)-15-(3-guanidinopropyl)-2,11,14,17,20-pentaoxo-12-(4-((*E*)-phenyldiazenyl)benzyl)-1,3,5,10,13,16,21-heptaazacyclopentacos-3-ene-9-carboxamide (32).



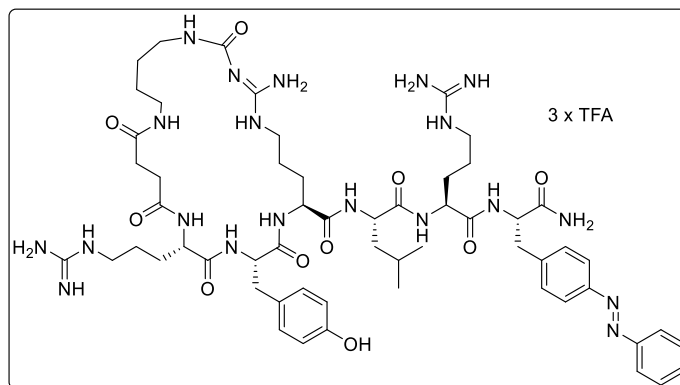
Yield: 61%. **¹H NMR** (600 MHz, DMSO-*d*₆) δ 10.18 (s, 1H), 9.18 (t, *J* = 10.2 Hz, 2H), 8.33 (s, 2H), 8.17 (s, 1H), 8.00 (d, *J* = 10.4 Hz, 2H), 7.95 – 7.71 (m, 6H), 7.62 – 7.51 (m, 5H), 7.51 – 6.67 (br, 10H), 7.43 (d, *J* = 8.3 Hz, 1H), 7.36 (s, 1H), 7.06 (s, 1H), 6.99 – 6.96 (m, 2H), 6.78 (dd, *J* = 41.6, 7.9 Hz, 1H), 6.63 (d, *J* = 8.2 Hz, 2H), 4.54 (s, 1H), 4.36 – 4.24 (m, 3H), 4.21 (q, *J* = 7.4 Hz, 1H), 4.08 (s, 1H), 3.23 – 2.92 (m, 10H), 2.85 (dt, *J* = 14.0, 7.0 Hz, 2H), 2.71 (dd, *J* = 13.9, 8.0 Hz, 1H), 2.34 (dd, *J* = 37.2, 11.8 Hz, 4H), 1.64 (s, 3H), 1.53 (t, *J* = 11.4 Hz, 4H), 1.50 – 1.29 (m, 12H), 0.84 (td, *J* = 20.3, 19.4, 6.5 Hz, 6H). **¹³C NMR** (151 MHz, DMSO) δ 173.1, 173.1, 172.5, 172.4, 171.4, 171.3, 171.1, 158.8, 158.6, 157.2, 156.3, 154.4, 154.2, 152.4, 151.1, 142.1, 131.9, 130.6, 130.5, 129.9, 129.4, 128.0, 127.6, 122.9, 122.9, 120.4, 120.3, 118.7, 116.7, 115.3, 54.4, 53.6, 52.8, 52.2, 51.6, 41.0, 40.9, 40.9, 40.8, 40.7, 39.3, 38.6, 37.3, 36.9, 31.6, 31.4, 29.4, 29.0, 27.0, 25.6, 25.3, 24.6, 23.6, 21.9. **HR-MS** (ESI): calcd. for C₅₇H₈₄N₂₀O₁₀ (M+H)⁺, *m/z* = 1209.6753, found 1209.6754.

(9*S*,12*S*,15*S*,*E*)-4-Amino-*N*-((*S*)-1-(((*S*)-1-(((*S*)-1-amino-3-(4-hydroxyphenyl)-1-oxopropan-2-yl)amino)-5-guanidino-1-oxopentan-2-yl)amino)-1-oxo-3-(4-((*E*)-phenyldiazenyl)phenyl)propan-2-yl)-15-(3-guanidinopropyl)-12-(4-hydroxybenzyl)-2,11,14,17,20-pentaoxo-1,3,5,10,13,16,21-heptaazacyclopentacos-3-ene-9-carboxamide (33).



Yield: 69%. **¹H NMR** (600 MHz, DMSO-*d*₆) δ 10.19 (s, 1H), 9.20 (d, *J* = 7.3 Hz, 2H), 9.11 (s, 1H), 8.47 – 8.25 (m, 3H), 8.03 (d, *J* = 7.9 Hz, 2H), 7.99 – 7.74 (m, 8H), 7.59 – 7.50 (m, 5H), 7.50 – 6.67 (br, 8H), 7.46 – 7.39 (m, 3H), 7.28 (t, *J* = 7.9 Hz, 1H), 7.15 (dd, *J* = 7.9, 6.0 Hz, 1H), 7.06 (d, *J* = 8.0 Hz, 1H), 7.01 – 6.97 (m, 4H), 6.79 – 6.68 (m, 1H), 6.67 – 6.58 (m, 4H), 4.65 (td, *J* = 8.6, 3.9 Hz, 1H), 4.42 – 4.31 (m, 2H), 4.30 – 4.18 (m, 2H), 4.15 – 4.05 (m, 1H), 3.25 (s, 2H), 3.17 – 3.03 (m, 6H), 2.86 (tt, *J* = 14.3, 8.0 Hz, 4H), 2.72 (ddd, *J* = 16.8, 13.0, 7.0 Hz, 2H), 2.34 (d, *J* = 22.1 Hz, 4H), 1.69 – 1.61 (m, 2H), 1.60 – 1.50 (m, 2H), 1.41 (t, *J* = 23.7 Hz, 12H). **HR-MS** (ESI): calcd. for C₆₀H₈₂N₂₀O₁₁ (M+2H)²⁺, *m/z* = 630.3309, found 630.3315.

(9*S*,12*S*,15*S*,*E*)-4-Amino-*N*-(((*S*)-1-(((*S*)-1-(((*S*)-1-amino-1-oxo-3-(4-((*E*)-phenyldiazenyl)phenyl)propan-2-yl)amino)-5-guanidino-1-oxopentan-2-yl)amino)-4-methyl-1-oxopentan-2-yl)-15-(3-guanidinopropyl)-12-(4-hydroxybenzyl)-2,11,14,17,20-penta-oxo-1,3,5,10,13,16,21-heptaazacyclopentacos-3-ene-9-carboxamide (34).



Yield: 58%. **¹H NMR** (600 MHz, DMSO-*d*₆) δ 10.33 (s, 1H), 9.20 (d, *J* = 30.3 Hz, 2H), 8.33 (s, 2H), 8.15 (s, 1H), 8.06 (d, *J* = 8.0 Hz, 1H), 7.99 (d, *J* = 7.7 Hz, 1H), 7.93 – 7.77 (m, 7H), 7.63 – 7.54 (m, 5H), 7.54 – 6.67 (br, 7H), 7.48 (s, 1H), 7.42 (d, *J* = 8.2 Hz, 2H), 7.29 (q, *J* = 7.0, 6.2 Hz, 1H), 7.17 (d, *J* = 3.9 Hz, 1H), 7.00 (d, *J* = 8.1 Hz, 2H), 6.83 – 6.70 (m, 1H), 6.64 (dd, *J* = 8.6, 2.4 Hz, 2H), 4.50 (td, *J* = 8.3, 5.0 Hz, 1H), 4.39 – 4.17 (m, 4H), 4.06 (s, 1H), 3.28 (d, *J* = 6.8 Hz, 2H), 3.25 – 3.16 (m, 1H), 3.15 – 3.03 (m, 6H), 2.97 – 2.89 (m, 2H), 2.88 – 2.71 (m, 2H), 2.45 – 2.22 (m, 4H), 1.75 (d, *J* = 8.9 Hz, 1H), 1.68 – 1.57 (m, 3H), 1.57 – 1.33 (m, 15H), 0.81 (dd, *J* = 15.3, 6.5 Hz, 6H). **¹³C NMR** (151 MHz, DMSO) δ 173.1, 172.9, 172.8, 172.5, 172.4, 172.4, 172.0, 171.7, 171.5, 171.4, 159.5, 159.3, 159.1, 158.9, 157.2, 157.2, 156.3, 154.4, 154.2, 154.0, 152.4, 152.2, 151.0, 142.2, 131.8, 130.7, 130.4, 129.9, 129.4, 128.1, 127.6, 122.8, 120.6, 120.4, 120.3, 118.6, 116.6, 115.4, 114.6, 55.3, 53.9, 53.5, 52.8, 52.2, 51.6, 41.0, 40.9, 40.8, 40.6, 40.5, 39.3, 38.6, 38.0, 36.1, 31.7, 31.5, 29.4, 29.2, 27.0, 25.6, 25.4, 24.7, 24.6, 23.6, 21.8. **HR-MS** (ESI): calcd. for C₅₇H₈₄N₂₀O₁₀ (M+2H)²⁺, *m/z* = 605.3415, found 605.3417.

3.10.3 Biological Investigation

3.10.3.1 Ligand Binding and Functional Characterization

Materials. Human pancreatic polypeptide (hPP) and porcine neuropeptide Y (pNPY) were purchased from SynPeptide (Shanghai, China). The synthesis of UR-AK86c was described previously.^[19] The syntheses of the radioligands [³H]UR-MK299^[33] and [³H]UR-KK200^[24] were described elsewhere. [³H]propionyl-pNPY (specific activity: 37.5 Ci/mmol, radiochemical purity: 99%) was prepared according to a previously reported procedure^[33] with minor modifications (solvent: DMF/NMP/H₂O/DIPEA 45:20:32:3 v/v/v/v (60 μL) instead of 0.1 M sodium borate buffer pH 8.5 (135 μL); propionyl-pNPY was used instead of pNPY for the determination of the molarity and specific activity; radiochemical yield: 26%). Dulbecco's modified Eagle's medium (DMEM) and HAM's F-12 medium were purchased from Sigma-Aldrich (Taufkirchen, Germany). Leibovitz' L-15 medium (L-15) was obtained from ThermoFisher Scientific (Nidderau, Germany). FCS and trypsin/EDTA were from Merck Biochrom (Darmstadt, Germany). BSA were from Serva (Heidelberg, Germany). Geneticin (G418) was purchased from Merck Biochrom or Fisher Scientific. Puromycin and zeocin were from InvivoGen (Toulouse, France) and furimazine stock solution from Promega (Mannheim, Germany). Hygromycin B was obtained from Carl Roth (Karlsruhe, Germany). D-luciferin was purchased from Thermo Fisher Scientific and coelenterazine h was obtained from Biosynth (Staad, Switzerland). The pcDNA3.1 vector was purchased from ThermoFisher Scientific and the pIRESpuro3 vector was a kind gift from Prof. Dr. Gunter Meister (University of Regensburg). The cDNA encoding the human Y₄R was from the Missouri cDNA Research Center (Rolla, MO, USA). The restriction enzymes *DpnI*, *HindIII*, *XbaI* and *SacII* were from New England Biolabs (Frankfurt am Main, Germany). Primers were obtained from Eurofins Genomics (Eurofins Genomics LLC, Ebersberg, Germany).

Cell Culture. Cells were cultured in 75 cm² flasks (Sarstedt, Nümbrecht, Germany) in a humidified atmosphere (95% air, 5% CO₂) at 37 °C. SK-N-MC neuroblastoma cells (obtained from the American Type Culture Collection, ATCC HTB-10) were grown in EMEM supplemented with 5% FCS. CHO-hY₂R cells (obtained from PerkinElmer, Perkin Elmer, Rodgau, Germany) were maintained in Ham's F-12 supplemented with 5% FCS and G418 (400 μg/mL). CHO-hY₄-G_{q5}-mtAEQ cells^[34] were cultured in HAM's F-12 supplemented with

10% FCS, hygromycin (400 $\mu\text{g}/\text{mL}$), zeocin (250 $\mu\text{g}/\text{mL}$) and G418 (400 $\mu\text{g}/\text{mL}$). HEC-1B-hY₅ cells^[35] were maintained in EMEM supplemented with 5% FCS and G418 (400 $\mu\text{g}/\text{mL}$). HEK293T-NlucN-mG_{si}/Y₄R-NlucC cells and HEK293T-CBRN-mG_{si}/Y₄R-CBRC cells were cultivated in DMEM supplemented with 10% FCS, puromycin (1 $\mu\text{g}/\text{mL}$) and G418 (600 $\mu\text{g}/\text{mL}$).

Molecular Cloning. For construction of the pcDNA3.1 Y₄R-NlucC vector, the human Y₄ receptor gene was amplified by PCR without stop codon and restriction sites of *Hind*III and *Xba*I were added to the N- and C-terminus, respectively. The receptor sequence was then cloned into the pcDNA3.1 H₁R-NlucC plasmid (containing G418 resistance) by replacing the H₁R gene by restriction digest with *Hind*III and *Xba*I as described previously.^[23] For pcDNA3.1 Y₄R-CBRC vector construction, the pcDNA3.1 Y₄R-NlucC vector was digested with *Xba*I and *Sac*II and then gel purified to remove the NlucC sequence. Required nucleotide overlaps were added to the CBRC sequence by PCR to perform a Gibson assembly protocol using the linearized pcDNA3.1 Y₄R vector and the DpnI-digested CBRC PCR product. For construction of the pIRESpuro3 CBRN-mG_{si} plasmid, nucleotide overlaps required for Gibson assembly were added to the CBRN sequence by PCR and the NlucN sequence was removed from the pIRESpuro3 NlucN-mG_{si} plasmid^[23] by PCR vector linearization and gel purification. Then, a Gibson assembly protocol was performed using the linearized pIRESpuro3 mG_{si} vector and the DpnI-digested CBRN PCR product. The plasmids encoding Y₄R-NlucC, Y₄R-CBRC and CBRN-mG_{si} constructs were verified by sequencing (Eurofins Genomics LLC, Ebersberg, Germany).

Generation of Stable HEK293T Transfectants: HEK293T-CBRN-mG_{si}/Y₄R-CBRC and HEK293T-NlucN-mG_{si}/Y₄R-NlucC Cells. In order to generate HEK293T cells stably expressing NlucN-mG_{si} and Y₄R-NlucC fusion proteins, the day prior to the transfection, the parental cell line, i.e. HEK293T-NlucN-mG_{si} cells,^[23] providing puromycin resistance, were seeded into a 6-well dish at a density of 0.3×10^6 cells/mL in DMEM supplemented with 10% FCS (2 mL/well). The cells were transfected with 2 μg of the pcDNA3.1 Y₄R-NlucC vector using the XtremeGene HP transfection reagent (Merck KGaA, Darmstadt, Germany) according to the manufacturer's protocol. To generate HEK293T cells stably expressing CBRN-mG_{si} and Y₄R-CBRC fusion proteins, HEK293T wildtype cells were first transfected

with 2 μg of the pIRESpuro3 CBRN-mG_{si} plasmid in an analogous transfection process and stabilized by puromycin antibiotic selection. Also in analogy, HEK293T-CBRN-mG_{si} cells were then transfected using 2 μg of the pcDNA3.1 Y₄R-CBRC plasmid and stabilized by G418 antibiotic selection. Afterwards, the cells were cultivated in DMEM supplemented with 10% FCS, 1 $\mu\text{g}/\text{mL}$ puromycin and 600 $\mu\text{g}/\text{mL}$ G418 for sustained selection pressure.

Y₄R Mini-G_{si} Protein Recruitment Assays (Agonist Mode). A day prior to the experiment, HEK293T-NlucN-mG_{si}/Y₄R-NlucC cells or HEK293T-CBRN-mG_{si}/Y₄R-CBRC cells were detached by trypsin treatment (0.05% trypsin, 0.02% EDTA in PBS) and centrifuged (700 g, 5 min). The cells were resuspended in Leibovitz' L-15 medium, supplemented with 10 mM HEPES (Serva, Heidelberg, Germany) and 5% FCS, to yield a cell density of 1.25×10^6 cells/mL. 100.000 cells (80 μL of the cell suspension) were seeded into the wells of a white flat-bottom 96-well microtiter plate (Merck KGaA, Darmstadt, Germany), followed by incubation overnight at 37 °C in a water-saturated atmosphere containing only atmospheric CO₂. On the day of the experiment, the culture medium was carefully removed by suction and the cells were carefully washed with FCS-free L-15 supplemented with 10 mM HEPES and 1% BSA (200 μL) and covered with FCS-free L-15 supplemented with 10 mM HEPES and 1% BSA (80 μL). 10 μL of a 10 mM solution of the CBR substrate D-luciferin in Hank's balanced salt solution (Gibco/Thermo Fisher Scientific) or 10 μL of the feed dilution of the Nluc substrate furimazine (obtained by diluting the furimazine stock 1:1000 with FCS-free L-15 supplemented with 10 mM HEPES) were added to each well and the plate was transferred to a pre-heated (37 °C) EnSpire plate reader (Perkin Elmer Inc., Rodgau, Germany). After recording the basal luminescence for 15 min, 10 μL of the Y₄R agonist feed solutions (prepared in L-15 10-fold concentrated compared to the final concentration) or 10 μL of the vehicle control were added and the luminescence was recorded for 45 min (note: the preparation of serial dilutions and the addition of the compounds to the cells were performed in the dark using a red LED ($\lambda = 650 \text{ nm}$) to maintain visibility for the operator). For Nluc assays, luminescence signals were measured with an integration time of 0.1 s per well and for CBR assays an integration time of 1 s per well was used. Data were analysed using GraphPad Prism 5 (GraphPad Software, San Diego, CA, USA). Absolute luminescence values were corrected for the slight inter-well variability caused by fluctuations in cell density and substrate concentration by dividing luminescences of each well by the baseline luminescence measured

in the same well just before agonist addition. Subsequently, inter-well corrected data were corrected for the baseline drift by dividing all data by the vehicle control. The maximum responses corresponding to the peak or plateau values occurring after the initial steep rise of the signal within 3.5-7.5 min (Figure S56) were normalized to the response of 1 μM hPP (100%) and the vehicle control (0%). The normalized responses were plotted against $\log(\text{concentration of } Y_4\text{R agonist})$ and the data were analyzed by a four-parameter logistic equation (GraphPad Prism 5) to obtain concentration-response curves yielding the pEC_{50} values. Efficacies α (maximum effect relative to 1 μM hPP) were calculated from the upper plateaus of the concentration-response curves.

$Y_4\text{R Ca}^{2+}$ -Aequorin Assay. The assay was performed with intact CHO-h $Y_4\text{RmtAEQ-G}_{q15}$ cells^[34] in agonist mode as previously reported.^[19] The preparation of serial dilutions (10-fold concentrated feed solutions) and the addition of the compounds to the cells were performed in the dark using a red LED ($\lambda = 650 \text{ nm}$) to maintain visibility for the operator. Measurements were performed with a GENius Pro plate reader (Tecan, Salzburg, Austria). Areas under the curve were calculated using GraphPad Prism 5.0 (GraphPad software). Fractional luminescences (calculated by dividing the area of peak 1 by the total area (peaks 1 and 2)) were normalized (100% = fractional luminescence obtained by 1 μM hPP, 0% = basal effect in the absence of agonist; GraphPad Prism 5.0), and relative responses were plotted against $\log(\text{concentration of agonist})$ followed by fitting according to a four-parameter logistic equation ($\log(\text{agonist})$ vs response - variable slope; GraphPad Prism 5.0) to obtain pEC_{50} values. Intrinsic activities α (maximum effect relative to 1 μM hPP) of (partial) agonists were calculated based on the upper plateaus of the concentration-response curves.

Radioligand Binding Assays. All radioligand competition binding studies were performed at intact cells at $23 \pm 1 \text{ }^\circ\text{C}$ using previously described procedures with the following general modification: the preparation of serial dilutions (10-fold concentrated feed solutions) and the addition of the compounds to the cells were performed in the dark using a red LED ($\lambda = 650 \text{ nm}$) to maintain visibility for the operator. Incubations were performed in the dark.

$Y_1\text{R}$ binding: Competition binding experiments at $Y_1\text{R}$ -expressing SK-N-MC neuroblastoma cells were performed as described previously using [^3H]UR-MK299 ($K_d = 0.044 \text{ nM}$, concentration: 0.15 nM) as radioligand.^[33] Due to low radioligand displacement at the highest

competitor concentration used (10 μ M), no pIC₅₀ values were determined for compounds **27**, **30** and **31**. In the case of compounds **20**, **25**, **28**, **29** and **32-34**, pIC₅₀ values were obtained from a linear Hill plot ($\log(B/(B_0 - B))$) plotted against $\log(\text{concentration competitor})$ followed by linear regression; B = specifically bound [³H]UR-MK299 in the presence of competitor, B_0 = specifically bound [³H]UR-MK299 in the absence of competitor; the intercept of the linear curve with the abscissas equals the pIC₅₀). pIC₅₀ values were converted to pK_i values according to the Cheng-Prusoff equation^[36] (logarithmic form).

Y₂R binding: Competition binding experiments at CHO-hY₂R cells were performed as previously reported using [³H]propionyl-pNPY ($K_d = 0.14$ nM, concentration: 0.5 nM) as radioligand.^[37] Due to low radioligand displacement at the highest competitor concentration used (10 μ M), no pIC₅₀ values were determined for the studied compounds (**25**, **27**, **30**, **31** and **33**).

Y₄R binding: Competition binding experiments at CHO-hY₄-G_{q15}-mtAEQ cells were performed as described previously using [³H]UR-KK200 ($K_d = 0.67$ nM,^[24] concentration: 1.0 nM) as radioligand.^[19] Total binding data, including total binding in the absence of competitor, were plotted against $\log(\text{concentration competitor})$ and analyzed by a four-parameter logistic equation ($\log(\text{inhibitor})$ vs response - variable slope, GraphPad Prism) followed by normalization (100% = “top” of the four-parameter logistic fit, 0% = unspecifically bound radioligand ligand) and analysis of the normalized data by a four-parameter logistic equation to obtain pIC₅₀ values. The latter were converted to pK_i values according to the Cheng-Prusoff equation^[36] (logarithmic form).

Y₅R binding: Competition binding experiments at HEC-1B-hY₅ cells were performed as described previously using [³H]propionyl-pNPY ($K_d = 11$ nM,^[25] concentration: 5 nM) as radioligand.^[24] Due to low radioligand displacement at the highest competitor concentration used (10 μ M), no pIC₅₀ values were determined for compounds **27**, **30** and **31**. In the case of compounds **20**, **25**, **28**, **29** and **32-34**, pIC₅₀ values were obtained from a linear Hill plot ($\log(B/(B_0 - B))$) plotted against $\log(\text{concentration competitor})$ followed by linear regression; B = specifically bound [³H]propionyl-pNPY in the presence of competitor, B_0 = specifically bound [³H]propionyl-pNPY in the absence of competitor; the intercept of the linear curve with the abscissas equals the pIC₅₀). pIC₅₀ values were converted to pK_i values according to the Cheng-Prusoff equation^[36] (logarithmic form).

3.10.3.2 Impedance Studies

General Information.

Materials. Human pancreatic polypeptide (hPP) was purchased from SynPeptide (Shanghai, China). HAM's F-12 medium, trypsin, PBS⁻, forskolin, L-glutamine, geneticin, penicillin and streptomycin were purchased from Sigma-Aldrich (Taufkirchen, Germany). Leibovitz's L-15 without phenol red was obtained from Thermo Fisher Scientific GmbH (Nidderau, Germany). Zeocin and Hygromycin B were from InvivoGen (Toulouse, France).

Cell Culture. All cell culture work was conducted inside a laminar flow hood (HERASafe KS/KSP class II biological safety cabinet, Thermo Fisher Scientific Inc., Waltham, USA). The solutions were autoclaved (DX-45, Systec Inc., Wetztenberg) at 120 °C for 20 min or sterile filtrated (pore size: 0.2 µm) unless they were supplied sterile by the manufacturer. Before getting into contact with the cells, media, buffer and measuring solutions were pre-warmed to 37 °C in a water bath (TW12, Julabo Inc., Seelbach). In routine culture, the CHO cells were seeded onto the bottom of polystyrene culture flasks with a growth area of 25 cm² or 75 cm² using 4 mL or 12 mL of culture medium respectively. Cells were cultivated in a humidified incubator (Heraeus Function Line, Thermo Fisher Scientific Inc., Waltham, USA) at 37 °C and in an atmosphere containing 5% CO₂. The CHO Y₄R cells were sub-cultivated once a week and the medium was exchanged after three days. The basal culture medium for routine culture was HAM's F-12 supplemented with 10% (v/v) FCS, 0.1 g/L penicillin, 0.1 g/L streptomycin and 5 g/L L-glutamine. Sub-cultivation was conducted according to the following standardized protocol. First medium was aspirated; the cell layer was then washed with phosphate buffered saline (PBS⁻; pH 7.4). The supernatant PBS⁻ was aspirated and the cells were incubated with 1 mL trypsin (0.05% (w/v) in PBS⁻) for 3 min at 37 °C and 5% CO₂. Tryptic digestion was stopped by an excess of culture medium (6 mL). The cell suspension was transferred into a centrifugation tube and centrifuged for 10 min (110 x g, rt, Heraeus Multifuge 1S-R, Thermo Fisher Scientific Inc., Waltham, USA). After aspiration of the supernatant, the cell pellet was resuspended in 3 mL of fresh medium and seeded into new flasks (1:10). The antibiotics Zeocin (250 µg/mL), Hygromycin B (400 µg/mL), and Geneticin (400 µg/mL) were used for selection.

Preparation of Electrode Arrays. 96-well electrode arrays with circular gold-film electrodes (NSP-96 CardioExcyte Sensor Plates 0.6 mm) were purchased from Nanion Technologies Inc., Munich. They were sterilized in Argon plasma (Argon Plasma Cleaner PDC 002, Harrick Plasma, Ithaca, USA) for 30 s and got pre-incubated with 50 μL /well HAM's F-12 medium for 2 h prior to cell inoculation to stabilize the electrode impedance. After aspiration of the pre-incubation medium, the wells of the electrode arrays were loaded with cell suspension yielding 100.000 cells/ cm^2 in each well. After 24 h the supernatant was exchanged by fresh medium and the cells were incubated for another 24 h at 37 °C and 5% CO_2 before the experiments were performed.

Setup for Impedance Measurements. All impedimetric measurements were performed with a CardioExcyte 96 (Nanion Technologies Inc., Munich, 56A) system. The complete device consists of a measurement unit (Figure S1A) accepting and contacting the 96well electrode array. Once the electrode array is loaded in the measurement unit, it is covered by a lid. Heating and ventilation systems (Figure S1B) together with a gas mixer (Figure S1C; ibidi GmbH, Gräfelfing) provide a physiological environment of 37 °C and an atmosphere with 80% humidity and no additional CO_2 . The experiment was controlled and data was collected by an application provided by the manufacturer (SpectraControl 1.4.0, Nanion Technologies Inc., Munich). The 96-well electrode arrays (NSP-96 CardioExcyte Sensor Plates 0.6 mm, Nanion Technologies Inc., Munich) were used with transparent and black multi-well plate bodies. Each well provides a volume of maximal 340 μL and a growth area of 34 mm^2 .

Impedance was recorded at an AC frequency of 12 kHz throughout all experiments. This frequency was identified as the frequency of maximum sensitivity. The time resolution of the measurement was 22 seconds. The amplitude of the alternating driving voltage was set to 40 mV which is non-invasive to the cells.

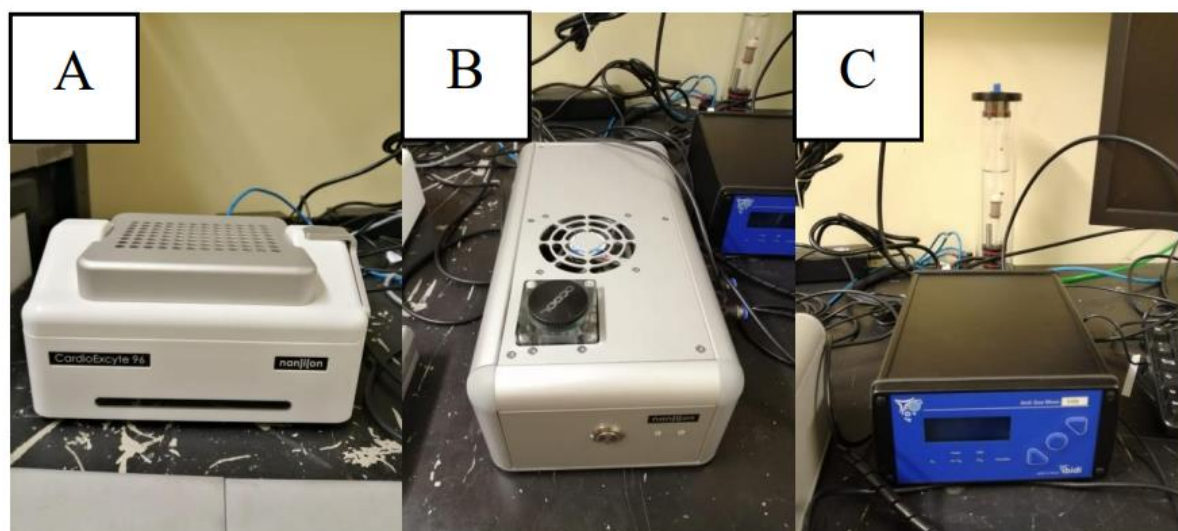


Figure S1. Tabletop measurement setup. **(A)** CardioExcyte 96 measurement unit that detects the complex impedance Z of 96-well electrode arrays. **(B)** Supply unit to adjust the temperature of the lid and of the measurement chamber. **(C)** Gas mixer to adjust the humidity and CO_2 of the atmosphere inside the measurement chamber.

Experimental Procedures

General Experimental Setup. It was mandatory to perform the experiments in a dark room with a red-light emitting diode (LED: 645 nm, 700 mA) as exclusive light source to prohibit unintended photoswitching of the ligands. Working solutions of the photochromic ligands were prepared in the dark and outside a sterile flow hood. Single LEDs (340 nm, 455 nm) or 96-well LED arrays (528 nm) were used as irradiation source. The LED-arrays were custom-made by the in-house electronics workshop (faculty for chemistry and pharmacy, University of Regensburg). Those parts of the electrode arrays that should not be exposed to light were covered by aluminum foil. Ligand solutions were warmed to 37 °C in a custom-made heating plate (machine shop, University of Regensburg) in the darkroom.

Dose Response Measurements. All dose response measurements were recorded using the same general protocol. After removal of the supernatant culture medium, each well was washed with L-15 (100 μL /well) and loaded with a final volume of 50 μL /well L-15 medium before baseline recording of the impedance at 12 kHz were started. Cells were pre-stimulated by 0.4 μM forskolin dissolved in L-15. Photochromic ligands were dissolved in L-15 medium containing 0.4 μM forskolin to keep the final forskolin concentration constant in all experiments. A negative control (DMSO, 0.01% (v/v)) and a positive control (hPP, 200 nM) were also prepared in L-15 medium. Aliquots of the photochromic ligands' stock solution

(50 μM in L-15) were irradiated with the corresponding wavelength in the dark room to receive a saturated solution of one isomer. Impedance was recorded while the cells were pre-stimulated with forskolin (0.4 μM). After equilibration of the impedance, the cells were stimulated with the various ligands in triplicates or the corresponding vehicle controls. For all graphical presentations, the impedance immediately before adding the photochromic ligands to the cells was set to zero.

Switching Experiments. *In situ* switching of photochromic ligands required identical experimental steps as described in the previous paragraph. The ligands were added in individual concentrations (**28**: 50 nM; **30**: 1 nM) to the wells in triplicate. The impedance was continuously recorded while the wells were irradiated with the appropriate wavelength to switch the ligand under study between its two isomers. At different time points, ranging from 25 min to 160 min the initial ligand exposure, parts of the electrode array were covered by aluminum foil, whereas remaining wells were irradiated with the corresponding wavelengths for 30 to 180 seconds. If toggling between two isoforms was investigated, the same wells were irradiated again but with the corresponding wavelength suitable for back switching.

Control Experiments. The electrode arrays were prepared as described above. They were either kept cell-free, just immersed in L-15 medium, or they were inoculated with a corresponding cell suspension to form a confluent cell monolayer on the planar gold-film electrodes. The cell populations were then irradiated with light of the appropriate wavelength and duration but in absence of the photochromic ligands. This experiment was meant to indicate any impact of the light itself on impedance recordings. In an inverse control format, the electrodes were kept cell-free but were flooded with the solutions of the photochromic ligands. Impedance was recorded before, after and during exposure to light of the appropriate wavelength and duration or while the electrodes were kept in the dark.

Washing Experiment. The cell-covered electrode arrays were prepared as described in section “switching experiments”. Prior to irradiation with light of the appropriate wavelength, a washing step was included to wash out unbound ligand. For this, the measurement was paused 20 minutes after ligand addition and the supernatant was aspirated. 100 μL of a washing solution (L-15 + 0.4 μM forskolin) were added and removed. Eventually, the wells were re-

filled with 200 μL of the washing buffer and data collection was continued. Approximately 17 minutes after addition of ligands, the cell-covered electrodes were either irradiated with 340 nm ($t = 1$ min) or with 455 nm ($t = 2$ min). 30 min later, those wells that had been irradiated with 340 nm first were now illuminated with 455 nm and vice versa.

3.11 Supporting Information

3.11.1 Purity

Purity of compounds was measured in DMSO (0.2 mM) on analytical RP-HPLC at 30 °C (flow: 0.3 mL/min, solvent A: H₂O (0.05% TFA), solvent B: MeCN; gradient A/B: 0-25 min: 90/10, 25-30 min: 2/98). Detection at 220 nm.

Compound 20

Purity: 98% (12% (*cis*-isomer) + 86% (*trans*-isomer))

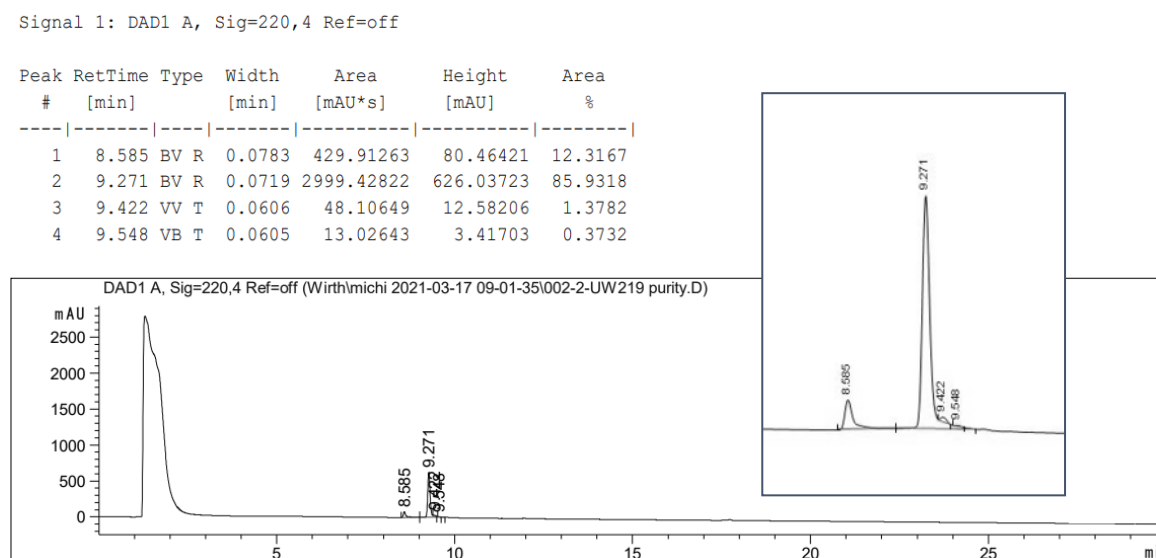


Figure S2. Purity of 20. Complete HPLC run and zoomed in view.

Compound 27

Purity: 97% (19% (*cis*-isomer) + 78% (*trans*-isomer))

Signal 1: DAD1 A, Sig=220,4 Ref=off

Peak #	RetTime [min]	Type	Width [min]	Area [mAU*s]	Height [mAU]	Area %
1	8.801	BV R	0.0909	979.70068	152.54715	19.4117
2	9.366	VV E	0.1277	132.40099	14.07552	2.6234
3	9.550	VB	0.0746	3934.85010	783.94788	77.9649

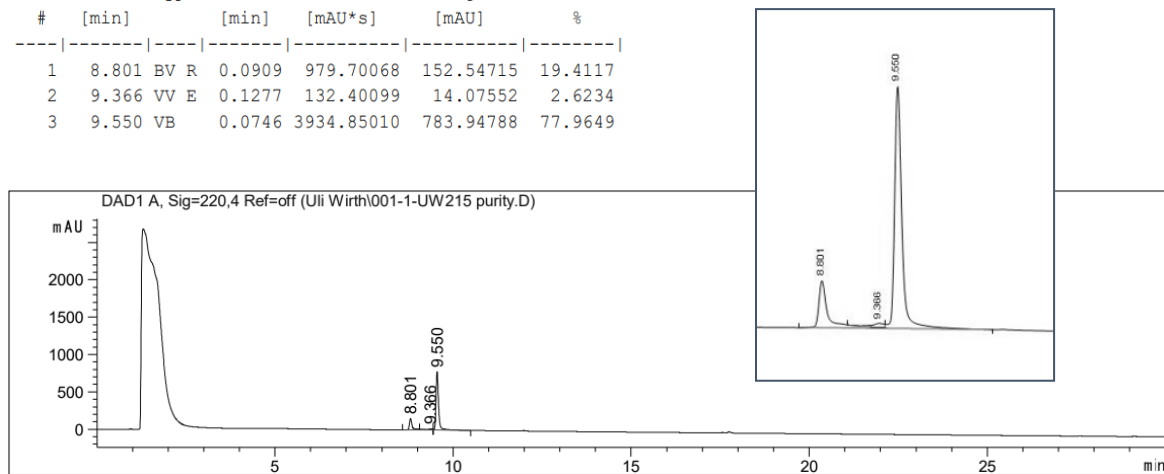


Figure S3. Purity of 27. Complete HPLC run and zoomed in view.

Compound 28

Purity: 99% (28% (*cis*-isomer) + 71% (*trans*-isomer))

Signal 1: DAD1 A, Sig=220,4 Ref=off

Peak #	RetTime [min]	Type	Width [min]	Area [mAU*s]	Height [mAU]	Area %
1	8.787	BV	0.0856	1110.29492	186.22455	27.7395
2	9.287	MM	0.0741	2837.13403	638.25336	70.8827
3	9.422	MM	0.0554	55.14565	12.40931	1.3778

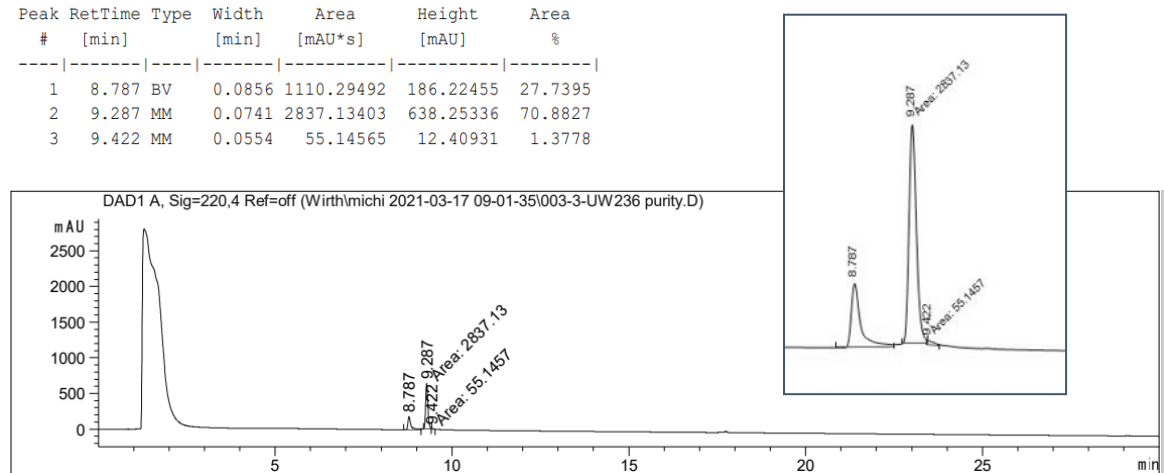


Figure S4. Purity of 28. Complete HPLC run and zoomed in view.

Compound 29

Purity: 97% (18% (*cis*-isomer) + 79% (*trans*-isomer))

Signal 1: DAD1 A, Sig=220,4 Ref=off

Peak #	RetTime [min]	Type	Width [min]	Area [mAU*s]	Height [mAU]	Area %
1	8.816	MM	0.0807	585.11053	120.90730	18.2696
2	9.390	MM	0.0755	2544.65967	562.05634	79.4547
3	9.543	MM	0.0643	48.04019	12.44841	1.5000
4	9.811	MM	0.0808	24.84307	5.12332	0.7757

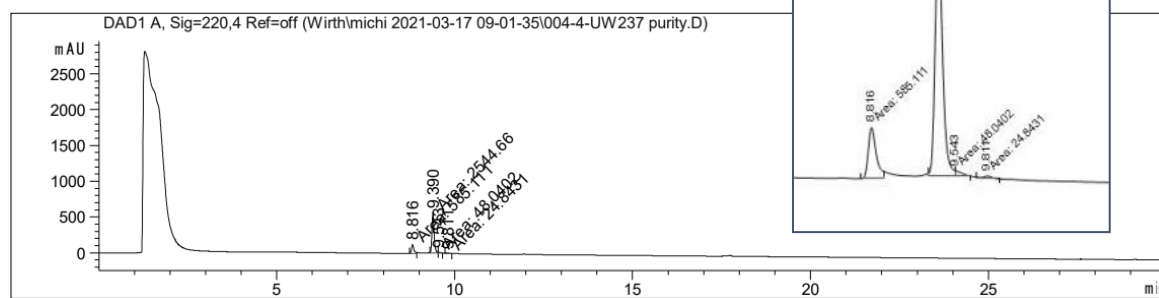


Figure S5. Purity of 29. Complete HPLC run and zoomed in view.

Compound 30

Purity: >99% (8% (*cis*-isomer) + 92% (*trans*-isomer))

Signal 1: DAD1 A, Sig=220,4 Ref=off

Peak #	RetTime [min]	Type	Width [min]	Area [mAU*s]	Height [mAU]	Area %
1	8.511	BB	0.0737	254.40007	51.47693	8.2173
2	9.388	BV R	0.0778	2841.49268	552.99078	91.7827

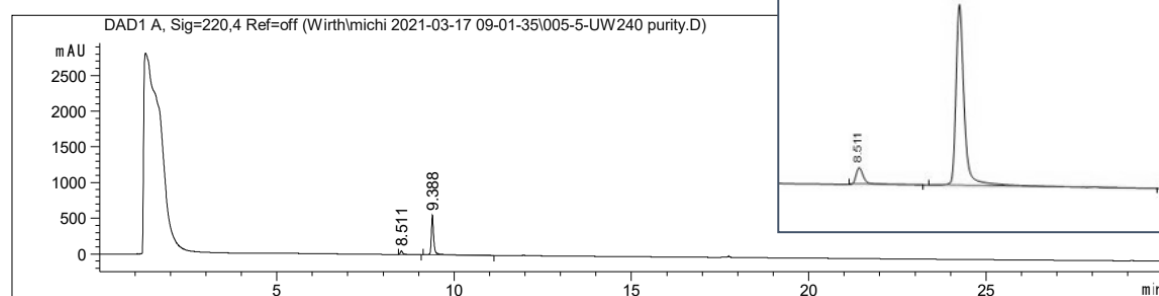


Figure S6. Purity of 30. Complete HPLC run and zoomed in view.

Compound 31

Purity: 98% (15% (*cis*-isomer) + 83% (*trans*-isomer))

Signal 1: DAD1 A, Sig=220,4 Ref=off

Peak #	RetTime [min]	Type	Width [min]	Area [mAU*s]	Height [mAU]	Area %
1	8.499	BV	0.0847	532.06866	93.10622	15.2194
2	9.447	VV R	0.0757	2903.39355	567.16821	83.0494
3	11.952	BB	0.0801	60.52050	11.75444	1.7311

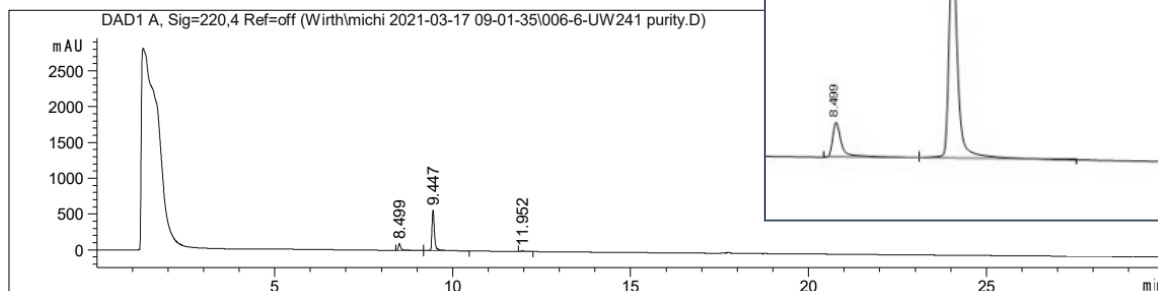


Figure S7. Purity of 31. Complete HPLC run and zoomed in view.

Compound 32

Purity: 97% (20% (*cis*-isomer) + 77% (*trans*-isomer))

Signal 1: DAD1 A, Sig=220,4 Ref=off

Peak #	RetTime [min]	Type	Width [min]	Area [mAU*s]	Height [mAU]	Area %
1	9.624	VV R	0.0644	946.47888	227.93115	20.4618
2	9.815	VB E	0.0814	37.37729	6.87379	0.8081
3	10.720	BV R	0.0736	3558.50073	744.72693	76.9309
4	11.022	BB	0.0627	41.05861	10.26344	0.8876
5	11.323	BV	0.0671	42.16544	9.62445	0.9116

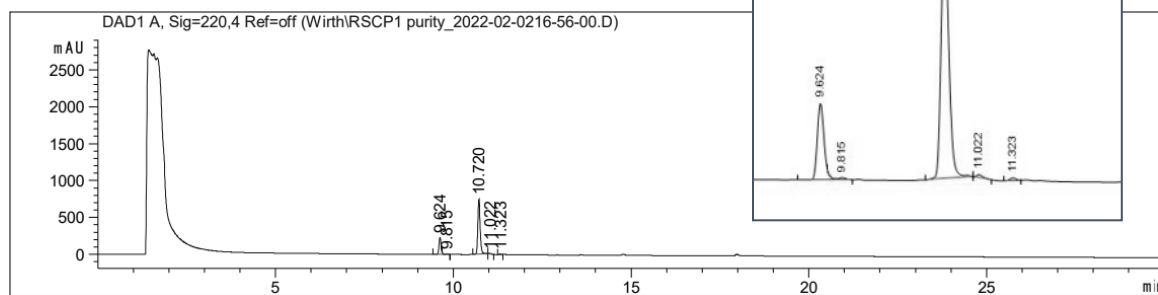


Figure S8. Purity of 32. Complete HPLC run and zoomed in view.

Compound 25

Purity: 95% (20% (*cis*-isomer) + 75% (*trans*-isomer))

Signal 1: DAD1 A, Sig=220,4 Ref=off

Peak #	RetTime [min]	Type	Width [min]	Area [mAU*s]	Height [mAU]	Area %
1	10.369	BB	0.1067	625.12036	90.32092	20.4991
2	11.295	MM	0.1010	2274.31982	375.28741	74.5799
3	11.413	MM	0.0531	150.06653	38.22523	4.9210

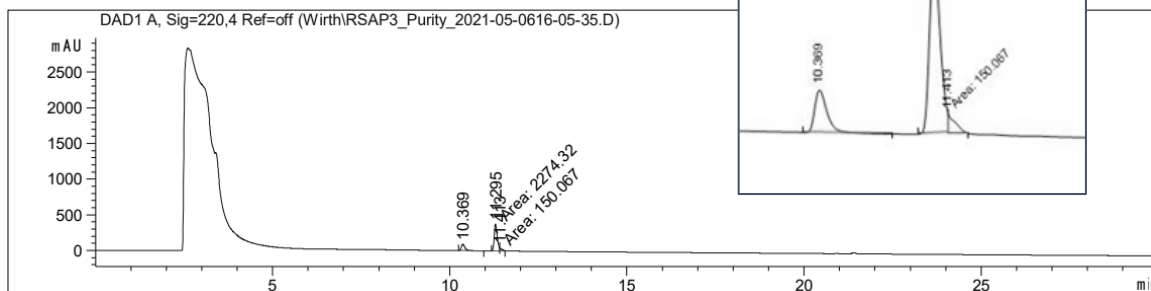


Figure S9. Purity of 25. Complete HPLC run and zoomed in view.

Compound 33

Purity: 97% (16% (*cis*-isomer) + 81% (*trans*-isomer))

Signal 1: DAD1 A, Sig=220,4 Ref=off

Peak #	RetTime [min]	Type	Width [min]	Area [mAU*s]	Height [mAU]	Area %
1	11.210	MM	0.1157	389.93976	56.18875	15.5710
2	12.192	MM	0.1044	2036.99817	325.24564	81.3408
3	12.361	MM	0.0964	77.33907	11.96274	3.0883

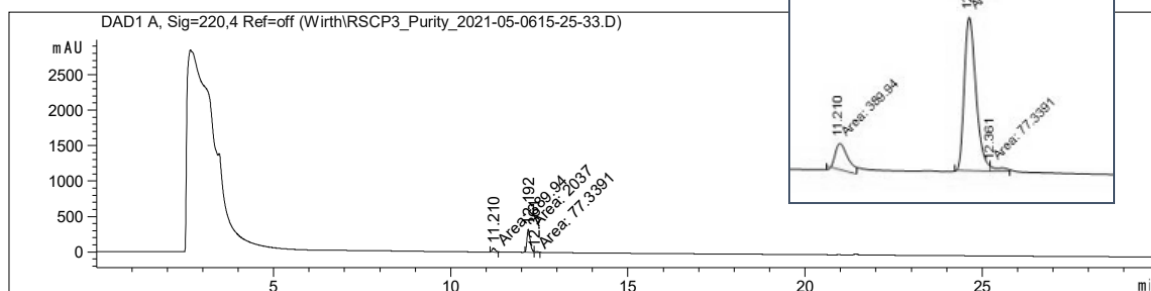


Figure S10. Purity of 33. Complete HPLC run and zoomed in view.

Compound 34

Purity: >99% (15% (*cis*-isomer) + 85% (*trans*-isomer))

Signal 1: DAD1 A, Sig=220,4 Ref=off

Peak #	RetTime [min]	Type	Width [min]	Area [mAU*s]	Height [mAU]	Area %
1	9.381	BB	0.0788	163.27571	30.32437	15.3987
2	10.564	BV R	0.0823	897.04865	162.73558	84.6013

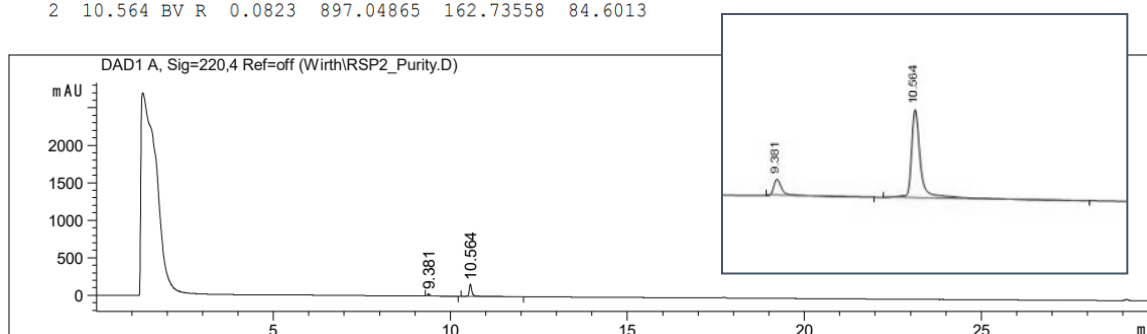


Figure S11. Purity of 34. Complete HPLC run and zoomed in view.

3.11.2 Photophysical Characterization

3.11.2.1 UV/Vis Spectra and Cycle Performance

UV/Vis spectra were measured in HEPES buffer (20 μ M + 0.1% DMSO). The spectra were measured in a quartz glass cuvette. First, the solution was illuminated with 340 nm for 10 s to switch to the *cis*-isomer. After measuring the UV/Vis spectrum of the *cis*-isomer, the solution was illuminated with 455 nm (**20**, **25**, **27-29**, **32-34**) or 528 nm (**30**, **31**), respectively, for 60 s and the spectrum for the *trans*-isomer was measured.

For the cycle performance the solution was irradiated alternating with 340 nm and 455 nm (**20**, **25**, **27-29**, **32-34**) or 528 nm (**30**, **31**), respectively. A UV/Vis spectrum was measured after each switching step. This was repeated ten times to show the stability of the compounds. The absorption of the maximum of the *trans*-isomer was plotted against the cycle number.

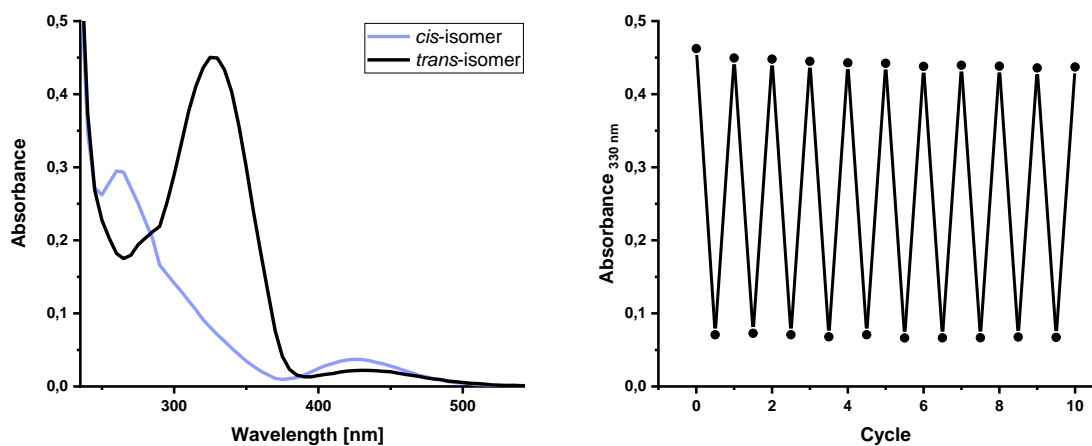


Figure S12. UV/Vis spectra and cycle performance of 20.

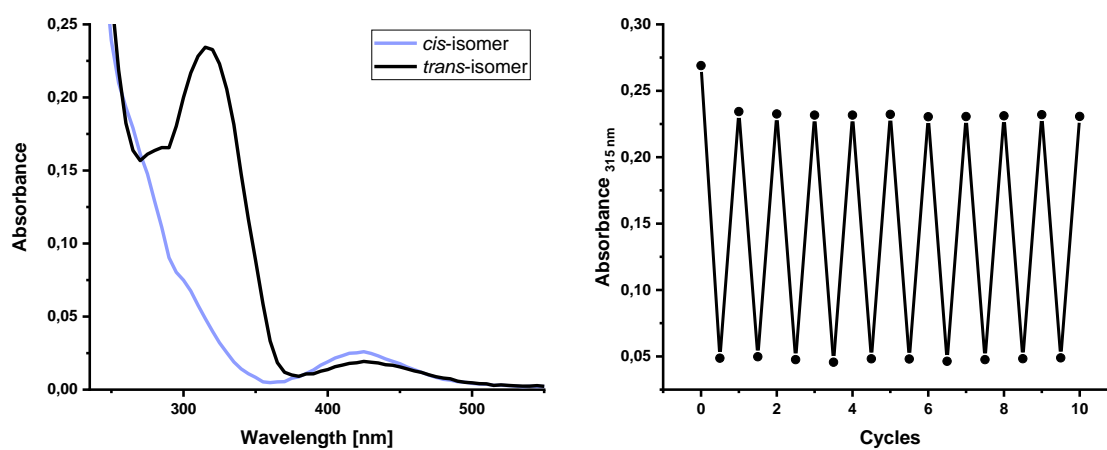


Figure S13. UV/Vis spectra and cycle performance of 27.

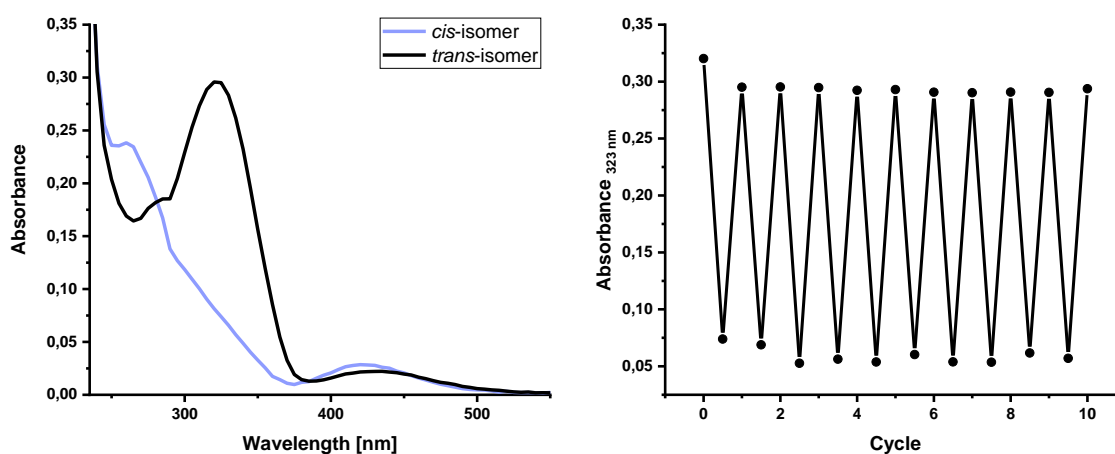


Figure S14. UV/Vis spectra and cycle performance of 28.

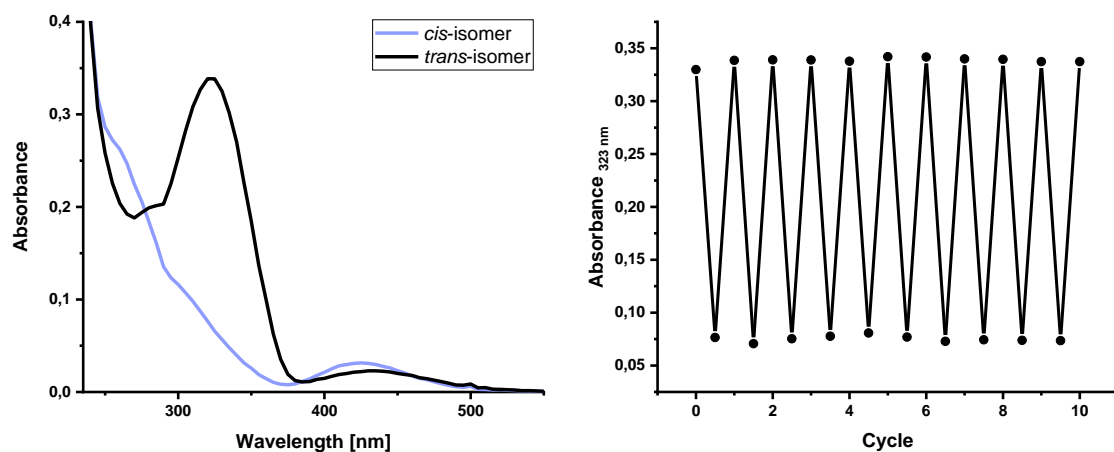


Figure S15. UV/Vis spectra and cycle performance of 29.

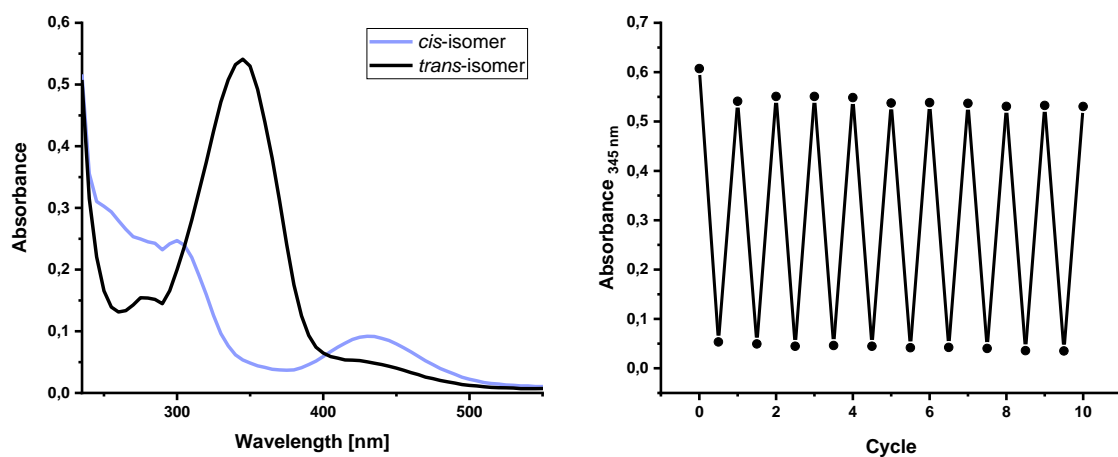


Figure S16. UV/Vis spectra and cycle performance of 30.

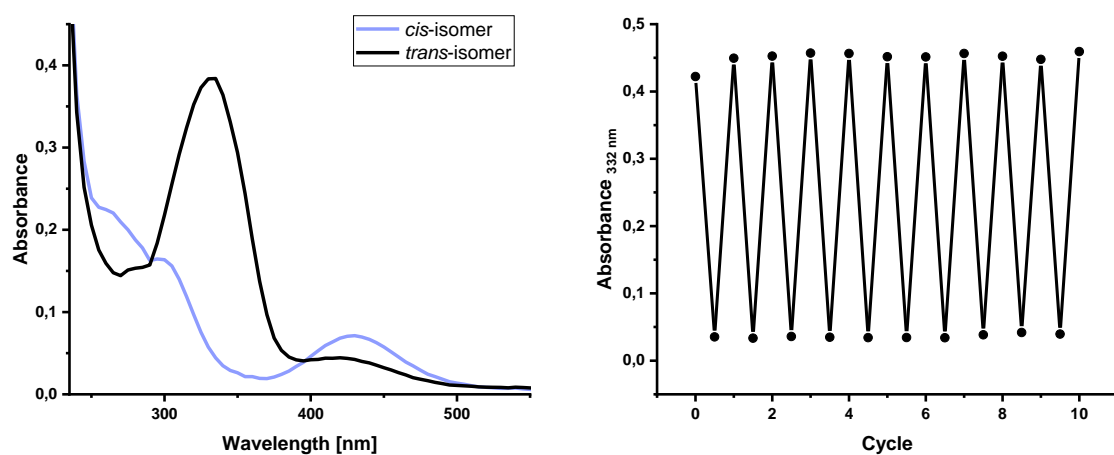


Figure S17. UV/Vis spectra and cycle performance of 31.

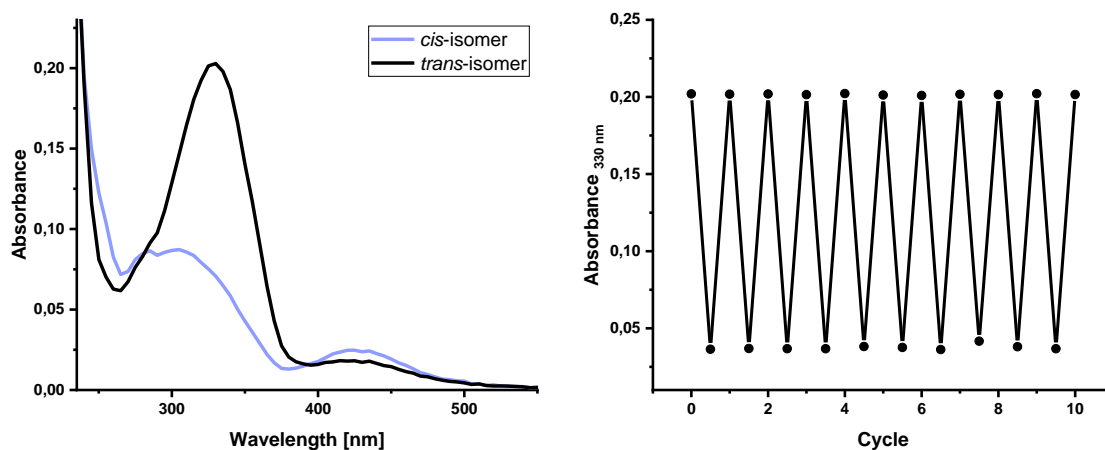


Figure S18. UV/Vis spectra and cycle performance of 32.

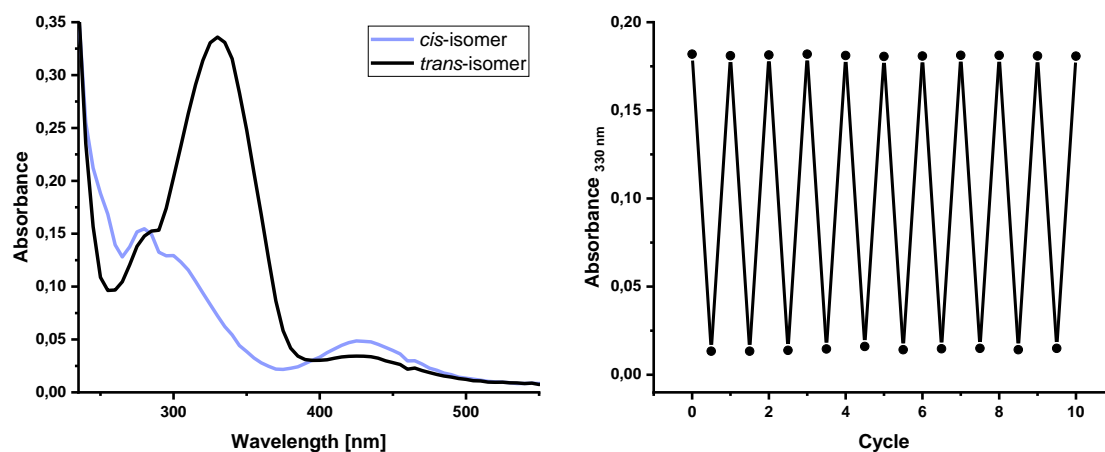


Figure S19. UV/Vis spectra and cycle performance of 25.

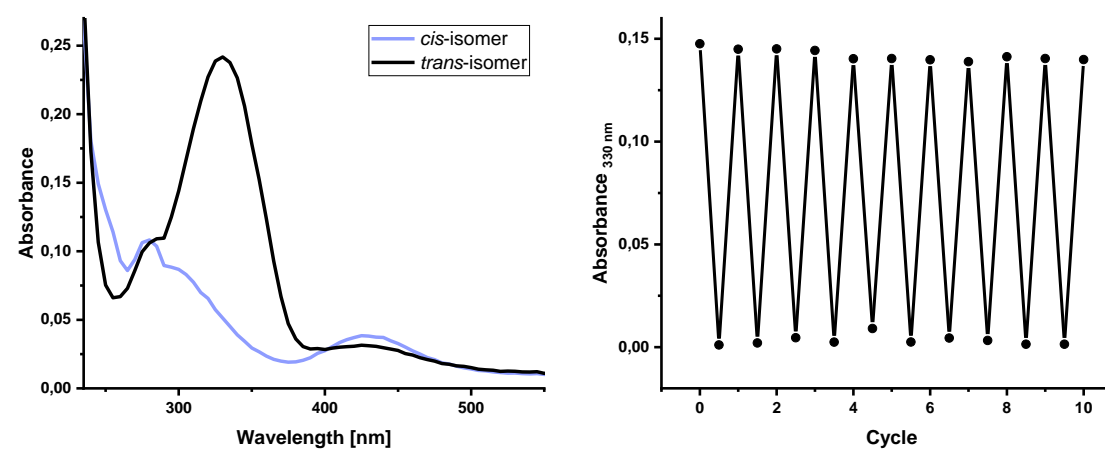


Figure S20. UV/Vis spectra and cycle performance of 33.

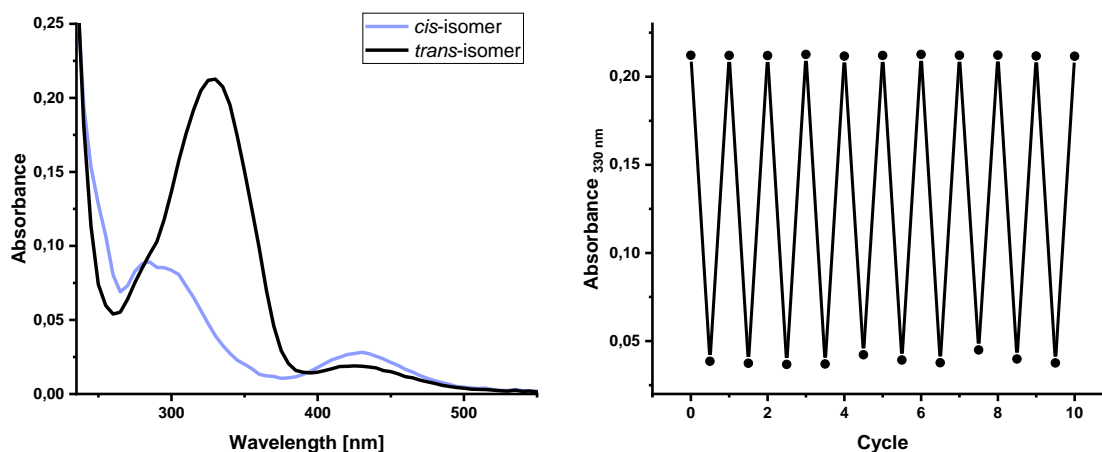


Figure S21. UV/Vis spectra and cycle performance of 34.

3.11.2.2 Photostationary States

Photostationary states (PSS) were measured by analytical HPLC (flow: 0.3 mL/min, solvent A: H₂O (0.05% TFA), solvent B: MeCN). To determine the photostationary state of the photoswitches the samples (0.1 mM in HEPES buffer + 1% DMSO) were irradiated first with 340 nm to get the *Z*-isomer. Afterwards, the sample was irradiated with 455nm or 528 nm, respectively, to get back to the *E*-isomer. The samples were measured at the isosbestic points.

Compound 20

Irradiation with 340 nm: ***cis*-Isomer: 90%** *trans*-Isomer: 10%

Signal 6: DAD1 F, Sig=284,4 Ref=off

Peak #	RetTime [min]	Type	Width [min]	Area [mAU*s]	Height [mAU]	Area %
1	7.983	MM	0.0736	522.76599	118.33800	89.9872
2	8.501	MM	0.0745	58.16745	13.02052	10.0128

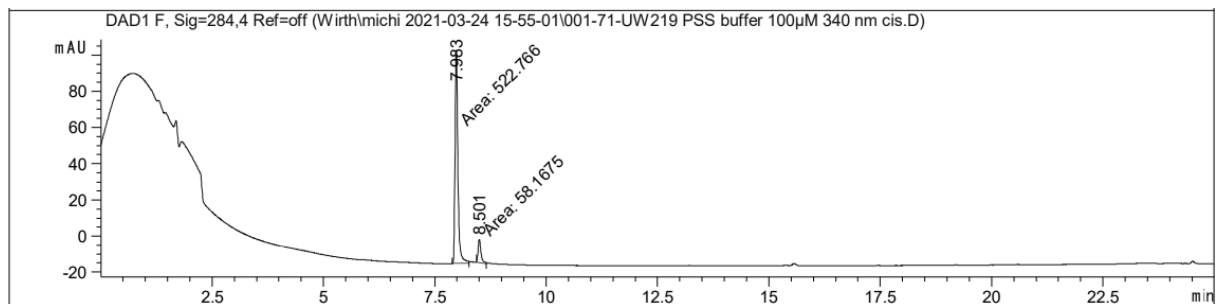


Figure S22. PSS of compound 20 after irradiation with 340 nm.

Irradiation with 455 nm: *cis*-Isomer: 16% ***trans*-Isomer: 88%**

Signal 6: DAD1 F, Sig=284,4 Ref=off

Peak #	RetTime [min]	Type	Width [min]	Area [mAU*s]	Height [mAU]	Area %
1	7.993	BB	0.0701	75.71635	16.32818	11.6829
2	8.533	BB	0.0685	572.38043	127.20951	88.3171

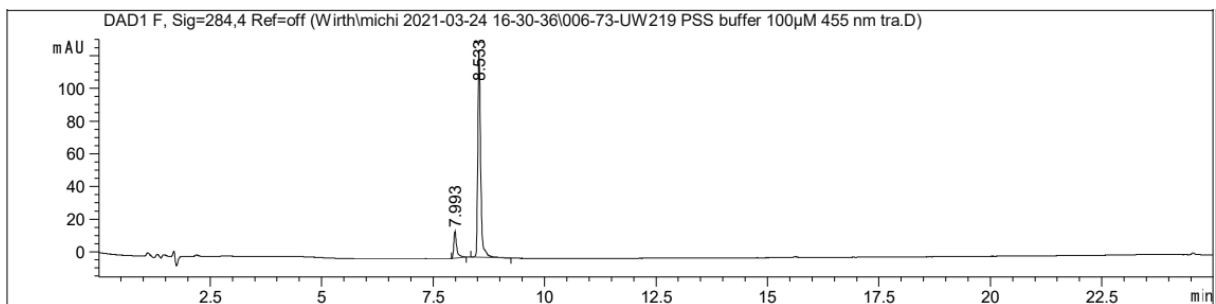


Figure S23. PSS of compound 20 after irradiation with 455 nm.

Compound 27

Irradiation with 340 nm: ***cis*-Isomer: 95%** *trans*-Isomer: 5%

Signal 5: DAD1 E, Sig=272,4 Ref=off

Peak #	RetTime [min]	Type	Width [min]	Area [mAU*s]	Height [mAU]	Area %
1	8.190	MM	0.0813	207.04970	42.42040	95.0248
2	8.769	MM	0.0882	10.84057	2.04771	4.9752

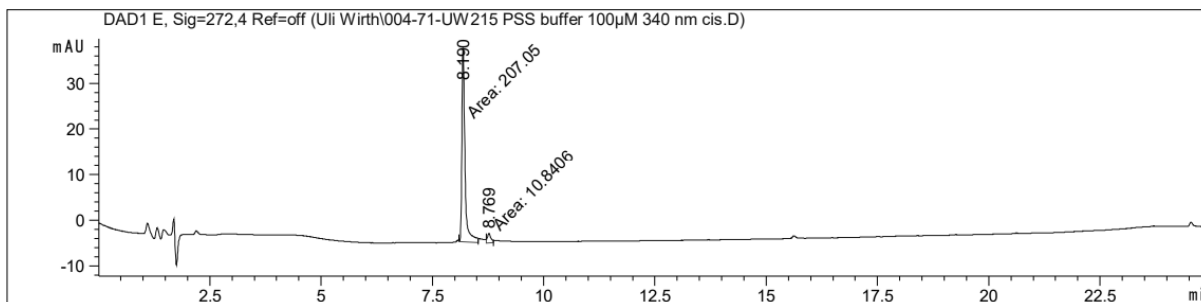


Figure S24. PSS of compound 27 after irradiation with 340 nm.

Irradiation with 455 nm: *cis*-Isomer: 26% ***trans*-Isomer: 74%**

Signal 5: DAD1 E, Sig=272,4 Ref=off

Peak #	RetTime [min]	Type	Width [min]	Area [mAU*s]	Height [mAU]	Area %
1	8.187	BB	0.0704	53.95904	11.16722	26.2556
2	8.764	BB	0.0716	151.55505	31.78581	73.7444

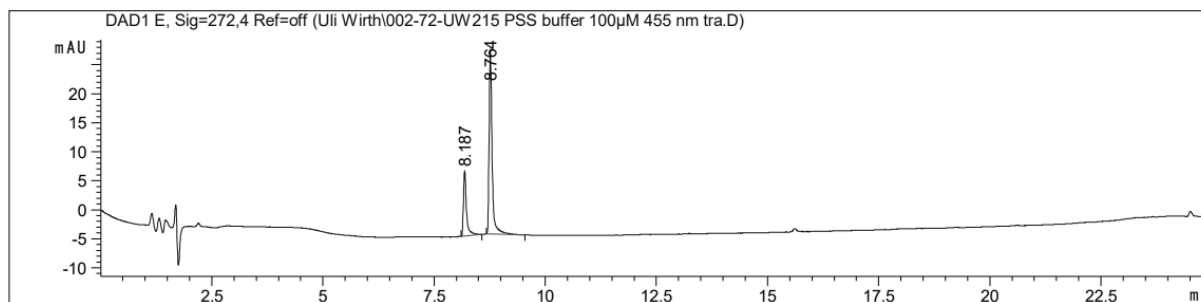


Figure S25. PSS of compound 27 after irradiation with 455 nm.

Compound 28

Irradiation with 340 nm: ***cis*-Isomer: 92%** *trans*-Isomer: 8%

Signal 7: DAD1 G, Sig=281,4 Ref=off

Peak #	RetTime [min]	Type	Width [min]	Area [mAU*s]	Height [mAU]	Area %
1	8.182	MM	0.0800	227.64291	47.45224	92.0375
2	8.546	MM	0.0819	19.69414	4.00768	7.9625

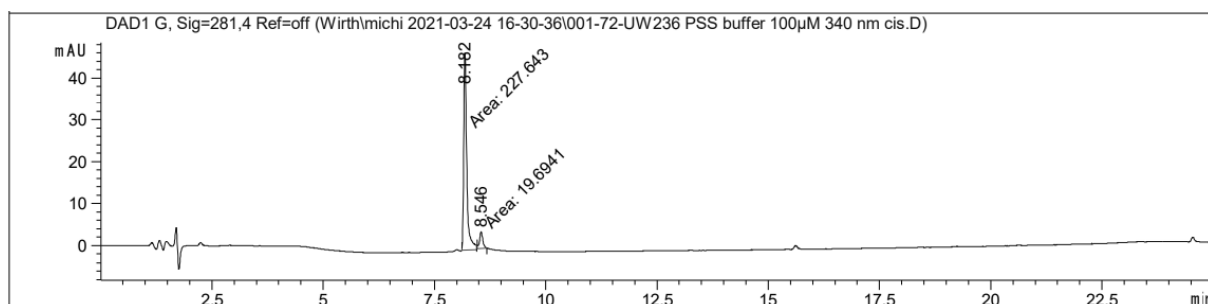


Figure S26. PSS of compound 28 after irradiation with 340 nm.

Irradiation with 455 nm: *cis*-Isomer: 22% ***trans*-Isomer: 78%**

Signal 7: DAD1 G, Sig=281,4 Ref=off

Peak #	RetTime [min]	Type	Width [min]	Area [mAU*s]	Height [mAU]	Area %
1	8.146	BV	0.0794	62.20841	11.44946	22.1682
2	8.512	VB	0.0803	218.41136	39.62774	77.8318

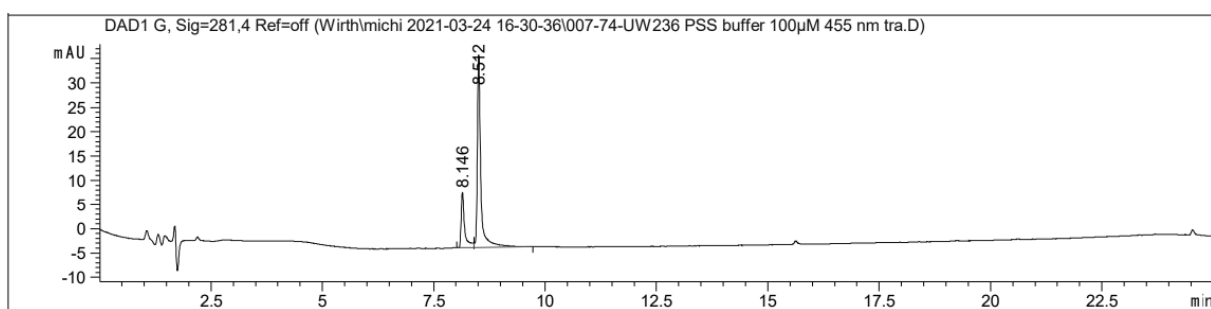


Figure S27. PSS of compound 28 after irradiation with 455 nm.

Compound 29

Irradiation with 340 nm: ***cis*-Isomer: 91%** *trans*-Isomer: 9%

Signal 8: DAD1 H, Sig=277,4 Ref=off

Peak #	RetTime [min]	Type	Width [min]	Area [mAU*s]	Height [mAU]	Area %
1	8.176	MM	0.0822	242.21330	49.08168	90.9130
2	8.608	MM	0.1006	24.20993	4.01205	9.0870

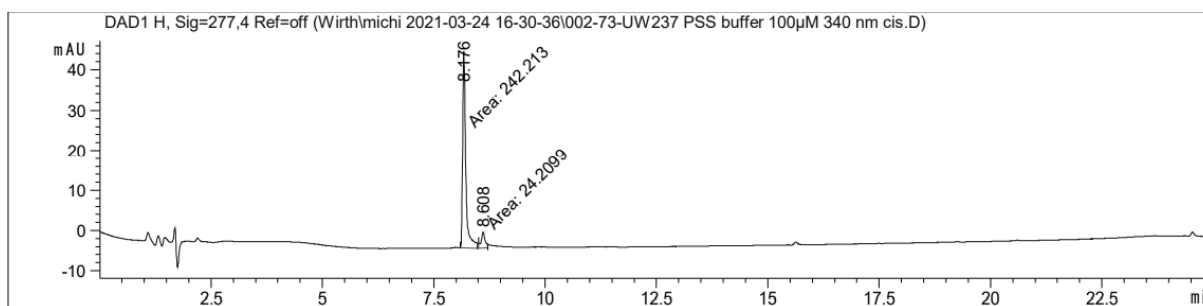


Figure S28. PSS of compound 29 after irradiation with 340 nm.

Irradiation with 455 nm: *cis*-Isomer: 22% ***trans*-Isomer: 78%**

Signal 8: DAD1 H, Sig=277,4 Ref=off

Peak #	RetTime [min]	Type	Width [min]	Area [mAU*s]	Height [mAU]	Area %
1	8.174	BB	0.0707	58.73814	12.51740	21.6601
2	8.600	BB	0.0731	212.44354	43.42910	78.3399

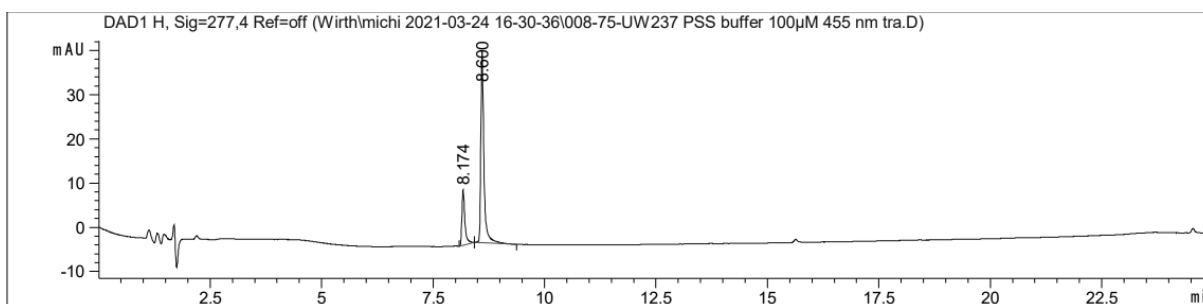


Figure S29. PSS of compound 29 after irradiation with 455 nm.

Compound 30

Irradiation with 340 nm: ***cis*-Isomer: 94%** ***trans*-Isomer: 6%**

Signal 4: DAD1 D, Sig=305,4 Ref=off

Peak #	RetTime [min]	Type	Width [min]	Area [mAU*s]	Height [mAU]	Area %
1	7.913	BB	0.0701	296.55350	63.90984	94.3661
2	8.600	BB	0.0829	17.70515	3.08698	5.6339

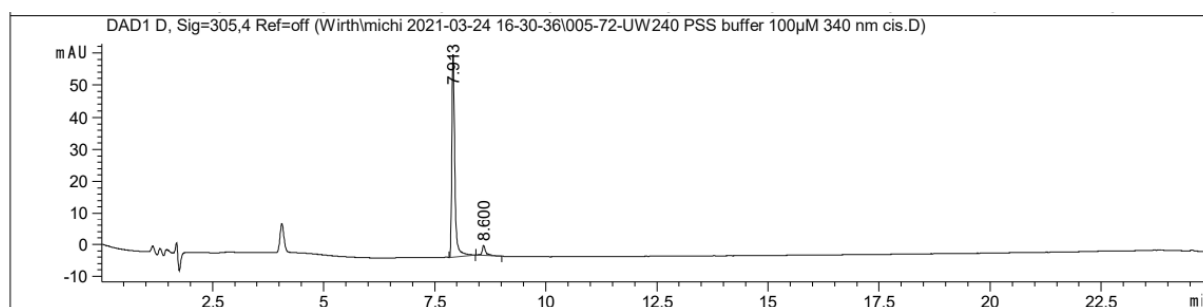


Figure S30. PSS of compound 30 after irradiation with 340 nm.

Irradiation with 528 nm: ***cis*-Isomer: 9%** ***trans*-Isomer: 91%**

Signal 4: DAD1 D, Sig=305,4 Ref=off

Peak #	RetTime [min]	Type	Width [min]	Area [mAU*s]	Height [mAU]	Area %
1	7.920	MM	0.0739	30.12749	6.79401	8.8177
2	8.609	MM	0.0856	311.54309	60.64463	91.1823

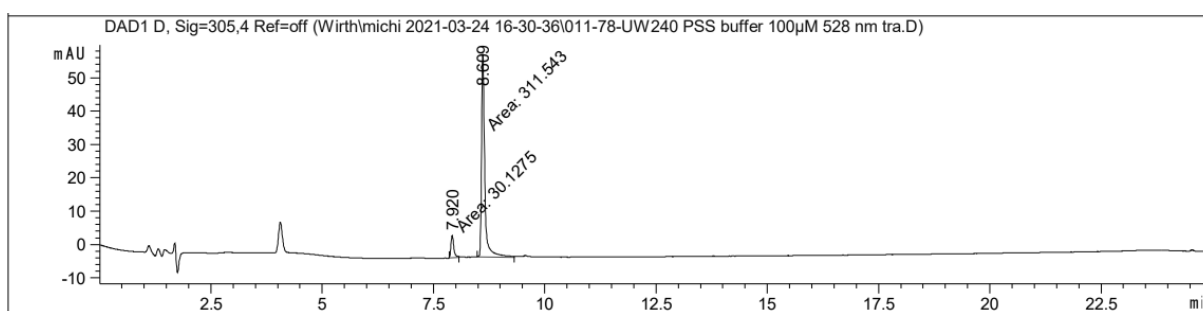


Figure S31. PSS of compound 30 after irradiation with 528 nm.

Compound 31

Irradiation with 340 nm: ***cis*-Isomer: 97%** *trans*-Isomer: 3%

Signal 3: DAD1 C, Sig=291,4 Ref=off

Peak #	RetTime [min]	Type	Width [min]	Area [mAU*s]	Height [mAU]	Area %
1	7.916	MM	0.0784	190.18820	40.43310	97.0643
2	8.655	MM	0.0897	5.75212	1.06862	2.9357

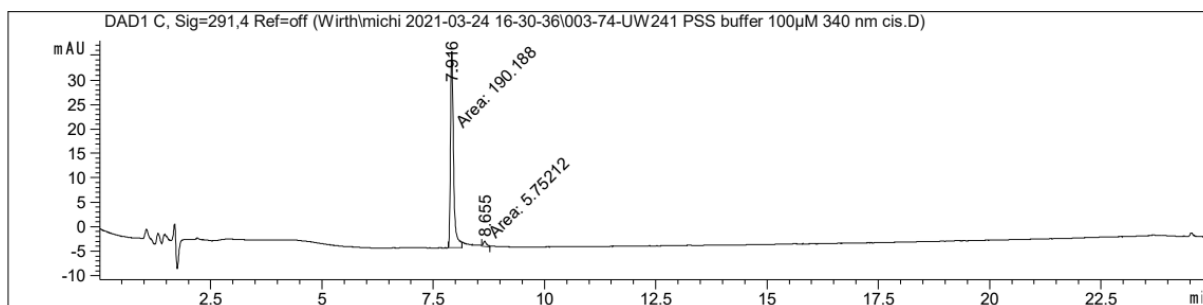


Figure S32. PSS of compound 31 after irradiation with 340 nm.

Irradiation with 528 nm: *cis*-Isomer: 10% ***trans*-Isomer: 90%**

Signal 3: DAD1 C, Sig=291,4 Ref=off

Peak #	RetTime [min]	Type	Width [min]	Area [mAU*s]	Height [mAU]	Area %
1	7.924	BB	0.0731	20.61293	4.21345	10.0587
2	8.667	BB	0.0746	184.31396	36.67817	89.9413

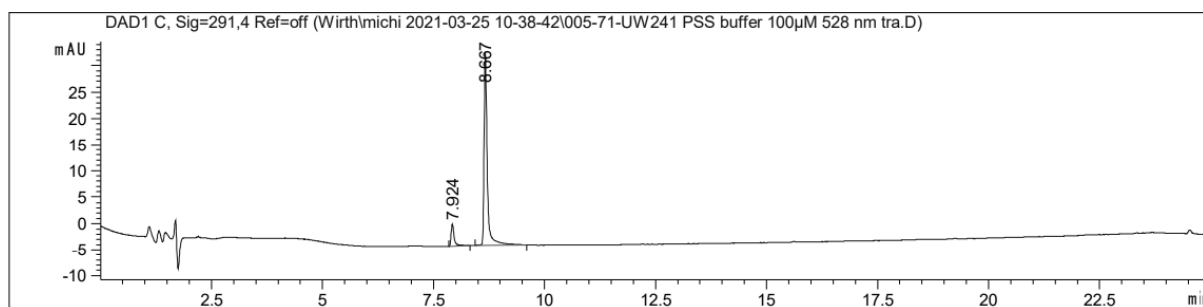


Figure S33. PSS of compound 31 after irradiation with 528 nm.

Compound 32

Irradiation with 340 nm: ***cis*-Isomer: 92%** *trans*-Isomer: 8%

Signal 7: DAD1 G, Sig=281,4 Ref=off

Peak #	RetTime [min]	Type	Width [min]	Area [mAU*s]	Height [mAU]	Area %
1	8.741	MM	0.0708	1085.10144	255.53123	92.0242
2	9.605	BB	0.0738	94.04707	18.97541	7.9758

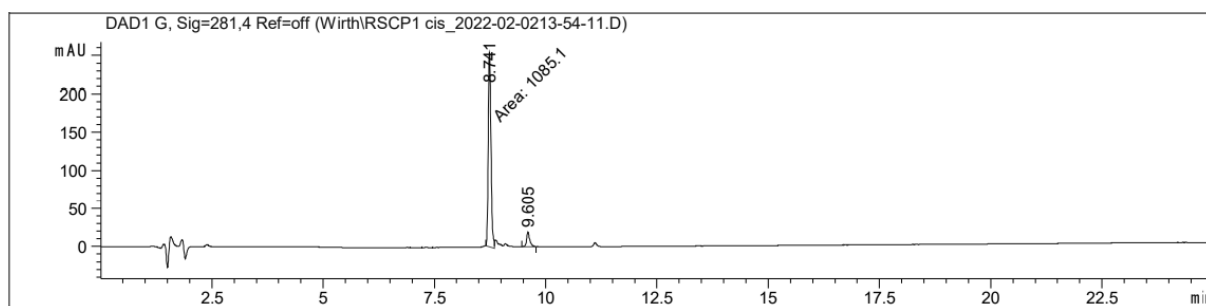


Figure S34. PSS of compound 32 after irradiation with 340 nm.

Irradiation with 455 nm: *cis*-Isomer: 22% ***trans*-Isomer: 78%**

Signal 7: DAD1 G, Sig=281,4 Ref=off

Peak #	RetTime [min]	Type	Width [min]	Area [mAU*s]	Height [mAU]	Area %
1	8.768	MM	0.0679	226.34534	55.57696	21.7608
2	9.584	MM	0.0748	813.80664	181.22363	78.2392

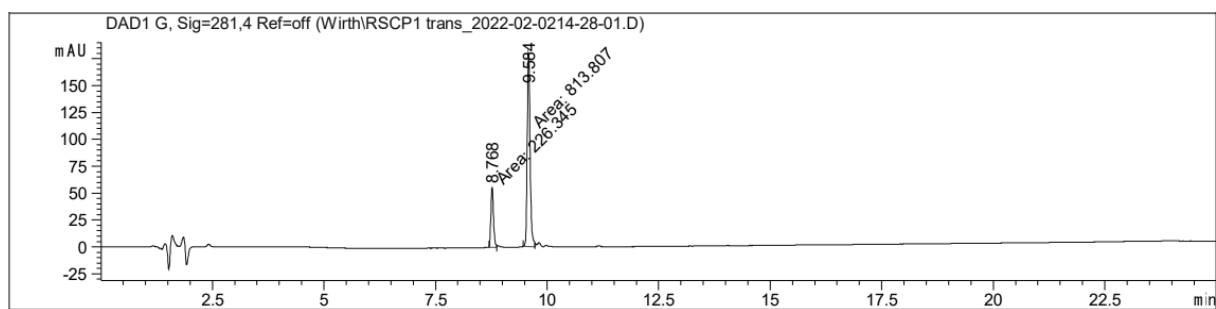


Figure S35. PSS of compound 32 after irradiation with 455 nm.

Compound 25

Irradiation with 340 nm: ***cis*-Isomer: 94%** *trans*-Isomer: 6%

Signal 3: DAD1 D, Sig=287,4 Ref=off

Peak #	RetTime [min]	Type	Width [min]	Area [mAU*s]	Height [mAU]	Area %
1	7.782	BB	0.0632	111.64442	27.61388	94.2154
2	8.533	BB	0.0645	6.85468	1.58347	5.7846

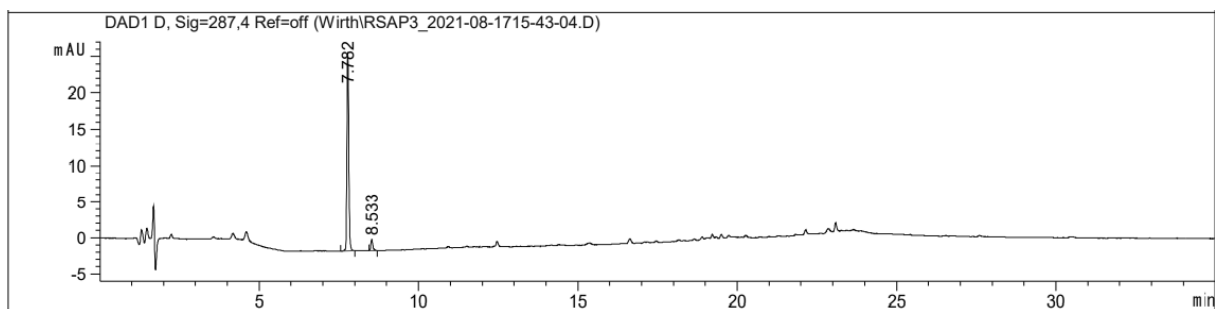


Figure S36. PSS of compound 25 after irradiation with 340 nm.

Irradiation with 455 nm: *cis*-Isomer: 19% ***trans*-Isomer: 81%**

Signal 3: DAD1 D, Sig=287,4 Ref=off

Peak #	RetTime [min]	Type	Width [min]	Area [mAU*s]	Height [mAU]	Area %
1	7.832	BB	0.0626	46.10271	11.54889	18.5700
2	8.574	BB	0.0646	202.16148	48.54773	81.4300

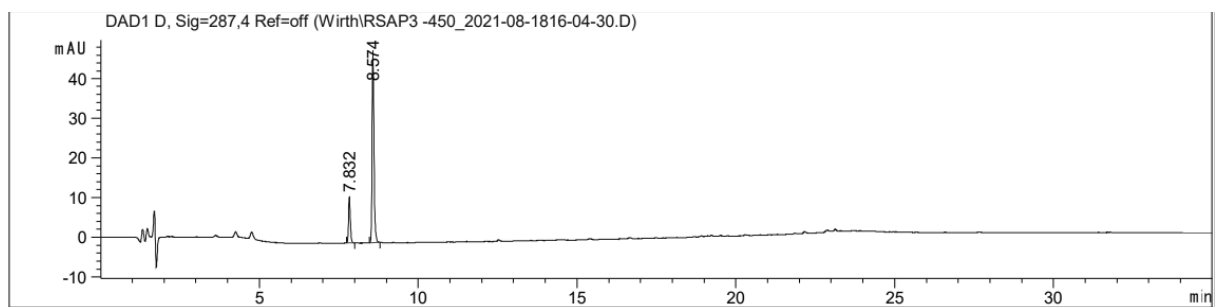
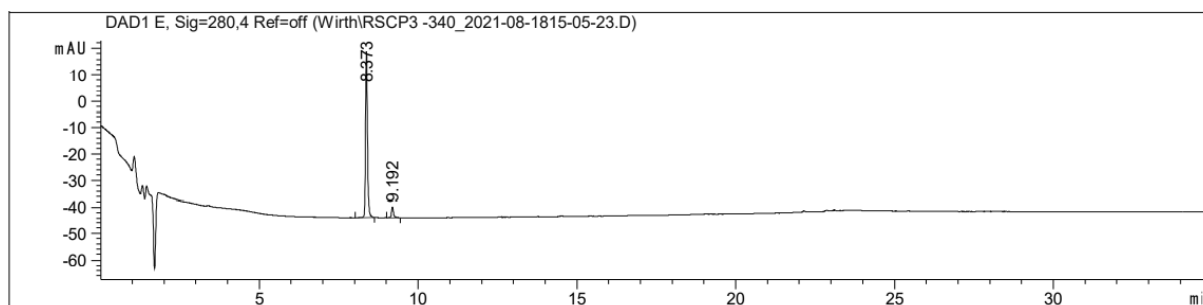


Figure S37. PSS of compound 25 after irradiation with 455 nm.

Compound **33**Irradiation with 340 nm: ***cis*-Isomer: 94%** *trans*-Isomer: 6%

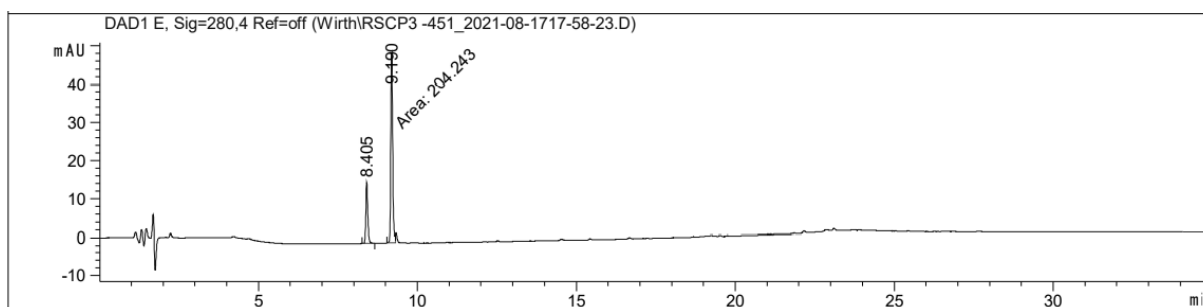
Signal 4: DAD1 E, Sig=280,4 Ref=off

Peak #	RetTime [min]	Type	Width [min]	Area [mAU*s]	Height [mAU]	Area %
1	8.373	BB	0.0637	266.82629	62.58050	93.5502
2	9.192	BB	0.0692	18.39638	4.03538	6.4498

Figure S38. PSS of compound **33** after irradiation with 340 nm.Irradiation with 455 nm: *cis*-Isomer: 25% ***trans*-Isomer: 75%**

Signal 4: DAD1 E, Sig=280,4 Ref=off

Peak #	RetTime [min]	Type	Width [min]	Area [mAU*s]	Height [mAU]	Area %
1	8.405	BB	0.0651	66.53974	15.80803	24.5731
2	9.190	MM	0.0686	204.24348	49.63858	75.4269

Figure S39. PSS of compound **33** after irradiation with 455 nm.

Compound 34

Irradiation with 340 nm: ***cis*-Isomer: 94%** *trans*-Isomer: 6%

Signal 4: DAD1 E, Sig=280,4 Ref=off

Peak #	RetTime [min]	Type	Width [min]	Area [mAU*s]	Height [mAU]	Area %
1	8.629	MM	0.0829	125.22134	25.18497	94.2025
2	9.523	MM	0.0840	7.70655	1.52892	5.7975

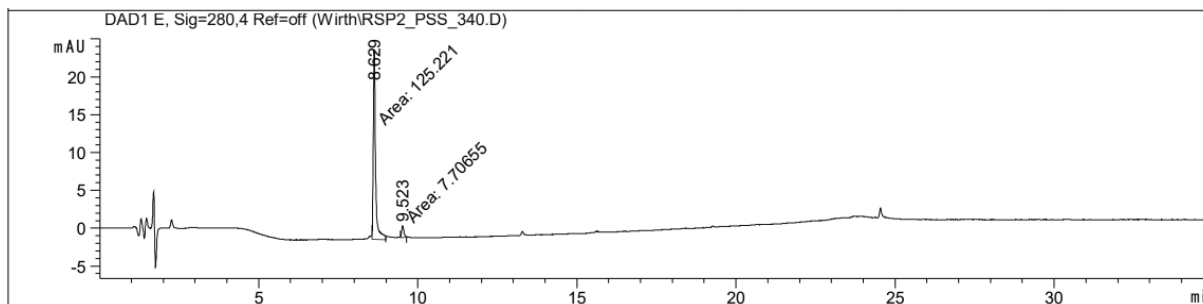


Figure S40. PSS of compound 34 after irradiation with 340 nm.

Irradiation with 455 nm: *cis*-Isomer: 22% ***trans*-Isomer: 78%**

Signal 4: DAD1 E, Sig=280,4 Ref=off

Peak #	RetTime [min]	Type	Width [min]	Area [mAU*s]	Height [mAU]	Area %
1	8.634	BB	0.0737	29.25062	5.90946	21.8040
2	9.493	BB	0.0766	104.90203	20.18746	78.1960

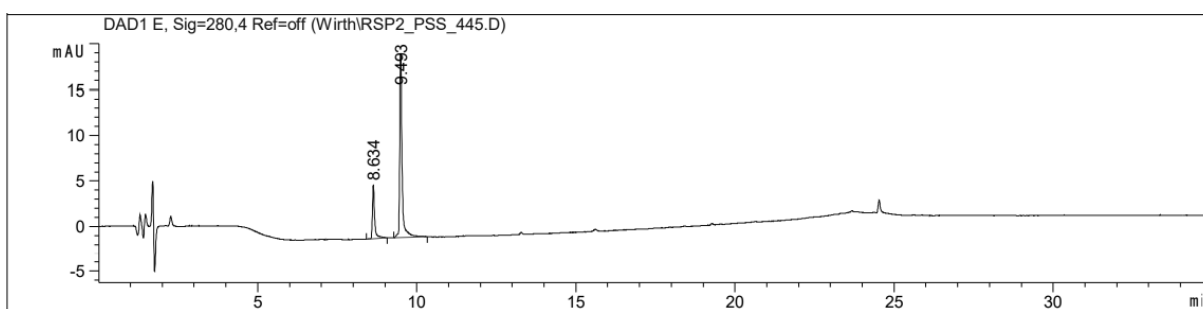


Figure S41. PSS of compound 34 after irradiation with 455 nm.

3.11.2.3 Thermal Half-lives

Thermal half-life was measured in a 96-well plate in a Thermo Scientific Multiskan® Spectrum at rt. The solutions (50 μM in HEPES buffer + 0.25% DMSO) were pre-irradiated with 340 nm. The absorption at 335 nm was measured every 3 h. The data was analyzed using Origin 2021.

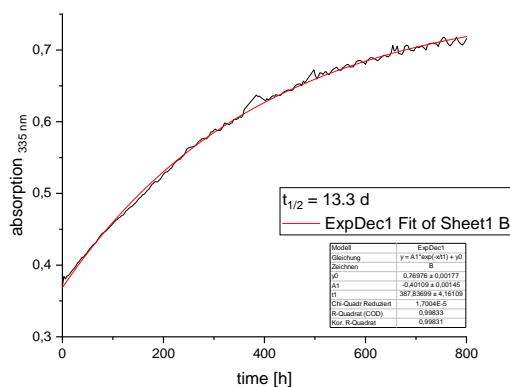


Figure S42. Thermal half-life of 20.

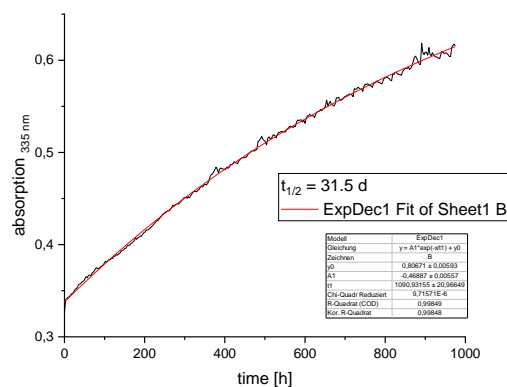


Figure S43. Thermal half-life of 27.

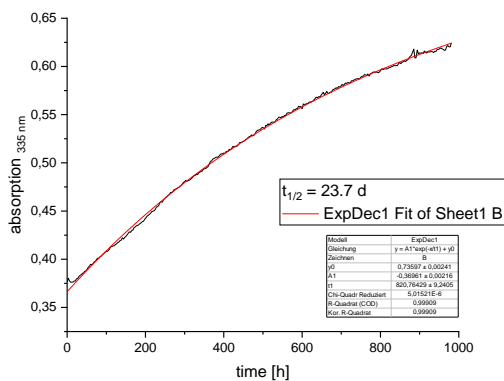


Figure S44. Thermal half-life of 28.

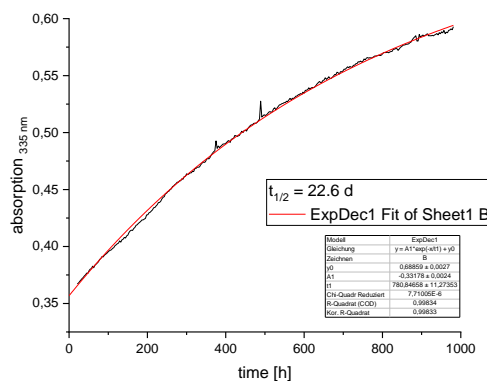


Figure S45. Thermal half-life of 29.

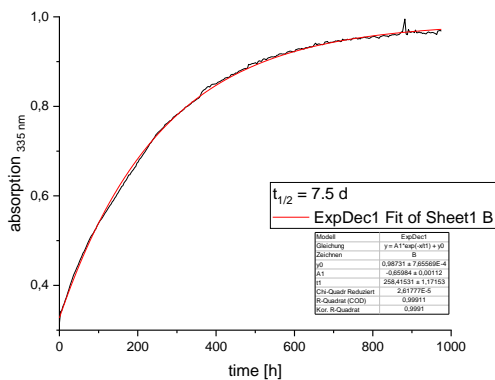


Figure S46. Thermal half-life of 30.

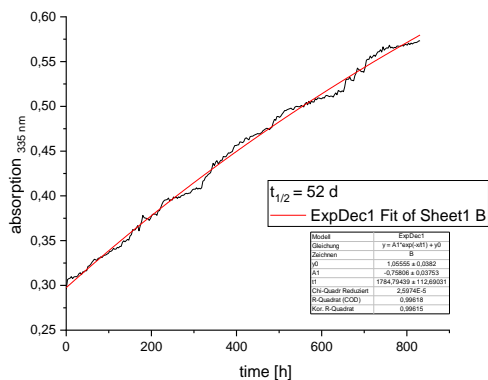


Figure S47. Thermal half-life of 31.

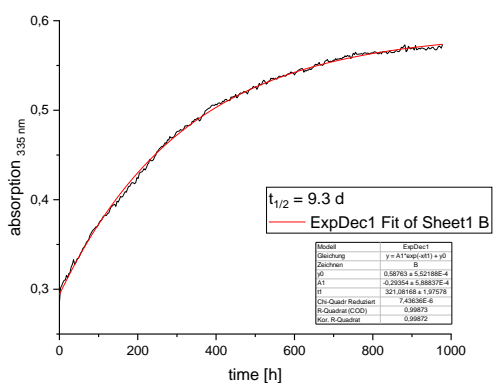


Figure S48. Thermal half-life of 32.

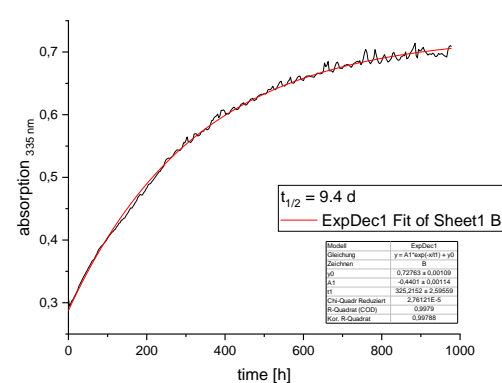


Figure S49. Thermal half-life of 25.

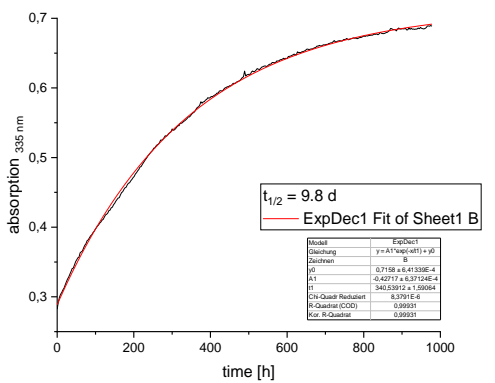


Figure S50. Thermal half-life of 33.

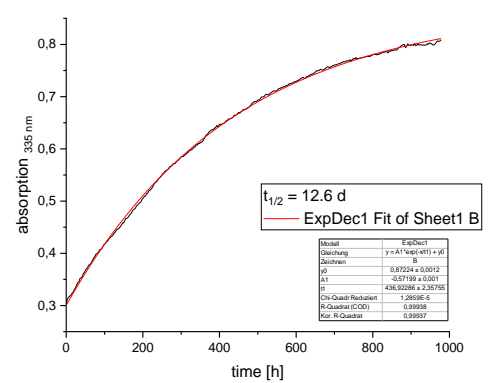


Figure S51. Thermal half-life of 34.

3.11.3 Supplementary Information to Ligand Binding and Functional Characterization

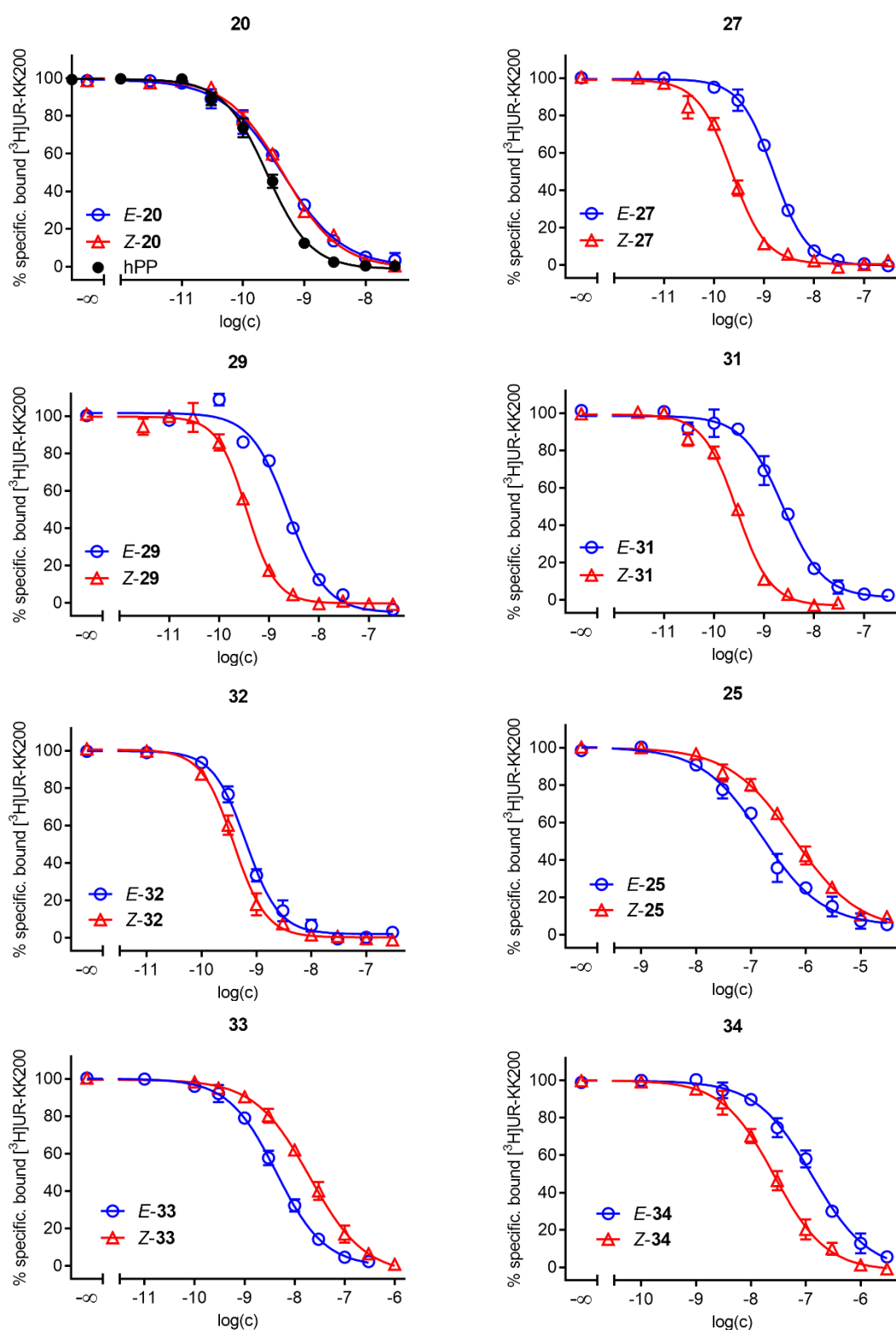


Figure S52. Competition binding curves of hPP and peptides **20**, **25**, **27**, **29**, **31-34** obtained from competition binding experiments with the Y_4R radioligand $[^3\text{H}]\text{UR-KK200}$ ($K_d = 0.67 \text{ nM}$, $^{[24]}c = 1 \text{ nM}$) performed at intact CHO-h Y_4R -mtAEQ-G $_{\text{qi}5}$ cells. Data represent mean values \pm SEM from three or four independent experiments (performed in triplicate).

Table S1. Y₁, Y₂, Y₄ and Y₅ receptor binding data of hPP, **1**, **20**, **25** and **27-34**.

compd.	pK _i ± SEM / K _i (nM) hY ₁ R ^[a]	pK _i ± SEM / K _i (nM) hY ₂ R ^[b]	pK _i ± SEM / K _i (nM) hY ₄ R ^[c]	pK _i ± SEM / K _i (nM) hY ₅ R ^[d]
hPP	440 ^[e]	>3000 ^[e]	10.02 ± 0.06 / 0.10	17 ^[e]
1	>3000 ^[f]	>3000 ^[f]	10.36 / 0.05 ^[f]	>3000 ^[f]
E-20	<6 / >1000	<6 / >1000	9.76 ± 0.01 / 0.17	<6 / >1000
Z-20	<6 / >1000	<6 / >1000	9.74 ± 0.05 / 0.18	<6 / >1000
E-27	n.d.	n.d.	9.21 ± 0.02 / 0.62	n.d.
Z-27	n.d.	n.d.	10.04 ± 0.05 / 0.092	n.d.
E-28	6.18 ± 0.08 / 690	<6 / >1000	8.37 ± 0.04 / 4.3	5.56 ± 0.05 / 2800
Z-28	6.59 ± 0.10 / 270	<6 / >1000	9.35 ± 0.05 / 0.45	5.77 ± 0.07 / 1700
E-29	6.12 ± 0.08 / 790	<6 / >1000	9.16 ± 0.09 / 0.73	<6 / >1000
Z-29	6.37 ± 0.01 / 430	<6 / >1000	9.86 ± 0.02 / 0.14	5.82 ± 0.02 / 1500
E-30	n.d.	n.d.	9.31 ± 0.06 / 0.50	n.d.
Z-30	n.d.	n.d.	10.19 ± 0.03 / 0.066	n.d.
E-31	n.d.	n.d.	9.03 ± 0.04 / 0.94	n.d.
Z-31	n.d.	n.d.	9.94 ± 0.03 / 0.11	n.d.
E-32	6.27 ± 0.01 / 540	<6 / >1000	9.58 ± 0.08 / 0.27	5.63 ± 0.05 / 2400
Z-32	6.15 ± 0.07 / 740	<6 / >1000	9.81 ± 0.05 / 0.16	5.75 ± 0.05 / 1800
E-25	<6 / >1000	n.d.	7.17 ± 0.066 / 69	<6 / >1000
Z-25	<6 / >1000	n.d.	6.61 ± 0.089 / 260	<6 / >1000
E-33	6.33 ± 0.04 / 480	n.d.	8.76 ± 0.090 / 1.8	5.59 ± 0.04 / 2600
Z-33	<6 / >1000	n.d.	8.07 ± 0.093 / 8.9	5.96 ± 0.05 / 1100
E-34	<6 / >1000	<6 / >1000	7.30 ± 0.050 / 51	5.63 ± 0.03 / 2400
Z-34	<6 / >1000	<6 / >1000	7.98 ± 0.07 / 11	6.02 ± 0.08 / 980

[a] Determined by competition binding with [³H]UR-MK299 ($K_d = 0.044$ nM,^[33] $c = 0.15$ nM) at hY₁R expressing SK-N-MC neuroblastoma cells. [b] Determined by competition binding with [³H]propionyl-pNPY ($K_d = 0.14$ nM,^[37] $c = 0.5$ nM) at CHO-hY₂R cells. [c] Data taken from Table 2. [d] Determined by competition binding with [³H]propionyl-pNPY ($K_d = 11$ nM,^[25] $c = 5$ nM) at HEC-1B-hY₅R cells. [e] Reported by Berlicki *et al.*, reported K_i values were converted to pK_i values.^[38] [f] Reported by Konieczny *et al.*^[19] Data represent mean values from at least three independent experiments performed in triplicate (standard error of the mean (SEM) given for Y₄R pK_i values). n.d.: not determined.

Concentration-response curves obtained from a hY₄R miniG_i recruitment assay performed with HEK293T-CBR-N-mG_{si}/Y₄R-CBR-C cells:

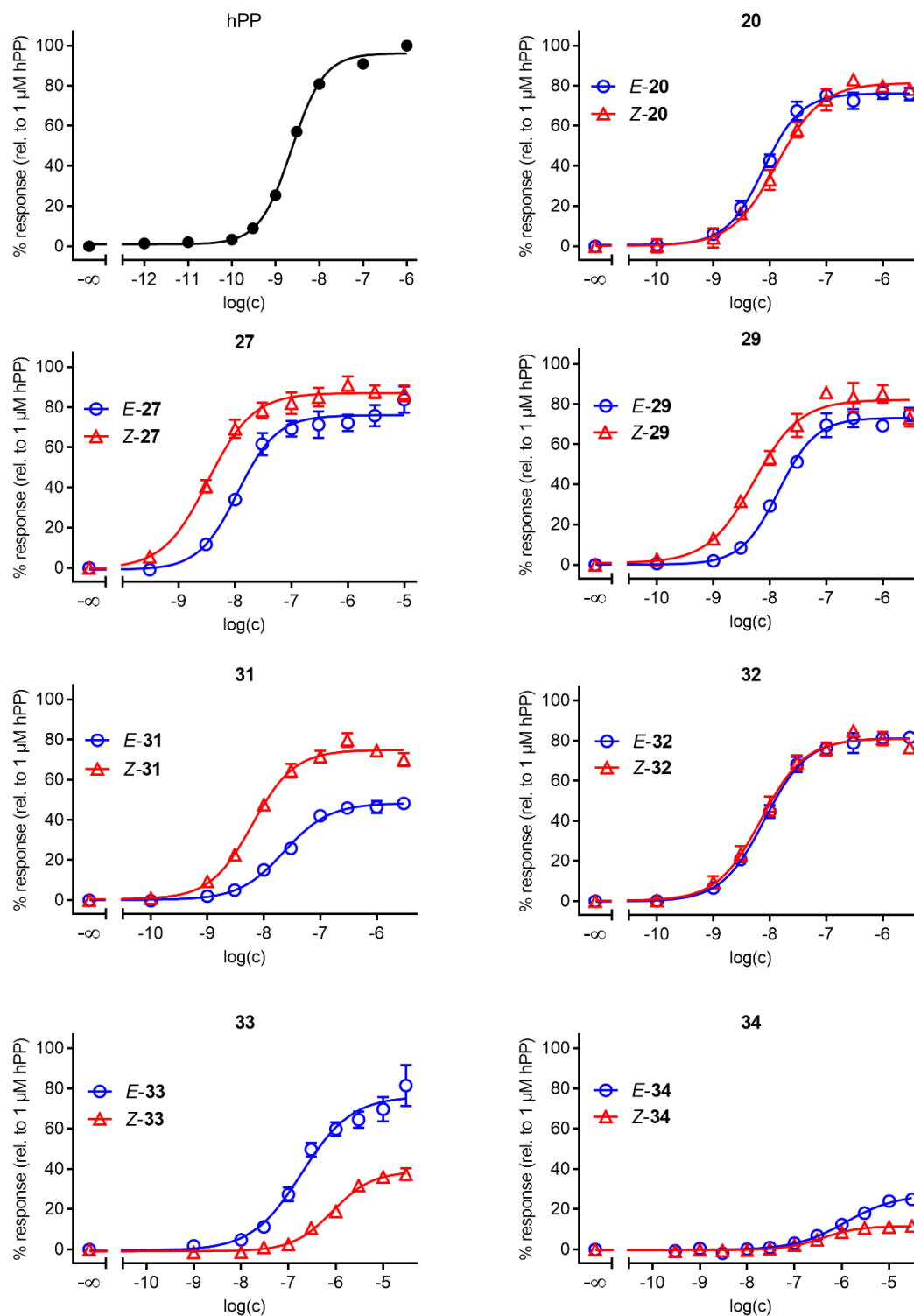
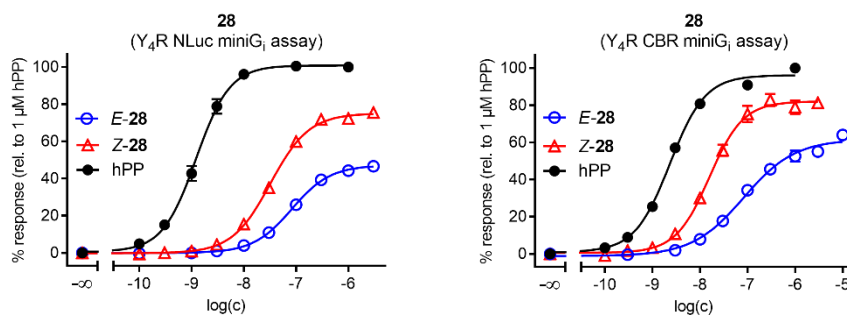


Figure S53. Concentration-response curves of hPP and **20**, **27**, **29** and **31-34** determined in a miniG_i protein recruitment assay performed with HEK293T-CBR-N-mG_{si}/Y₄R-CBR-C cells. Data represent mean values from at least three independent experiments performed in triplicate.

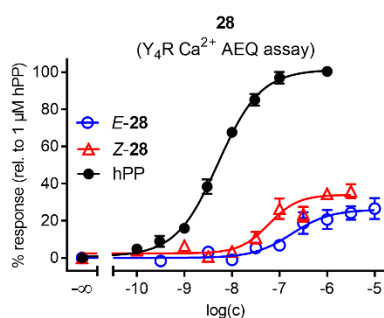
Comparison: Agonistic potencies and intrinsic activities of **28** obtained from a hY₄R miniG_i recruitment assay performed with HEK293T-NlucN-mG_{si}/Y₄R-NlucC and HEK293T-CBRN-mG_{si}/Y₄R-CBR-C cells:



	Nluc miniG _i assay		CBR miniG _i assay	
	<i>E</i> -28	<i>Z</i> -28	<i>E</i> -28	<i>Z</i> -28
pEC ₅₀ ± SEM / EC ₅₀ (nM)	7.086 ± 0.001 / 82	7.49 ± 0.01 / 32	7.08 ± 0.02 / 84	7.79 ± 0.04 / 16
efficacy E ± SEM	47 ± 1	75 ± 1	62 ± 2	83 ± 3

Figure S54. Concentration-response curves of **28** and hPP determined in a miniG_i protein recruitment assay performed with HEK293T-NlucN-mG_{si}/Y₄R-NlucC cells (left) and HEK293T-CBRN-mG_{si}/Y₄R-CBRC cells (right). Data represent mean values from at least three independent experiments performed in triplicate. The corresponding pEC₅₀ values and intrinsic activities are summarized in the table.

Concentration-response curves of **28** obtained from Ca²⁺-aequorin assay performed with intact CHO-hY₄RmtAEQ-G_{q5} cells:



	<i>E</i> -28	<i>Z</i> -28
pEC ₅₀ ± SEM / EC ₅₀ (nM)	6.76 ± 0.07 / 181	7.23 ± 0.10 / 62.7
efficacy E ± SEM	23 ± 5	36 ± 2

Figure S55. Concentration-response curves of **28** determined in a Ca²⁺-aequorin assay performed with intact CHO-hY₄RmtAEQ-G_{q5} cells. Data represent mean values from at least three independent experiments performed in triplicate. The corresponding pEC₅₀ values and intrinsic activities are summarized in the table.

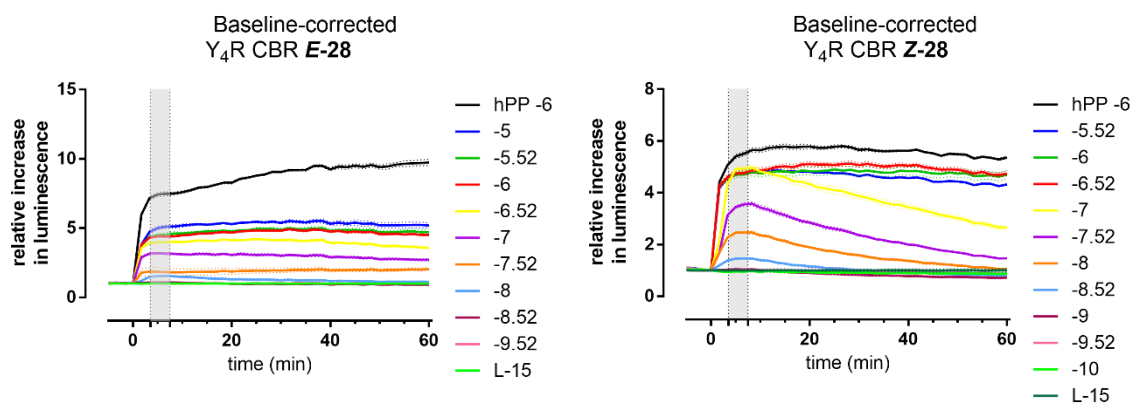


Figure S56. Luminescence signal time courses of hPP (1 μ M, black lines) and *E-28* and *Z-28* (different concentrations represented by different colors) from a mini- G_{si} protein recruitment assay performed with HEK293T-CBRN-m G_{si} /Y₄R-CBRC cells. The signal of the plateau or peak occurring after the initial step rise of the luminescence within 3.5-7.5 min (time window indicated a shaded area), was used for the analysis.

3.11.4 Supplementary Information to Impedance Studies

Impedance-based dose response curves with wild type CHO cells. Figure S57 shows the stimulation of wild type CHO K1 cells with **28** *E/Z* and **30** *E/Z* with respect to the response of CHO Y₄R cells incubated with 0.1 μ M hPP. The dose-response relationships are based on impedance readings at an AC frequency of 12 kHz.

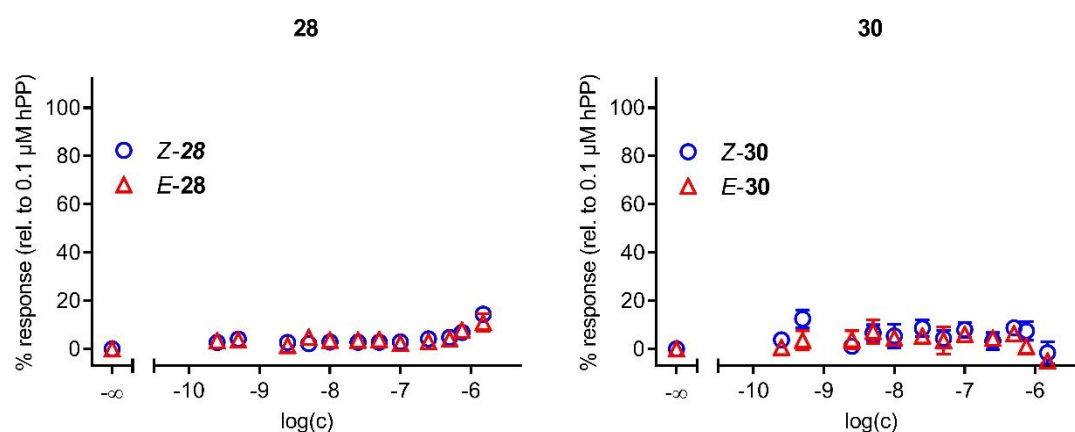


Figure S57. Dose-response curves of *E/Z*-isomers of **28** and **30** obtained by AUC calculation of impedance time courses at 12 kHz performed on wild type CHO K1 cells. HPP response measured on CHO NPY Y₄ cells. Data represent mean values \pm SEM from at least three independent experiments performed in triplicate.

Concentration dependency of the impedance time courses. Figure S58 shows data from one typical experiment conducted to record the concentration dependency of the impedance time courses of CHO Y₄R cells stimulated with different concentrations of **Z-30** (left) or **E-30** (right). After baseline measurements, the cells were pre-stimulated with forskolin (0.4 μM, 50 μL) at time point t = -30 min. Both isomers of **30** were added to the cells in different concentrations at t = 0. The dose-response relationship (Figure 6) was established by calculating the area under the curve (AUC) for the individual time series between the time points 20 min and 40 min for at least three individual experiments.

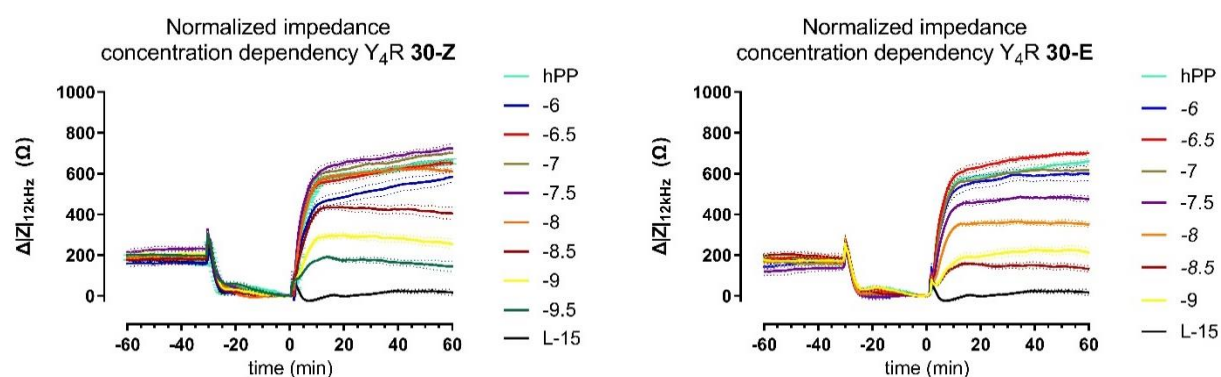


Figure S58. Impedance time course of CHO Y₄R cells at an AC frequency of 12 kHz. Pre-stimulation with forskolin (50 μL, 0.4 μM) started at t = -30 min. Stimulation with different concentrations of **Z-30** (left) and **E-30** (right) was initiated at t = 0. L-15 served as negative and hPP (0.1 μM) as positive controls. Mean ± SEM.

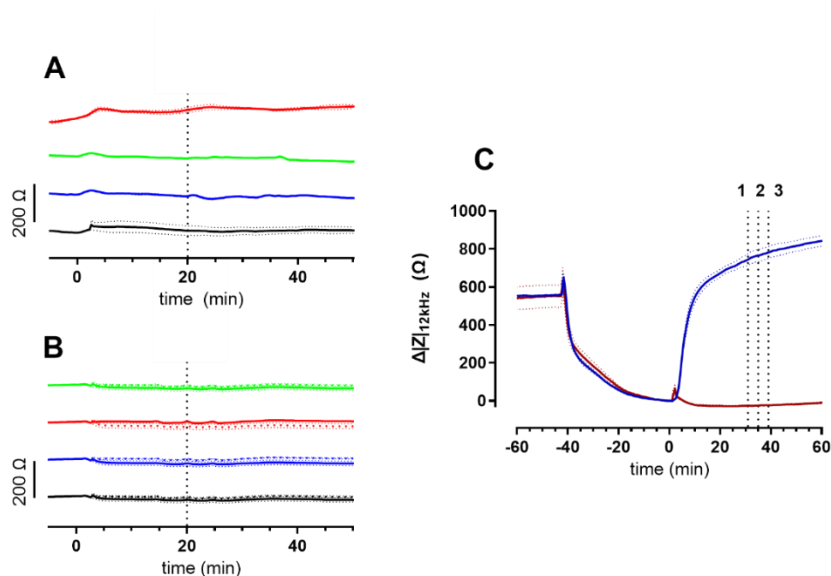
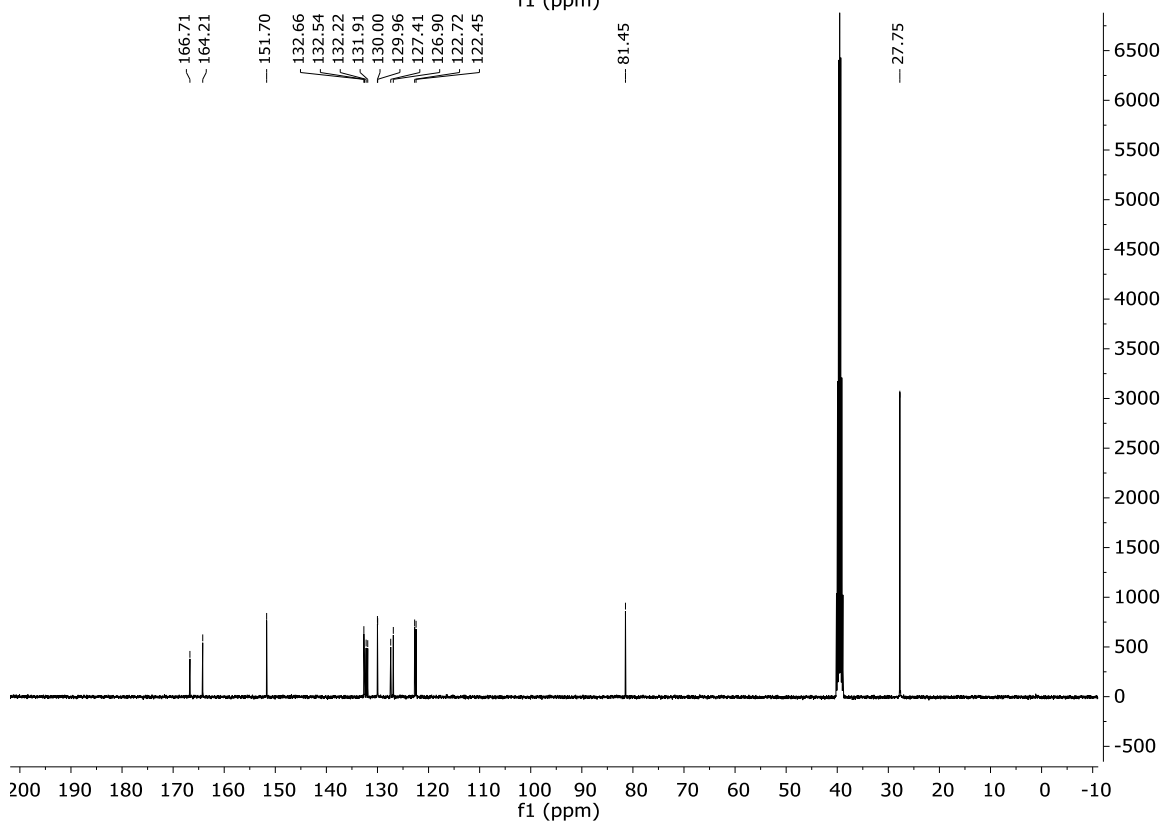
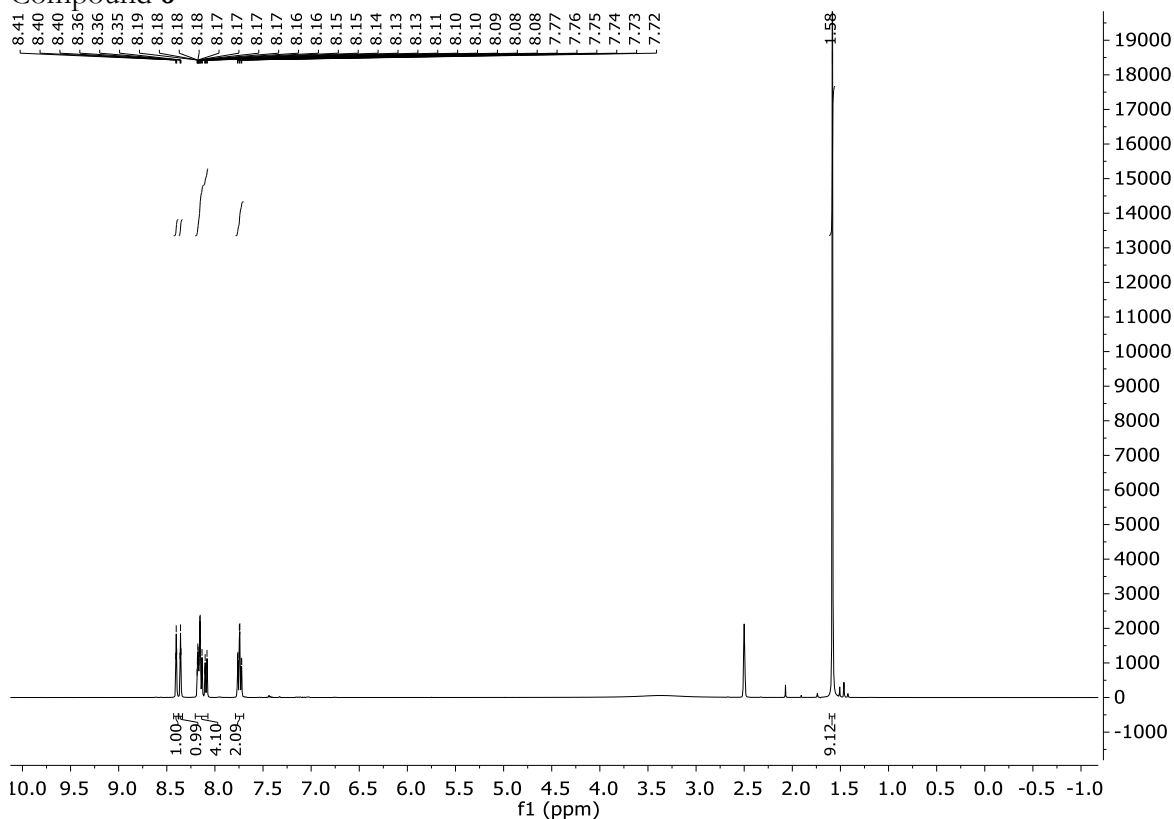


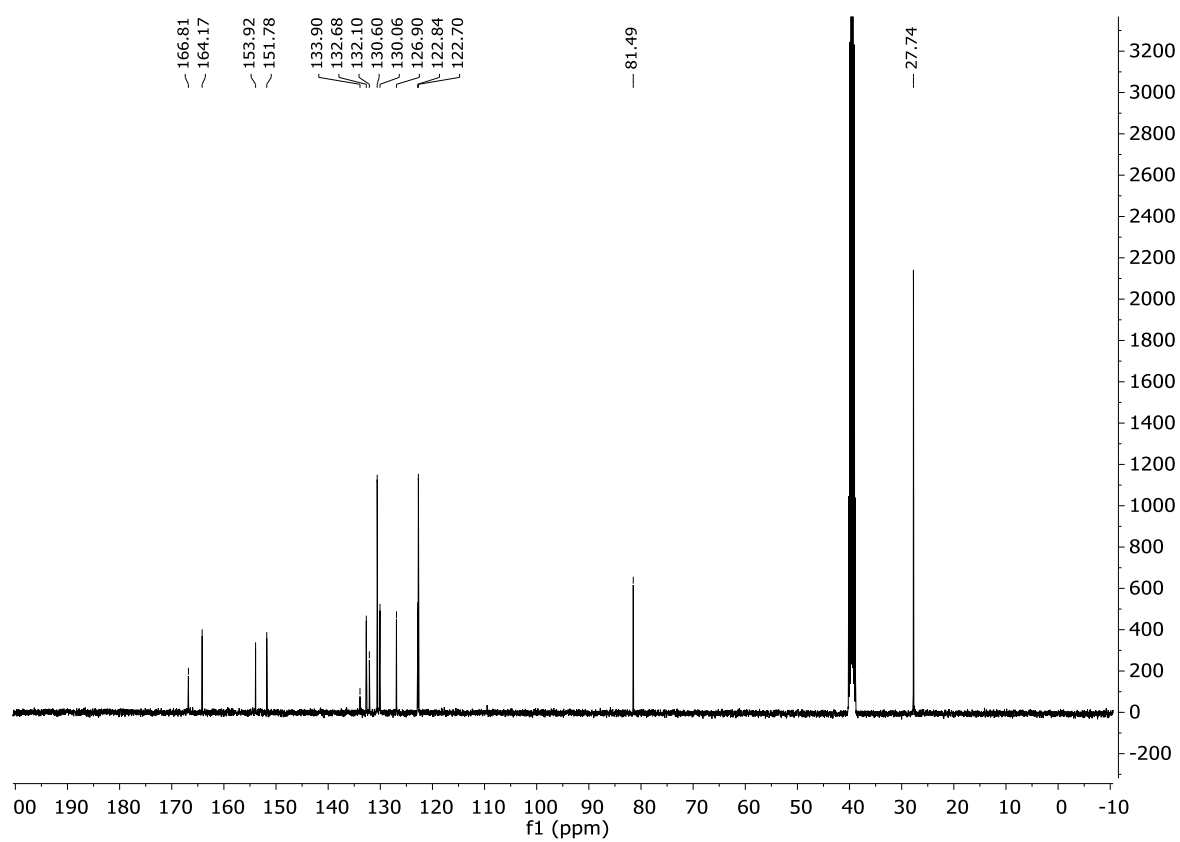
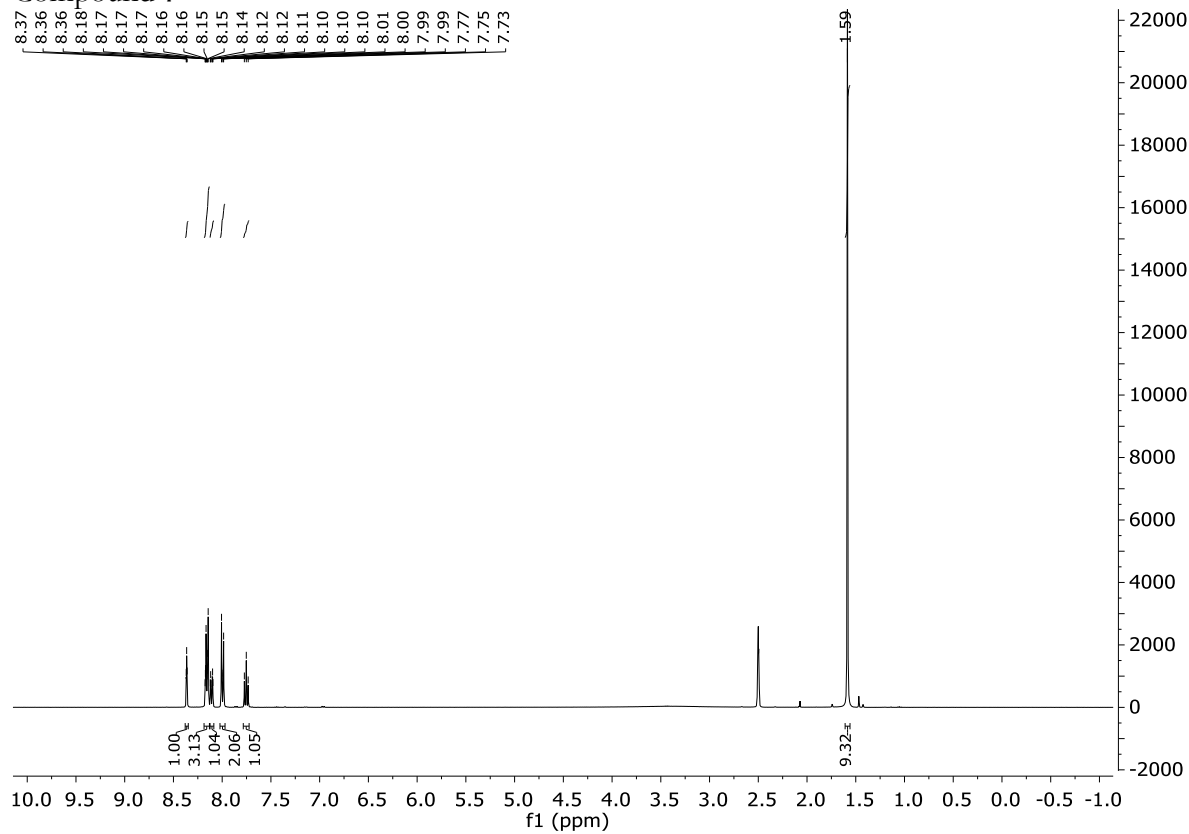
Figure S59. Time courses of impedance (12 kHz) during control experiments. **(A)** Influence of irradiation on cells without agonists. CHO-Y₄R cells were kept in the dark (black) or were irradiated with wavelengths as defined by the color code (blue: 455 nm; green: 340 nm; red: 528 nm) at the time indicated by the dashed vertical line. **(B)** Time courses of impedance for cell-free (!) electrodes in contact to both isomers of **28** and **30** ($c = 50$ nM). (i) The two isomers of **28** (black, dashed/solid) and **30** (blue, dashed/solid) were not exposed to light for the entire observation time. (ii) The two isomers of **28** (red, dashed/solid) and **30** (green, dashed/solid) were irradiated with the wavelength required for their individual photoisomerization (*E*-**28/30**: 340 nm; *Z*-**28**: 455 nm; *Z*-**30**: 528 nm) at the time indicated by the dashed vertical line. The scale bar corresponds to a change in impedance magnitude $\Delta|Z|$ of 200 Ω . Mean \pm SEM ($n=3$). **(C)** Influence of irradiation on cells stimulated with a non-photochromic ligand or a vehicle control. The blue curve represents the cells stimulated with hPP (100 nM) whereas the red line stands for cells incubated with a vehicle control (DMSO, $c = 0.01\%$ (v/v)). The vertical, dashed lines depict the time point of illumination with either (i) 455 nm at line 1, (ii) 528 nm at line 2 or (ii) 340 nm at line 3. Cells were pre-stimulated with forskolin (0.4 μM , $t = -40$). MEAN \pm SEM ($n=3$).

3.11.5 NMR Spectra

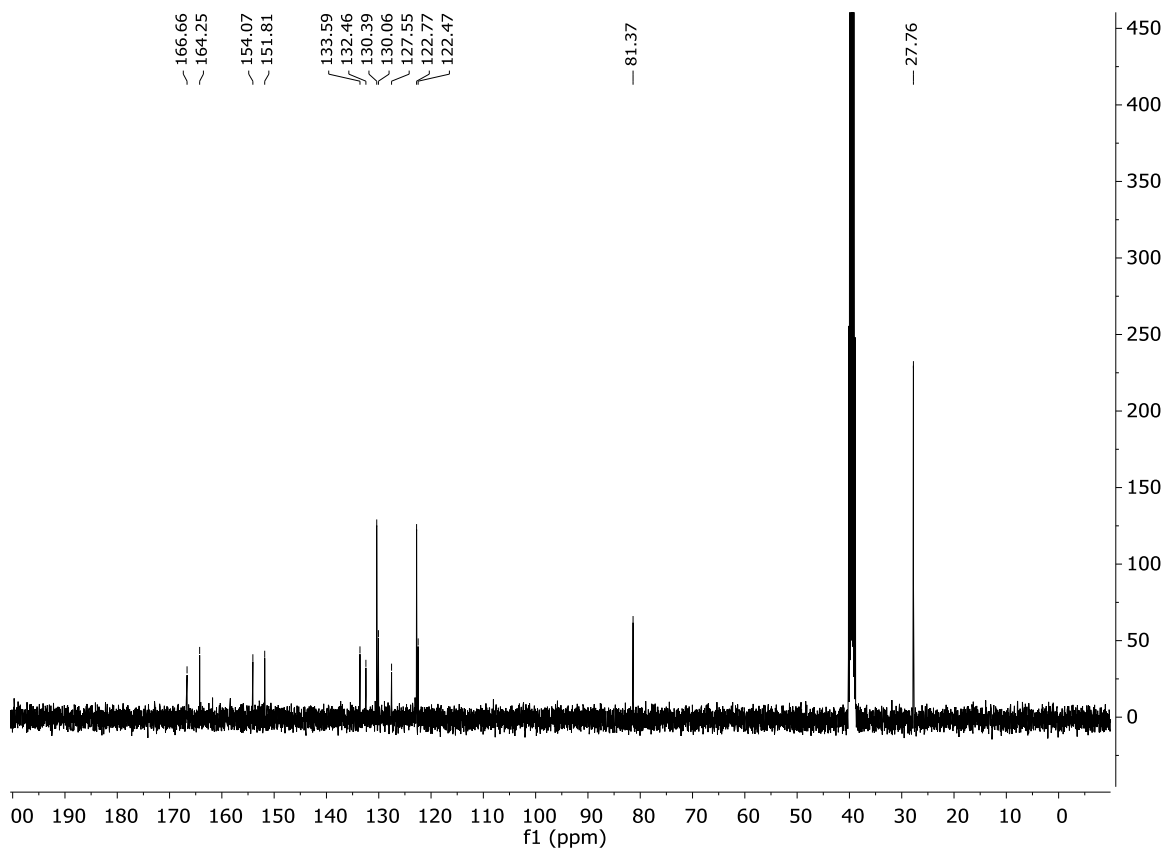
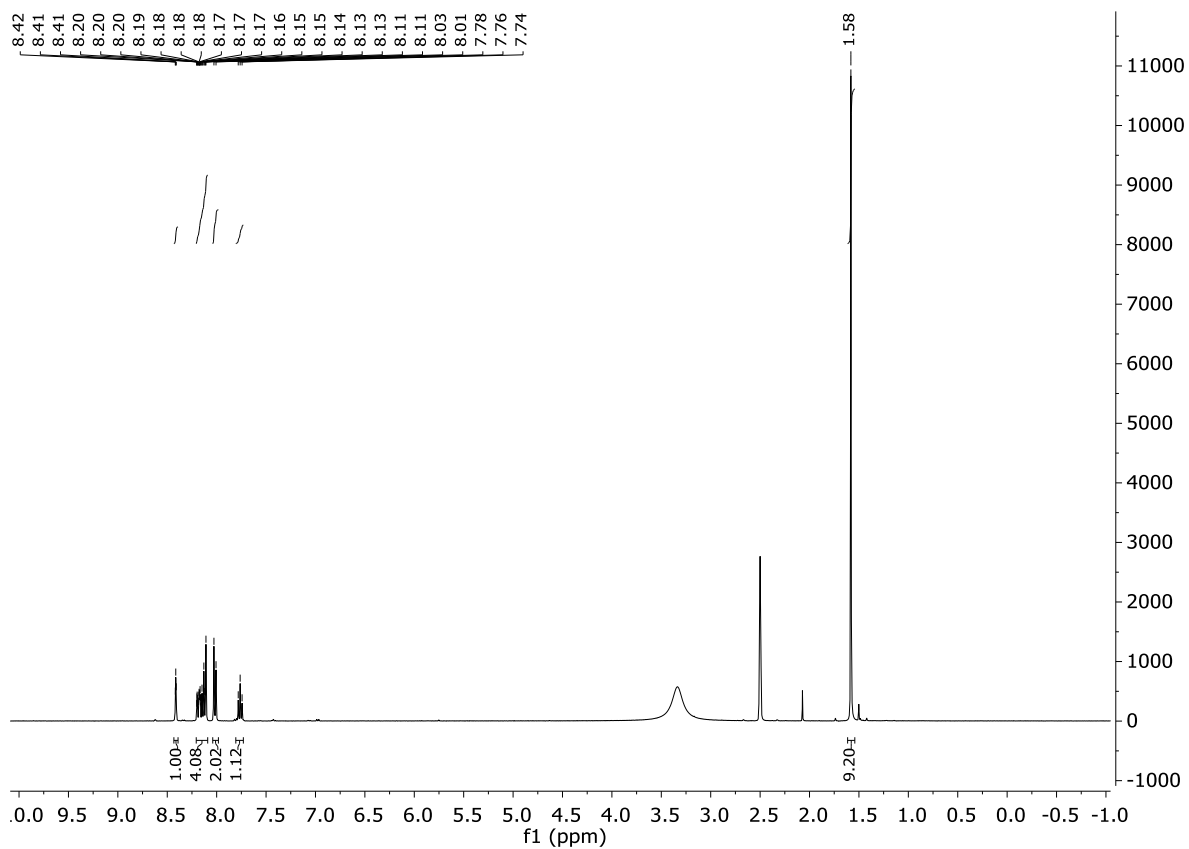
Compound 6



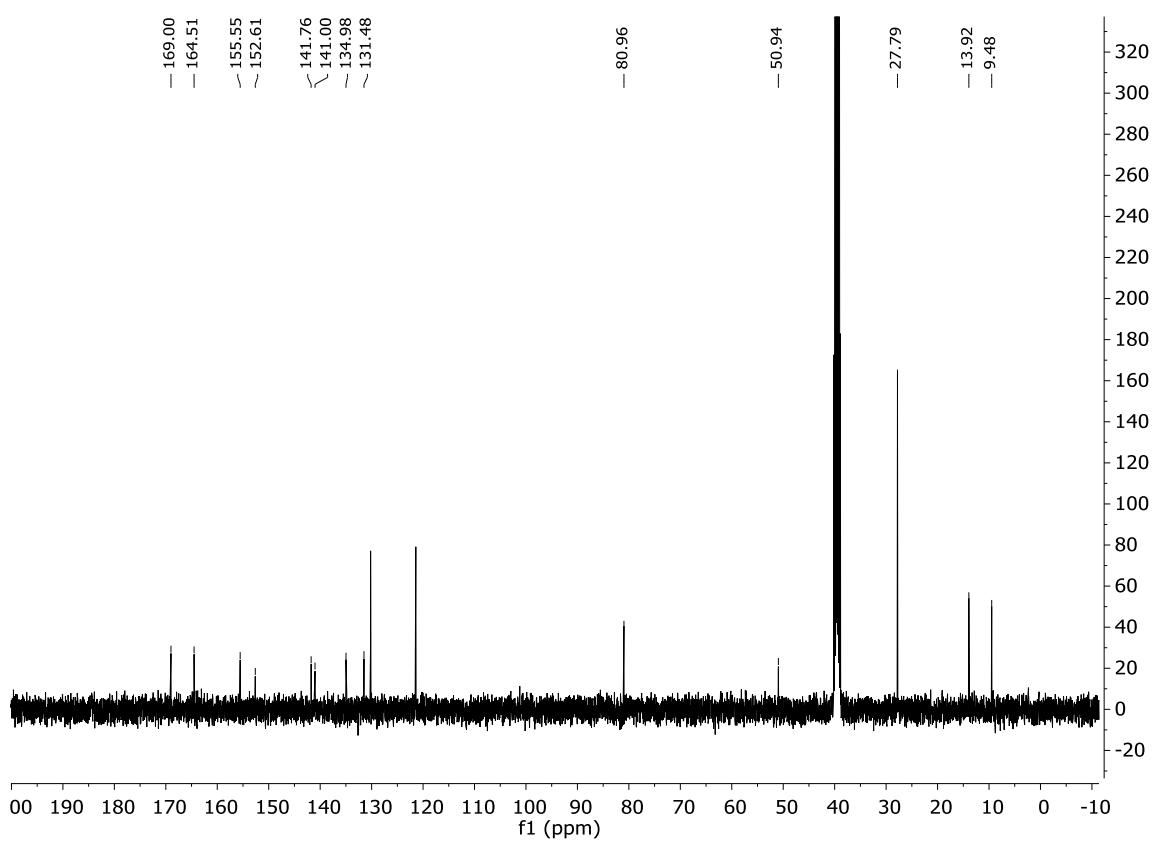
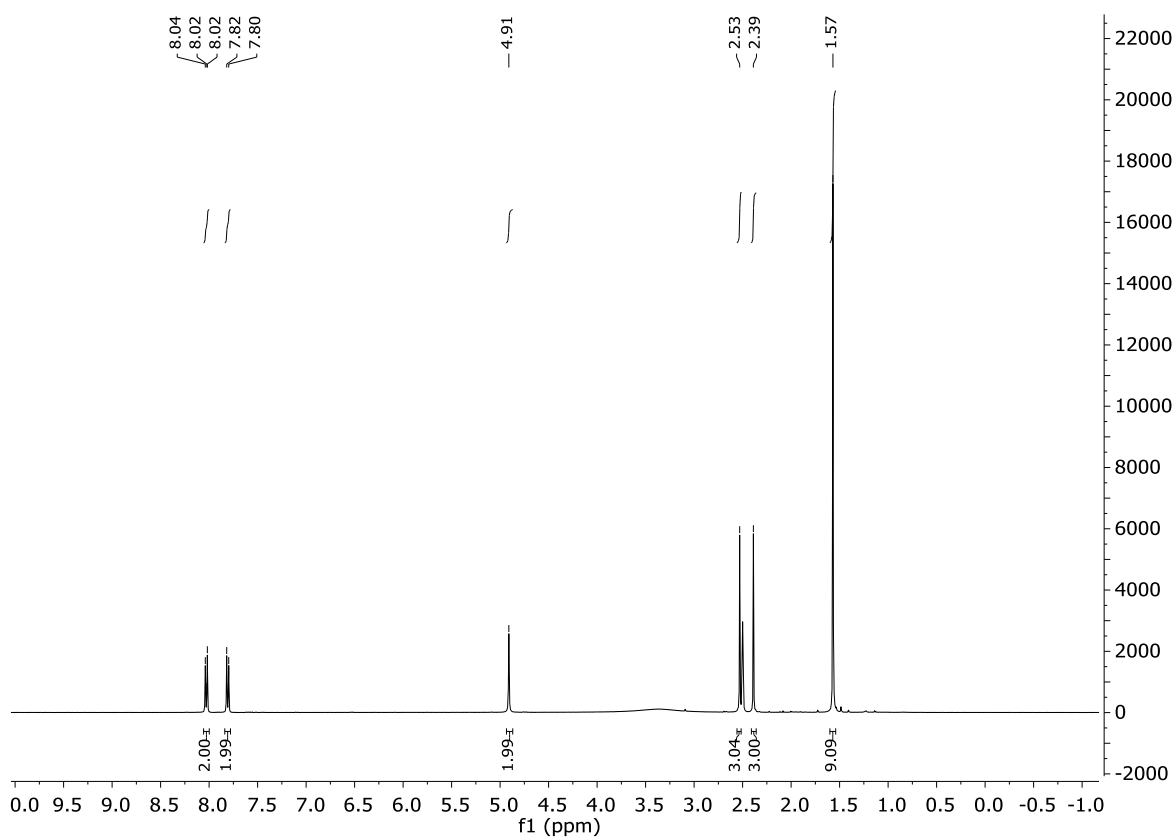
Compound 7



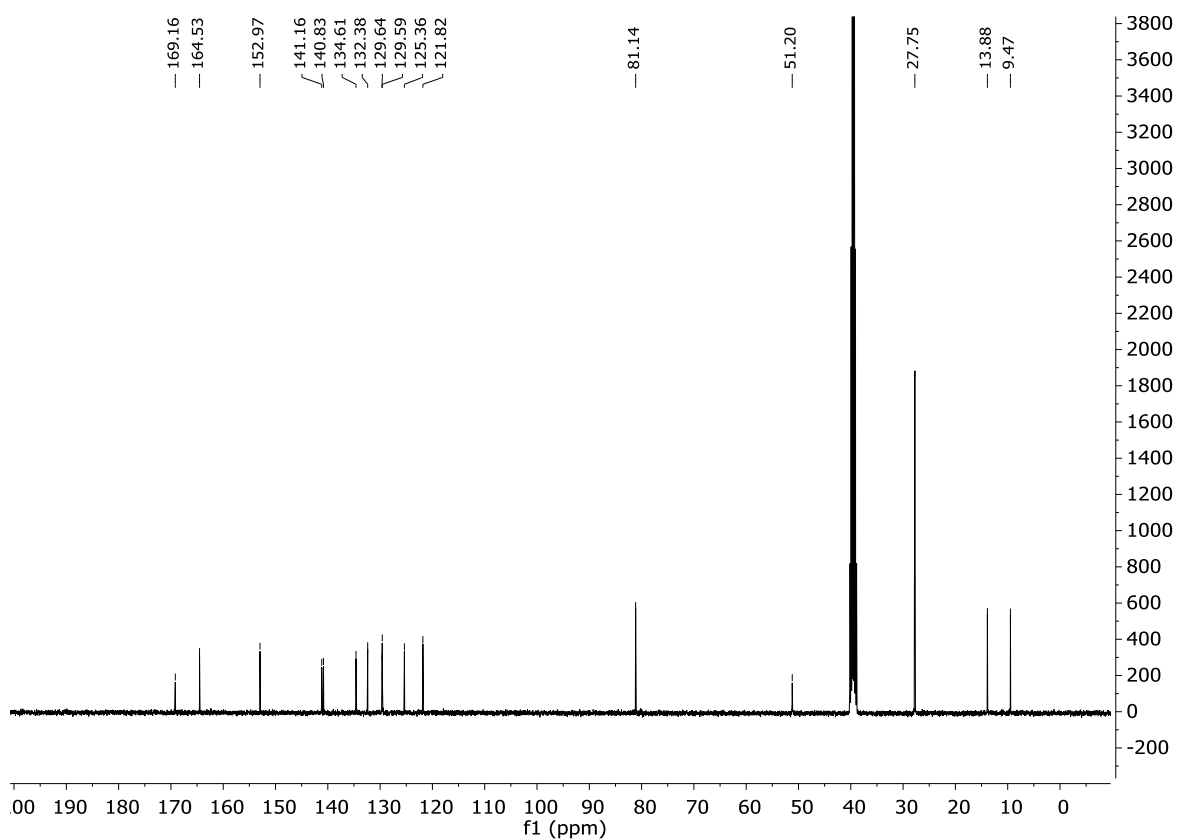
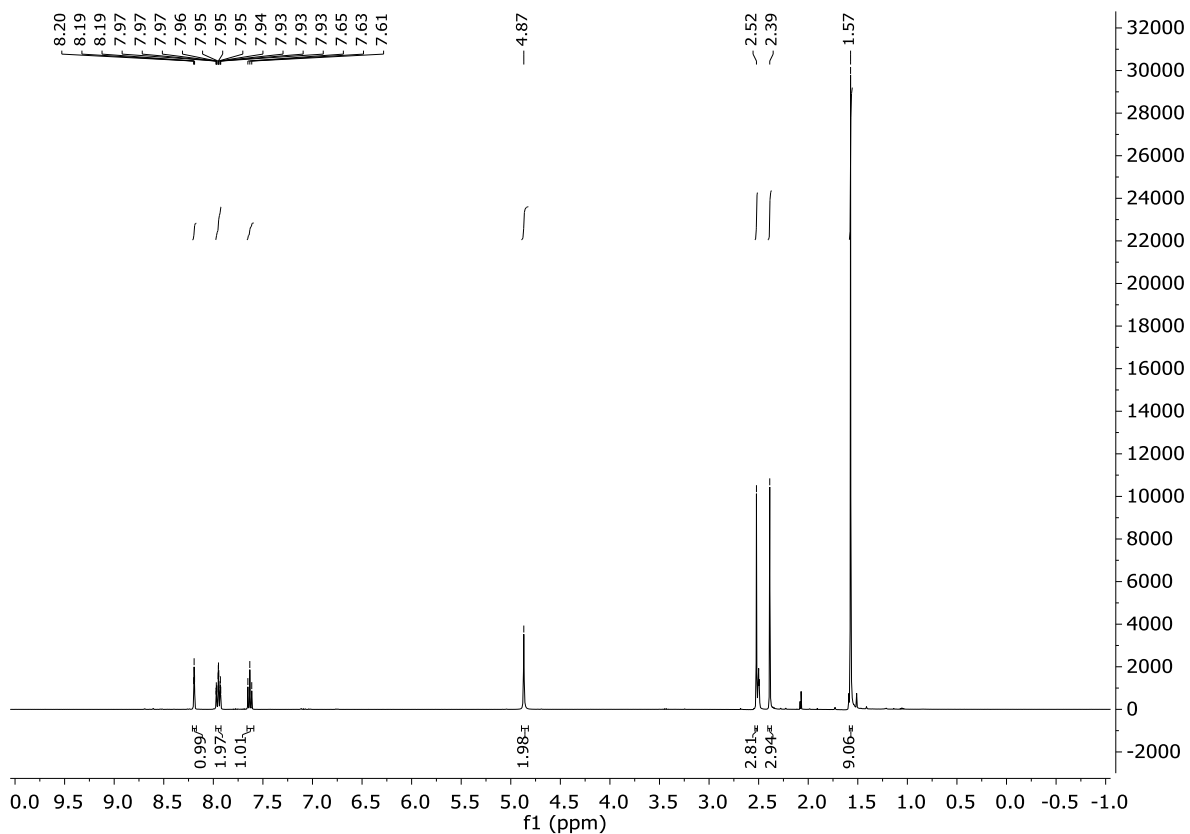
Compound 8



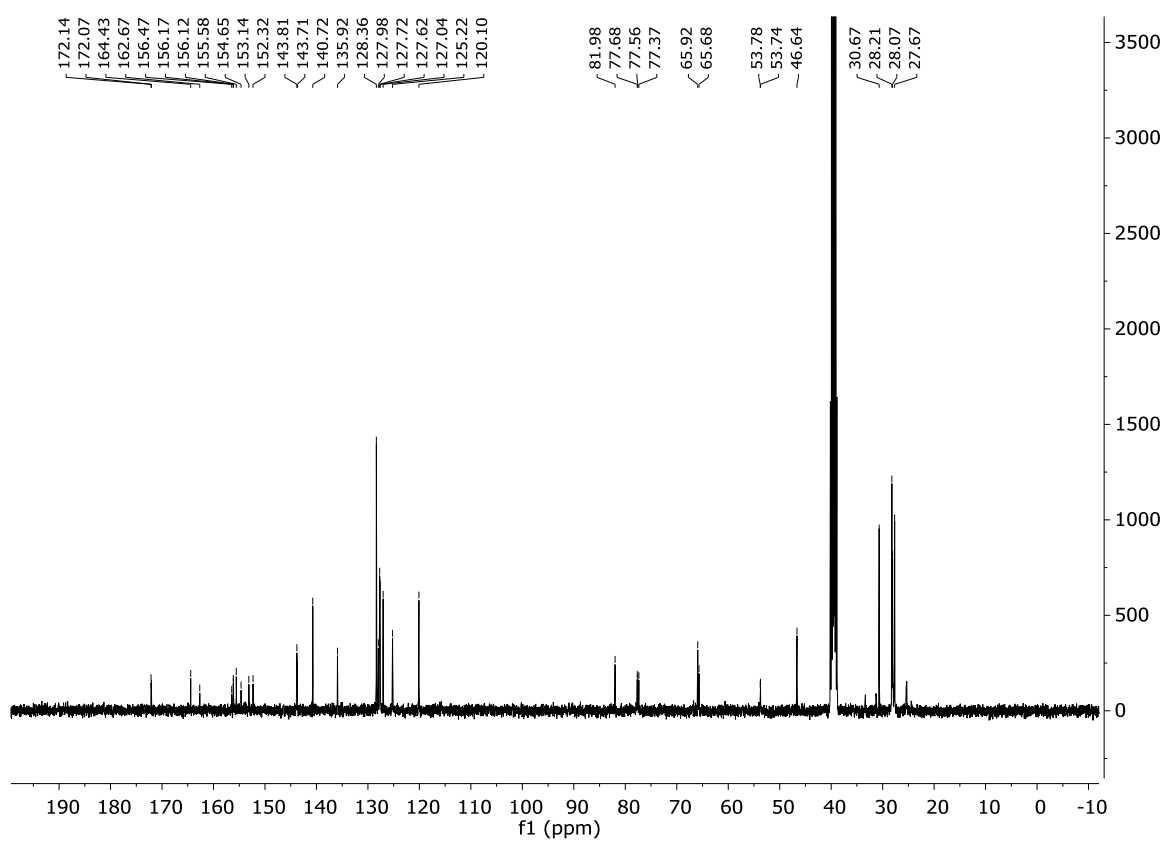
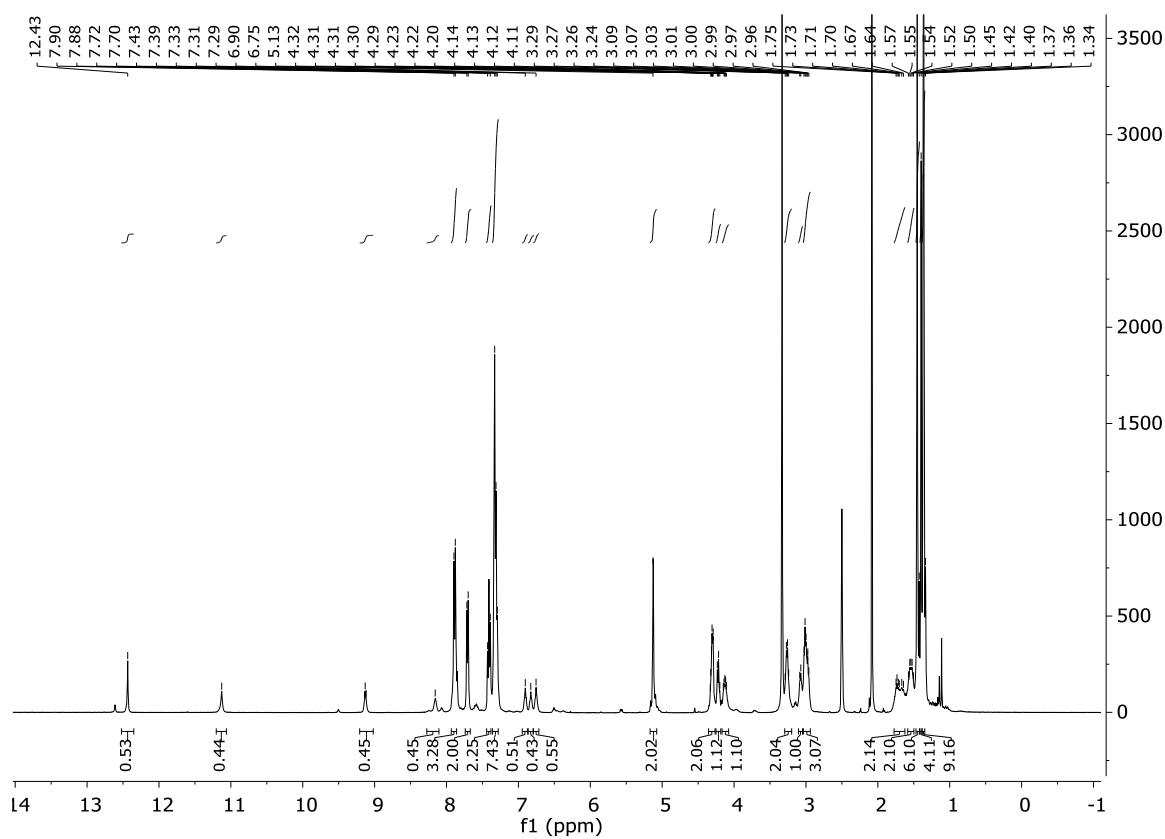
Compound 12



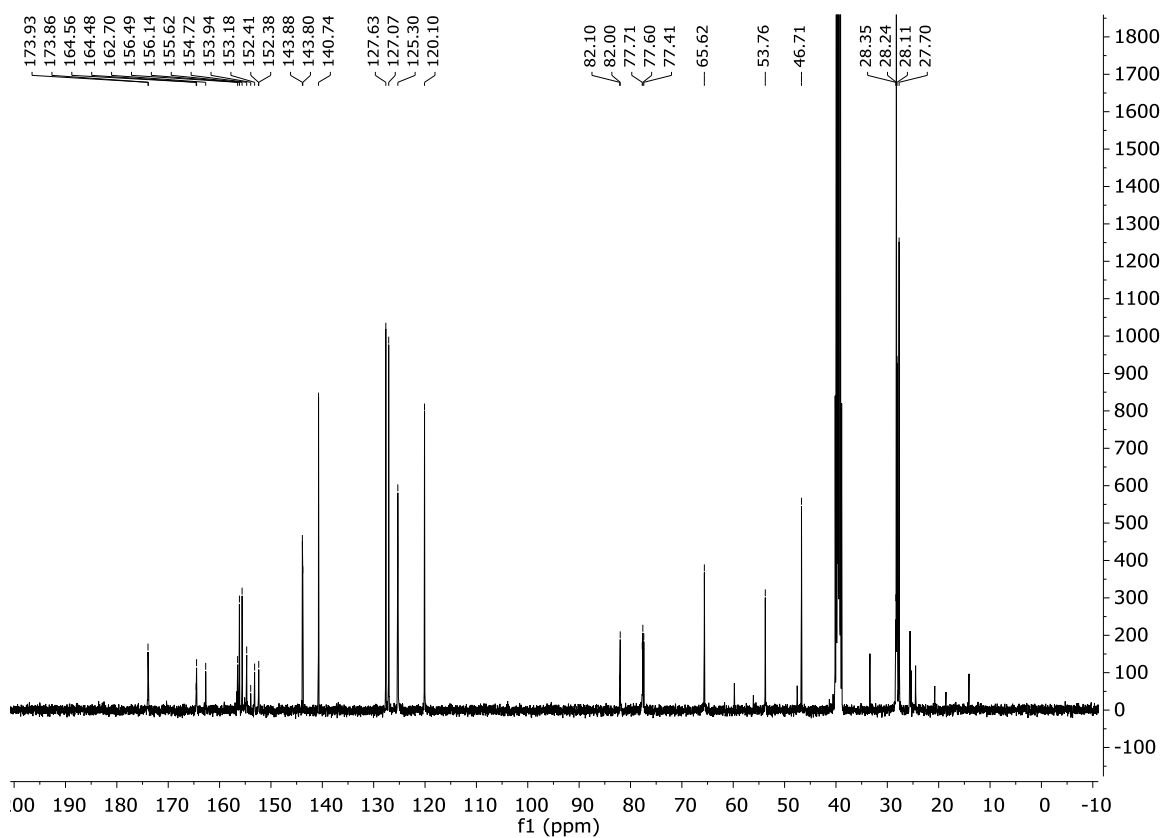
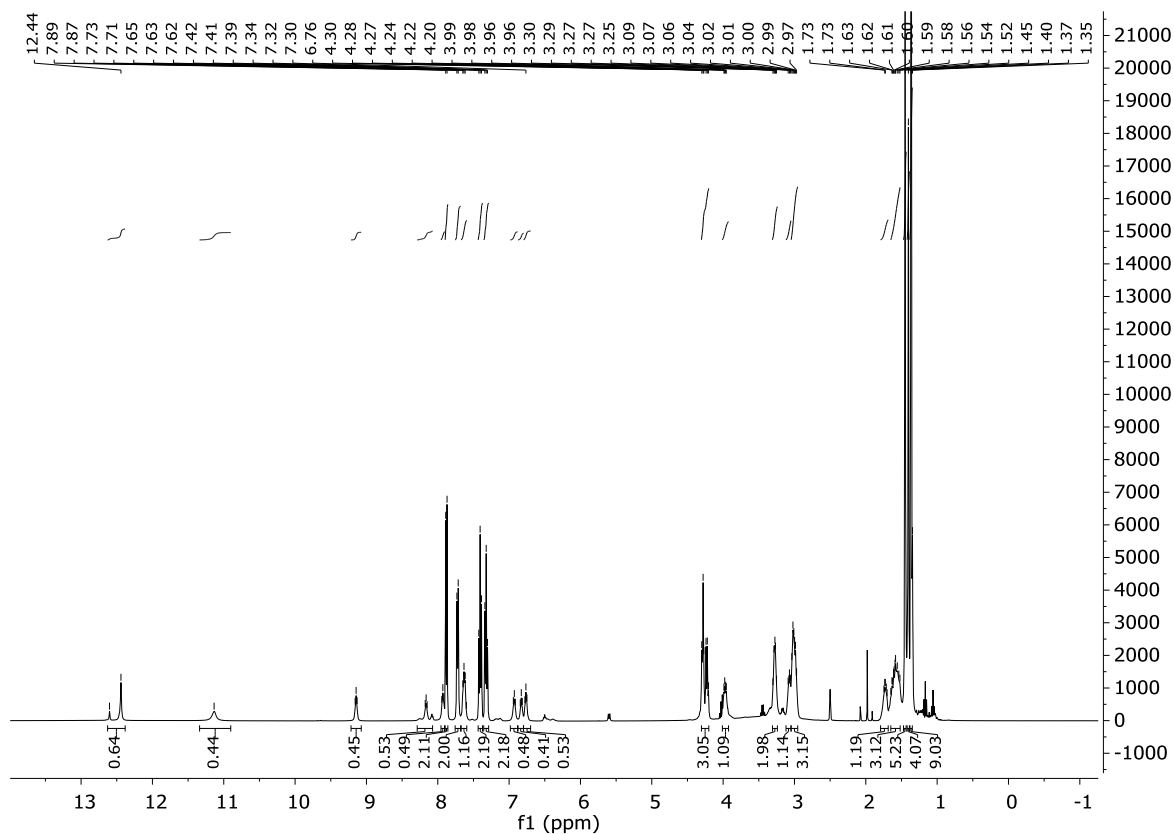
Compound 13



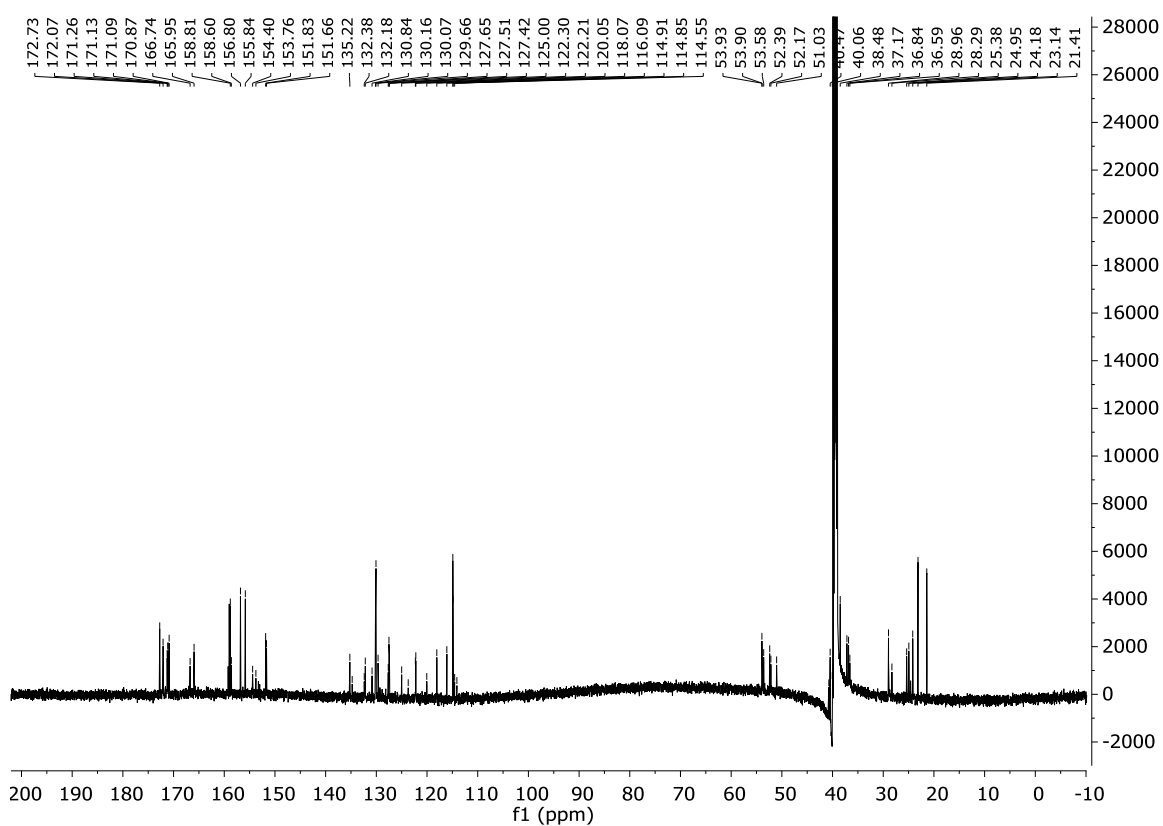
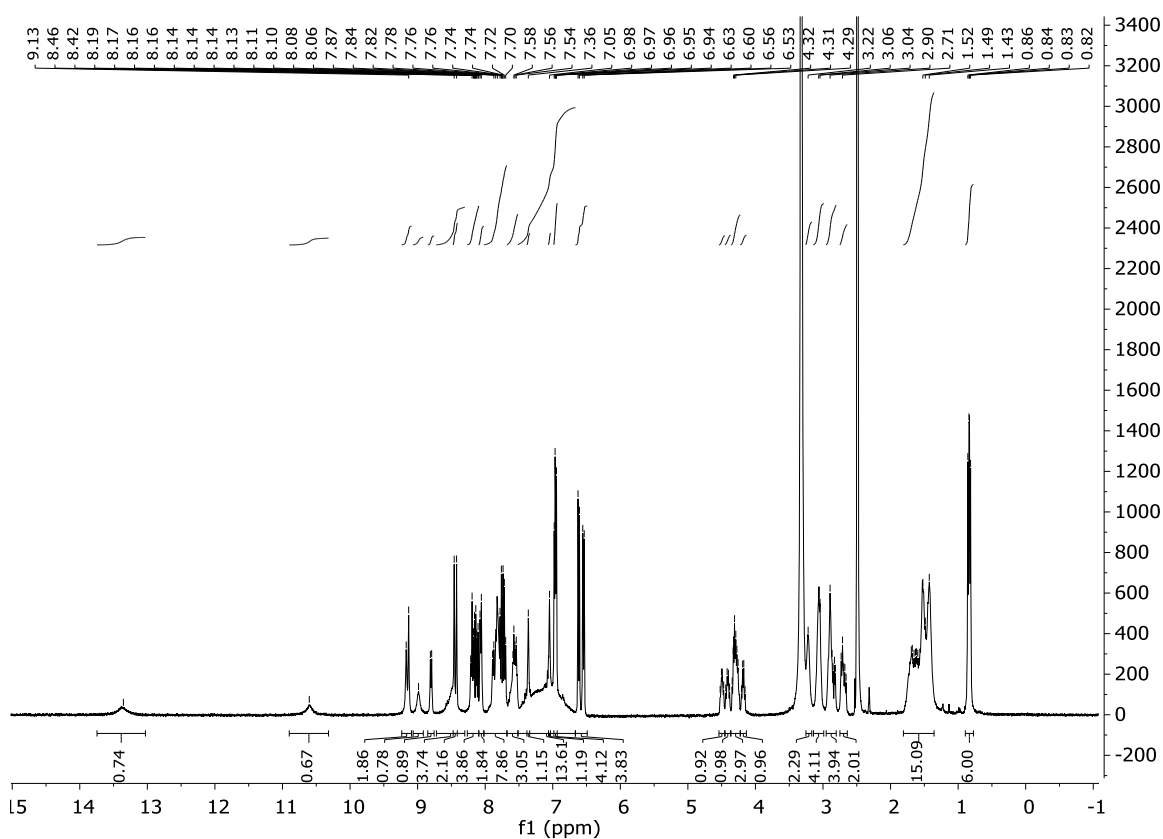
Compound 41



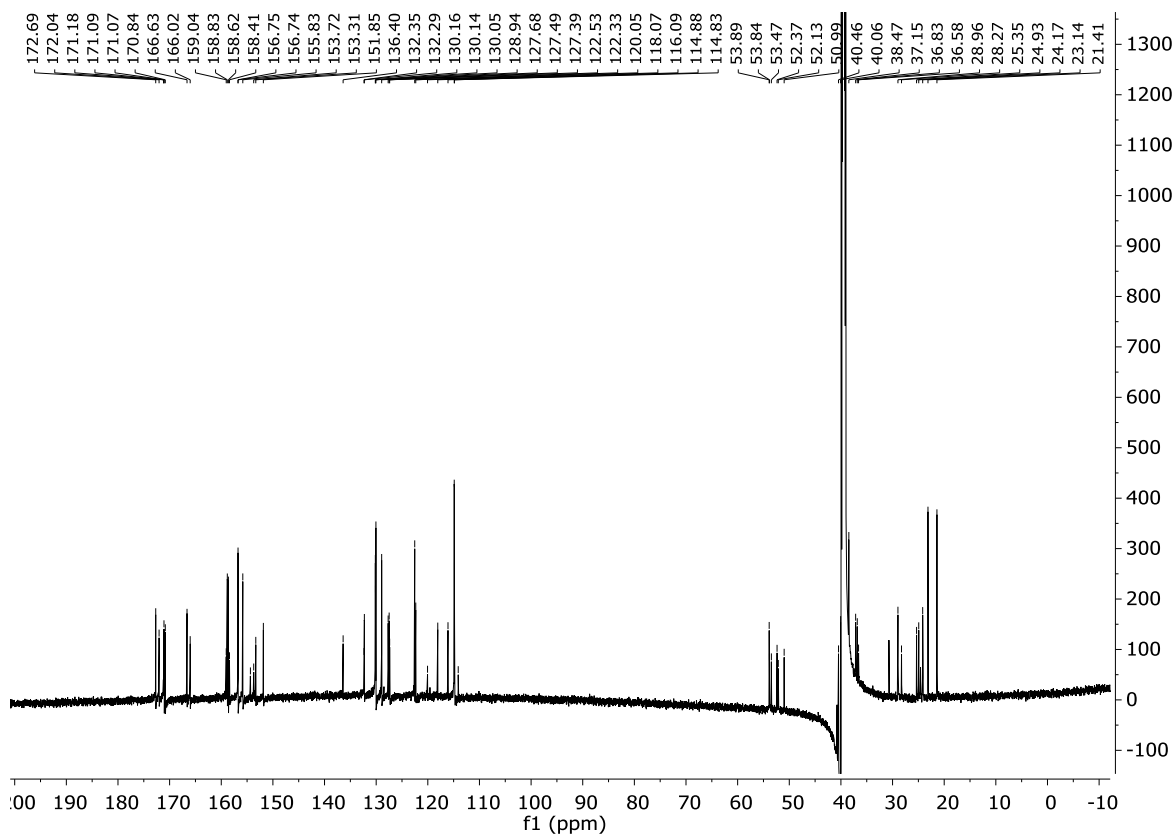
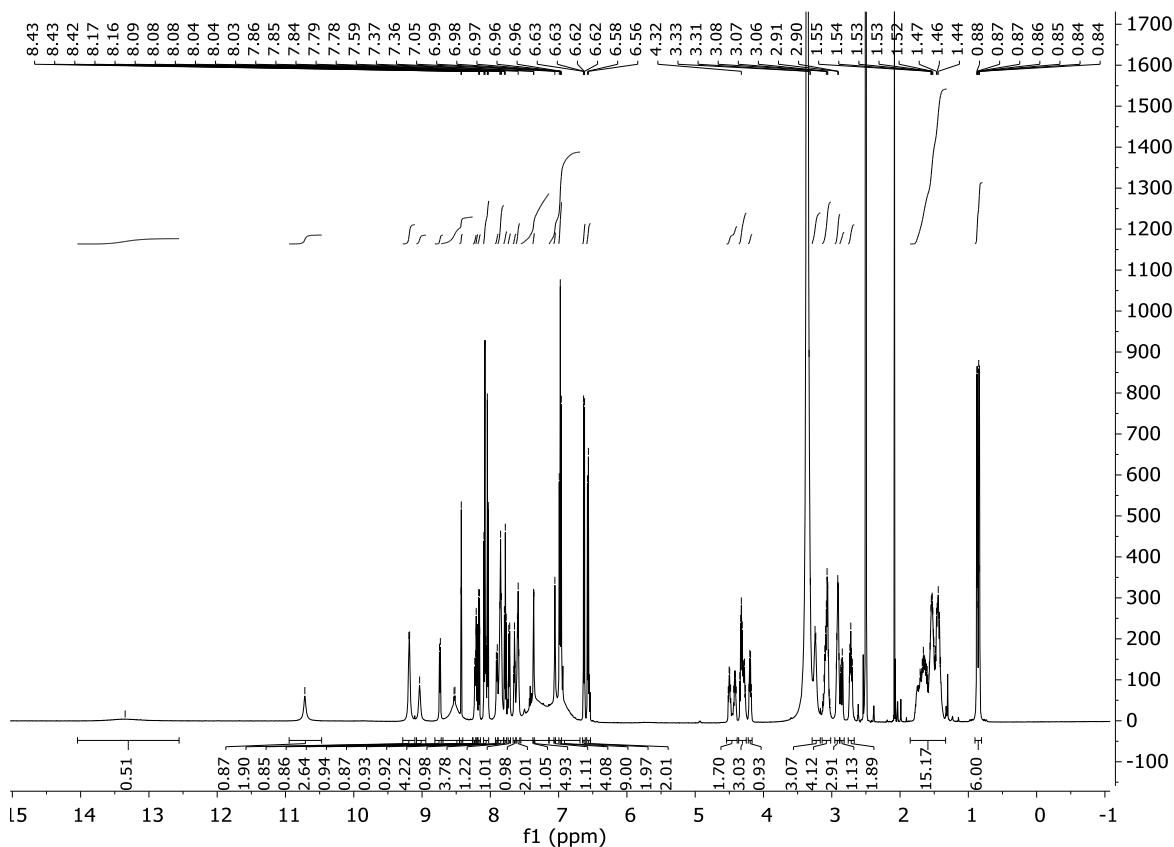
Compound 17



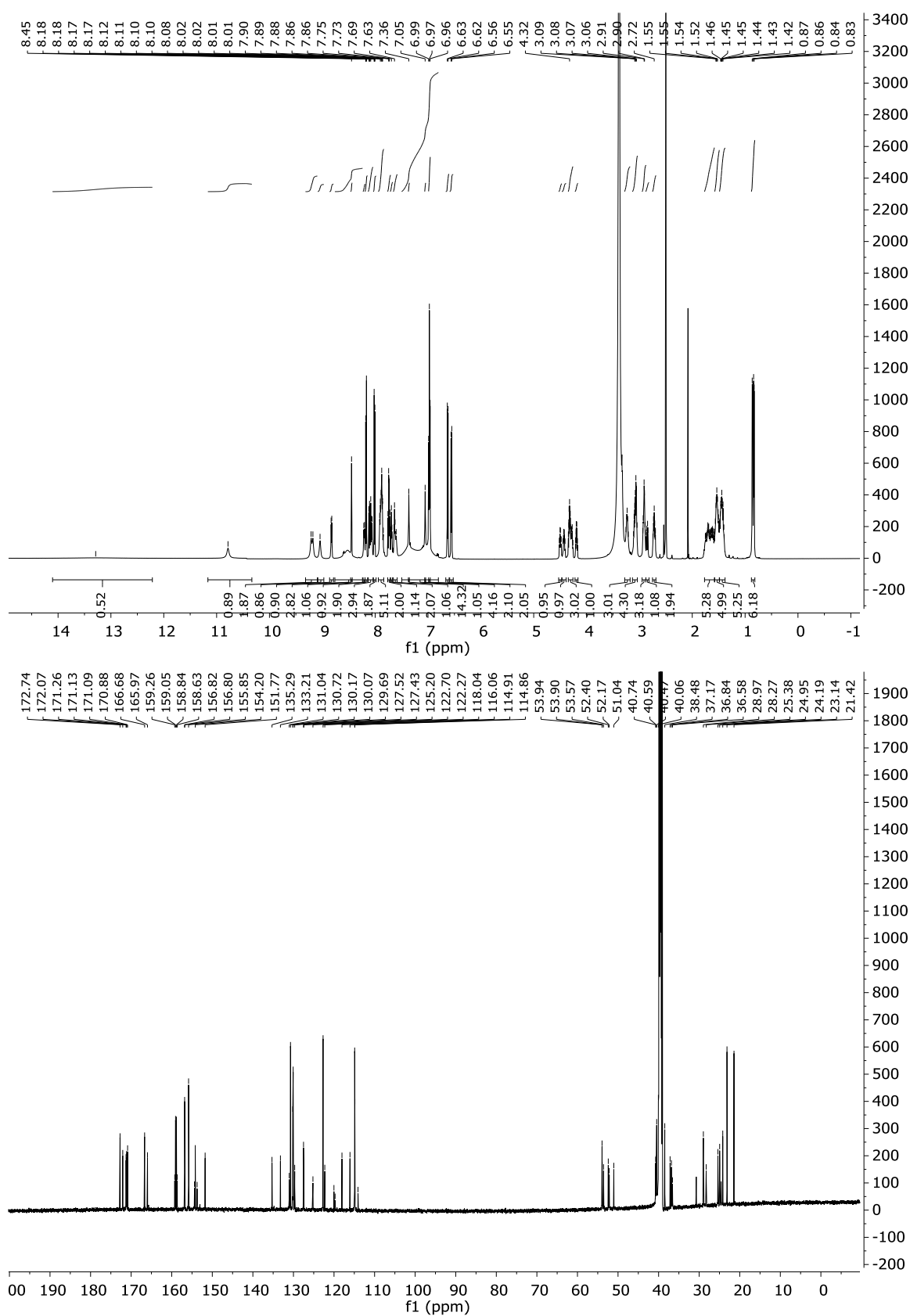
Compound 19



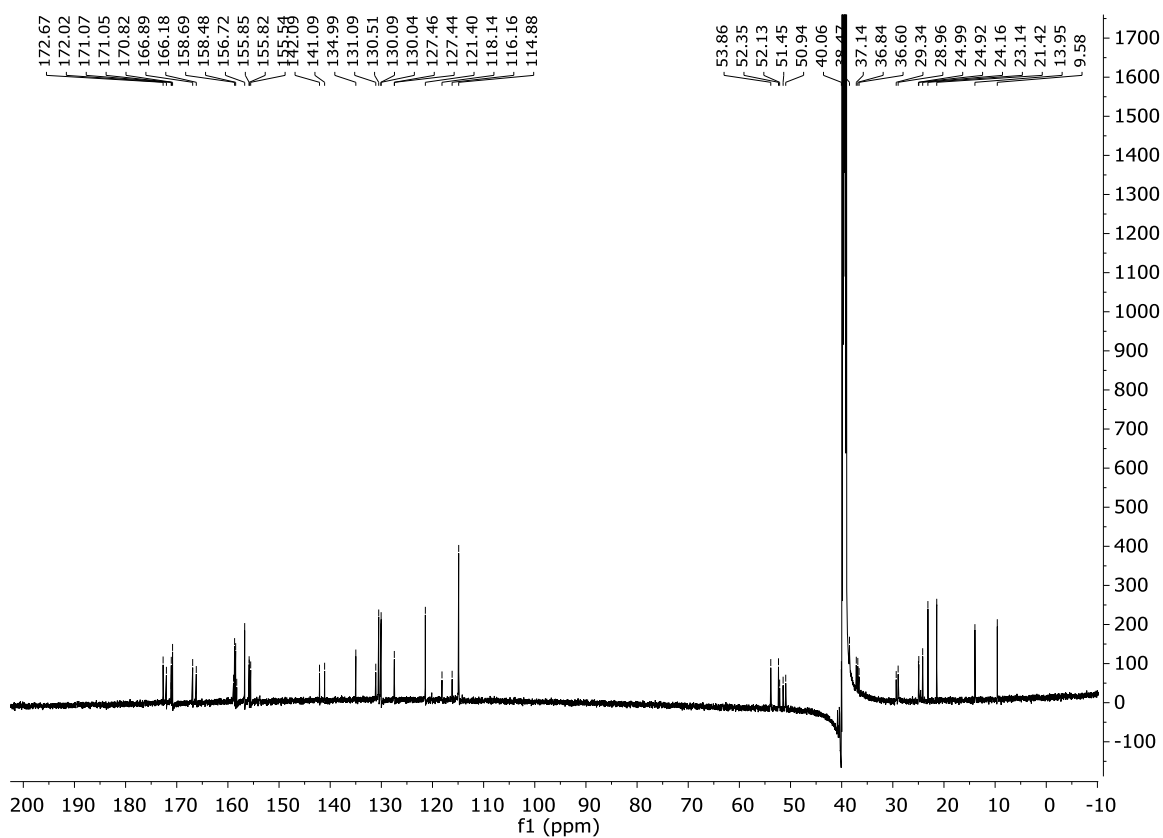
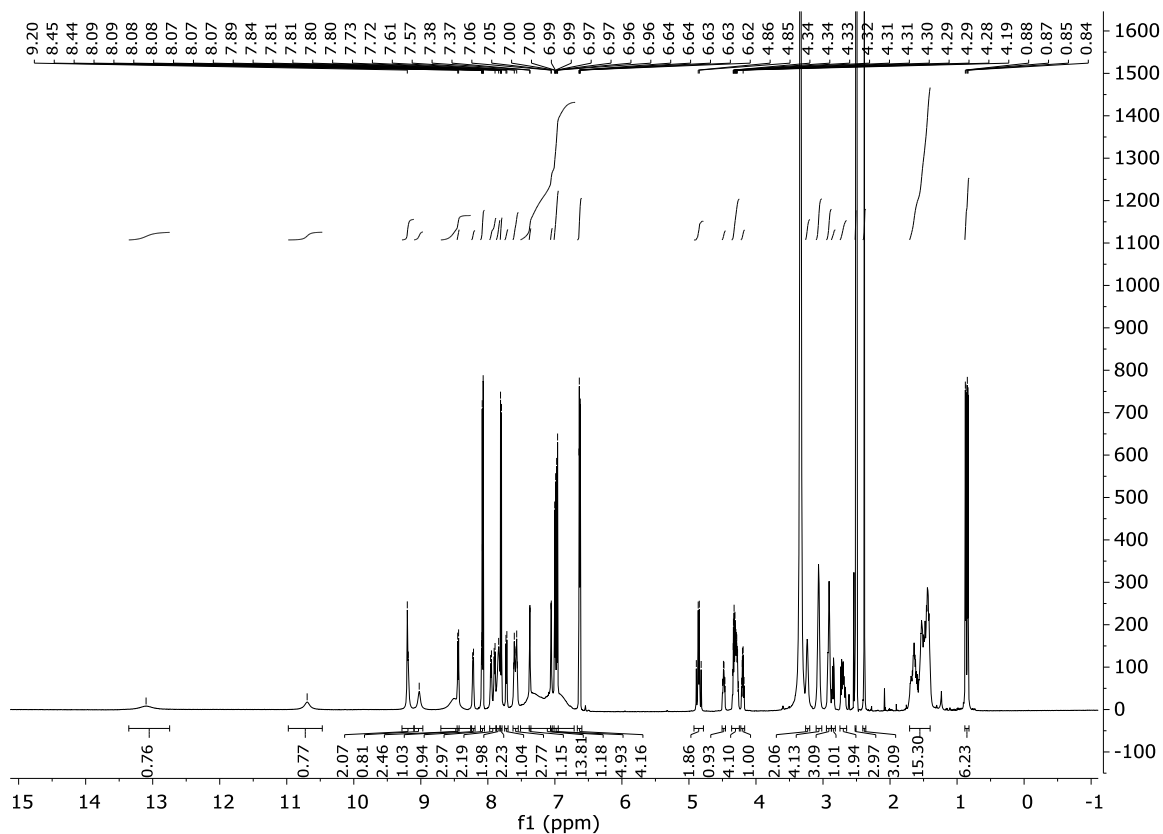
Compound 20



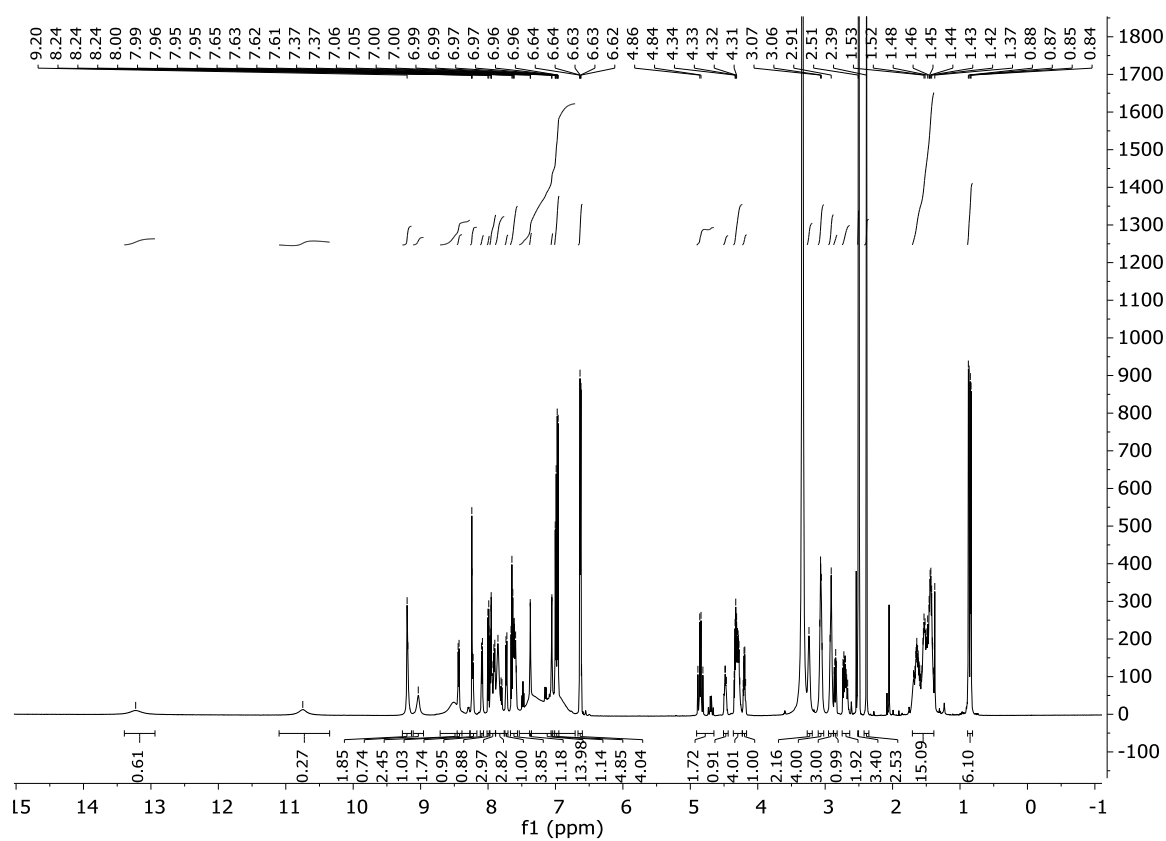
Compound 21



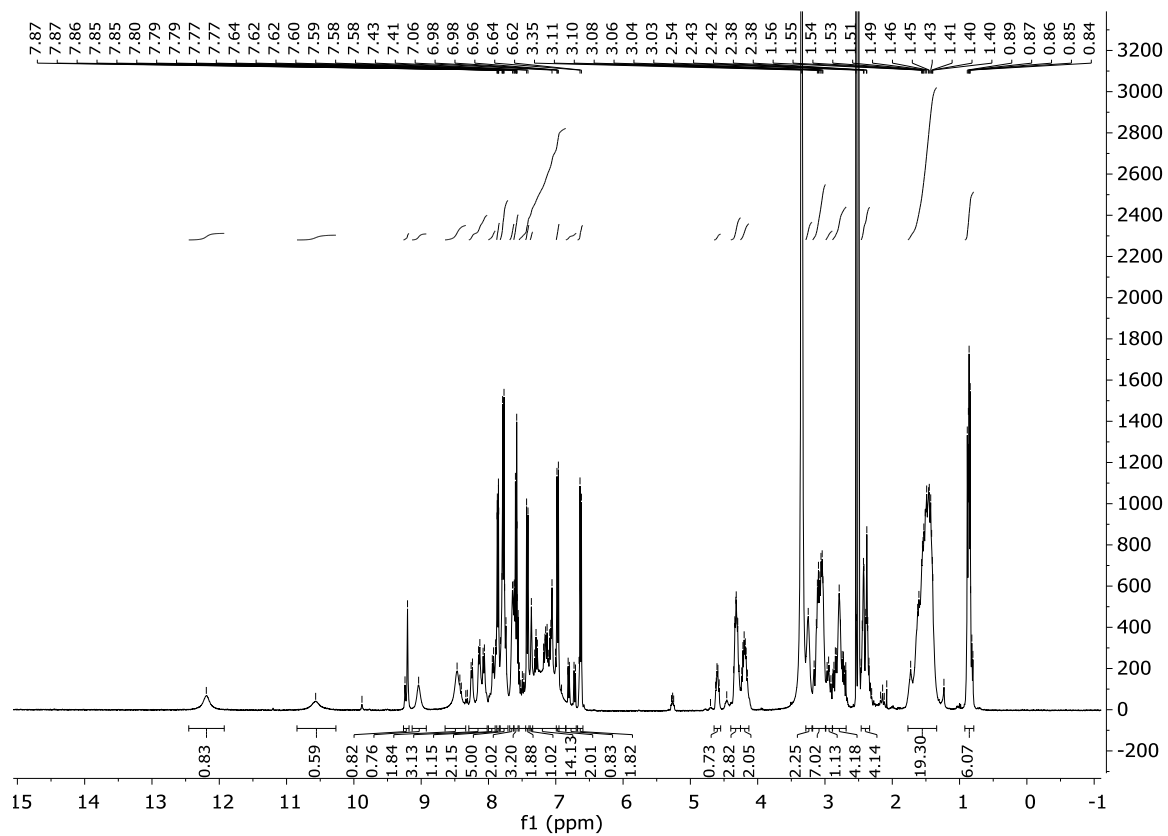
Compound 22



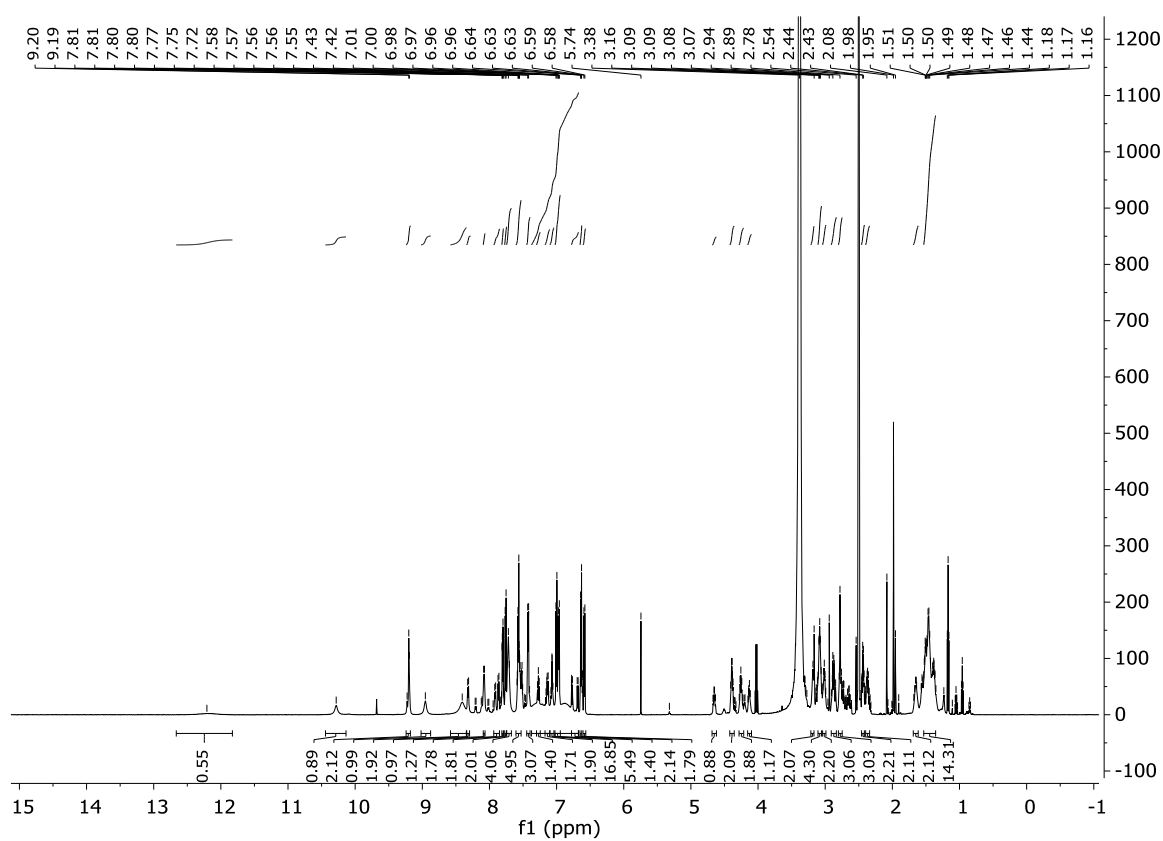
Compound 23



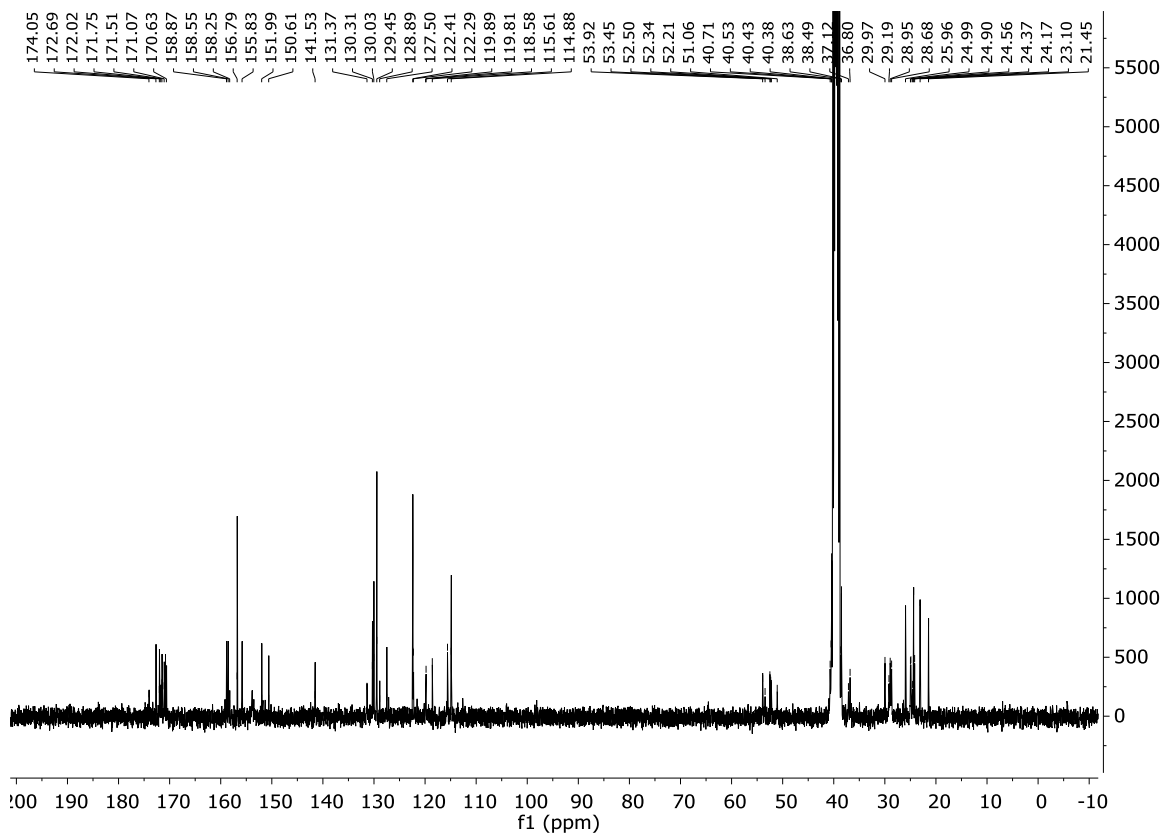
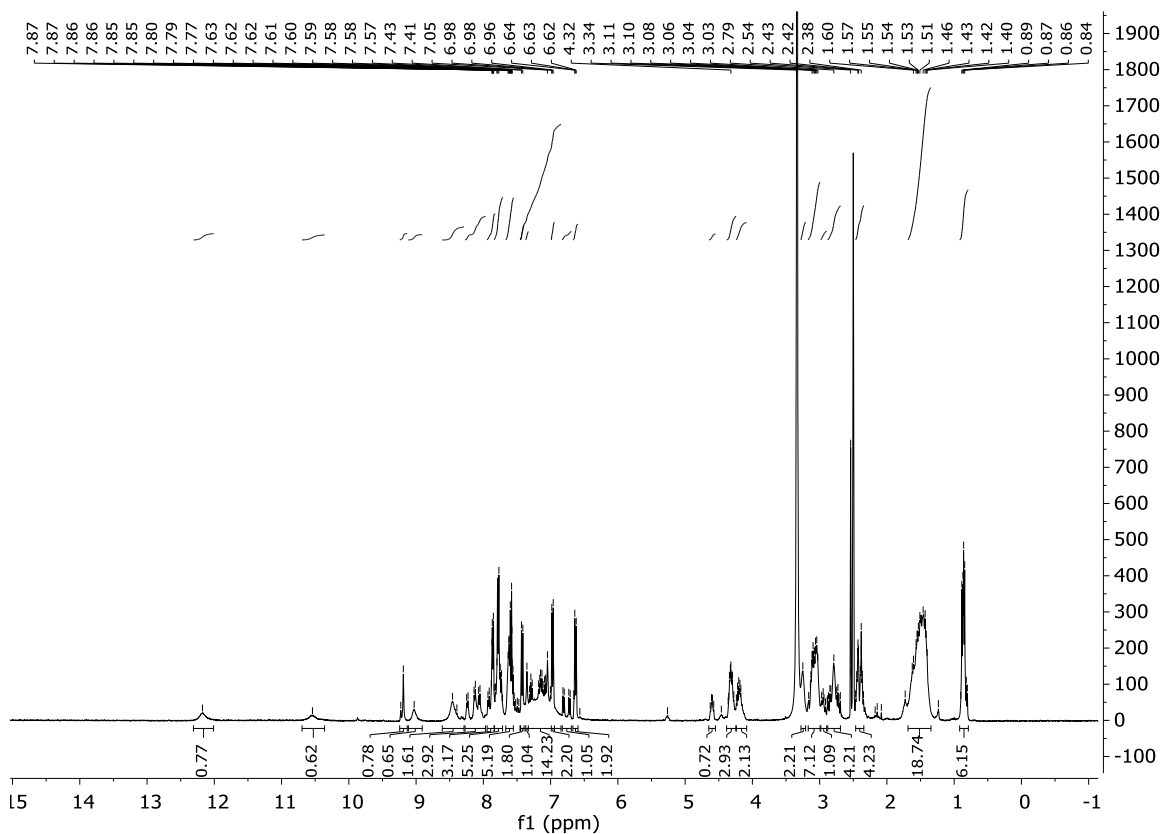
Compound 24



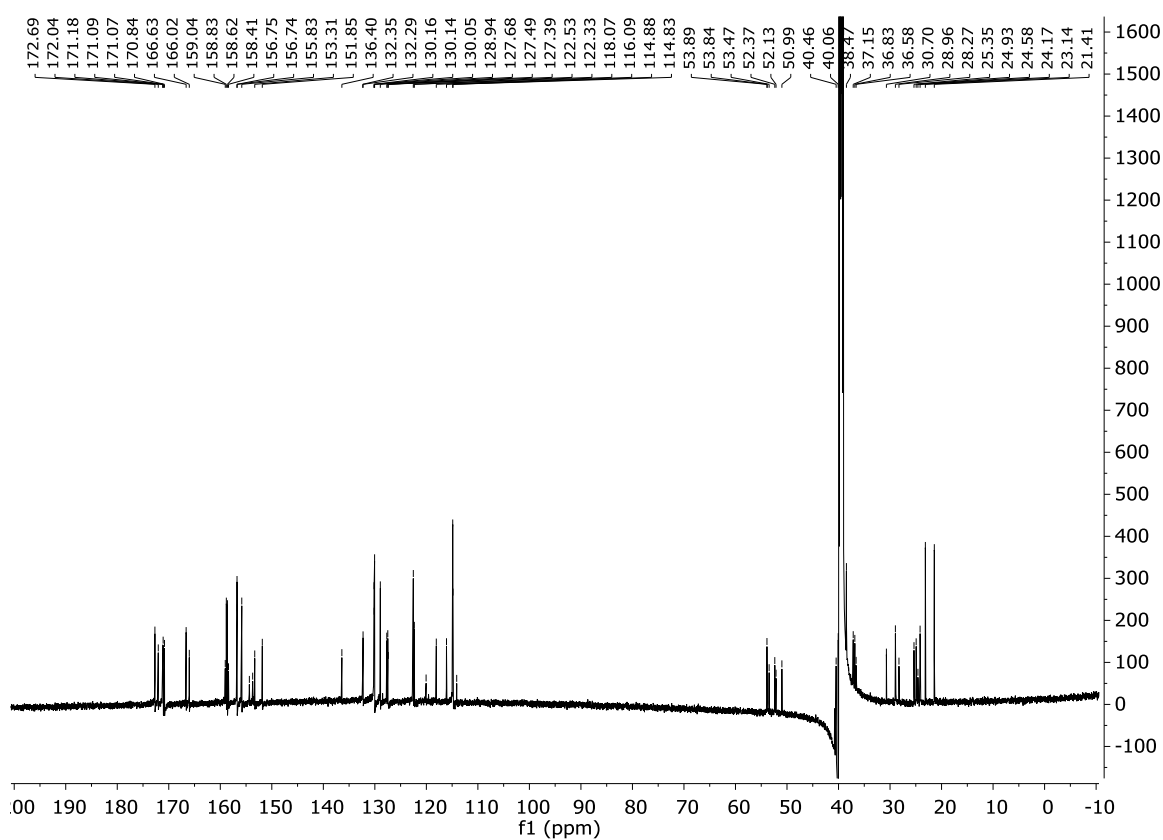
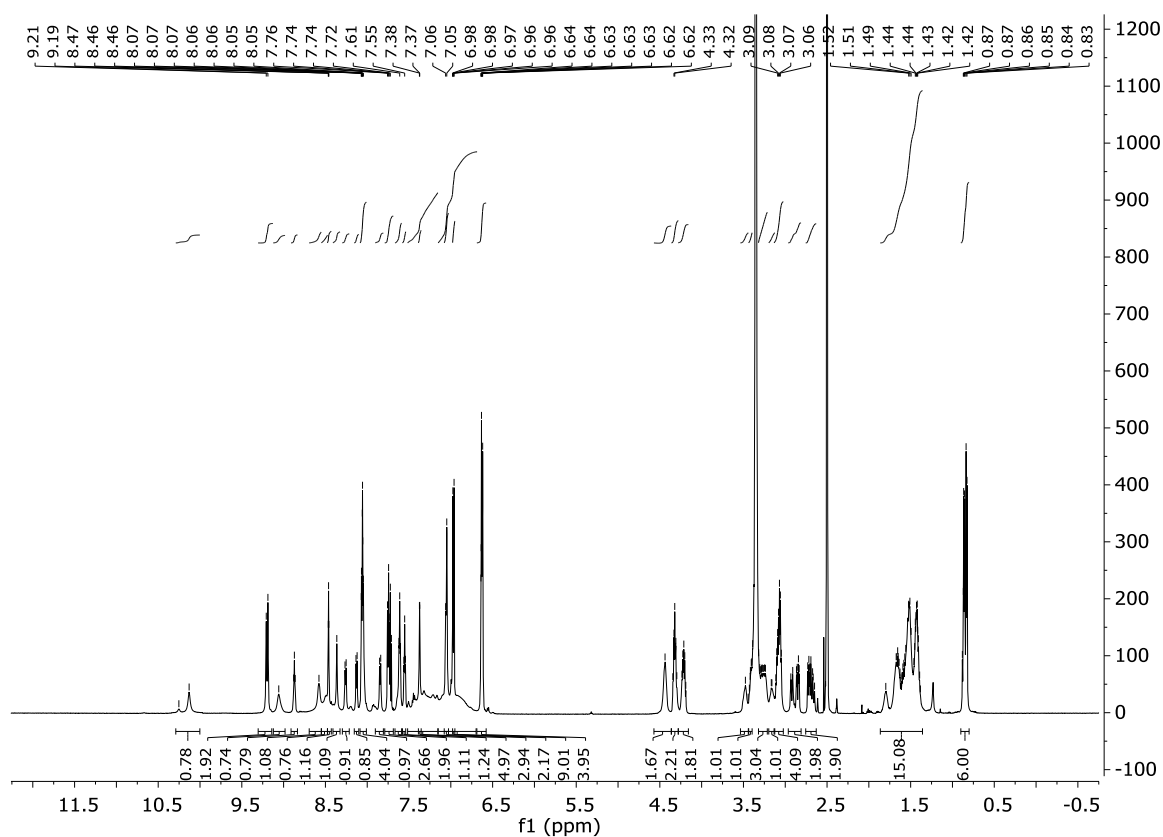
Compound 25



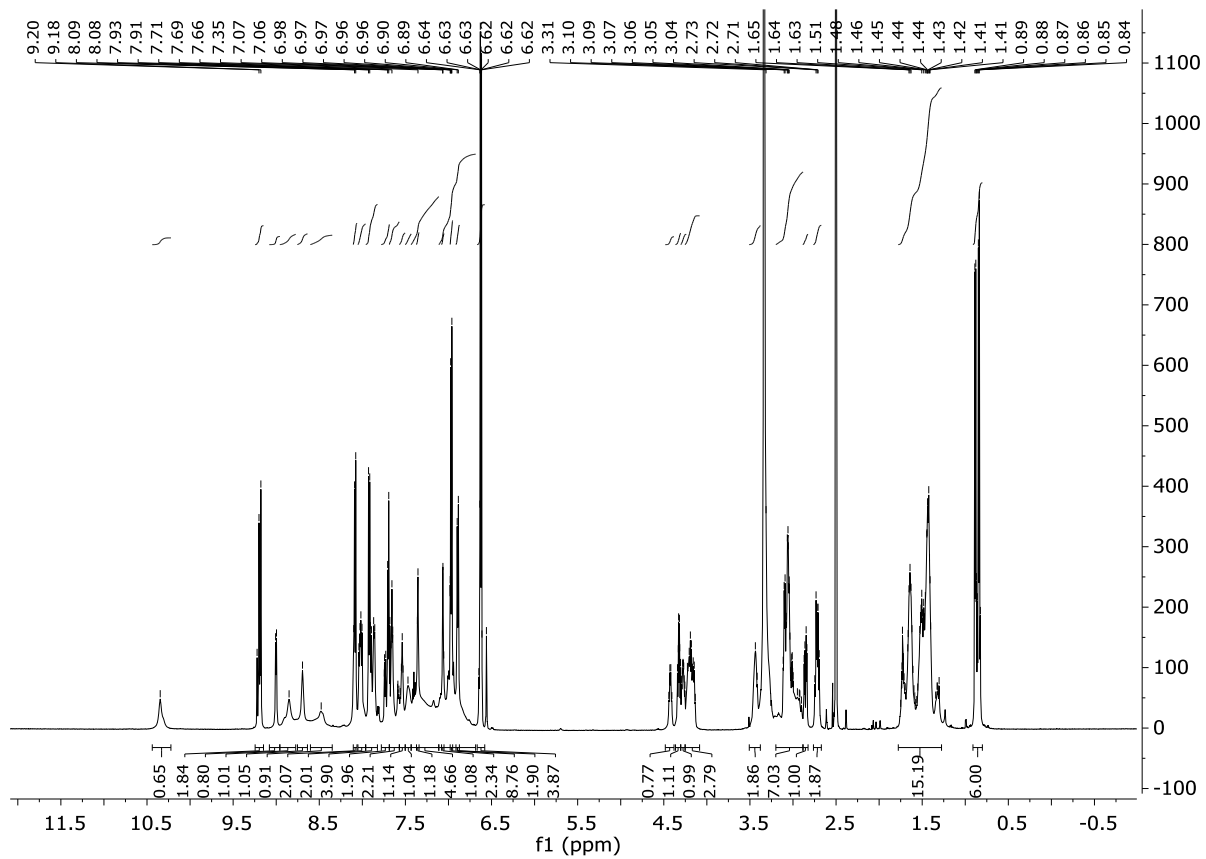
Compound 26



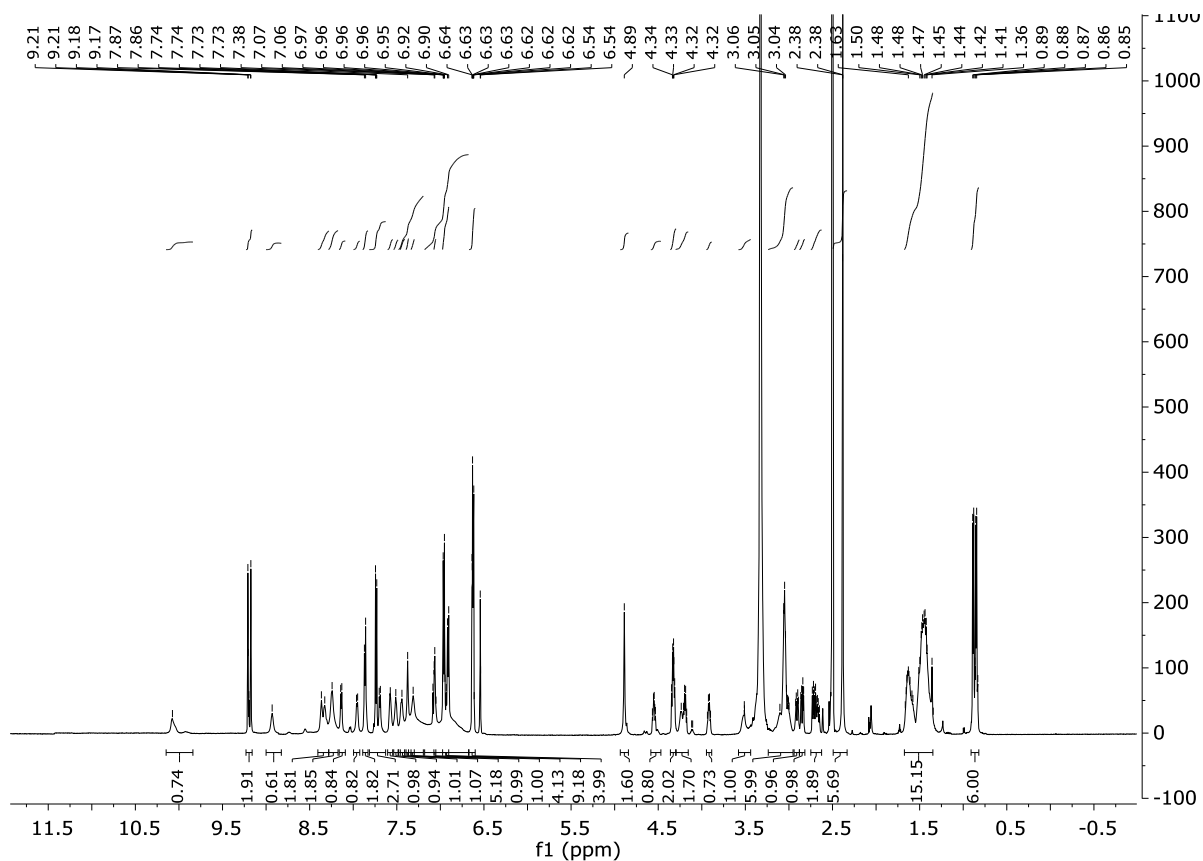
Compound 27



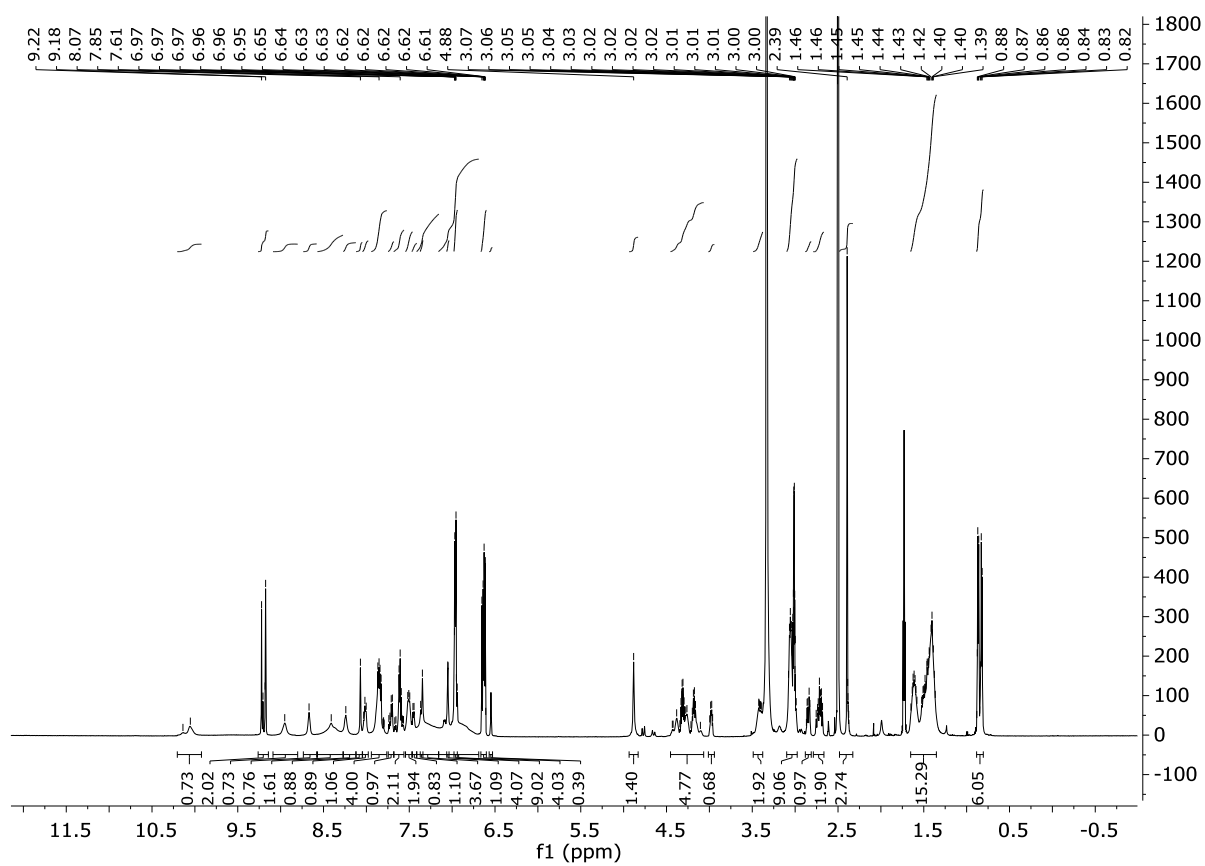
Compound 28



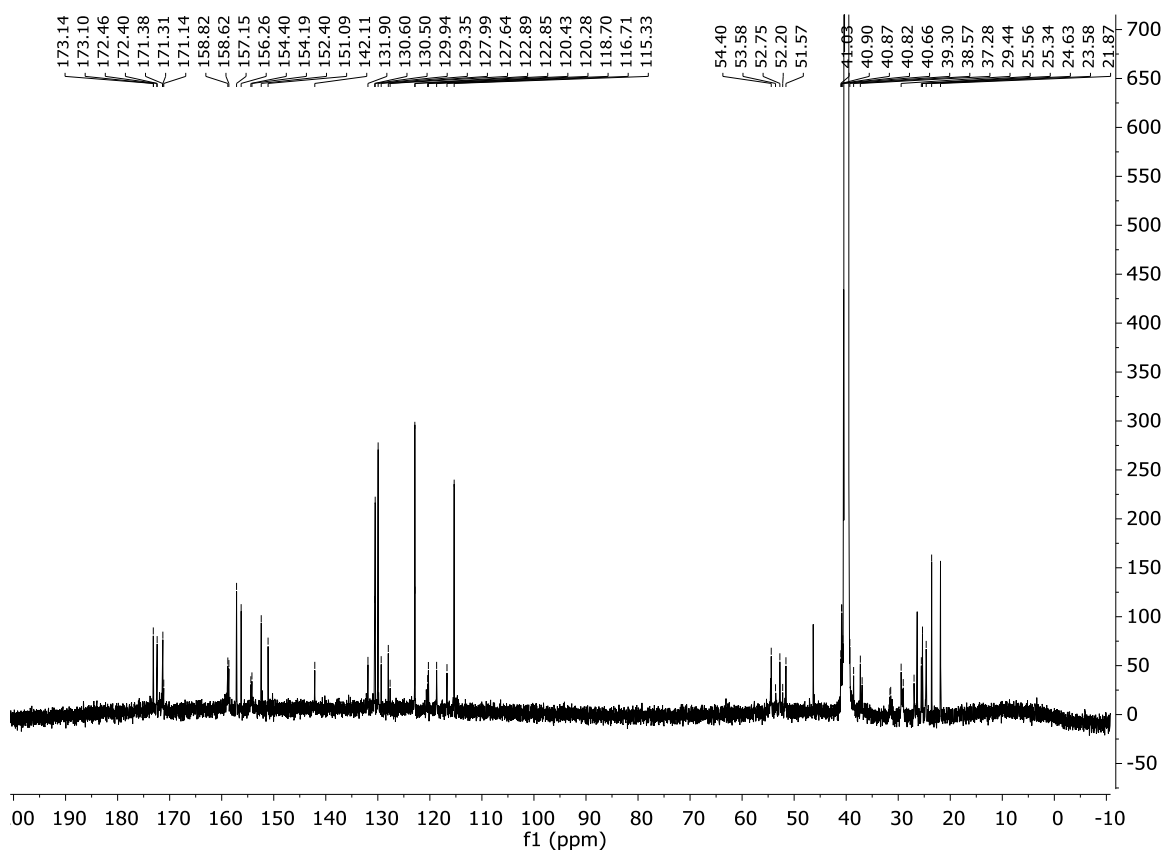
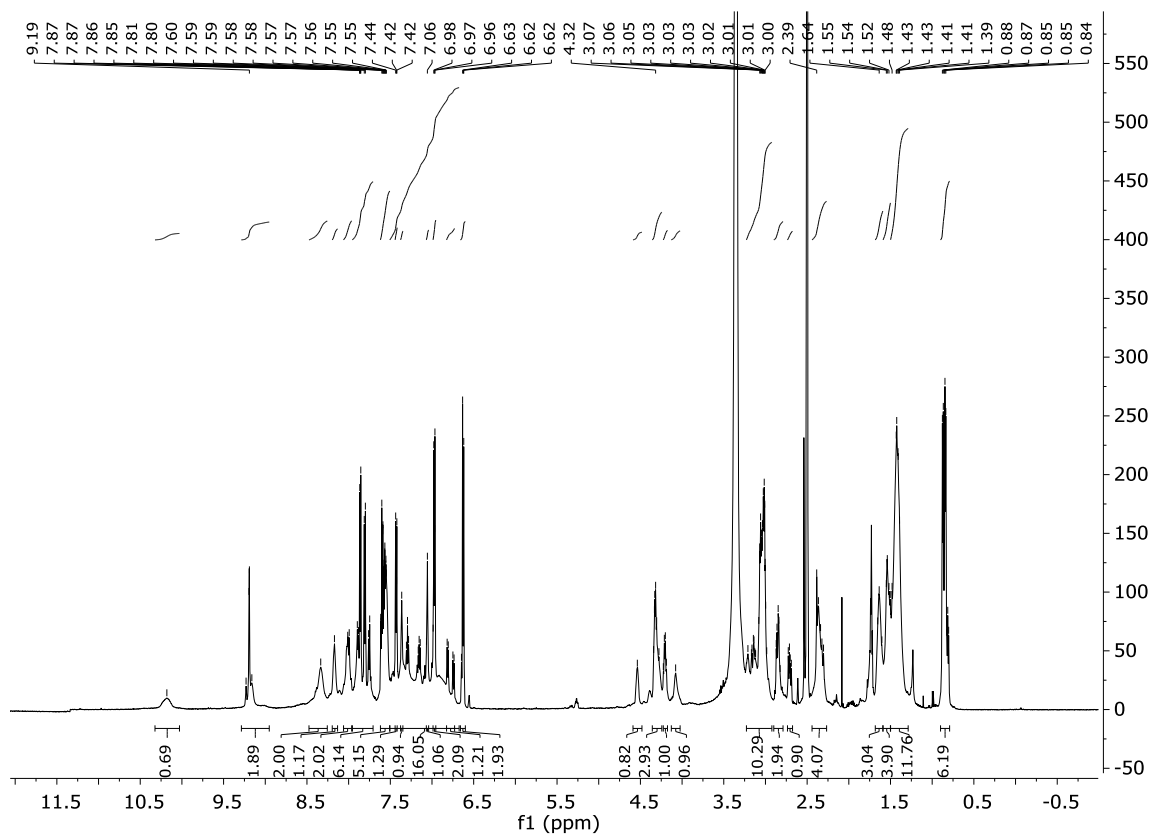
Compound 30



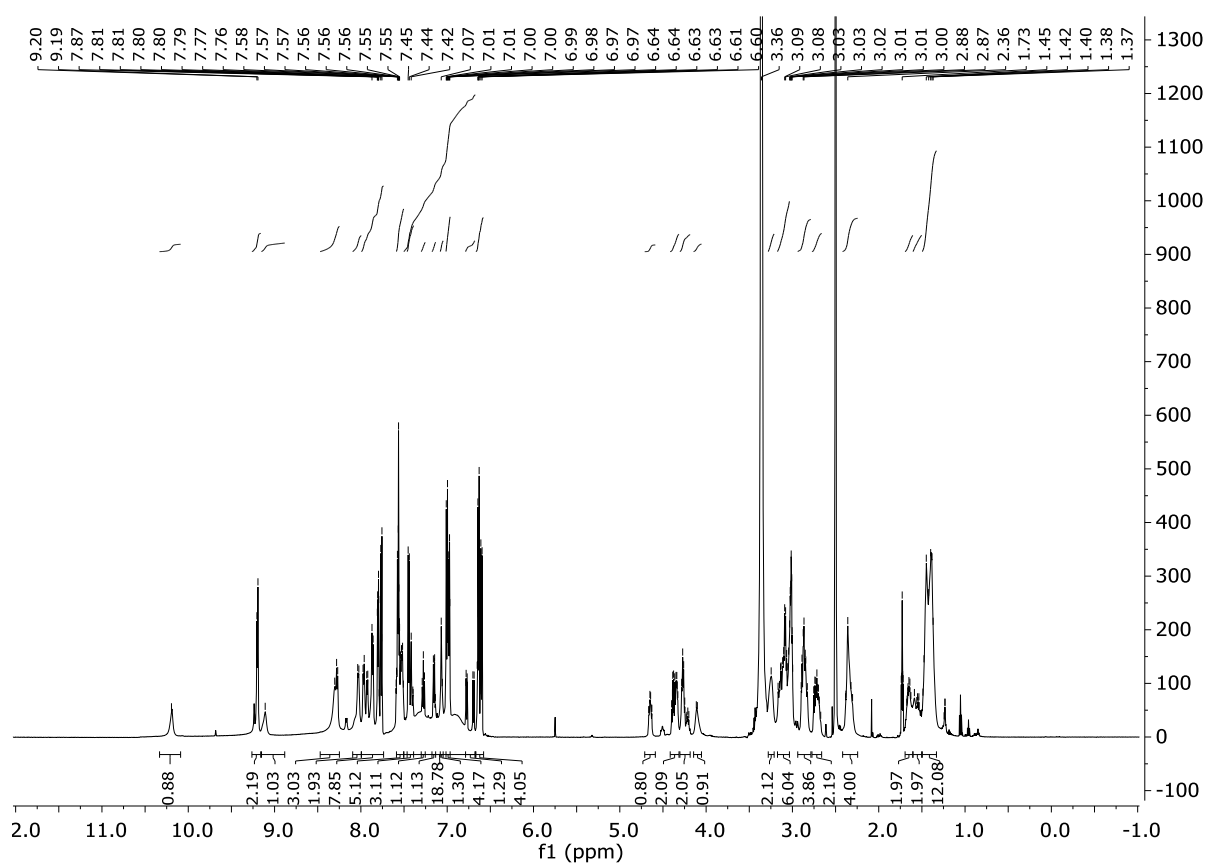
Compound 31



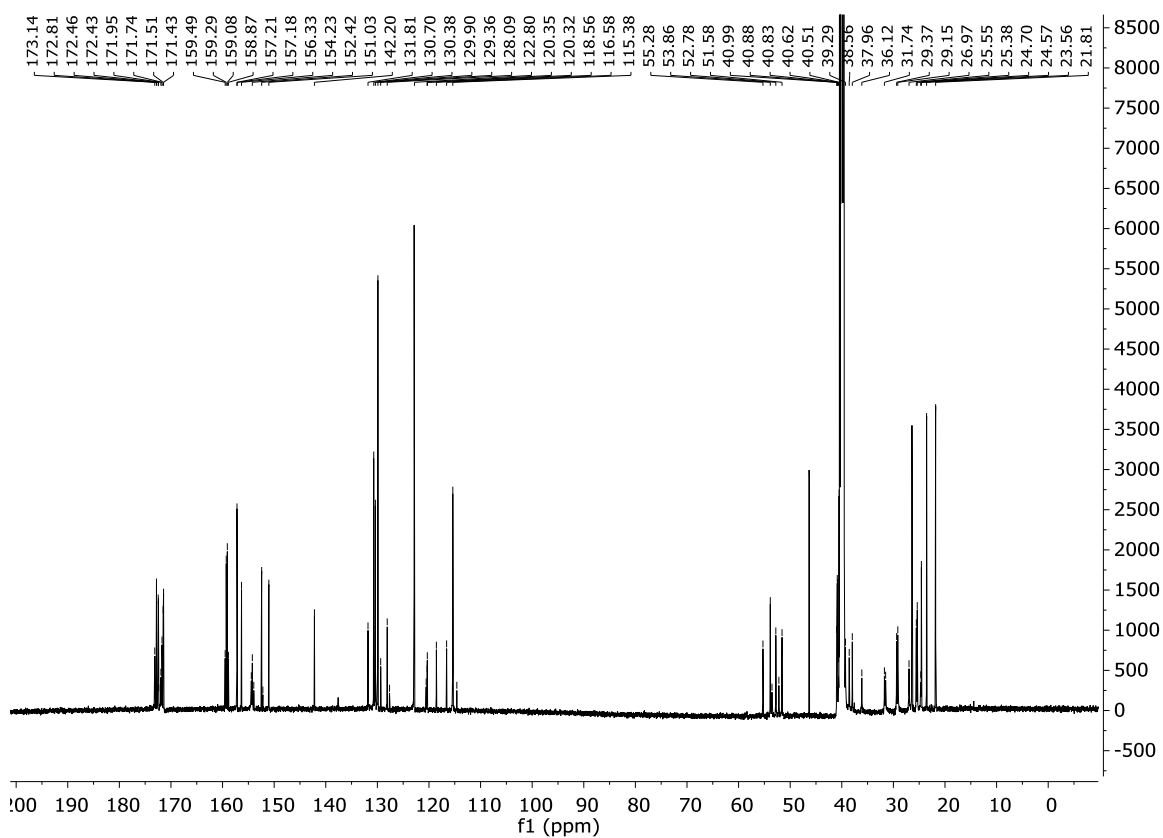
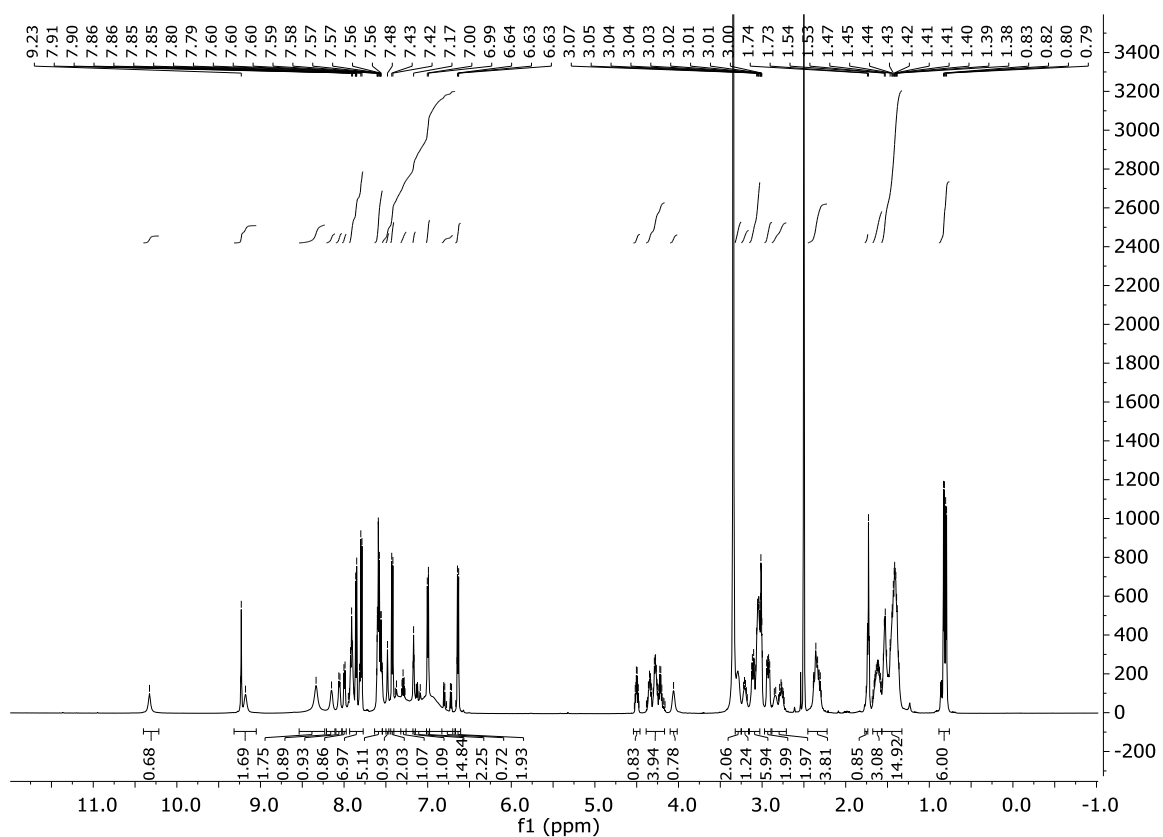
Compound 32



Compound 33



Compound 34



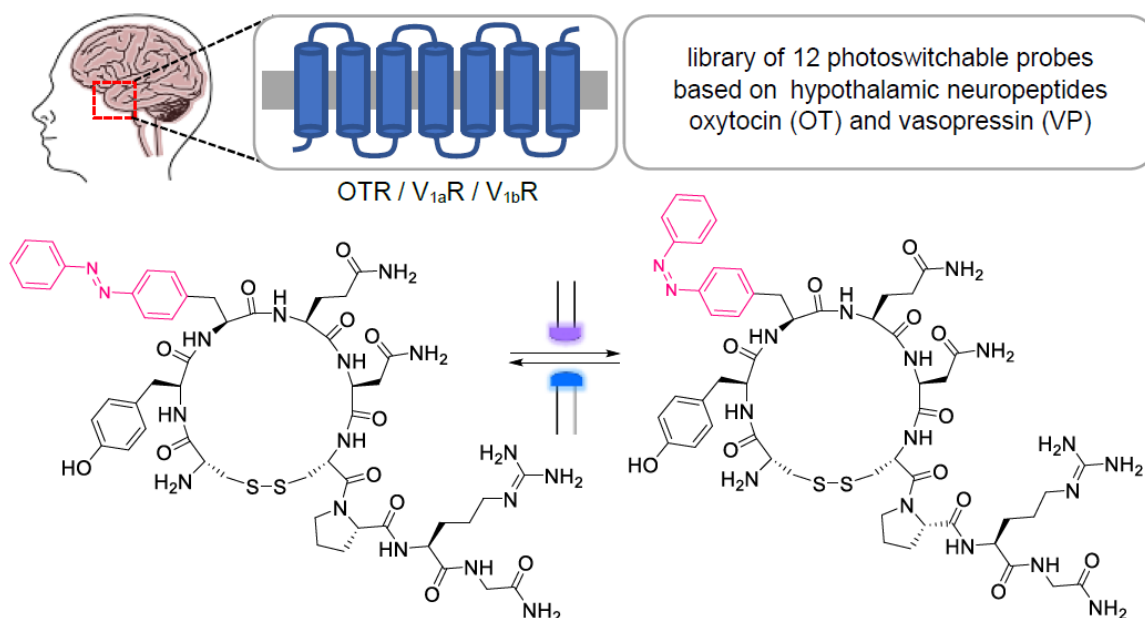
3.12 References

- [1] K. Sriram, P. A. Insel, *Mol. Pharmacol.* **2018**, *93*, 251-258.
- [2] L. A. Catapano, H. K. Manji, *Biochim. Biophys. Acta* **2007**, *1768*, 976-993.
- [3] F. Reimann, F. M. Gribble, *Diabetologia* **2016**, *59*, 229-233.
- [4] T. Schoneberg, A. Schulz, H. Biebermann, T. Hermsdorf, H. Rompler, K. Sangkuhl, *Pharmacol. Ther.* **2004**, *104*, 173-206.
- [5] R. M. Eglen, *Comb. Chem. High Throughput Screen.* **2005**, *8*, 311-318.
- [6] K. Lundstrom, *Future Med. Chem.* **2013**, *5*, 523-538.
- [7] N. A. Balenga, E. Martinez-Pinilla, J. Kargl, R. Schroder, M. Peinhaupt, W. Platzer, Z. Balint, M. Zamarbide, I. G. Dopeso-Reyes, A. Ricobaraza, J. M. Perez-Ortiz, E. Kostenis, M. Waldhoer, A. Heinemann, R. Franco, *Br. J. Pharmacol.* **2014**, *171*, 5387-5406.
- [8] S. Lieb, S. Michaelis, N. Plank, G. Bernhardt, A. Buschauer, J. Wegener, *Pharmacol. Res.* **2016**, *108*, 65-74.
- [9] C. W. Scott, M. F. Peters, *Drug Discov. Today* **2010**, *15*, 704-716.
- [10] M. Skiba, J. A. Stolwijk, J. Wegener, *Methods Cell Biol.* **2022**, *169*, 221-236.
- [11] J. A. Stolwijk, M. Skiba, C. Kade, G. Bernhardt, A. Buschauer, H. Hubner, P. Gmeiner, J. Wegener, *Integr Biol.* **2019**, *11*, 99-108.
- [12] J. Wegener, S. Zink, P. Rosen, H. Galla, *Pflugers Arch.* **1999**, *437*, 925-934.
- [13] S. Lieb, T. Littmann, N. Plank, J. Felixberger, M. Tanaka, T. Schafer, S. Krief, S. Elz, K. Friedland, G. Bernhardt, J. Wegener, T. Ozawa, A. Buschauer, *Pharmacol. Res.* **2016**, *114*, 13-26.
- [14] A. Duran-Corbera, M. Faria, Y. Ma, E. Prats, A. Dias, J. Catena, K. L. Martinez, D. Raldua, A. Llebaria, X. Rovira, *Angew. Chem. Int. Ed.* **2022**, *61*, e202203449.
- [15] D. Lachmann, C. Studte, B. Mannel, H. Hubner, P. Gmeiner, B. König, *Chem. Eur. J.* **2017**, *23*, 13423-13434.
- [16] J. Morstein, G. Romano, B. E. Hetzler, A. Plante, C. Haake, J. Levitz, D. Trauner, *Angew. Chem. Int. Ed.* **2022**, *61*, e202117094.
- [17] M. Ricart-Ortega, J. Font, A. Llebaria, *Mol. Cell. Endocrinol.* **2019**, *488*, 36-51.
- [18] S. Panarello, X. Rovira, A. Llebaria, X. Gómez-Santacana, in *Molecular Photoswitches*, **2022**, pp. 921-944.
- [19] A. Konieczny, M. Conrad, F. J. Ertl, J. Gleixner, A. O. Gattor, L. Gratz, M. F. Schmidt, E. Neu, A. H. C. Horn, D. Wifling, P. Gmeiner, T. Clark, H. Sticht, M. Keller, *J. Med. Chem.* **2021**, *64*, 16746-16769.
- [20] B. Priewisch, K. Rück-Braun, *J. Org. Chem.* **2005**, *70*, 2350-2352.
- [21] F. Paternostre, Marie-Therese; Cintrat, Jean-Christophe; Valery, Celine; Roux, Stephane; Rousseau, Bernard; Ijsselstijn, Maarten; Cherif-Cheikh, Roland; Artzner, *New Octapeptide Compounds, Their Preparation, Self-Assembly Properties and Use as Ligands of Somatostatin Receptor Subtypes 2 and/ or 5*, **2009**, WO2010037930.
- [22] M. Keller, K. K. Kuhn, J. Einsiedel, H. Hubner, S. Biselli, C. Mollereau, D. Wifling, J. Svobodova, G. Bernhardt, C. Cabrele, P. M. Vanderheyden, P. Gmeiner, A. Buschauer,

- J. Med. Chem.* **2016**, *59*, 1925-1945.
- [23] C. Höring, U. Seibel, K. Tropmann, L. Grätz, D. Mönnich, S. Pitzl, G. Bernhardt, S. Pockes, A. Strasser, *Int. J. Mol. Sci.* **2020**, *21*, 8440.
- [24] K. K. Kuhn, T. Ertl, S. Dukorn, M. Keller, G. Bernhardt, O. Reiser, A. Buschauer, *J. Med. Chem.* **2016**, *59*, 6045-6058.
- [25] S. Dukorn, T. Littmann, M. Keller, K. Kuhn, C. Cabrele, P. Baumeister, G. Bernhardt, A. Buschauer, *Bioconj. Chem.* **2017**, *28*, 1291–1304.
- [26] S. Rajagopal, S. Ahn, D. H. Rominger, W. Gowen-MacDonald, C. M. Lam, S. M. Dewire, J. D. Violin, R. J. Lefkowitz, *Mol. Pharmacol.* **2011**, *80*, 367-377.
- [27] T. P. Tenakin, *A pharmacology primer - Techniques for more effective and strategic drug discovery*, Academic Press, **2014**.
- [28] M. Grundmann, E. Kostenis, *Methods Mol. Biol.* **2015**, *1272*, 199-213.
- [29] L. M. Bohn, L. Zhou, J. H. Ho, *Methods Mol. Biol.* **2015**, *1335*, 177-189.
- [30] S. Arndt, J. Seebach, K. Psathaki, H. J. Galla, J. Wegener, *Biosens. Bioelectron.* **2004**, *19*, 583-594.
- [31] G. Hayes, T. J. Biden, L. A. Selbie, J. Shine, *Mol. Endocrinol.* **1992**, *6*, 920-926.
- [32] E. Tran, Y. Fang, *J. Recept. Signal Transduct. Res.* **2009**, *29*, 154-162.
- [33] M. Keller, S. Weiss, C. Hutzler, K. K. Kuhn, C. Mollereau, S. Dukorn, L. Schindler, G. Bernhardt, B. König, A. Buschauer, *J. Med. Chem.* **2015**, *58*, 8834–8849.
- [34] R. Ziemek, E. Schneider, A. Kraus, C. Cabrele, A. G. Beck-Sickinger, G. Bernhardt, A. Buschauer, *J. Recept. Signal Transduct. Res.* **2007**, *27*, 217–233.
- [35] C. Moser, G. Bernhardt, J. Michel, H. Schwarz, A. Buschauer, *Can. J. Physiol. Pharmacol.* **2000**, *78*, 134–142.
- [36] C. Yung-Chi, W. H. Prusoff, *Biochem. Pharmacol.* **1973**, *22*, 3099–3108.
- [37] A. Konieczny, D. Braun, D. Wifling, G. Bernhardt, M. Keller, *J. Med. Chem.* **2020**, *63*, 8198–8215.
- [38] Ł. Berlicki, M. Kaske, R. Gutiérrez-Abad, G. Bernhardt, O. Illa, R. M. Ortuño, C. Cabrele, A. Buschauer, O. Reiser, *J. Med. Chem.* **2013**, *56*, 8422–8431

CHAPTER 4

4 Photoswitchable Probes of Oxytocin and Vasopressin



This chapter is a submitted manuscript.

This chapter was done in collaboration with the group of Prof. M. Muttenthaler (Institut für Biologische Chemie, Universität Wien, Österreich).

U. Wirth performed the synthesis, (photo-)chemical characterization; and biological evaluation of all compounds under the supervision of K. Raabe.

U. Wirth, K. Raabe and Prof. Muttenthaler wrote the manuscript draft.

Prof. König and Prof. Muttenthaler supervised the project.

4.1 Introduction

Oxytocin (OT) and vasopressin (VP) are hypothalamic neuropeptides and responsible for a myriad of processes in the central as well as peripheral nervous system.^[1–4] Although OT is widely known as the ‘love hormone’ due to its important role in social bonding and maternal behavior, its functions are much more diverse, being the key molecule in regulating several other physiological functions such as uterine contractions and breast feeding.^[5–9] The less famous but not less important VP regulates water homeostasis^[1,10–12] and blood pressure,^[13–15] and is also involved in social behavior, that can be described as opposing or complementary to OT including aggression and fear.^[1,16,17] OT and VP are paralogues that consist of nine amino acids cyclized by a disulfide bridge between position 1 and 6 and an exocyclic three-residue C-terminal tail. The two nonapeptides differ in only two amino acids (Figure 1, highlighted in purple), VP containing Phe³ and Arg⁸ instead of Ile³ and Leu⁸ in OT.^[10,18] In mammals, they act *via* four receptors, OTR, V_{1a}R, V_{1b}R and V₂R, all belonging to the class A of G protein-coupled receptors (GPCRs).^[19,20] Due to the high sequence- and structural- similarity between the receptors, OT and VP are also able to activate VPRs and OTR, respectively and *in vivo* differences in signaling are mainly attributed to differences in receptor expression levels.^[21–23] Hence, OT and VP are unspecific and represent poor pharmacological tools and drug leads for systemic administration.^[24] Nonetheless, OT is clinically used to induce and progress labor and to prevent post-partum bleeding,^[25,26] whereas VP is used to medicate postoperative gastrointestinal bleeding or for the treatment of vasodilatory shock.^[27,28] Beyond that, OT and VP and their receptors are being investigated in their involvement in autism, schizophrenia and Prader-Willi syndrome presenting potential targets and treatment options to improve the social deficits related to such neurodevelopmental disorders.^[2,29–32]

A lot of effort has been put into the development of receptor-selective agonists and antagonists, with the goal of elucidating the potential of receptor subtype-specific therapeutic intervention.^[23,33] While this has advanced the field substantially over the last three decades, these probes do not provide sufficient spatiotemporal resolution as often required to dissect the neuronal circuits in the brain. This problem can be tackled by the application of photopharmacology.^[33–35] With light as an external and orthogonal stimulus, spatiotemporal control over the receptor ligands can be obtained, as demonstrated with several small-molecule ligands^[36–38] and, to a lesser extent, with peptide ligands^[39,40], e.g. for the photoregulation of the glucagon-like-peptide-1-receptor,^[41] the natriuretic peptide receptor A,^[42] or for the clathrin-mediated endocytosis.^[43]

To obtain light-responsive probes, a photochromic moiety must be incorporated in or attached to a ligand. Azobenzenes, the most widely used photoswitches, allow rapid and reversible switching between their *trans*- and *cis*-isomer resulting in significant changes in molecular geometry.^[34,44,45] Ideally, the activity is toggled between agonism and antagonism or between an inactive state and an active state (either agonism or antagonism).^[34,46] The principle of photopharmacology has been applied to several GPCRs, including the dopamine receptors,^[47,48] the μ -opioid receptor,^[49,50] the histamine H₃ receptor^[51] and β_2 -receptor.^[52] Herein, we report the synthesis, photochemical characterization and biological evaluation of the first photoswitchable OT- and VP-derivatives. Different design strategies were applied and led to a series of photoprobes based on the structures of OT and VP. In a pharmacological evaluation these compounds were tested regarding if receptor activation occurs and, more importantly, if photoswitching the probe results in an altered activation profile leading to the desired light-controllable tool.

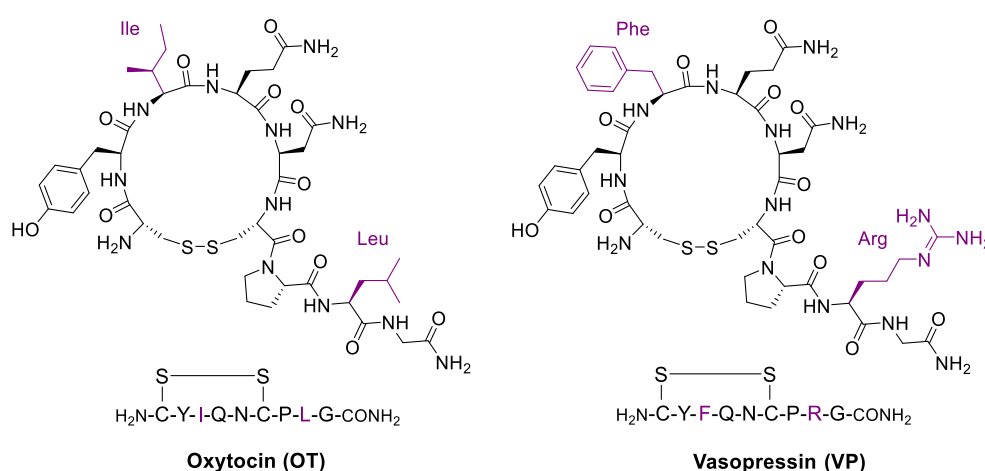
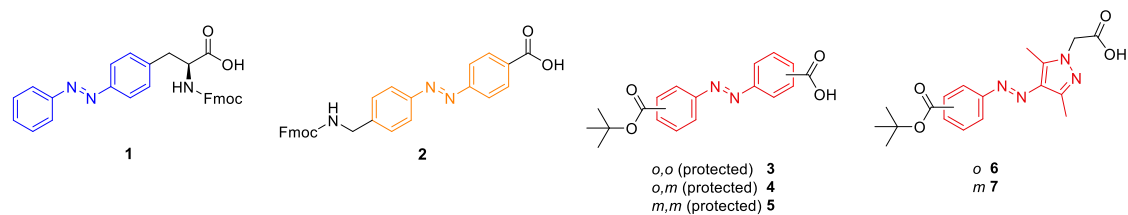


Figure 1. Chemical Structures of OT and VP. Highlighted in purple are the two amino acids that differ in the sequence.

4.2 Design

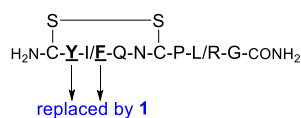
OT and VP are highly sensitive to structural modifications often resulting in substantial drops in affinity and activity upon even subtle changes, rendering it a challenging molecular class to work with.^[24] We therefore explored different modification strategies as well as several photoswitch designs ranging from conservative to more drastic modifications, namely the replacement of an aromatic amino acid by a photoswitchable amino acid, modifications in the exocyclic tail and the most drastic, the replacement of the disulfide bond by a photoswitchable moiety (Figure 2). In the first approach, we replaced the aromatic amino acid at position 2 in OT and position 3 in VP with the photoswitch **1**, resulting in peptides **8** and **12**, respectively. Photoswitch **1** contains the photoresponsive moiety in the side chain of the amino acid, which should not disrupt the core structures of OT and VP too much. In the second approach, we modified the C-terminal tail of OT and VP: Substitution of Pro⁷ with photoswitch **1** resulted in peptide **9** with a photoswitchable side chain. Furthermore, photoswitch **2** was incorporated into the peptide backbone *via* a linear connection of both sides of the azobenzene core structure replacing Pro⁷ to obtain a more pronounced geometric change at the C-terminal tail, resulting in peptides **11** and **14**. To compensate for the larger size of the photoswitch compared to Pro⁷, we additionally removed residue 8 in the probe design, leading to peptides **10** and **13**. In the third approach, we targeted the disulfide bond and replaced it with a photoswitch. For this strategy, we only focused on VP, as even small changes in ring size in OT result in a loss of affinity and activity at OTR.^[53,54] VP and VPRs are more forgiving to ring size or disulfide bond modifications, as demonstrated by the discovery of linear antagonists for the VPRs.^[55-57] We used azobenzenes **3-5** and arylazopyrazoles **6** and **7** with different substitution patterns to create a small library of 'disulfide-mimetics' and ring sizes for VP. Arylazopyrazoles often have improved photophysical properties like higher photostationary states (PSS) or longer thermal half-lives, compared to azobenzenes, which make them an interesting structure for our purpose.^[58]

A: Photoswitches

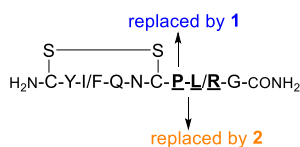


B: Modification strategies

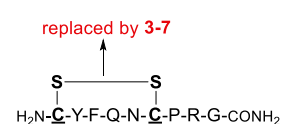
replacement of aromatic amino acid



modifications at position 7 (and 8)



SS-mimetics



C: Photoprobes

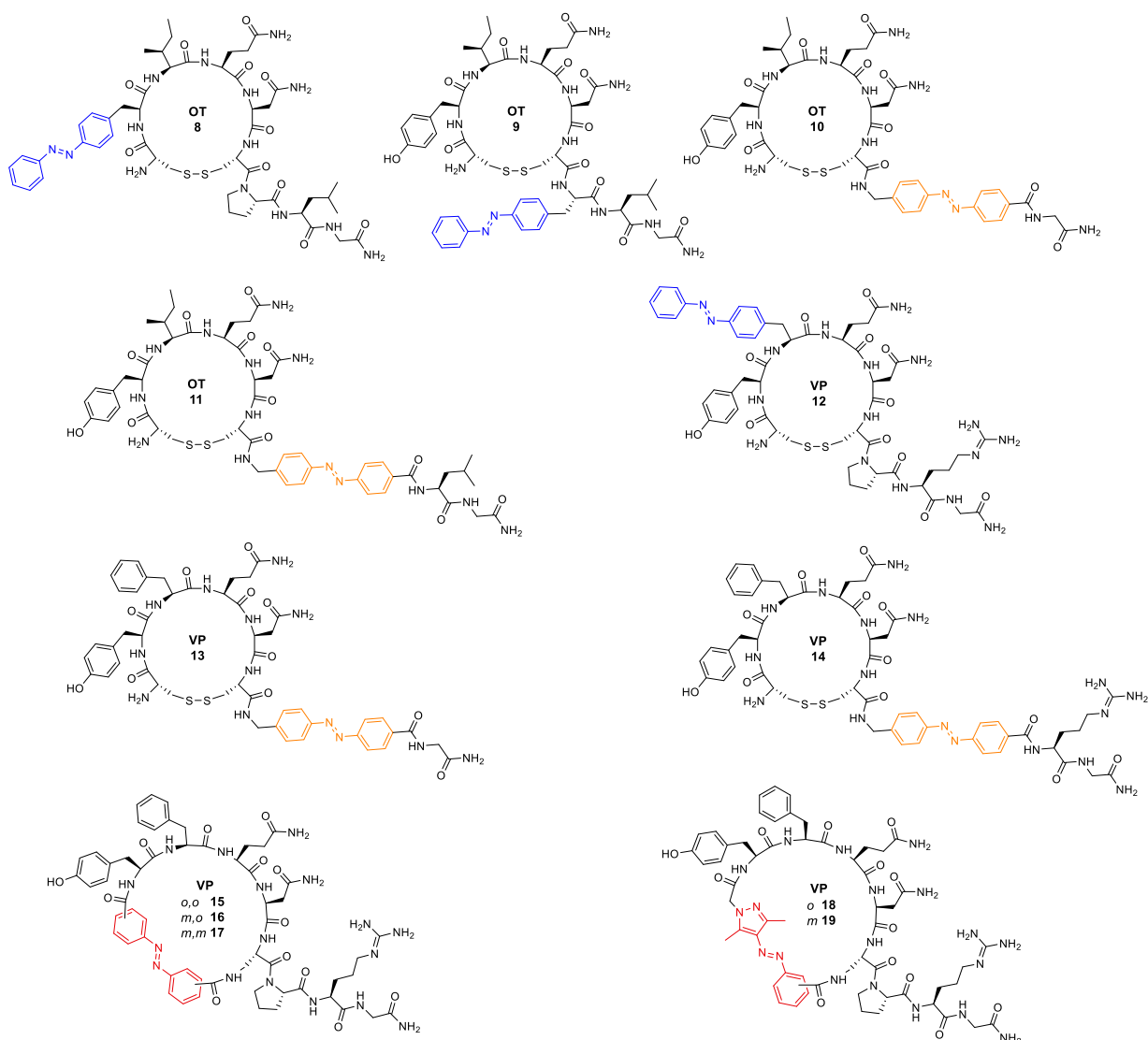
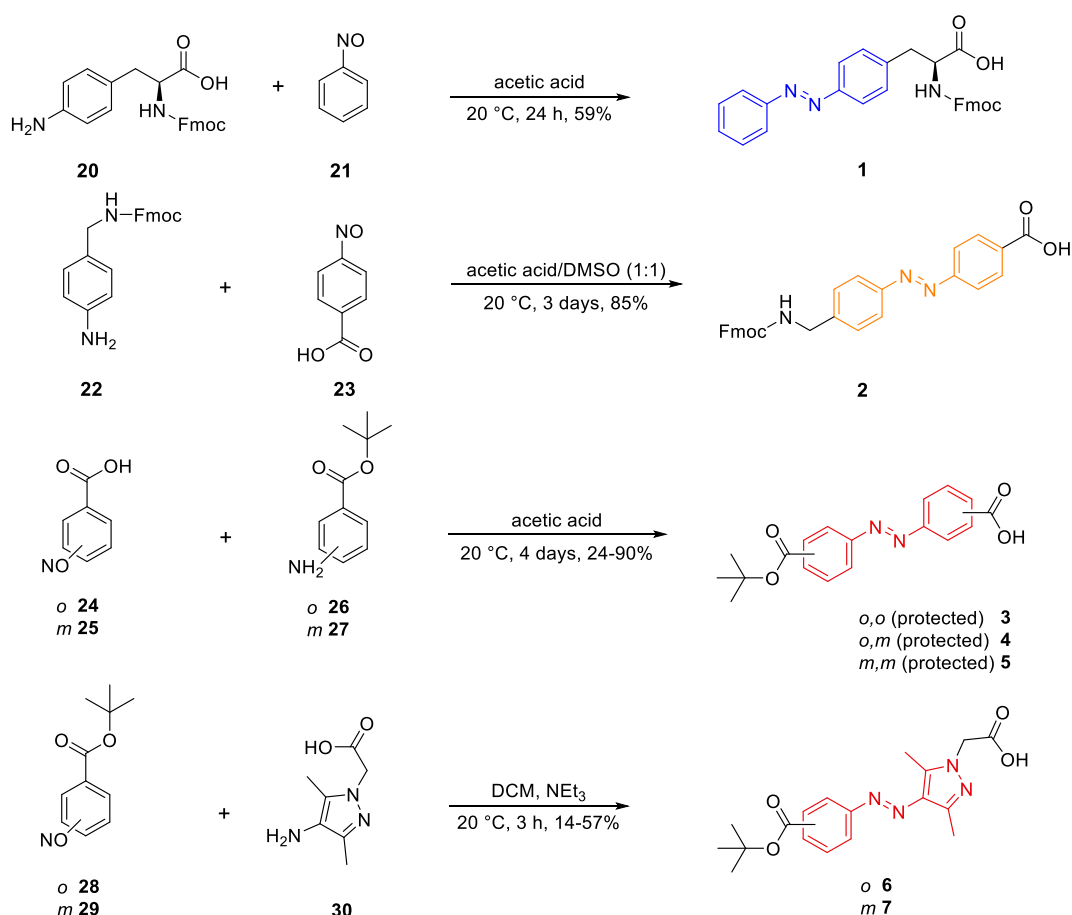


Figure 2. Overview of photoswitches and OT/VP photoprobe design strategies. **(A)** Selected photochromic moieties for the incorporation into the peptides. **(B)** Different approaches for the modifications in OT and VP. **(C)** Synthesized photoswitchable OT (8-11) and VP (12-19) derivatives.

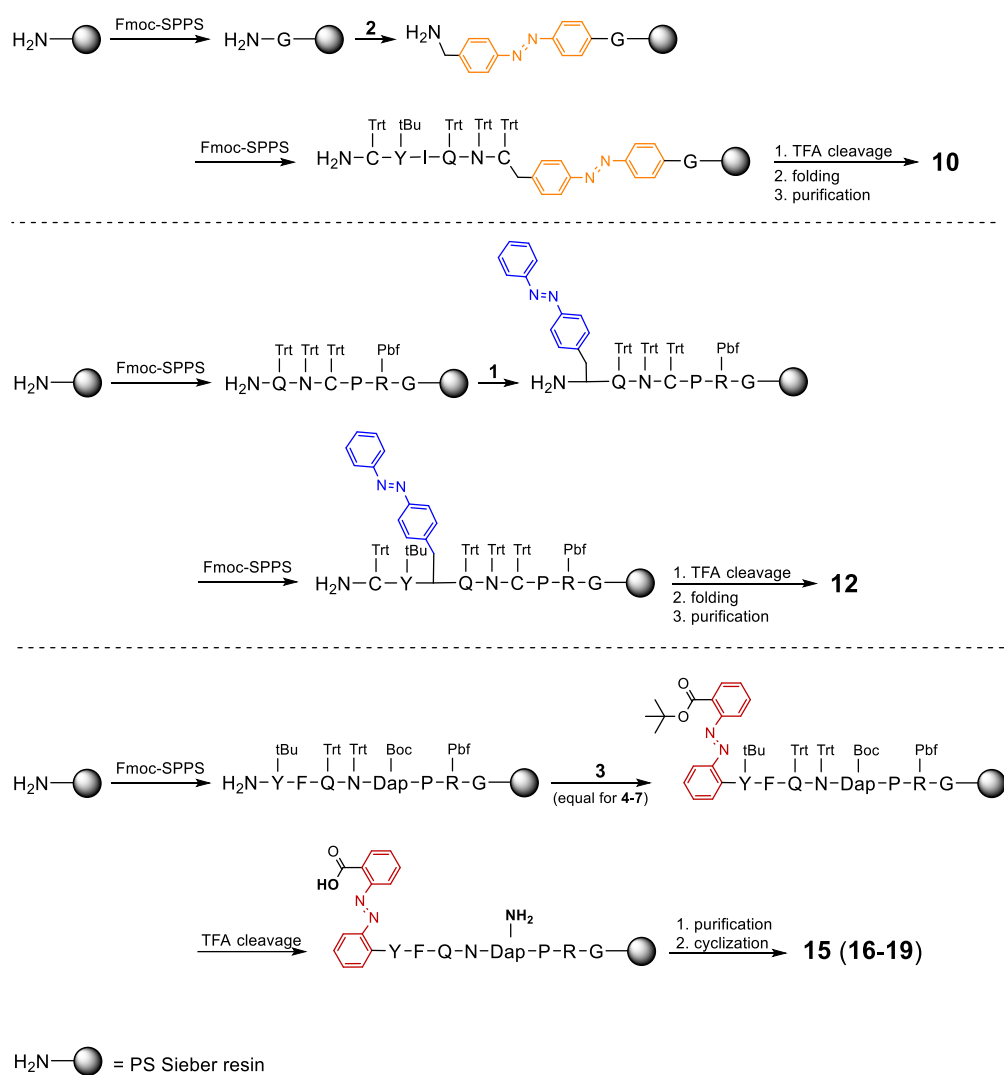
4.3 Synthesis

Photoswitches **1** and **2** were synthesized using a Mills reaction (Scheme 1). Starting from amino-phenylalanine **20** and nitrosobenzene **21** the photoswitchable derivative of Fmoc-protected phenylalanine **1** was synthesized to replace either Tyr² or Pro⁷ in OT¹ or Phe³ in VP.^[59] Photoswitch **2** to replace Pro⁷ and to mimic the backbone was also synthesized *via* a Mills reaction from **22** and **23**.^[60] Photoswitches **3-7** containing a free and a protected carboxylic acid moiety were synthesized to replace the disulfide-bond. The required nitroso compounds **24**, **25**, **28** and **29** were produced from the corresponding amines in an oxidation reaction with oxone.^[61] The Mills reaction that afforded the azobenzenes **3-5** was done in acetic acid over 4 days. For the preparation of the arylazopyrazoles **6** and **7**, the Mills reaction was performed under basic conditions with triethylamine in dichloromethane (DCM).



Scheme 1. Synthetic schemes to produce photoswitches 1-7.

The peptide precursors were assembled *via* manual Fmoc-solid phase peptide synthesis (Fmoc-SPPS) using a Sieber amide resin (selected routes, Scheme 2) and HBTU/HOBt/DIPEA as coupling reagents for the natural amino acids as well as for **1** and **2** and DMF/NMP (8:2 v/v) as the solvent. For photoswitches **5-7**, PyBOP/HOBt/DIPEA was used. Photoswitches **3** and **4** with *ortho*-substitution could not be coupled to the peptide with PyBOP due to an immediate decomposition once the active ester was formed; therefore, *N,N'*-diisopropylcarbodiimide (DIC) was used instead since it does not form an active ester. All natural amino acids were double coupled with 5-fold excess for 45 min at 35 °C. Single coupling using 3-fold excess for overnight at 35 °C was applied for **1-7**. After the last coupling step, all peptides were cleaved from the resin and globally deprotected using TFA/DCM/triisopropylsilane/H₂O (50/46/2/2, v/v) at 20 °C for 4-5 h followed by the addition of water and lyophilization. Subsequently, the precursor peptides of **8-14** containing cysteines were folded using DMSO as the oxidizing agent, followed by lyophilization and purification by preparative HPLC. The linear precursors of peptides **15-19** not containing cysteines were first purified by preparative HPLC, before cyclization in solution using PyBOP/HOBt/DIPEA as coupling reagents at a peptide concentration of 5 mM in DMF/NMP (8:2 v/v). Purification of the cyclized peptides was performed using preparative C₁₈-RP-HPLC. The overall yields of **8-14** containing the disulfide bridge ranged between 2–5% and the yields of the linear precursors of peptides **15-17** containing an azobenzene 8–17%. Precursors to peptides **18** and **19** with an arylazopyrazole afforded the best yields with 32% and 68%. The cyclization yields of **15-19** ranged between 23–60%. The poor yields can be explained by partial reduction of the azo bond by for example triisopropylsilane (TIPS) that is used as a scavenger but can also act as a mild reducing agent. Removal of TIPS, however, was not possible as we otherwise detected the trityl protecting groups by mass spectrometry. The better yields for the arylazopyrazoles are due to the electron rich pyrazole moiety preventing the azo bond from reduction.^[62]



Scheme 2. Synthetic strategies to generate OT/VP photoprobes. Reagents and conditions: SPPS: amino acid coupling: Fmoc-amino acid/HBTU/HOBt/DIPEA (5/5/4.9/10 eq.), DMF/NMP (8:2), 35 °C, 2 × 45 min (double coupling), Fmoc deprotection: 20% piperidine in DMF/NMP (8:2), 20 °C, 2 × 10 min; photoswitch **1** or **2**/HBTU/HOBt/DIPEA (3/3/2.95/6 eq.), DMF/NMP (8:2), 35 °C, 24 h (single coupling), Fmoc deprotection: 20% piperidine in DMF/NMP (8:2), 20 °C, 2 × 10 min; cleavage from resin and side chain deprotection: TFA/DCM/TIPS/H₂O (50/46/2/2, v/v), 20 °C, 4-5 h; folding: MeCN/phosphate buffer (pH = 7.4) (7/3) + 10% DMSO, 20 °C, O/N; photoswitches **3** or **4**/DIC (3/3 eq.), DMF/NMP (8:2), 35 °C, 24 h (single coupling), photoswitches **5-7**/PyBOP/HOBt/DIPEA (3/3/3/6 eq.), DMF/NMP (8:2), 35 °C, 24 h (single coupling); purification on preparative HPLC; cyclization: PyBOP/HOBt/DIPEA (5/5/10 eq.), DMF/NMP (8:2), 20 °C, 24 h. Dap = diaminopropionic acid. Protecting groups: Trt = trityl, tBu = tert-butyl, Pbf = 2,2,4,6,7-pentamethylidihydrobenzofuran-5-sulfonyl, Boc = *tert*-butyloxycarbonyl. (For routes towards peptides **8**, **9**, **11**, **13** and **14**, see supporting information Scheme S1).

4.4 Photophysical Characterization

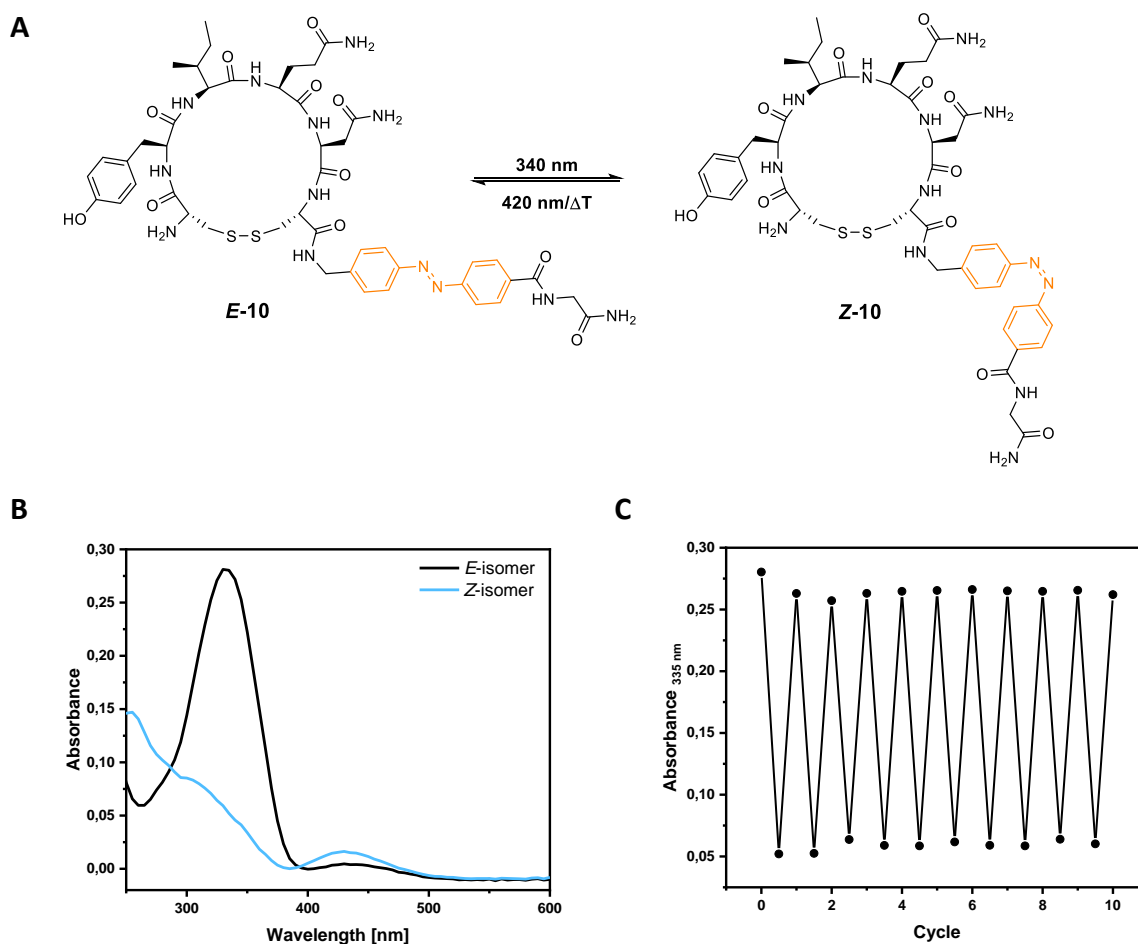


Figure 3. Representative photocharacterization of photoprobe **10**. **(A)** Light-induced *E/Z*-photoisomerization. **(B)** UV/Vis spectra of *E/Z*-isomers. **(C)** Cycle performance. Results are of photoprobe **10** (20 μ M) in HEPES buffer (25 mM HEPES, 2.5 mM CaCl_2 , 1 mM MgCl_2 , pH = 7.4) + 0.1% DMSO. Photoprobes **8**, **9** and **11-19** displayed similar photophysical properties (SI Figures S13-S24).

All photoprobes were investigated regarding their photophysical properties in aqueous buffer to imitate the conditions of the biological functional assays. The UV/Vis spectra displayed the typical absorptions of the *trans*-isomer (Figure 3, black curve) and *cis*-isomer (blue curve). All compounds could be switched to the *cis*-isomer by irradiation with 340 nm. Compounds **8-17** containing an azobenzene were switched back to the *trans*-isomer by irradiation at 420 nm. The arylazopyrazole-containing compounds **18** and **19** could be reverted to the *trans* isomer at 528 nm. Switching was repeated over ten cycles demonstrating that the compounds exhibit high fatigue resistance. The PSS when switched to the *cis*-isomer were throughout good with 81–95%. Switching back to the *trans*-isomer worked also well for most compounds, only the

peptides containing the photoswitchable phenylalanine **8**, **9** and **12** had PSSs below 80% and peptide **15** containing the *ortho*, *ortho* substituted azobenzene had a PSS of 69% (Table 1). Interestingly, peptide **E-15** was slightly more polar than **Z-15**, whereas with all the other peptides the *cis*-isomers were slightly more polar (assessed by analytical C₁₈-RP-HPLC). The thermal half-lives, describing how fast the meta-stable *cis*-isomer was switching back to the *trans*-isomer, ranged between 12 h and 54 days (Table 1).

Table 1. Summary of the photophysical properties of switchable photoprobes **8-19**.^[a]

Compound	λ_{\max} (<i>trans</i>) [nm]	λ_{\max} (<i>cis</i>) [nm]	λ_{iso} [nm]	$t_{1/2}$ [days] ^[b]	PSS (<i>E</i> \rightarrow <i>Z</i>) ^[c]	PSS (<i>Z</i> \rightarrow <i>E</i>) ^[c]
8	328	430	277, 395	5.5	94%	72%
9	330	428	281, 391	3.0	93%	77%
10	332	430	285, 393	1.7	86%	81%
11	333	430	285, 396	1.2	87%	85%
12	330	430	281, 390	3.0	95%	74%
13	332	425	285, 405	0.5	85%	79%
14	332	430	285, 400	1.4	81%	86%
15	320	440	277, 380	2.7	88%	69%
16	320	430	277, 390	3.1	89%	83%
17	323	425	274, 375	28.6	93%	88%
18	340	427	293, 403	6.6	94%	82%
19	333	431	285, 402	54.5	93%	87%

[a] Isomerization was obtained by irradiation with 340 nm (*Z*-isomer) and 420 nm for **8-17** and 528 nm for **18** and **19** (*E*-isomer), respectively. Concentration: 20 μM in HEPES buffer (25 mM HEPES, 2.5 mM CaCl₂, 1 mM MgCl₂, pH = 7.4) + 0.1% DMSO. [b] Pre-irradiation with 340 nm. [c] PSS determination was done by analytical C₁₈-RP-HPLC at the appropriate isosbestic points.

4.5 Biological Investigation

We pharmacologically characterized the photoswitchable OT/VP derivatives **8-19** at the human OTR, V_{1a}R, or V_{1b}R using HEK293 cells overexpressing the respective receptor subtype using a commercially available IP-One accumulation assay (Cisbio) for G_q-coupled receptors.^[63] V₂R was not evaluated since this receptor subtype is not present in the brain. The endogenous ligands OT (OTR) and VP (V_{1a}R, V_{1b}R) were used as reference compounds. The *cis* and *trans* isomer of each photoswitchable peptide were measured separately following prior irradiation of the dilution series at the appropriate wavelength (Table 1). All compounds were initially measured at two concentrations (100 nM and 10 μM) and a full dose-response curve was generated for any active compound.

Table 2 and 3 summarize the EC₅₀ and E_{max} values of the three modification strategies including OT (**8-11**) and VP derivatives (**12-14**) at OTR, V_{1a}R or V_{1b}R. We first report the impact of the photoswitch incorporation compared to OT and VP followed by the differences between the

cis (*Z*) and *trans* (*E*) isomers. In the first strategy, we focused on the aromatic residues at position 2 and 3 of the macrocycle. OT-based peptide **8**, with the photoswitch **1** incorporated at Tyr², displayed a substantial drop in potency compared to OT (more than 1400-fold) with an EC₅₀ in the 3-4 μM range, additionally displaying partial agonism (E_{max} 35-45%). The drop in activity is likely due to the larger size of the azobenzene that replaced Tyr² which also lacks a hydroxyl group that can act as a H-donor.^[64] Displacement of Phe³ in VP with photoswitch **1** (peptide **12**) also displayed reduced potency at V_{1a}R (>1000-fold compared to VP), but at V_{1b}R it was quite potent (**Z-12**, EC₅₀ 20.2 nM, full agonist, 6-fold less potent than VP), supporting the note that V_{1b}R is more tolerant to modifications than V_{1a}R. The second modification strategy focused on the three-residue C-terminal tail. OT-derived peptides **9**, **10** and **11** were modified at Pro⁷ either by substitution with photoswitch **1** (peptide **9**) or in a linear fashion with photoswitch **2** (peptides **10** and **11**). This modification strategy was better tolerated, resulting in only a 12-fold potency decrease for **Z-10** and a 55-fold decrease for **Z-9** and **Z-11** compared to OT at OTR, with E_{max} ranging between 75–92%. Linear photoswitch **2** was also introduced into VP (peptides **13** and **14**) resulting in a complete loss of potency at V_{1a}R at concentrations up to 10 μM (Figure S51) and a 700–2000-fold reduced potency at V_{1b}R. The reason why this strategy was not so well tolerated at the VPRs, is likely due to the removal (**13**) or shift of positively-charged Arg⁸ (**14**) which is important for the formation of ionic interactions with the receptors.^[65,66] The third modification strategy focused on the disulfide bond of VP. The series of disulfide-mimetics **15-19** resulted in complete loss of activity up to a concentration of 10 μM at both V_{1a}R and V_{1b}R (Figure S52). Even though we stated that VP and VPRs are more forgiving the azobenzene or arylazopyrazole motifs are probably too big and rigid to be used here as disulfide-bond mimetics.

Table 2. OTR potencies (EC_{50}) and efficacies (E_{max}) of OT and **8-11**.^[a]

OTR			
	$EC_{50} \pm SEM$ [nM]	$E_{max} \pm SEM$ [%]	E/Z ratio EC_{50}
OT	2.46 ± 0.58	100	-
E-8	4501 ± 1014	45 ± 3	1.3
Z-8	3496 ± 1887	35 ± 1	
E-9	346 ± 30	89 ± 1	2.5
Z-9	136 ± 6	90 ± 1	
E-10	94.6 ± 19	80 ± 1	3.1
Z-10	30.7 ± 4	92 ± 0	
E-11	263 ± 21	75 ± 1	2.0
Z-11	134 ± 17	86 ± 1	

[a] Determined in an IP-One accumulation assay performed with stable HEK293 cell lines expressing hOTR. Efficacies were determined relative to the effect of OT. Data represent mean values from at least three independent experiments performed in triplicate (standard error of the mean (SEM)).

Table 3. V_{1aR} and V_{1bR} potencies (EC_{50}) and efficacies (E_{max}) of VP and **12-14**.^[a]

	V_{1aR}			V_{1bR}		
	$EC_{50} \pm SEM$ [nM]	$E_{max} \pm SEM$ [%]	E/Z ratio EC_{50}	$EC_{50} \pm SEM$ [nM]	$E_{max} \pm SEM$ [%]	E/Z ratio EC_{50}
VP	0.64 ± 0.09	100	-	3.33 ± 0.48	100	-
E-12	722 ± 53	104 ± 1	2.0	107 ± 13	95 ± 1	5.3
Z-12	1439 ± 108	99 ± 1		20.2 ± 6	95 ± 1	
E-13	>10 μ M	-	-	11260 ± 1829	45 ± 3	1.6
Z-13	>10 μ M	-	-	7228 ± 1575	52 ± 5	
E-14	>10 μ M	-	-	4967 ± 754	48 ± 2	2.1
Z-14	>10 μ M	-	-	2373 ± 607	67 ± 2	

[a] Determined in an IP-One accumulation assay performed with stable HEK293 cell lines expressing h V_{1aR} and h V_{1bR} . Efficacies were determined relative to the effect of VP. Data represent mean values from at least three independent experiments performed in triplicate (standard error of the mean (SEM)).

The most promising candidates with a reasonable activation ability were peptides **9**, **10**, and **11** at OTR and **12** at V_{1bR} . Peptides **9**, **10**, and **11** derived from the second modification strategy (Pro⁷) and peptide **12** from the first modification strategy (Phe³). Substitution of Pro⁷ with the azobenzene photoswitch in the side chain position (**9**) was still a full agonist with an EC_{50} of 136 nM for **Z-9** and 346 nM for **E-9**, providing a 2.5-fold potency difference between the two

isomers at OTR. Peptides **10** and **11** have the photoswitch incorporated within the backbone instead of Pro⁷ with **11** containing Leu⁸, whereas in **10** Leu⁸ was removed. Both derivatives were still potent agonists, with the shorter peptide **10** being the more potent and better design. Peptide **10** displayed a 3.1-fold potency difference between the two isomers, with an EC₅₀ of 94.6 nM for *E*-**10** and 30.7 nM for *Z*-**10** (Figure 4). The longer peptide **11** displayed a 2-fold potency difference, with EC₅₀ values of 263 nM for *E*-**11** and 134 nM for *Z*-**11**. Peptide **10** was therefore the best candidate from the OT-design series (Figure 4A). Peptide **12** was the best candidate from the VP-derived series, having the azobenzene moiety in the sidechain instead of Phe³, displaying a 5.3-fold potency difference, with an EC₅₀ of 107 nM for *E*-**12** and 20.2 nM for *Z*-**12** at V_{1b}R (Figure 4B).

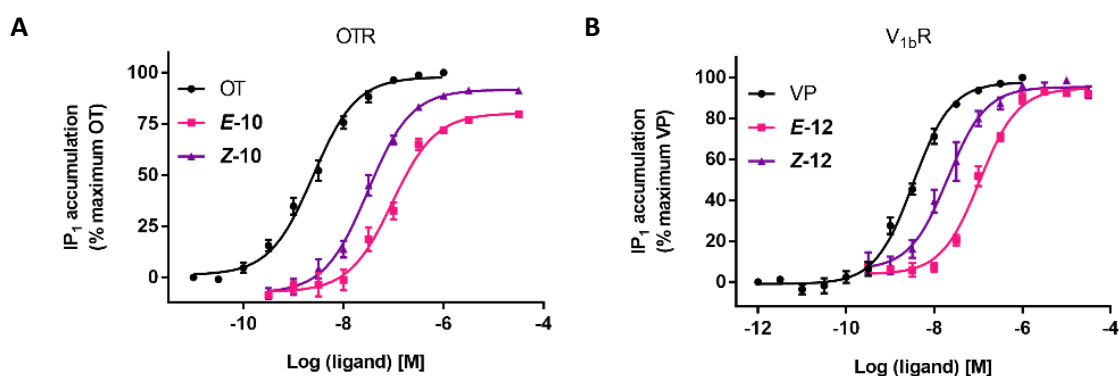


Figure 4. Full-dose-response curves. **(A)** Both isomers of **10** and OT at the OTR. **(B)** Both isomers of **12** and VP at V_{1b}R. For the full-dose-response-curves of **8**, **9** and **11-14** see SI Figure S50. Data represent mean values \pm SEM from at least three independent experiments performed in triplicate.

Since the structural changes could also result in an agonist-to-antagonist switch, we also tested all inactive compounds for their ability to antagonize V_{1a}R as it represents the most important VPR. This was done *via* co-addition and prior mixing of VP (EC₆₀ of 1 nM) and the potential antagonists **13-19**. V_{1a}R antagonist Atosiban was used as a positive control.^[67] IP₁ accumulation was measured at 10 and 100 μ M (**13-19**). Peptides **13** and **14** displayed some antagonistic activity (VP displacement of 76% and 85% at 10 μ M) which was quite weak compared to Atosiban (VP displacement of 86% at 1 μ M). The disulfide-mimetics **16-19** were mostly inactive at these concentrations displaying very poor antagonism (Figure 5). Only disulfide-mimetic **15** with the *ortho/ortho* substitution at the azobenzene (closest/smallest ring structure) displayed some antagonistic properties at 10 μ M.

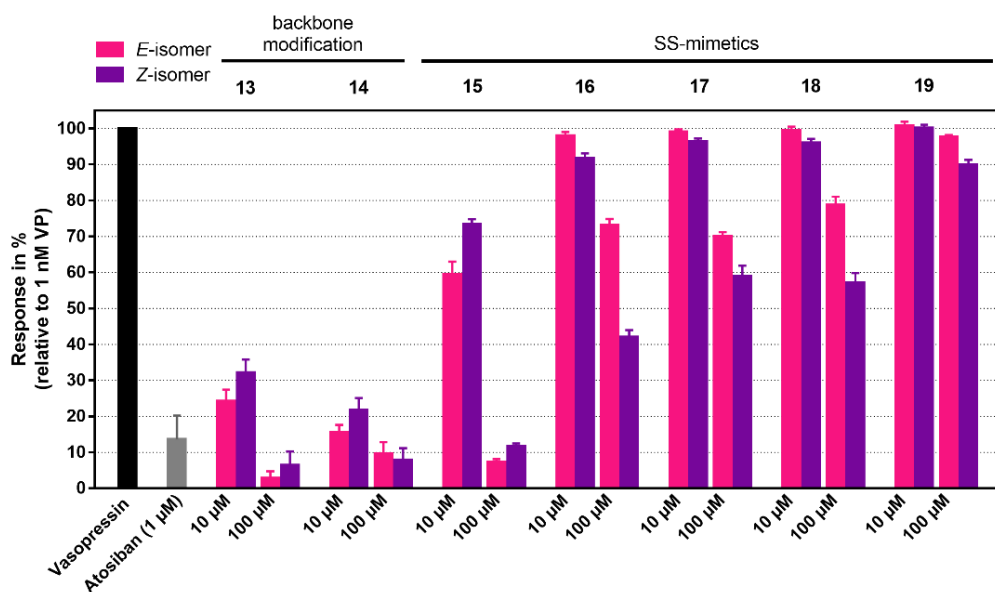


Figure 5. Antagonistic activities at the $V_{1a}R$. VP displacement of positive control atosiban and **13-19** was determined in an IP-One accumulation assay with stable HEK293 cell lines overexpressing $hV_{1a}R$ by co-addition (premixed) of VP (1 nM) and atosiban (1 μ M) or potential antagonists **13-19** (10 and 100 μ M). Data represent mean \pm SEM from at least three independent experiments, each performed in triplicate.

Because of their involvement in various disorders OT, VP and their receptors are of great interest for research.^[1-4] A lot of effort has been put into the development of receptor-selective agonists and antagonists, but these ligands lack spatiotemporal precision that is required to dissect the OT/VP-dependent neuronal circuits of the brain.^[23,33] Still, to this day, no photoswitchable probes targeting these receptors have been developed. Here, we present the first photoswitchable OT and VP derivatives. With **10** and **12** we were able to identify compounds that display a good difference between the two isomers and, despite OTs and VPs sensitivity towards structural changes, an only slightly reduced potency compared to the endogenous ligands. OT-derived compound **10** showed a 3-fold difference between the two isoforms at the OTR and VP-derived compound **12** a 5-fold difference at the $V_{1b}R$ regarding potency. These compounds do not represent a full on/off-switch but at certain concentrations, they can enable different activation profiles of the receptors. For example, the *E*-form of compound **12** added in a concentration of 10 nM activated the receptor to 7%, whereas the *Z*-form activated it to 40%. These differences in activation could allow for the utilization in *in vitro* and *ex vivo* assays. Additionally, the insights into the structure-activity relationships derived from this work help to come up with new modifications that improve these windows and achieve higher fold differences. Especially, compounds **10** and **12** represent good starting points for further fine tuning the photopharmacological properties. New alterations could be,

e.g., changing the photochromic moiety to, e.g., arylazopyrazoles, different substituents and/or varying the substitution patterns on the phenyl rings. These findings in our work may encourage further research and pave the way to find cutting-edge photocontrollable peptides for the investigation of dynamic and kinetic processes upon activation of OT and VP receptors.

4.6 Conclusion

We herein describe the successful synthesis of the first photoswitchable OT- and VP-derivatives by incorporating photochromic moieties into different sites of their scaffolds. All compounds exhibited good photochemical properties such as reversible switching, high fatigue resistance, good PSS, and thermal half-lives long enough for the biological investigations. Activation studies were performed on the three G_q-coupled receptors OTR, V_{1a}R or V_{1b}R in a functional IP-One accumulation assay. Overall, we observe a reduced potency compared to the endogenous ligands OT and VP because of the high sensitivity of these peptides to structural modifications. Nevertheless, with peptide **10** we found an OT derivative with a potency in the nano molar range at OTR. This compound displayed a 3.1-fold difference between *cis* and *trans* isomer. Even more interesting, however, was VP-derived peptide **12** with an only 6-fold reduced potency compared to endogenous VP at the V_{1b}R and a 5.3-fold difference between the two isoforms. Knowing what modifications were tolerated by which receptor builds the foundation to design a new generation of photoswitchable OT and VP derivatives with the chance to incorporate other photochromic moieties to finetune the properties of the bioactive photoresponsive molecule.

4.7 Experimental Part

4.7.1 General Information

Starting materials and commercial reagents were purchased from Acros, Alfa Aesar, Fisher, Fluka, Fluorochem, Merck (Sigma-Aldrich), TCI and VWR and were used without further purification. Solvents were used in p.a. quality or dried according to common procedures if necessary. All reactions with oxygen- or moisture-sensitive reagents were carried out in glassware that was dried before use by heating under vacuum. Dry nitrogen or argon were used as inert gas atmosphere. NMR spectra were measured at room temperature (20 °C) using a Bruker Avance 400 (400 MHz for ^1H and 101 MHz for ^{13}C) or a Bruker Avance 600 (600 MHz for ^1H and 151 MHz for ^{13}C) NMR spectrometer. All chemical shifts are reported in δ -scale as parts per million [ppm] (multiplicity, coupling constant J, number of protons) relative to the solvent residual peaks. Coupling constants J are given in Hertz [Hz]. Abbreviations used for signal multiplicity: ^1H -NMR: s = singlet, d = doublet, dd = doublet of doublets, ddd = doublet of doublets of doublets, dt = doublet of triplets, t = triplet, td = triplet of doublets, q = quartet, and m = multiplet. Mass spectra were recorded on an Agilent Q-TOF 6540 UHD, Finnigan MAT SSQ 710 A, Jeol AccuTOF GCX or ThermoQuest Finnigan TSQ 7000 spectrometer. Absorption spectra were recorded on a UV/VIS Agilent Cary 50 spectrometer. Thermal half-lives were measured on a 96-well plate in a Thermo Scientific Multiskan® Spectrum. Analytical TLC was performed on silica gel coated alumina plates (MN precoated TLC-sheets ALUGRAM® Xtra SIL G/UV254). Visualization was done using UV-light (254 nm or 366 nm) or staining with ninhydrin solution. Column chromatography was performed on a Biotage Isolera One automated flash purification system with UV/Vis detector. Analytical RP-HPLC was carried out on an Agilent 1220 Infinity LC System (column: P/No 00F-4251-B0, Phenomenex Luna® 3 μm C18(2) 100 Å, LC column 150 x 2.0 mm). Purification by preparative HPLC was conducted on a preparative HPLC Agilent 1260 Infinity LC System (column: P/No 00G-4253-P0-AX, Phenomenex Luna® 10 μm C18(2) 100 Å, LC column 250 x 21.2 mm). The eluent systems were used as specified. After the purification process, solvents were removed by lyophilization. Switching experiments were done with a 340 nm LED (SSC VIOSYS CUD4AF1B, 500 mA, 55 mW), 420 nm LED (ILH-XC01-S410-SC211-WIR200, 800 mA, 440 mW) and 528 nm LED (OSRAM Oslon SSL 80 green, 500 mA, 34 mW).

(E)-3-((3-(tert-Butoxycarbonyl)phenyl)diazenyl)benzoic acid (5). Yield: 24%.

¹H NMR (400 MHz, DMSO-d₆) δ 8.38 (dt, *J* = 17.9, 1.9 Hz, 2H), 8.24 – 8.05 (m, 4H), 7.74 (td, *J* = 7.8, 2.0 Hz, 2H), 1.58 (s, 9H). ¹³C NMR (101 MHz, DMSO) δ 166.7, 164.2, 151.7, 132.7, 132.5, 132.2, 131.9, 130.0, 130.0, 127.4, 126.9, 122.7, 122.5, 81.5, 27.8. **ESI-MS:** *m/z* (%) = 327.14 (M+H)⁺.

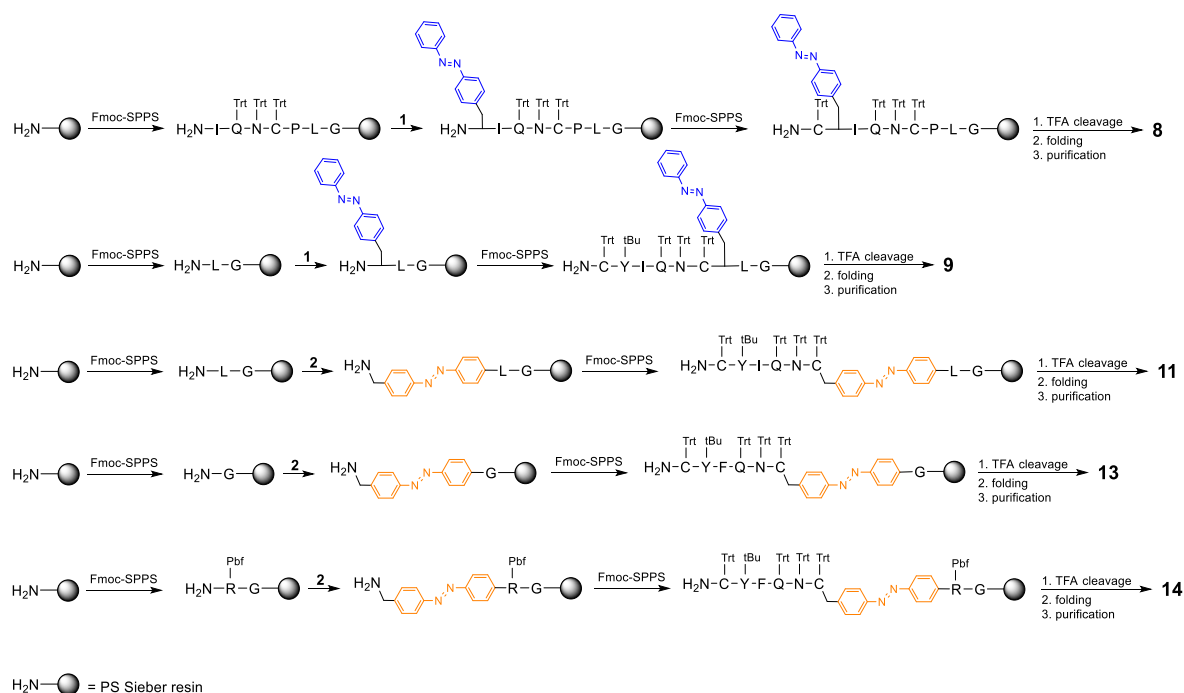
General procedure for the synthesis of arylazopyrazoles 6 and 7. Compound **28** or **29** (1.0 eq.) in DCM was added to (4-amino-3,5-dimethyl-1*H*-pyrazol-1-yl)acetic acid dihydrochloride hydrate (**30**) (1.0 eq.) dissolved in DCM. Then NEt₃ was added dropwise until the solution turned yellow. The mixture was stirred for 3 h at 20 °C. The solvent was removed *in vacuo* and the crude product was purified by column chromatography (MeCN/EtOH, 0-30%).

(E)-2-(4-((2-(tert-Butoxycarbonyl)phenyl)diazenyl)-3,5-dimethyl-1*H*-pyrazol-1-yl)acetic acid (6). Yield: 14%. ¹H NMR (400 MHz, DMSO-d₆) δ 7.59 (ddd, *J* = 15.3, 7.4, 1.5 Hz, 2H), 7.51 (dd, *J* = 8.1, 1.3 Hz, 1H), 7.45 (td, *J* = 7.4, 1.4 Hz, 1H), 4.95 (s, 2H), 2.48 (s, 3H), 2.33 (s, 3H), 1.46 (s, 9H). ¹³C NMR (101 MHz, DMSO) δ 169.2, 166.6, 151.6, 141.4, 141.2, 135.2, 131.3, 130.6, 128.8, 128.8, 117.7, 81.4, 50.6, 27.8, 13.7, 9.5. **ESI-MS:** *m/z* (%) = 359.17 (M+H)⁺.

(E)-2-(4-((3-(tert-Butoxycarbonyl)phenyl)diazenyl)-3,5-dimethyl-1*H*-pyrazol-1-yl)acetic acid (7). Yield: 57%. ¹H NMR (400 MHz, DMSO-d₆) δ 8.19 (t, *J* = 1.8 Hz, 1H), 7.95 (ddt, *J* = 9.7, 7.8, 1.2 Hz, 2H), 7.63 (t, *J* = 7.8 Hz, 1H), 4.87 (s, 2H), 2.52 (s, 3H), 2.39 (s, 3H), 1.57 (s, 9H). ¹³C NMR (101 MHz, DMSO) δ 169.2, 164.5, 153.0, 141.2, 140.8, 134.6, 132.4, 129.6, 129.6, 125.4, 121.8, 81.1, 51.2, 27.8, 13.9, 9.5. **ESI-MS:** *m/z* (%) = 359.17 (M+H)⁺.

General procedure for peptide synthesis. Peptides were synthesized by manual SPPS according to the Fmoc strategy using Fmoc-PS-Sieber Resin. 5-mL Discardit II syringes equipped with polyethylene frits were used as reaction vessels. DMF/NMP (8:2 v/v) was used as solvent for the coupling reactions and the cleavage of Fmoc groups. For initial Fmoc deprotection of the resin and swelling, the resin was treated with 20% piperidine in solvent at 20 °C for 2 × 20 min. Protected natural L-amino acids were used in 5-fold excess and preactivated with HBTU (4.9 eq.)/HOBt (5 eq.)/DIPEA (10 eq.) in polypropylene reaction vessels for 1 min prior to addition to the resin (volume of the solvent: ca. 2.2 mL/mmol Fmoc-amino acid). In the case of standard Fmoc-amino acids, “double” coupling (2 × 40 min) was

performed at 35 °C. Photoswitch **1** and **2** were used in 3-fold excess, preactivated with HBTU (2.95 eq.)/HOBT (3 eq.)/DIPEA (6 eq.) (volume of solvent: ca. 1.6 mL/mmol of amino acid), and the reaction was performed at 35 °C for overnight (“single” coupling). During coupling reactions, syringes were shaken using a HLC BlockThermostate and ThermoMixer. After completed coupling of an Fmoc-amino acid, the resin was washed with solvent (4 × 5 mL) and treated with 20% piperidine in DMF/NMP (8:2 v/v) at 20 °C for 2 × 10 min followed by washing the resin with solvent (6 × 5 mL). For the peptides containing cysteines **8-14**, the last step was the Fmoc deprotection of the last cysteine residue. For the linear precursors of peptides containing a photoswitch in the cyclic part **15-19**, after the final Fmoc deprotection of the final amino acid photoswitches **5-7** were preactivated with PyBOP (3 eq.)/HOBT (3 eq.)/DIPEA (6 eq.) and photoswitches **3** and **4** were preactivated with DIC (3 eq.), all photoswitches were used in 3-fold excess and were added to the resin and the reaction proceeded at 35 °C for overnight. Afterwards, for all peptides, the resin was washed with solvent (6×) and CH₂Cl₂ (4×) followed by TFA cleavage off the resin and global deprotection of the amino acid side chains with TFA/CH₂Cl₂/TIPS/H₂O (50/46/2/2, v/v) at 20 °C for 4-5 h. The collected liquid phases were combined in a round-bottom flask and water was added which was followed by lyophilization with subsequent purification of the linear precursors of peptides **15-19** by preparative HPLC (column: Phenomenex Luna® 10 μm C18(2) 100 Å, 250 x 21 mm; flow: 22 mL/min, solvent A: H₂O (0.05% TFA), solvent B: MeCN; gradient A/B: 0-20 min: 97/3, 20-25 min: 2/98) after lyophilization. For the peptides containing cysteines **8-14**, oxidative folding was carried out after lyophilization in acetonitrile/phosphate buffer (pH 7.4) and 10% DMSO at 20 °C overnight and subsequent purification by preparative HPLC (column: Phenomenex Luna® 10 μm C18(2) 100 Å, 250 x 21 mm; flow: 22 mL/min, solvent A: H₂O (0.05% TFA), solvent B: MeCN; gradient A/B: 0-20 min: 97/3, 20-25 min: 2/98). The overall yield is based on the used resin and resin loading.



Scheme S1. Synthesis of peptides **8**, **9**, **11**, **13** and **14**. Protecting groups: Trt = trityl, ^tBu = *tert*-butyl, Pbf = 2,2,4,6,7-pentamethylidihydrobenzofuran-5-sulfonyl.

Nomenclature

Azb = Azobenzene

S = side chain (photoswitch **1**)

Azp = Arylazopyrazole

L = linear (photoswitch **2**)

Dap = diaminopropionic acid

C = cyclic (photoswitches **3-7**)

[AzbS²]-OT (8). Overall yield: 4%. HPLC (gradient: 0-15 min: MeCN/H₂O + 0.05% TFA 10/90 – 98/2, 15-20 min: 98/2): t_R: *cis*-isomer: 8.5 min, *trans*-isomer: 9.4 min. HR-MS (ESI): calculated m/z for C₄₉H₇₀N₁₄O₁₁S₂ (M+2H)²⁺: 548.2468; observed: 548.2479.

[AzbS⁷]-OT (9). Overall yield: 3%. HPLC (gradient: 0-15 min: MeCN/H₂O + 0.05% TFA 10/90 – 98/2, 15-20 min: 98/2): t_R: *cis*-isomer: 8.9 min, *trans*-isomer: 9.8 min. HR-MS (ESI): calculated m/z for C₅₃H₇₂N₁₄O₁₂S₂ (M+H)⁺: 1161.4968; observed: 1161.4972.

[Azbl^{7/8}]-OT (10). Overall yield: 2%. **HPLC** (gradient: 0-15 min: MeCN/H₂O + 0.05% TFA 10/90 – 98/2, 15-20 min: 98/2): t_R: *cis*-isomer: 7.6 min, *trans*-isomer: 7.9 min. **HR-MS** (ESI): calculated m/z for C₄₆H₅₉N₁₃O₁₁S₂ (M+2H)²⁺: 517.7022; observed: 517.7028.

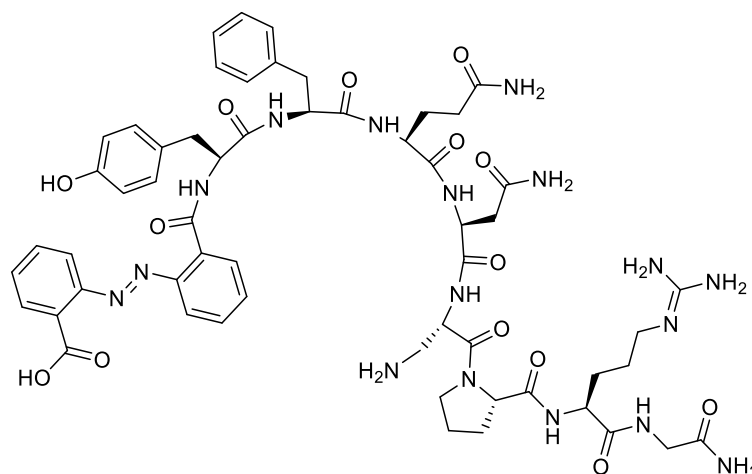
[Azbl⁷]-OT (11). Overall yield: 3%. **HPLC** (gradient: 0-15 min: MeCN/H₂O + 0.05% TFA 10/90 – 98/2, 15-20 min: 98/2): t_R: *cis*-isomer: 8.5 min, *trans*-isomer: 8.9 min. **HR-MS** (ESI): calculated m/z for C₅₂H₇₀N₁₄O₁₂S₂ (M+2H)²⁺: 574.2442; observed: 574.2451.

[Azbs³]-VP (12). Overall yield: 5%. **HPLC** (gradient: 0-15 min: MeCN/H₂O + 0.05% TFA 10/90 – 98/2, 15-20 min: 98/2): t_R: *cis*-isomer: 7.3 min, *trans*-isomer: 8.3 min. **HR-MS** (ESI): calculated m/z for C₅₂H₆₉N₁₇O₁₂S₂ (M+2H)²⁺: 594.7449; observed: 594.7461.

[Azbl^{7/8}]-VP (13). Overall yield: 5%. **HPLC** (gradient: 0-15 min: MeCN/H₂O + 0.05% TFA 10/90 – 98/2, 15-20 min: 98/2): t_R: *cis*-isomer: 7.9 min, *trans*-isomer: 8.0 min. **HR-MS** (ESI): calculated m/z for C₄₉H₅₇N₁₃O₁₁S₂ (M+2H)²⁺: 534.6944; observed: 534.6954.

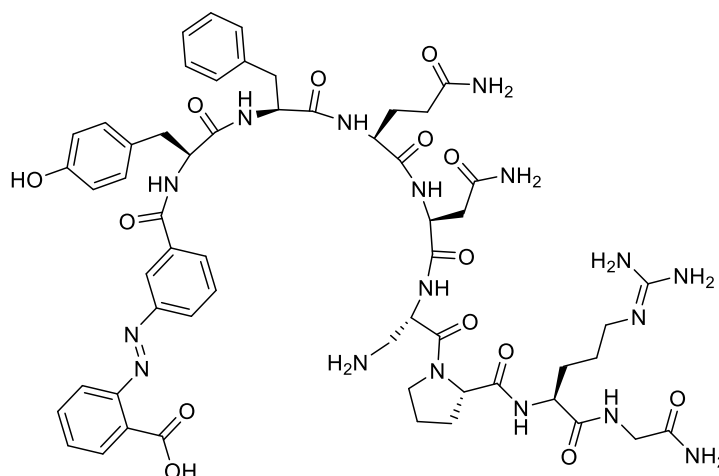
[Azbl⁷]-VP (14). Overall yield: 4%. **HPLC** (gradient: 0-15 min: MeCN/H₂O + 0.05% TFA 10/90 – 98/2, 15-20 min: 98/2): t_R: *cis*-isomer: 7.4 min, *trans*-isomer: 7.5 min. **HR-MS** (ESI): calculated m/z for C₅₅H₆₉N₁₇O₁₂S₂ (M+2H)²⁺: 612.7449; observed: 612.7458.

open[Azbc(*o,o*)¹,Dap⁶]-VP (linear precursor to 15).



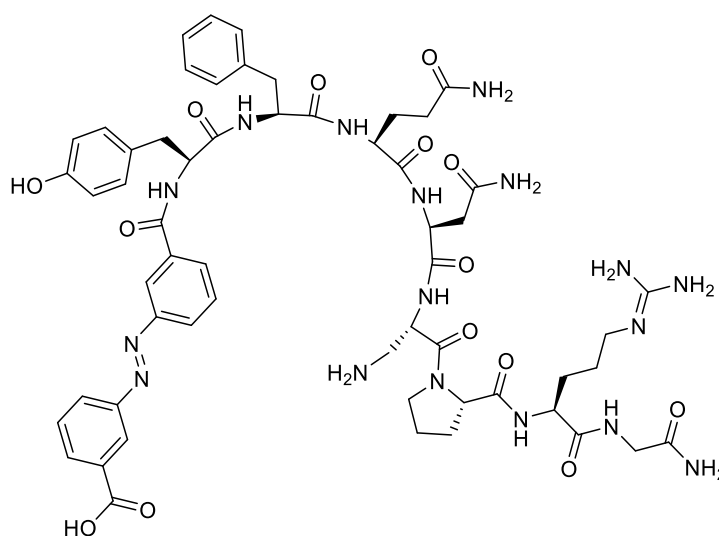
Overall yield: 8%

HR-MS (ESI): calculated m/z for C₅₇H₇₁N₁₇O₁₄ (M+2H)²⁺: 609.7756; observed: 609.7766.

open[AzbC(*m,o*)¹,Dap⁶]-VP (linear precursor to 16).

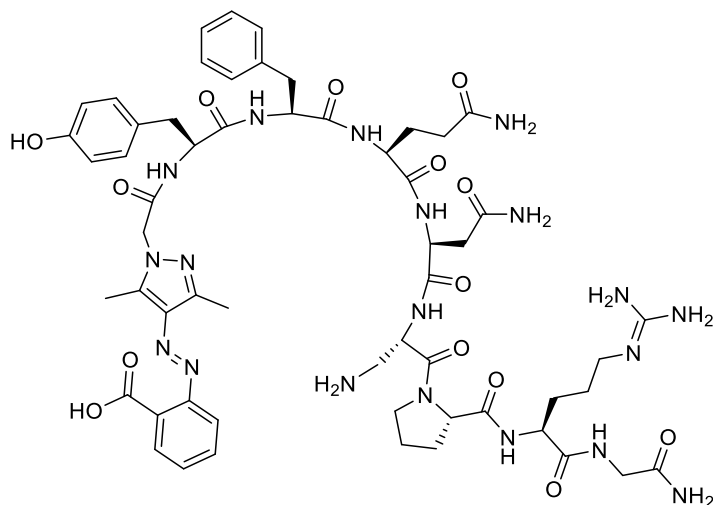
Overall yield: 17%

HR-MS (ESI): calculated m/z for $C_{57}H_{71}N_{17}O_{14}$ ($M+2H$)²⁺: 609.7756; observed: 609.7767.

open[AzbC(*m,m*)¹,Dap⁶]-VP (linear precursor to 17).

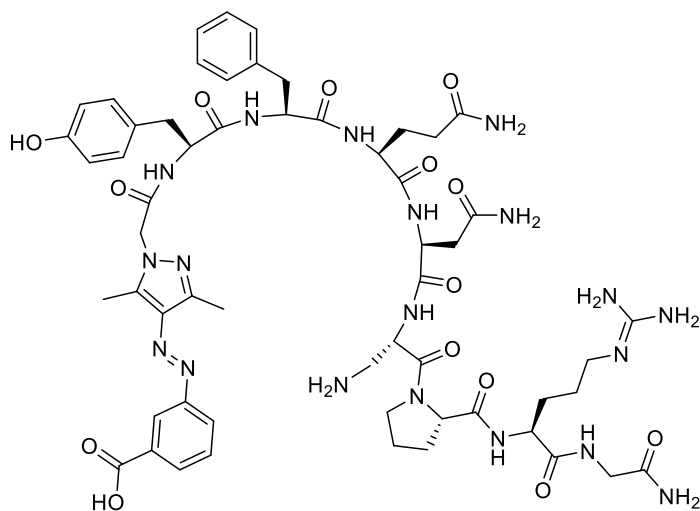
Overall yield: 14%

HR-MS (ESI): calculated m/z for $C_{57}H_{71}N_{17}O_{14}$ ($M+2H$)²⁺: 609.7756; observed: 609.7763.

open[AzpC(*o*)¹,Dap⁶]-VP (linear precursor to 18).

Overall yield: 32%

HR-MS (ESI): calculated m/z for $C_{57}H_{75}N_{19}O_{14}$ ($M+2H$)²⁺: 625.7943; observed: 625.7956.

open[AzpC(*m*)¹,Dap⁶]-VP (linear precursor to 19).

Overall yield: 68%

HR-MS (ESI): calculated m/z for $C_{57}H_{75}N_{19}O_{14}$ ($M+2H$)²⁺: 625.7943; observed: 625.7952.

General procedure for the cyclization of peptides 15-19. Linear precursors of peptides **15-19** (1 eq.), HOBT (5 eq.) and DIPEA (10 eq.) were dissolved in DMF/NMP 8:2 v/v (100 μ L/ μ mol of peptide) in an Eppendorf tube. Under stirring, a solution of PyBOP (5 eq.) in DMF/NMP 8:2 v/v (100 μ L/ μ mol of peptide) was added, and the mixture was stirred at 20 °C overnight. The crude product was purified by preparative HPLC (column: Phenomenex Luna® 10 μ m C18(2) 100 Å, 250 x 21 mm; flow: 22 mL/min, solvent A: H₂O (0.05% TFA), solvent B: MeCN; gradient A/B: 0-20 min: 97/3, 20-25 min: 2/98).

[AzbC(*o,o*)¹,Dap⁶]-VP (15). Cyclization yield: 23%. **HPLC** (gradient: 0-15 min: MeCN/H₂O + 0.05% TFA 10/90 – 98/2, 15-20 min: 98/2): t_R: *cis*-isomer: 8.5 min, *trans*-isomer: 8.3 min. **HR-MS** (ESI): calculated m/z for C₅₇H₆₉N₁₇O₁₃ (M+2H)²⁺: 600.7703; observed: 600.7711.

[AzbC(*m,o*)¹,Dap⁶]-VP (16). Cyclization yield: 45%. **HPLC** (gradient: 0-15 min: MeCN/H₂O + 0.05% TFA 10/90 – 98/2, 15-20 min: 98/2): t_R: *cis*-isomer: 8.3 min, *trans*-isomer: 8.7 min. **HR-MS** (ESI): calculated m/z for C₅₇H₆₉N₁₇O₁₃ (M+2H)²⁺, m/z 600.7703; observed: 600.7717.

[AzbC(*m,m*)¹,Dap⁶]-VP (17). Cyclization yield: 48%. **HPLC** (gradient: 0-15 min: MeCN/H₂O + 0.05% TFA 10/90 – 98/2, 15-20 min: 98/2): t_R: *cis*-isomer: 8.1 min, *trans*-isomer: 8.6 min. **HR-MS** (ESI): calculated m/z for C₅₇H₆₉N₁₇O₁₃ (M+2H)²⁺: 600.7703; observed: 600.7713.

[AzpC(*o*)¹,Dap⁶]-VP (18). Cyclization yield: 60%. **HPLC** (gradient: 0-15 min: MeCN/H₂O + 0.05% TFA 10/90 – 98/2, 15-20 min: 98/2): t_R: *cis*-isomer: 7.7 min, *trans*-isomer: 8.2 min. **HR-MS** (ESI): calculated m/z for C₅₇H₇₃N₁₉O₁₃ (M+2H)²⁺: 616.7890; observed: 616.7902.

[AzpC(*m*)¹,Dap⁶]-VP (19). Cyclization yield: 57%. **HPLC** (gradient: 0-15 min: MeCN/H₂O + 0.05% TFA 10/90 – 98/2, 15-20 min: 98/2): t_R: *cis*-isomer: 7.6 min, *trans*-isomer: 8.2 min. **HR-MS** (ESI): calculated m/z for C₅₇H₇₃N₁₉O₁₃ (M+2H)²⁺: 616.7890; observed: 616.7902.

4.7.3 Pharmacology

Cell culture. The stable HEK 293 cell lines overexpressing either hOTR, hV_{1a}R, or hV_{1b}R were stored at -80 °C in 700 µL freezing medium (FBS with 10% DMSO). After quick thawing, the cells were transferred into a cell culture flask containing 10 mL of Dulbecco's modified eagle medium with 10% FBS, 2 mM glutamine and 1 mM sodium pyruvate and incubated at 37 °C for 24 h. The old medium was aspirated to remove the DMSO and 10 mL of fresh medium were transferred into the flask. In addition to the growth medium, 160 µL of a 50 mg/mL G-418 solution were added. Since the stable cell lines carry a neomycin-geneticin resistance gene alongside the gene for the receptor of interest, the G-418 antibiotic was included with the medium when working with the stable cell lines. They were incubated at 37 °C and 5% CO₂ to a confluency of 70–100%. Cells were split after three to four days. The medium was removed, and cells were detached using 3 mL of trypsin-EDTA solution followed by 9 mL of fresh medium. The cells were pipetted up and down to detach all of them. After centrifugation (178 *g*, 1000 rpm, 3 min), the cells were resuspended in 1 mL of medium, counted with the Neubauer counting chamber and plated in 384-well plates.

Preparation of ligands. A two-fold concentrated dilution series in stimulation buffer was prepared for each isomer. To get to the respective *Z*-isomer of each compound, the highest concentrated dilution was irradiated with 340 nm for 1 min in an Eppendorf Tube. Thereafter, the dilution series was prepared, and the Eppendorf tubes were covered with aluminum foil. The solutions of *E*-isomers were not irradiated prior to the dilution.

IP-One assay (CisBio HTRF® IP-One Assay). Agonist mode. Measurement of OTR, V_{1a}R and V_{1b}R activation was done with the IP-One HTRF assay from CisBio. The experiments were done according to the manufacturer's protocol. Cells were seeded into a white 384-well plate with F-bottom (10,000 cells/well) and incubated for 48 h at 37 °C and 5% CO₂. The medium was removed and 5 µL of stimulation buffer was added to each well, followed by 15 min incubation at 37 °C and 5% CO₂. Subsequently, 5 µL of compound dilution prepared with stimulation buffer was added. The plate was incubated for 1 h at 37 °C and 5% CO₂. After the incubation time, 5 µL IP1-d2 conjugate and 5 µL anti-IP1-cryptate-TB conjugate dissolved in lysis buffer, were added to each well and incubated for another 60 min at 20 °C. Fluorescence emission measurements at 615 nm and 665 nm were performed using a Spark Multimode plate reader (Tecan, Männedorf, Switzerland) at an excitation wavelength

of 340 nm. Results were analyzed as a ratio of fluorescence intensities of 665 nm to 615 nm and normalized to OT and VP. **Antagonist mode.** To assess the antagonistic properties of compounds **13-19**, a four-fold concentrated dilution series in stimulation buffer was prepared for each isomer. Separately, a four-fold concentrated VP solution was prepared (4 nM, final concentration 1 nM). A 1:1 mixture of VP solution and the diluted ligand was made to end up with a two-fold concentration of both compounds. The following steps were conducted as described above for the agonist mode. The FRET ratios (665 nm/615 nm) were calculated and obtained values were normalized to the basal activity value (0%) and maximal effect of VP (100%). Atosiban was used as the positive control.

4.8 Supporting Information

4.8.1 Purity

Purity was determined by analytical RP-HPLC at 220 nm.

Purity: **99%** (*cis*-Isomer: 27% + *trans*-isomer: 73%)

Signal 2: DAD1 B, Sig=220,4 Ref=off

Peak #	RetTime [min]	Type	Width [min]	Area [mAU*s]	Height [mAU]	Area %
1	8.507	BV R	0.0645	937.61279	217.43913	26.5484
2	9.381	VV R	0.0672	2580.50317	586.88135	73.0668
3	13.137	BB	0.1036	13.58862	2.04224	0.3848

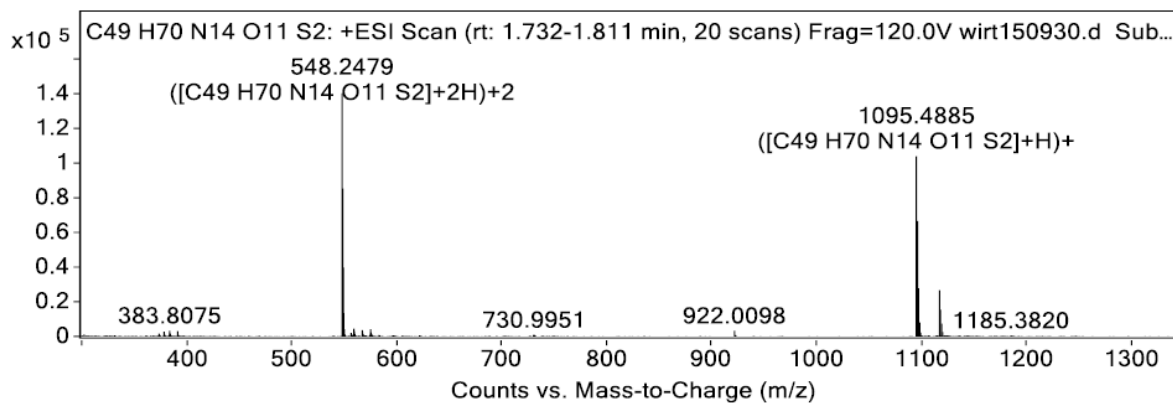
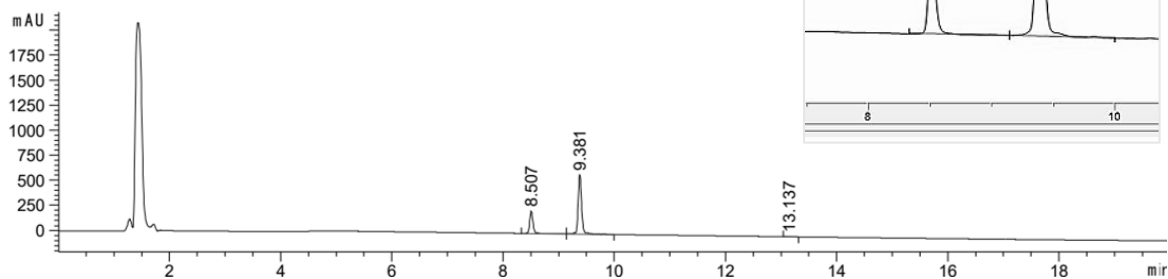


Figure S1. Analytical C_{18} -RP-HPLC trace and high-resolution mass spectrum of **8**.

Purity: **96%** (*cis*-Isomer: 22% + *trans*-isomer: 74%)

Signal 2: DAD1 B, Sig=220,4 Ref=off

Peak #	RetTime [min]	Type	Width [min]	Area [mAU*s]	Height [mAU]	Area %
1	7.500	MM	0.0664	51.19547	12.85047	3.8045
2	8.880	BB	0.0607	302.78906	75.67075	22.5012
3	9.774	VB R	0.0633	991.67480	244.42427	73.6943

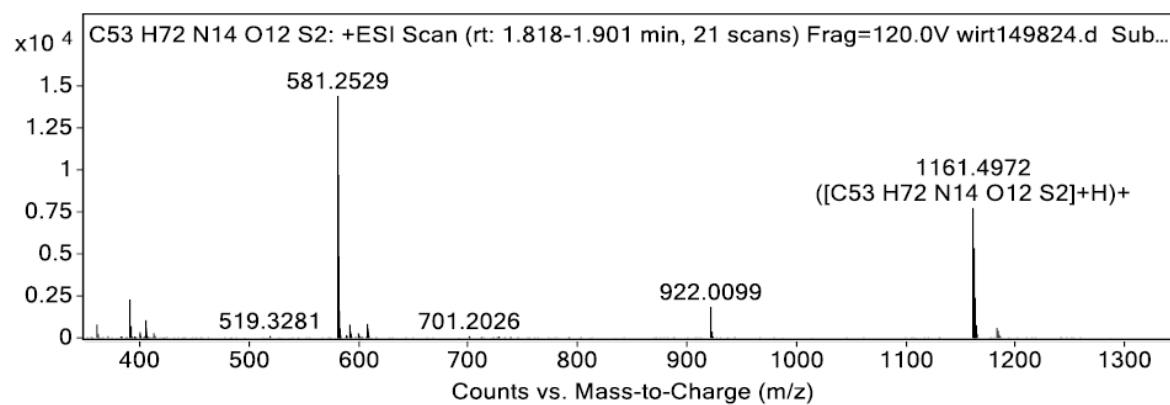
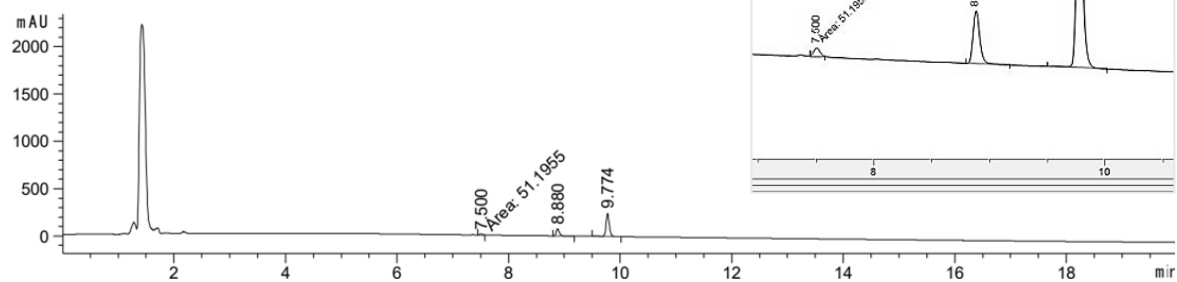
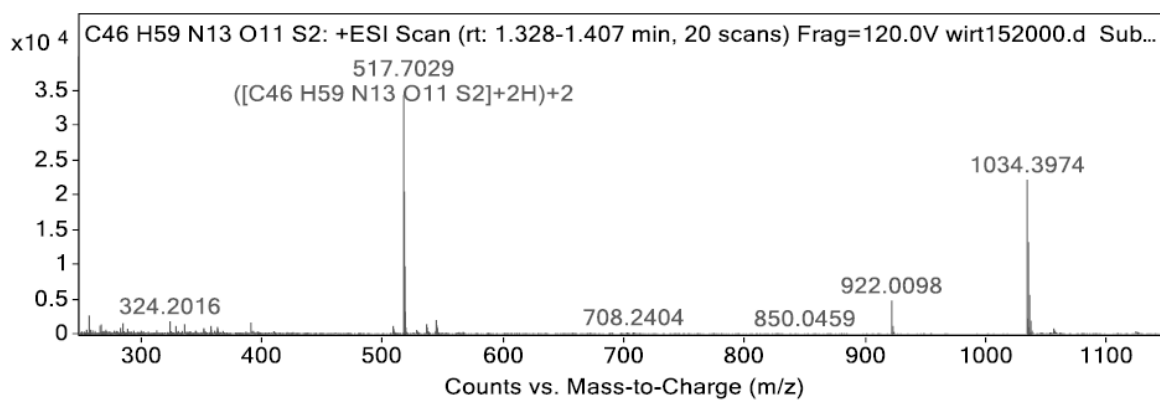
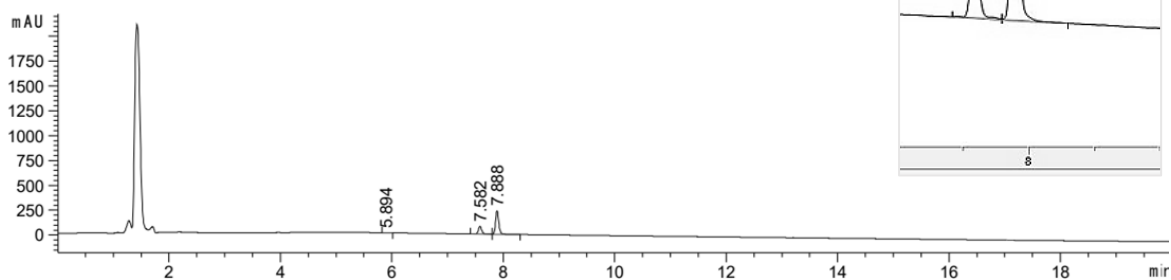


Figure S2. Analytical C₁₈-RP-HPLC trace and high-resolution mass spectrum of **9**.

Purity: **99%** (*cis*-Isomer: 26% + *trans*-isomer: 74%)

Signal 2: DAD1 B, Sig=220,4 Ref=off

Peak #	RetTime [min]	Type	Width [min]	Area [mAU*s]	Height [mAU]	Area %
1	5.894	BB	0.0792	6.42033	1.26486	0.4999
2	7.582	VV R	0.0666	333.65219	76.87822	25.9803
3	7.888	VB	0.0623	944.17615	237.92987	73.5197

**Figure S3.** Analytical C_{18} -RP-HPLC trace and high-resolution mass spectrum of **10**.

Purity: **99%** (*cis*-Isomer: 16% + *trans*-isomer: 83%)

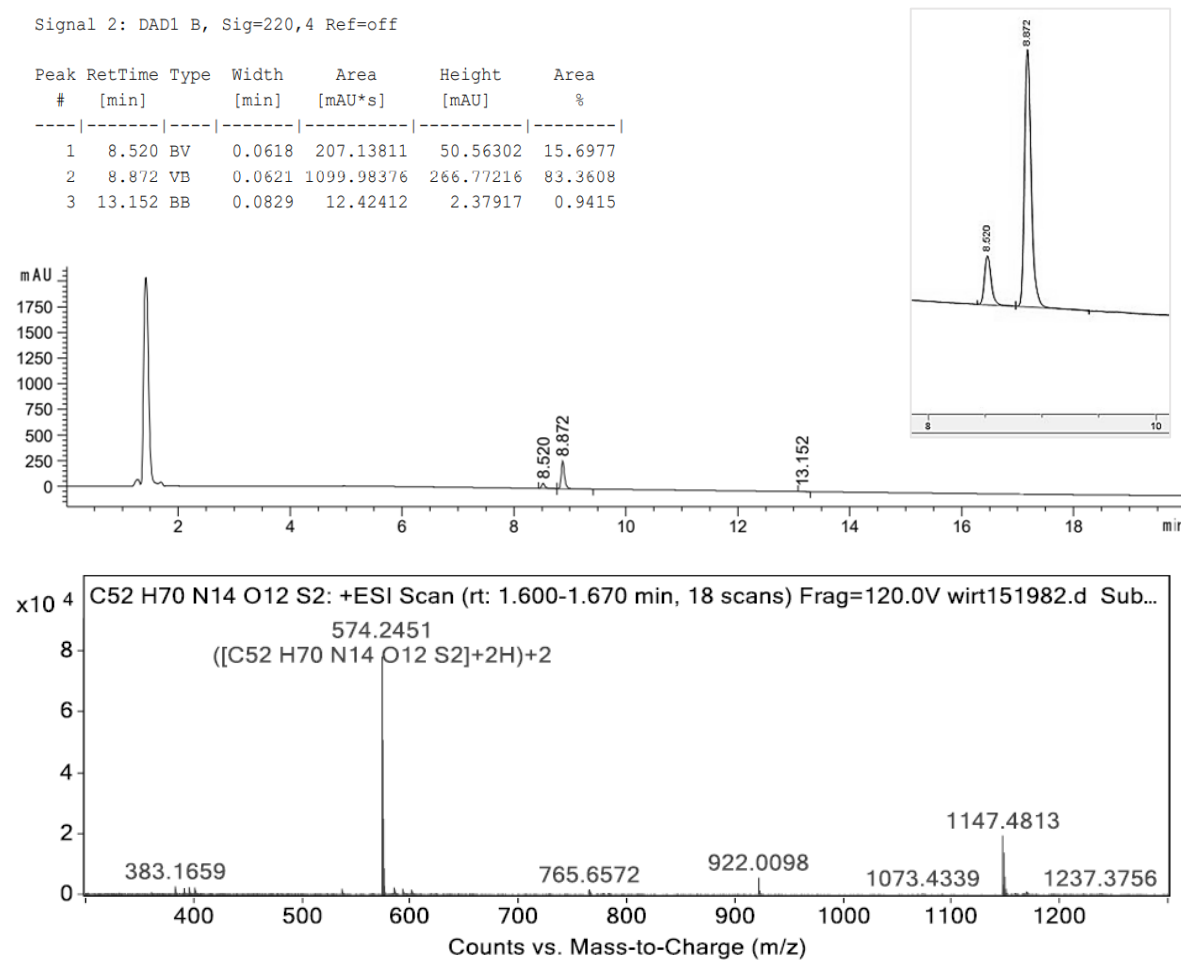
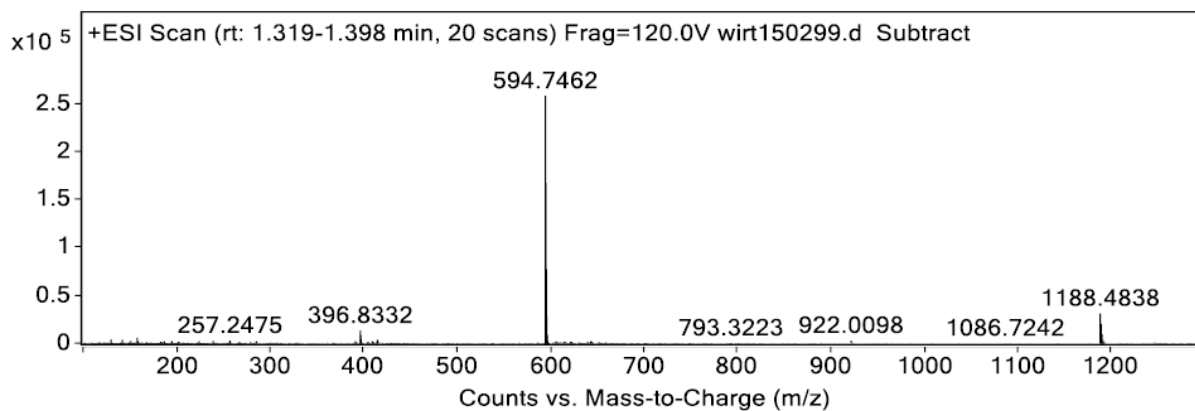
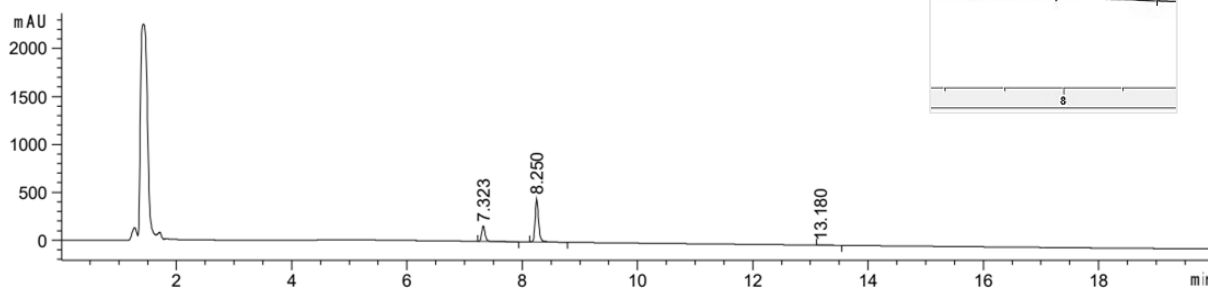


Figure S4. Analytical C₁₈-RP-HPLC trace and high-resolution mass spectrum of **11**.

Purity: **99%** (*cis*-Isomer: 26% + *trans*-isomer: 74%)

Signal 2: DAD1 B, Sig=220,4 Ref=off

Peak #	RetTime [min]	Type	Width [min]	Area [mAU*s]	Height [mAU]	Area %
1	7.323	BB	0.0645	664.36975	159.92587	25.8232
2	8.250	BB	0.0659	1898.35449	444.14838	73.7867
3	13.180	BB	0.0810	10.03463	1.92021	0.3900

**Figure S5.** Analytical C₁₈-RP-HPLC trace and high-resolution mass spectrum of **12**.

Purity: **98%** (*cis*-Isomer: 18% + *trans*-isomer: 81%)

Signal 2: DAD1 B, Sig=220,4 Ref=off

Peak #	RetTime [min]	Type	Width [min]	Area [mAU*s]	Height [mAU]	Area %
1	6.827	VB	0.0654	19.16032	4.35307	0.9534
2	7.855	BV	0.0616	360.17862	92.14953	17.9224
3	8.027	VB	0.0599	1622.89905	412.86786	80.7549
4	13.198	BB	0.0954	7.42210	1.11909	0.3693

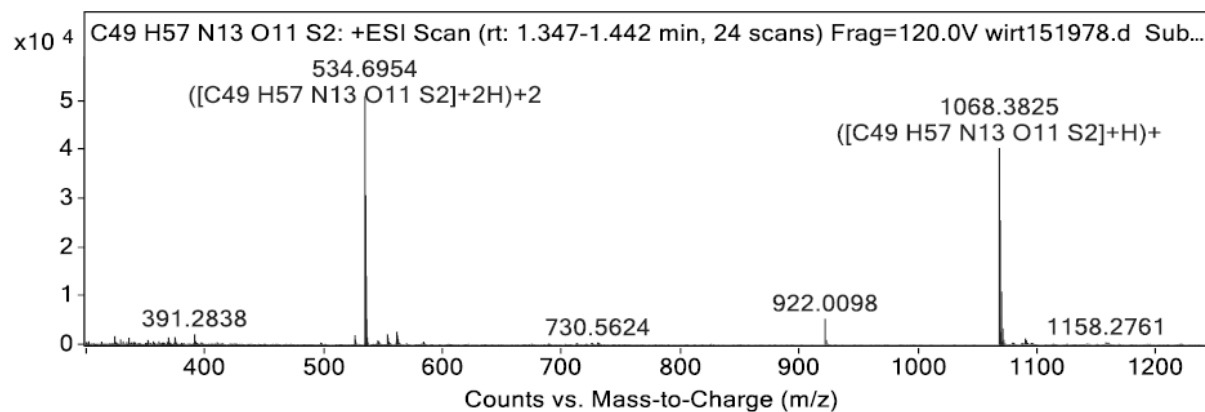
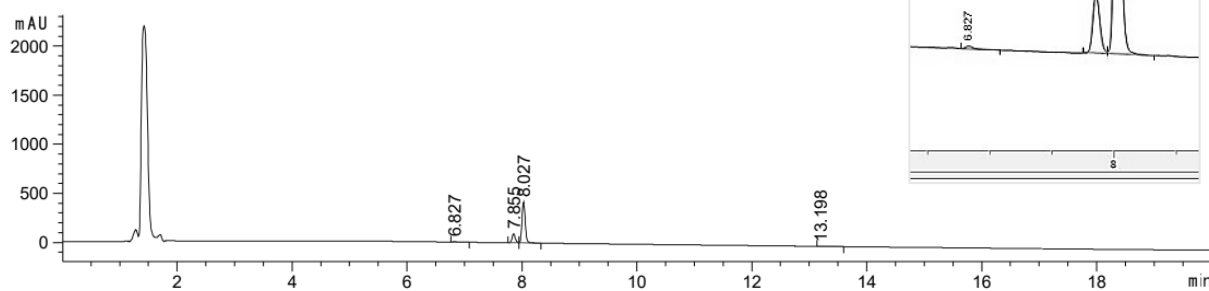


Figure S6. Analytical C₁₈-RP-HPLC trace and high-resolution mass spectrum of **13**.

Purity: **99%** (*cis*-Isomer: 13% + *trans*-isomer: 87%)

Signal 2: DAD1 B, Sig=220,4 Ref=off

Peak #	RetTime [min]	Type	Width [min]	Area [mAU*s]	Height [mAU]	Area %
1	7.368	BV E	0.0602	298.77222	75.39442	13.1674
2	7.504	VB R	0.0645	1963.04138	472.67993	86.5145
3	13.198	BB	0.0905	7.21912	1.16171	0.3182

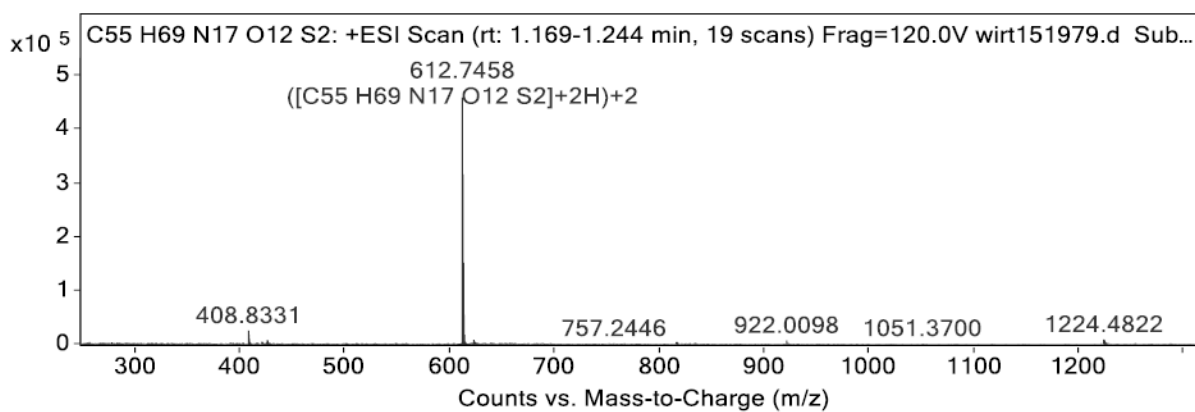
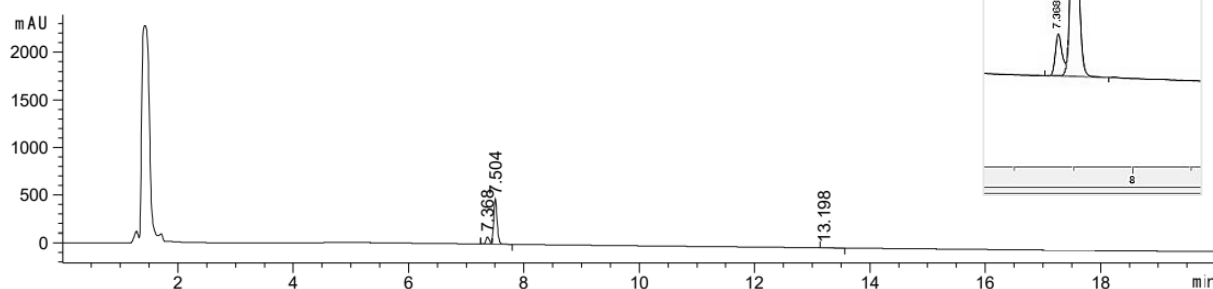


Figure S7. Analytical C_{18} -RP-HPLC trace and high-resolution mass spectrum of **14**.

Purity: **99%** (*cis*-Isomer: 29% + *trans*-isomer: 70%)

Signal 2: DAD1 B, Sig=220,4 Ref=off

Peak #	RetTime [min]	Type	Width [min]	Area [mAU*s]	Height [mAU]	Area %
1	3.957	BB	0.0885	27.36912	4.80377	1.2536
2	8.267	BV	0.0645	1525.45618	367.16348	69.8716
3	8.470	VB	0.0610	630.40137	156.56445	28.8748

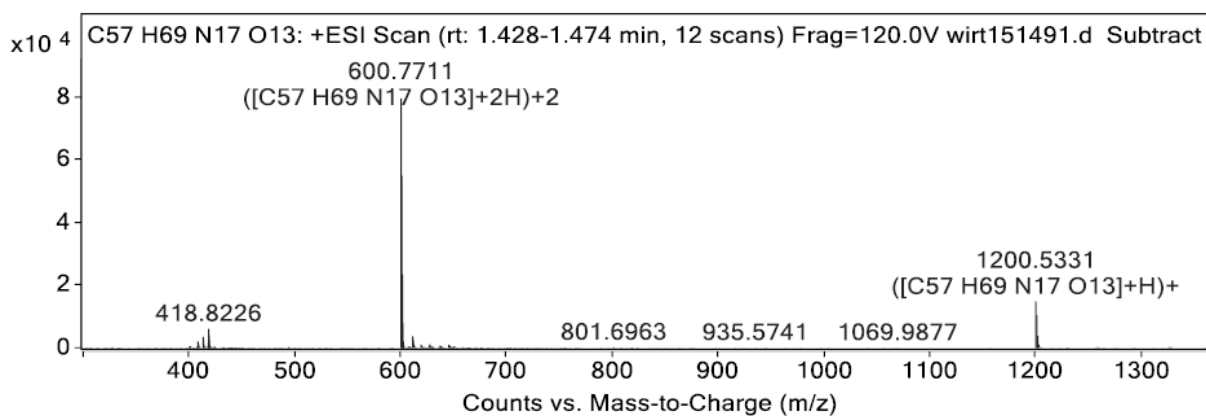
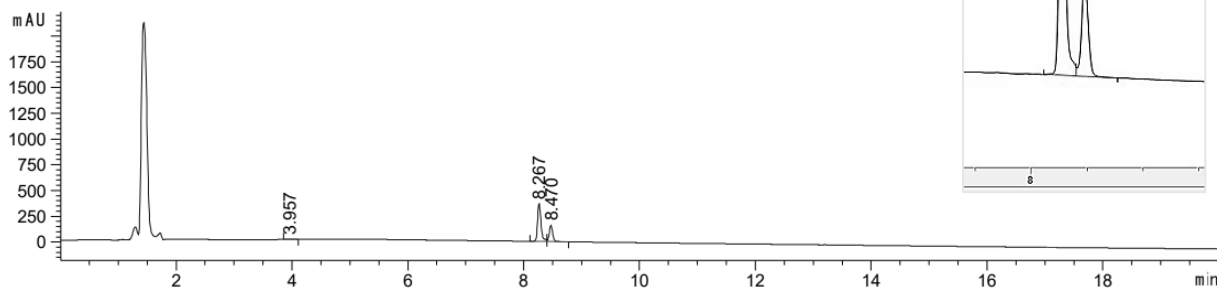
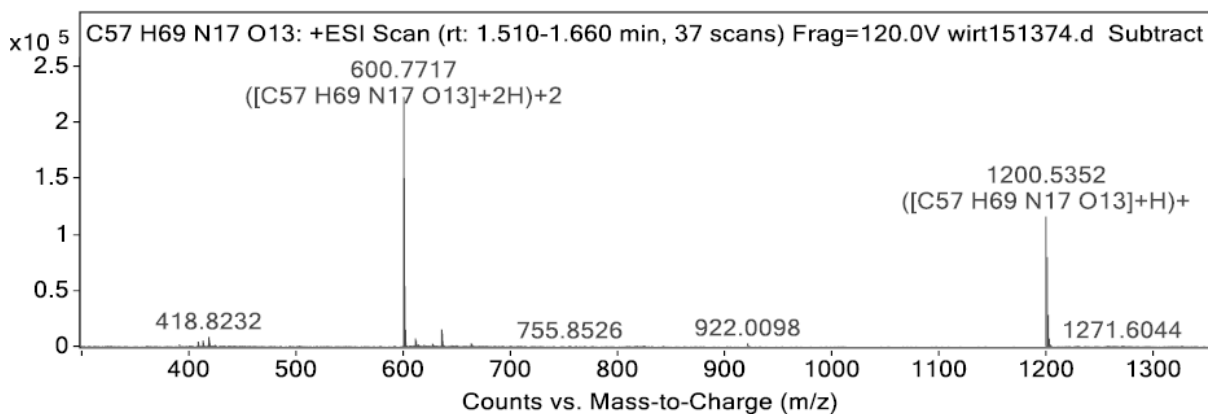
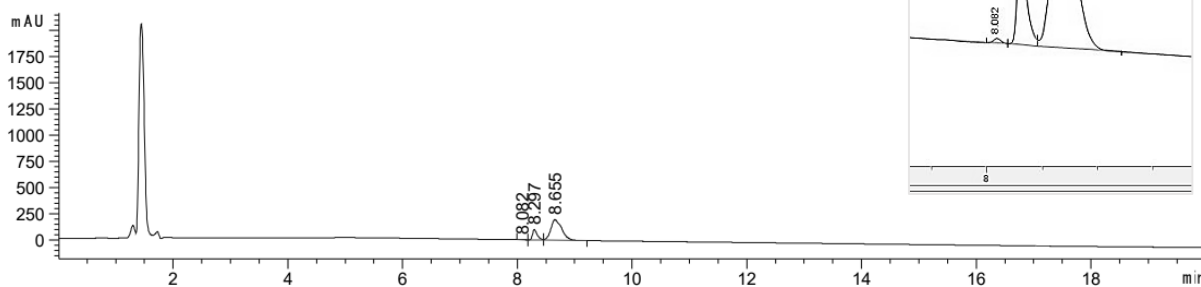


Figure S8. Analytical C_{18} -RP-HPLC trace and high-resolution mass spectrum of **15**.

Purity: **99%** (*cis*-Isomer: 18% + *trans*-isomer: 81%)

Signal 2: DAD1 B, Sig=220,4 Ref=off

Peak #	RetTime [min]	Type	Width [min]	Area [mAU*s]	Height [mAU]	Area %
1	8.082	BV	0.0732	21.57994	4.55996	0.6797
2	8.297	VV	0.0876	566.69836	97.78909	17.8485
3	8.655	VB	0.1871	2586.77246	194.57198	81.4718

**Figure S9.** Analytical C₁₈-RP-HPLC trace and high-resolution mass spectrum of **16**.

Purity: **99%** (*cis*-Isomer: 13% + *trans*-isomer: 87%)

Signal 2: DAD1 B, Sig=220,4 Ref=off

Peak #	RetTime [min]	Type	Width [min]	Area [mAU*s]	Height [mAU]	Area %
1	8.050	BV	0.0916	297.20914	47.13602	13.4929
2	8.641	VB	0.0657	1905.49341	447.25916	86.5071

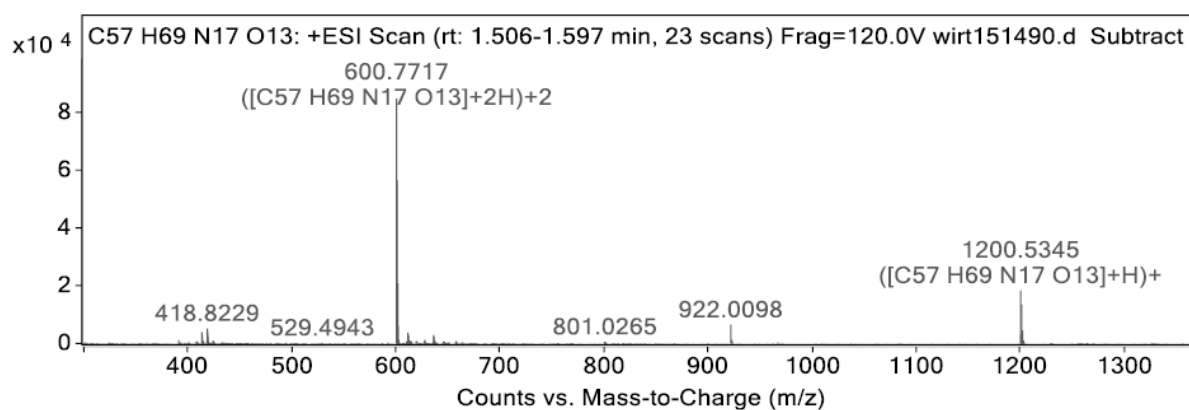
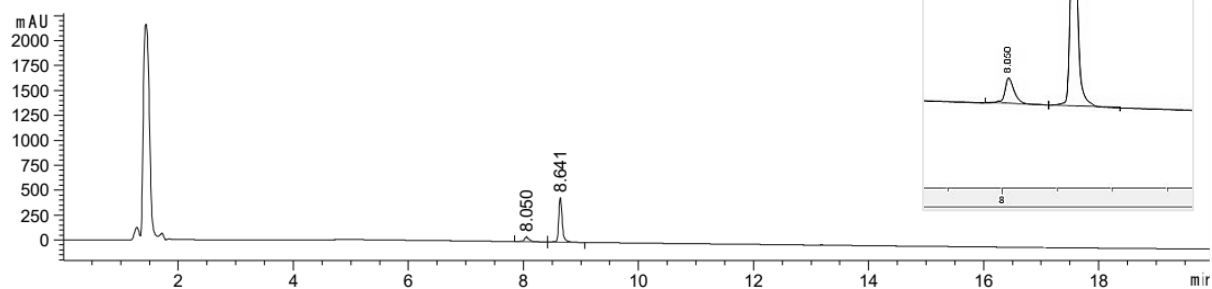
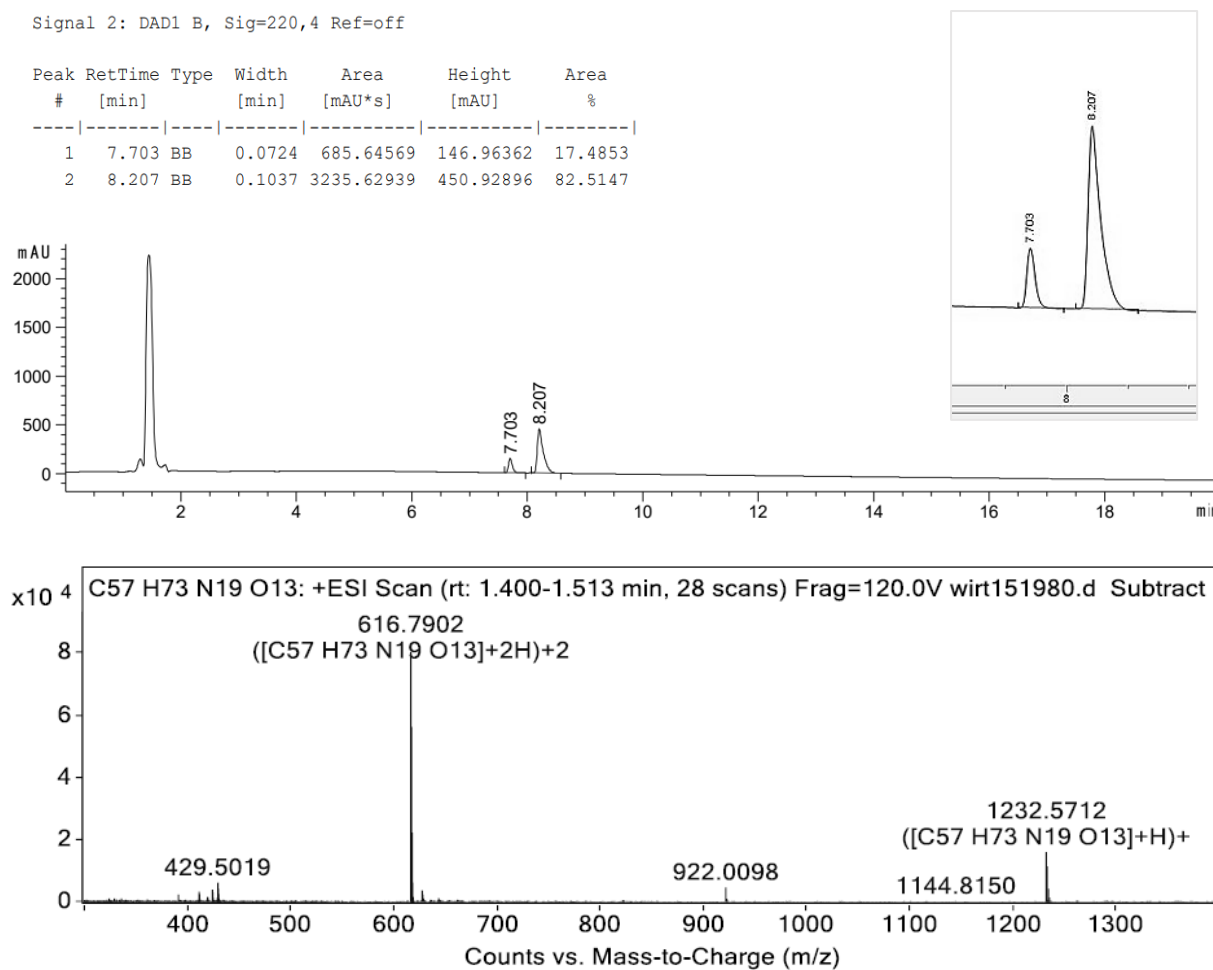


Figure S10. Analytical C_{18} -RP-HPLC trace and high-resolution mass spectrum of **17**.

Purity: **99%** (*cis*-Isomer: 17% + *trans*-isomer: 83%)**Figure S11.** Analytical C_{18} -RP-HPLC trace and high-resolution mass spectrum of **18**.

Purity: **99%** (*cis*-Isomer: 25% + *trans*-isomer: 75%)

Signal 2: DAD1 B, Sig=220,4 Ref=off

Peak #	RetTime [min]	Type	Width [min]	Area [mAU*s]	Height [mAU]	Area %
1	7.632	BB	0.0874	873.05621	146.69434	24.6998
2	8.231	BB	0.0637	2661.60620	650.82031	75.3002

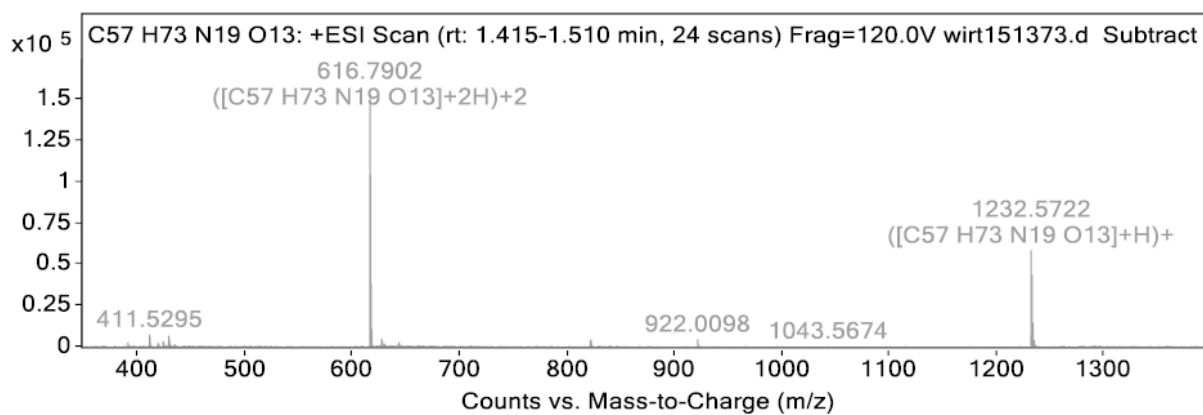
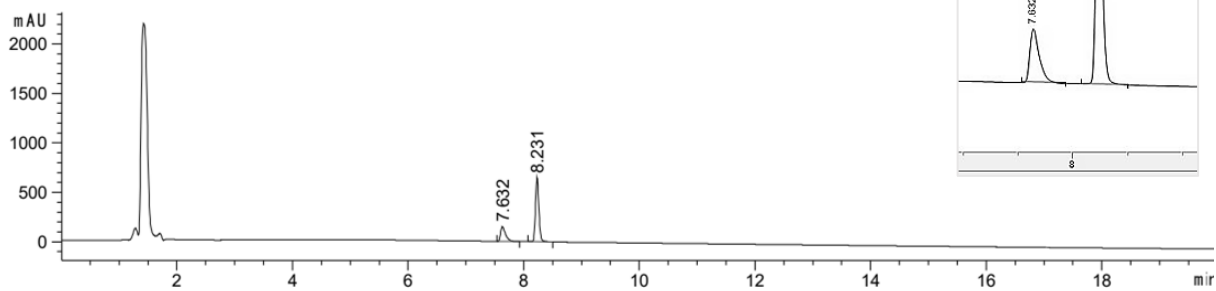


Figure S12. Analytical C₁₈-RP-HPLC trace and high-resolution mass spectrum of **19**.

4.8.2 Photophysical Characterization

4.8.2.1 UV/Vis Spectra and Cycle Performance

UV/Vis spectra were measured in HEPES buffer (20 μ M + 0.1% DMSO). The spectra were measured in quartz glass cuvettes. First, the solution was illuminated with 340 nm for 10 s to switch to the *cis*-isomer. After measuring the UV/Vis spectra of the *cis*-isomers, the solution was illuminated at 420 nm (**8-17**) or 528 nm (**18** and **19**) for 60 s, respectively, and the spectra for the *trans*-isomer were measured.

To assess the cycle performance, the solutions were irradiated alternating with 340 nm and 420 nm (**8-17**) or 528 nm (**18** and **19**). A UV/Vis spectrum was measured after each switching step. This was repeated ten times to show the stability of the compounds. The absorption of the maximum of the *trans*-isomer was plotted against the cycle number.

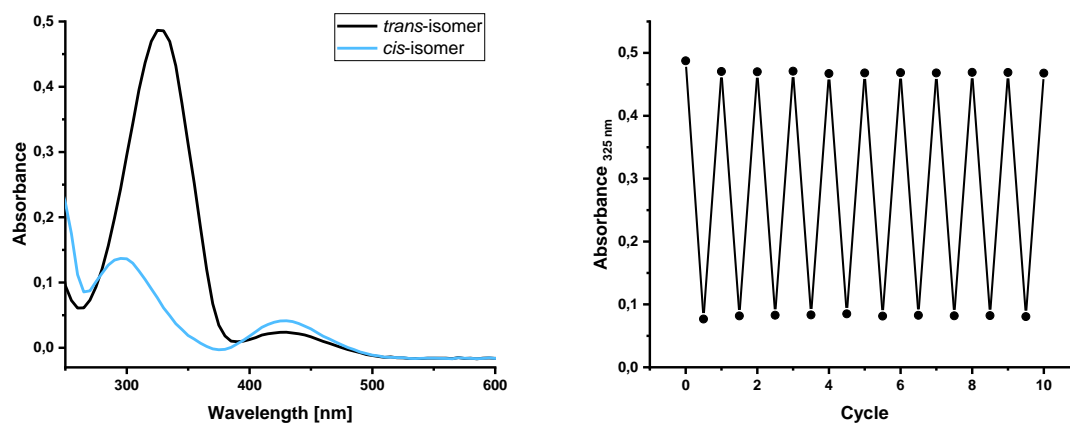


Figure S13. UV/Vis spectra and cycle performance of **8**.

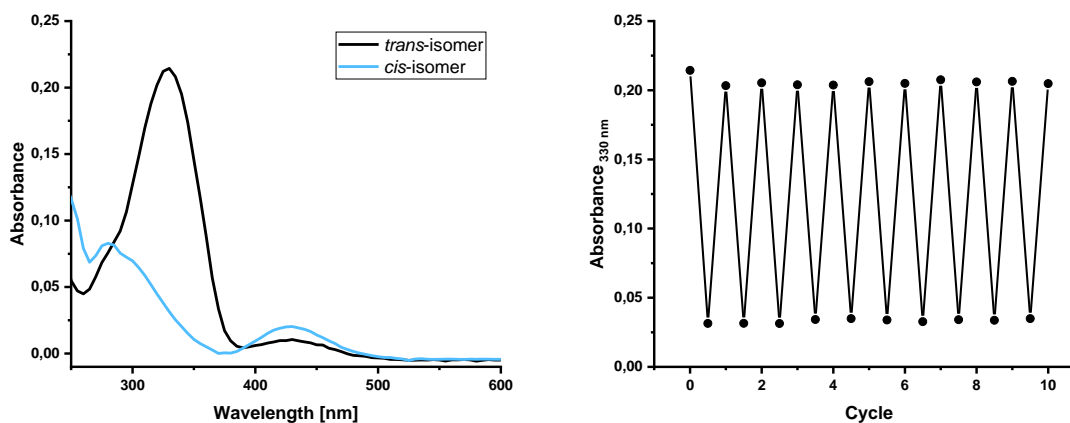


Figure S14. UV/Vis spectra and cycle performance of **9**.

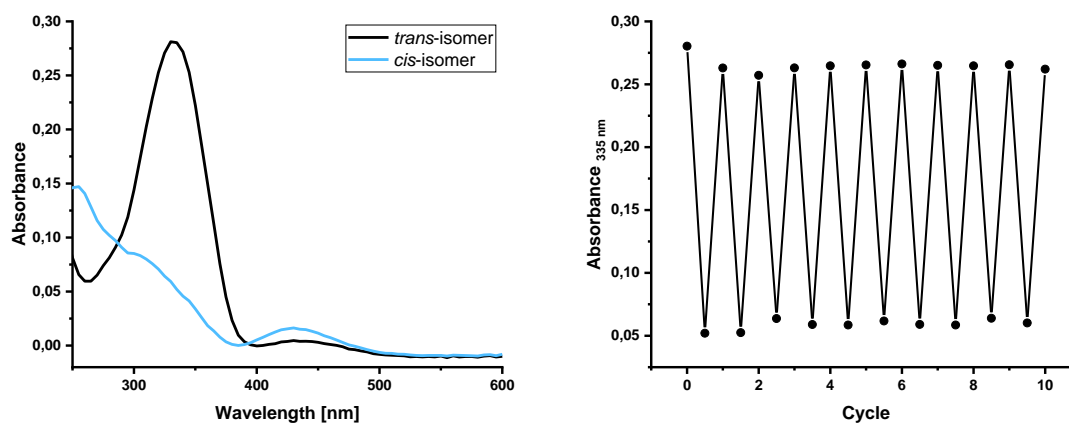


Figure S15. UV/Vis spectra and cycle performance of 10.

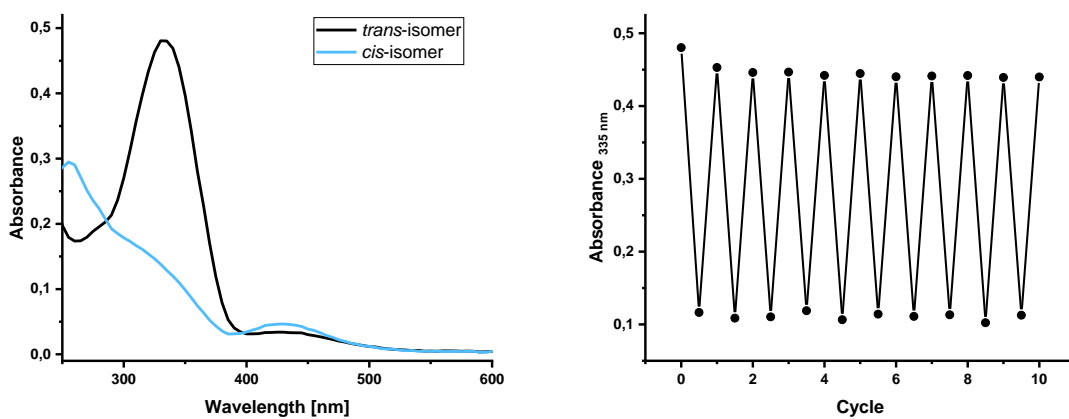


Figure S16. UV/Vis spectra and cycle performance of 11.

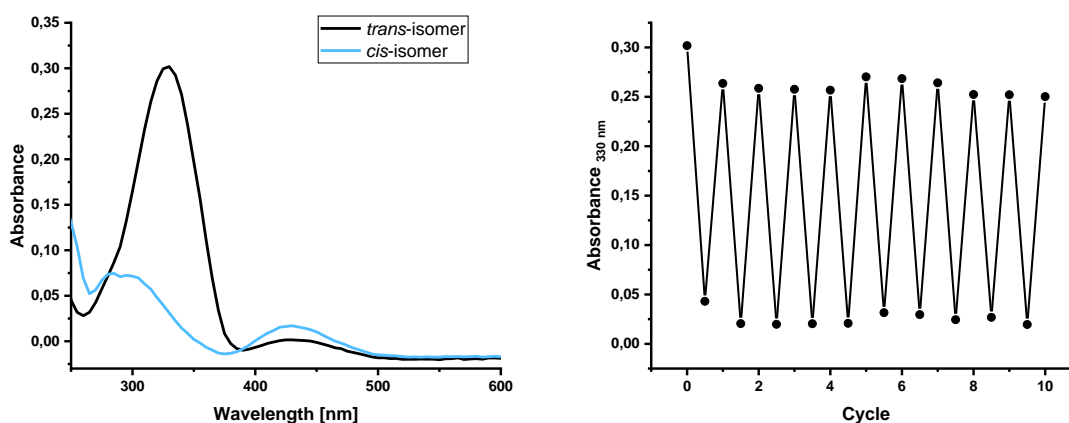


Figure S17. UV/Vis spectra and cycle performance of 12.

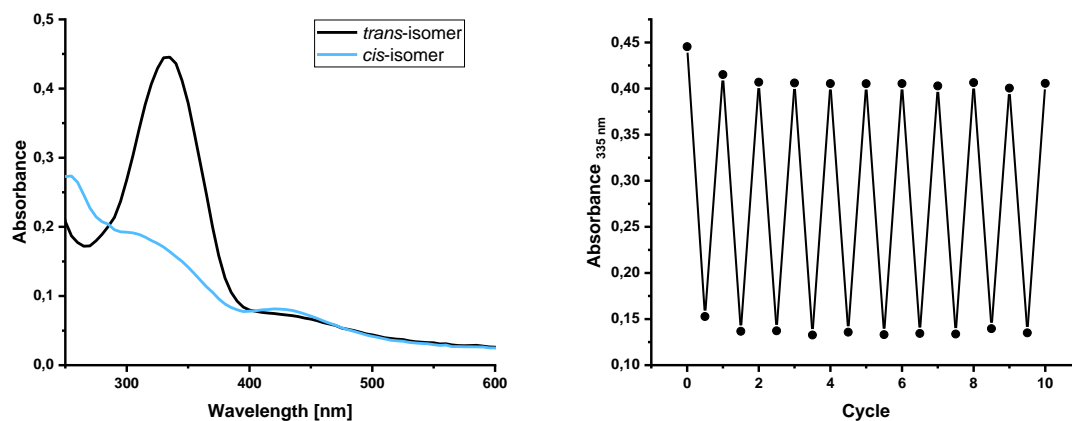


Figure S18. UV/Vis spectra and cycle performance of 13.

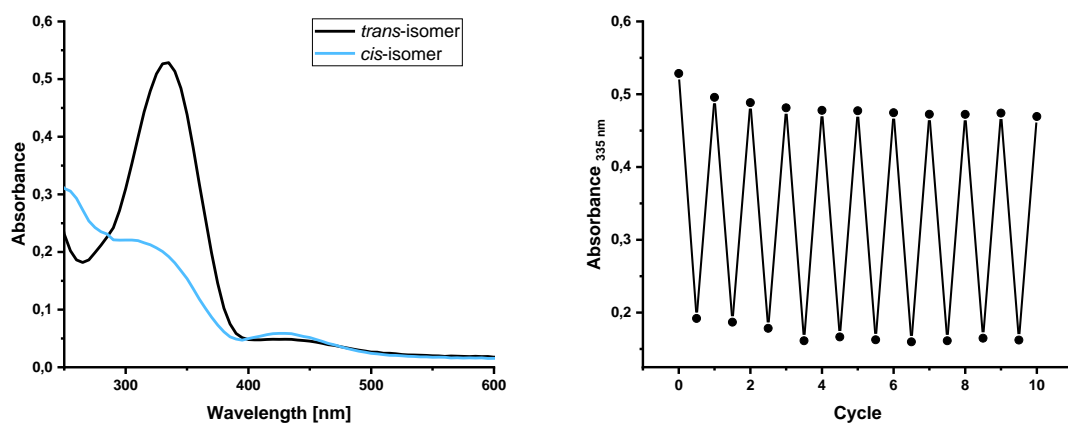


Figure S19. UV/Vis spectra and cycle performance of 14.

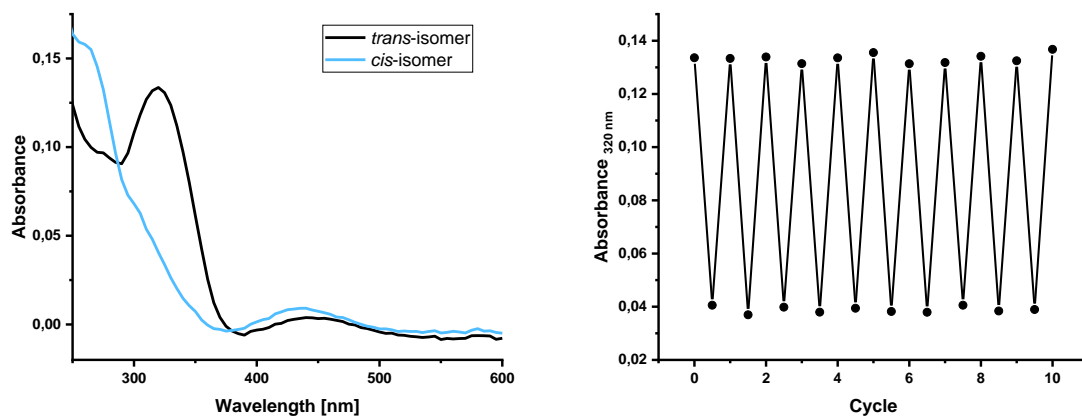


Figure S20. UV/Vis spectra and cycle performance of 15.

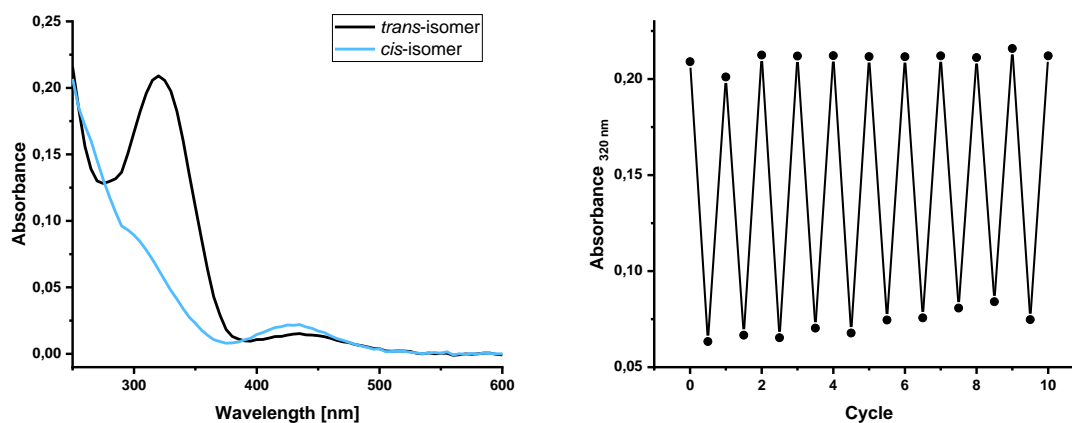


Figure S21. UV/Vis spectra and cycle performance of 16.

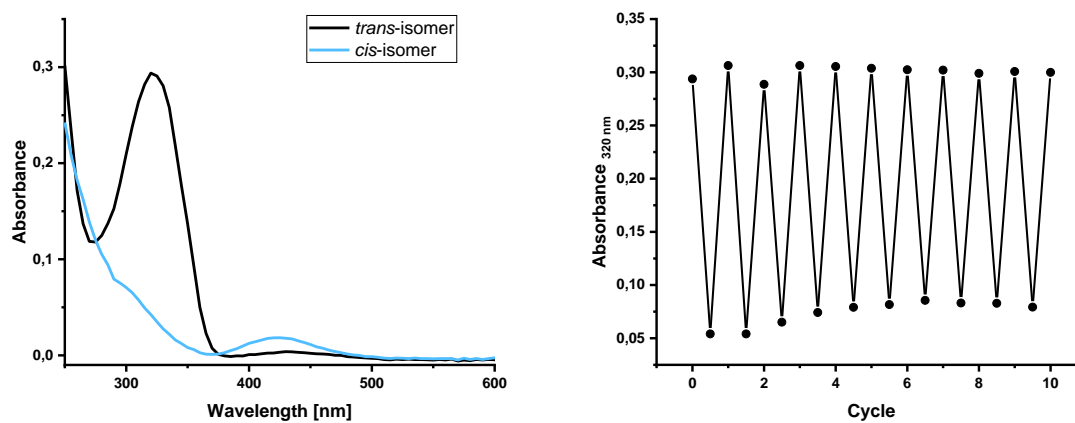


Figure S22. UV/Vis spectra and cycle performance of 17.

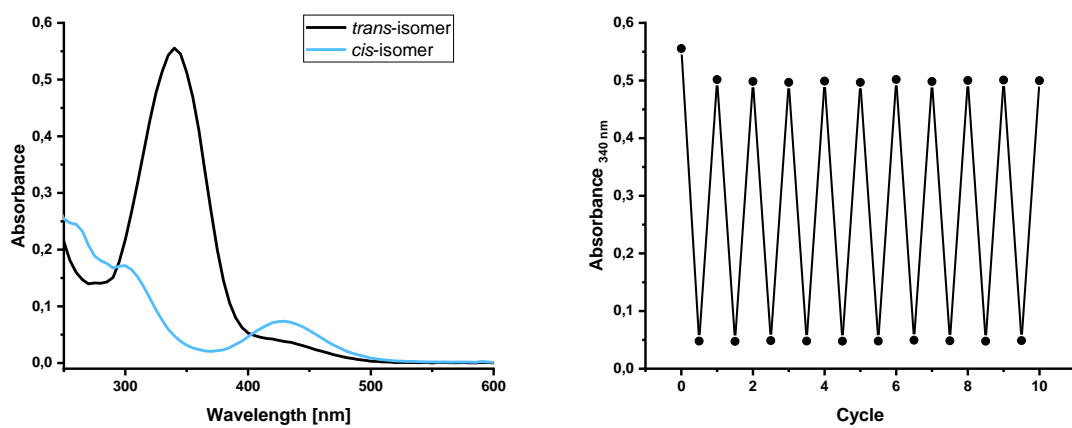


Figure S23. UV/Vis spectra and cycle performance of 18.

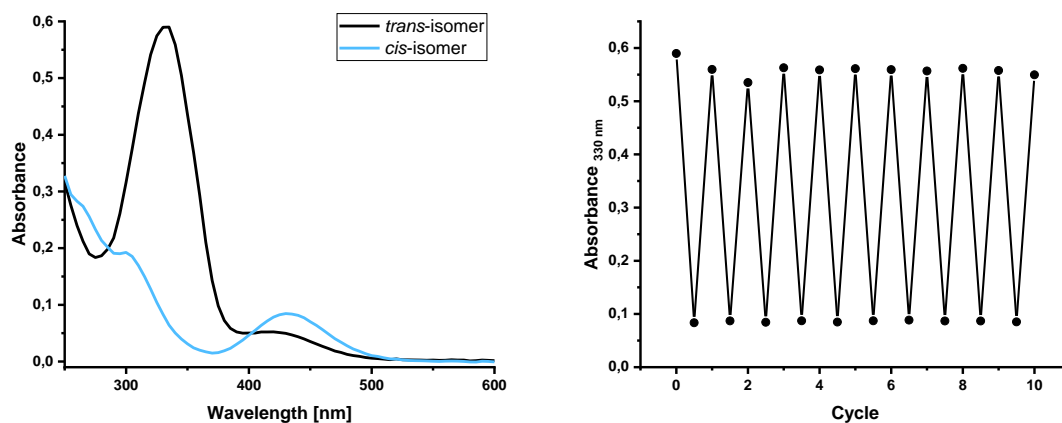


Figure S24. UV/Vis spectra and cycle performance of 19.

4.8.2.2 Photostationary States

Photostationary states (PSS) were measured on analytical C₁₈-RP-HPLC (flow: 0.3 mL/min, solvent A: H₂O (0.05% TFA), solvent B: MeCN). To determine the PSS of the photoswitches the samples (in 0.1 mM in HEPES buffer + 1% DMSO) were irradiated first with 340 nm to get the *Z*-isomer. Afterwards, the sample was irradiated with 420 nm (**8-17**) or 528 nm (**18** and **19**), respectively, to get back to the *E*-isomer. The samples were measured at the isosbestic points.

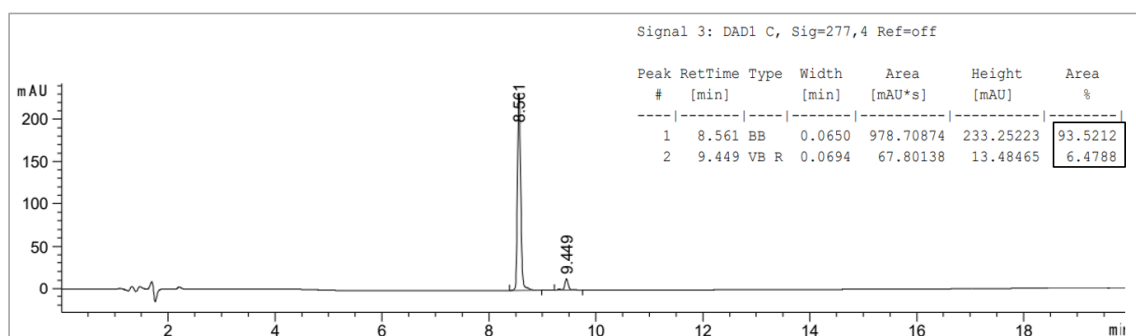


Figure S25. PSS of compound 8 after irradiation with 340 nm.

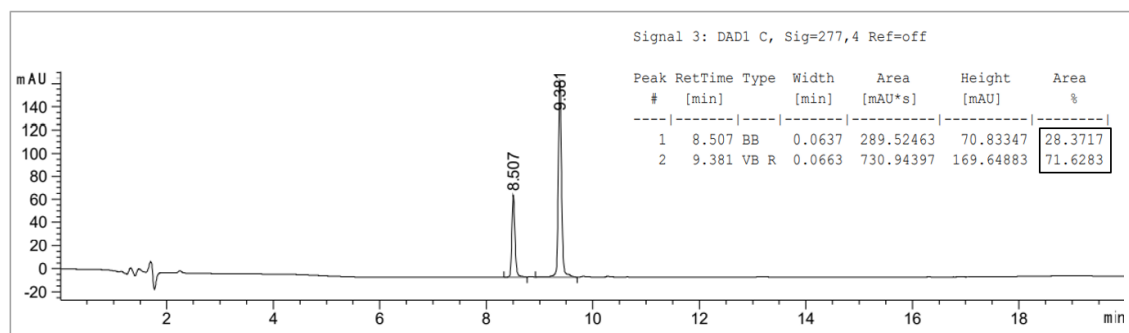


Figure S26. PSS of compound **8** after irradiation with 420 nm.

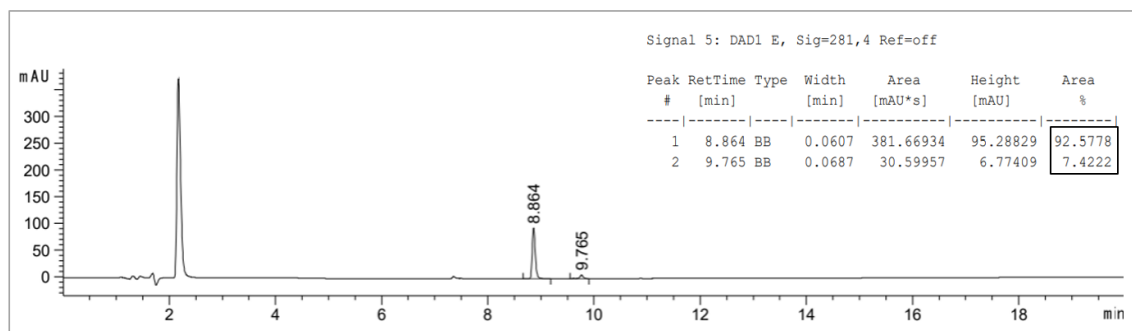


Figure S27. PSS of compound **9** after irradiation with 340 nm.

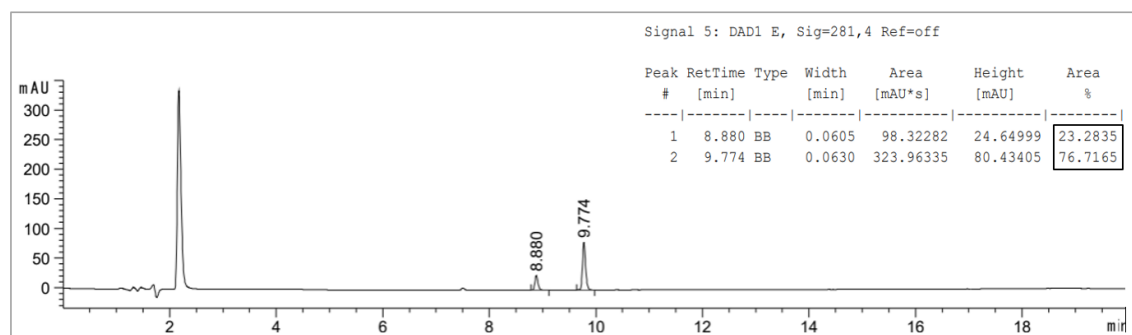


Figure S28. PSS of compound **9** after irradiation with 420 nm.

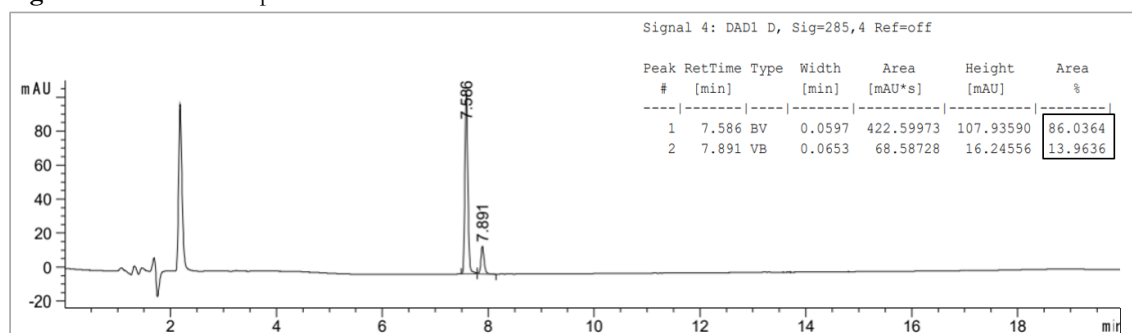
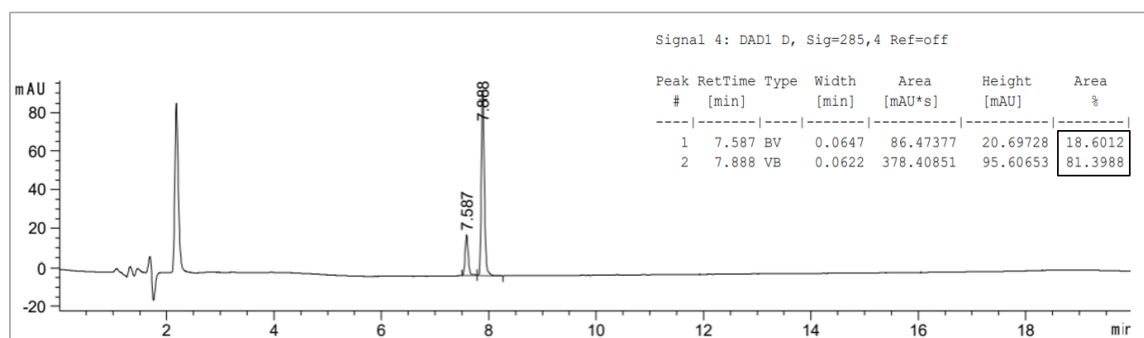
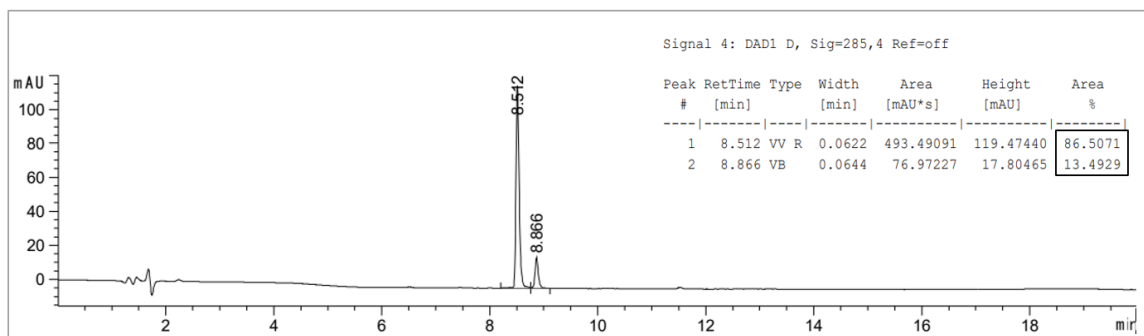
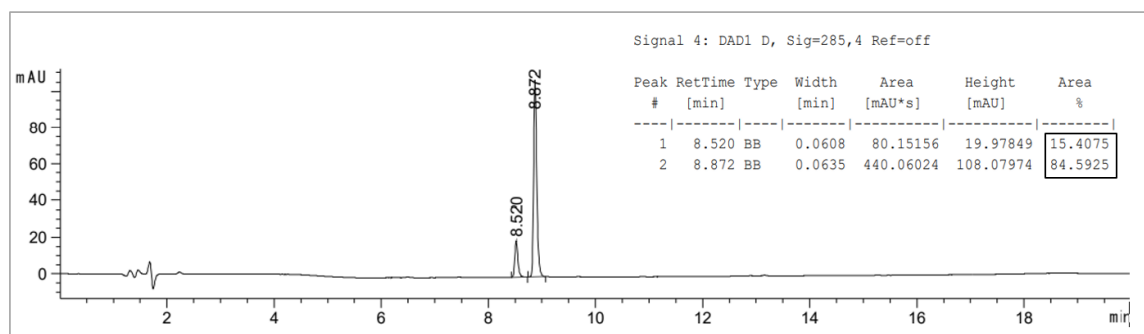
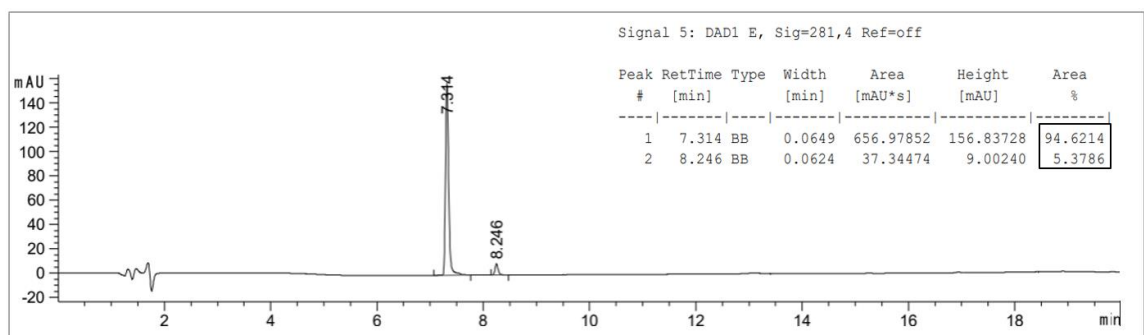
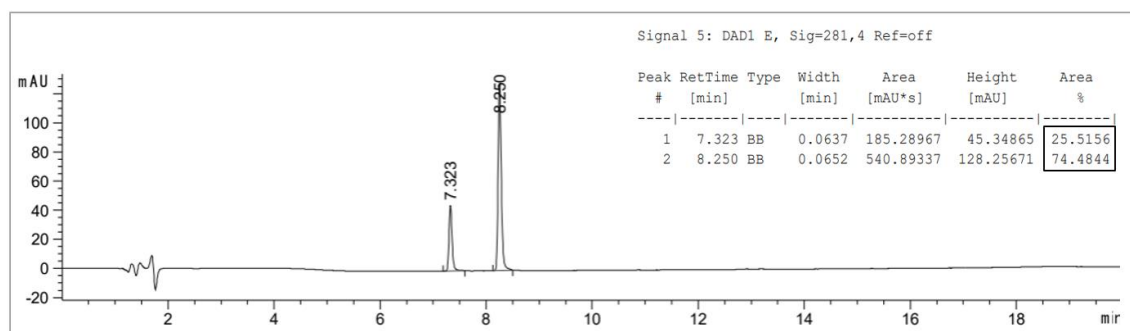
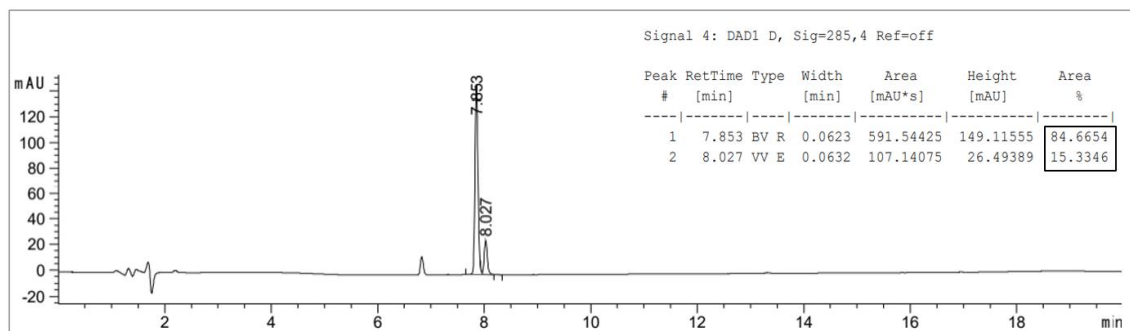
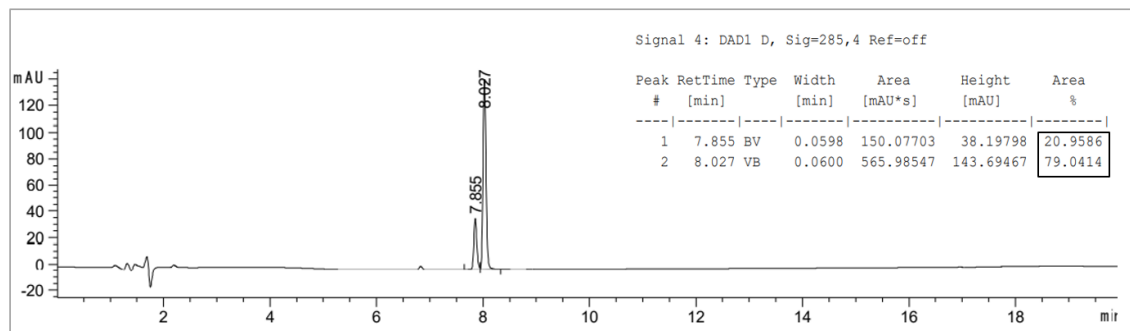
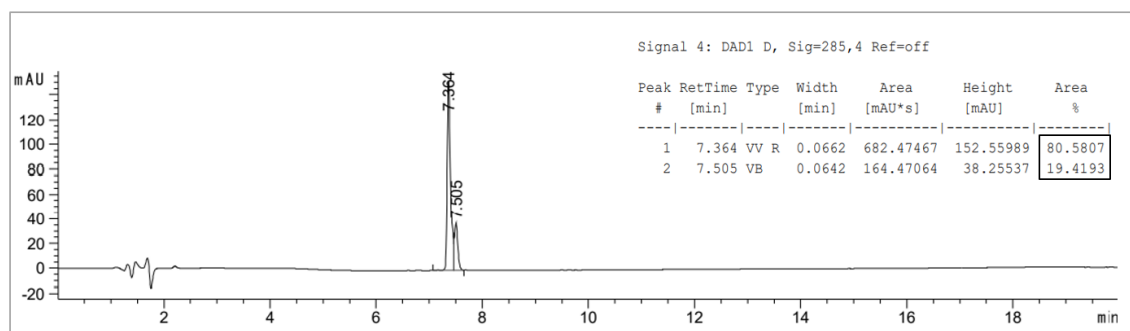


Figure S29. PSS of compound **10** after irradiation with 340 nm.

Figure S30. PSS of compound **10** after irradiation with 420 nm.Figure S31. PSS of compound **11** after irradiation with 340 nm.Figure S32. PSS of compound **11** after irradiation with 420 nm.Figure S33. PSS of compound **12** after irradiation with 340 nm.

Figure S34. PSS of compound **12** after irradiation with 420 nm.Figure S35. PSS of compound **13** after irradiation with 340 nm.Figure S36. PSS of compound **13** after irradiation with 420 nm.Figure S37. PSS of compound **14** after irradiation with 340 nm.

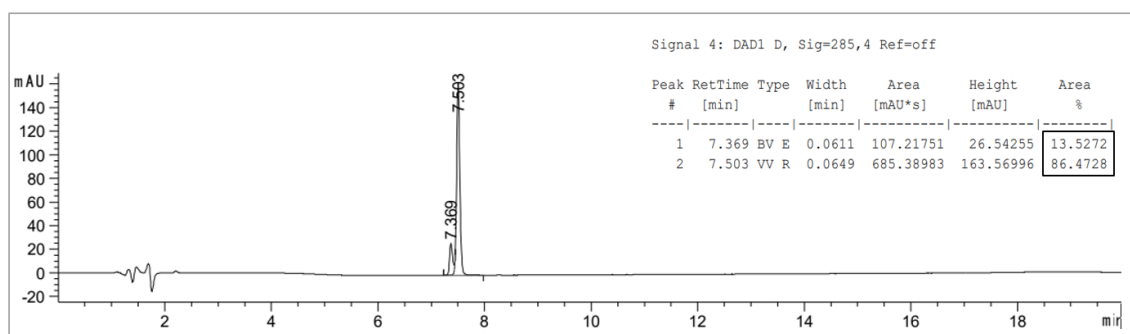


Figure S38. PSS of compound **14** after irradiation with 420 nm.

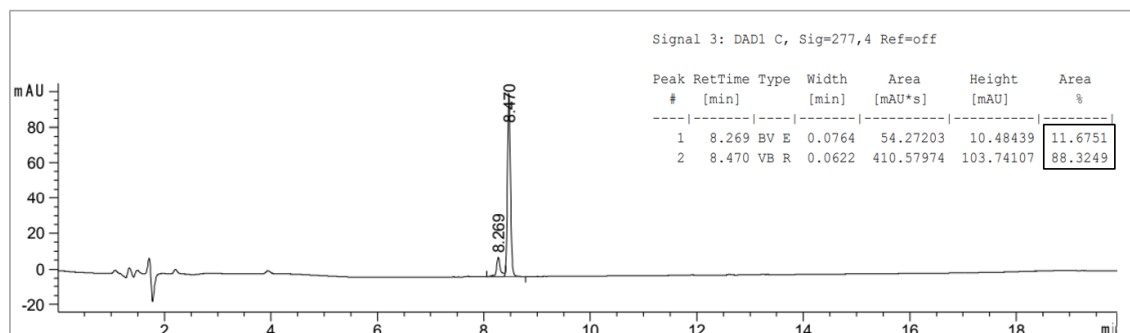


Figure S39. PSS of compound **15** after irradiation with 340 nm (here: *cis*-isomer has longer retention times than *trans*-isomer).

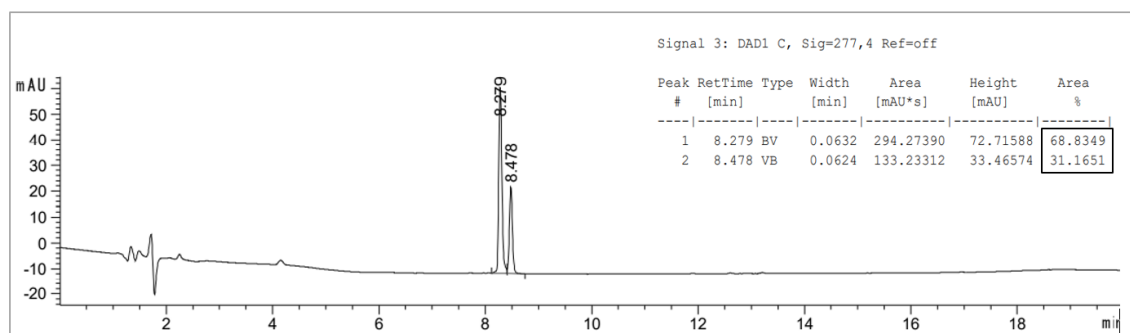


Figure S40. PSS of compound **15** after irradiation with 420 nm (here: *cis*-isomer has longer retention times than *trans*-isomer).

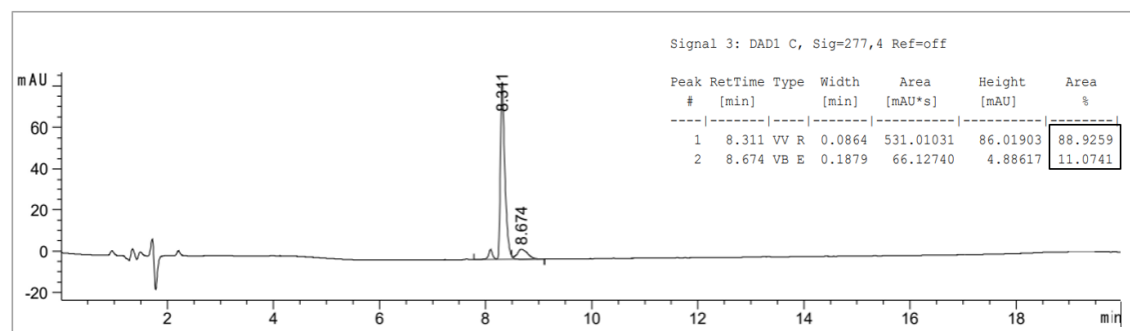


Figure S41. PSS of compound **16** after irradiation with 340 nm.

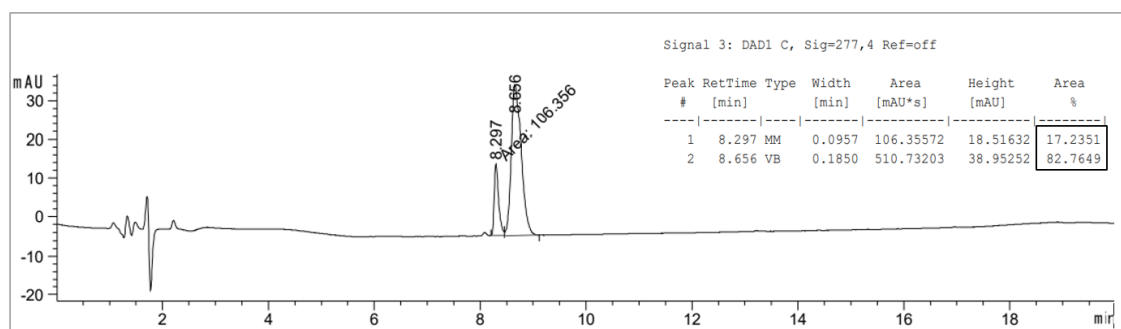


Figure S42. PSS of compound 16 after irradiation with 420 nm.

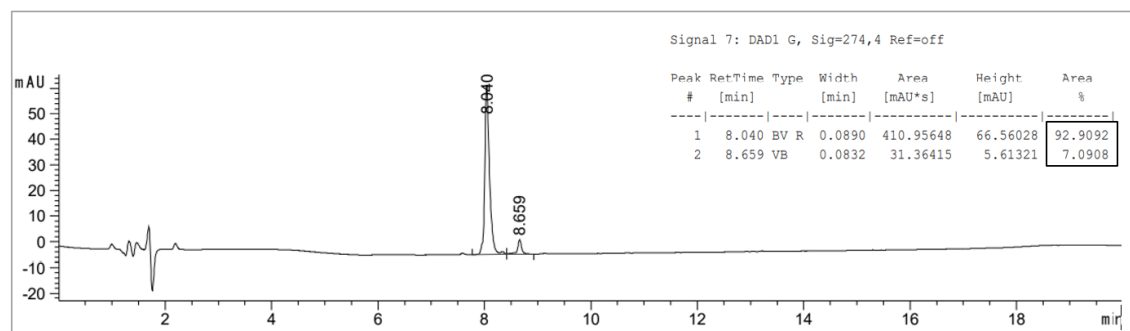


Figure S43. PSS of compound 17 after irradiation with 340 nm.

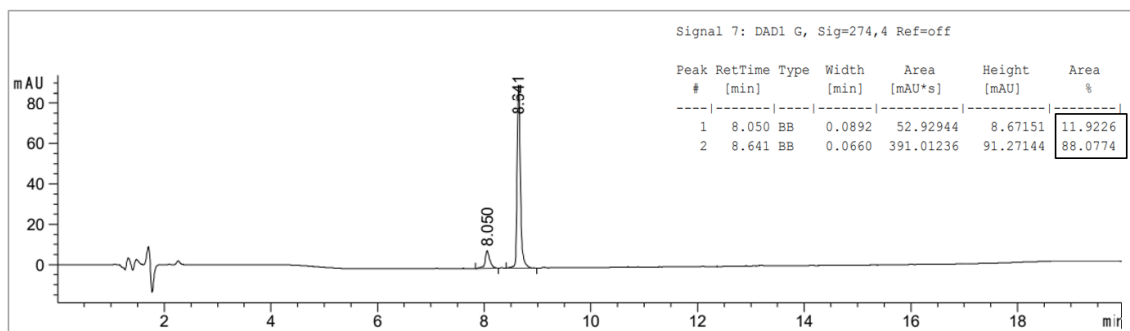


Figure S44. PSS of compound 17 after irradiation with 420 nm.

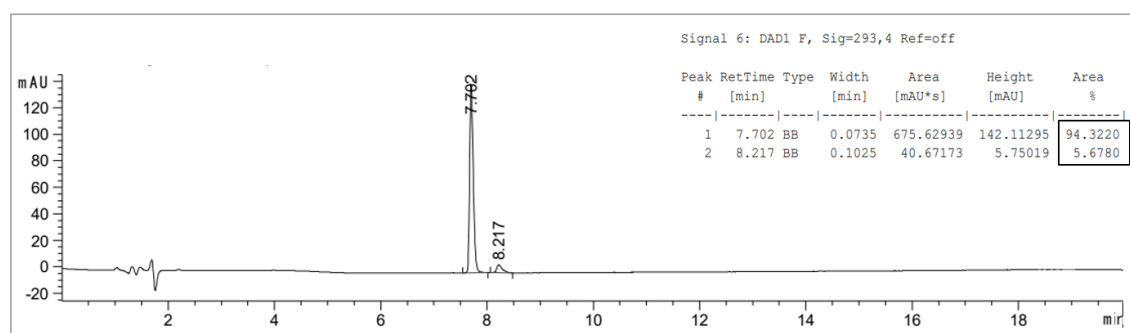


Figure S45. PSS of compound 18 after irradiation with 340 nm.

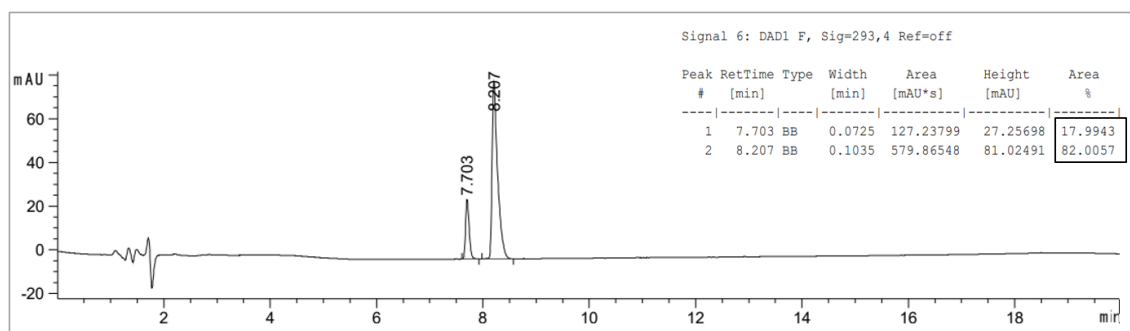


Figure S46. PSS of compound **18** after irradiation with 420 nm.

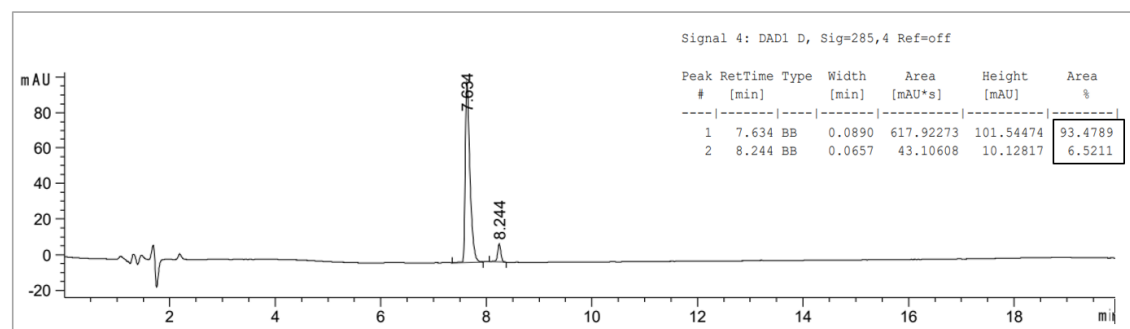


Figure S47. PSS of compound **19** after irradiation with 340 nm.

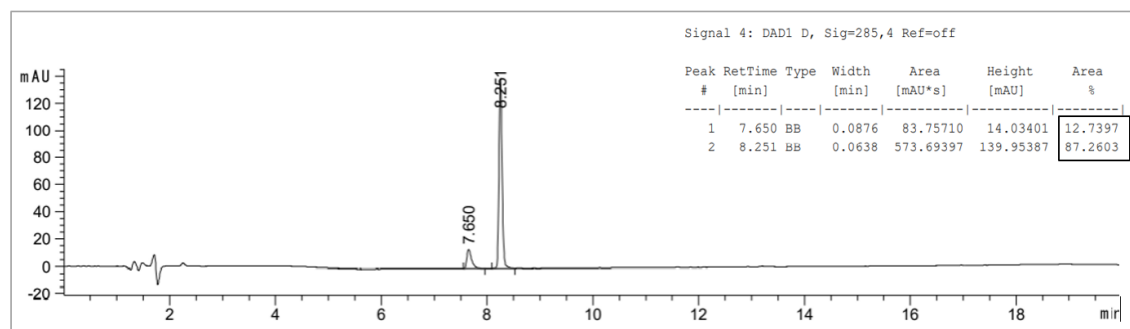
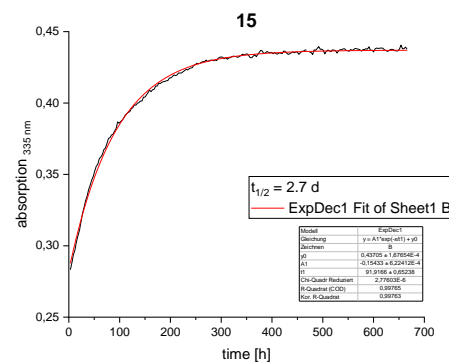
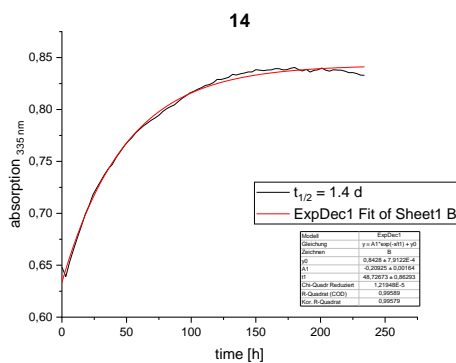
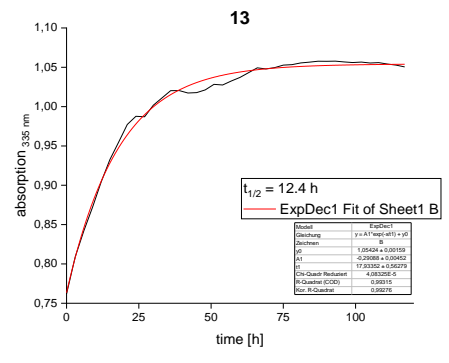
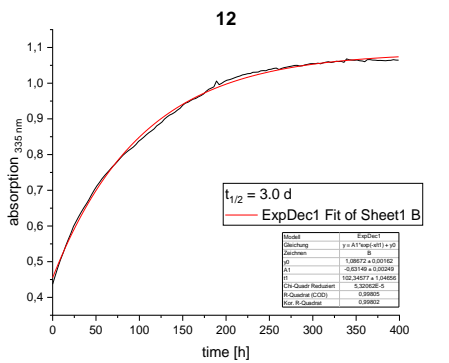
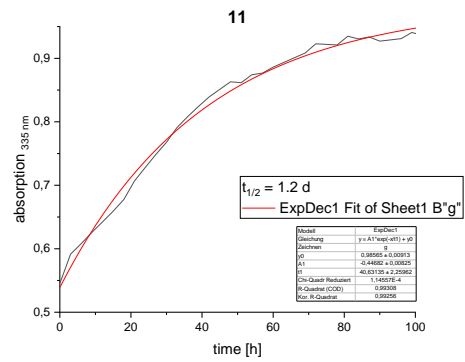
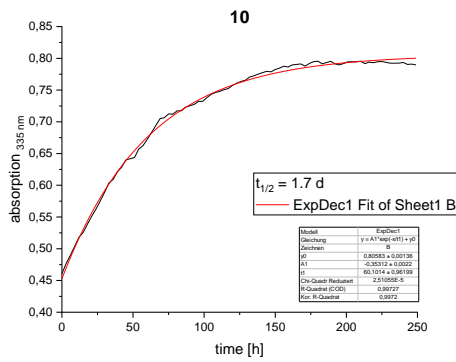
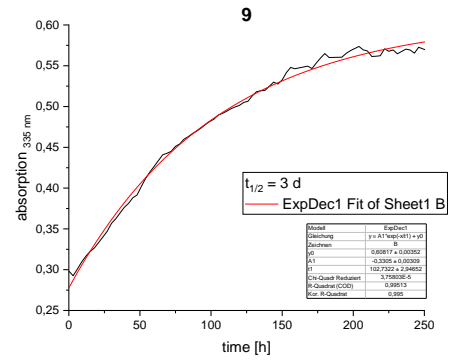
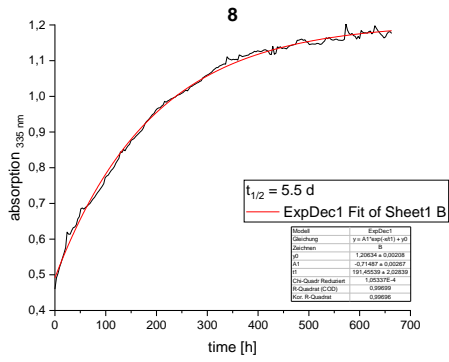


Figure S48. PSS of compound **19** after irradiation with 420 nm.

4.8.2.3 Thermal Half-lives

Thermal half-life was measured in a 96-well plate in a Thermo Scientific Multiskan® Spectrum at 25 °C. The solutions (50 μM in HEPES buffer + 0.25% DMSO) were pre-irradiated with 340 nm. The absorption at 335 nm was measured every 3 h. The data was analyzed using Origin 2021.



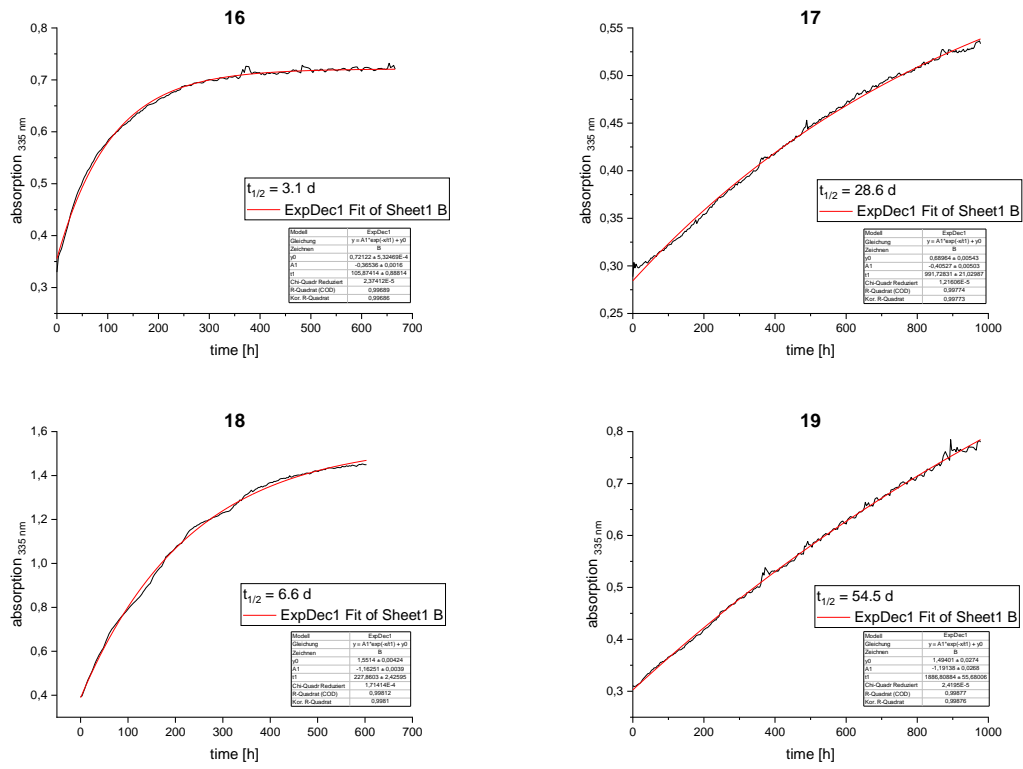


Figure S49. Thermal half-lives of compounds 8-19.

4.8.3 Supplementary Figures

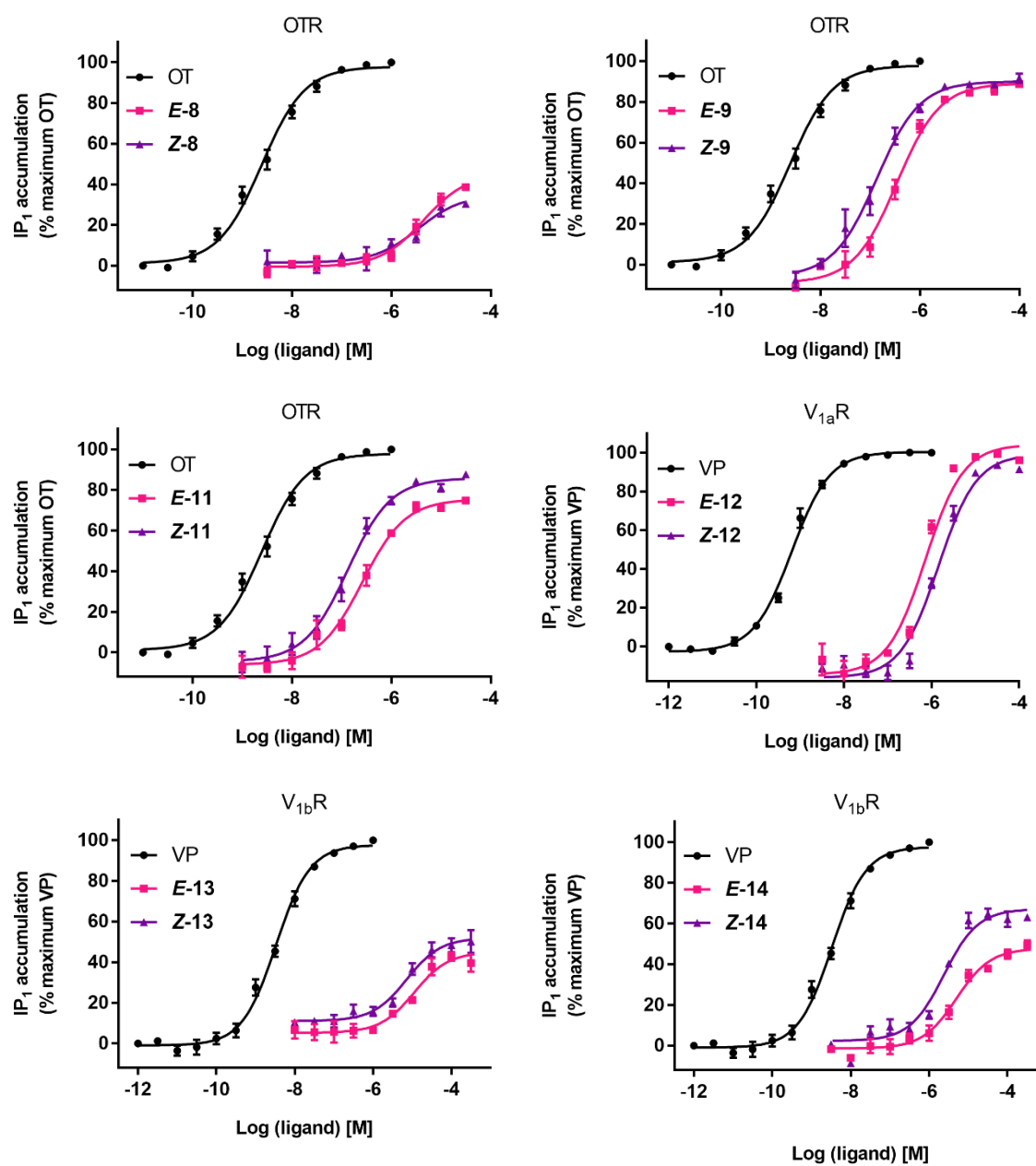


Figure S50. Full-dose-response curves of 19, 20, 22-25 at the respective receptor. Data represent mean values \pm SEM from at least three independent experiments performed in triplicate.

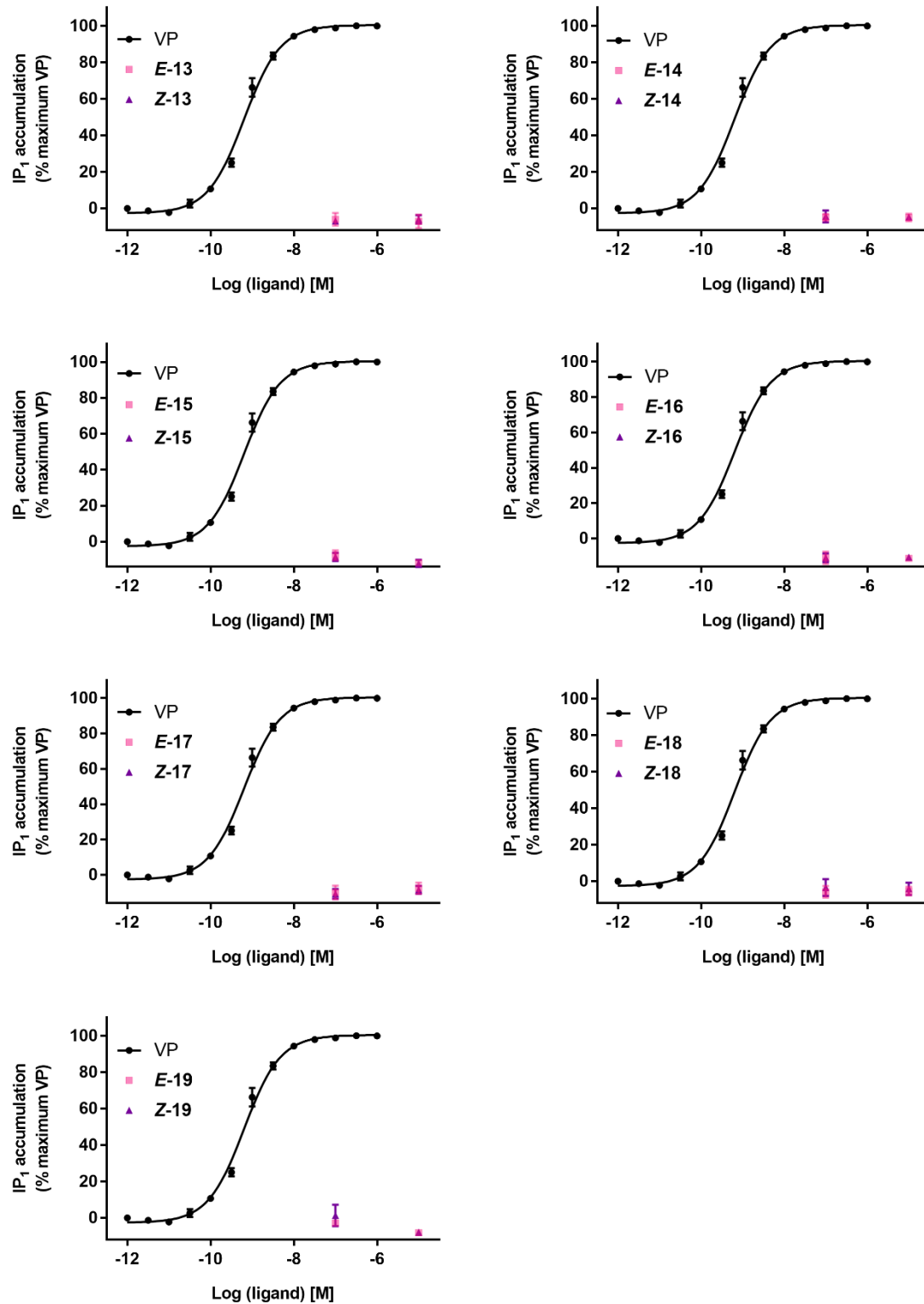


Figure S51. Two-point evaluation of compounds 13-19 at the V_{1a}R. Data represent mean values \pm SEM from at least three independent experiments performed in triplicate.

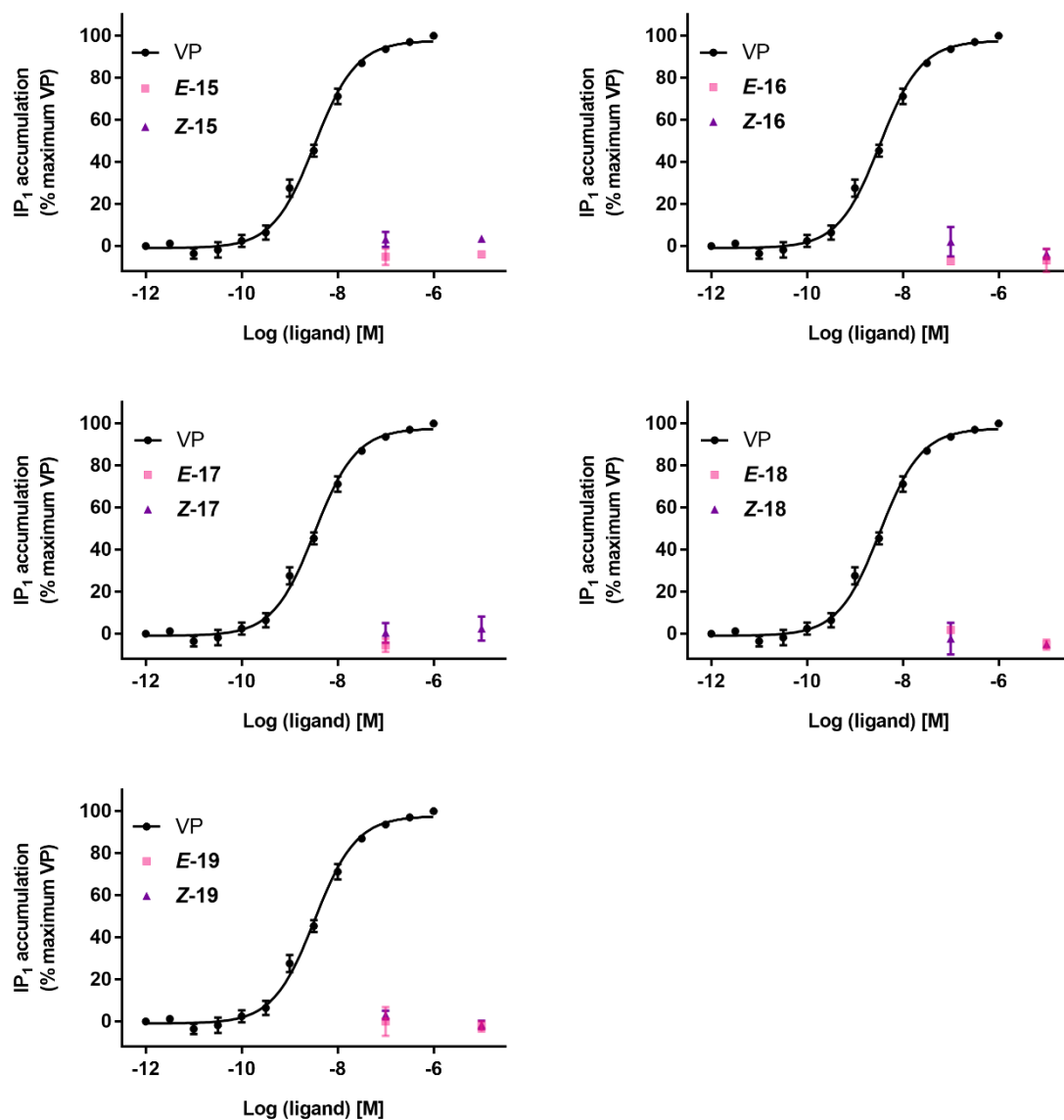
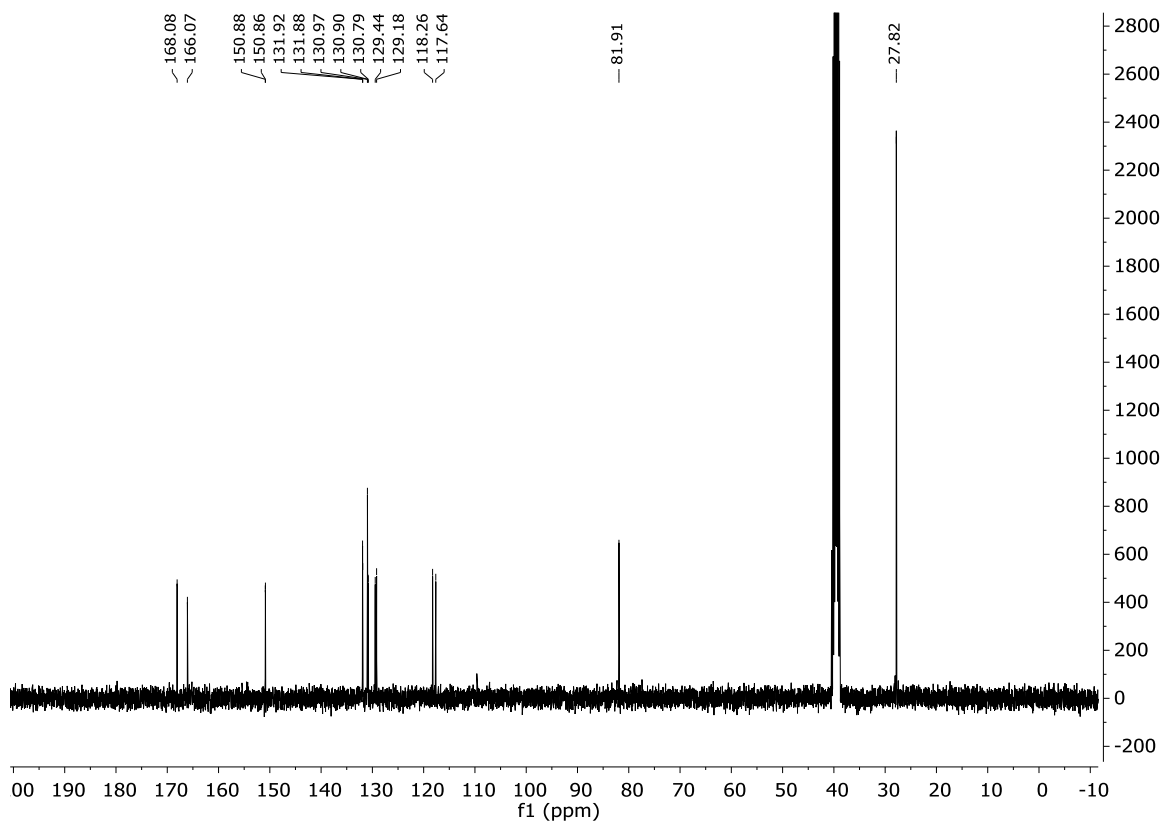
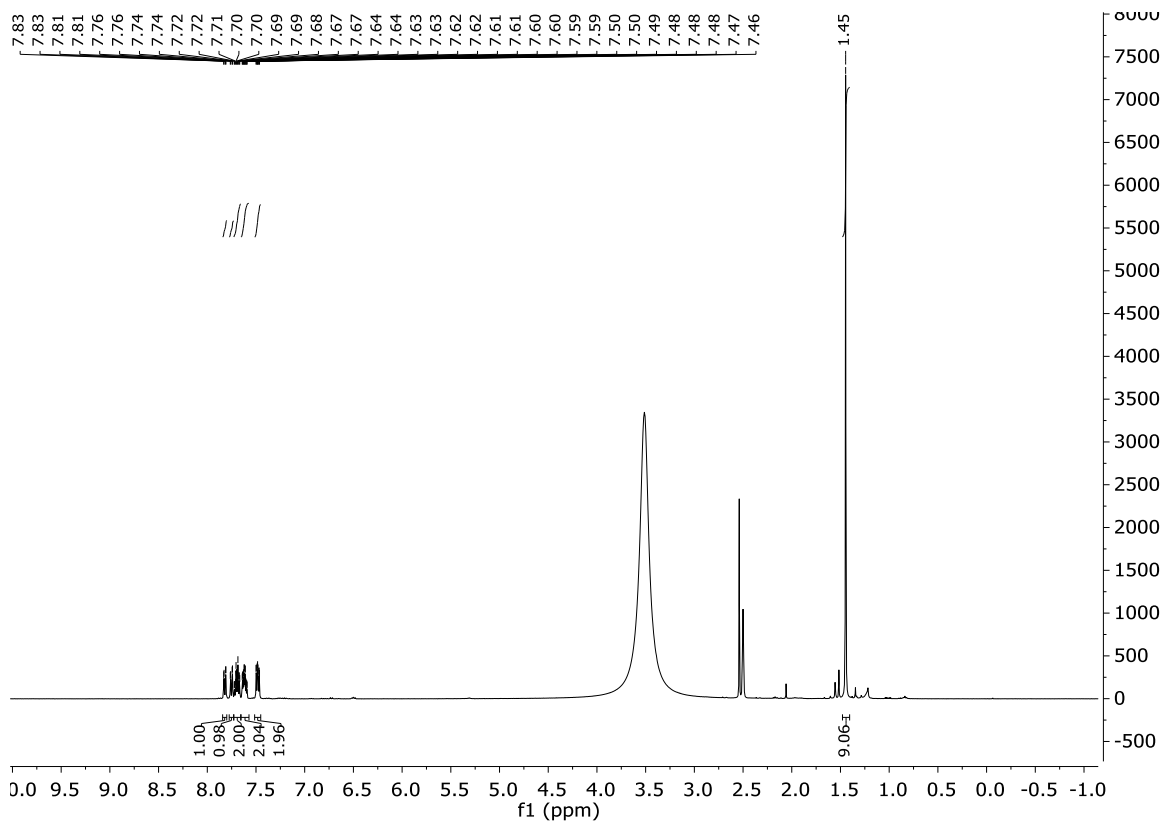


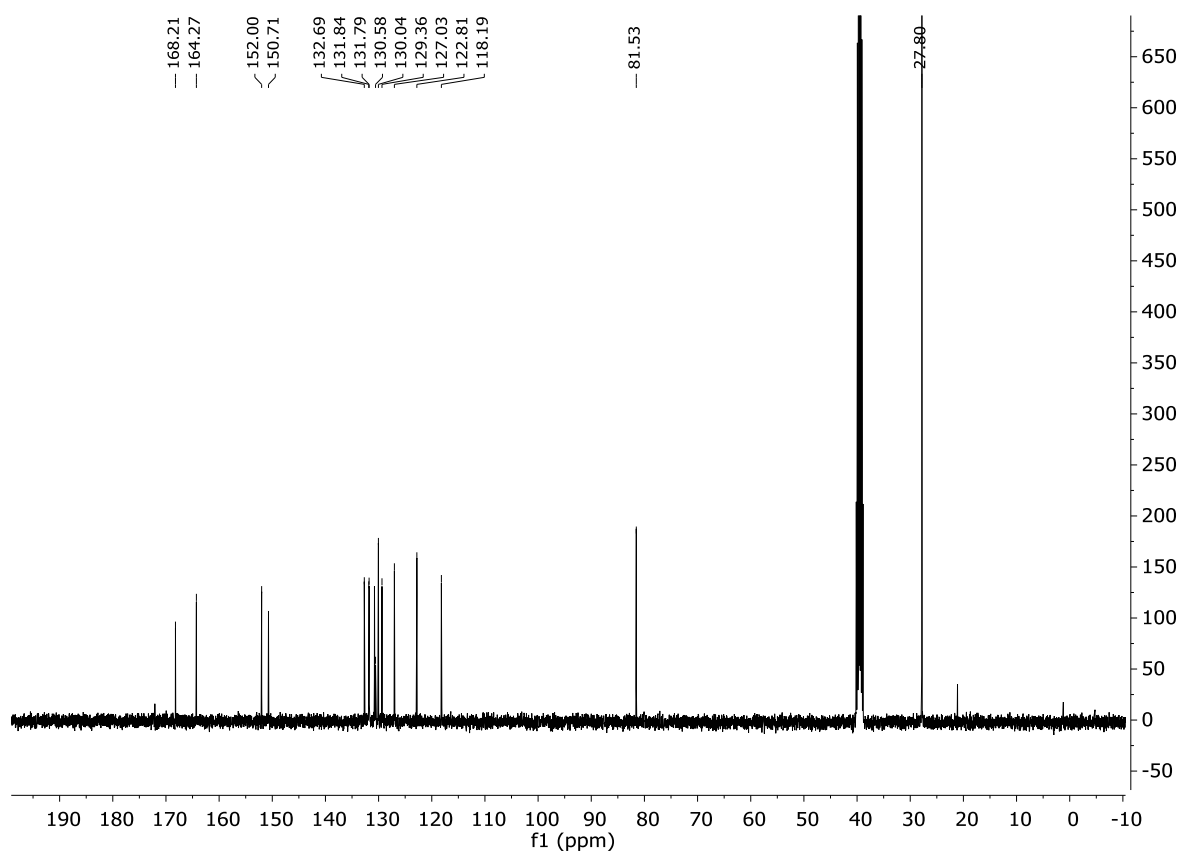
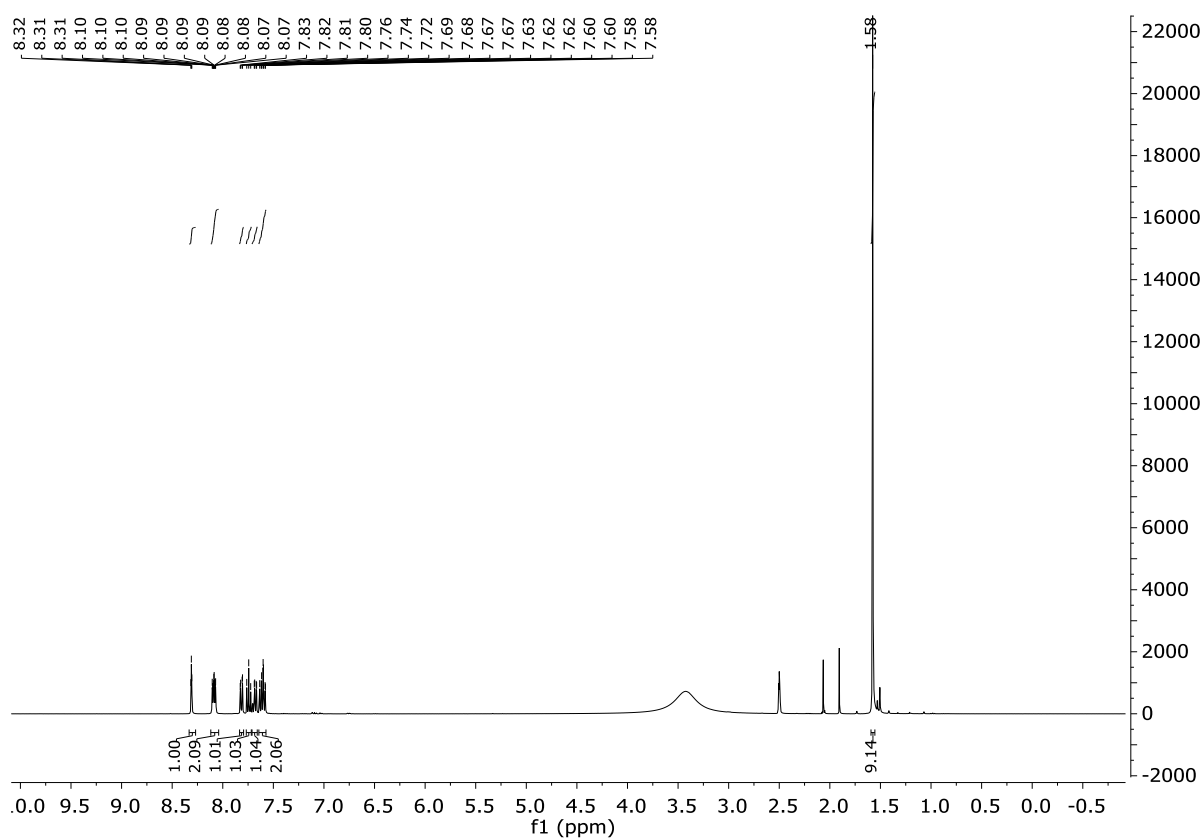
Figure S52. Two-point evaluation of compounds 15-19 at the V_{1b}R. Data represent mean values \pm SEM from at least three independent experiments performed in triplicate.

4.8.4 NMR Spectra

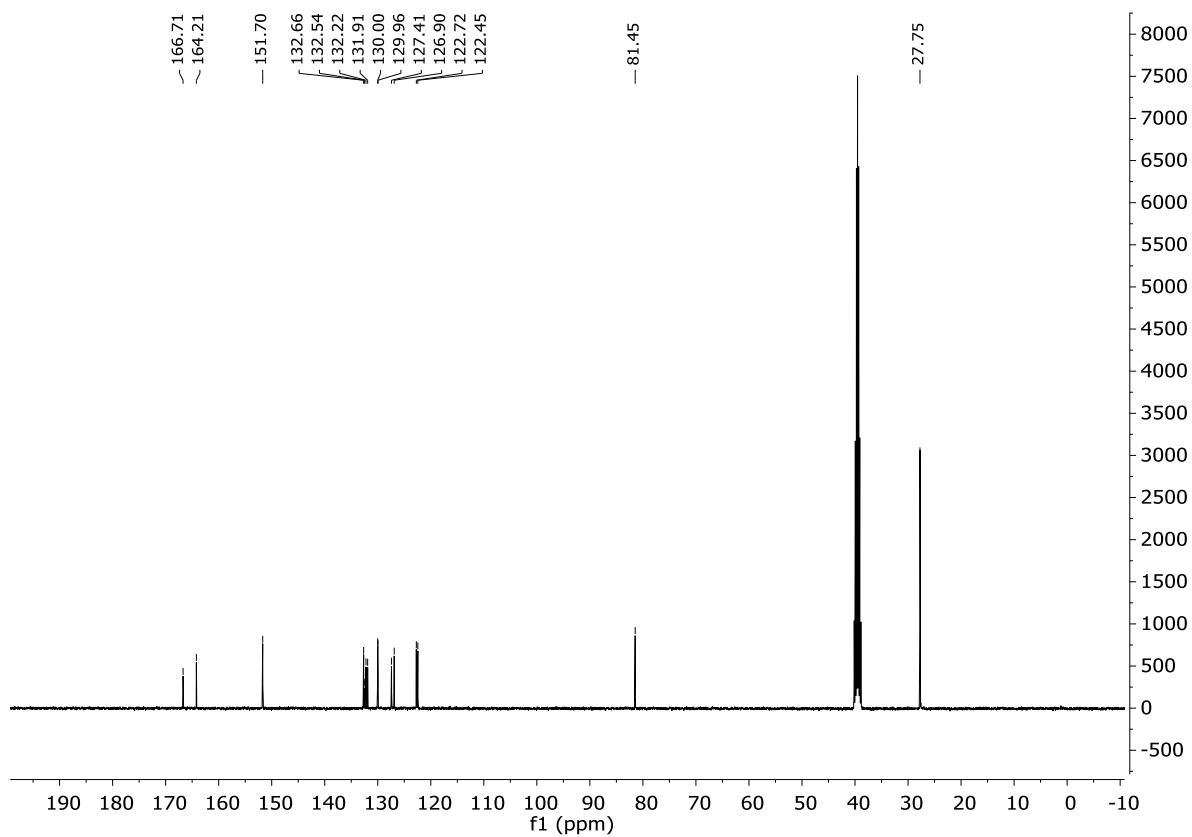
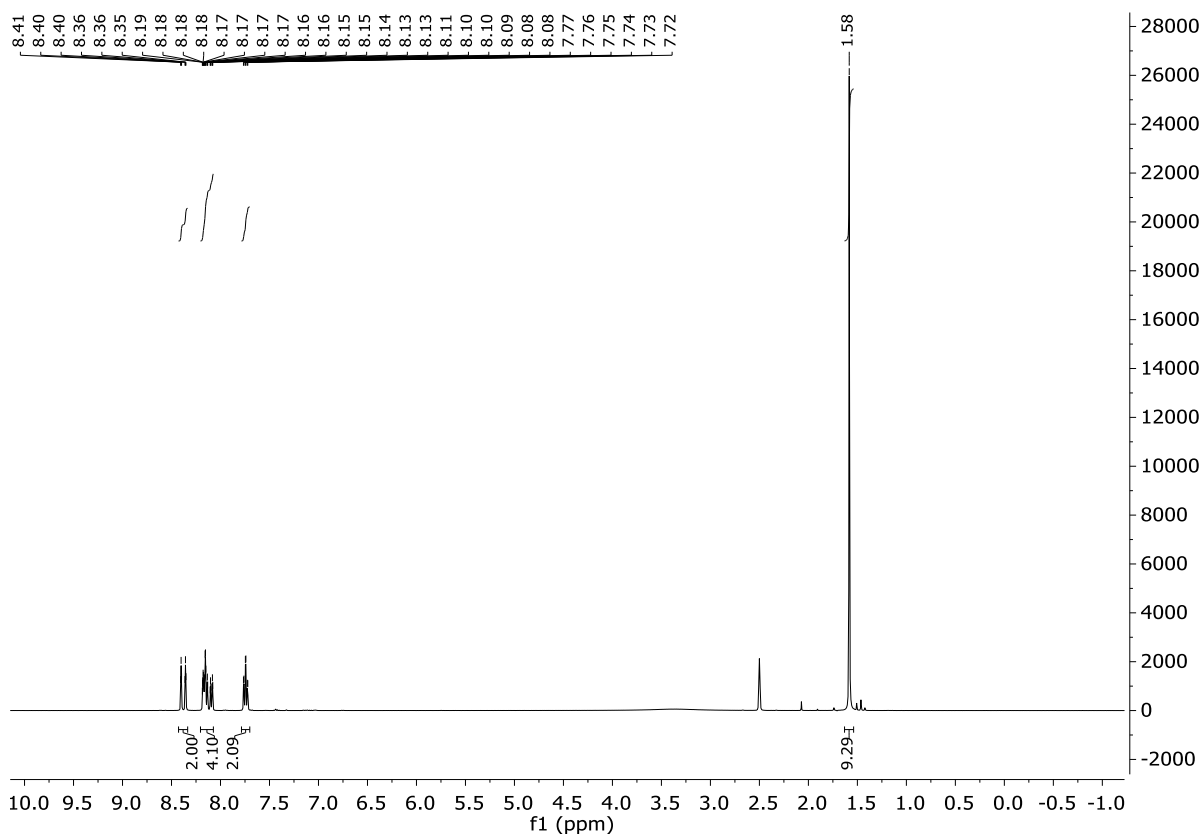
Compound 3



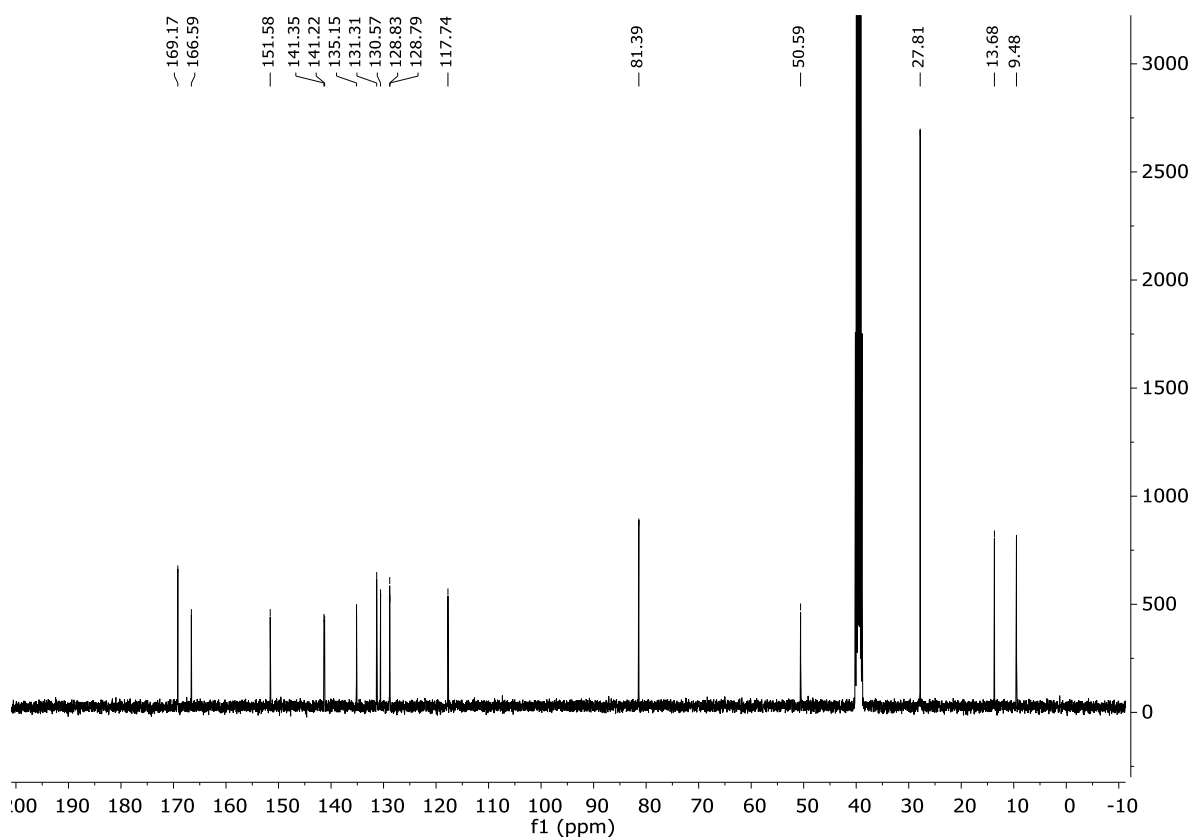
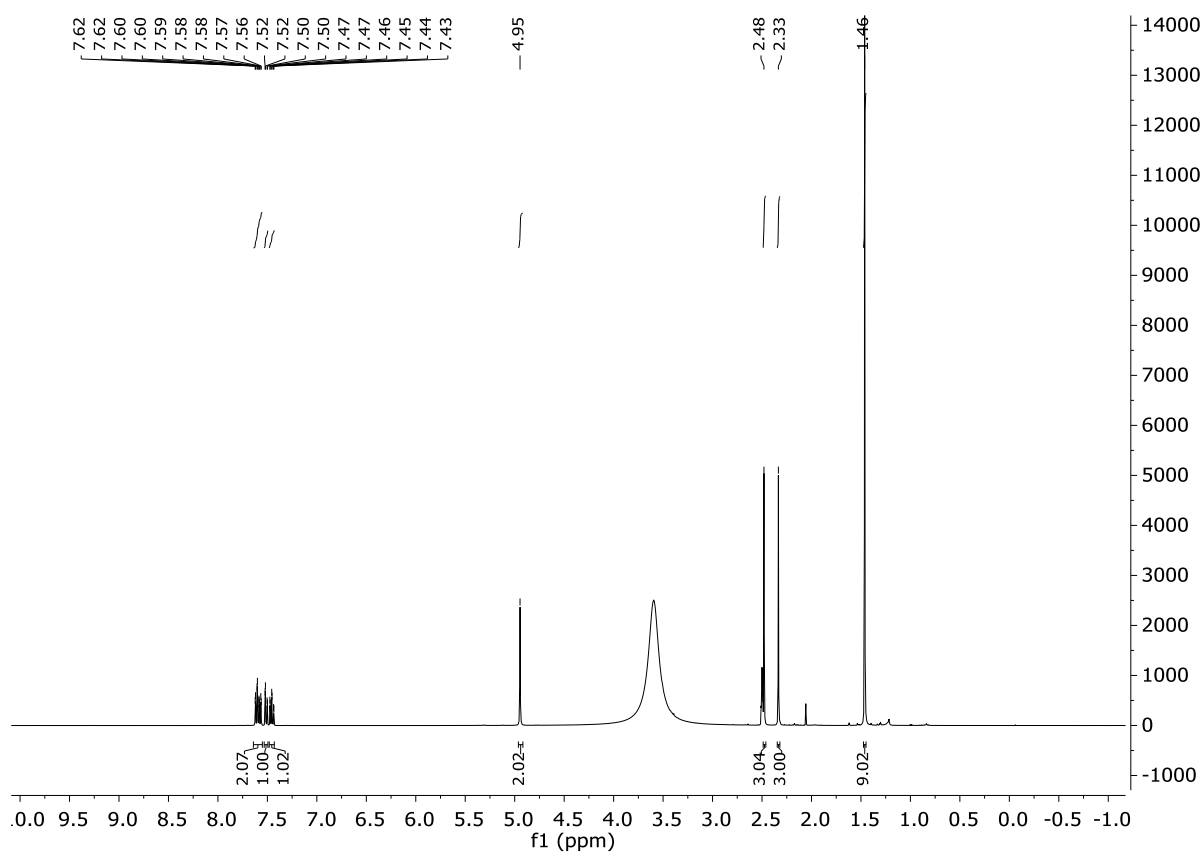
Compound 4



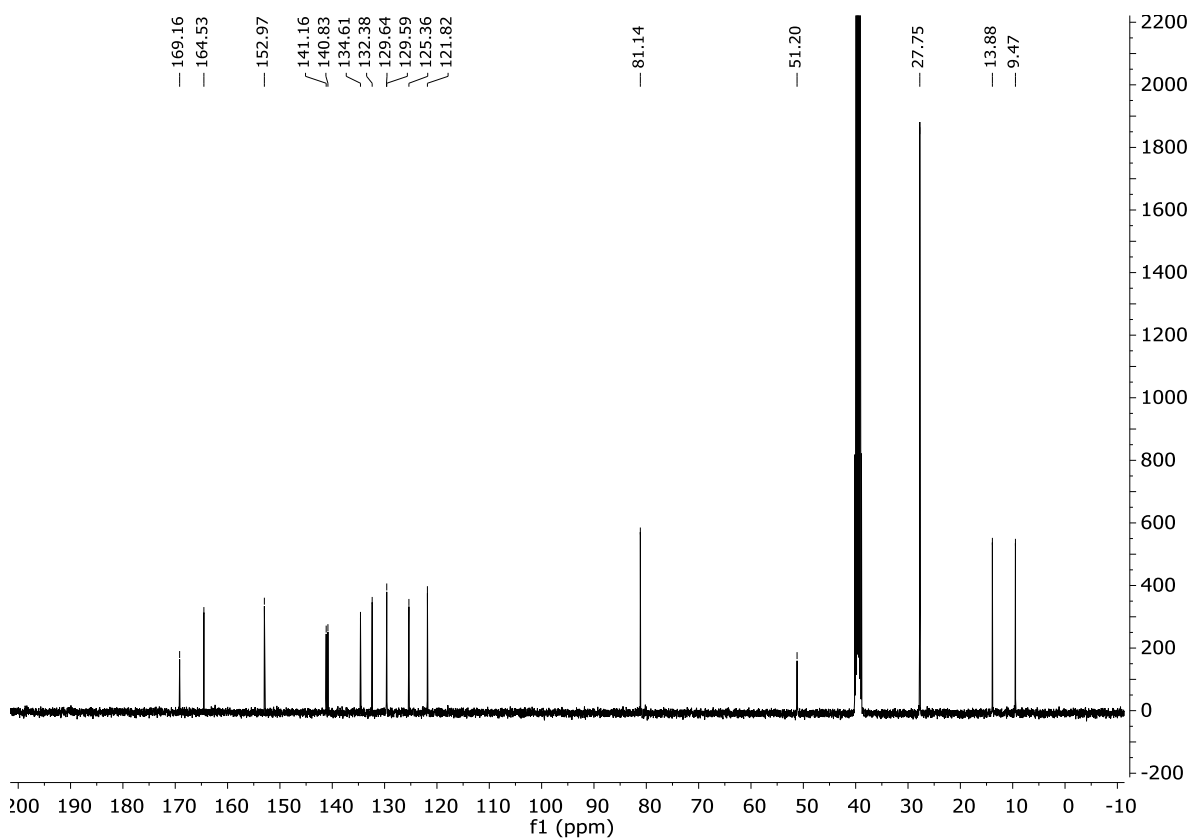
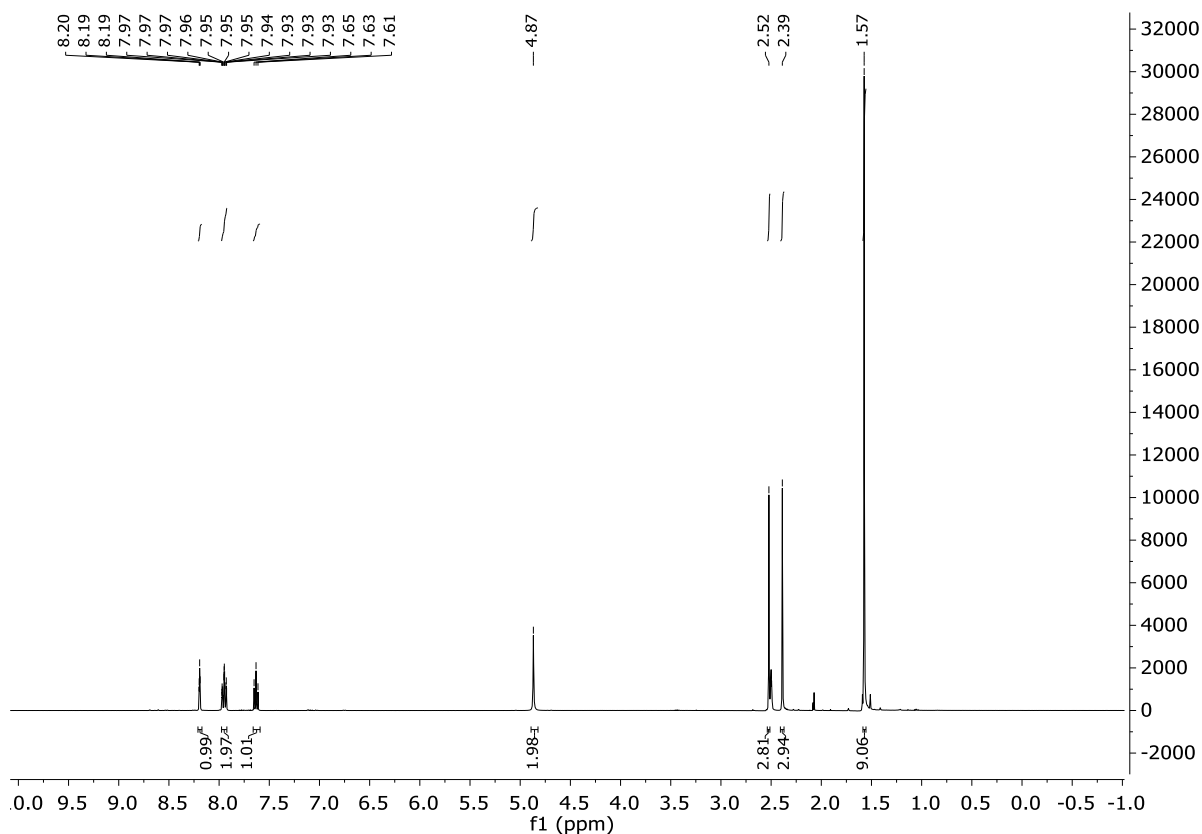
Compound 5



Compound 6



Compound 7



4.9 References

- [1] E. E. Benarroch, *Neurology* **2013**, *80*, 1521–1528.
- [2] A. Meyer-Lindenberg, G. Domes, P. Kirsch, M. Heinrichs, *Nat. Rev. Neurosci.* **2011**, *12*, 524–538.
- [3] M. Heinrichs, B. von Dawans, G. Domes, *Front. Neuroendocrinol.* **2009**, *30*, 548–557.
- [4] T. R. Insel, *Neuron* **2010**, *65*, 768–779.
- [5] J. P. Burkett, L. J. Young, *Psychopharmacology* **2012**, *224*, 1–26.
- [6] Z. R. Donaldson, L. J. Young, *Science* **2008**, *322*, 900–904.
- [7] G. Gimpl, F. Fahrenholz, *Physiol. Rev.* **2001**, *81*, 629–683.
- [8] A. Patin, D. Scheele, R. Hurlemann, *Curr. Top. Behav. Neurosci.* **2018**, *35*, 389–420.
- [9] J. B. Zik, D. L. Roberts, *Psychiatry Res.* **2015**, *226*, 31–37.
- [10] D. A. Baribeau, E. Anagnostou, *Front. Neurosci.* **2015**, *9*, 335.
- [11] Maciej Serda, F. G. Becker, M. Cleary, R. M. Team, H. Holtermann, D. The, N. Agenda, P. Science, S. K. Sk, R. Hinnebusch, R. Hinnebusch A, I. Rabinovich, Y. Olmert, D. Q. G. L. Q. Uld, W. K. H. U. Ri, V. Lq, W. K. H. Frxqwu, E. Zklfk, L. V Edvhg, R. Q. Wkh, F. G. Becker, N. Aboueldahab, R. Khalaf, L. R. De Elvira, T. Zintl, R. Hinnebusch, M. Karimi, S. M. Mousavi Shafae, D. O 'driscoll, S. Watts, J. Kavanagh, B. Frederick, T. Norlen, A. O'Mahony, P. Voorhies, T. Szayna, N. Spalding, M. O. Jackson, M. Morelli, B. Satpathy, B. Muniapan, M. Dass, P. Katsamunski, Y. Pamuk, A. Stahn, E. Commission, T. E. D. Piccone, M. K. Annan, S. Djankov, M. Reynal-Querol, M. Couttenier, R. Soubeyran, P. Vym, E. Prague, World Bank, C. Bodea, N. Sambanis, A. Florea, A. Florea, M. Karimi, S. M. Mousavi Shafae, N. Spalding, N. Sambanis, *ح. فاطمی, Clin. Sci.* **1981**, *61*, 343–354.
- [12] E. Kozniowska, K. Romaniuk, *J. Physiol. Pharmacol.* **2008**, *59*, 109–116.
- [13] P. M. Smith, A. V. Ferguson, *Neuroendocrinology* **1997**, *66*, 130–135.
- [14] F. M. Abboud, J. S. Floras, P. E. Aylward, G. B. Guo, B. N. Gupta, P. G. Schmid, *J. Vasc. Res.* **1990**, *27*, 106–115.
- [15] T. A. Koshimizu, Y. Nasa, A. Tanoue, R. Oikawa, Y. Kawahara, Y. Kiyono, T. Adachi, T. Tanaka, T. Kuwaki, T. Mori, S. Takeo, H. Okamura, G. Tsujimoto, *Proc. Natl. Acad. Sci.* **2006**, *103*, 7807–7812.
- [16] H. K. Caldwell, H. J. Lee, A. H. Macbeth, W. S. Young, *Prog. Neurobiol.* **2008**, *84*, 1–24.
- [17] D. Viviani, R. Stoop, *Prog. Brain Res.* **2008**, *170*, 207–218.
- [18] B. Jurek, I. D. Neumann, *Physiol. Rev.* **2018**, *98*, 1805–1908.
- [19] A. S. Hauser, M. M. Attwood, M. Rask-Andersen, H. B. Schiöth, D. E. Gloriam, *Nat. Rev. Drug Discov.* **2017**, *16*, 829–842.
- [20] C. W. Gruber, M. Muttenthaler, M. Freissmuth, *Curr. Pharm. Des.* **2010**, *16*, 3071–3088.
- [21] M. Manning, S. Stoev, B. Chini, T. Durroux, B. Mouillac, G. Guillon, *Prog. Brain Res.* **2008**, *170*, 473–512.
- [22] B. Chini, M. Manning, G. Guillon, *Prog. Brain Res.* **2008**, *170*, 513–517.
- [23] B. Chini, M. Manning, *Biochem. Soc. Trans.* **2007**, *35*, 737–741.
- [24] M. Muttenthaler, Å. Andersson, I. Vetter, R. Menon, M. Busnelli, L. Ragnarsson, C. Bergmayr, S. Arrowsmith, J. R. Deuis, H. S. Chiu, N. J. Palpant, M. O'brien, T. J. Smith, S. Wray, I. D. Neumann, C. W. Gruber, R. J. Lewis, P. F. Alewood, *Sci. Signal.* **2017**, *10*,

- eaan3398.
- [25] D. A. Wing, L. Sheibani, *Expert Opin. Pharmacother.* **2015**, *16*, 1657–1668.
- [26] L. Sentilhes, B. Merlot, H. Madar, F. Sztark, S. Brun, C. Deneux-Tharoux, *Expert Rev. Hematol.* **2016**, *9*, 1043–1061.
- [27] N. Japundžić-Žigon, M. Lozić, O. Šarenac, D. Murphy, *Curr. Neuropharmacol.* **2019**, *18*, 14–33.
- [28] M. W. Dünser, V. Wenzel, A. J. Mayr, W. R. Hasibeder, *Drugs* **2003**, *63*, 237–256.
- [29] M. Rae, M. Lemos Duarte, I. Gomes, R. Camarini, L. A. Devi, *Br. J. Pharmacol.* **2021**, *179*, 1544–1564.
- [30] J. L. Miller, R. Tamura, M. G. Butler, V. Kimonis, C. Sulsona, J. A. Gold, D. J. Driscoll, *Am. J. Med. Genet. A* **2017**, *173*, 1243–1250.
- [31] D. Gulliver, E. Werry, T. A. Reekie, T. A. Katte, W. Jorgensen, M. Kassiou, *Trends Pharmacol. Sci.* **2019**, *40*, 22–37.
- [32] E. A. D. Hammock, L. J. Young, *Philos. Trans. R. Soc. B Biol. Sci.* **2006**, *361*, 2187–2198.
- [33] M. Manning, A. Misicka, A. Olma, K. Bankowski, S. Stoev, B. Chini, T. Durroux, B. Mouillac, M. Corbani, G. Guillon, *J. Neuroendocrinol.* **2012**, *24*, 609–628.
- [34] J. Broichhagen, J. A. Frank, D. Trauner, *Acc. Chem. Res.* **2015**, *48*, 1947–1960.
- [35] W. Szymański, J. M. Beierle, H. A. V. Kistemaker, W. A. Velema, B. L. Feringa, *Chem. Rev.* **2013**, *113*, 6114–6178.
- [36] M. Ricart-Ortega, J. Font, A. Llebaria, *Mol. Cell. Endocrinol.* **2019**, *488*, 36–51.
- [37] K. Hüll, J. Morstein, D. Trauner, *Chem. Rev.* **2018**, *118*, 10710–10747.
- [38] M. Wijtmans, I. Josimovic, H. F. Vischer, R. Leurs, *Curr. Opin. Pharmacol.* **2022**, *63*, 102192.
- [39] R. J. Mart, R. K. Allemann, *Chem. Commun.* **2016**, *52*, 12262–12277.
- [40] L. Albert, O. Vázquez, *Chem. Commun.* **2019**, *55*, 10192–10213.
- [41] J. Broichhagen, T. Podewin, H. Meyer-Berg, Y. Von Ohlen, N. R. Johnston, B. J. Jones, S. R. Bloom, G. A. Rutter, A. Hoffmann-Röder, D. J. Hodson, D. Trauner, *Angew. Chemie Int. Ed.* **2015**, *54*, 15565–15569.
- [42] T. Podewin, J. Broichhagen, C. Frost, D. Groneberg, J. Ast, H. Meyer-Berg, N. H. F. Fine, A. Friebe, M. Zacharias, D. J. Hodson, D. Trauner, A. Hoffmann-Röder, *Chem. Sci.* **2017**, *8*, 4644–4653.
- [43] L. Nevola, A. Martín-Quirós, K. Eckelt, N. Camarero, S. Tosi, A. Llobet, E. Giralt, P. Gorostiza, *Angew. Chemie Int. Ed.* **2013**, *52*, 7704–7708.
- [44] A. A. Beharry, G. A. Woolley, *Chem. Soc. Rev.* **2011**, *40*, 4422–4437.
- [45] H. M. D. Bandara, S. C. Burdette, *Chem. Soc. Rev.* **2012**, *41*, 1809–1825.
- [46] W. A. Velema, W. Szymanski, B. L. Feringa, *J. Am. Chem. Soc.* **2014**, *136*, 2178–2191.
- [47] D. Lachmann, C. Studte, B. Männel, H. Hübner, P. Gmeiner, B. König, *Chem. Eur. J.* **2017**, *23*, 13423–13434.
- [48] P. C. Donthamsetti, N. Winter, M. Schönberger, J. Levitz, C. Stanley, J. A. Javitch, E. Y. Isacoff, D. Trauner, *J. Am. Chem. Soc.* **2017**, *139*, 18522–18535.
- [49] M. Schönberger, D. Trauner, *Angew. Chem. Int. Ed.* **2014**, *53*, 3264–3267.
- [50] R. Lahmy, H. Hübner, M. F. Schmidt, D. Lachmann, P. Gmeiner, B. König, *Chem. Eur. J.* **2022**, *28*, e202201515.
- [51] N. J. Hauwert, T. A. M. Mocking, D. Da Costa Pereira, A. J. Kooistra, L. M. Wijnen,

- G. C. M. Vreeker, E. W. E. Verweij, A. H. De Boer, M. J. Smit, C. De Graaf, H. F. Vischer, I. J. P. De Esch, M. Wijtmans, R. Leurs, *J. Am. Chem. Soc.* **2018**, *140*, 4232–4243.
- [52] A. Duran-Corbera, J. Catena, M. Otero-Viñas, A. Llebaria, X. Rovira, *J. Med. Chem.* **2020**, *63*, 8458–8470.
- [53] M. Muttenthaler, A. Andersson, A. D. De Araujo, Z. Dekan, R. J. Lewis, P. F. Alewood, *J. Med. Chem.* **2010**, *53*, 8585–8596.
- [54] A. D. de Araujo, M. Mobli, J. Castro, A. M. Harrington, I. Vetter, Z. Dekan, M. Muttenthaler, J. Wan, R. J. Lewis, G. F. King, S. M. Brierley, P. F. Alewood, *Nat. Commun.* **2014**, *5*, 3165.
- [55] M. Manning, W. A. Klis, M. Kruszynski, J. P. Przybylski, A. Olma, N. C. Wo, G. H. Pelton, W. H. Sawyer, *Int. J. Pept. Protein Res.* **1988**, *32*, 455–467.
- [56] M. Manning, S. Stoev, A. Kolodziejczyk, W. A. Klis, M. Kruszynski, A. Misicka, A. Olma, *J. Med. Chem.* **1990**, *33*, 3079–3086.
- [57] M. Manning, J. P. Przybylski, A. Olma, W. A. Klis, M. Kruszynski, N. C. Wo, G. H. Pelton, W. H. Sawyer, *Nat.* **1987**, *329*, 839–840.
- [58] C. E. Weston, R. D. Richardson, P. R. Haycock, A. J. P. White, M. J. Fuchter, *J. Am. Chem. Soc.* **2014**, *136*, 11878–11881.
- [59] F. Paternostre, Marie-Therese; Cintrat, Jean-Christophe; Valery, Celine; Roux, Stephane; Rousseau, Bernard; Ijsselstijn, Maarten; Cherif-Cheikh, Roland; Artzner, *New Octapeptide Compounds, Their Preparation, Self-Assembly Properties and Use as Ligands of Somatostatin Receptor Subtypes 2 and/or 5*, **2009**, WO2010037930.
- [60] L. Albert, J. Xu, R. Wan, V. Srinivasan, Y. Dou, *Chem. Sci* **2017**, *8*, 4612–4618.
- [61] B. Priewisch, K. Rück-Braun, *J. Org. Chem.* **2005**, *70*, 2350–2352.
- [62] M. J. Fuchter, *J. Med. Chem* **2020**, *63*, 11436–11447.
- [63] L. Nørskov-Lauritsen, A. R. B. Thomsen, H. Bräuner-Osborne, *Int. J. Mol. Sci.* **2014**, *15*, 2554–2572.
- [64] J. G. Meyerowitz, M. J. Robertson, X. Barros-Álvarez, O. Panova, R. M. Nwokonko, Y. Gao, G. Skiniotis, *Nat. Struct. Mol. Biol.* **2022**, *29*, 274–281.
- [65] J. Rodrigo, A. Pena, B. Murat, M. Trueba, T. Durroux, G. Guillon, D. Rognan, *Mol. Endocrinol.* **2007**, *21*, 512–523.
- [66] M. Thibonnier, P. Coles, D. M. Conarty, C. L. Plesnicher, M. Shoham, *J. Pharmacol. Exp. Ther.* **2000**, *294*, 195–203.
- [67] M. Manning, S. Stoev, B. Chini, T. Durroux, B. Mouillac, G. Guillon, *Prog. Brain Res.* **2008**, *170*, 473–512.
- [68] B. Priewisch, K. Rück-Braun, *J. Org. Chem.* **2005**, *70*, 2350–2352.

SUMMARY

5 Summary

This thesis presents the development of new photoswitchable compounds including design, synthesis, photophysical characterization and their biological application in GABA_A and G protein-coupled receptors.

Chapter 1 describes the synthesis of a photoswitchable potentiator of the GABA_A receptor. The design is based on the known nonbenzodiazepine abecarnil from the β -carboline family. In an azologization approach, the ether bond between the phenyl rings was replaced by an azo group and azocarnil was generated. The design was further supported by molecular docking studies that predicted that the compound is still active, and that the *cis* isomer shows more interactions with the benzodiazepine binding site than the *trans* isomer and therefore is the more active isomer. These first indications were confirmed by electrophysiological investigations. Patch-clamp measurements showed that the *cis* isomer of azocarnil increased the amplitude of the gabaergic currents in cultured hippocampal neurons, whereas the *trans* isomer did not influence these currents. By blocking the ion channel after the experiments with the known GABA_A receptor inhibitor bicuculline a decrease in the amplitude was observed which proved that the currents are of gabaergic origin. Additionally, azocarnil did not change glutamatergic currents indicating selectivity towards the GABA_A receptor. After these successful *in vitro* studies testing of azocarnil *in vivo* in mice is ongoing.

The synthesis and biological evaluation of covalent binding photochromic ligands for the β_2 -adrenergic receptor, a G protein-coupled receptor, which could potentially be used for single molecule spectroscopy is reported in **chapter 2**. The design of the covalent photoswitchable ligands was inspired by the reported covalent compounds FAUC50 and FAUC37 which consist of a pharmacophore, a phenyl linker, and a covalent warhead. The phenyl linker was replaced by an arylazopyrazole moiety which was connected to the covalent warhead *via* a variable linker. The selected pharmacophores were the endogenous ligand norepinephrine and the high-affinity synthetic ligand BI-167107. The choice for the covalent tether fell on maleimides and disulfides which interact with a free cysteine that was engineered to the receptor by point mutation. After combining these units in different ways, we tested the compounds regarding their ability to activate the wild-type β_2 -adrenergic receptor. It turned out that all compounds displayed agonistic properties. Subsequently, the ligands were tested in an enhanced bystander BRET assay on the mutated receptor. By addition of washing and blocking steps it was ensured that only the recruitment of β -arrestin of covalently bound

ligands were measured. One compound that showed the biggest difference between the isomers was selected to be tested for *in situ* switching. The gain and loss in activity upon irradiation during the assay showed that switching while covalently bound to the receptor is presumably possible.

In **chapter 3**, macrocyclic peptidic photochromic ligands based on reported UR-AK86c were developed that target the NPY Y₄ receptor, a G protein-coupled receptor. The photoswitchable moiety was installed as an amino acid side chain or in the cyclic part to maximize the effect upon *cis/trans* isomerization. The ligands exhibited excellent photophysical properties and were first tested in classical labeled biological assays to test their affinity and activation ability. Most compounds displayed affinities in the sub nanomolar range with a difference between the two isomers up to almost 10-fold. The differences in potency were less distinctive and reached up to 5-fold. The most promising compounds were subjected to electric cell-substrate impedance sensing (ECIS), a label-free holistic method that integrates over the entire cell body and the entire signalling cascade. These measurements demonstrated that *in situ* switching enabled real-time monitoring of GPCR signaling. By adding a washing step after the addition of ligand and subsequent switching we observed that switching is still possible which led us to the assumption that the switching process is taking place inside the binding pocket of the receptor. This was the first time that photochromic molecules were combined with ECIS measurements and since this method is broadly applicable it may be also used to unravel mechanistic details of receptor activation or signaling of other types of receptors.

Chapter 4 deals with photoswitchable probes of the cyclic hypothalamic neuropeptides oxytocin (OT) and vasopressin (VP). OT and VP act *via* four receptors, OTR, V_{1a}R, V_{1b}R and V₂R, all belonging to the class of G protein-coupled receptors. Based on these endogenous ligands three different design strategies were applied that ranged from conservative to more drastic modifications. Photochromic moieties were incorporated as an amino acid side chain, in a linear way in the exocyclic tail and in the cyclic structure motif. The photoswitchable peptides were assembled by solid phase peptide synthesis. The investigation of the photophysical properties revealed high fatigue resistances, good photostationary states for the *trans* to *cis* isomerization and thermal half-lives long enough for the length of the biological assays. The photoprobes were tested in an IP1 accumulation assay regarding their ability to activate the respective receptor. For most compounds a substantial or complete loss of activity was observed as OT and VP are prone to lose their activity upon structural changes. Two

compounds however stood out with only a slightly reduced potency compared to the endogenous ligand at the OTR and V_{1b}R, respectively. Additionally, they displayed 3- to 5-fold differences in the EC₅₀ values between the *trans* and *cis* isomer.

ZUSAMMENFASSUNG

6 Zusammenfassung

Diese Dissertation behandelt die Entwicklung neuer photoschaltbarer Verbindungen einschließlich Design, Synthese, photophysikalische Charakterisierung und ihre biologische Anwendung in GABA_A und G Protein-gekoppelten Rezeptoren.

Kapitel 1 beschreibt die Synthese eines photoschaltbaren Potentiators des GABA_A-Rezeptors. Das Design basiert auf dem bekannten Nicht-Benzodiazepin Abecarnil aus der Familie der β -Carboline. In einem Azologisierungsansatz wurde die Etherbindung zwischen den Phenylringen durch eine Azogruppe ersetzt und Azocarnil entstand. Das Design wurde durch molekulare Docking-Studien noch weiter unterstützt, die vorhersagten, dass die Verbindung immer noch aktiv ist und dass das *cis*-Isomer mehr Wechselwirkungen mit der Benzodiazepin-Bindungsstelle zeigt als das *trans*-Isomer und daher das aktivere Isomer ist. Diese ersten Hinweise wurden durch elektrophysiologische Untersuchungen bestätigt. Patch-Clamp-Messungen zeigten, dass das *cis*-Isomer von Azocarnil die Amplitude der gabaergen Ströme in kultivierten Hippocampus-Neuronen erhöhte, während das *trans*-Isomer diese Ströme nicht beeinflusste. Durch die Blockierung des Ionenkanals nach den Experimenten mit dem bekannten GABA_A-Rezeptor Inhibitor Bicucullin wurde eine Abnahme der Amplitude beobachtet, was beweist, dass die Ströme gabaergen Ursprungs sind. Außerdem veränderte Azocarnil die glutamatergen Ströme nicht, was auf eine Selektivität gegenüber dem GABA_A-Rezeptor hindeutet. Nach diesen erfolgreichen *in vitro* Studien wird Azocarnil aktuell auch *in vivo* an Mäusen getestet.

In **Kapitel 2** wird über die Synthese und biologische Bewertung kovalent bindender photochromer Liganden für den β 2-adrenergen Rezeptor, einen G Protein-gekoppelten Rezeptor, berichtet, die potenziell für die Einzelmolekülspektroskopie verwendet werden könnten. Das Design der kovalenten photoschaltbaren Liganden wurde von den bekannten kovalenten Verbindungen FAUC50 und FAUC37 inspiriert, die aus einem Pharmakophor, einem Phenyl-Linker und einer reaktiven Kopfgruppe bestehen. Der Phenyl-Linker wurde durch eine Arylazopyrazol-Einheit ersetzt, die über einen variablen Linker mit reaktiven Gruppe verbunden war. Als Pharmakophore wurden der endogene Ligand Norepinephrin und der hochaffine synthetische Ligand BI-167107 ausgewählt. Die Wahl für den kovalenten Tether fiel auf Maleinimide und Disulfide, die mit einem freien Cystein reagieren können, das durch Punktmutation in den Rezeptor eingebaut wurde. Nachdem diese Einheiten auf unterschiedliche Weise kombiniert wurden, wurden die Verbindungen auf ihre Fähigkeit, den

Wildtyp des β 2-adrenergen Rezeptor zu aktivieren, getestet. Es zeigte sich, dass alle Verbindungen agonistische Eigenschaften aufwiesen. Anschließend wurden die Liganden in einem verstärkten Bystander-BRET-Assay an dem mutierten Rezeptor getestet. Durch zusätzliche Wasch- und Blockierungsschritte wurde sichergestellt, dass nur die Rekrutierung von β -Arrestin von kovalent gebundenen Liganden gemessen wurde. Eine Verbindung, die den größten Unterschied zwischen den Isomeren aufwies, wurde ausgewählt, um auf *In situ*-Schalten getestet zu werden. Die Aktivitätszunahme und der Aktivitätsverlust bei Bestrahlung während des Assays zeigten, dass ein Schalten auch während der kovalenten Bindung an den Rezeptor vermutlich möglich ist.

In **Kapitel 3** wurden makrozyklische peptidische photochrome Liganden basierend auf UR-AK86c entwickelt, die auf den NPY Y₄-Rezeptor, einen G Protein-gekoppelten Rezeptor, abzielen. Die photoschaltbare Einheit wurde als Aminosäureseitenkette oder im zyklischen Teil eingebaut, um die Wirkung der *cis/trans*-Isomerisierung zu maximieren. Die Liganden wiesen ausgezeichnete photophysikalische Eigenschaften auf und wurden zunächst in klassischen markierten biologischen Assays auf ihre Affinität und Aktivierungsfähigkeit hin getestet. Die meisten Verbindungen wiesen Affinitäten im subnanomolaren Bereich auf, wobei der Unterschied zwischen den beiden Isomeren bis zu 10-fach war. Die Unterschiede in der Potenz waren weniger ausgeprägt und erreichten bis zu 5-fache Unterschiede. Die vielversprechendsten Verbindungen wurden in einem elektrischen Zell-Substrat-Impedanzsensor (ECIS) untersucht, einer markierungsfreien ganzheitlichen Methode, die den gesamten Zellkörper und die gesamte Signalkaskade erfasst. Diese Messungen zeigten, dass das *In situ*-Schalten eine Echtzeitüberwachung der GPCR-Signalübertragung ermöglicht. Durch Hinzufügen eines Waschschriffs nach der Ligandenzugabe und anschließendem Schalten konnte beobachtet werden, dass das Schalten immer noch möglich ist, was uns zu der Annahme veranlasste, dass der Schaltprozess innerhalb der Bindungstasche des Rezeptors stattfindet. Dies war das erste Mal, dass photochrome Moleküle mit ECIS-Messungen kombiniert wurden, und da diese Methode breit anwendbar ist, kann sie auch dazu verwendet werden, mechanistische Details der Rezeptoraktivierung oder der Signalübertragung bei anderen Rezeptortypen zu entschlüsseln.

Kapitel 4 beschäftigt sich mit photoschaltbaren Derivaten der zyklischen hypothalamischen Neuropeptide Oxytocin (OT) und Vasopressin (VP). OT und VP wirken über vier Rezeptoren, OTR, V_{1a}R, V_{1b}R und V₂R, die alle zur Klasse der G Protein-gekoppelten Rezeptoren gehören. Auf der Grundlage dieser endogenen Liganden wurden drei verschiedene Designstrategien

angewandt, die von konservativen bis zu drastischeren Modifikationen reichten. Die photochromen Einheiten wurden als Aminosäureseitenkette, linear in den exozyklischen Teil und in das zyklische Strukturmotiv eingebaut. Die photoschaltbaren Peptide wurden durch Festphasen-Peptidsynthese hergestellt. Die Untersuchung der photophysikalischen Eigenschaften ergab eine hohe Ermüdungsbeständigkeit, gute photostationäre Zustände für die *trans*-zu-*cis*-Isomerisierung und thermische Halbwertszeiten, die für die Dauer der biologischen Assays ausreichen. Die photoschaltbaren Liganden wurden in einem IP1-Akkumulationsassay auf ihre Fähigkeit zur Aktivierung des jeweiligen Rezeptors getestet. Bei den meisten Verbindungen wurde ein erheblicher oder vollständiger Aktivitätsverlust beobachtet, da OT und VP bei strukturellen Veränderungen dazu neigen, ihre Aktivität zu verlieren. Zwei Verbindungen zeichneten sich jedoch durch eine nur geringfügig reduzierte Potenz im Vergleich zum endogenen Liganden am OTR bzw. V_{1b}R aus. Außerdem wiesen sie 3- bis 5-fache Unterschiede bei den EC₅₀-Werten zwischen dem *trans*- und dem *cis*-Isomer auf.

APPENDIX

7 Appendix

7.1 Abbreviations

aa	amino acid
AC	alternating current
AcOH	acetic acid
AMPA receptor	α -amino-3-hydroxy-5-methyl-4-isoxazolepropionic acid receptor
AP5	(2R)-amino-5-phosphonovaleric acid
AR	adrenergic receptor
Arg	arginine
Asn	asparagine
ATP	adenosine triphosphate
BI	Boehringer Ingelheim
BnBr	benzyl bromide
Boc	<i>tert</i> -butyloxycarbonyl
BRET	bioluminescence resonance energy transfer
BSA	bovine serum albumin
BTMA-ICl ₂	benzyltrimethylammonium dichloroiodate
C	cysteine
cAMP	cyclic adenosine monophosphate
carb	carbamoyleated
CB ₁	cannabinoid receptor 1
CBR	click beetle red luciferase
CBRC	C-terminal fragment of the CBR, 148 amino acids
CBRN	N-terminal fragment of the CBR, 417 amino acids
CNQX	6-cyano-7-nitroquinoxaline-2,3-dione
Cov _{max}	maximum covalent binding level
CXCR3	chemokine receptor CXCR3
Cys	cysteine
Dap	diaminopropionic acid
DIC	<i>N,N'</i> -diisopropylcarbodiimide
DIPEA	<i>N,N</i> -diisopropylethylamine
DIV	days in vitro
DMCM	methyl 6,7-dimethoxy-4-ethyl- β -carboline-3-carboxylate

DMF	dimethyl formamide
DMP	Dess-Martin periodinane
DMSO	dimethyl sulfoxide
<i>E</i>	entgegen
EC ₅₀	half maximal effective concentration
ECL	extracellular loop
EDTA	ethylenediaminetetraacetic acid
EGTA	ethylene glycol-bis(β -aminoethyl ether)- <i>N,N,N',N'</i> -tetraacetic acid
EtOH	ethanol
FBS	fetal bovine serum
FCS	fetal calf serum
fmoc	fluorenylmethoxycarbonyl
FRET	fluorescence resonance energy transfer
GABA	γ -aminobutyric acid
Gln	glutamine
Gly	glycine
GPCR	G-protein coupled receptor
GTP	guanosine-5'-triphosphate
H	histidine
HBTU	2-(1 <i>H</i> -benzotriazol-1-yl)-1,1,3,3-tetramethyluronium hexafluorophosphate
HEPES	4-(2-hydroxyethyl)-1-piperazineethanesulfonic acid
HEK	human embryonic kidney
His	histidine
HOBt	hydroxybenzotriazole
hOTR	human oxytocin receptor
HPLC	high performance liquid chromatography
hPP	human pancreatic polypeptide
H ₃ R	histamine H ₃ receptor
hV _{1a} R	human vasopressin receptor 1a
hV _{1b} R	human vasopressin receptor 1b
Ile	isoleucine
IP	inositol phosphate
IP1	inositol monophosphate

K	lysine
Leu	leucine
Lys	lysine
MeCN	acetonitrile
MeOH	methanol
mEPSCs	miniature excitatory postsynaptic currents
MesCl	mesyl chloride
<i>m</i>	<i>meta</i>
MeCN	acetonitrile
mGlu ₅	metabotropic glutamate receptor 5
mIPSCs	miniature inhibitory postsynaptic currents
NE	norepinephrine
Nluc	Nanoluciferase
NlucN	N-terminal fragment of the Nluc, 159 amino acids
NlucC	C-terminal fragment of the Nluc, 11 amino acids
NMDA receptor	<i>N</i> -methyl-D-aspartate receptor
NMP	<i>N</i> -methyl-2-pyrrolidone
NMR	nuclear magnetic resonance
<i>o</i>	<i>ortho</i>
OR	opioid receptor
OT	oxytocin
OTR	oxytocin receptor
<i>p</i>	<i>para</i>
Pbf	2,2,4,6,7-pentamethyldihydrobenzofuran-5-sulfonyl
PDB	protein data bank
PE	petroleum ether
Phe	phenylalanine
pNPY	porcine neuropeptide Y
Pro	proline
PS	polystyrene
PSS	photostationary state
PTX	picROTOXIN
PyBOP	benzotriazol-1-yloxytripyrrolidinophosphonium hexafluorophosphate
RP	reverse phase

rt	room temperature
SEM	standard error of the mean
SPPS	solid phase peptide synthesis
$t_{1/2}$	thermal half-life
^t Bu	<i>tert</i> -butyl
TCCA	trichloroisocyanuric acid
TFA	trifluoroacetic acid
TIPS	triisopropylsilane
TM	transmembrane
Tris	tris(hydroxymethyl)aminomethane
Trp	Tryptophane
Trt	trityl
TTX	tetrodotoxin
Tyr	tyrosine
VP	vasopressin
V _{1a} R	vasopressin receptor 1a
V _{1b} R	vasopressin receptor 1b
V ₂ R	vasopressin receptor 2
Z	impedance
Z	zusammen
Zn	zinc

7.2 Curriculum Vitae

Personal Data

Name: Ulrike Wirth
Date and place of birth: 17.12.1993; Altötting
Marital Status: Unmarried
Nationality: German

Education

11/2018 – 03/2023 **Ph.D. in Organic Chemistry**
Institute of Organic Chemistry, University of Regensburg
“Photochromic Molecules for Biological Applications”
Supervisor: Prof. Dr. Burkhard König (Regensburg)

10/2016 – 09/2018 **Master of Science in Chemistry**
Institute of Organic Chemistry, University of Regensburg
Master thesis: *“Photochromic Modulators for the GABA_A Receptor”*
Supervisor: Prof. Dr. Burkhard König (Regensburg)

10/2013 – 09/2016 **Bachelor of Science in Chemistry**
Institute of Organic Chemistry, University of Regensburg
Bachelor thesis: *“Palladium catalyzed hydrogenolysis of benzylic alcohols”*
Supervisor: Prof. Dr. Ivana Fleischer (Regensburg)

10/2012 – 09/2013 **Bachelor of Science in Molecular Biotechnology**
TU-Munich, Freising

09/2004 – 07/2012 **Allgemeine Hochschulreife**
Maria-Ward-Gymnasium Altötting

Memberships

2020 – present	Gesellschaft Deutscher Chemiker (GDCh, German Chemical Society)
03/2019 – 08/2022	DFG – Graduate Training Group GRK 1910 “Medicinal Chemistry of Selective GPCR Ligands”

Conferences

05/2018	3rd Modulight Meeting (oral presentation) Regensburg, Germany
11/2018	2nd International Symposium on Photopharmacology (poster presentation) Vic, Spain
09/2022	8th Weizmann Summer School “Advances in Drug Discovery” (poster presentation) Prague, Czech Republic
09/2022	19th Ischia Advanced School of Organic Chemistry (poster presentation) Ischia, Italy
2019 – 2021	Seminar Days of the GRK 1910 (oral presentations) Erlangen, Regensburg, Germany

DANKSAGUNG

8 Danksagung

Mein besonderer Dank gilt meinem Doktorvater Prof. Dr. Burkhard König für die Betreuung meiner Dissertation mit einer sehr interessanten und vielseitigen Themenstellung. Ich bedanke mich für seine Unterstützung und seine stets offene Tür bei Problemen jeglicher Art.

Für die Übernahme des Zweitgutachtens möchte ich Dr. Max Keller danken. Weiterhin geht mein Dank an Prof. Dr. Joachim Wegener und Apl. Prof. Dr. Rainer Müller, dass sie sich die Zeit genommen haben in meinem Prüfungsausschuss mitzuwirken.

Außerdem möchte ich Dr. Galyna Malieieva, Prof. Dr. Pau Gorostiza, Prof. Dr. Piotr Bregestovski, Prof. Dr. Carme Rovira, Dr. Alba Nin-Hill, Prof. Dr. Ulrich Zeilhofer, Matteo Ranucci, Dr. Steffen Feustel, Prof. Dr. Peter Gmeiner, Dr. Harald Hübner, Julia Erl, Carina Höring, Dr. Max Keller, Prof. Dr. Joachim Wegener, Konstantin Raabe und Prof. Dr. Markus Muttenthaler für die gute Zusammenarbeit in diversen Projekten danken. Dem Graduiertenkolleg 1910 „Medicinal Chemistry of Selective GPCR Ligands“ möchte ich für die finanzielle Unterstützung und die interessanten GRK Retreats danken.

Ich danke auch Barbara, Britta, Julia, Ernst, Rudi, Regina, Petra und Simone für jegliche Hilfe und Unterstützung in technischen, organisatorischen, chromatographischen und bürokratischen Angelegenheiten.

Ich danke den Mitgliedern der Zentralen Analytik und der NMR-Abteilung der Universität Regensburg für eine stets zügige Bearbeitung von Aufträgen.

Bei meinen Praktikanten und Bacheloranden Thilo Reiter, Nicolas Müller, Lukas Steigleder, Markus Meier, Regina Deubelli, Christina Auer, Anna Feilhuber und Sara Alami möchte ich mich für die Mitarbeit bedanken. Auch Ritu Singh möchte ich Danke sagen für die gute Zusammenarbeit während ihrer Masterarbeit.

Ganz besonders danken möchte ich allen ehemaligen und aktuellen Mitgliedern des AK Königs für das angenehme Arbeitsklima, die Aktivitäten drumherum und die ein oder andere Party, allen voran meinen Laborkollegen Ranit, Alessa, Michela und Lea, dem besten Beerpong Team und Gewinner der Herzen Peppersweet und Karsten.

Von ganzem Herzen danke ich meiner Familie, vorallem meinen Eltern und meiner Schwester für ihre Unterstützung.

Danke

Eidesstattliche Erklärung

- (1) Ich erkläre hiermit an Eides statt, dass ich die vorliegende Arbeit ohne unzulässige Hilfe Dritter und ohne Benutzung anderer als der angegebenen Hilfsmittel angefertigt habe; die aus anderen Quellen direkt oder indirekt übernommenen Daten und Konzepte sind unter Angabe des Literaturzitats gekennzeichnet.
- (2) Bei der Auswahl und Auswertung folgenden Materials haben mir die nachstehend aufgeführten Personen in der jeweils beschriebenen Weise unentgeltlich geholfen:
 1. Gekennzeichnete Experimente, Untersuchungen oder Berechnungen in Kapitel 1 wurden von G. Malieieva und A. Nin-Hill durchgeführt.
 2. Gekennzeichnete Experimente, Untersuchungen oder Berechnungen in Kapitel 2 wurden von S. Feustel und M. Schmidt durchgeführt.
 3. Gekennzeichnete Experimente oder Untersuchungen in Kapitel 3 wurden von R. Singh, J. Erl und C. Höring durchgeführt.
 4. Gekennzeichnete Experimente oder Untersuchungen in Kapitel 4 wurden von K. Raabe durchgeführt.
- (3) Weitere Personen waren an der inhaltlich-materiellen Herstellung der vorliegenden Arbeit nicht beteiligt. Insbesondere habe ich hierfür nicht die entgeltliche Hilfe eines Promotionsberaters oder anderer Personen in Anspruch genommen. Niemand hat von mir weder unmittelbar noch mittelbar geldwerte Leistungen für Arbeiten erhalten, die im Zusammenhang mit dem Inhalt der vorgelegten Dissertation stehen.
- (4) Die Arbeit wurde bisher weder im In- noch im Ausland in gleicher oder ähnlicher Form einer anderen Prüfungsbehörde vorgelegt.

Regensburg, der 15.02.2023

